Boundaries, Braneworlds, and Black Holes:

Applications of the AdS/BCFT Correspondence

by

Christopher Neil Waddell

B.Sc., McGill University, 2017

A THESIS SUBMITTED IN PARTIAL FULFILLMENT OF
THE REQUIREMENTS FOR THE DEGREE OF

DOCTOR OF PHILOSOPHY

in

The Faculty of Graduate and Postdoctoral Studies

(Physics)

THE UNIVERSITY OF BRITISH COLUMBIA

(Vancouver)

August 2023

The following individuals certify that they have read, and recommend to the Faculty of Graduate and Postdoctoral Studies for acceptance, the dissertation entitled:

Boundaries, Braneworlds, and Black Holes: Applications of the AdS/BCFT Correspondence

submitted by Christopher Neil Waddell in partial fulfillment of the requirements for the degree of Doctor of Philosophy in Physics.

Examining Committee:

Mark Van Raamsdonk, Professor, Physics, UBC
Supervisor

Moshe Rozali, Professor, Physics, UBC
Supervisory Committee Member

Marcel Franz, Professor, Physics, UBC
University Examiner

Jim Bryan, Professor, Mathematics, UBC
University Examiner

Michael Gutperle, Professor, Physics, University of California, Los Angeles
External Examiner

Additional Supervisory Committee Members:

Gordon Semenoff, Professor, Physics, UBC
Supervisory Committee Member

Gary Hinshaw, Professor, Physics, UBC
Supervisory Committee Member

Abstract

The AdS/CFT correspondence is a far-reaching equivalence between theories of quantum gravity in spacetimes with negative cosmological constant, such as anti-de Sitter (AdS) space, and lower-dimensional, non-gravitational quantum systems, such as conformal field theories (CFTs). In this thesis, we will use a version of AdS/CFT applicable to boundary conformal field theories (BCFTs) to investigate the physics of supersymmetric gauge theories, and to develop holographic models for cosmology and black hole physics. We make frequent use of an ansatz for holographic BCFT wherein AdS spacetime ends on a surface called an end-of-the-world (ETW) brane, and of the Ryu-Takayanagi (RT) formula for holographic entanglement entropy.

We first study the N = 4 supersymmetric Yang-Mills (SYM) theory on a half-space, with boundary conditions preserving scale invariance and half of the original supersymmetry. We calculate a conjectured renormalization group (RG) monotone called boundary F for the most general such boundary conditions using the RT formula. In some cases, we perform an exact calculation using supersymmetric localization, and find exact agreement for the leading large N term as a function of the 't Hooft coupling.

Next, we introduce a toy model for cosmological physics in the framework of AdS/CFT, wherein a 4D cosmology resides on an ETW brane propagating behind the horizon in a black hole microstate. We study the time-dependent physics of the behind-the-horizon region in such microstates, finding that it can often be probed by the time-dependence of entanglement entropy for sufficiently large CFT subsystems. We investigate the plausibility of obtaining localized 4D gravity on the ETW brane in both effective and microscopic versions of this model.

Last, we consider a doubly-holographic model of a radiating black hole,

and apply the RT formula to analyze the time-dependence of the fine-grained entropy of its radiation. We obtain an analogue of the Page curve consistent with unitarity due to a phase transition between RT surfaces, after which the radiation system encodes part of the black hole interior.

Lay Summary

Some quantum mechanical systems have the surprising property that, when the interactions between particles in these systems are tuned to be very strong, they appear to encode gravitational physics in a space with more dimensions. We use this fact to learn about an important quantum system that exhibits this "holographic" property, calculating a quantity which can help to map the space of possible boundary conditions for this system. We also consider the possibility that special high-energy states of such quantum systems may encode the physics of a universe broadly similar to our own, beginning with a "big bang" and recollapsing to a "big crunch". Lastly, we study a holographic quantum system describing a black hole emitting radiation, demonstrating that information which fell into such a black hole will eventually find its way out.

Preface

This is a manuscript-style thesis, whose main content consists of previously published work which is reproduced here verbatim.

Chapters 1 and 2 of this work are an original synthesis of the relevant literature, providing the necessary context and technical prerequisites for later chapters. Section 1.7, which states the objectives of this thesis, is a paraphrasis of the abstracts of the works appearing in this thesis, which were largely written with or by my co-authors in these works.

A version of Chapter 3 was published in [1], in collaboration with Mark Van Raamsdonk. We jointly carried out the holographic calculation found in Section 3.4, and collaborated in writing the material appearing in Sections 3.1, 3.2, 3.3, 3.4, and 3.7. I was solely responsible for the exact calculation using supersymmetric localization found in Section 3.5 and Appendix B.6, as well as the analysis of Section 3.4.3 and 3.6, and Appendices B.4, B.5, and B.7. I am the author of these sections and appendices (with the exception of the finite N comparison appearing in Section 3.5).

A version of Chapter 4 was published in [2], in collaboration with Sean Cooper, Moshe Rozali, Brian Swingle, Mark Van Raamsdonk, and David Wakeham. I was resonsible for the analysis of Ryu-Takayanagi surfaces in dimension $d + 1 = 5$ found in Section 4.3.2, as well as the argument for the cosmological interpretation discussed in Section 4.7; I am the author of the material found in both of these sections.

A version of Chapter 5 was published in [3]; I am the sole author of this material, though I thank Mark Van Raamsdonk for collaboration at an early stage of this work.

A version of Chapter 6 was published in [4], in collaboration with Mark Van Raamsdonk, much of the analysis and the writing of the main body of

this paper (found here in Sections 6.1, 6.2, 6.3 and 6.4) being shared. The elements of this work for which I am solely responsible include the analysis of families of boundary conditions corresponding to arbitrarily large AdS regions (Section 6.4.3 and Appendix E.4), perturbations to these families (Section 6.4.4 and Appendix E.5), the analysis of wedge and multi-wedge holography (Section 6.6 and Appendix E.6), and the proof that the scale of the internal space cannot be suppressed relative to the AdS scale (Appendix E.1), as well as the writing of Sections 6.4.3, 6.4.4, 6.6, 6.7, and all appendices for this chapter.

A version of Chapter 7 was published in [5], in collaboration with Moshe Rozali, James Sully, Mark Van Raamsdonk, and David Wakeham. In addition to participating in the conceptual discussions which lead to this work, I was involved in the gravitational calculation for the static case found in Section 7.3, and am the sole author of Section 7.4.2.

The works [6–8], also completed during the course of my PhD program, will not appear in this thesis.

Table of Contents

List of Figures

Acknowledgements

It is a rare pleasure to have the opportunity to acknowledge and thank the people who have helped me along the way, in a public document that somebody might even read. Having spent the past few years doing something I love in a beautiful city with wonderful people, I have many to thank.

Firstly, I would like to thank my supervisor, Mark Van Raamsdonk, who has been a font of good ideas and intuition. That I have found myself in the right place at the right time to be able to learn from Mark is a happenstance for which I am constantly delighted and thankful. Landing in the right place was made possible with substantial help and/or advice from Robert Brandenberger, Vojkan Jakšić, Alex Maloney, and Andreas Warburton.

As a graduate student, I have greatly benefited from input and insights from my other senior collaborators, Moshe Rozali and Brian Swingle, and various other teachers and mentors, including Mona Berciu, Gary Hinshaw, Gary Horowitz, and Gordon Semenoff.

Next in the quasi-feudal academic hierarchy come the many post-docs; I would like to especially thank Panos Betzios, Aidan Chatwin-Davies, Felix Haehl, Arjun Kar, Charles Marteau, Léo Mangeolle (my KITP roomie), Jason Pollack, Ying Zhao, and particularly Lampros Lamprou, Felipe Rosso, and Jamie Sully. The large cohort of amazing post-docs at UBC throughout my time here has been a secret weapon in my education.

I have had the joy of interacting with and learning from many other students over the past few years, including Stefano Antonini, Suzanne Bintanja, Omar Chammaa, Eric Hansen, Pronobesh Maity, Jane Panangaden, Renaud Raquépas, Oscar Sprumont, and Jordan Wilson-Gerow. My undergraduate survival can be largely attributed to Theo Tomalty, who graciously spent many late nights on Rue Milton comparing problem sets over military-grade

lapsang souchong.

Some of my most emphatic shout-outs are reserved for the many other inhabitants of Hennings 418, namely Jonah Berean-Dutcher, Shovon Biswas, Sean Cooper, Pompey Leung, Alex May, Dominik Neuenfeld, Wyatt Reeves, Abhisek Sahu, Petar Simidzija, David Wakeham, and Rana Zibakhsh. Physics is very fun, but it's even better when shared, and nothing beats standing at a blackboard and repeatedly drawing pictures of cylinders with friends. I would like to single out Alex May, Petar Simidzija, and David Wakeham, my approximate academic cohort, who have been three different instruction manuals for how to do good physics.

The work discussed in this thesis has benefited from the input and insights of many others, including Ahmed Almheiri, Tarek Anous, Jordan Cotler, Davide Gaiotto, Jaume Gomis, Michael Gutperle, Tom Hartman, Eliot Hijano, Kristan Jensen, Andreas Karch, Shiraz Minwalla, Volker Schomerus, and Tadashi Takayanagi, all of whom have been acknowledged in the original papers.

I would also like to acknowledge funding from the National Sciences and Engineering Research Council of Canada, via the CGS-M, PGS-D, and CGS-D programs, and support from the Graduate Fellowship Program of the Kavli Institute for Theoretical Physics, by way of the National Science Foundation under Grant No. NSF PHY-1748958.

My siblings – Jane and Meghan – have wildly discrepant levels of enthusiasm for physics, though this appears uncorrelated with their consistent support for me.

My parents, to whom I dedicate this thesis, deserve special acknowledgment; they taught me to love knowledge for its own sake, to relish all things counter-intuitive and bizarre, and to follow my bliss well outside the realm of practicality. They taught me most of what I know, 300+ page theses about quantum gravity notwithstanding.

I also can't help but thank William Boan and Louis Zhao, the only two non-physicists to have read all of my papers on the arXiv (to gleefully scour for typos).

Last, I thank Soma Dalai: it's a gift to live in a hologram with you.

To my parents, for obvious reasons.

Part I

Invitation

Chapter 1

Introduction

This is a thesis about quantum gravity and its applications. Some of these applications will be commonsense, as in our investigations of black holes and cosmological spacetimes: both entail strong gravitational fields varying on microscopic scales, so it is sensible that quantum gravitational phenomena will come into play. Other applications are perhaps surprising; through *holography*, we will be able to use gravitational physics to study quantum mechanical systems with no explicit gravitational degrees of freedom at all. Since we are interested in quantum gravity, we should clarify what this phrase means, and why it is worth studying; this chapter will provide a user-friendly overview of our motivation and some of the relevant concepts, while the following chapter will cover some more technical preliminaries. Rather than attempting to make our coverage systematic, we emphasize material which will be most relevant for later chapters.

1.1 Why quantize gravity?

In the pursuit of a theory describing gravitational phenomena in a quantum mechanical framework, the most naïve approach one might consider is to simply quantize small fluctuations of spacetime, along with whatever other quantum fields may be present, on a fixed background, utilizing the standard techniques of quantum field theory; we might refer to such a gestalt as *semi-classical*. This perturbative approach, while entirely consistent (see e.g. [10, 11]), is incomplete, in the sense that it is unable to make predictions about the outcome of certain experiments, which may involve high-energy particles or strong gravitational fields.

To preview why this might be the case, one need only observe that

the gravitational coupling governing graviton-graviton interactions is Newton's gravitational constant G, which has mass dimension $[G] = -(D-2)$ in D spacetime dimensions. In the machinery of perturbative quantum field theory, this suggests that Einstein gravity is (perturbatively) *non-renormalizable*;[1] a graviton scattering amplitude with centre of mass energy E may be computed as a power series in the ratio of the energy to the Planck mass E/m_p, and therefore breaks down at the Planck scale. Such considerations suggest that gravity is best understood from the Wilsonian viewpoint, as an *effective field theory* with a cutoff at or somewhat below the Planck scale. Following this philosophy, we should start by positing a symmetry group that should be present in the theory (here diffeomorphism and Lorentz invariance), and write down the most general Lagrangian consistent with these symmetries, with coefficients fixed by dimensional analysis up to $O(1)$ factors.[2] This procedure allows one to make predictions for the outcome of low-energy experiments; to understand high-energy experiments, where new physics is expected to play an important role, one requires an *ultraviolet (UV) completion* of the effective field theory.

1.2 String theory

The above discussion motivates the pursuit of a UV complete quantum mechanical theory which reproduces ordinary Einstein gravity at low energies. At present, perhaps the most promising candidate for such a theory is *string theory*, which is believed to be UV finite (see e.g. [14–17]) and which has long been understood to naturally incorporate a graviton in its spectrum [18–20].

While modern string theory is a vast and rich discipline, encompassing a variety of physical objects and phenomena, a natural starting point for the study of string theory is the quantization of the classical theory of a

[1] It is a logical possibility that Einstein gravity, while being *perturbatively* non-renormalizable, secretly corresponds to an RG flow with a UV fixed point; this paradigm is referred to as *asymptotic safety* [12].

[2] Conspicuously, this philosophy is in dramatic contradiction to the observed value of the cosmological constant; this is the *cosmological constant problem*, see e.g. [13].

propagating string. The fundamental degrees of freedom in this theory describe the embedding of a two-dimensional surface, the *string worldsheet*, into a D-dimensional spacetime, the *target space*; the action principle then requires that the area of the resultant embedding should be extremized. To fully define the classical theory, we must also specify boundary conditions for the embedding functions; these can correspond to either open or closed strings. In the former case, the possibility of a fixed boundary condition for some coordinates, implying that the string endpoint is constrained to lie in some $(p+1)$-dimensional surface in spacetime, presages the existence of extended objects known as *Dp-branes* on which fundamental strings can end.

Canonically quantizing the classical theory, one finds an infinite tower of states, with masses separated by a large energy scale (the *string scale*), with a finite number of particles at each mass level. In the versions of this theory enjoying *supersymmetry*, a symmetry relating bosonic and fermionic degrees of freedom, the lowest mass level consists of massless states, which include a vector boson for the open string and a graviton for the closed string. It can be shown that the low-energy effective field theories describing the tree-level physics of the massless spectrum of various supersymmetric string theories are ten-dimensional supersymmetric theories of gravity, known as *supergravity* theories.

For superstring theory to be well-defined at the quantum level, it transpires that the number of spacetime dimensions must be equal to $D = 10$. This suggests that, if string theory were to describe a universe like our own, some of the spatial dimensions must be *compactified* to microscopic scales, an idea we will return to shortly. Beyond ensuring the theory's consistency, the introduction of compactified extra dimensions leads to interesting phenomenological consequences, given that the geometry of these extra dimensions plays a role in determining the particle spectrum as seen by a 4D observer via the *Kaluza-Klein (KK) mechanism* [21, 22].

One of the most important developments in the study of string theory has been the elucidation of the central role played by D-branes [23]; rather than the rigid surfaces appearing in the classical theory, D-branes have been

understood to correspond to dynamical, fluctuating objects on which additional fields may reside. A particularly interesting example is the D3-brane appearing in the superstring theory known as *type IIB string theory*; the low-energy effective action of a stack of D3-branes, capturing the physics of massless open string modes, is a special gauge theory known as $\mathcal{N} = 4$ *supersymmetric Yang-Mills (SYM) theory*. This fact plays a crucial role in motivating the AdS/CFT correspondence, elaborated on in the following section.

1.3 Holography

There have long been intimations that the fundamental quantum description of gravity should be *holographic*, in the sense that the physics of a gravitating region may be best described in terms of degrees of freedom associated to the region's boundary. In 1972, Bekenstein argued on the basis of a simple thought experiment that, to avoid violations of the second law of thermodynamics, one should associate a thermodynamic entropy to a black hole proportional to its horizon area in Planck units [24, 25]. Taking this idea seriously suggests a holographic entropy bound which must be satisfied by *any* quantum mechanical theory which contains black holes: thermodynamic entropy that can be put into a gravitating region cannot exceed the area of that region, since otherwise one could create a black hole within the region by adding enough additional matter, violating a generalized version of the second law of thermodynamics [26]. The surprising implication is that the number of degrees of freedom required to describe a gravitating region quantum mechanically scales with the area of the region's boundary, in stark contrast to the volume-extensive entropy scaling of typical quantum mechanical systems. This type of reasoning led 't Hooft, and later Susskind, to argue for a "holographic principle" governing quantum gravity [27, 28]. Only a few years later, this principle received beautiful microscopic incarnation, in the form of the AdS/CFT correspondence [29].

The AdS/CFT correspondence

An interesting observation in physics is that different regimes of a physical theory may be most naturally described in terms of different degrees of freedom; for example, Yang-Mills theory can be thought of as a theory of glueballs at strong coupling. A remarkable and surprising fact is that, when we consider certain conventional quantum systems in a strong coupling limit, the natural degrees of freedom in which to formulate the theory are inherently geometrical. In some cases, the dynamics of these degrees of freedom may even be governed by Einstein gravity.

The *AdS/CFT correspondence*, more inclusively referred to as holography or *gauge/gravity duality*, describes a precise equivalence between two quantum mechanical theories [29–31]. In the canonical version of AdS/CFT, one of these two theories, sometimes referred to as the *bulk* theory, is a $(d+1)$-dimensional theory of quantum gravity in a negatively curved, or *anti-de Sitter (AdS)*, spacetime. The other, equivalent theory, often referred to as the *boundary theory*, is a conventional, non-gravitational, d-dimensional theory known as a *conformal field theory (CFT)*; this name refers to the presence of a collection of symmetries of the theory, known as conformal symmetries, which includes scale invariance in addition to the standard Poincaré invariance of local quantum field theory. The boundary theory is so-named because it can be thought of as residing on the (conformal) boundary of the bulk AdS spacetime, thereby providing a precise realization of the holographic principle. As this boundary theory becomes increasingly strongly coupled, the corresponding bulk theory becomes increasingly well-approximated by classical supergravity.

Though its earliest and most precise manifestations provide a relationship between specific, microscopic supersymmetric gauge theories and superstring theories, the AdS/CFT correspondence has long been understood to apply much more broadly; effective field theories in AdS are believed to give rise to approximate conformal field theories on very general grounds, and conditions under which a conformal field theory should admit such a bulk description, namely for a conformal field theory to be *holographic*, have

been proposed [32] and extensively studied (see e.g. [33–38]).

The development of an increasingly detailed understanding of the mapping between theories related by AdS/CFT duality, colloquially referred to as the *holographic dictionary*, has permitted unprecedented computational control in understanding both quantum gravitational systems and strongly coupled quantum field theories. One of the most important entries in this dictionary, the *GKPW dictionary* [30, 31], can be used to make explicit the relationship between a variety of physical data appearing in theories related by holographic duality, from correlation functions of local operators to information theoretic quantities. As such, the AdS/CFT dictionary has led to a variety of revolutionary insights, from properties of quantum mechanical black holes to the emergence of spacetime, and even to applications well beyond the traditional purview of quantum gravity (see e.g. the reviews [39, 40]).

It from qubit

One of most elegant and exciting programs in the study of AdS/CFT has been guided by the realization that, even without detailed input regarding the structure of a holographic CFT, certain basic properties of information processing in quantum mechanical systems may be responsible, via the duality, for basic properties of gravitational physics. An early suggestion of the role played by *quantum entanglement* in the state of a holographic CFT was the observation that a particular highly entangled state of such a theory could encode the physics of a two-sided black hole, whose two asymptotic regions are connected by a spatial *wormhole* [41]. Further progress was permitted by a groundbreaking result of Ryu and Takayanagi [42], who conjectured a powerful generalization of Bekenstein's formula for the entropy of a black hole in the context of AdS/CFT. The *Ryu-Takayanagi (RT) formula* equates the *von Neumann entropy* of spatial subregions of the boundary CFT, which can be used to characterize the amount of entanglement between degrees of freedom inside and outside of these subregions, to the area of certain extremal surfaces in the bulk theory, thereby "geometrizing" the

entanglement structure of holographic states.

A particularly influential application of the Ryu-Takayanagi formula has been to argue more broadly that the connectivity of spacetime may arise from the entanglement structure of the underlying holographic degrees of freedom [43–45]. This philosophy represents a fundamental reversal of the puzzle of reconciling gravity and quantum mechanics, suggesting that the geometrical structure so central to Einstein's theory of gravity is precisely a manifestation of the fundamentally quantum property of entanglement.

1.4 Black holes

Black holes are among the most fundamental objects in any theory of quantum gravity; indeed, the effort to establish a theoretical framework capable of describing the quantum physics of black holes has been an important engine driving the pursuit of a UV completion for gravity. In spite of this motivation, a key theme of quantum gravity research in recent years has been the surprising extent to which foundational and previously inexplicable features of quantum black holes, from their unitary dynamics to a precise accounting of their microstates, appear to be recoverable from semi-classical methods.

As mentioned above, reconciling the existence of black holes with the laws of thermodynamics appears to require one to associate a thermodynamic entropy to a black hole which is proportional to its area in Planck units [24]. Circumstantial evidence for this proposal was granted by the discovery of the *laws of black hole mechanics* [46], theorems governing the behaviour of black holes in classical gravity which suggest an analogy with typical thermodynamic systems. In the context of statistical mechanics, thermodynamic entropy admits an interpretation as counting the microstates of a theory corresponding to some collection of fixed macroscopic observables. However, in classical gravity, the interpretation of a putative thermodynamic entropy is mysterious, as classical black holes satisfy *no-hair theorems* [47–49] which imply that they are completely characterized by a small number of charges, and therefore appear to permit no distinct microstates. This observation

indicates that a statistical interpretation of the black hole entropy should necessarily invoke quantum mechanics.

Indeed, stronger support for understanding black holes as genuine thermodynamic systems came from Hawking's calculation of the spectrum of radiation emitted by a quantum mechanical black hole [50], based on a semi-classical treatment of quantum fields propagating on a black hole background. This analysis suggested that black holes radiate with a perfect blackbody spectrum, with an associated entropy given precisely by the aforementioned area law, often referred to as the *Bekenstein-Hawking formula* for the entropy. An alternative derivation of the Bekenstein-Hawking entropy formula was later given by Gibbons and Hawking [51], making use of a Euclidean version of Feynman's path integral formalism applied to semi-classical gravity. These results invite an interpretation of black hole physics which is now sometimes referred to as the *central dogma of black hole mechanics* [52]: we should think of a black hole as a regular quantum mechanical system interacting with its environment, with roughly one degree of freedom per unit area in Planck units.

This understanding of black hole microphysics has found explicit realization in string theory and AdS/CFT. An important result of Strominger and Vafa [53] provided a precise microstate-counting interpretation of the Bekenstein-Hawking formula for a particular class of supersymmetric black holes in string theory; this result has since been substantially generalized, including to account for subleading corrections to the black hole entropy formula (see [54] for a review). In AdS/CFT, black holes may be understood as corresponding to thermal states of a holographic CFT [55], and the Bekenstein-Hawking entropy formula appears as a special case of the Ryu-Takayanagi formula applied to these states.

Despite these advances, a long outstanding question regarding black hole physics follows from a disquieting consequence of Hawking's calculation, namely a tension between effective field theory and unitarity, sometimes termed the *black hole information problem*: given that the radiation emitted by an evaporating black hole is thermal, its evolution appears to transform a pure state prior to black hole formation into a mixed state after its

complete evaporation, violating unitarity [56]. A useful diagnostic for the deviation from unitarity is the von Neumann entropy of the radiation, which here can be thought of as measuring the amount of entanglement between the radiation and the black hole, or more generally, as characterizing the degree of uncertainty in the underlying quantum state of the radiation. In unitary quantum mechanics, the von Neumann entropy would rise with the early emission of Hawking radiation, saturate at the value of the Bekenstein-Hawking entropy, and decrease to zero when the black hole evaporates, following a profile known as the *Page curve* [57, 58]. The inflection point of this curve, occurring at a time referred to as the *Page time*, must demarcate the onset of physics not accounted for in Hawking's analysis.

An especially striking statement of the black hole information problem is known as the *firewall paradox*, which suggests that preserving both unitarity and semi-classical physics in weakly-curved spacetime necessarily implies the existence of extremely high-energy excitations at the horizon of an old black hole [59, 60] (see also [61, 62]). This conclusion arises from a thought experiment regarding the distribution of entanglement between a black hole and its environment. To comply with unitarity, quantum information must escape in the radiation emitted from a black hole after the Page time, implying that a photon emitted at late times should be maximally entangled with the early Hawking radiation. Basic quantum mechanical constraints then imply that the entanglement between this photon and all modes in the black hole interior must be completely severed, at the price of dramatic consequences at the horizon. Refined versions of the firewall paradox remain unresolved at the time of writing, though an intriguing principle for addressing this problem, the *ER=EPR* proposal of Maldacena and Susskind [45], suggests a means for circumventing the paradox may be to posit that the early radiation modes and the interior modes should be identified, with the two seemingly disparate spacetime regions that these modes occupy being connected by microscopic wormholes.

Recent developments have shed significant light on many of these issues, suggesting that, in defiance of long-held expectations, a careful effective field theory calculation can reproduce a unitary Page curve [9, 63–67]. In

particular, a subtle modification of the formula used to compute the entropy of Hawking radiation appears to be necessary when applied to gravitational systems; this alteration can be motivated by the observation that the Euclidean gravitational path integrals which can be used to compute these entropies must include additional, previously neglected saddle-point configurations referred to as *replica wormholes* [65, 66]. A model for understanding the modified entropy formula without recourse to the Euclidean gravitational path integral has also been provided by [67], which makes concrete the idea that exponentially small quantum overlaps in the naïvely orthogonal wavefunctions of effective field theory excitations in the black hole interior can explain the need for a correction to Hawking's calculation.[3] A counter-intuitive consequence of these findings has been the conclusion that an experimenter acting only on the Hawking radiation of an old black hole can in principle instantaneously manipulate objects in its interior.

1.5 Braneworlds

As mentioned previously, the consistency of string theory relies on the existence of extra spacetime dimensions; consequently, taking seriously the idea that string theory could describe our universe, one seemingly requires some of these dimensions to be compact in order to avoid conflict with observation. A naïve expectation is that these extra dimensions must be very small to avoid detection in high-energy collider experiments.[4] However, an interesting alternative to compactification, often referred to as the *RSII model*,[5] was offered by Randall and Sundrum [72]; in this model, one envisions low-energy observers localized to a four-dimensional membrane which cuts off a five-dimensional AdS spacetime near its conformal boundary. In contrast to

[3] Very recently, a careful treatment of these overlaps has apparently enabled a precise accounting for the Bekenstein-Hawking entropy at the level of effective field theory [68, 69].

[4] An early challenge to this expectation was raised by Arkani-Hamed, Dimopoulous, and Dvali, who proposed that a compactification manifold could have sizes up to 1 mm if gravity is the only known force capable of probing the extra dimensions [70].

[5] An earlier instantiation of this model, the RSI model, involved a compact extra dimension, and was intended to solve the hierarchy problem regarding the large discrepancy between the Planck scale and the electroweak scale [71].

the simplest compactifications appearing in string theory, the RSII model is what is known as a *warped compactification*, meaning that the local geometry in the full spacetime depends non-trivially on one's location in the extra dimensions.

Studying the classical gravitational fluctuations around the background RSII geometry, one finds a massless graviton in the spectrum, whose wavefunction is localized to the brane. There is additionally a continuum of Kaluza-Klein modes with arbitrarily small mass, but the suppression of the wavefunctions of these modes at the brane ensures that corrections to 4D gravity for brane-localized observers remain small. Given that the RSII background corresponds to a piece of AdS, the physics of this model has a natural interpretation in AdS/CFT [73–76]; one can think of cutting off AdS by placing a *Planck brane* near its boundary as tantamount to introducing a UV cutoff in the dual CFT, and coupling this theory to dynamical 4D gravity. With the possibility of localizing gravity to a membrane in a higher-dimensional theory arose a substantial industry of studying phenomena like black holes, gravitational waves, and cosmology on Randall-Sundrum branes, sometimes referred to as *braneworlds* in this context; see [77] for a review.

A more precise proposal for embedding the RSII idea in string theory came from Karch and Randall [78, 79], who considered putting an d-dimensional AdS brane (rather than a flat brane) in $(d+1)$-dimensional AdS; in this model, one obtains a non-zero gap in the Kaluza-Klein spectrum, but 4D gravity is only "locally localized", because the graviton obtains a small mass. The Karch-Randall set-up is expected to arise from a holographic theory where conformal symmetry is partially broken by a boundary or defect, perhaps arising from the low-energy physics of stacks of intersecting D-branes in string theory; consequently, it represents one of the first suggestions that holographic systems with boundaries may have interesting applications.

1.6 Boundaries

Much less central than the developments mentioned so far within the realm of quantum gravity is a subgenre of holographic literature concerned with extending the AdS/CFT dictionary to encompass holographic quantum field theories with boundaries. A particularly tractable class of quantum field theories with boundaries are *boundary conformal field theories (BCFTs)*; these theories are well-motivated and widely studied in the context of condensed matter physics [80–85], providing insight into quantum systems with impurities or finite size effects. In 2D, BCFTs are also of direct relevance to perturbative string theory, providing a description of the worldsheet theory in the presence of a D-brane boundary condition; see [86] for a review. The subject of the holographic correspondence for boundary conformal field theories sometimes goes by the title of the *AdS/BCFT correspondence*.

A crucial feature of the proposed holographic duals for BCFTs, including the effective model of [78, 87, 88] as well as microscopic realizations in supergravity, is that the bulk theory involves a spacetime which ends on a surface known as an *end-of-the-world (ETW) brane*, or which smoothly degenerates in a macroscopic "ETW brane region". In addition to allowing one to use the tools of AdS/CFT to study the physics of field theories with boundaries, the possibility of introducing a new gravitating object in the bulk enriches the space of physical systems that one can study in the quantum gravity theory; as in the aforementioned braneworld scenarios, black holes or entire universes may reside on an ETW brane.

1.7 This thesis

Our objectives in this thesis will be three-fold.

First, in Chapter 3, we will apply a microscopic version of the AdS/BCFT correspondence to investigate the physics of the celebrated $\mathcal{N} = 4$ supersymmetric Yang-Mills theory with gauge group $U(N)$. We consider the full space of conformally invariant boundary conditions for this theory which preserve half of the original supersymmetry, as classified by Gaiotto and

Witten [89, 90]. These boundary conditions arise from string theory constructions involving D3-branes ending on collections of 5-branes. The theories obtained for each choice of boundary condition are characterized by a quantity called *boundary* F, conjectured to decrease under renormalization group flows triggered by deformations with boundary-localized operators. We perform a holographic calculation of boundary F for all such theories by evaluating the entanglement entropy for a half-ball centered on the BCFT boundary using the Ryu-Takayanagi formula in the dual solutions of type IIB supergravity. For a subset of these boundary conditions, we also calculate boundary F exactly by evaluating the hemisphere partition function using supersymmetric localization. We find that the leading term at large N in the supergravity and localization results agree exactly as a function of the 't Hooft coupling λ.

Second, in Chapters 4, 5, and 6, we will propose and study a microscopic quantum mechanical model for cosmological physics which embeds the braneworld paradigm into the framework of AdS/BCFT, commenting on how field theory observables may be used to probe the cosmological evolution, and investigating whether localized 4D gravity can be achieved in either effective or microscopic versions of this model. In Chapter 4, we explore the possibility that certain high-energy holographic CFT states correspond to black hole microstates with a geometrical behind-the-horizon region, modelled by a portion of a second asymptotic region terminating at an ETW brane. We study the time-dependent physics of this behind-the-horizon region, whose ETW boundary geometry takes the form of a closed FRW spacetime. We show that in many cases, this behind-the-horizon physics can be probed directly by looking at the time dependence of entanglement entropy for sufficiently large spatial CFT subsystems. In Chapter 5, we consider simple generalizations of this set-up with an additional interface brane propagating in the bulk. We find that solutions with a viable cosmological interpretation for the ETW brane, wherein gravity is localized, exist only if our model is further generalized, for example by including an Einstein-Hilbert term in the ETW brane action. In Chapter 6, we return to the solutions of type IIB string theory dual to $\mathcal{N} = 4$ supersymmetric

Yang-Mills theory on half of $\mathbb{R}^{1,3}$ with half-supersymmetric boundary conditions which were used for the holographic calculations in an earlier chapter. We show that, by choosing the boundary conditions appropriately, the ETW brane region appearing in the supergravity solutions can be pushed arbitrarily far towards the "missing" asymptotic boundary, recovering an arbitrarily large wedge of Poincaré $AdS_5 \times S^5$, a pre-condition for gravity localization in such theories.

Finally, in Chapter 7, following [9, 63, 64], we introduce and study various holographic systems which can describe evaporating black holes. The systems we consider are boundary conformal field theories for which the number of local degrees of freedom on the boundary (c_{bdy}) is large compared to the number of local degrees of freedom in the bulk CFT (c_{bulk}). We consider states where the boundary degrees of freedom on their own would describe an equilibrium black hole, but the coupling to the bulk CFT degrees of freedom allows this black hole to evaporate. The Page time for the black hole is controlled by the ratio $c_{\text{bdy}}/c_{\text{bulk}}$. Using both holographic calculations and direct CFT calculations, we study the evolution of the entanglement entropy for the subset of the radiation system (i.e. the "bulk" CFT) at a distance $d > a$ from the boundary, with fixed a. We find that the entanglement entropy for this subsystem increases until time $t = a + t_{\text{Page}}$ and then undergoes a phase transition, after which the entanglement wedge of the radiation system includes the black hole interior. Remarkably, this occurs even if the radiation system is initially at the same temperature as the black hole so that the two are in thermal equilibrium. In this case, even though the black hole does not lose energy, it "radiates" information through interaction with the radiation system until the radiation system contains enough information to reconstruct the black hole interior.

Chapter 2

The Theoretical Minimum

In this chapter, we aim to provide the minimal number of definitions and technicalities required to understand subsequent chapters, as well as a brief introduction to some of the standard "lore" which will be useful to contextualize our results.

2.1 Gravity

While our investigations utilize the AdS/CFT correspondence, which defines a theory of *quantum* gravity, we will often be interested in studying the case that the gravity side of the duality is in the *classical* regime, with vanishingly small string coupling constant and a string length suppressed relative to the curvature scale of the background. It is therefore useful to recall some features of the relevant classical gravity theories and their solutions. We focus here on a class of solutions of Einstein gravity with negative cosmological constant which are central to the study of AdS/CFT, and a particular ten-dimensional supergravity theory which will be the context for gravity calculations in later chapters. We will draw upon material from [91–96] in this section.

2.1.1 Anti-de Sitter

Anti-de Sitter (AdS) space is the maximally symmetric solution of the vacuum Einstein equations with negative cosmological constant Λ,[6] arising from

[6] We will sometimes refer to this solution as *pure AdS* to distinguish it from the asymptotically AdS spacetimes considered momentarily.

the Einstein-Hilbert Lagrangian density with cosmological constant term

$$\mathcal{L}_{\text{EH}} = \frac{1}{16\pi G}\left(R - 2\Lambda\right) . \tag{2.1}$$

The $(d+1)$-dimensional space AdS_{d+1} is naturally realized as a hyperboloid embedded in flat space $\mathbb{R}^{2,d}$,[7] whose locus in the flat coordinates X^M is

$$\eta_{MN}X^M X^N = -L_{\text{AdS}}^2 , \qquad \eta = \text{diag}(-1,-1,\underbrace{1,\ldots,1}_{d}) . \tag{2.2}$$

Here, L_{AdS} is called the *AdS radius*, and sets the curvature scale of the spacetime; it is related to the cosmological constant Λ by

$$\Lambda = -\frac{d(d-1)}{2L_{\text{AdS}}^2} . \tag{2.3}$$

This embedding makes manifest that the isometries of AdS_{d+1} form the *conformal group* $SO(2,d)$ of d-dimensional Minkowski space, to be introduced in Section 2.2.1, here realized as Lorentz transformations in the embedding space $\mathbb{R}^{2,d}$.[8]

Pure AdS: global coordinates

The geometry obtained from the above embedding has closed timelike curves, so we are typically interested in passing to the *universal covering space*; in pedestrian terms, we would like to decompactify a timelike direction. To do this, it is useful to introduce *global coordinates* $(\rho, t, \hat{x}^i)$ via the coordinate transformation

$$\begin{aligned} X^{-1} &= L_{\text{AdS}}\cosh(\rho)\sin(t) \\ X^0 &= L_{\text{AdS}}\cosh(\rho)\cos(t) \\ X^i &= L_{\text{AdS}}\sinh(\rho)\hat{x}^i , \end{aligned} \tag{2.4}$$

[7] We choose to denote the dimensionality of AdS by $d+1$ in preparation for its appearance in the context of AdS/CFT.

[8] Our embedding construction gives Lorentzian AdS_{d+1}; to obtain Euclidean AdS_{d+1}, also known as *hyperbolic space*, we should instead embed in $\mathbb{R}^{1,d+1}$. The isometry group of Euclidean AdS_{d+1} is then $SO(1,d+1)$.

with $\hat{x}^i$ a vector on the unit S^{d-1} such that $\sum_{i=1}^{d} \hat{x}_i^2 = 1$. In these coordinates, one arrives at the metric

$$ds^2 = L_{\text{AdS}}^2 \big[-\cosh^2(\rho) dt^2 + d\rho^2 + \sinh^2(\rho) d\Omega_{d-1}^2 \big] , \tag{2.5}$$

and one can then readily pass to the universal covering space by extending to the non-compact interval $t \in \mathbb{R}$.

Taking the radial coordinate transformation $r = \tan(\rho)$, the same space can be parametrized by new global coordinates $(r, t, \hat{x}^i)$, with metric

$$ds^2 = L_{\text{AdS}}^2 \left[-f(r) dt^2 + \frac{dr^2}{f(r)} + r^2 d\Omega_{d-1}^2 \right] , \quad f(r) = \left(1 + \frac{r^2}{L_{\text{AdS}}^2} \right) . \tag{2.6}$$

It is perhaps easiest to study the global structure of AdS by making an alternative change of radial coordinates $\tan\vartheta = \sinh\rho$, obtaining a third set of global coordinates

$$ds^2 = \frac{L_{\text{AdS}}^2}{\cos^2\vartheta} \left[-dt^2 + d\vartheta^2 + \sin^2\vartheta d\Omega_{d-1}^2 \right] . \tag{2.7}$$

Evidently, there is a second order pole at $\vartheta = \pi/2$; this is the *conformal boundary* of the spacetime. To conformally compactify, we can multiply the metric by a *defining function* with a second order zero at $\vartheta = \pi/2$. The ambiguity in choosing such a defining function manifests in a rescaling ambiguity $g_{\mu\nu}(x) \sim \Omega(x)^2 g_{\mu\nu}(x)$ of the d-dimensional metric of the conformal boundary, which one therefore thinks of as a *conformal structure* rather than a fixed (pseudo-)Riemannian manifold. The conformal compactification of AdS_{d+1} is the manifold-with-boundary obtained via this procedure.

Our three choices of global coordinates above all cover an identical manifold, which we refer to as *global AdS*. It is often useful to visualize global AdS, via conformal compactification, as a solid cylinder (with some of the sphere directions suppressed for $d > 2$); see Figure 2.1. One can justify this by considering the expression (2.7) with the overall conformal factor neglected. Here, the radial coordinate ϑ is identified with the radial direc-

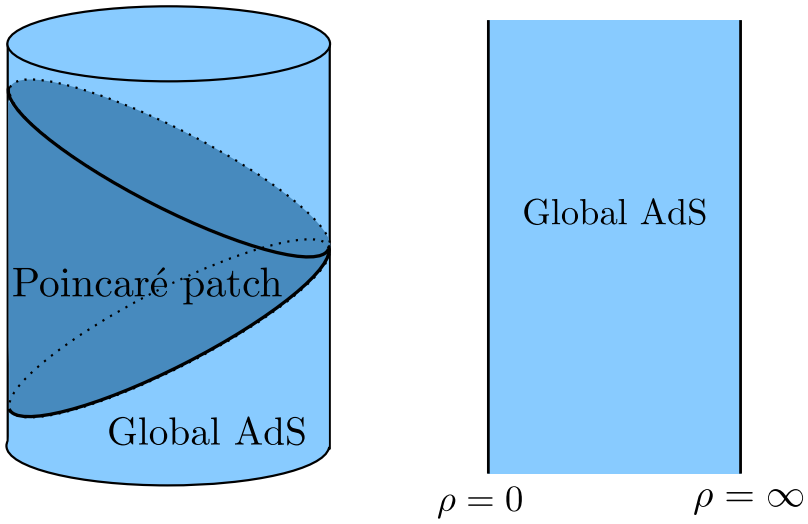

Figure 2.1: (Left) Solid cylinder (light and navy blue) representing the conformal compactification of AdS, with the Poincaré patch shaded (navy blue). This diagram suppresses some sphere directions for $d+1 > 3$. (Right) Penrose diagram for global AdS.

tion of the cylinder, t is identified with the axial direction,[9] and one of the spherical directions appears as an S^1. Suppressing all spherical directions, we obtain the Penrose diagram of global AdS shown in Figure 2.1.

It is often stated that global AdS is "like a box", in the sense that a massive observer moving in AdS can send a light ray toward the conformal boundary and receive its reflection in finite proper time (assuming reflecting boundary conditions). However, the trajectories of massive particles cannot reach the conformal boundary, so the space is complete with respect to timelike geodesics.

[9] A similar cylinder picture can be used to visualize Euclidean AdS, obtained via the Wick rotation $\tau = it$.

Pure AdS: Poincaré coordinates

It is often useful to instead consider the AdS geometry in *Poincaré coordinates*, in which case the metric is given by

$$ds^2 = \frac{L_{\text{AdS}}^2}{z^2}\left[dz^2 - dt^2 + d\vec{x}^2\right], \tag{2.8}$$

where the conformal boundary is now located at $z = 0$. These coordinates exchange the spherical S^{d-1} symmetry of global AdS for a planar $\mathbb{R}^{d-1}$ symmetry. The Poincaré coordinates only cover a portion of global AdS, the so-called *Poincaré patch*[10], illustrated in Figure 2.1. The metric degenerates at $z = \infty$, referred to as the *Poincaré horizon*.

Asymptotically anti-de Sitter spacetimes

In the context of holography, one is often interested in spacetimes with AdS asymptotics; we refer to a spacetime as *asymptotically locally AdS* if it is conformally compact and satisfies the equation $R_{\mu\nu} = -dg_{\mu\nu}$ at leading order near the conformal boundary. Such a spacetime is *asymptotically globally AdS* if it additionally has the boundary topology of global AdS, namely the cylinder $\mathbb{R} \times S^{d-1}$. We will sometimes use the phrase *asymptotically AdS (AAdS)* in place of asymptotically locally AdS.

The metric in the neighbourhood of the conformal boundary in such spacetimes may be expressed in *Fefferman-Graham coordinates* as

$$ds^2 = \frac{L^2}{z^2}\left[dz^2 + \Gamma_{\mu\nu}(z,x)dx^\mu dx^\nu\right], \tag{2.9}$$

where the function $\Gamma_{\mu\nu}(z,x)$ has the near boundary expansion

$$\Gamma_{\mu\nu}(z,x) = g^{(0)}_{\mu\nu}(x) + O(z^2). \tag{2.10}$$

In particular, $g^{(0)}_{\mu\nu}(x)$ is a representative of the boundary conformal structure for the spacetime; in AdS/CFT, we will see that this can be thought of as

[10] The Poincaré patch in Euclidean signature covers the entirety of Euclidean AdS, with the Poincaré horizon $z = \infty$ equivalent to the origin of global coordinates $\rho = r = \vartheta = 0$.

the spacetime background for a holographic quantum field theory.

AdS black holes

A particularly interesting asymptotically locally AdS spacetime is the *AdS black hole*, sometimes known as the *eternal AdS black hole* or the *AdS Schwarzschild* spacetime; in Schwarzschild coordinates, the metric of this spacetime takes the form

$$\begin{aligned} ds^2 &= L_{\text{AdS}}^2 \left[-f(r)dt^2 + \frac{dr^2}{f(r)} + r^2 d\Omega_{d-1}^2 \right] , \\ f(r) &= \frac{r^2}{L_{\text{AdS}}^2} + 1 - \frac{r_H^{d-2}}{r^{d-2}} \left(\frac{r_H^2}{L_{\text{AdS}}^2} + 1 \right) . \end{aligned} \tag{2.11}$$

There is a coordinate horizon at $r = r_H$, where $f(r) = 0$ and the metric degenerates.

Much like the asymptotically flat Schwarzschild black hole, the AdS Schwarzschild black hole permits a two-sided maximal extension, as can be analyzed by switching to *Kruskal coordinates*

$$U = -e^{-2(t-r_*)} , \quad V = e^{2(t+r_*)} , \tag{2.12}$$

where $r_* = \int_0^r \frac{dr'}{f(r')} + C$ is a *tortoise coordinate*, with the integration constant C chosen to enforce the reality of the Kruskal coordinates outside the horizon.[11] In these coordinates, the metric takes the form

$$ds^2 = L_{\text{AdS}}^2 \left[-\frac{f}{4} e^{-4r_*} dU dV + r^2 d\Omega_{d-1}^2 \right] . \tag{2.13}$$

The Penrose diagram for the AdS black hole is shown in Figure 2.2.

Another black hole which is an asymptotically locally AdS spacetime is

[11] The tortoise coordinate implicitly depends on a choice of contour around the simple pole at $r = r_H$, and the integral $\int_0^r \frac{dr'}{f(r')}$ will typically take imaginary values for $r > r_H$; we may choose C to ensure that $r_*(r)$ is real when $r > r_H$.

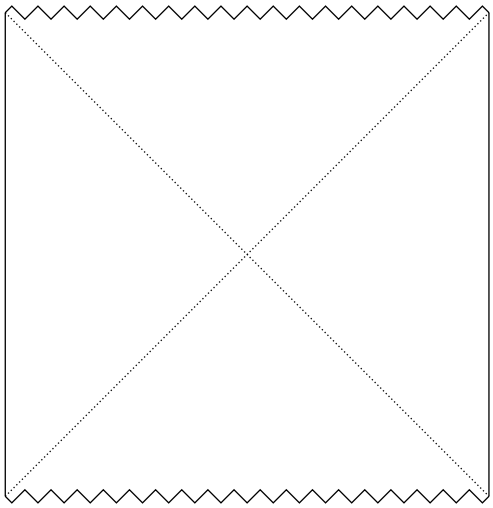

Figure 2.2: Penrose diagram for the maximally extended AdS Schwarzschild black hole. The geometry includes two exterior asymptotic regions, as well as past and future singularities. The horizons are denoted by dotted lines. In dimensions $d+1 > 3$, the past and future singularities curve upward and downward respectively compared to what is illustrated here.

the *planar AdS black hole*, whose metric is

$$ds^2 = \frac{L_{\text{AdS}}^2}{z^2}\left(-f(z)dt^2 + \frac{dz^2}{f(z)} + d\vec{x}_{d-1}^2\right), \qquad f(z) = 1 - \frac{z^d}{z_H^d}. \tag{2.14}$$

The planar AdS black hole can be obtained as a limit $r_H/L_{\text{AdS}} \to \infty$, letting $z \sim L_{\text{AdS}}/r$; when the black hole becomes very large, the horizon appears locally flat.

2.1.2 Type IIB supergravity

The *type IIB supergravity (SUGRA)* theory is a ten-dimensional theory of gravity; in the string theory context, it arises as an effective description of the massless sector of the type IIB superstring. The field content of this theory consists of:

- A metric g_{MN}

- Two real scalars $C_{(0)}$ (the *axion*) and Φ (the *dilaton*), sometimes combined into a complex scalar (the *axion-dilaton*)

$$\tau = C_{(0)} + ie^{-\Phi} \tag{2.15}$$

- Two two-form fields $B_{(2)}$ (the *NS-NS two-form*) and $C_{(2)}$ (the *R-R two-form*)
- One four-form field $C_{(4)}$ (the *R-R 4-form*) whose field strength satisfies a self-duality condition defined below
- Two left-handed Majorana-Weyl fermions Ψ_I^M (the *gravitinos*) and two right-handed Majorana-Weyl fermions λ_I (the *dilatinos*).

Various relevant conventions pertaining to the parameters of the type IIB supergravity and string theory in the context of the AdS/CFT correspondence can be found in Appendix B.1.

As usual, taking an exterior derivative of the p-form $C_{(p)}$ yields a $(p+1)$-form field strength $F_{(p)} = dC_{(p)}$. It is convenient to define combined field strength tensors

$$\begin{aligned} H_{(3)} &= dB_{(2)} \,, \quad \tilde{F}_{(3)} = F_{(3)} - C_{(0)}H_{(3)} \,, \\ \tilde{F}_{(5)} &= F_{(5)} - \frac{1}{2}C_{(2)} \wedge H_{(3)} + \frac{1}{2}B_{(2)} \wedge F_{(3)} \,; \end{aligned} \tag{2.16}$$

in particular, the action for type IIB supergravity is most readily expressed in terms of the combined field strengths, as is the self-duality condition imposed on the field strength associated to the four-form

$$\tilde{F}_5 = *\tilde{F}_5 \,. \tag{2.17}$$

Action and supersymmetry

There is an important subtlety in formulating an action principle for this theory, since we have a self-duality condition on the five-form field strength, which cannot arise as an equation of motion. However, one can derive the

equations of motion from a (string frame) action whose bosonic part is

$$2\kappa_0^2 S_{IIB} = \int d^{10}x\sqrt{-g}\Bigg[e^{-2\Phi}\left(R + 4\partial_M\Phi\partial^M\Phi - \frac{1}{2}|H_{(3)}|^2\right) - \frac{1}{2}|F_{(1)}|^2 - \frac{1}{2}|\tilde{F}_{(3)}|^2 - \frac{1}{4}|\tilde{F}_{(5)}|^2\Bigg] - \frac{1}{2}\int C_{(4)} \wedge H_{(3)} \wedge F_{(3)} \,, \quad (2.18)$$

and then enforce self-duality of $\tilde{F}_5$ *a posteriori* as a separate condition. Here, κ_0^2 is a gravitational constant which is related to the ten-dimensional (Einstein frame) Newton constant in (2.20).

The type IIB theory is invariant under various global supersymmetry transformations, which can be parametrized by a 16-component (complex) Weyl spinor of $SO(1,9)$; the theory consequently has 32 real supersymmetries. We refrain from recording these transformations here, though they can be found in the works [97–99] which introduced the type IIB theory; in our conventions, the supersymmetry transformations for the fermions can be found in [95]. Notably, the action written above is not invariant under all of these supersymmetries off-shell.

String frame and Einstein frame

The gravitational kinetic term in the above action has an additional factor of the dilaton $e^{-2\Phi}$ compared to the typical Einstein-Hilbert action; however, it is possible to perform a field redefinition of the metric to recover the latter, at the expense of modifying the remaining kinetic terms. The asymptotic value Φ_∞ of the dilaton sets the magnitude of the string coupling $g = e^{\Phi_\infty}$, which appears in the topological expansion of the worldsheet path integral. To convert from the *string frame* to the *Einstein frame*, one simply redefines the metric

$$g_{\mu\nu}^{(\mathrm{SF})} \to g_{\mu\nu}^{(\mathrm{EF})} \equiv e^{(\Phi_\infty - \Phi)/2} g_{\mu\nu}^{(\mathrm{SF})} \,. \quad (2.19)$$

We typically suppress the labels SF and EF when the frame is clear from context. This redefinition of the metric yields

$$\frac{1}{2\kappa_0^2}\int d^{10}x\,\sqrt{-g}e^{-2\Phi}R \to \frac{1}{2\kappa^2}\int d^{10}x\,\sqrt{-g}\left(R-\frac{9}{2}\partial_\mu\Phi\partial^\mu\Phi\right) \tag{2.20}$$

where the right-hand side is implicitly in terms of the Einstein frame metric. The ten-dimensional Newton constant G_{10}, the couplings κ_0^2 and κ^2 in the string frame and Einstein frame actions, the string coupling g, and the string length $\ell_s = \sqrt{\alpha'}$ are related by

$$16\pi G_{10} = 2\kappa^2 = 2\kappa_0^2 g^2 = (2\pi)^7(\alpha')^4 g^2\,. \tag{2.21}$$

D3-branes, D5-branes, and NS5-branes

Type IIB string theory describes various extended objects which are charged under the various gauge fields in the theory; in general, a p-brane is the source for a $(p+1)$-form gauge field $A_{(p+1)}$, with the coupling given schematically by the pullback to the worldvolume M_{p+1} of the brane

$$S \sim Q_p \int_{M_{p+1}} A_{(p+1)}\,, \tag{2.22}$$

where Q_p is the charge. Since we have seen that the spectrum of type IIB supergravity includes zero-form, two-form, and four-form gauge fields, we anticipate the existence of D(-1)-branes, D1-branes, and D3-branes in the theory; in fact, there are additional branes which are magnetically charged under some of these fields. In later chapters, we will be most concerned with the following branes:

- The D3-brane, electrically charged under the R-R four-form $C_{(4)}$
- The D5-brane, magnetically charged under the R-R two-form $C_{(2)}$
- The NS5-brane, magnetically charged under the NS-NS two-form $B_{(2)}$.

In supergravity, the manifestation of these branes is the existence of solitonic solutions, known as *black brane* solutions, which carry the appro-

priate charges (as computed by integrating the appropriate flux over an S^{8-p} surrounding the brane in the transverse space). Solutions relevant for Dp-branes in the theory are

$$\begin{aligned} ds_{10}^2 &= \frac{1}{\sqrt{H_p(r)}}\eta_{\mu\nu}dx^\mu dx^\nu + \sqrt{H_p(r)}(dr^2 + r^2 d\Omega_{8-p}^2)\,, \\ e^\Phi &= gH_p(r)^{(3-p)/4}\,, \qquad B_{MN} = 0\,, \\ C_{(p+1)} &= \left(\frac{1}{H_p(r)} - 1\right) dx^0 \wedge dx^1 \wedge \ldots \wedge dx^p\,, \end{aligned} \tag{2.23}$$

with $H_p(r) = 1 + \left(\frac{L_p}{r}\right)^{7-p}$ and

$$L_p^{7-p} = (4\pi)^{(5-p)/2}\Gamma\left(\frac{7-p}{2}\right) gN(\alpha')^{(7-p)/2}\,, \tag{2.24}$$

where N is interpreted as the number of coincident Dp-branes (quantized in the full string theory). On the other hand, solutions relevant to the NS5-branes are

$$\begin{aligned} ds^2 &= \frac{1}{H_5(r)^{1/4}}\eta_{\mu\nu}dx^\mu dx^\nu + H_5(r)^{3/4}(dr^2 + r^2 d\Omega_3^2)\,, \\ e^\Phi &= gH_5(r)^{1/2}\,, \quad B_{(6)} = \left(\frac{1}{H_5(r)} - 1\right) dx^0 \wedge \ldots \wedge dx^5\,, \end{aligned} \tag{2.25}$$

with $H_5(r) = 1 + \frac{L_5^2}{r^2}$ and $L_5^2 = \alpha' N$, and N the number of NS5-branes. Here, the six-form field $B_{(6)}$ is obtained by dualizing $B_{(2)}$.

2.2 Conformal field theory

In this section, we provide a brief introduction to the notion of a particular class of quantum field theories known as *conformal field theories* (*CFTs*). We restrict our presentation to some definitions and basic properties, since this is all that we will require in the remainder of this thesis. Our focus will be on the case of dimension $d > 2$, since two-dimensional conformal field theories have an enhanced symmetry and consequently a special mathemat-

ical structure which will not be relevant for our purposes. In this thesis, we will be specifically interested in CFTs defined by a path integral; while this assumption may not be necessary to formulate some general properties, we will assume it here when convenient. An introduction to the path integral methods used throughout this thesis can be found in Appendix A.1.

2.2.1 Conformal field theory: preliminaries

Our exposition in this section will draw from [100–105]; these references may be consulted for additional background. Further details relevant to conformal field theory are collected in Appendix A.2.

The conformal algebra

The symmetry algebra of a conformal field theory in flat space is the *conformal algebra*, with non-vanishing commutators

$$\begin{aligned}
[D, P_\mu] &= iP_\mu \,, \\
[D, K_\mu] &= -iK_\mu \,, \\
[K_\mu, P_\nu] &= 2i(\eta_{\mu\nu} D - L_{\mu\nu}) \,, \\
[K_\rho, L_{\mu\nu}] &= i(\eta_{\rho\mu} K_\nu - \eta_{\rho\nu} K_\mu) \,, \\
[P_\rho, L_{\mu\nu}] &= i(\eta_{\rho\mu} P_\nu - \eta_{\rho\nu} P_\mu) \,, \\
[L_{\mu\nu}, L_{\rho\sigma}] &= i(\eta_{\nu\rho} L_{\mu\sigma} + \eta_{\mu\sigma} L_{\nu\rho} - \eta_{\mu\rho} L_{\nu\sigma} - \eta_{\nu\sigma} L_{\mu\rho}) \,,
\end{aligned} \tag{2.26}$$

where $\eta_{\mu\nu}$ denotes the flat Lorentzian (or Euclidean) metric. In a conformal field theory, this algebra is realized by charges associated to conserved currents which can be constructed by contracting the energy-momentum tensor $T^{\mu\nu}$ with vector fields ξ^μ which satisfy

$$\partial_\mu \xi_\nu + \partial_\nu \xi_\mu = \frac{2}{d} \eta_{\mu\nu} \partial_\rho \xi^\rho \,. \tag{2.27}$$

This equation is known as the *conformal Killing equation*, and its solutions are referred to as *conformal Killing vectors*.[12] The significance of such vectors is that they generate the *conformal isometries* of flat space, which can be thought of as diffeomorphisms from flat space to itself which preserve the metric up to a local rescaling. Conservation and tracelessness of the energy-momentum tensor in conformal field theory,

$$\partial_\mu T^{\mu\nu} = 0\,, \qquad T^\mu_\mu = 0\,, \qquad \text{(operator equation)} \tag{2.28}$$

ensure the conservation of the associated charges when ξ^μ is a conformal Killing vector. When interpreting these conformal isometries as transformations on the fields in a theory, the generators are represented by differential operators which satisfy the conformal algebra.

The last two commutation relations in the algebra (2.26) encode the Poincaré (or Euclidean) subalgebra, generated by momentum generators P_μ and Lorentz (or rotation) generators $L_{\mu\nu}$. The additional generators in the conformal algebra are the generator of *dilations* D, associated to the vector field which generates scale transformations $x^\mu \to \lambda x^\mu$, and the generator of *special conformal transformations (SCTs)* K_μ, associated to the vector field which generates the transformations

$$x^\mu \to \frac{x^\mu + b^\mu x^2}{1 + 2b\cdot x + b^2 x^2}\,. \tag{2.29}$$

The SCTs may be understood as corresponding to a translation conjugated by an inversion $x^\mu \to \frac{x^\mu}{x^2}$, which itself is not a globally well-defined diffeomorphism of flat space.

It is edifying to repackage some of these generators as

$$\begin{aligned} J_{\mu\nu} &= L_{\mu\nu}\,, & J_{-1,0} &= D\,, \\ J_{-1,\mu} &= \frac{1}{2}(P_\mu - K_\mu)\,, & J_{0,\mu} &= \frac{1}{2}(P_\mu + K_\mu)\,, \end{aligned}$$

[12] The subset of solutions for which the right-hand side of the conformal Killing equation vanishes are the *Killing vectors*, corresponding to Poincaré (Euclidean) transformations in flat Lorentzian (Euclidean) space.

whereby one can demonstrate that the conformal algebra is manifestly $\mathfrak{so}(2,d)$ or $\mathfrak{so}(1,d+1)$ in Lorentzian and Euclidean signature respectively,

$$[J_{ab}, J_{cd}] = i(\eta_{ad}J_{bc} + \eta_{bc}J_{ad} - \eta_{ac}J_{bd} - \eta_{bd}J_{ac}) \,. \tag{2.30}$$

Representations: primaries and descendants

To define a quantum field theory, one can begin by choosing a background for the theory and specifying a collection of local fields transforming in representations of a given symmetry group. These fields can appear in correlation functions, as computed by the Euclidean path integral, which are consequently constrained by symmetry. One may then choose a foliation of the background, with slices related by an isometry (or a conformal isometry in the case of a CFT), interpreted as the generator of Euclidean "time". The Hilbert space is constructed with respect to this foliation, which is referred to as a *quantization* of the theory, by slicing the path integral. Euclidean correlators with field insertions may be interpreted as time-ordered vacuum expectation values of local operators with respect to Euclidean time. Under suitable technical assumptions, this approach can be used to construct a well-defined, unitary Lorentzian theory, whose correlation functions can be obtained from the Euclidean correlators by analytic continuation. In this subsection, we will discuss what it means to have local operators transforming in representations of the conformal symmetry algebra.

Suppose that the conformal algebra $\mathfrak{so}(1,d+1)$ that acts on the algebra of local operators in Euclidean signature is represented by the generators $(\mathcal{P}_\mu, \mathcal{L}_{\mu\nu}, \mathcal{D}, \mathcal{K}_\mu)$. Given that $(\mathcal{L}_{\mu\nu}, \mathcal{D}, \mathcal{K}_\mu)$ is the subalgebra of the conformal algebra associated to transformations of the plane which keep the origin fixed, we can define the operator content of the theory by positing the existence of local operators $\{O^a(0)\}$ at the origin transforming in irreducible representations of this subalgebra, then define $O^a(x) = e^{x\cdot P}O^a(0)e^{-x\cdot P}$. In particular, we can take the Cartan subalgebra to be generated by $(\mathcal{L}_{\mu\nu}, \mathcal{D})$; noting that $\mathcal{K}_\mu$ acts as a lowering operator for $\mathcal{D}$, we can seek lowest weight

representations generated by *primary operators* $O^a(0)$ satisfying

$$\begin{aligned} [\mathcal{L}_{\mu\nu}, O^a(0)] &= (S_{\mu\nu})^a{}_b O^b(0) \\ [\mathcal{D}, O^a(0)] &= \Delta O^a(0) \qquad\qquad \text{(operator equations)} \\ [\mathcal{K}_\mu, O^a(0)] &= 0\,. \end{aligned} \tag{2.31}$$

Here, $S_{\mu\nu}$ are some finite-dimensional representation matrices for $\mathfrak{so}(d)$, and Δ is the *scaling dimension* (or *conformal dimension*) of O^a.

The rest of the corresponding irreducible representation consists of *descendant operators*, which can be obtained by acting on $O^a(0)$ with the raising operator P_μ (via the commutator). This has the effect of taking derivatives of the operator $O^a(x)$ at $x = 0$, and thereby raising the scaling dimension $\Delta \to \Delta + 1$; for example, one has

$$[P_\mu, O^a(x)] = \partial_\mu O^a(x)\,. \qquad \text{(operator equation)} \tag{2.32}$$

Quantization

A standard choice of quantization for conformal field theories in flat space is *radial quantization*, in which we foliate the Euclidean plane by concentric spheres S^{d-1} centred at the origin. This is particularly convenient in CFT because the dilation operator $\mathcal{D}$ generates (Euclidean) evolution between the leaves of this foliation.

Another appealing property of radial quantization arises from the observation that d-dimensional punctured Euclidean flat space is conformally equivalent to the Euclidean cylinder $\mathbb{R} \times S^{d-1}$, with the radial coordinate r of flat space and the axial coordinate τ of the cylinder related by $r = e^\tau$:

$$ds^2_{\mathbb{R}\times S^{d-1}} = d\tau^2 + d\Omega^2_{d-1} = \frac{1}{r^2}\left(dr^2 + r^2 d\Omega^2_{d-1}\right) \propto ds^2_{\mathbb{R}^d}\,. \tag{2.33}$$

Consequently, as explained in Appendix A.2, the correlation functions in a conformal field theory defined on the former space are determined by those on the latter; for example, using the r coordinate for both the plane and the

cylinder as above, we have for scalar operators[13]

$$\begin{aligned}\frac{\langle O_1(r_1,\hat{x}_1^i)\dots O_n(r_n,\hat{x}_n^i)\rangle_{\mathbb{R}\times S^{d-1}}}{\langle 1\rangle_{\mathbb{R}\times S^{d-1}}} \\ = \left(\prod_{i=1}^n r_i^{\Delta_i}\right)\frac{\langle O_1(r_1,\hat{x}_1^i)\dots O_n(r_n,\hat{x}_n^i)\rangle_{\mathbb{R}^d}}{\langle 1\rangle_{\mathbb{R}^d}}\,.\end{aligned} \tag{2.34}$$

The map between the two spaces sends concentric spheres S^{d-1} centred at the origin to the spherical slices of the cylinder at fixed Euclidean time τ; consequently, the radially quantized theory in flat space is related to the theory on the cylinder with the standard quantization.

The choice of quantization fixes a notion of conjugation for Euclidean operators; as an example, if $O_L(t,\hat{x}^i)$ denotes a Hermitian scalar operator in the Lorentzian theory on the cylinder with the standard quantization, then the analytic continuation $\tau = it$ to Euclidean signature implies the conjugation rule for Euclidean operators

$$O_E(\tau,\hat{x}^i)^\dagger = O_E(-\tau,\hat{x}^i)\,. \tag{2.35}$$

More generally, we may be interested in operators which have Lorentz indices, and which consequently accumulate additional imaginary factors upon analytic continuation of the time-like indices; for example, the Lorentzian vector operator $O_L^\mu(t,\hat{x}^i)$ undergoes analytic continuation

$$O_E^0(\tau,\hat{x}^i) = -iO_L^0(t,\hat{x}^i)\,,\quad O_E^i(\tau,\hat{x}^i) = O_L^i(t,\hat{x}^i)\,. \tag{2.36}$$

For these more general operators, conjugation acts on the Euclidean operators as

$$O_E^{\mu_1\dots\mu_n}(\tau,\hat{x}^i)^\dagger = \Theta^{\mu_1}_{\nu_1}\dots\Theta^{\mu_n}_{\nu_n}O_E^{\nu_1\dots\nu_n}(-\tau,\hat{x}^i)\,, \tag{2.37}$$

where $\Theta^\mu_\nu = \delta^\mu_\nu - 2\delta^\mu_0\delta^0_\nu$ may be interpreted as a time-reflection.

Using the relationship (2.34) between correlators on the cylinder and flat space, we observe that, for a given operator $O(r,\hat{x}^i)$ in the flat space

[13]The explicit denominators in this expression account for the possibility of a *Weyl anomaly* $\langle 1\rangle_{\mathbb{R}\times S^{d-1}} \neq \langle 1\rangle_{\mathbb{R}^d}$.

theory, we can formally define another operator $O_{\text{cyl}}(r, \hat{x}^i) \equiv r^{\Delta} O(r, \hat{x}^i)$ in the *flat space* theory whose correlators can precisely reproduce those of the original operator on the cylinder; using this identification, and demanding that O_{cyl} satisfy the conjugation rules for the cylinder outlined above, we can obtain the conjugation rules for the corresponding flat space operators in radial quantization. In particular, for scalar operators, we obtain (now using Cartesian coordinates on the plane for convenience)

$$O(x^\mu)^\dagger = x^{-2\Delta} O(x^\mu / x^2) \,, \tag{2.38}$$

while for operators with spin, we obtain

$$O^{\mu_1 \dots \mu_n}(x^\mu)^\dagger = I^{\mu_1}_{\nu_1}(x) \dots I^{\mu_n}_{\nu_n}(x) x^{-2\Delta} O^{\nu_1 \dots \nu_n}(x^\mu / x^2) \,, \tag{2.39}$$

where $I^\mu_\nu(x) = \delta^\mu_\nu - \frac{2x^\mu x_\nu}{x^2}$.

Having established a notion of conjugation compatible between Euclidean and Lorentzian signature, we can begin to address the question of necessary conditions for a Euclidean CFT to have a well-defined, unitary Lorentzian continuation. A basic requirement of unitarity is that the norm of all states in the Hilbert space must be positive definite; in Euclidean signature, this corresponds to the statement of *reflection positivity*, which demands that time reflection-symmetric correlators must be positive

$$\langle 0 | O(\tau_n, \hat{x}^i_n) \dots O(\tau_1, \hat{x}^i_1) O(-\tau_1, \hat{x}^i_1) \dots O(-\tau_n, \hat{x}^i_n) | 0 \rangle \geq 0 \,. \tag{2.40}$$

The operator-state correspondence

In any quantum field theory, one can associate a state $|O\rangle$ in the radially quantized Hilbert space to any local operator $O(x)$ in the theory: given a sphere S^{d-1}_R of radius R centred at the origin, we can simply choose the state $|O\rangle$ on S^{d-1}_R which is prepared by the Euclidean path integral on the ball B^d_R with a single insertion of $O(0)$ at the origin. Explicitly, we may define

$|O\rangle$ by requiring that, for any state $|\phi_0\rangle$ in the Hilbert space,

$$\langle\phi_0|O\rangle = \int^{\phi(r=R)=\phi_0} \mathcal{D}\phi\, e^{-S[\phi]} O(0)\,. \tag{2.41}$$

In a conformal field theory, the converse is also true. Given an eigenstate of the dilatation operator $|O\rangle$ with eigenvalue Δ, we can compute the overlap with any other state $|\Psi\rangle$ by a Euclidean path integral

$$\begin{aligned}\langle\Phi|O\rangle &= e^{(R-r)\Delta}\langle\Phi|e^{-(R-r)D}|O\rangle \\ &= e^{(R-r)\Delta}\int d\phi_1\langle\phi_1|O\rangle\int d\phi_2\langle\Phi|\phi_2\rangle\int_{\phi(r)=\phi_1}^{\phi(R)=\phi_2}\mathcal{D}\phi e^{-S[\phi]}\,,\end{aligned} \tag{2.42}$$

for any $r < R$. In the limit $r \to 0$, the insertion of the state $|O\rangle$ in the path integral can be replaced by a local operator. We can extend this correspondence to all states in the Hilbert space by linearity (and limits).

The operator-state correspondence helps us to organize the Hilbert space of the theory into representations of the conformal algebra. In particular, the map implies the following:

- The identity operator $\mathbb{1}$ corresponds to the vacuum state $|0\rangle$.
- A primary operator $O^a(x)$ of conformal dimension Δ transforming in a representation of $\mathfrak{so}(d)$ with representation matrices $S_{\mu\nu}$ corresponds to a state $|O^a\rangle$ satisfying

$$K_\mu|O^a\rangle = 0\,, \quad D|O^a\rangle = \Delta|O^a\rangle\,, \quad \mathcal{L}_{\mu\nu}|O^a\rangle = (S_{\mu\nu})^a_{\ b}|O^b\rangle\,. \tag{2.43}$$

- Descendant operators of $O^a(x)$ correspond to descendant states

$$P_\mu|O\rangle,\ P_\mu P_\nu|O\rangle\,,\ \ldots \tag{2.44}$$

  A primary state and its descendants together form an irreducible representation of the conformal algebra, sometimes called a *conformal multiplet*.

Operator product expansion

The primary operators in a CFT satisfy a fusion algebra, referred to as the *operator product expansion (OPE)*

$$O_i^a(x_1)O_j^b(x_2) = \sum_k [C_{ijk}(x_{12}, \partial_2)]_c^{ab} O_k^c(x_2) \qquad \text{(operator equation)} \quad (2.45)$$

valid as an operator statement (i.e. provided we do not have an insertion within the smallest ball containing the two operators on the left-hand side). Here, we are in Euclidean signature, and $C_{ijk}(x_{12}, \partial_2)$ denotes a differential operator which may also have Lorentz representation indices.

The existence of an operator product expansion should hold in a general quantum field theory for arbitrary local operators; however, in conformal field theory, conformal invariance significantly constrains this OPE, and in particular the differential operators $C_{ijk}(x_{12}, \partial_2)$, such that the contributions of descendant operators in the OPE are entirely fixed by the contribution of the corresponding primary. Moreover, the OPE is easily proven in CFT as a consequence of the operator-state correspondence, given that $O_i(x_1)O_j(x_2)|0\rangle$ is a state in the Hilbert space and therefore admits an expansion in terms of primary states $O_k(x_2)|0\rangle$ and their descendants. The operator statement is obtained by considering inner products between these states and any other states built from acting on the vacuum with local operators outside of a ball containing x_1 and x_2.

CFT correlators

Often, the field theory observables we are interested in are correlation functions of local operators; in CFT, these are highly constrained by symmetry, as manifested through Ward identities, which specify how the symmetry generators act when inserted in correlation functions with local primaries. If the CFT is defined by a path integral, correlators arise from operator insertions

$$\langle O_1(x_1) \dots O_n(x_n) \rangle = \int \mathcal{D}\Phi e^{-S[\Phi]}\, O_1(x_1) \dots O_n(x_n)\,, \qquad (2.46)$$

where the $O_i(x_i)$ on the right-hand side are functions constructed from the fields Φ and their derivatives; in this case, the Ward identities can be shown to arise from a (non-anomalous) symmetry of the action. Given a choice of quantization, these objects are interpreted as time-ordered vacuum expectation values, with respect to the Euclidean time of the quantization

$$\langle O_1(x_1)\dots O_n(x_n)\rangle \equiv \langle 0|\mathcal{T}\{O_1(x_1)\dots O_n(x_n)\}|0\rangle\,. \tag{2.47}$$

Rather than revisit the derivation of low-point conformal correlators, which can be found in e.g. [101], we simply state the results. It suffices to consider correlation functions of primary operators, since general correlators can be generated from these via insertions of P^μ, using the Ward identities. In the following, we denote the Euclidean distance $x_{12} \equiv |x_1 - x_2|$ for convenience.

In conformal field theory, one-point functions of non-trivial primary operators vanish identically

$$\langle O(x)\rangle = \begin{cases} 0 & O \neq \mathbb{1} \\ 1 & O = \mathbb{1} \end{cases}\,. \tag{2.48}$$

Scalar primary two-point functions are fixed up to a proportionality constant C_O

$$\langle O_i(x_1)O_j(x_2)\rangle = \begin{cases} \frac{C_O}{x_{12}^{2\Delta}} & \Delta_i = \Delta_j \equiv \Delta \\ 0 & \Delta_i \neq \Delta_j \end{cases}\,; \tag{2.49}$$

we can eliminate the factor C_O by choosing a normalized basis of primary operators, i.e. by rescaling the O_i. On the other hand, the scalar primary three-point function is of the form

$$\langle O_i(x_1)O_j(x_2)O_k(x_3)\rangle = \frac{C_{ijk}}{x_{12}^{\Delta_i+\Delta_j-\Delta_k}x_{23}^{\Delta_j+\Delta_k-\Delta_i}x_{31}^{\Delta_k+\Delta_i-\Delta_j}}\,, \tag{2.50}$$

where the coefficients C_{ijk} represent genuine physical data about the theory equivalent to that contained in the OPE.

Up to this point, the spatial dependence of the correlation functions has

been completely determined by conformal invariance; it is said that these correlators are fixed by *kinematic* considerations, rather than depending on the particular theory of interest, i.e. the *dynamics*. By contrast, the scalar primary four-point function involves a function of the *conformal cross-ratios*

$$u = \frac{x_{12}^2 x_{34}^2}{x_{13}^2 x_{24}^2}\,, \qquad v = \frac{x_{23}^2 x_{14}^2}{x_{13}^2 x_{24}^2}\,, \tag{2.51}$$

the two independent quantities constructed from (x_1, x_2, x_3, x_4) which can be demonstrated to be invariant under conformal transformations. For example, one can verify that the four-point function of a single scalar primary

$$\langle O(x_1)O(x_2)O(x_3)O(x_4)\rangle = \frac{g(u,v)}{x_{12}^{2\Delta}x_{34}^{2\Delta}} \tag{2.52}$$

has the required symmetry properties for any function g. For a given theory, we will see momentarily how the function g is related to other data constituting the theory.

The OPE can be used to reduce high-point correlation functions to lower-point correlation functions. An important example of this is the four-point function; applying the OPE to the four-point function of a single scalar primary, one obtains

$$\langle \overbrace{O(x_1)O}(x_2)\overbrace{O(x_3)O}(x_4)\rangle = \frac{1}{x_{12}^{2\Delta_O}x_{34}^{2\Delta_O}}\sum_{O'} C_{OOO'}^2 g_{\Delta_{O'},\ell_{O'}}(x_i)\,,$$

where we have indicated pairwise contraction using the OPE, the sum is over primaries, and we have defined the objects

$$g_{\Delta,\ell}(x_i) \equiv x_{12}^{2\Delta_O}x_{34}^{2\Delta_O} C_a(x_{12},\partial_2)C_b(x_{34},\partial_4)\frac{I^{ab}(x_{24})}{x_{24}^{2\Delta}}\,, \tag{2.53}$$

where $I^\mu_\nu(x)$ is as introduced below (2.39). These objects are known as *conformal blocks*; it can be shown that they depend only on the invariant cross-ratios (u, v), and therefore that the function $g(u, v)$ appearing in (2.52)

can be expressed as

$$g(u,v) = \sum_{O'} C^2_{OOO'} g_{\Delta_O,\ell_O}(u,v)\,. \tag{2.54}$$

In this sense, the conformal blocks form a basis for the space of conformally invariant four-point functions.

The order of contractions with the OPE used above is sometimes referred to as the *S-channel*; however, we could choose to expand the four-point function in another channel, using a different sequence of contractions, thereby obtaining a different expression involving different coefficients and conformal blocks. The consistency of these two expansions, referred to as *crossing symmetry*, enforces powerful constraints on permissible CFT data.

We note in passing that correlation functions for operators with spin are somewhat more complicated, though still constrained. As an example, the two-point function of a spin-ℓ symmetric traceless tensor is

$$\langle O^{\mu_1\ldots\mu_\ell}(x) O_{\nu_1\ldots\nu_\ell}(0)\rangle = C_O \left(\frac{I^{(\mu_1}_{\nu_1}(x)\ldots I^{\mu_\ell)}_{\nu_\ell}(x)}{x^{2\Delta}} - (\text{traces}) \right)\,, \tag{2.55}$$

where the subtraction is intended to ensure that this object is traceless in both the μ-indices and the ν-indices.

The bootstrap philosophy

It is worth briefly mentioning an important perspective on conformal field theory informed by the *conformal bootstrap* program, which seeks to explore and characterize the space of legitimate conformal field theories by deriving consequences from simple consistency conditions, like unitarity and crossing symmetry, and possibly additional assumptions, such as restricting to large N or holographic CFTs, or demanding superconformal symmetry.

From this perspective, a general CFT can be thought of as being determined by the following data:[14]

[14] It is currently unknown whether additional non-local information needs to be specified in dimension $d > 2$.

- A list of local primary operator scaling dimensions and spins $\{(\Delta, s)\}$, and possibly other quantum numbers if we would like to impose additional structure (e.g. R-charges in the case of a superconformal field theory). This data is sometimes referred to as the *spectrum* of the theory, and encodes the kinematics.

- A list of OPE coefficients $\{c_{ijk}\}$, which encodes the dynamics.

The conformal bootstrap then proceeds by imposing certain consistency conditions on this data, thereby ruling out regions of the parameter space. In general, there is no known set of sufficient consistency conditions for the existence of a CFT that can be easily implemented in the bootstrap approach.

2.2.2 Boundary conformal field theory

Having provided an overview of the subject of conformal field theory, we can turn to a generalization, *boundary conformal field theory (BCFT)*, which will be most relevant in the following chapters. Roughly speaking, a BCFT can be obtained from a CFT by introducing a codimension-1 boundary, thereby reducing the symmetry of the theory; a detailed discussion of BCFT in arbitrary dimension can be found in [80, 106]. For simplicity of presentation, we will restrict our discussion to the case of a planar boundary in flat Euclidean space $\mathbb{R}^d$.

Suppose that we decompose the coordinates of $\mathbb{R}^d$ as

$$\mathbf{x} \equiv (x_1, \ldots, x_{d-1}) \,, \qquad y \equiv x_d \,, \tag{2.56}$$

and introduce a spatial boundary at $y = 0$, so that our background now corresponds to the half-space $H\mathbb{R}^d$ defined by $y \geq 0$. As observed in [80], such a boundary remains invariant under an $SO(1, d)$ subgroup of the original conformal group, generated by the $(d-1)$-dimensional Poincaré transformations on the transverse coordinates $\mathbf{x}$ together with the usual inversion $x^\mu \to x^\mu / x^2$. We may then define a BCFT on the half-space by specifying the spectrum of primary CFT bulk operators, transforming as in (2.31)

under the residual conformal group, and their OPE coeffiients, along with some additional boundary data, which we discuss momentarily. Typically, we will be interested in the case where a BCFT is defined with reference to a particular CFT on the original space by imposing suitable boundary conditions on the CFT bulk fields and possibly introducing additional degrees of freedom at the boundary, such that the resulting theory respects the $SO(1,d)$ symmetry.

Given that a general transformation from the residual conformal group applied to points x_1, x_2 induce transformations of the form

$$(x_1 - x_2)^2 \to \frac{(x_1 - x_2)^2}{\Omega(x_1)\Omega(x_2)}\,, \qquad y_i \to \frac{y_i}{\Omega(x_i)} \tag{2.57}$$

for some conformal factor Ω, we see that the cross-ratios

$$\xi \equiv \frac{(x_1 - x_2)^2}{4y_1 y_2}\,, \qquad v^2 \equiv \frac{(x_1 - x_2)^2}{(x_1 - x_2)^2 + 4y_1 y_2} = \frac{\xi}{\xi + 1} \tag{2.58}$$

are invariant. The reduced symmetry now permits non-vanishing one-point functions for primary scalar fields of the form

$$\langle O(x) \rangle = \frac{A_O}{(2y)^\Delta}\,. \tag{2.59}$$

If we choose to normalize the CFT bulk operators by specifying the two-point functions in the original CFT, then the constants A_O appearing in the one-point functions are physically meaningful, depending generically on the operator $O(x)$ and its boundary condition. Moreover, the two-point function of quasi-primary bulk CFT operators may now be proportional to a function of the invariant cross-ratio defined above, and is not necessarily vanishing for operators with distinct scale dimension or spin. For example, the scalar-scalar two-point function takes the form

$$\langle O_1(x_1) O_2(x_2) \rangle = \frac{1}{(2y_1)^{\Delta_1}(2y_2)^{\Delta_2}} f_{12}(\xi)\,, \tag{2.60}$$

where the function f_{12} is constrained by the OPE.

As we mentioned above, one must also specify additional boundary data in order to determine the BCFT. In addition to the bulk CFT operators, we may generically have a spectrum of local boundary operators $\hat{O}_I(\mathbf{x})$ (where the circumflex connotes quantities at the boundary). These boundary operators, which are specified by their own scaling dimensions and OPE, also form a basis for the BCFT, in the sense that one has a *boundary operator expansion (BOE)* analogous to the OPE

$$O_i(x) = \sum_J \frac{B_i^J}{(2y)^{\Delta_i - \hat{\Delta}_J}} \hat{O}_J(\mathbf{x}) + (\text{descendants}) \,. \tag{2.61}$$

In particular, $A_O = B_O^1$. The BOE also constrains the function f_{12} appearing in the CFT bulk two-point function. More generally, correlation functions may be decomposed in either bulk or boundary channels, providing general crossing-symmetry constraints which must be satisfied by the dynamical BCFT data.

To summarize, the BCFT is characterized by the spectrum of bulk operators and their OPE coefficients, the spectrum of boundary operators and their OPE coefficients, and the bulk-boundary two-point function coefficients.

2.3 Supersymmetry

The notion of *supersymmetry*, a type of spacetime symmetry which interrelates bosonic and fermionic degrees of freedom, plays an integral role in the study of string theory and of AdS/CFT. Supersymmetry can also serve as a powerful tool for simplifying calculations and obtaining exact results in otherwise intractable systems like strongly coupled gauge theories. Our objective in this section will be to introduce the concept of supersymmetry and the terminology which will be important in the remainder of this thesis; to achieve this concisely, we largely focus our presentation on the case of Lorentzian signature. Our discussion will draw on material from the references [96, 107–113].

2.3.1 Supersymmetry algberas in 3D and 4D

We begin with a discussion of the 3D and 4D supersymmetry algebras. Our exposition will focus on the case of the supersymmetric extensions of the Poincaré algebra, relevant to theories in flat space (and conformal theories in conformally flat spaces).

Supersymmetry algebra in 4D

The supersymmetric extension of the 4D Poincaré algebra is obtained by augmenting the Poincaré algebra by additional fermionic supersymmetry generators, which obey the algebra

$$\{Q^A_\alpha, \tilde{Q}_{\dot{\alpha}B}\} = 2\delta^A_B \sigma^\mu_{\alpha\dot{\alpha}} P_\mu \,, \quad \{Q^A_\alpha, Q^B_\beta\} = 2\epsilon_{\alpha\beta} Z^{AB} \,, \tag{2.62}$$

where $\tilde{Q}_{\dot{\alpha}I} = (Q^I_\alpha)^\dagger$.[15] Here, $\sigma^\mu = (1, \vec{\sigma})$ are the Pauli matrices, P^μ are the momentum generators, and the elements of the anti-symmetric tensor Z^{IJ} are referred to as *central charges*, since they commute with all of the generators. Note that the Greek indices are two-component spinor indices, which are raised and lowered with the anti-symmetric symbol $\epsilon_{\alpha\beta}$ and its inverse, while the uppercase Latin indices run in the list $\{1, \ldots, \mathcal{N}\}$, and are raised and lowered with δ_{AB} and its inverse. In particular, we have $4\mathcal{N}$ real supersymmetries in 4D. The remainder of the super-Poincaré algebra is fixed by noting that the supercharges transform as Weyl spinors under $\mathfrak{so}(1,3)$, and commute with translations.

In a supersymmetric theory, the supersymmetry generators may transform under a bosonic symmetry referred to as an *R-symmetry*. Formally, the R-symmetry is the subgroup of outer automorphisms of the super-Poincaré algebra which leave the Poincaré subgroup invariant. As an example, we observe that a supersymmetric theory with $\mathcal{N} > 1$ has a manifest $SU(\mathcal{N})$ R-symmetry, with supercharges Q transforming in the fundamental representation. We will see that in superconformal field theories, R-symmetries

[15] Because Weyl spinors are self-conjugate in 4D Euclidean spacetime, this conjugation relation no longer holds in Euclidean signature. A useful reference for supersymmetry in general signature can be found in [114].

are promoted to a more central role: they will generate inner automorphisms of the superconformal algebra. As with any global symmetry, R-symmetries may become anomalous in a quantum theory.

Supersymmetry algebra in 3D

The 3D super-Poincaré algebra is most easily expressed in terms of real (Majorana) supercharges[16] satisfying

$$\{Q_\alpha^A, Q_\beta^B\} = 2\gamma^\mu_{\alpha\beta}\delta^{AB}P_\mu + 2\epsilon_{\alpha\beta}Z^{AB}\,, \tag{2.63}$$

where Greek and uppercase Latin indices are again spinor indices and supersymmetry labels in $\{1,\ldots,\mathcal{N}\}$ respectively. The remainder of the commutation relations are fixed in an analogous way to those in 4D. Also as in the 4D case, Z^{AB} denotes an anti-symmetric tensor of central charges. In 3D, we have $2\mathcal{N}$ real supercharges.

For $\mathcal{N}=2$ supersymmetry, it is sometimes convenient to consider complex supercharges by taking complex linear combinations

$$Q_\alpha = \frac{1}{\sqrt{2}}(Q^1_\alpha + iQ^2_\alpha)\,, \quad \tilde{Q}_\alpha = \frac{1}{\sqrt{2}}(Q^1_\alpha - iQ^2_\alpha)\,. \tag{2.64}$$

The SUSY algebra may then be expressed as

$$\{Q_\alpha, \tilde{Q}_\beta\} = 2\sigma^\mu_{\alpha\beta}P_\mu + 2i\epsilon_{\alpha\beta}Z\,, \quad \{Q_\alpha, Q_\beta\} = \{\tilde{Q}_\alpha, \tilde{Q}_\beta\} = 0\,, \tag{2.65}$$

with $Z = Z^{21} = -Z^{12}$. In this basis, we can easily observe the diagonal $U(1)$ R-symmetry

$$Q_\alpha \to e^{i\theta}Q_\alpha\,, \quad \tilde{Q}_\alpha \to e^{-i\theta}\tilde{Q}_\alpha\,. \tag{2.66}$$

For $\mathcal{N}=4$ supersymmetry, we have an $SO(4) \cong SU(2)\times SU(2)$ R-symmetry. This can be understood by considering 3D $\mathcal{N}=4$ theories as

[16] In Euclidean signature, it is not possible to impose a Majorana condition in 3D. Consequently, the minimal amount of supersymmetry is $\mathcal{N}=2$ in Euclidean. A statement of the 3D $\mathcal{N}=2$ Euclidean super-Poincaré algebra can be found in [115].

dimensional reductions of 6D $\mathcal{N} = 1$ theories; one factor of $SU(2)$ arises from the R-symmetry of the 6D theory, while the second factor of $SU(2)$ arises from the rotation group of the reduced dimensions [116].

2.3.2 Supersymmetry representations in 4D

When introducing representations of the super-Poincaré algebra, it is often convenient to distinguish between massless and massive representations; we consider each in turn. To streamline our discussion, we will focus on the representation theory of states in the Hilbert space of a Lorentzian quantum field theory, rather than on supersymmetry transformations of fields and supersymmetric actions of these fields; we will discuss the latter for the specific case of $\mathcal{N} = 4$ supersymmetric Yang-Mills in a later subsection.

Massless representations

For massless representations, it is convenient to boost to a frame where the momentum is $P^\mu = (E, 0, 0, E)$,[17] and study the representations of the supersymmetry subalgebra in this frame. The supersymmetry algebra then includes the anti-commutator

$$\{Q^A_\alpha, \tilde{Q}_{\dot{\alpha}B}\} = \begin{pmatrix} 4E & 0 \\ 0 & 0 \end{pmatrix}_{\alpha\dot{\beta}} \delta^A_B \,. \tag{2.67}$$

In particular, we observe that $\{Q^A_2, (Q^A_2)^\dagger\} = 0$, which requires these generators to identically vanish on the representation, and thus (via the other anti-commutators) that all of the central charges also vanish.

The remaining generators Q^A_1 and $\tilde{Q}_{\dot{1}A}$ obey the algebra of fermionic creation and annihilation operators, up to rescaling by $\sqrt{2E}$; the real and imaginary parts of these generators satisfy the Clifford algebra associated to the Euclidean rotation group $SO(2\mathcal{N})$, and the non-trivial supersymmetry generators act as raising and lowering operators for the helicity. We can thus consider a $2^{\mathcal{N}}$-dimensional representation of this algebra, obtained by acting

[17] Namely, to choose a state within a given Lorentz orbit with these quantum numbers for the components of P^μ.

on a highest helicity state $|h\rangle$ with the lowering operators Q_1^A. In actuality, CPT symmetry requires that the spectrum should be symmetric under a sign reversal of the helicity; consequently, we will obtain either a $2^{\mathcal{N}}$-dimensional representation or a $2^{\mathcal{N}+1}$-dimensional representation, depending on whether we need to append the CPT conjugate states.

Constructing the massless irreducible multiplets for $\mathcal{N} = 1$ supersymmetry in this way, we obtain the following multiplets with helicities not exceeding one, labelled by the helicities $(\lambda, \lambda + \frac{1}{2})$ of the states in the multiplet:

- The *chiral multiplet* $(-\frac{1}{2}, 0) \oplus (0, \frac{1}{2})$, consisting of a complex scalar and a Weyl fermion.
- The *vector multiplet* $(-1, -\frac{1}{2}) \oplus (\frac{1}{2}, 1)$, sometimes called the *gauge multiplet*, consisting of a vector boson and a Weyl fermion in the adjoint of the gauge group.

Multiplets with states of helicity greater than one, including the *gravitino* and *graviton multiplets*, are of relevance in the supergravity context.

We also record here the multiplets with states whose helicity does not exceed one for the case of $\mathcal{N} = 2$ and $\mathcal{N} = 4$ extended supersymmetry:

- The $\mathcal{N} = 2$ *gauge/vector multiplet* $(-1, -\frac{1}{2}, -\frac{1}{2}, 0) \oplus (0, \frac{1}{2}, \frac{1}{2}, 1)$, consisting of one vector, two Weyl fermions, and one complex scalar.
- The $\mathcal{N} = 2$ *hypermultiplet* $(-\frac{1}{2}, 0, 0, \frac{1}{2}) \oplus (-\frac{1}{2}, 0, 0, \frac{1}{2})$, consisting of two Weyl fermions and two complex scalars.
- The $\mathcal{N} = 4$ *gauge/vector multiplet* $(-1, 4\times-\frac{1}{2}, 6\times0, 4\times\frac{1}{2}, 1)$, consisting of a vector, four Weyl fermions, and three complex scalars.

Both $\mathcal{N} = 1$ chiral multiplets and $\mathcal{N} = 2$ hypermultiplets will sometimes be referred to as *matter multiplets*, in contrast to the vector multiplets appearing in the supersymmetric gauge theories we consider.

Massive representations

When considering massive representations, we boost to a frame with $P^\mu = (M, 0, 0, 0)$; the supersymmetry algebra now includes the anti-commutator

$$\{Q^A_\alpha, \tilde{Q}_{\dot{\beta}B}\} = 2M\delta_{\alpha\dot{\beta}}\delta^A_B \,. \tag{2.68}$$

We can begin by considering the case of minimal $\mathcal{N} = 1$ supersymmetry, where the supersymmetry algebra does not include central charges. The supercharges may then be identified with fermionic creation and annihilation operators as in the massless case, though now we have two uncoupled fermionic oscillators for $\mathcal{N} = 1$ supersymmetry. Consequently, we find the following multiplets with helicities not exceeding one:

- The *chiral multiplet* $(-\frac{1}{2}, 0, 0, \frac{1}{2})$, consisting of a complex scalar and Weyl fermion.
- The *vector/gauge multiplet* $(-1, -\frac{1}{2}, -\frac{1}{2}, 0) \oplus (0, \frac{1}{2}, \frac{1}{2}, 1)$, consisting of a massive gauge field, a massive Dirac fermion, and a real complex scalar.

Considering now the case of extended supersymmetry, we first observe that an arbitrary anti-symmetric matrix Z^{AB} can be block-diagonalized to the form

$$Z = \begin{cases} \mathrm{diag}(\epsilon Z_1, \ldots, \epsilon Z_r) & \mathcal{N} = 2r \text{ even} \\ \mathrm{diag}(\epsilon Z_1, \ldots, \epsilon Z_r, 0) & \mathcal{N} = 2r + 1 \text{ odd} \end{cases} , \tag{2.69}$$

where Z_i are (real) constants and ϵ^{ab} is the anti-symmetric tensor (with indices suppressed in our expression). An enlightening form of the algebra can consequently be obtained by rotating the supercharges by a $SU(\mathcal{N})_R$ transformation in order to block-diagonalize the matrix of central charges Z^{ab}. Letting barred indices $\bar{a}, \bar{b}$ run over the 2×2 blocks, and thus in the range $\{1, \ldots, r\}$ with $r \equiv \lfloor \frac{\mathcal{N}}{2} \rfloor$, and defining

$$\mathcal{Q}^{\bar{a}}_{\alpha\pm} \equiv \frac{1}{2}(Q^{1\bar{a}}_\alpha \pm \sigma^0_{\alpha\dot{\beta}}(Q^{2\bar{a}}_\beta)^\dagger) \,, \tag{2.70}$$

we have non-vanishing anti-commutators

$$\{\mathcal{Q}^{\bar{a}}_{\alpha\pm}, (\mathcal{Q}^{\bar{b}}_{\beta\pm})^\dagger\} = \delta^{\bar{a}}_{\bar{b}}\delta^{\beta}_{\alpha}(M \pm Z_{\bar{a}})\,. \tag{2.71}$$

The fact that this is again positive-definite for $a = b$ and $\alpha = \beta$ implies the *BPS bound*

$$M \geq |Z_{\bar{a}}|\,. \tag{2.72}$$

When one or more of these bounds is saturated, the corresponding supercharges must vanish by the same logic as in the massless case; the result is that the naive size $2^{2\mathcal{N}}$ of the representation is reduced, yielding a *shortened* or *BPS multiplet*. The number of vanishing supercharges determines the degree of shortening; for example, one saturated BPS inequality results in a $\frac{1}{2}$-BPS multiplet (dimension $2^{2\mathcal{N}-2}$), while two saturated inequalities results in a $\frac{1}{4}$-BPS multiplet (dimension $2^{2\mathcal{N}-4}$). In the extreme cases where r BPS inequalities are saturated, one refers to the representation as an *ultrashort multiplet*. In practice, the presence of shortened representations in a supersymmetric theory is often essential for providing computational control, the reason being that the BPS requirement prevents the spectrum of short representations from receiving perturbative quantum corrections. A review of the massive multiplets for $\mathcal{N} = 2$ and $\mathcal{N} = 4$ theories can be found in e.g. [111].

Decomposing representations of extended supersymmetry

It is manifest from the form of the super-Poincaré algebras with $\mathcal{N} = \mathcal{N}_1$ and $\mathcal{N} = \mathcal{N}_2$ that the former is a subalgebra of the latter when $\mathcal{N}_1 < \mathcal{N}_2$. Consequently, irreducible representations of the super-Poincaré algebra with $\mathcal{N} = \mathcal{N}_2$ decompose into multiple irreducible representations of the super-Poincaré algebra with $\mathcal{N} = \mathcal{N}_1$. Some examples relevant for later chapters are as follows:

- One $\mathcal{N} = 4$ vector multiplet in the adjoint of gauge group G decomposes to:

  - One adjoint $\mathcal{N} = 2$ vector multiplet
  - One adjoint $\mathcal{N} = 2$ hypermultiplet.

- One $\mathcal{N} = 2$ vector multiplet in the adjoint of gauge group G decomposes to:
  - One adjoint $\mathcal{N} = 1$ vector multiplet
  - One adjoint $\mathcal{N} = 1$ chiral multiplet.

- One $\mathcal{N} = 2$ hypermultiplet in representation R decomposes to:
  - Two $\mathcal{N} = 1$ chiral multiplets in reprsentation R.

2.3.3 Supersymmetry representations in 3D

In this subsection, we will focus on the cases of 3D $\mathcal{N} = 2$ and $\mathcal{N} = 4$ supersymmetry which will be relevant in later sections. A discussion of 3D $\mathcal{N} = 1$ multiplets can be found in [113]; notably, this amount of supersymmetry is only possible in Lorentzian signature, whereas in Euclidean signature the minimal amount of supersymmetry is $\mathcal{N} = 2$.

While one can obtain representations of the supersymmetry algebra in a similar way to the 4D case, the representations of 3D $\mathcal{N} = 2$ and $\mathcal{N} = 4$ supersymmetry are most easily obtained by dimensional reduction of 4D $\mathcal{N} = 1$ or $\mathcal{N} = 2$ supersymmetry respectively; concretely, this amounts to choosing a 4D $\mathcal{N} = 1$ representation on fields, dimensionally reducing to 3D, and observing how the resulting fields transform under the reduced Lorentz group $SO(1,3) \to SO(1,2)$ or the corresponding spin group. The dimensional reduction preserves the number of real supercharges; for example, at the level of the algebra, dimensionally reducing in the x^2 direction corresponds to considering representations for which the quantum number associated with the component P^2 is fixed to some value Z, in which case the 4D $\mathcal{N} = 1$ supersymmetry algebra can be written as

$$\{Q_\alpha, (Q_\beta)^\dagger\} = 2\sigma^\mu_{\alpha\beta} P_\mu + 2i\epsilon_{\alpha\beta} Z \,, \tag{2.73}$$

where $\mu \in (0, 1, 3)$. We recognize this as the 3D $\mathcal{N} = 2$ algebra with a particular choice of basis for the gamma matrices.

We refrain from presenting the full analysis here, instead recording the relevant results. For the case of $\mathcal{N} = 2$ supersymmetry, one obtains the following multiplets:[18]

- The *chiral multiplet*, obtained from a 4D $\mathcal{N} = 1$ chiral multiplet, consisting of a complex scalar and a complex Weyl fermion.
- The *vector multiplet*, obtained from a 4D $\mathcal{N} = 1$ vector multiplet, consisting of a vector, a complex Weyl fermion, and a real scalar in the adjoint of the gauge group.

On the other hand, for the case of 3D $\mathcal{N} = 4$ supersymmetry, one has the following representations:

- The *vector multiplet*, obtained from a 4D $\mathcal{N} = 2$ vector multiplet, consisting of a 3D $\mathcal{N} = 2$ vector and a 3D $\mathcal{N} = 2$ hypermultiplet.
- The *hypermultiplet*, obtained from a 4D $\mathcal{N} = 2$ hypermultiplet, consisting of two 3D $\mathcal{N} = 2$ chiral multiplets.

2.3.4 Superconformal algebras in 3D and 4D

In 3D and 4D,[19] the conformal algebra admits a supersymmetric extension to the so-called *superconformal algebras* with various amounts of supersymmetry. The superconformal algebras consist of two types of fermionic generators, which are spinors of the d-dimensional Lorentz group: supercharges Q^A (and possibly $\tilde{Q}_A$) whose anti-commutators include the momentum P_μ, and the supercharges S^A (and possibly $\tilde{S}_A$) whose anti-commutators include the special conformal generator K_μ.[20] The 3D superconformal group with $\mathcal{N}$ supercharges Q is denoted $OSp(\mathcal{N}|4)$, while the 4D superconformal algebra

[18] In 3D, there are also multiplets known as *linear multiplets*, in which global currents appear.

[19] The classification of superconformal algebras was given by Nahm in [117]; in particular, such algebras are only possible in dimension $d \leq 6$.

[20] We neglect spinor indices for the fermionic generators in this subsection.

is denoted by $SU(2,2|\mathcal{N})$ (or $PSU(2,2|\mathcal{N})$ in the case $\mathcal{N}=4$). We will omit the corresponding algebras here; useful references include [96, 118–120]. We can, however, schematically summarize the algebra as follows:

$$\begin{aligned} &[D,Q] = -\frac{i}{2}Q\,, \quad [D,S] = \frac{i}{2}S\,, \quad [K,Q] \approx S\,, \quad [P,S] \approx Q\,, \\ &\{Q,Q\} \approx P\,, \qquad \{S,S\} \approx K\,, \quad \{Q,S\} \approx L + D + R\,. \end{aligned} \tag{2.74}$$

The precise form of these commutation relations will generally be different in different dimensions, but the above indicates which charges appear in a given commutator or anti-commutator. The bosonic charges R correspond to generators of the R symmetry algebra.

As in the case of conformal symmetry, one is interested in constructing representations by considering local primary operators, annihilated by K_μ, whose behaviour at the origin is

$$[\mathcal{L}_{\mu\nu}, \mathcal{O}^a(0)] = (\mathcal{S}_{\mu\nu})^a_{\ b}\mathcal{O}^b(0)\,, \quad [D, \mathcal{O}^a(0)] = \Delta\mathcal{O}^a(0)\,, \tag{2.75}$$

meaning that $\mathcal{O}^a(0)$ transforms in a representation of "scale + Lorentz". In superconformal field theories, we are interested in constructing representations from operators which additionally satisfy

$$[S^A, \mathcal{O}^a(0)]_\pm = [\tilde{S}_A, \mathcal{O}^a(0)]_\pm = 0\,, \tag{2.76}$$

where $\pm$ denotes that we should either take commutators or anti-commutators, depending on whether $\mathcal{O}^a(0)$ is bosonic or fermionic. Such an operator is referred to as a *superconformal primary operator*. Note that all superconformal primary operators are also conformal primaries, as can be established from the definitions and the fact that $\{S, \tilde{S}\} \sim K$.

Superconformal descendant operators can be obtained by acting with the generators P^μ and Q^A; in particular, acting on a superconformal primary with one of the supercharges Q gives rise to a *super-descendant operator* $\mathcal{O}' = [Q, \mathcal{O}]_\pm$. Super-descendant operators are themselves conformal primary operators; a superconformal multiplet therefore consists of many conformal multiplets related by supersymmetry.

An important subclass of superconformal primary operators are the *chiral primary operators*, which additionally satisfy

$$[Q^A, \mathcal{O}]_\pm = 0 \tag{2.77}$$

for at least one A and one spinor component. Such operators are BPS, in the sense that they give rise to shorter representations of supersymmetry, consisting of fewer conformal primaries. One significant property of chiral primaries is that their dimensions do not receive quantum corrections, as they are protected by the R-symmetry.

2.3.5 4D $\mathcal{N} = 4$ supersymmetric Yang-Mills theory

The 4D $\mathcal{N} = 4$ supersymmetric Yang-Mills (SYM) theory is a prototypical superconformal field theory, and has particular importance in the holographic context. The 4D SYM theory is most readily obtained from dimensional reduction of the 10D $\mathcal{N} = 1$ Yang-Mills theory [121], whose field content consists of the gauge field A^M and the Majorana-Weyl gaugino Ψ, and whose action is given by

$$S = \frac{1}{g_{\text{YM}}^2} \int d^{10}x \, \text{tr} \left(\frac{1}{2} F_{MN} F^{MN} - i \bar{\Psi} \Gamma^M D_M \Psi \right) . \tag{2.78}$$

Here, uppercase Latin indices are 10D (flat Lorentzian) spacetime indices, and Γ^M are the 10D Dirac matrices; the overbar on Ψ denotes the Dirac conjugate, and D_M is the gauge-covariant derivative.

Dimensionally reducing by requiring the fields to only depend on coordinates $(x^0, \ldots, x^3)$, the 10D Lorentz group breaks to a subgroup

$$SO(1,9) \to SO(1,3) \times SO(6)_R \, . \tag{2.79}$$

The gauge field decomposes into a 4D gauge field A^μ and six real scalars $(A^4, \ldots, A^9)$, which we may rename Φ^i for convenience (up to rescaling by g_{YM}). The Majorana-Weyl fermion decomposes into four conjugate Weyl spinors λ^a, such that Ψ transforms in the $(2,1,4) \oplus (1,2,\bar{4})$ of $SO(1,3) \times$

$SO(6)_R$. One then obtains an action whose purely bosonic part is

$$S = \int d^4x \, \mathrm{tr} \Bigg(\frac{1}{2g^2_{\mathrm{YM}}} F_{\mu\nu} F^{\mu\nu} + \sum_i D_\mu \Phi^i D^\mu \Phi^i - \frac{g^2_{\mathrm{YM}}}{2} \sum_{i,j} [\Phi^i, \Phi^j]^2 \Bigg) . \quad (2.80)$$

Operator spectrum

We briefly discuss the spectrum of local gauge-invariant operators in the quantum theory. The general such operator is either the trace of a product of the elementary fields, referred to as a *single-trace operator*, or the product of single-traces, referred to as a *multi-trace operator*. We will focus the discussion here on the single-trace operators; in the *'t Hooft limit*

$$\lambda \equiv g^2_{\mathrm{YM}} N \text{ fixed} , \qquad N \to \infty , \quad (2.81)$$

which will be relevant in the holographic context, correlation functions involving multi-traces will be suppressed by powers of N relative to those involving single-traces.

Given that the 4D $\mathcal{N} = 4$ superalgebra has 16 real supercharges, a generic (long) representation of the superconformal algebra consists of 2^{16} conformal primaries, with helicities in half-integer increments spanning $\{\lambda - 4, \ldots, \lambda + 4\}$ for λ the helicity of the primary with lowest conformal dimension. As discussed previously, one can also have short representations and ultra-short representations.

A special class of superconformal primary operators introduced in Section 2.3.4 are the chiral primaries; we will follow [107] in presenting the known spectrum of chiral primary operators of the $\mathcal{N} = 4$ $SU(N)$ supersymmetric Yang-Mills theory, though a straightforward systematic way of computing the full spectrum is not known. Given that the field strength $F_{\mu\nu}$ and fermions λ_a are found to arise in the action of supersymmetry on the fundamental fields, it turns out that the lowest components of the chiral primary representations are built from the scalars Φ^i. We therefore begin

by considering operators of the form

$$\tilde{O}^{i_1 \dots i_n} = \mathrm{tr}(\Phi^{i_1} \dots \Phi^{i_n}) \,, \tag{2.82}$$

where the i_j are free indices. Since in fact we also observe commutators of Φ^i arising in the action of supersymmetry on the fields, we can further restrict to linear combinations of these operators which symmetrize the indices, sometimes denoted using the *symmetrized trace* as

$$O^{i_1 \dots i_n} = \mathrm{str}(\Phi^{i_1} \dots \Phi^{i_n}) \,. \tag{2.83}$$

The linear combinations of such primary scalar operators which are traceless with respect to contractions of any two indices are precisely the chiral primaries; we can unambiguously use the notation $O^{i_1 \dots i_n}$ to refer to such traceless linear combinations.

It can be shown that the dimension of $O^{i_1 \dots i_n}$ defined in this way, as determined from the superconformal algebra, is $[O_n] = n$, coinciding with the value in free field theory. Notably, for finite N, short chiral primary representations are built from these operators with n in the range $n \in \{2, \dots, N\}$; this is because the product of more than N commuting $N \times N$ matrices can be written as a sum of products of traces of fewer matrices.[21]

Non-perturbative features

In the string theory context, the $\mathcal{N} = 4$ $U(N)$ SYM theory arises as a description of the low-energy physics of a stack of N coincident D3-branes in type IIB string theory. An important conjecture about the $\mathcal{N} = 4$ SYM theory is that it is in fact UV finite, and retains exact conformal symmetry at the quantum level.

The SYM theory is believed to exhibit an exact $SL(2, \mathbb{Z})$ global symmetry, known as *Montonen-Olive duality* or *S-duality*, whereby the complexified

[21] We have focused our discussion on single-trace operators, but the spectrum of $\mathcal{N} = 4$ SYM also includes multi-trace operators, including chiral primary multi-traces; see e.g. [122] for details.

coupling

$$\tau = \frac{\theta_I}{2\pi} + \frac{4\pi i}{g^2} \tag{2.84}$$

undergoes a Möbius transformation

$$\tau \to \frac{a\tau + b}{c\tau + d}\,, \quad ad - bc = 1\,, \quad a, b, c, d \in \mathbb{Z}\,. \tag{2.85}$$

In particular, this group of transformations is generated by the shift $\tau \to \tau + 1$ and the S-duality transformation $\tau \to -1/\tau$; the former is known to hold, while the latter is conjectured. As can be seen by applying the S-duality transformation in the case $\theta_I = 0$, S-duality is a *strong-weak coupling duality* or a *non-perturbative duality*.

2.3.6 Supersymmetric localization

The existence of supersymmetry in a theory sometimes permits an exact calculation of protected quantities in the theory, using a technique called *supersymmetric localization*. We will give a cursory review of the general theory behind supersymmetric localization; a useful introduction can be found in [123], while [124] provides a very comprehensive overview of relevant techniques.

Supersymmetry on curved backgrounds

A starting point for most computations involving supersymmetric localization is to put a supersymmetric theory of interest on a compact (Euclidean) manifold M; doing so assists the convergence of the path integral by explicitly removing IR divergences. We would like the theory on M to have the same UV behaviour as our original theory in flat space, and to preserve supersymmetry. However, naïvely covariantizing the original Lagrangian, while providing a suitable curved space generalization of the original theory, may explicitly break supersymmetry; moreover, a generic curved manifold may not permit supersymmetry.

One systematic approach to placing a given supersymmetric theory on a curved manifold is to consider an expansion of both the covariantized super-

symmetry transformations and the Lagrangian in inverse powers of the curvature scale r on the manifold, enforcing order-by-order that the supersymmetry algebra closes and the theory is supersymmetric. Under favourable circumstances, this expansion will truncate and yield an exactly supersymmetric theory. An alternative approach, due to Festuccia and Seiberg [125], is to first directly couple the flat space theory to supergravity, then take a rigid limit $G \to 0$ to decouple dynamical gravity and recover a fixed background. Demanding that the background preserve supersymmetry leads to the requirement that the gravitino and its supersymmetry variation should vanish; the latter condition directly imposes that the spinor parameter generating supersymmetry must satisfy a differential equation known as the *generalized Killing spinor equation*. This suggests an obstruction to defining a supersymmetric theory on manifolds which do not admit solutions to this equation.

A relevant example of a supersymmetric theory on a curved background is the case of the $\mathcal{N} = 4$ SYM theory on S^4. Expressing the action in terms of the fields of 10D $\mathcal{N} = 1$ SYM from which the 4D theory is a dimensional reduction, one arrives at the compact expression

$$S_E = \frac{1}{g^2_{\mathrm{YM}}} \int d^4x \sqrt{g}\, \mathrm{tr} \left(\frac{1}{2} F_{MN} F^{MN} - \Psi \Gamma^M D_M \Psi + \frac{2}{r^2} \Phi_i \Phi^i \right) , \quad (2.86)$$

where r denotes the radius of the S^4, such that the Ricci curvature is given by $R = \frac{12}{r^2}$, and covariant derivatives are now also geometrically covariant. The supersymmetry transformations, parametrized by a Majorana-Weyl spinor parameter ε, can be found in [126]. Similar considerations for 3D $\mathcal{N} = 2$ theories on S^3 can be found in [127].

General theory of supersymmetric localization

We now turn to a bird's-eye view of the argument underpinning supersymmetric localization. It will be most conceptually straightforward to formulate the logic in the arena of standard finite-dimensional integrals, but the extension to quantum field theory path integrals is entirely analogous.

Suppose that we are interested in computing an integral of the form

$$Z = \int dxd\theta\, e^{-S_E[x,\theta]}\,, \tag{2.87}$$

where x and θ are bosonic and fermionic coordinates respectively; we can think of this as an integration over a Grassmann-odd line bundle with canonical measure, where x are coordinates on the base space and θ are coordinates on the fibre. Suppose further that the function S_E is invariant under a fermionic symmetry, as implemented by a differential operator Q on superspace (x,θ) which is a linear combination of derivatives: $QS_E = 0$. The square of Q either vanishes, or is a bosonic symmetry of S_E which we may denote by δ_B.

Consider next the deformed integral

$$Z(t) = \int dxd\theta\, e^{-S_E[x,\theta]-tQV[x,\theta]}\,, \qquad \delta_B V = 0\,, \qquad QV \geq 0\,, \tag{2.88}$$

where V is some function invariant under the bosonic symmetry obtained by squaring Q. Taking a t-derivative, we obtain

$$\frac{\partial Z}{\partial t} = -\int dxd\theta\, QVe^{-S_E-tQV} = -\int dxd\theta\, Q\left(Ve^{-S_E-tQV}\right)\,. \tag{2.89}$$

Since Q is a total derivative operator, this manifestly vanishes, assuming suitable behaviour of the functions S_E and V at infinity. We may therefore conclude that $Z(t)$ is independent of t; we are hence free to evaluate $Z(0)$ by considering the limit $\lim_{t\to\infty} Z(t)$, which we can compute by a saddle-point approximation which becomes exact in the limit.

In detail, denoting by (x_0,θ_0) a zero of QV, and parametrizing

$$x = x_0 + \frac{\hat{x}}{\sqrt{t}}\,, \qquad \theta = \theta_0 + \frac{\hat{\theta}}{\sqrt{t}}\,, \tag{2.90}$$

we may write

$$S_E + tQV = S_E[x_0,\theta_0] + (QV)_2[x_0,\theta_0;\hat{x},\hat{\theta}] + O(t^{-1/2})\,, \tag{2.91}$$

where $(QV)_2$ is the term in QV which is second order in $(\hat{x}, \hat{\theta})$. We then have

$$Z = \lim_{t\to\infty} Z(t) = \sum_{(x_0,\theta_0)\text{ zeros}} \frac{e^{-S_E[x_0,\theta_0]}}{\mathrm{SDet}(QV)_2[x_0,\theta_0]}\,, \tag{2.92}$$

where the quantity SDet, which can be thought of as a one-loop determinant in the field theory version of this argument, is defined by[22]

$$\frac{1}{\mathrm{SDet}(QV)_2[x_0,\theta_0]} = \int d\hat{x}d\hat{\theta}\; e^{-(QV)_2[x_0,\theta_0;\hat{x},\hat{\theta}]}\,, \tag{2.93}$$

and can be evaluated by Gaussian integration.

It is clear from the derivation of this result that a similar argument applies not only to Euclidean partition functions, but to correlation functions of supersymmetric observables with suitable asymptotic behaviour in field space.

2.4 The AdS/CFT correspondence

The AdS/CFT correspondence can be viewed as the statement that *any* conformal field theory on a suitable d-dimensional spacetime background B can be interpreted as a theory of quantum gravity in an asymptotically $\mathrm{AdS}_{d+1}\times M$ spacetime with B the conformal boundary of the AdS_{d+1} factor, where M is compact (or perhaps trivial). The fact that B is the conformal boundary of the AdS spacetime motivates our use of the phrase *boundary theory* to refer to the CFT, and *bulk theory* to refer to the quantum gravity theory. In some cases, the bulk quantum gravity theory may look like general relativity, perhaps coupled to a small number of additional light fields, at low energies; in others, the theory might look much more complicated, with infinite towers of massless higher spin fields.

More broadly, AdS/CFT is something of a misnomer, as some version of holographic duality may be applicable in situations where the boundary theory is not strictly conformal. Some examples are as follows:

[22] We have used here that the canonical measure on the integration space, involving an appropriately graded version of the Pfaffian, satisfies $dxd\theta = d\hat{x}d\hat{\theta}$.

- The term *AdS/BCFT correspondence* is sometimes applied in situations where conformal invariance is partially broken by the presence of boundaries or interfaces in the boundary theory.
- Bulk theories with non-trivial profiles for matter fields which backreact on the geometry can describe *holographic RG flows*.
- A holographic dual interpretation has been proposed for some theories of *matrix quantum mechanics*.
- In some low-dimensional examples, an equivalence has been established between a bulk theory of quantum gravity and a dual *ensemble* of quantum theories.

Given that we do not have a fully independent definition of string theory beyond the regime of string worldsheet perturbation theory, one common perspective is to understand the CFT as providing a non-perturbative, UV complete *definition* of a quantum gravity theory. However, even in the absence of a non-perturbative definition of string theory, we should be able to describe bulk physics below the string scale within the framework of effective field theory (EFT). In this case, the AdS/CFT correspondence provides a map from bulk EFT physics to physics in an underlying CFT.

An alternative perspective is that two dual quantum mechanical descriptions exist, and in particular that there should be some intrinsically bulk definition of the UV complete theory; in this case, AdS/CFT can be viewed as an exact isomorphism between Hilbert spaces respecting the dynamics. The subject of AdS/CFT is concerned both with situations in which a precise microscopic duality is identified, and the more "bottom-up" approach of bulk effective field theory. In both cases, understanding features of the holographic map has been a longstanding goal of research in AdS/CFT; in this section, we will make note of some important entries in the holographic dictionary. Our discussion will rely on material found in [52, 93, 96, 107, 128–131].

2.4.1 Fundamentals of the AdS/CFT dictionary

An equivalence between two quantum theories is established if the Hilbert spaces and operator algebras can be shown to be isomorphic. We shall see that two of the central pillars of our current understanding of the AdS/CFT dictionary are a map between bulk and boundary Hilbert spaces, and a map between path integrals.

Equivalence of Hilbert spaces

One statement of the equivalence of Hilbert spaces between bulk and boundary theories related by holographic duality is that there exists an isomorphism

$$V : \mathcal{H}_{\text{AdS-QG}} \to \mathcal{H}_{\text{CFT}} \,, \tag{2.94}$$

where $\mathcal{H}_{\text{AdS-QG}}$ and $\mathcal{H}_{\text{CFT}}$ are the bulk and boundary Hilbert spaces respectively, such that

$$V \circ U_{\text{AdS-QG}} = U_{\text{CFT}} \circ V \,, \tag{2.95}$$

where the U are unitary operators implementing the $SO(2,d)$ symmetries in the two theories.[23] Such a map V evidently preserves representations of $SO(2,d)$. Hamiltonian evolution is an example of one of these unitaries U, so that in particular the spectrum of the Hamiltonian is preserved via the isomorphism. We will revisit the spectrum in more granular detail when we consider the effective approach to AdS/CFT below.

This statement is satisfactory when we have a UV complete theory in the bulk, but we can make a slightly different statement applying to bulk effective field theory around an asymptotically AdS background. In this case, one anticipates that there exists an *injection* between Hilbert spaces

$$V : \mathcal{H}_{\text{AdS-EFT}} \to \mathcal{H}_{\text{CFT}} \,. \tag{2.96}$$

Such a map may or may not be an isometry, namely a map which preserves

[23] We note that the $U_{\text{AdS-QG}}$ are still physical symmetries rather than gauge symmetries in the bulk theory; at the semi-classical level, they can be thought of as related to diffeomorphisms that act non-trivially on the boundary.

the inner product, and therefore satisfies $V^\dagger V = 1$. A statement like (2.95) can no longer be precisely true, since for example some of the $SO(2,d)$ transformations in the CFT could raise the energy of a state beyond the regime of validity of effective field theory. As we will briefly return to below, the map V is best understood in the language of *quantum error correction*.

Equivalence of path integrals

In the AdS/CFT correspondence, every bulk field in AdS_{d+1} is associated to a corresponding gauge-invariant boundary operator,[24] including the following important examples:

- Bulk scalar fields correspond to boundary scalar operators;
- Bulk vector fields correspond to boundary current operators;
- The bulk metric corresponds to the boundary stress tensor.

The conformal dimension Δ of the CFT operator is related to the mass m of the corresponding bulk field; for example, one has for scalar operators[25]

$$m^2 = \Delta(\Delta - d)\,. \tag{2.97}$$

As is clear from our examples, the spin of the CFT operator is fixed by the spin of the corresponding bulk field (as reflected in the Lorentz index structure).

Concretely, the boundary condition for a field ϕ corresponds to a *source* $\phi^{(0)}$ for the associated operator O, meaning a deformation of the CFT action by a term

$$S_{\mathrm{CFT}} \to S_{\mathrm{CFT}} + \int d^d x \sqrt{|g(x)|}\phi^{(0)}(x)O(x)\,, \tag{2.98}$$

with a precise identification made via the relation

$$\phi^{(0)}(x) = \lim_{z\to 0} z^{-\Delta}\phi(z,x)\,, \tag{2.99}$$

[24] When dimensionally reducing $\mathrm{AdS}_{d+1}\times M$ with compact M to AdS_{d+1}, one obtains a tower of Kaluza-Klein modes; each mode is associated to a different CFT operator.

[25] A dictionary for general operators can be found in [107].

where z denotes the holographic coordinate in Fefferman-Graham coordinates introduced in (2.9), and x schematically denotes the remaining bulk coordinates and the boundary coordinates they induce.

Much of the basic content of the AdS/CFT correspondence is contained in the *Gubser-Klebanov-Polyakov-Witten (GKPW) dictionary* [30, 31]

$$Z_{\text{grav}}[\phi^{(0)}(x)] \stackrel{!}{=} Z_{\text{CFT}}[\phi^{(0)}] \,, \tag{2.100}$$

where the left hand side is the Euclidean gravitational path integral with appropriate boundary conditions for the fields ϕ,

$$Z_{\text{grav}}[\phi^{(0)}(x)] \equiv \int_{\phi(z,x)\sim z^{\Delta}\phi^{(0)}(x)} \mathcal{D}g\mathcal{D}\phi \, e^{-S_E[g,\phi]} \,, \tag{2.101}$$

and the right hand side is a *generating functional* for the CFT

$$\begin{aligned} Z_{\text{CFT}}[\phi^{(0)}(x)] &= \int \mathcal{D}\varphi \, e^{-S_{\text{CFT}}[\varphi] - \int d^d x \sqrt{|g|}\phi^{(0)}(x)\mathcal{O}(x)} \\ &= \langle e^{-\int d^d x \sqrt{|g|}\phi^{(0)}(x)\mathcal{O}(x)} \rangle_{\text{CFT}} \,. \end{aligned} \tag{2.102}$$

We have focused on a Euclidean statement of the GKPW dictionary and the relationship between bulk fields and boundary sources, though it is possible to formulate a similar duality between path integrals with more general contours (see e.g. [132, 133]).

Formally, both sides of (2.100) are divergent; one expects UV divergences in the CFT correlators, as well as long-distance divergences from the infinite-volume asymptotically AdS region in the bulk. The disparate origins of these divergences hint at the notion of *UV/IR duality* in AdS/CFT, and the heuristic that the holographic direction in the bulk geometrizes the spectrum of energy scales for processes in the CFT. The GKPW formula can be more carefully defined by making use of *holographic renormalization*, wherein a cutoff surface is chosen in the bulk to regulate calculations and local counterterms are introduced on this surface to cancel divergent quantities as the cutoff is removed; see [92] for an introduction.

Differentiating a generating functional with respect to sources is a route

to calculating correlation functions, and part of the utility of the GKPW dictionary is that it permits CFT correlators to be extracted from a bulk calculation

$$\langle O_1(x_1)\dots O_n(x_n)\rangle = \frac{(-1)^n}{Z_{\text{grav}}[0]}\frac{\delta^n Z_{\text{grav}}[\phi_1^{(0)},\dots,\phi_n^{(0)}]}{\delta\phi_1^{(0)}(x_1)\dots\delta\phi_n^{(0)}(x_n)}\Big|_{\phi_i^{(0)}=0}. \tag{2.103}$$

An alternative but equivalent [134] formulation is the so-called *extrapolate dictionary*, which directly relates bulk and boundary correlators via

$$\begin{aligned}&\langle O_1(x_1)\dots O_n(x_n)\rangle_{\text{CFT}}\\ &\qquad = \lim_{z\to 0} z^{-(\Delta_1+\dots+\Delta_n)}\langle O_1(z,x_1)\dots O_n(z,x_n)\rangle_{\text{grav}}\,.\end{aligned} \tag{2.104}$$

In practice, we often consider the semi-classical regime (with small Newton constant G), such that we can approximate bulk path integral calculations by a classical saddle-point approximation. This is the basis for the common claim that bulk geometries are dual to CFT states; the bulk geometry in question is the leading classical saddle appearing in a bulk path integral calculation, and the CFT state is obtained by cutting open the corresponding Euclidean CFT path integral. The semi-classical limit also allows us to compute CFT correlation functions by performing perturbative quantum field theory on a fixed background, using Feynman diagrams which are referred to as *Witten diagrams* in the AdS context, and then differentiating the result with respect to the functions $\phi^{(0)}$ appearing in the boundary conditions.

2.4.2 Microscopic AdS/CFT

The paradigmatic example of an exact equivalence between microscopic theories in the context of AdS/CFT, which will be of interest to us later in this thesis, is the following [29]:

> The $\mathcal{N} = 4$ supersymmetric Yang-Mills theory with gauge group $SU(N)$ and Yang-Mills coupling g_{YM} is dynamically equivalent to type IIB string theory, with string length ℓ_s and string

coupling g, on $\mathrm{AdS}_5 \times S^5$ with (string frame) curvature scale $L^{(\mathrm{SF})}_{\mathrm{AdS}}$ and N units of $F_{(5)}$ flux on S^5. The relationship between field theory and string theory parameters is

$$g^2_{\mathrm{YM}} = 4\pi g\,, \qquad \lambda \equiv g^2_{\mathrm{YM}} N = (L^{(\mathrm{SF})}_{\mathrm{AdS}}/\ell_s)^4\,. \tag{2.105}$$

This correspondence is motivated by the equivalence of open and closed string descriptions of the physics of N coincident D3-branes in type IIB string theory. It will also sometimes be convenient to introduce the quantity $\alpha' \equiv \ell_s^2$. The Planck scale is related to the string scale by $\ell_p = g^{1/4}\ell_s$, so one can think of the large N limit as ensuring a hierarchy between the AdS scale and the Planck scale. Our conventions for this iteration of the AdS/CFT correspondence are available for reference in Appendix B.1.

Parameter regimes

The regime of *classical (type IIB) supergravity* is

$$\lambda \gg 1 \quad \text{and} \quad N \to \infty \qquad \longleftrightarrow \qquad g \to 0 \quad \text{and} \quad \ell_s/L^{(\mathrm{SF})}_{\mathrm{AdS}} \ll 1\,. \tag{2.106}$$

Setting the string coupling to zero truncates the string loop perturbative expansion to tree-level, while suppressing the string length relative to the curvature scale suppresses higher derivative α' corrections in the action.

On the other hand, one can maintain the large N limit while relaxing the condition of large λ to obtain the regime of *classical string theory*

$$\lambda = O(1) \text{ and } N \to \infty \quad \longleftrightarrow \quad g \to 0 \text{ and } \ell_s/L^{(\mathrm{SF})}_{\mathrm{AdS}} = O(1)\,, \tag{2.107}$$

or one can consider general (λ, N) to recover the regime of truly *quantum string theory*. While the latter regime is not well understood on the bulk side, the AdS/CFT correspondence as stated above has been conjectured to hold for arbitrary parameter values.

AdS/CFT is sometimes referred to as a *strong-weak coupling duality*; more precisely, we see that the CFT is strongly coupled ($\lambda \gg 1$) precisely

when the bulk theory is weakly-curved ($\ell_s \ll L_{\rm AdS}^{(\rm SF)}$) and vice versa. This mutual incompatibility of the regimes of validity of perturbation theory in Yang-Mills and classical type IIB supergravity poses a challenge for verifying the AdS/CFT correspondence, but also provides a direct route toward calculating non-perturbative effects through controlled calculations on the opposite side of the duality.

Operator spectrum matching

The microscopic AdS/CFT duality as stated above has been subjected to extensive numerical checks; an incomplete list can be found in [107]. We will briefly review a check at the level of the spectrum, since this will provide insights relevant beyond this particular microscopic iteration of AdS/CFT.

Although one would like to be able to compare the full spectrum of $\mathcal{N} = 4$ SYM and type IIB string theory on $\mathrm{AdS}_5 \times S^5$, it is not known how to compute the spectrum when stringy effects become important, namely for energies above the inverse string length $E \gtrsim 1/\ell_s$. Consequently, one can only compare spectra well below this scale, where the classical supergravity approximation is valid. Though the results should correspond to results at large coupling in the CFT, one can compare these directly for operators with protected dimensions, including chiral primary operators.

To compute the spectrum of type IIB supergravity on $\mathrm{AdS}_5 \times S^5$, one first writes the 10D fields in terms of spherical harmonics on the S^5

$$\phi(x^\mu, \hat{y}^i) = \sum_{k=0}^{\infty} \phi_k(x^\mu) Y_k(\hat{y}^i) \,, \tag{2.108}$$

where x^μ are the AdS_5 coordinates, $\hat{y}^i$ are coordinates on S^5 (such that $\sum_{i=1}^6 (\hat{y}^i)^2 = 1$), and Y_k are spherical harmonics. One then expands the Kaluza-Klein modes $\phi_k(x^\mu)$ in fluctuations around the AdS_5 background, and then diagonalizes the equations for the fluctuations. It transpires that these fluctuations can be organized into chiral representations of the superconformal transformations, with chiral primaries corresponding to linear combinations of the metric and self-dual four form. These represen-

tations can therefore be matched to the $\frac{1}{2}$-BPS chiral representations of $SU(N)$ $\mathcal{N} = 4$ SYM theory discussed in Section 2.3.5. Notably, in the supergravity calculation, the effective masses of the Kaluza-Klein modes are unbounded, whereas the chiral primary operator dimensions range from $n \in \{2, \ldots, N\}$; this reflects the fact that the supergravity approximation breaks down when the KK mass scale becomes of order the string scale, or when $n \sim L_{\mathrm{AdS}}/\ell_s = \lambda^{1/4} \ll N$. The supergravity calculation should account for the entire spectrum below the string scale, and it appears to be precisely matched to the spectrum of chiral primary representations in $\mathcal{N} = 4$ SYM; this suggests firstly that all non-chiral primary operators in SYM acquire parametrically large anomalous dimensions, at least of order $\lambda^{1/4}$, and secondly that all states above the string scale should necessarily appear in long multiplets.

2.4.3 Effective AdS/CFT

Much of the power of the AdS/CFT correspondence relies on the fact that many of the features observed in the above microscopic example appear to have a much broader range of applicability; indeed, it is typical to think of an *arbitrary* CFT as defining a possibly very exotic theory of gravity. We are most interested in those gravitational theories which reduce to general relativity, possibly coupled to a small number of light, weakly-interacting fields,[26] at low energies;[27]consequently, an important program within AdS/CFT is to establish a set of necessary and sufficient conditions to impose on a CFT that ensure this property in the dual.

Generalized free theories

A useful point of reference in the following discussion is the case of a free field theory in the bulk, which will define a *generalized free field theory* in the

[26]One may also be interested in the case of strong interactions, see e.g. [135].

[27]The phrase *sub-AdS locality* is sometimes used to signify the validity of effective field theory between the AdS scale and some parametrically larger cutoff scale.

boundary via the extrapolate dictionary.[28] Before considering a free field, we can begin by considering an even simpler system, namely one-particle quantum mechanics in AdS_{d+1}; a pedagogical account is provided in [131]. One can identify differential operators $(\mathcal{D}, \mathcal{P}_\mu, \mathcal{K}_\mu, \mathcal{L}_{\mu\nu})$ in AdS_{d+1} which implement the conformal algebra $\mathfrak{so}(2,d)$; in particular, we can choose $\mathcal{D}$ to be the generator of global time translations, and therefore interpret it as the AdS Hamiltonian. One may then construct irreducible representations of this algebra by first identifying a primary wavefunction satisfying $\mathcal{K}_\mu \psi_0 = 0$, then acting on ψ_0 with general products of $\mathcal{P}_\mu$ to produce wavefunctions

$$(\mathcal{P}_\mu \mathcal{P}^\mu)^n \mathcal{P}_{\mu_1} \dots \mathcal{P}_{\mu_\ell} \psi_0 \,. \tag{2.109}$$

Letting Δ denote the $\mathcal{D}$ eigenvalue of ψ_0, these wavefunctions have energy $E_{n,\ell} = \Delta + 2n + \ell$ with respect to the operator $\mathcal{D}$. For fixed n and ℓ, we can choose to consider linear combinations $\psi_{n,\ell,J}$ of the states (2.109) transforming in irreducible representations of $\mathfrak{so}(d)$ labelled by additional angular momentum quantum numbers J. For a fixed Δ, we can arrange for all $\psi_{n,\ell,J}$ to be orthonormal.

Having understood single-particle quantum mechanics in AdS, we can turn to free field theory. The canonical quantization of a free scalar field in the bulk proceeds by introducing an expansion[29]

$$\phi(t, \vartheta, \hat{x}^i) = \sum_{n,\ell,J} \psi_{n,\ell,J}(t, \vartheta, \hat{x}^i) a_{n,\ell,J} + \psi^*_{n,\ell,J}(t, \vartheta, \hat{x}^i) a^\dagger_{n,\ell,J} \,. \tag{2.110}$$

Here, the orthonormalized solutions to the Klein-Gordon equation $\psi_{n,\ell,J}$ are precisely the one-particle wavefunctions obtained for $m^2 = \Delta(\Delta - d)$, and $a^\dagger_{n,\ell,J}$ and $a_{n,\ell,J}$ are creation and annihilation operators satisfying

$$[a_{n_1,\ell_1,J_1}, a^\dagger_{n_2,\ell_2,J_2}] = \delta_{n_1 n_2} \delta_{\ell_1 \ell_2} \delta_{J_1 J_2} \,. \tag{2.111}$$

Following the standard approach to free quantum field theory, one can define

[28] Of course, this will not define a genuine CFT dual unless we have a perturbative graviton in the bulk and therefore a boundary stress tensor.

[29] We are using here the global AdS coordinates introduced in equation (2.7).

a Fock space including all multi-particle excitations.

To understand the corresponding boundary theory, we can apply the extrapolate dictionary to $\phi(t, \vartheta, \hat{x}^i)$, thereby obtaining a boundary operator $O(t, \hat{x}^i)$ expressed as a linear combination of the operators $a_{n,\ell,J}$ and $a^\dagger_{n,\ell,J}$. More generally, we can also apply the extrapolate dictionary to the descendant fields obtained by acting on the expression (2.110) with the differential operators $\mathcal{P}_\mu$, and also to normal-ordered products of bulk fields obtained this way.[30] Some immediate consequences of this procedure are as follows:

- Operators which produce single-particle excitations in the bulk correspond to the primary operator O of dimension Δ and its descendants $O_{n,\ell,J}$, which have dimension $\Delta + 2n + \ell$ and spin ℓ. These are the analogues of single-trace operators for the generalized free field theory.

- Operators which produce multi-particle excitations in the bulk correspond to products of $O_{n,\ell,J}$. The conformal dimension of such operators is simply the sum of conformal dimensions of the constituent single-particle operators, since energies are additive in the bulk free field theory. These are the analogues of multi-trace operators for the generalized free field theory.

- The simplest multi-trace operators are the double-trace operators, denoted by $[OO]_{n,\ell,J}$, which arise from the product of O and $O_{n,\ell,J}$. These operators are the only operators appearing in the OPE of O with itself.

- The three-point function of O with itself vanishes, because vacuum expectation values involving precisely three creation/annihilation operators in the bulk must vanish.

- Higher-point correlation functions factorize, in the sense that they are equal to a sum over products of two-point functions, with all possible pairwise contractions included in the sum. This is because free field theory correlators are computed by Wick contractions, as a consequence of the algebra (2.111).

[30] See [131] for a careful explanation.

Gapped large N theories

We would like to move beyond the case of bulk free field theory, allowing general semi-classical bulk physics including both perturbative gravity and interactions. The natural constructions to produce this bulk physics are known as *gapped large N CFTs*, which are families of d-dimensional CFTs satisfying the following conditions (paraphrased from [130]):[31]

- There exists a finite set of primary operators $\{O_i\}$ with scaling dimensions $\{\Delta_i\}$, referred to as *single-trace*, which, when normalized such that $\langle OO\rangle = O(N^0)$, have the property that

$$\langle O_i O_j O_k\rangle = O(N^{-1})\,. \tag{2.112}$$

  These operators are interpreted as the primary operators dual to the fundamental fields ϕ_i in the bulk which create single-particle states.

- There exists a unique single-trace spin-2 primary operator of dimension $\Delta = d$, the *energy-momentum tensor* $T_{\mu\nu}$, which has two-point function $\langle TT\rangle \sim N$.

- For any collection of $n = O(N^0)$ single-trace primaries $\{O_{i_1}, \ldots, O_{i_n}\}$, there exists an associated *multi-trace* primary $O_{i_1 \ldots i_n}$ whose scaling dimension is

$$\Delta_{i_1} + \ldots + \Delta_{i_n} + O(N^{-1})\,. \tag{2.113}$$

  These operators are dual to operators which create multi-particle states in the bulk.

- Correlation functions of the single-trace and multi-trace operators defined above agree with the factorized (generalized free field) result at leading order in $1/N$.

[31] As stated here, this definition is appropriate for capturing effective field theory in AdS_{d+1}; to accommodate the possibility of a higher-dimensional bulk with a compact internal space giving rise to towers of Kaluza-Klein modes, we should also permit towers of single-trace operators with $O(1)$ spacing of their conformal dimensions.

- All operators with $\Delta = O(N^0)$ are the above-mentioned single-trace and multi-trace primaries and descendants.

The proposal that gapped large N theories should ensure bulk semi-classical physics was put forward in [32], and has since been subject to various tests and refinements (see e.g. [34–38, 136–139]).

In this more general language, bulk free field theory may be thought of formally as a theory at infinite N, whereas perturbative interactions in the bulk are captured by the large N expansion. Many of the features of the generalized free field case, including the Fock space structure, the suppression of three-point functions, and the factorization of higher-point correlation functions, are therefore required to hold at leading order in $1/N$. That single-trace and multi-trace primaries and their descendants are the only operators with $O(1)$ scaling dimension reflects the expectation that all bulk states up to some cutoff scale are described by EFT excitations.

Our definition is broad enough to allow for any low-energy effective field theory with gravity; in particular, it could include higher spin fields in the low-energy spectrum, which could arise for example as excited string modes. On the other hand, it may also be desirable to require a parametric separation for higher spin fields, demanding that the low-energy theory in the bulk should resemble Einstein gravity. In the context of $\mathcal{N} = 4$ SYM, establishing such a parametric separation, namely demanding that $\ell_s \ll L_{\rm AdS}$, required a strongly coupled field theory. It transpires that the analogous criterion in the context of the abstract gapped large N CFTs introduced here is the existence of a *single-trace higher spin gap*, namely a parametrically large $\Delta_{\rm gap}$, with $1 \ll \Delta_{\rm gap} \ll N$, such that there do not exist primaries with dimension $\Delta < \Delta_{\rm gap}$ and spin greater than two.

For a generic gapped large N CFT with a higher spin gap, we can summarize the important regimes in the spectrum in terms of the bulk physics they describe as follows:

- $\Delta \ll \Delta_{\rm gap}$: Effective field theory excitations, including perturbative gravitons. In string theory language, this is the part of the spectrum lying well below the string scale, where classical supergravity is valid.

This regime may include Kaluza-Klein excitations, with large dimension $1 \ll \Delta \ll \Delta_{\text{gap}}$.

- $\Delta_{\text{gap}} \lesssim \Delta \ll N$: "Stringy" and/or higher-spin excitations. These are massive states that would be found in the spectrum of perturbative string theory.

- $\Delta \sim N$: An intermediate regime of the spectrum associated to bulk physics including non-perturbative objects like D-branes. CFT operators with scaling dimension in this regime are sometimes referred to as "hefty operators".

- $\Delta \sim N^2$: Black hole states.[32] CFT operators with scaling dimension in this regime are sometimes referred to as "heavy operators".

Notably, high-energy states of the theory are interpreted as black hole microstates; we turn to a discussion of black holes in the context of AdS/CFT presently.

2.4.4 Black holes in AdS/CFT

One of the most important applications of the AdS/CFT correspondence has been to the study of black hole physics. Historically, the behaviour of quantum black holes has been mysterious, since a semi-classical calculation due to Hawking appeared to suggest the break down of unitarity [50, 56]. In AdS/CFT, unitarity is inherent in the CFT description, and an important question, which has not been fully answered at the time of writing despite much recent progress [9, 63–67], is how the bulk perspective of the black hole evolution is able to account for this.

We have already discussed how black holes appear as high-energy microstates of holographic theories; in this subsection, we will mention two other important appearances of black holes in the context of AdS/CFT. We first consider the black holes which arise in computations in the *canonical*

[32] Small black holes may appear in the spectrum below $\Delta \sim N^2$, when the bulk energy scale exceeds the Planck mass; for example, in the microscopic version of AdS/CFT discussed earlier, one has small black holes appearing at $\Delta \sim N^{1/4}$ and above [140].

ensemble of the CFT, where we are able to treat the bulk semi-classically. We then describe a particular, special microstate of the two-fold tensor product of a CFT, known as the *thermofield double*, describing a two-sided black hole in the bulk; this state has been an invaluable laboratory for black hole physics and the emergence of geometry in AdS/CFT.

Canonical ensemble

As discussed in Appendix A.1, the *thermal partition function* of a quantum field theory quantized on the surface Σ_{d-1} at inverse termperature β can be computed via the Euclidean path integral on $\Sigma_{d-1} \times S^1_\beta$, with S^1_β the *thermal circle* of circumference β. Via the GKPW dictionary (2.100), we have the equivalence of path integrals

$$Z_{\text{grav}} = Z_{\text{CFT}}[\Sigma_{d-1} \times S^1_\beta] \,, \tag{2.114}$$

where the bulk path integral includes an integration over suitable asymptotically AdS Euclidean metrics with conformal boundary $\Sigma_{d-1} \times S^1_\beta$. We will restrict our consideration to the case of pure gravity, and focus on $\Sigma_{d-1} = S^{d-1}$ for concreteness.

In the limit of vanishing Newton constant $G \to 0$, when semi-classical gravity is valid in the bulk, we recall that the bulk path integral should be well-approximated by

$$Z_{\text{grav}} = \sum_{\text{saddles}} e^{-S_E[\text{saddle}]} \,, \tag{2.115}$$

where we are summing over Euclidean gravity solutions with the required boundary conditions, evaluating the on-shell Euclidean action S_E for each. We neglect loop corrections for the moment; they contribute to the exponential at order $O((L^{d-1}_{\text{AdS}}/G)^0)$, whereas the on-shell Euclidean action contributes at order $O(L^{d-1}_{\text{AdS}}/G)$.

The simplest such saddle in the case of the thermal partition function is *Euclidean thermal AdS*, whose metric is precisely that of pure Euclidean

AdS,

$$ds^2 = L_{\text{AdS}}^2 \left[f(r) d\tau^2 + \frac{dr^2}{f(r)} + r^2 d\Omega_{d-1}^2 \right] , \quad f(r) = 1 + \frac{r^2}{L_{\text{AdS}}^2} , \tag{2.116}$$

but subject to the identification $\tau \sim \tau + \beta$ in Euclidean time. We note that a closed path which wraps the τ direction is not contractible in the bulk; this is most easily visualized for AdS_3, where thermal AdS has the topology of a solid torus, as shown in Figure 2.3.

An alternative saddle is the *Euclidean black hole*, sometimes called the *Euclidean cigar*, with metric

$$\begin{aligned} ds^2 &= L_{\text{AdS}}^2 \left[f(r) d\tau^2 + \frac{dr^2}{f(r)} + r^2 d\Omega_{d-1}^2 \right] , \\ f(r) &= \frac{r^2}{L_{\text{AdS}}^2} + 1 - \frac{r_H^{d-2}}{r^{d-2}} \left(\frac{r_H^2}{L_{\text{AdS}}^2} + 1 \right) , \end{aligned} \tag{2.117}$$

where we still demand periodicity $\tau \sim \tau + \beta$. Unlike thermal AdS, the Euclidean black hole has the topology of $\text{Disk}_\beta \times S^{d-1}$ as shown in Figure 2.3, with a closed path wrapping the τ direction now contractible in the bulk. The solution $r = r_H$ to the equation $f(r) = 0$ gives the position of the Euclidean horizon, which can be thought of as the origin of the disk. Demanding that the solution has no conical singularity at this horizon, one discovers that the inverse temperature β and the horizon of the black hole r_H are related by

$$\beta = \frac{4\pi r_H L_{\text{AdS}}^2}{(d-2) L_{\text{AdS}}^2 + d r_H^2} . \tag{2.118}$$

This expression is readily inverted to deduce the horizon position in terms of β,

$$\frac{r_H}{L_{\text{AdS}}} = \frac{2\pi L_{\text{AdS}} \pm \sqrt{4\pi^2 L_{\text{AdS}}^2 - d(d-2)\beta^2}}{d\beta} . \tag{2.119}$$

Since r_H is real, we immediately observe that there is a minimum possible

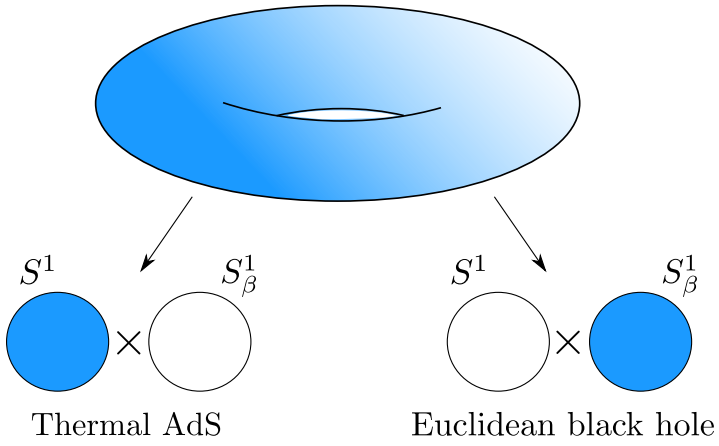

Figure 2.3: Solid torus representing the Euclidean gravity solutions appearing as saddle points in the calculation of the thermal partition function in $d+1=3$. For thermal AdS, loops in the thermal direction are non-contractible while loops in the spatial S^1 direction are contractible, whereas the opposite holds for the Euclidean black hole.

temperature, or maximum possible β, given by

$$\beta_{\max} = \frac{2\pi L_{\text{AdS}}}{\sqrt{d(d-2)}}\,. \tag{2.120}$$

Moreover, for a given β below this maximum, we see that there are in fact two Euclidean black hole solutions corresponding to the two signs in (2.119); we refer to these as the *large* and *small black holes* at a given temperature.[33]

To determine which saddle dominates the canonical ensemble, one can evaluate the on-shell Euclidean action for each; the saddle with least action will dominate.[34] As noted above, for low temperatures $\beta > \beta_{\max}$, no black hole saddles exist, and thermal AdS always dominates the canonical ensemble. Moreover, for $\beta < \beta_{\max}$, it can be shown that the large black hole

[33] In the $d=2$ case of AdS_3, 2.119 has only one positive solution, so there are no small black holes.

[34] Care must be taken to regulate large volume divergences in AdS; this can be achieved by cutting off the solutions at the surface $z=\epsilon$ in Fefferman-Graham coordinates, calculating the difference between on-shell actions for two solutions subject to this cutoff, and taking the limit $\epsilon \to 0$ to obtain a finite difference.

always has lower action than the small black hole. Comparing the on-shell action between the large black hole and thermal AdS for $\beta < \beta_{\max}$, one finds

$$\Delta S_E = \frac{\beta r_H^{d-2} \mathrm{Vol}(S^{d-1})}{16\pi G} \left(1 - \frac{r_H^2}{L_{\mathrm{AdS}}^2}\right) , \tag{2.121}$$

and therefore, using (2.119), one observes an exchange of dominance from thermal AdS to the large black hole as we lower β below the critical value

$$\beta_{\mathrm{c}} = \frac{2\pi L_{\mathrm{AdS}}}{d-1} . \tag{2.122}$$

This exchange is known as the *Hawking-Page transition* [141].[35]

In addition to the partition function, it is interesting to consider how the thermal entropy varies with β. For the Euclidean black hole, we can use a standard thermodynamic relation and $Z_{\mathrm{grav}} \approx e^{-S_E[\mathrm{saddle}]}$ to compute

$$S = (1 - \beta\partial_\beta) \ln Z = \frac{A_H}{4G} + \dots , \quad A_H = r_H^{d-1} \mathrm{Vol}(S^{d-1}) . \tag{2.123}$$

This is the famous *Bekenstein-Hawking* area law for the entropy of a black hole [24, 25, 50], which states the proportionality between the thermodynamic entropy and the horizon area. On the other hand, a similar calculation for thermal AdS would yield vanishing entropy, which we expect to become $O((L_{\mathrm{AdS}}^{d-1}/G)^0)$ with the inclusion of quantum corrections (due to thermal gravitons). Consequently, the thermal entropy at the Hawking-Page transition jumps from $O((L_{\mathrm{AdS}}^{d-1}/G)^0)$ to $O(L_{\mathrm{AdS}}^{d-1}/G)$, indicating a large number of high-energy states that become populated at high temperatures. This is related to a confinement-deconfinement transition in the dual CFT [55].

[35] It is worth noting that the Hawking-Page transition is absent in the case of the planar AdS black hole, which always dominates the canonical ensemble for the theory on flat space $\Sigma_{d-1} = \mathbb{R}^{d-1}$. The interpretation is that, although we have set the radius R of the S^{d-1} on which the CFT is quantized to one in the above analysis, it is the dimensionless parameter β/R which controls the Hawking-Page transition, and thus sending $R \to \infty$ enforces that we are always below this transition.

The eternal AdS black hole and the thermofield double state

We have seen that thermal physics at temperatures above the Hawking-Page transition is dominated by the Euclidean black hole in the bulk, meaning that the Euclidean CFT partition function corresponds to a Euclidean gravity partition function whose leading saddle is this black hole. An interesting result can be obtained by slicing this Euclidean CFT path integral to define a state on two copies of Σ_{d-1}; as argued in Appendix A.1, this defines a particular entangled state known as the *thermofield double state*

$$|\mathrm{TFD}_\beta\rangle_{12} \equiv \sum_n e^{-\beta E_n/2}|E_n\rangle_1|E_n\rangle_2 \tag{2.124}$$

in the two-fold tensor product of the CFT. This state can be thought of as a canonical purification of the thermal state on Σ_{d-1}; when we perform a partial trace of the pure state $|\mathrm{TFD}_\beta\rangle\langle\mathrm{TFD}_\beta|$ over one CFT, we recover precisely the thermal density matrix ρ_β on the remaining CFT.

Considering the corresponding slicing of the bulk path integral, we find that this path integral prepares a state of the eternal AdS black hole geometry introduced in Section 2.1.1, obtained by performing the analytic continuation $\tau \to it$; this is known as the *Hartle-Hawking state* [142]. This path integral manipulation suggests the proposal, due to Maldacena [41], that the full Lorentzian geometry, including the black hole interior, is holographically dual to the thermofield double state of two CFTs with temperature above the Hawking-Page transition.

This is a remarkable claim; as we will return to shortly, we anticipate that the thermal density matrix obtained by tracing out either of the two entangled CFTs describes only the physics occurring outside the black hole horizon, in one of the two exterior regions. The existence of a smooth interior connecting these regions must then be intimately related to the pattern of quantum entanglement found in the thermofield double state; we will explore the notion of entanglement and its relevance to AdS/CFT further in the next subsection.

2.4.5 Quantum information in AdS/CFT

Quantum information theory is an enormous discipline, and its applications to AdS/CFT have been widespread.[36] For the purposes of this thesis, we will need relatively modest input from quantum information theory; we will focus our presentation on perhaps the most basic measure of correlations between quantum subsystems known as *entanglement entropy*.

Von Neumann entropy

For a quantum mechanical system with Hilbert space $\mathcal{H}$, the *von Neumann entropy* associated to a density matrix ρ on $\mathcal{H}$ is defined by

$$S(\rho) = -\mathrm{tr}(\rho \ln \rho)\,. \tag{2.125}$$

The von Neumann entropy quantifies both classical and quantum uncertainty present in the state ρ. As such, the minimum possible entropy occurs when $\rho = |\Psi\rangle\langle\Psi|$ is a pure state, in which case

$$S(|\Psi\rangle\langle\Psi|) = 0\,, \tag{2.126}$$

while the maximum possible entropy in a d-dimensional Hilbert space occurs when $\rho = \frac{1}{d}\mathbb{1}$ is maximally mixed, in which case

$$S\big(\frac{1}{d}\mathbb{1}\big) = \ln d\,. \tag{2.127}$$

A case of particular interest is when the density matrix ρ is obtained from a pure state by tracing out some of the degrees of freedom in the system. In particular, suppose that we have a bipartite system AB with factorizing Hilbert space $\mathcal{H}_{AB} = \mathcal{H}_A \otimes \mathcal{H}_B$, and a pure state $|\Psi\rangle$ of the full Hilbert space $\mathcal{H}_{AB}$. We can then obtain a density matrix on the subsystem A by

[36] A high-level summary of the applications of quantum information theory to quantum gravity appears in [143].

performing a partial trace

$$\rho_A = \mathrm{tr}_B(|\Psi\rangle\langle\Psi|)\,. \tag{2.128}$$

In this context, the von Neumann entropy of the state ρ_A is referred to as the *entanglement entropy*, since it reflects the degree of entanglement between A and B in the state $|\Psi\rangle$. When A and B are unentangled in $|\Psi\rangle$, then ρ_A is pure, whereas when $|\Psi\rangle$ is a state with a pattern of entanglement like that of $\frac{1}{\sqrt{d}}\sum_{i=1}^{d}|a_i\rangle\otimes|b_i\rangle$, with $\{a_i\}$ and $\{b_i\}$ orthonormal bases for $\mathcal{H}_A$ and $\mathcal{H}_B$,[37] then ρ_A is maximally mixed.

We will often be interested in the entanglement entropy of spatial subregions in the context of quantum field theory, for example in the case of a holographic CFT. In fact, this quantity is technically not well-defined, essentially because the Hilbert space does not factorize into $\mathcal{H}_A$, $\mathcal{H}_{\bar{A}}$ associated with an open region A and the interior of its complement. If we attempted to choose a lattice regularization and then take a continuum limit, we would find the entanglement entropy to be UV-divergent, reflecting the generic presence of short-range entanglement in quantum field theory.[38][39] However, as a result of the universal structure of these divergences, emerging from the fact that all finite energy states in QFT have the entanglement structure of the vacuum state in the limit of short distances, one can introduce UV regulators and compute quantities, like differences in the entanglement entropy of a fixed subregion for different quantum states, which remain finite when the regulator is removed.

It is important to note that the von Neumann entropy is not a thermodynamic entropy, in the sense that it does not count microstates consistent with a list of macroscopic data. For this reason, the von Neumann entropy is

[37] If $\mathcal{H}_A$ and $\mathcal{H}_B$ have different dimension, then the rank of ρ_A is at most equal to the smaller dimension. In particular ρ_A cannot be maximally mixed when the A Hilbert space is larger than the B Hilbert space.

[38] In the language of algebraic QFT, the von Neumann algebra associated to a subregion in quantum field theory is a type III factor, which has neither a well-defined density matrix nor entropy.

[39] Additional technical challenges arise when attempting to define a notion of subregion entanglement entropy in the context of gauge theory.

also sometimes called a *fine-grained entropy*: it is a property of a particular density matrix. A *coarse-grained* or *thermodynamic entropy* may instead be defined with respect to a collection $\mathbf{a} = (a_1, \ldots, a_n)$ of expectation values of macroscopic observables $\{A_1, \ldots, A_n\}$ by

$$S_{\text{thermo}}(\mathbf{a}) \equiv \max_{\rho \in A_{\mathbf{a}}} S(\rho) \,, \qquad A_{\mathbf{a}} \equiv \{\rho : \text{tr}(\rho A) = a_i\} \,. \tag{2.129}$$

In words, it is obtained by maximizing the von Neumann entropy with respect to density matrices with the appropriate expectation values for the operators A_i.

Entanglement entropy in AdS/CFT

A remarkable entry in the AdS/CFT dictionary, which can be derived from a careful treatment of the equivalence of path integrals and an application of the replica trick [65, 66, 144–146], is the *Ryu-Takayanagi formula* [42] and its various generalizations (e.g. [145, 147–149]), which relate the von Neumann entropy of a boundary subregion to the area of an extremal surface in the bulk.[40] The original proposal of Ryu and Takayanagi, relevant to the special case of holographic states with classical, static, asymptotically AdS duals, stated that the von Neumann entropy associated to the subregion A should be given by

$$S(\rho_A) = \min_{X_A} \frac{\mathcal{A}[X_A]}{4G} \tag{2.130}$$

where the minimization is over surfaces X_A, contained in some static slice Σ whose boundary contains A, which are homologous to A, meaning that there exists a *homology surface* H_A whose boundary is $\partial H_A = A \cup X_A$. A prototypical example of the application of this formula is to the thermofield double state on two copies of a holographic CFT, which we saw in the previous subsection is dual to an eternal AdS black hole. In this case, the entanglement entropy of the reduced density matrix on the left CFT is simply the von Neumann entropy of the thermal state of this CFT, which we have seen is given by the Bekenstein-Hawking formula, which here precisely

[40] A useful overview of the RT formula and its generalizations can be found in [150].

coincides with the Ryu-Takayanagi formula.

A useful generalization of the RT formula due to Hubeny, Rangamani, and Takayanagi, known as the *HRT formula* [147], applies to any classical, asymptotically AdS spacetime satisfying the null energy condition. The statement of the HRT formula is superficially identical to (2.130), with the caveat that the minimization is now with respect to all bulk extremal surfaces X_A homologous to A, rather than all surfaces restricted to a particular static slice. The HRT formula admits a convenient reformulation due to Wall, known as the *maximin formulation* [148], which states

$$S(\rho_A) = \max_{\Sigma} \min_{X_A \subset \Sigma} \frac{\mathcal{A}[X_A]}{4G} \,. \tag{2.131}$$

In words, the maximin formula instructs one to first select a Cauchy slice Σ and minimize with respect to homologous surfaces $X_A \subset \Sigma$, and then to maximize the result over all possible Σ.

It is sometimes of interest to consider corrections to the holographic entanglement entropy formula, including higher derivative corrections to the gravitational action and quantum corrections from propagating quantum fields. In this case, an expression which accounts for leading order corrections is provided by [145, 151]

$$S[\rho_A] = \frac{\mathcal{A}_{\text{gen}}[X_A]}{4G} + S[\rho_{H_A}] \equiv S_{\text{gen}}[X_A] \,, \tag{2.132}$$

where X_A is precisely the surface appearing in the HRT formula for a given background, H_A is a homology surface for X_A, $\mathcal{A}_{\text{gen}}$ is a generalized area which accounts for higher derivative corrections, and $S[\rho_{H_A}]$ is the von Neumann entropy of the semi-classical bulk fields in the region H_A. An important upgrade of this formula, known as the *Engelhardt-Wall formula* or sometimes simply the *gravitational entropy formula* [149], proposes modifying (2.132) by replacing X_A with the *quantum extremal surface* which minimizes the generalized entropy. Here, a quantum extremal surface X_A is simply a surface homologous to A for which the generalized entropy is extremized. This improvement has played a significant role in recent progress in

understanding the black hole information paradox; importantly, it is needed in situations where quantum corrections need not be small, but can rather compete with the area term in the generalized entropy formula. It is also significant in this context that the surface X_A appearing in the extremization procedure need not be connected, but can contain disconnected components which therefore allow for H_A to include disconnected *entanglement island* regions; such surfaces are important for restoring a unitary Page curve in holographic models of black hole evaporation.

Bulk reconstruction

A primary goal in the study of AdS/CFT is to understand how bulk physics is encoded in the boundary theory. To this end, a basic question is whether, given a CFT state and a choice of boundary spatial subregion A at fixed time, there exists some bulk subregion whose semi-classical physics is entirely reconstructible from data contained within A. Concretely, one might require that any element of the algebra of bulk local operators within this subregion can be expressed in terms of the algebra of boundary local operators in the region A. The existence of such a bulk subregion is not guaranteed *a priori* due to the inherently non-local nature of the AdS/CFT correspondence; it is a manifestation of a property of the correspondence sometimes referred to as *subregion duality*.

Perhaps the most intuitive guess for the relevant bulk subregion is a region known as the *causal wedge* of A, defined by

$$C[A] = J^+[D(A)] \cap J^-[D(A)]\,, \tag{2.133}$$

where $D(A)$ denotes the *domain of dependence* of A, defined as the spacetime region consisting of points p such that all causal curves through p intersect A, and $J^\pm[S]$ denote the bulk future/past light cones of boundary region S. We can think about the causal wedge as the collection of points in the bulk which lie on causal curves whose endpoints are in the domain of dependence of A. The fact that causality permits a probe to be sent from and back to $D(A)$ via any point in the causal wedge is at least suggestive that physics within

this wedge may be reconstructible on $D(A)$, and therefore in principle on A. An explicit demonstration of causal wedge reconstructibility is provided by the *HKLL procedure* [152], which makes use of the extrapolate dictionary to relate bulk and boundary operators.

In fact, general arguments making use of the Ryu-Takayanagi formula suggest that a generically larger region[41] known as the *entanglement wedge* of A should be reconstructible within A; this region is defined by

$$E[A] \equiv D[H_A] \,, \tag{2.134}$$

where H_A denotes a homology surface appearing in the HRT formula. Notably, whereas the definition of the causal wedge forbids reconstruction of physics at bulk spacetime points behind causal horizons, such points may lie within the entanglement wedge of a boundary subregion; in particular, the entanglement wedge of the entire boundary is necessarily the entire bulk spacetime.

A naïve puzzle posed by the entanglement wedge reconstruction paradigm is illustrated in Figure 2.4, which demonstrates a situation in which a tripartition of the boundary into subregions A, B, and C might permit some bulk points to be reconstructible on AB, BC, or AC but not A, B, or C individually. Such considerations have led to the realization that the AdS/CFT map has the structure of a *quantum error correcting code*, where quantum information may be simultaneously stored in an entangled state of multiple quantum subystems, thereby protecting against errors within individual subsystems. This is formalized by the existence of an embedding

$$V : \mathcal{H}_{\text{AdS-EFT}} \to \mathcal{H}_{\text{CFT}} \,, \tag{2.135}$$

where in this context the image of the EFT Hilbert space $V(\mathcal{H}_{\text{AdS-EFT}})$ is referred to as a *code subspace* of the CFT Hilbert space. A pedagogical introduction to this subject can be found in [130].

[41] The containment $C[A] \subseteq E[A]$ can be derived subject to certain physical assumptions, including the null energy condition.

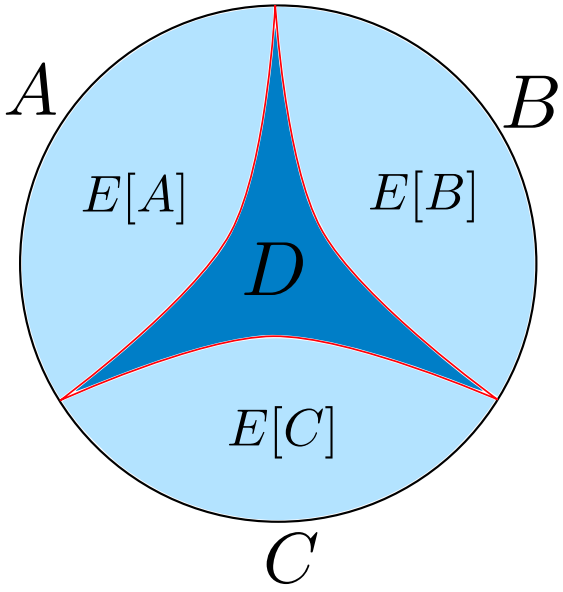

Figure 2.4: Time slice of a static bulk configuration illustrating a puzzle for entanglement wedge reconstruction. The CFT is partitioned into three regions, A, B, and C. Ryu-Takayanagi surfaces are shown in red. The bulk region D (dark blue) is not contained in the entanglement wedges of A, B, or C (light blue), but is contained in the entanglement wedge of e.g. AB, which is equal to $E[A] \cup E[B] \cup D$.

Part II

Boundaries

Chapter 3

Boundary F in $\mathcal{N} = 4$ Supersymmetric Yang-Mills Theory

3.1 Introduction

Conformal field theories in various dimensions may be characterized by a parameter, sometimes known as $\tilde{F}$ or "generalized F", that characterizes the number of local degrees of freedom [153–158]. This is equal to the central charge c for two-dimensional CFTs, and the Weyl-anomaly coefficient a for four-dimensional CFTs. In general, $\tilde{F}$ may be defined from a regulator-independent term in the sphere free energy, or alternatively from a universal term in the vacuum entanglement entropy for a ball-shaped region. The $\tilde{F}$ parameter is conjectured to decrease under renormalization group (RG) flows between conformal fixed points. This has been proven in two, three, and four dimensions as the c-theorem [153], F-theorem [154, 155, 159], and a-theorem [156, 157], respectively.

A similar parameter, boundary $\tilde{F}$, may be defined for boundary conformal field theories (BCFTs) [84, 160–162].[42] It can be understood as a measure of the number of local degrees of freedom associated with the bound-

[42] We recall that a BCFT is a local quantum field theory defined on a manifold with boundary such that the theory on a half-space preserves the conformal invariance of a CFT in one lower dimension (see e.g. [80, 106, 163, 164]). Each BCFT is associated with some bulk CFT which governs the short-distance behavior of local bulk correlators. Some BCFTs may be naturally understood by starting with this bulk CFT and choosing some boundary conditions for the fields. More generally, we can couple in (arbitrarily numerous) additional boundary degrees of freedom.

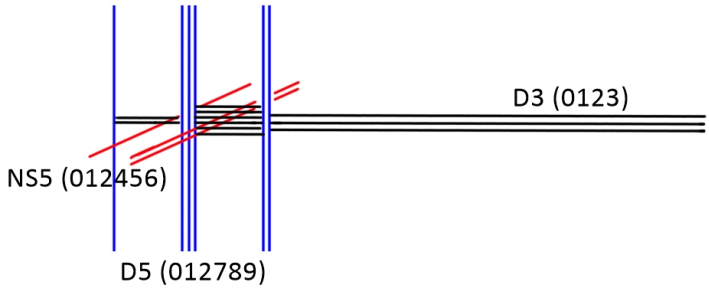

Figure 3.1: D-brane construction of a half-supersymmetric BCFT whose bulk CFT is $\mathcal{N} = 4$ SYM theory.

ary.[43] Boundary $\tilde{F}$ may be defined from the partition function of the BCFT on a hemisphere, or from the vacuum entanglement entropy of a half-ball centered on the boundary. It is conjectured to decrease under boundary RG flows (where a UV BCFT is perturbed by a relevant boundary operator) [162, 165–168]; this has been proven as the g-theorem in two dimensions [84, 160, 169] and the b-theorem in three dimensions [170, 171], but remains a conjecture (the boundary F theorem) for four-dimensional BCFTs.

It is interesting to characterize the possible BCFTs that are associated with a particular bulk CFT, and specifically to understand which values of boundary $\tilde{F}$ are possible. This is understood for minimal model CFTs in two dimensions, but relatively few results are available for more complicated CFTs or CFTs in higher dimensions. The main goal of this chapter is to investigate the possible values of boundary F in a very special higher-dimensional example where we take the bulk CFT to be $U(N)$ $\mathcal{N} = 4$ supersymmetric Yang-Mills (SYM) theory and we constrain the BCFT to preserve half of the supersymmetry.

This rich class of theories was classified by Gaiotto and Witten in [89, 90]. These theories preserve an $OSp(4|4)$ subgroup of the original 4D superconformal symmetry group $PSU(2,2|4)$; they are four-dimensional BCFTs with the maximum possible supersymmetry. Many of these theories de-

[43] This quantity can be negative; in this case, we can understand the boundary condition as removing some of the bulk degrees of freedom near the boundary.

scribe the decoupled low-energy physics of coincident D3-branes in type IIB string theory ending in various ways on stacks of D5-branes and NS5-branes, possibly with additional D3-branes stretched between the five-branes, as depicted in Figure 3.1. As for their $\mathcal{N} = 4$ SYM parent, the associated half-supersymmetric BCFTs are holographic; their vacuum states are dual to solutions of type IIB supergravity preserving $SO(3) \times SO(3) \times SO(3,2)$ symmetry. These solutions were described in [172–175].

In this chapter, we calculate boundary F for a general $OSp(4|4)$-symmetric BCFTs whose bulk CFT is $U(N)$ $\mathcal{N} = 4$ SYM theory. First, we perform a holographic calculation, making use of the Ryu-Takayanagi (RT) formula to calculate the vacuum entanglement entropy for a half-ball. This was done in [162] for a particular type of boundary condition associated with nk D3-branes ending on k D5-branes;[44] we extend these calculations to the most general case, arising from the brane construction in Figure 3.1 with arbitrary numbers and configurations of branes. The result is given as equation (3.73) in Section 3.4.2.

Next, we calculate boundary F exactly by evaluating the hemisphere partition function using supersymmetric localization, for the class of boundary conditions arising from D3-branes ending on only D5-branes or only NS5-branes, in all possible ways.[45] These results are given as equation (3.118) for boundary conditions associated with NS5-branes and (3.120) for boundary conditions associated with D5-branes.

We compare the localization results, which should be exact, to the supergravity calculations, which are expected to be valid at large N and large 't Hooft coupling λ. The results agree precisely in a limit where a certain set of integers characterizing the theory (roughly, the number of D3-branes ending on each five-brane in the string theory picture and the non-zero differences between these numbers) are large. Perhaps surprisingly, we find that this agreement holds exactly as a function of the 't Hooft coupling λ,

[44] Similar calculations were performed in [176] for 3D superconformal theories and in [177] for 3D BCFTs.

[45] Localization calculations of F for related 3D SCFTs were performed in [176], and calculations of the interface entropy for supersymmetric Janus interfaces in 4D $\mathcal{N} = 2$ SCFTs were performed in [178].

suggesting a non-renormalization theorem governing the α' corrections in the string theory calculation.

Making use of our results, we analyze in Section 3.6 the distribution of possible values of boundary F for various classes of boundary conditions. For the most general boundary conditions associated with D5-branes and NS5-branes, we can have arbitrarily large values of boundary F for a given N and λ, in accord with the fact that we can couple in a 3D SCFT with an arbitrarily large number of degrees of freedom. For the theories associated with NS5-branes only or D5-branes only (which may be interpreted as boundary conditions for $\mathcal{N} = 4$ SYM theory without added degrees of freedom), we find that boundary F is bounded, but can take positive or negative values. For boundary conditions associated with D5-branes only, we find that F is typically negative at small 't Hooft coupling, consistent with the fact that these boundary conditions are associated with scalar vevs that diverge near the boundary and give spatially dependent mass terms that effectively remove some of the bulk CFT degrees of freedom. For NS5-brane boundary conditions, we find that boundary F is positive for small λ but that an increasing proportion of these boundary conditions become negative as λ grows.[46]

3.2 Background

In this section, we review some relevant background material on boundary F and on half-supersymmetric BCFTs associated with the $\mathcal{N} = 4$ SYM theory.

[46] For $\lambda > 4\pi N$, we can make an S-duality transformation that maps a theory with NS5 boundary conditions to a theory with D5 boundary conditions and $\lambda < 4\pi N$, so it is expected that the proportion of NS5 boundary conditions with negative boundary F grows with λ; likewise, the proportion of D5 boundary conditions with positive boundary F should grow with λ.

3.2.1 Boundary entropy and boundary free energy

In a d-dimensional CFT, the vacuum state entanglement entropy of a ball-shaped region of radius R has the general UV divergence structure

$$S[B_R^{d-1}] = a_{d-2}\,(R/\epsilon)^{d-2} + a_{d-4}\,(R/\epsilon)^{d-4} + \ldots + \begin{cases} 4(-1)^{\frac{d-2}{2}} A \ln(R/\epsilon) & 2 \mid d \\ (-1)^{\frac{d-1}{2}} F & 2 \nmid d \end{cases}, \quad (3.1)$$

where ϵ is a UV regulator. The coefficients a_i are generally scheme-dependent, and arise from integration of local geometric quantities over the entangling surface, while the coefficients A and F are universal, i.e. independent of the regularization scheme. In particular, the quantity A coincides with the A-type trace anomaly in even dimensions, while F is the sphere free energy $F = -\ln Z[S^d]$; this equivalence is established by the relation

$$S[B_R^{d-1}]_{\text{univ}} = \ln Z[S_R^d]_{\text{univ}} \quad (3.2)$$

of Casini, Huerta, and Myers for sphere entanglement entropy and the sphere partition function in CFT [179]. These universal terms are conjectured to be RG monotones in arbitrary dimension [158, 180–182]; this has been proven in dimensions $d = 2, 3$, and 4, with the results referred to as the (Zamolodchikov) c-theorem [153], the F-theorem [154, 155, 159], and the a-theorem [156, 157] respectively. The conjectured extension to arbitrary dimension is sometimes referred to as the generalized F-theorem.

In the BCFT case, we may instead consider the entanglement entropy of a half-ball region centred at the BCFT boundary (see Figure 3.2). The entanglement entropy now has divergences of d-dimensional and $(d-1)$-

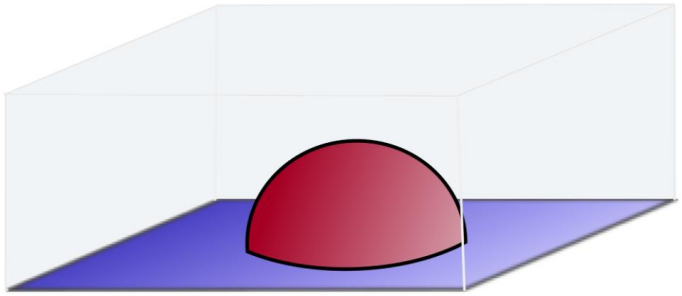

Figure 3.2: Set-up for calculation of boundary F, showing the entangling surface for a half-ball region centred at the boundary for a BCFT on half of $\mathbb{R}^{1,3}$.

dimensional origin, taking the form

$$S[HB_R^{d-1}] = \tilde{a}_{d-2}\,(R/\epsilon)^{d-2} + \tilde{a}_{d-3}\,(R/\epsilon)^{d-3} + \ldots + \begin{cases} 4(-1)^{\frac{d-2}{2}} A \ln(R/\epsilon) + (-1)^{\frac{d-2}{2}} \tilde{F} & 2 \mid d \\ 4(-1)^{\frac{d-3}{2}} \tilde{A} \ln(R/\epsilon) + (-1)^{\frac{d-1}{2}} F & 2 \nmid d \end{cases} . \quad (3.3)$$

The coefficient $\tilde{F}$ in this expression is not universal, insofar as the logarithmic term changes by a constant when we change regulators. However, by analogy to the two-dimensional case [183], one may define the "boundary entropy"

$$S_\partial(R) \equiv S^{(\mathrm{BCFT})}[HB_R^{d-1}] - \frac{1}{2} S^{(\mathrm{CFT})}[B_R^{d-1}] \,, \quad (3.4)$$

where $S^{(\mathrm{CFT})}$ denotes the entanglement entropy calculated in the ambient CFT for a region far from the boundary.[47] Given that the divergences with d-dimensional origin cancel in this subtraction, we recover boundary entropy

[47] In practice, $S^{(\mathrm{CFT})}$ may be calculated in the theory without a boundary. For example, in our holographic calculation, we compute $S^{(\mathrm{CFT})}$ using the RT formula in the $\mathrm{AdS}_5 \times S^5$ geometry.

of the form

$$S_\partial(R) = \tilde{a}_{d-3}\,(R/\epsilon)^{d-3} + \tilde{a}_{d-5}\,(R/\epsilon)^{d-5} + \ldots + \begin{cases} (-1)^{\frac{d-2}{2}}\tilde{F} & 2 \mid d \\ 4(-1)^{\frac{d-3}{2}}\tilde{A}\ln(R/\epsilon) & 2 \nmid d \end{cases} . \quad (3.5)$$

In particular, $\tilde{F}$ and $\tilde{A}$ are universal terms appearing in the expression for $S_\partial(R)$. The coefficient $\tilde{A}$ occurring for odd dimensions is related to the boundary Weyl anomaly in BCFT, using a similar argument to that of [179] (see also [167, 171, 184, 185]). In general, as for the CFT case, the boundary entropy can be related to the logarithm of the partition function via

$$S_\partial(R)_{\text{univ}} = \left(\ln Z[HS^d_R] - \frac{1}{2}\ln Z[S^d_R]\right)_{\text{univ}} . \quad (3.6)$$

This quantity has also been conjectured to satisfy an RG monotonicity theorem in various dimensions [162, 165–168] (see [87, 88, 186] for proposed holographic g-functions); this has been proven in dimensions $d = 2$ and $d = 3$, with the results referred to as the g-theorem [84, 160, 169] and the b-theorem [170, 171].[48]

In this chapter, we will be specifically concerned with the case $d = 4$, where we have

$$S_\partial(R) = S_1\frac{R}{\epsilon} + S_{\text{univ}} . \quad (3.7)$$

Defining

$$F_\partial \equiv -S_{\text{univ}} , \quad (3.8)$$

the universal quantity F_∂ appearing in the boundary entropy is referred to as "boundary F" or the "boundary free energy". The boundary free energy was conjectured to satisfy an RG monotonicity theorem in [162, 166]. Note

[48] In fact, the b-theorem establishes the monotonicity of the Weyl anomaly coefficient on a dimension-2 submanifold in arbitrary dimension.

that we may extract F_∂ from the boundary entropy by

$$F_\partial = \lim_{\epsilon \to 0} \left(R \frac{d}{dR} - 1 \right) S_\partial(R) \,. \tag{3.9}$$

In the $d = 4$ case, one finds exactly [185]

$$F_\partial = - \lim_{\epsilon \to 0} \left(\ln Z[HS^4_R] - \frac{1}{2} \ln Z[S^4_R] \right) \,. \tag{3.10}$$

3.2.2 Half-supersymmetric BCFTs from $\mathcal{N} = 4$ SYM

In this section, we review the boundary conformal field theories constructed from $\mathcal{N} = 4$ SYM that preserve half of the supersymmetry and an $OSp(4|4)$ subgroup of the superconformal symmetry group $PSU(2,2|4)$ of $\mathcal{N} = 4$ SYM. The classification of these theories is due to Gaiotto and Witten; see [89, 90] for details. Our conventions are similar to those of [187].

Starting with the four-dimensional $\mathcal{N} = 4$ SYM theory on $\mathbb{R}^{1,3}$, we can introduce a planar boundary at $x^3 = 0$, and consider boundary conditions preserving the subset of conformal transformations which leave this plane fixed. Specifically, we are interested in half-BPS boundary conditions which preserve an $OSp(4|4)$ superconformal subgroup of the initial superconformal group $PSU(2,2|4)$. We will also consider the addition of extra degrees of freedom at this boundary such that the full theory preserves the same symmetry.

The bosonic sector of the residual symmetry group corresponds to

$$\mathfrak{so}(2,3) \times \mathfrak{so}(3) \times \mathfrak{so}(3) \,. \tag{3.11}$$

To reflect this reduction in R-symmetry, it is convenient to decompose the scalars Φ^i of the $\mathcal{N} = 4$ theory as triples

$$(X^1, X^2, X^3) \equiv (\Phi^4, \Phi^5, \Phi^6) \,, \qquad (Y^1, Y^2, Y^3) \equiv (\Phi^7, \Phi^8, \Phi^9) \,, \tag{3.12}$$

and the fermions as[49]

$$\Psi_{\pm} \equiv \frac{1}{2}\left(1 \pm \Gamma_{3456}\right)\Psi \,. \tag{3.14}$$

The four-dimensional $\mathcal{N}=4$ vector multiplet decomposes with respect to the reduced symmetry group into two different multiplets, naturally interpreted from the perspective of the three-dimensional $\mathcal{N}=4$ supersymmetry algebra as

$$\text{hyper} \,:\, \Psi_{-}\,,\; A_3\,,\; X^i\,, \qquad \text{vector} \,:\, \Psi_{+}\,,\; A_{0,1,2}\,,\; Y^i\,. \tag{3.15}$$

The various theories we consider arise from the low-energy physics of string theory configurations with D3-branes ending on and stretched between both D5-branes and NS5-branes. We consider first boundary conditions involving only D5-branes or only NS5-branes before considering the general case.

Single NS5-brane boundary conditions

For the boundary condition corresponding to D3-branes ending on a single NS5-brane in the (012789) directions, Neumann boundary conditions are imposed on the three-dimensional vector multiplet and Dirichlet conditions on the hypermultiplet, i.e.

$$\text{NS5} \,:\qquad F_{3\mu}| = X^i| = D_3 Y^i| = 0\,, \qquad \Psi_{-}| = 0\,. \tag{3.16}$$

Here, the vertical line denotes that the fields are evaluated at $x_3 = 0$.

D5-brane boundary conditions

For boundary conditions associated with the D3-branes ending on one or more D5-branes in the (012456) directions, we have a Dirichlet condition on

[49] Here, our notation reflects the fact that $\mathcal{N}=4$ SYM theory may be understood as the dimensional reduction of ten-dimensional supersymmetric Yang-Mills theory. There exists a family of inequivalent $OSp(4|4)$ subalgebras related by $U(1)$ outer automorphisms of $\mathfrak{psu}(2,2|4)$ [89], and we are choosing a particular one which preserves SUSY generators ε satisfying

$$\Gamma_{3456}\varepsilon = \varepsilon\,. \tag{3.13}$$

.

the three-dimensional vector multiplet and a (generalized) Neumann condition on the hypermultiplet,

$$\text{D5}: \qquad F_{\mu\nu}| = D_3 X_i| - \frac{i}{2}\epsilon_{ijk}[X_j, X_k]| = Y_i| = 0\,, \qquad \Psi_+| = 0\,. \quad (3.17)$$

This is a generalization of the Dirichlet boundary condition, sometimes referred to as a "Nahm pole" boundary condition, since the scalar fields X^i are seen to satisfy the Nahm equation in the vicinity of the boundary, with solution

$$X^i = \frac{t^i}{x^3}\,, \qquad [t^i, t^j] = i\epsilon^{ijk}t^k\,. \quad (3.18)$$

Here t^i can be $SU(2)$ generators in an arbitrary N-dimensional representation. Choosing the irreducible representation gives a boundary condition that corresponds to N D3-branes along the (0123) directions ending on a single D5-brane. The non-commuting configuration of scalar matrices describe a non-commutative geometry corresponding to a string theory picture where the D3-branes flare out to form a "fuzzy funnel" [188] as they approach the D5-brane.

Taking t^i to correspond to a more general reducible representation of the $SU(2)$ with irreducible representations of size p_i gives a boundary condition related to a more general brane configuration where groups of p_i D3-branes each end on a single D5-brane.

General D5-NS5 boundary conditions

We now describe the more general theories that arise from configurations with both D5-branes and NS5-branes. It is convenient to consider first N_{D5} D5-branes and N_{NS5} NS5-branes at distinct locations in the x^3 direction, with the D5s stretched along the (012456) directions and the NS5s stretched along the (012789) directions. Next, we consider N semi-infinite D3-branes stretched in the (0123) directions, extending to $x^3 = \infty$, each ending on some five-brane. Finally, we can have additional D3-branes of finite extent in x^3 stretched between some of the five-branes. An example is shown in Figure 3.3.

As explained in [90], the low-energy physics of such configurations does not depend on the specific positions of the five-branes along the x^3 direction, and is even unchanged if we rearrange the five-branes relative to one another, taking into account the fact that when a D5-brane is moved past an NS5-brane towards the direction of larger x^3, we create and additional D3-brane stretched between the D5 and NS5 [189]. We consider brane configurations related by such re-arrangements as being part of an equivalence class.

The distinct IR superconformal BCFTs that can arise from these brane configurations are in one-to-one correspondence with equivalence classes that obey certain additional constraints [90].[50] The distinct theories satisfying the constraints may be represented by brane configurations of the type shown in Figure 3.3, where we have n_i D3-branes immediately to the right of the i^{th} NS5-brane counted from the left, and M_i D5-branes that intersect these, with the constraint that

$$M_i \geq 2n_i - n_{i+1} - n_{i-1} \qquad i = 1 \dots N_{NS5} - 1 \tag{3.19}$$

taking $n_0 = 0$. Additional D5-branes sit to the right of all NS5-branes, and we have a constraint that the net number of D3-branes ending on each D5-brane from the right (i.e. the number on the right minus the number on the left) increases from left to right.

The constraints (3.19) are equivalent to the requirement that by moving all D5-branes to the right of all NS5-branes (while preserving their order) as in Figure 3.3 (bottom), the net number K_i of D3-branes ending from the right on the i^{th} NS5-brane (starting from the left) is positive and non-decreasing with i. By construction, the net number $\tilde{L}_i$ of D3-branes ending from the right on the ith D5-brane (starting from the left) is also non-decreasing with i, and satisfies $\tilde{L}_i > -N_{NS5}$. The quantities $L_i = \tilde{L}_i + N_{NS5}$ are then positive and increasing with i; the action of S-duality simply exchanges $\{K_i\} \leftrightarrow \{L_i\}$. The parameters K_i and $\tilde{L}_i$ (or alternatively L_i), known as "linking numbers," are closely related to the parameters appearing

[50] Configurations which do not obey the constraints may fail to have a supersymmetric vacuum or may give rise to theories which factorize into a superconformal BCFT and some other 3D SCFT.

in the dual supergravity solutions.[51]

We can read off the linking numbers without re-ordering the branes by defining K_i in general to be the net number of D3-branes ending on the i^{th} NS5-brane from the right plus the total number of D5-branes to the left of this NS5, and defining $\tilde{L}_i$ to be the net number of D3-branes ending on the i^{th} D5-brane from the right minus the total number of NS5-branes to the right of this D5. With this definition, we can check that the linking numbers do not change as we move a D5-brane past an NS5-brane. It follows that the NS5-brane linking numbers K_i can be expressed in terms of M_i and n_i as

$$K_i = n_i - n_{i-1} + \sum_{j=1}^{i-1} M_j \ . \tag{3.20}$$

Conversely, we have that M_i is the number of D5-branes with linking number $\tilde{L} = i - N_{NS5}$ while

$$n_j = \sum_{i=1}^{j} (K_i + (i-j)M_i) \ , \tag{3.21}$$

so the requirement that n_j should be positive may be expressed as a constraint on the linking numbers.

It will also be useful to note that the rank of the gauge group for our $\mathcal{N} = 4$ SYM theory is related to the linking numbers by

$$N = \sum_i K_i + \sum_i \tilde{L}_i \ . \tag{3.22}$$

We can understand the field theory corresponding to such brane configurations as follows [90]. The semi-infinite D3-branes give rise to the bulk $\mathcal{N} = 4$ theory. Some subset of these end on D5-branes, so we have D5-brane boundary conditions as above for a subset of fields. These break the gauge symmetry from $U(N)$ to some subgroup $U(n)$ where $n \equiv n_{N_{NS5}}$ corresponds to the number of D3-branes intersecting the rightmost NS5-brane. The simplest situation is where these n D3-branes simply end on a single NS5-brane

[51] Here, the parameters (L_i, K_i) were introduced in [90] while the alternative $(\tilde{L}_i, K_i)$ were used in [174].

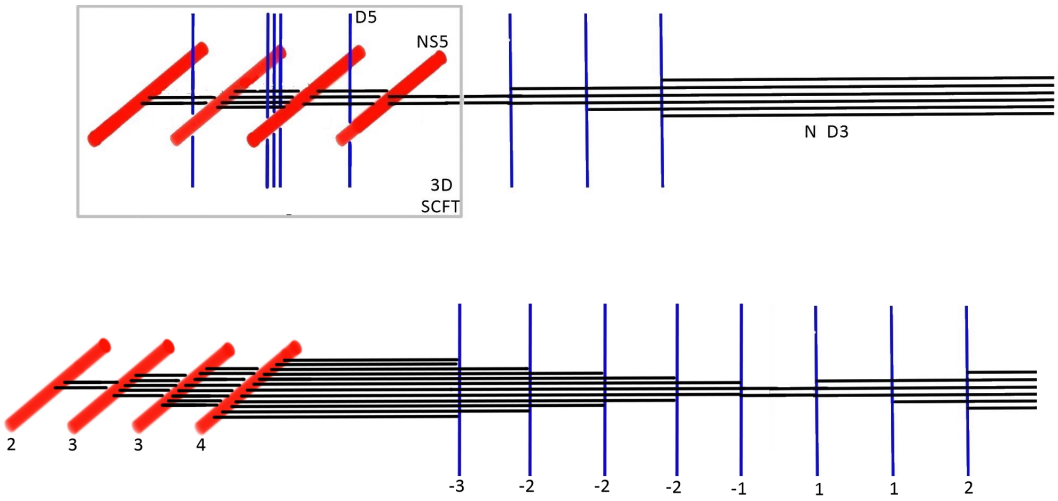

Figure 3.3: (Top) General brane configuration associated to a half-SUSY BCFT whose bulk CFT is $\mathcal{N} = 4$ SYM theory. For this configuration, we have $\vec{n} = (2, 4, 3, 4)$ and $\vec{M} = (1, 3, 1)$. (Bottom) the same configuration after a rearrangement of branes. Linking numbers K_i and $\tilde{L}_i$ for the five-branes are shown. (Apologies to M.C. Escher.)

with no additional branes to the left. This defines some particular BCFT with unbroken $U(n)$ gauge symmetry. The more general theories can be understood as coupling this theory to a 3D SCFT with global $U(n)$ symmetry, arising from the low-energy dynamics of the brane configuration between the leftmost and rightmost NS5-brane.

The 3D superconformal theories that are coupled at the boundary arise from the IR limit of certain 3-dimensional linear quiver gauge theories [90, 175], where we have gauge group $U(n_1) \times \cdots \times U(n_{N_{NS5}-1})$, and

- One 3D $\mathcal{N} = 4$ gauge multiplet for each gauge group factor $U(n_i)$ (coming from strings that start and end on D3-branes stretched between NS5s);

- One 3D $\mathcal{N} = 4$ bifundamental hypermultiplet for each neighbouring pair of gauge group factors $U(n_i) \times U(n_{i+1})$ (coming from strings that begin and end on D3-branes on either side of an NS5-brane);

- One 3d $\mathcal{N} = 4$ fundamental hypermultiplet for each D5-brane between NS5-branes (coming from 3-5 strings);
- An additional n 3d $\mathcal{N} = 4$ hypermultiplets in the fundamental of $U(n_{N_{NS5}-1})$.

We have a global symmetry $\{\prod_i U(M_i)\} \times U(n)$ under which the various fundamental hypermultiplets transform. See [90] for additional details.

3.3 Dual gravity solutions

Through the AdS/CFT correspondence, the vacuum states of the $OSp(4|4)$-symmetric BCFTs descending from $U(N)$ $\mathcal{N} = 4$ SYM theory correspond to $OSp(4|4)$-symmetric solutions of type IIB supergravity. The general local solutions with this symmetry were constructed by D'Hoker, Estes, and Gutperle in [172, 173] by solving the BPS equations. The $SO(3,2) \times SO(3) \times SO(3)$ global symmetry is reflected in the fact that the solutions are

$$\mathrm{AdS}_4 \times S_1^2 \times S_2^2 \,, \tag{3.23}$$

fibred over a Riemann surface Σ. Such solutions turn out to be uniquely characterized by specifying a pair of harmonic functions h_1, h_2 on Σ. The requirement that the solutions are non-singular imposes the extra constraint that the poles of h_i lie on the boundary of Σ, and flux-quantization conditions place additional constraints on the locations of these poles. Ultimately, the harmonic functions h_i and thus the entire supergravity solutions are determined by the locations of the poles.

This set of solutions includes geometries dual to the BCFTs we are interested in, but also geometries dual to $\mathcal{N} = 4$ SYM theories with planar codimension-one defects or interfaces between $\mathcal{N} = 4$ SYM theories with different parameters. Those solutions corresponding to the BCFT case were specifically analyzed in [174] (see also [175]).

3.3.1 General local solution

We now review explicitly the solutions of [172–174]; our conventions for type IIB string theory parameters and their relation to $\mathcal{N}=4$ SYM theory parameters are summarized in Appendix B.1.

To describe the solutions, we take Σ to be the first quadrant of the plane, with complex coordinate $w = re^{i\theta} = x + iy$ and metric

$$ds^2_\Sigma = 4\rho^2 |dw|^2 \,. \tag{3.24}$$

The solutions are expressed in terms of harmonic functions h_1, h_2 on Σ.

The full metric for the ten-dimensional solution takes the form

$$ds^2 = f_4^2 ds^2_{\mathrm{AdS}_4} + f_1^2 ds^2_{S^2_1} + f_2^2 ds^2_{S^2_2} + ds^2_\Sigma \,, \tag{3.25}$$

where f_1, f_2, f_4 are real-valued functions on Σ, and $ds^2_{\mathrm{AdS}_4}$ and $ds^2_{S^2_i}$ are metrics for AdS_4 and two-spheres with unit radius.

The metric functions and dilaton field can be expressed via a set of real functions

$$\begin{aligned} W &\equiv \partial_w h_1 \partial_{\bar{w}} h_2 + \partial_w h_2 \partial_{\bar{w}} h_1 \\ N_i &\equiv 2h_1 h_2 |\partial_w h_i|^2 - h_i^2 W \qquad (i = 1, 2) \end{aligned} \tag{3.26}$$

in terms of which the dilaton is

$$e^{2\Phi} = e^{4\phi} = \frac{N_2}{N_1} \,, \tag{3.27}$$

and the Einstein frame metric factors are

$$\rho^2 = e^{-\frac{\Phi}{2}} \frac{\sqrt{-N_2 W}}{h_1 h_2} \,, \qquad f_1^2 = 2e^{\frac{\Phi}{2}} h_1^2 \sqrt{-\frac{W}{N_1}} \,, \tag{3.28}$$

$$f_2^2 = 2e^{-\frac{\Phi}{2}} h_2^2 \sqrt{-\frac{W}{N_2}} \,, \qquad f_4^2 = 2e^{-\frac{\Phi}{2}} \sqrt{-\frac{N_2}{W}} \,. \tag{3.29}$$

The solutions also have a non-trivial NS-NS three-form field strengths and R-R three-form and five-form field strengths. We do not need these for our

analysis, but review them in Appendix B.2 for completeness.

3.3.2 Supergravity solutions: $\mathrm{AdS}_5 \times S^5$

It is useful to begin by describing the solution corresponding to $\mathrm{AdS}_5 \times S^5$. Making use of polar coordinates on Σ, we have

$$h_1 = \frac{L_{\mathrm{AdS}}^2}{4}\frac{1}{\sqrt{g}}\cos\theta\left(\frac{r}{r_0}+\frac{r_0}{r}\right)\,, \quad h_2 = \frac{L_{\mathrm{AdS}}^2}{4}\sqrt{g}\sin\theta\left(\frac{r}{r_0}+\frac{r_0}{r}\right)\,, \tag{3.30}$$

where g is the string coupling. Using

$$\partial_w\partial_{\bar{w}} f = \frac{1}{4}\left[\frac{1}{r}\partial_r(r\partial_r f)+\frac{1}{r^2}\partial_\theta^2 f\right]\,, \tag{3.31}$$

we find that

$$W = -\frac{L_{\mathrm{AdS}}^4}{16r^2}\sin(2\theta)\,, \quad \frac{1}{g}N_2 = gN_1 = \frac{L_{\mathrm{AdS}}^8}{1024 r_0^4}\sin(2\theta)\frac{(r^2+r_0^2)^4}{r^6}\,. \tag{3.32}$$

This gives a constant dilaton $e^{2\phi} = e^{\Phi} = g$ and a metric

$$\begin{aligned} ds^2 = L_{\mathrm{AdS}}^2\Bigg\{ &\left[d\theta^2+\sin^2(\theta)d\Omega_2^2+\cos^2(\theta)d\Omega_2^2\right] \\ &+\left[\frac{dr^2}{r^2}+\frac{(r^2+r_0^2)^2}{4r_0^2r^2}\left(\frac{1}{u^2}(du^2-dt^2+d\vec{x}^2)\right)\right]\Bigg\}\,. \end{aligned} \tag{3.33}$$

The first term in square brackets is the metric of a unit five-sphere while the second term in square brackets is the metric for AdS_5 with unit AdS radius; the latter can be checked by the change of coordinates

$$z = u\frac{2rr_0}{r^2+r_0^2}\,, \qquad x_\perp = u\frac{r^2-r_0^2}{r_0^2+r^2}\,, \tag{3.34}$$

after which this factor becomes

$$\frac{1}{z^2}(dz^2+dx_\perp^2-dt^2+d\vec{x}^2)\,. \tag{3.35}$$

We see that the parameter $L_{\rm AdS}$ corresponds to the AdS radius in Einstein frame, the parameter g corresponds to the string coupling, and the parameter r_0 is only associated with our choice of coordinates, with $r = r_0$ corresponding to the plane $x_\perp = 0$ in Fefferman-Graham coordinates.

3.3.3 Supergravity solutions: general BCFT solutions

The general solution we consider may be expressed most simply using Cartesian coordinates (x, y) on the first quadrant as[52]

$$\begin{aligned} h_1 &= \frac{\pi \ell_s^2}{2} \frac{x}{\sqrt{g}} + \frac{\ell_s^2}{4} \sum_A \frac{c_A}{\sqrt{g}} \ln \left(\frac{(x + l_A)^2 + y^2}{(x - l_A)^2 + y^2} \right) \\ h_2 &= \frac{\pi \ell_s^2}{2} \sqrt{g} y + \frac{\ell_s^2}{4} \sum_B d_B \sqrt{g} \ln \left(\frac{x^2 + (y + k_B)^2}{x^2 + (y - k_B)^2} \right) . \end{aligned} \tag{3.36}$$

We see that l_A give the location of poles of h_1 on the x axis, while k_A give the location of poles of h_2 on the y-axis.

Near $r = \infty$, these functions asymptote to

$$\begin{aligned} h_1 &= \frac{\ell_s^2}{\sqrt{g}} \left(\frac{\pi}{2} r + \frac{1}{r} \sum_A c_A l_A \right) \cos\theta + O(r^{-2}) \\ h_2 &= \ell_s^2 \sqrt{g} \left(\frac{\pi}{2} r + \frac{1}{r} \sum_B d_B k_B \right) \sin\theta + O(r^{-2}) . \end{aligned} \tag{3.37}$$

Using these asymptotic expressions in the general equations for the metric and dilaton, we find that the asymptotic metric is $\mathrm{AdS}_5 \times S^5$, with Einstein frame AdS length

$$L_{\rm AdS}^4 = 4\pi \ell_s^4 (\sum_A c_A l_A + \sum_B d_B k_B) \tag{3.38}$$

and asymptotic dilaton $e^\Phi = g$. In the asymptotic $\mathrm{AdS}_5 \times S^5$ region, our

[52] Here, we assume that l_A and k_B are distinct. Alternatively, we could omit the coefficient $c_A/\sqrt{g}$ and $d_B\sqrt{g}$ (which we will see are quantized in string theory solutions) and allow specific l_A to appear with some multiplicity. The solutions described in [174] have set $g = 1$; we have used the symmetry $\phi \to \phi + \phi_0$, $B_{(2)} \to e^{\phi_0} B_{(2)}$, $C_{(2)} \to e^{-\phi_0} C_{(2)}$ to write the solution for general asymptotic string coupling $g = e^{\Phi_\infty}$.

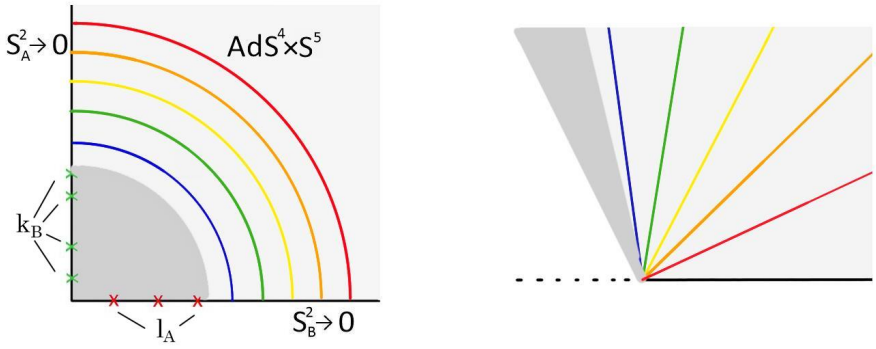

Figure 3.4: (Left) The dual geometries are $AdS_4 \times S^2 \times S^2$ fibred over the quadrant shown, with the first and second S^2 contracting to zero on the y- and x-axes respectively. (Right) The geometries can be understood as corresponding to a portion of Poincaré $AdS_5 \times S^5$ with Poincaré angle $\Theta > \Theta_*$, capped off by an "end-of-the-world" brane (shaded grey region) where the internal space degenerates smoothly. Arcs for large r correspond to $AdS_4 \times S^5$ slices of the $AdS_5 \times S^5$ region.

coordinate choice here matches with the coordinates of the previous section if we choose

$$r_0 = \frac{L^2_{\text{AdS}}}{2\pi\ell_s^2} \,. \tag{3.39}$$

From (B.5), the rank of the gauge group is related to the parameters in the solution by

$$N = \sum_A c_A l_A + \sum_B d_B k_B \,. \tag{3.40}$$

As shown in Figure 3.4, the large r part of the geometry (where r is the radial coordinate on the quadrant) corresponds to a portion of Poincaré $AdS_5 \times S^5$ with Poincaré angle near $\pi/2$. From (3.34) we have that the Poincaré angle is related to r by

$$\tan\Theta = \frac{1}{2}\left(\frac{r}{r_0} - \frac{r_0}{r}\right) \,. \tag{3.41}$$

The small r region corresponds to an "end-of-the-world" brane in the full geometry where the internal space degenerates smoothly, apart from D5-

brane throats associated with the singularities at $x = l_A, y = 0$ and NS5-brane throats associated with the singularities at $y = k_A, x = 0$.

Using (B.8) and the result (4.14) from [174] for the flux integral, we find that the number of units of D5-brane flux associated to the singularity at l_A is

$$N_{D5}^{(A)} = \frac{1}{\sqrt{g}} c_A \, . \tag{3.42}$$

Similarly, from (B.9) and the result (4.13) from [174], we have that the number of units of NS5-brane flux associated with the singularity at k_B is

$$N_{NS5}^{(B)} = \sqrt{g} d_B \, . \tag{3.43}$$

By analyzing the five-form fluxes in the solution, [174] determined that the number of units of five-form flux (the flux associated with D3-branes) *per five-brane* coming from the D5-branes in the A^{th} stack and the NS5-branes in the B^{th} stack are

$$\begin{aligned} N_{D3}^{A} &= \hat{l}_A - \frac{2}{\pi} \sum_B N_{NS5}^{(B)} \arctan\left(g \frac{\hat{k}_B}{\hat{l}_A} \right) \, . \\ \hat{N}_{D3}^{B} &= \hat{k}_B + \frac{2}{\pi} \sum_A N_{D5}^{(A)} \arctan\left(g \frac{\hat{k}_B}{\hat{l}_A} \right) \end{aligned} \tag{3.44}$$

where we have defined $\hat{k}_B = k_B/\sqrt{g}$ and $\hat{l}_A = \sqrt{g} l_A$.

In string theory, N_{D3}^A and $\hat{N}_{D3}^B$ should be quantized, so while we have a supergravity solution for any choice of $\{l_A\}$ and $\{k_A\}$, the allowed values corresponding to string theory solutions are discrete. We see that for sufficiently small g, the parameters $\hat{l}_A$ and $\hat{k}_B$ should be integers up to small corrections.

Relating supergravity parameters and gauge theory parameters

As pointed out in [174], it is natural to identify the numbers on the left in (3.44) with the linking numbers that specify the BCFT,[53] where we have

$$\begin{aligned} \{\tilde{L}_i\} &= \{N^A_{D3} \text{ with multiplicity } N^{(A)}_{D5}\} \\ \{K_i\} &= \{\hat{N}^B_{D3} \text{ with multiplicity } N^{(B)}_{NS5}\}\,. \end{aligned} \tag{3.45}$$

Alternatively, we can take l_A with multiplicity $N^{(A)}_{D5}$ and k_B with multiplicity $N^{(B)}_{NS5}$ in the original definition of h_i, setting $c_A/\sqrt{g} = d_B\sqrt{g}$=1. In this case, we find the original linking numbers (L_A, K_A) of Gaiotto and Witten can be related simply to the supergravity parameters as

$$\begin{aligned} L_A &= \sqrt{g}l_A + \frac{2}{\pi}\sum_B \arctan\frac{l_A}{k_B}\,. \\ K_B &= \frac{k_B}{\sqrt{g}} + \frac{2}{\pi}\sum_A \arctan\frac{k_B}{l_A}\,, \end{aligned} \tag{3.46}$$

where the poles l_A, k_B are now appearing with multiplicity (i.e. they need not all be distinct). The sum in the first expression has a geometric interpretation as the acute angle between the x-axis and the line segment from $(l_A, 0)$ to $(0, k_B)$, summed over k_B, while the sum in the second expression is the acute angle between the y axis and the segment from $(0, k_B)$ to $(l_A, 0)$, summed over l_A. We note that (3.46) are invariant under the S-duality transformations $\{L_A\} \leftrightarrow \{K_B\}$, $\{l_A\} \leftrightarrow \{k_B\}$, $g \leftrightarrow 1/g$.

In order to find the supergravity solution corresponding to the vacuum state of a particular BCFT defined by linking numbers $\{\tilde{L}_A\}$ and $\{K_A\}$, we need to use (3.44) to solve for the parameters $\{\hat{l}_A\}$ and $\{\hat{k}_B\}$, though it is not clear how to do this explicitly in general. An interesting check is that for any linking numbers that can be expressed in terms of supergravity parameters as in 3.44, the field theory constraint that the quantities (3.21) must be positive (so that the brane configuration can be represented as in the top of Figure 3.3) is automatically satisfied, as we show in Appendix

[53] Recall that these corresponded to the number of D3-branes ending on each five-brane in the bottom picture of Figure 3.3.

B.4.

We note that the final terms in the two equations in (3.44) are bounded in magnitude by the total number of NS5-branes and D5-branes respectively. Thus, when the linking numbers (D3-branes per five-brane) are all large compared with the total number of five-branes, the solution will have $\hat{k}_B \sim K_B$ and $\hat{l}_A \sim L_A$, and we can find the corrections to these leading order expressions perturbatively in $1/K$ and/or $1/L$. Similarly, when the asymptotic string coupling g is taken small with fixed linking numbers, we will have $\hat{k}_B \sim K_B + \mathcal{O}(g)$ and $\hat{l}_A \sim L_A + \mathcal{O}(g)$.

3.4 Holographic computation of boundary F

In this section, we perform a holographic computation of boundary F for the general BCFTs defined by a set of linking numbers $\{K_i, \tilde{L}_i\}$. This was done for the special case of N D3-branes ending on k D5-branes (linking numbers $K_i = 0, L_i = N/k$ with multiplicity k) in [162]; similar calculations of F in 3D superconformal theories were performed in [176].

As we have described earlier, boundary F may be computed either by evaluating the partition function for the theory on a hemisphere, or by calculating the vacuum entanglement entropy for a half-ball centered on the boundary. Either of these may be computed holographically using the dual gravity solutions; the two calculations give rise to the same final expression for boundary F in terms of the harmonic functions h_1 and h_2. In our presentation, we will holographically calculate the entanglement entropy, using the Ryu-Takayanagi formula [42, 147]

$$S(A) = \frac{\text{Area}(\tilde{A})}{4G} \ , \tag{3.47}$$

where $\tilde{A}$ is the minimal area codimension-two extremal surface homologous to the half-ball region on the boundary of AdS, computed using the Einstein-frame metric. The boundary F is then extracted by subtracting off half of the entanglement entropy for a ball-shaped region in $\mathcal{N} = 4$ SYM and keeping the universal piece, as in equations (3.4,3.7,3.8).

In the ten-dimensional geometry, the extremal surface we need to consider is codimension-two in the full spacetime. It wraps both of the internal S^2, and the directions spanned by the Riemann surface Σ, so that the surface is specified by describing a codimension-two locus in each AdS_4 slice. It turns out that the appropriate extremal surface to compute the entanglement entropy of a half-ball region of radius R centred at the BCFT boundary is just the one described by the hemisphere $\{t = t_0, u^2 + \vec{x}^2 = R^2, u > 0\}$ in each AdS_4 slice, which we recall had metric

$$ds^2_{AdS_4} = \frac{1}{u^2}\left(du^2 - dt^2 + d\vec{x}^2\right) , \qquad \vec{x} = (x_1, x_2) . \tag{3.48}$$

Indeed, one can verify that the surface $u^2+\vec{x}^2 = R^2$ is extremal in AdS from the Euler-Lagrange equations; this holds in any dimension, provided we let $\vec{x}$ denote the $d-2$ transverse coordinates. Moreover, in the boundary coordinates $(t, \vec{x}, x_\perp)$ of the half-space $H\mathbb{R}^{1,3}$, our extremal surface asymptotes to the entangling surface $\{t = t_0, x_\perp^2 + \vec{x}^2 = R^2, x_\perp < 0\}$.

The area of the extremal surface diverges as usual, but we will regulate this by placing a cutoff at $z = \epsilon$ in Fefferman-Graham coordinates. Subtracting off half of the area of the RT surface for a ball of radius R in $\mathcal{N} = 4$ SYM theory with the same regulator, we will obtain a result that is finite in the limit $\epsilon \to 0$.

Regulated areas

Representing the AdS_4 metric as

$$\begin{aligned} ds^2_{AdS_4} &= \frac{1}{u^2}(-dt^2 + du^2 + d\vec{x}^2) \\ &= \frac{1}{\rho^2\cos^2\theta_P}(-dt^2 + d\rho^2 + \rho^2 d\theta_P^2 + \rho^2\sin^2\theta_P d\phi^2) , \end{aligned} \tag{3.49}$$

we have that the extremal surface is at $\rho = R$ and fixed t. The eight-dimensional area of this surface is

$$\text{Area} \;=\; 64\pi^2 \int \frac{r dr d\theta d\phi \sin\theta_P d\theta_P}{\cos^2\theta_P} \rho^2 f_1^2 f_2^2 f_4^2 , \tag{3.50}$$

where the regulator $z = \epsilon$ in Fefferman-Graham coordinates corresponds to a restriction $\theta_P < \theta_P^\epsilon(r,\theta)$. The regularization procedure is described in detail in Appendix B.3. After subtracting off the regulated area of the RT surface for a ball of radius R in $\mathcal{N}=4$ SYM theory and removing the regulator, we find from the definitions (3.4,3.7,3.8) that

$$F_\partial = -\lim_{\Lambda\to\infty}\frac{256\pi^3}{G}\left[\int_0^\Lambda dr\int_0^{\frac{\pi}{2}} d\theta\, r h_1 h_2 \partial_w\partial_{\bar w}(h_1h_2) - \int_{r_0}^\Lambda dr\int_0^{\frac{\pi}{2}} d\theta\, r h_1^{\rm AdS} h_2^{\rm AdS}\partial_w\partial_{\bar w}(h_1^{\rm AdS}h_2^{\rm AdS})\right], \quad (3.51)$$

where $h_i^{\rm AdS}$ are the harmonic functions corresponding to pure $\mathrm{AdS}_5\times S^5$. We can easily evaluate the second term explicitly using the explicit expressions in Section 3.3.2, to give

$$F_\partial = \lim_{\Lambda\to\infty}\Big\{-\frac{256\pi^3}{G}\int_0^\Lambda dr\int_0^{\frac{\pi}{2}} d\theta\, r h_1 h_2\partial_w\partial_{\bar w}(h_1h_2) - \frac{\pi}{8}N\Lambda^2 - \frac{1}{4}N^2\ln\left(\frac{\Lambda^2\pi}{N}\right)\Big\}, \quad (3.52)$$

where we have used (B.5). Alternatively, we can combine the integrands to obtain a convergent integral,

$$F_\partial = -\frac{\pi^3}{G}\int_\Sigma d^2x\{h_1h_2\partial_w\partial_{\bar w}(h_1h_2) - \mathcal{J}_0\} \quad (3.53)$$

where (recalling the definition of r_0 in (3.39))

$$\mathcal{J}_0 = \begin{cases} 0 & r < r_0 \\ h_1^{\rm AdS}h_2^{\rm AdS}\partial_w\partial_{\bar w}(h_1^{\rm AdS}h_2^{\rm AdS}) = -\frac{L_{\rm AdS}^8\sin^2(2\theta)(r^2+r_0^2)^2}{512 r_0^2 r^4} & r \geq r_0 \end{cases}. \quad (3.54)$$

3.4.1 Boundary free energy: the integral

In this section, we will evaluate the integral (3.52) for the general solution (3.36) in order to calculate the boundary free energy F_∂ in the supergravity

approximation. We note that the metric, expressed in terms of the parameters (c_A, d_A, l_A, k_A), does not depend on the string coupling g, so we can work with $g = 1$. However, when expressing the results in terms of the natural field theory parameters, some g-dependence will appear.

In terms of the parameters (c_A, d_A, l_A, k_A), we have

$$F_\partial(c_A, d_A, l_A, k_A) = -2\pi \lim_{\Lambda\to\infty} \Big\{ \mathcal{I}(c_A, d_A, k_A, l_A, \Lambda) + \frac{1}{16} N\Lambda^2 + \frac{1}{8\pi} N^2 \ln\left(\frac{\Lambda^2\pi}{N}\right) \Big\}, \quad (3.55)$$

where we define

$$\begin{aligned} &\mathcal{I}(c_A, d_A, k_A, l_A, \Lambda) \\ &\quad = \int d^2w \left\{ \hat{h}_1 \hat{h}_2 \partial_w \partial_{\bar{w}} (\hat{h}_1 \hat{h}_2) \right\} \\ &\quad = \frac{1}{4} \int_0^\Lambda r dr \int_0^{\frac{\pi}{2}} d\theta \left\{ \hat{h}_1 \hat{h}_2 \left(\frac{1}{r} \partial_r (r \partial_r (\hat{h}_1 \hat{h}_2)) + \frac{1}{r^2} \partial_\theta^2 (\hat{h}_1 \hat{h}_2) \right) \right\} \end{aligned} \quad (3.56)$$

with

$$\begin{aligned} \hat{h}_1 &= r\cos(\theta) + \sum_A \frac{c_A}{2\pi} \ln\left(\frac{r^2 + 2rl_A\cos(\theta) + l_A^2}{r^2 - 2rl_A\cos(\theta) + l_A^2} \right) \\ \hat{h}_2 &= r\sin(\theta) + \sum_A \frac{d_A}{2\pi} \ln\left(\frac{r^2 + 2rk_A\sin(\theta) + k_A^2}{r^2 - 2rk_A\sin(\theta) + k_A^2} \right) . \end{aligned} \quad (3.57)$$

We note that the factors of ℓ_s present in h_1 and h_2 have cancelled in those from the Einstein frame expression for G taken from Appendix B.1.

There are no terms independent of c_A and d_A, so we can express the full

result as

$$\begin{aligned}\mathcal{I}(c_A, d_A, k_A, l_A, \Lambda) = &\sum_A c_A \mathcal{I}^c_A + \sum_A d_A \mathcal{I}^d_A + \sum_{A,B} c_A c_B \mathcal{I}^{cc}_{AB} \\ &+ \sum_{A,B} d_A d_B \mathcal{I}^{dd}_{AB} + \sum_{A,B} c_A d_B \mathcal{I}^{cd}_{AB} + \sum_{A,B,C} c_A c_B d_C \mathcal{I}^{ccd}_{ABC} \\ &+ \sum_{A,B,C} c_A d_B d_C \mathcal{I}^{cdd}_{ABC} + \sum_{A,B,C,D} c_A c_B d_C d_D \mathcal{I}^{ccdd}_{ABCD} \,. \end{aligned} \tag{3.58}$$

Integration techniques

There are various tricks that facilitate evaluation of the integral. First, it is helpful to use Stokes' theorem in order to rewrite the integral as a simpler integral plus a term that can be expressed as a boundary integral. We have

$$\begin{aligned} &4\mathcal{I}(c_A, d_A, k_A, l_A, \Lambda) \\ &\quad = \int_0^\Lambda r dr \int_0^{\frac{\pi}{2}} \left\{ -\hat{h}_2^2 \left(\partial_r \hat{h}_1 \partial_r \hat{h}_1 + \frac{1}{r^2} \partial_\theta \hat{h}_1 \partial_\theta \hat{h}_1 \right) \right\} \\ &\quad + \int_0^{\frac{\pi}{2}} d\theta \left\{ \hat{h}_1 \hat{h}_2^2 r \partial_r \hat{h}_1 \right\}_{r=\Lambda} + \int_0^\Lambda dr \left\{ -\hat{h}_1 \hat{h}_2^2 \frac{1}{r} \partial_\theta \hat{h}_1 \right\}_{\theta=0} \\ &\quad - \int_0^\Lambda dr \left\{ -\hat{h}_1 \hat{h}_2^2 \frac{1}{r} \partial_\theta \hat{h}_1 \right\}_{\theta=\pi/2} . \end{aligned} \tag{3.59}$$

In evaluating the various pieces, it is helpful to differentiate with respect to the parameters k_A or l_A in order to convert the logarithms into rational functions of r. The resulting expressions can be expressed in a partial fraction expansion, with denominators that are polynomials in r and $\cos(\theta)$ and numerators that are constant or linear functions of $\cos(\theta)$. After evaluating the integrals of the various parts, we can antidifferentiate with respect to k_A or l_A to obtain the final results.

We now present results for the various parts of the integral.

Linear terms

The terms linear in c_A or d_A are:

$$\mathcal{I}^c_A = -\frac{1}{16} l_A \, \Lambda^2 + \frac{{l_A}^3}{24} \tag{3.60}$$

and

$$\mathcal{I}^d_A = -\frac{1}{16} k_A \, \Lambda^2 + \frac{{k_A}^3}{24} \, . \tag{3.61}$$

Quadratic terms

For the terms quadratic in c_A and/or d_A, we find

$$\begin{aligned} \pi \, \mathcal{I}^{cc}_{AB} = -\frac{1}{4} l_A \, l_B \, \ln(\Lambda) - \frac{3}{16} l_A \, l_B + \frac{1}{32} (l_A + l_B)^2 \ln\Big((l_A + l_B)^2\Big) \\ - \frac{1}{32} (l_A - l_B)^2 \ln\Big((l_A - l_B)^2\Big) \end{aligned} \tag{3.62}$$

$$\begin{aligned} \pi \, \mathcal{I}^{dd}_{AB} = -\frac{1}{4} k_A \, k_B \, \ln(\Lambda) - \frac{3}{16} k_A \, k_B + \frac{1}{32} (k_A + k_B)^2 \ln\Big((k_A + k_B)^2\Big) \\ - \frac{1}{32} (k_A - k_B)^2 \ln\Big((k_A - k_B)^2\Big) \end{aligned} \tag{3.63}$$

and

$$\pi \, \mathcal{I}^{cd}_{AB} = -\frac{1}{2} \, l_A \, k_B \, \ln(\Lambda) - \frac{3}{8} l_A \, k_B + \frac{1}{4} \, k_B \, l_A \, \ln\left({k_B}^2 + {l_A}^2\right) \, . \tag{3.64}$$

Cubic terms

For the cubic terms, it is simpler to first give the derivatives with respect to one of the parameters. We have:

$$\begin{aligned}\pi^2 \frac{d}{dk_C}\mathcal{I}^{ccd}_{ABC} = \frac{1}{8}\left(\frac{{l_A}^2}{{k_C}^2+{l_A}^2}+\frac{{l_B}^2}{{k_C}^2+{l_B}^2}\right)\ln\left(\frac{(l_A-l_B)^2}{(l_A+l_B)^2}\right)\\ -\frac{1}{8}\left(\frac{l_A\,l_B}{{k_C}^2+{l_A}^2}+\frac{l_A\,l_B}{{k_C}^2+{l_B}^2}\right)\ln\left(\left({l_A}^2-{l_B}^2\right)^2\right)\\ +\frac{1}{4}\frac{l_A\,l_B}{{k_C}^2+{l_B}^2}\ln\left({k_C}^2+{l_A}^2\right)+\frac{1}{4}\frac{l_A\,l_B}{{k_C}^2+{l_A}^2}\ln\left({k_C}^2+{l_B}^2\right)\ .\end{aligned} \tag{3.65}$$

We can integrate this with respect to k_C, requiring that the result vanishes at $k_C = 0$. The result is conveniently written in terms of the Bloch-Wigner dilogarithm[54]

$$D(z) = \mathrm{Im}(\mathrm{Li}_2(z)) + \arg(1-z)\log|z|\ . \tag{3.66}$$

Here, Li_2 is the dilogarithm function defined as

$$\mathrm{Li}_2(z) = \sum_{n=1}^{\infty}\frac{z^n}{n^2} = -\int_0^z \frac{dt}{t}\log(1-t)\ . \tag{3.67}$$

Our result is simply

$$\mathcal{I}^{ccd}_{ABC} = \frac{l_A}{4\pi^2}\left\{D\left[\frac{l_B-ik_C}{l_A+l_B}\right]+D\left[\frac{l_B-ik_C}{l_B-l_A}\right]\right\}+\{l_A\leftrightarrow l_B\}\ . \tag{3.68}$$

The diagonal terms $l_B = l_A$ simplify to

$$\mathcal{I}^{ccd}_{AAC} = \frac{l_A}{2\pi^2}D\left[\frac{1}{2}-\frac{i}{2}\frac{k_C}{l_A}\right]\ . \tag{3.69}$$

[54]This is Jamie Sully's favorite dilogarithm. We thank him for making us aware of it and extolling its virtues.

Quartic terms

We find that

$$\begin{aligned}
&\frac{d}{dk_C}\frac{d}{dk_D}\mathcal{I}^{ccdd}_{ABCD} \\
&\quad= \frac{1}{8\pi^3}\Bigg\{\frac{l_A\, l_B}{\left({k_C}^2+{l_B}^2\right)\left({k_D}^2+{l_A}^2\right)}\ln\left(\frac{\left({l_A}^2-{l_B}^2\right)^2\left({k_C}^2-{k_D}^2\right)^2}{\left({k_C}^2+{l_A}^2\right)^2\left({k_D}^2+{l_B}^2\right)^2}\right) \\
&\qquad+\frac{l_A\, l_B}{\left({k_D}^2+{l_B}^2\right)\left({k_C}^2+{l_A}^2\right)}\ln\left(\frac{\left({l_A}^2-{l_B}^2\right)^2\left({k_C}^2-{k_D}^2\right)^2}{\left({k_C}^2+{l_B}^2\right)^2\left({k_D}^2+{l_A}^2\right)^2}\right) \\
&\qquad+\frac{{l_A}^2}{\left({k_D}^2+{l_A}^2\right)\left({k_C}^2+{l_A}^2\right)}\ln\left(\frac{(l_A+l_B)^2}{(l_A-l_B)^2}\right) \\
&\qquad+\frac{{l_B}^2}{\left({k_D}^2+{l_B}^2\right)\left({k_C}^2+{l_B}^2\right)}\ln\left(\frac{(l_A+l_B)^2}{(l_A-l_B)^2}\right)\Bigg\}.
\end{aligned} \tag{3.70}$$

We now need to integrate this with respect to k_C and k_D. This time, the result involves the trilogarithm function $\mathrm{Li}_3(z)$ in addition to dilogarithms and elementary functions. Taking guidance from the cubic terms, which could be written simply in terms of the Bloch-Wigner dilogarithm, we can make the guess that the full result here may be obtained by keeping only the terms with trilogarithms, and replacing each trilogarithm with the combination

$$\mathcal{L}(z) = Re(\mathrm{Li}_3(z) - \ln|z|\mathrm{Li}_2(z) + \frac{1}{3}\ln^2|z|\mathrm{Li}_1(z)) \tag{3.71}$$

which has been shown to be real analytic on $\mathbb{C}-\{0,1\}$ and continuous everywhere, and to obey various nice relations such as $\mathcal{L}(1/z)=\mathcal{L}(z)$. This

turns out to be correct. The full result for the integral is

$$
\begin{aligned}
&8\pi^3\,\mathcal{I}^{ccdd}_{ABCD} \\
&\quad= \mathcal{L}\left(\frac{(k_C+il_A)\,(k_D+il_B)}{(k_D+il_A)\,(k_C+il_B)}\right)+\mathcal{L}\left(\frac{(k_C+il_A)\,(k_D+il_B)}{(k_D-il_A)\,(k_C-il_B)}\right) \\
&\qquad-\mathcal{L}\left(\frac{(k_C+il_A)\,(k_D-il_B)}{(k_D+il_A)\,(k_C-il_B)}\right)-\mathcal{L}\left(\frac{(k_C+il_A)\,(k_D-il_B)}{(k_D-il_A)\,(k_C+il_B)}\right) \\
&\qquad+\mathcal{L}\left(\frac{(k_D+il_A)\,(l_B-ik_C)}{(k_C+k_D)\,(l_A+l_B)}\right)+\mathcal{L}\left(\frac{(l_A+ik_D)\,(k_C-il_B)}{(k_C-k_D)\,(l_A-l_B)}\right) \\
&\qquad-\mathcal{L}\left(\frac{(l_A+ik_D)\,(k_C+il_B)}{(k_C-k_D)\,(l_A+l_B)}\right)-\mathcal{L}\left(\frac{(l_A+ik_D)\,(k_C+il_B)}{(k_C+k_D)\,(l_A-l_B)}\right) \\
&\qquad+\{l_A\leftrightarrow l_B\}\,.
\end{aligned}
\tag{3.72}
$$

We note that the first two lines are already invariant under $\{l_A \leftrightarrow l_B\}$. The diagonal terms can be recovered by taking a limit in the above expression.

3.4.2 Full result

Combining all terms, we can now write the full result for F_∂ (in the supergravity approximation) associated to the theory whose vacuum has supergravity dual labeled by $\mathcal{P} \equiv \{c_A, d_A, l_A, k_A\}$. The result is

$$
\begin{aligned}
F_\partial(\mathcal{P}) \;=\;& \frac{3}{8}N^2+\frac{1}{4}N^2\ln\left(\frac{N}{\pi}\right)-\frac{\pi}{12}\sum_A c_A l_A^3-\frac{\pi}{12}\sum_B d_B k_B^3 \\
&-\frac{1}{16}\sum_{A,B} c_A c_B\Big\{(l_A+l_B)^2\ln\left((l_A+l_B)^2\right) \\
&\qquad\qquad -(l_A-l_B)^2\ln\left((l_A-l_B)^2\right)\Big\} \\
&-\frac{1}{16}\sum_{A,B} d_A d_B\Big\{(k_A+k_B)^2\ln\left((k_A+k_B)^2\right) \\
&\qquad\qquad -(k_A-k_B)^2\ln\left((k_A-k_B)^2\right)\Big\} \\
&-\frac{1}{2}\sum_{A,B} c_A d_B\left\{l_A k_B\ln\left(l_A^2+k_B^2\right)\right\} \\
&-\frac{1}{\pi}\sum_{A,B,C} c_A c_B d_C l_A\left\{D\left[\frac{l_B-ik_C}{l_A+l_B}\right]+D\left[\frac{l_B-ik_C}{l_B-l_A}\right]\right\}
\end{aligned}
$$

$$
\begin{aligned}
&-\frac{1}{\pi}\sum_{A,B,C} d_A d_B c_C k_A \left\{ D\left[\frac{k_B - i l_C}{k_A + k_B}\right] + D\left[\frac{k_B - i l_C}{k_B - k_A}\right]\right\} \\
&-\frac{1}{2\pi^2}\sum_{A,B,C,D} c_A c_B d_C d_D \Bigg\{ \mathcal{L}\left(\frac{(k_C + i l_A)(k_D + i l_B)}{(k_D + i l_A)(k_C + i l_B)}\right) \\
&\quad + \mathcal{L}\left(\frac{(k_C + i l_A)(k_D + i l_B)}{(k_D - i l_A)(k_C - i l_B)}\right) - \mathcal{L}\left(\frac{(k_C + i l_A)(k_D - i l_B)}{(k_D + i l_A)(k_C - i l_B)}\right) \\
&\quad - \mathcal{L}\left(\frac{(k_C + i l_A)(k_D - i l_B)}{(k_D - i l_A)(k_C + i l_B)}\right) + \mathcal{L}\left(\frac{(k_D + i l_A)(l_B - i k_C)}{(k_C + k_D)(l_A + l_B)}\right) \\
&\quad + \mathcal{L}\left(\frac{(l_A + i k_D)(k_C - i l_B)}{(k_C - k_D)(l_A - l_B)}\right) - \mathcal{L}\left(\frac{(l_A + i k_D)(k_C + i l_B)}{(k_C - k_D)(l_A + l_B)}\right) \\
&\quad - \mathcal{L}\left(\frac{(l_A + i k_D)(k_C + i l_B)}{(k_C + k_D)(l_A - l_B)}\right)\Bigg\}\,,
\end{aligned}
\tag{3.73}
$$

where we recall that

$$
N = \sum_A c_A l_A + \sum_B d_B k_B\,. \tag{3.74}
$$

We can express the results in terms of field theory parameters using the correspondence described in Section 3.3.3.

D5-branes only

We now consider various special cases. For theories descending from string theory configurations with only D3-branes and D5-branes, the result simplifies to

$$
\begin{aligned}
F_\partial = \frac{3}{8}N^2 - \sum_A \frac{\pi}{12} c_A l_A^3 - \sum_{A,B} \frac{1}{16} c_A c_B \Bigg\{ &(l_A + l_B)^2 \ln\left(\pi \frac{(l_A + l_B)^2}{N}\right) \\
&- (l_A - l_B)^2 \ln\left(\pi \frac{(l_A - l_B)^2}{N}\right)\Bigg\}\,.
\end{aligned}
\tag{3.75}
$$

Expressed purely in terms of the linking numbers L_A (which coincide with $\tilde{L}_A$ in this case), this is

$$F_\partial = \frac{N^2}{4}\left(\frac{3}{2} + \ln\left(\frac{\lambda}{4\pi^2}\right)\right) - \frac{\pi^2 N}{3\lambda}\sum_A L_A^3 - \frac{1}{16}\sum_{A,B}\Big\{(L_A+L_B)^2\ln\left((L_A+L_B)^2\right) - (L_A-L_B)^2\ln\left((L_A-L_B)^2\right)\Big\}. \quad (3.76)$$

We recall that in the brane construction, $\{L_A\}$ represents the numbers of D3-branes ending on each individual D5-brane, such that $\sum_A L_A = N$. When we have N D3-branes ending on N_5 D5-branes with N/N_5 D3-branes ending on each D5, the result simplifies further to

$$F_\partial = \frac{N^2}{8}\left[3 - \frac{8\pi^2}{3\lambda}\frac{N^2}{N_5^2} - 2\ln\left(\frac{16\pi^2}{\lambda}\frac{N^2}{N_5^2}\right)\right]. \quad (3.77)$$

This result corresponds to the case considered previously in [162]; our result agrees precisely with that computation.

NS5-branes only

For boundary conditions associated with only NS5-branes, we find that

$$F_\partial = \frac{3}{8}N^2 - \sum_A \frac{\pi}{12}d_A k_A^3 - \sum_{A,B}\frac{1}{16}d_A d_B\Big\{(k_A+k_B)^2\ln\left(\pi\frac{(k_A+k_B)^2}{N}\right) - (k_A-k_B)^2\ln\left(\pi\frac{(k_A-k_B)^2}{N}\right)\Big\}. \quad (3.78)$$

We can check that this may also be obtained from the D5-brane result by S-duality, manifested in the transformations $l_A \to k_A$, $c_A \to d_A$, $g \to 1/g$ (or $\lambda \to 16\pi^2 N^2/\lambda$). Expressed purely in terms of the linking numbers K_A,

this gives

$$F_\partial = \frac{N^2}{4}\left(\frac{3}{2} + \ln\left(\frac{4N^2}{\lambda}\right)\right) - \frac{\lambda}{48N}\sum_A K_A^3 - \frac{1}{16}\sum_{A,B}\Big\{(K_A+K_B)^2\ln\left((K_A+K_B)^2\right) - (K_A-K_B)^2\ln\left((K_A-K_B)^2\right)\Big\}, \quad (3.79)$$

where $\{K_A\}$ represents the numbers of D3-branes ending on each individual NS5-brane, as for the D5-brane case above. In the case corresponding to N D3-branes ending on N_5 NS5-branes with N/N_5 D3-branes ending on each NS5, the result simplifies to

$$F_\partial = \frac{N^2}{8}\left[3 - \frac{\lambda}{6N_5^2} - 2\ln\left(\frac{\lambda}{N_5^2}\right)\right]. \quad (3.80)$$

Both D5-branes and NS5-branes

In the special cases with either D5-branes or NS5-branes only, we were able to write an explicit expression for F_∂ in terms of variables in the brane constructions, i.e. the five-brane charges and linking numbers. For the most general constructions involving both D5-branes and NS5-branes, however, we do not know how to analytically invert the relations between supergravity and field theory variables. In scenarios of interest, we can always choose some field theory parameters, try to solve for the SUGRA parameters numerically, and then evaluate F_∂.

3.4.3 Validity of the supergravity approximation

The results of this section are based on the supergravity approximation to the dual gravity solutions and on the leading order RT formula without α'-corrections or quantum corrections. However, we expect that the solution and the RT formula receive both string loop and α'-corrections. These will correct our result, unless the corrections vanish, for example due to some

supersymmetric non-renormalization theorem.

Taking into account α' and string loop corrections, the purely gravitational sector of the effective action in string frame takes the schematic form

$$S \sim \int dx\, \sqrt{g}\Big[e^{2\phi}\left(\alpha' R + (\alpha' R)^2 + \ldots\right) + e^{4\phi}\left(\alpha' R + (\alpha' R)^2 + \ldots\right) + \ldots\Big]\,, \quad (3.81)$$

though certain terms vanish in type IIB supergravity due to constraints of supersymmetry.

This implies that the α'-corrections will be suppressed if the *string frame* Ricci curvature obeys

$$\alpha' R \ll 1\,, \quad (3.82)$$

whereas string loop corrections will be suppressed if

$$e^{2\phi} \ll 1\,. \quad (3.83)$$

For large N and large λ, we anticipate that these expressions should hold in the asymptotically AdS region, but might break down in the vicinity of the five-brane throats.

In order to estimate the expected size of the corrections to the supergravity results, we can employ the following general procedure:

- For an arbitrary fixed set of parameters, determine the region near a given five-brane stack where these correction terms would naively have a similar order of magnitude to the leading supergravity results.
- Find the size of the supergravity contribution to F_∂ from this region. Assuming that the corrections have a similar order of magnitude, we will take this as an estimate of size of the correction terms. Terms in the supergravity result that are parametrically larger than this will be considered reliable.

The details of this analysis are provided in Appendix B.5. As a specific example of the results, we find that for the theory corresponding to N

D3-branes ending on a single stack of $\tilde{L} = N/N_5$ D5-branes, the expected contribution from the part of the D5-brane throat where the string frame curvature is large is

$$\begin{cases} O(N_5^2) & \tilde{L} \sim 1 \\ O\left((N_5 \ln \tilde{L})^2\right) & \tilde{L} \gg 1 \end{cases} . \tag{3.84}$$

Thus, we might expect corrections to the supergravity result (3.77) at this order.

For the case of N D3-branes ending on a single stack of $K = N/N_5$ NS5-branes, the string frame curvature is only large in the vicinity of the NS5-brane throat provided that $N_{NS5} \sim 1$, in which case the expected contribution to F_∂ from this region is $O(N^2)$. Additionally, the expected contribution from the region in which the dilaton is large is

$$\begin{cases} O\left(\left(N_5^2 \ln\left(K^2/N_5^2\right)\right)^2\right) & K \gg N_5 \\ O(N_5^4) & K \sim N_5 \\ O(N^2) & K \ll N_5 \end{cases} . \tag{3.85}$$

Thus, we might expect corrections to the supergravity result (3.80) at this order.

In the next section, we will be able to calculate boundary F exactly using supersymmetric localization, for boundary conditions associated either with only D5-branes or only NS5-branes. We will see that the supergravity results are actually more reliable than our analysis suggests.

3.5 Localization calculation

In the above analysis, we have extracted the value of F_∂ by holographically computing the entanglement entropy for a half-ball centred at the field theory boundary. However, we recall that F_∂ is also related to the partition

function for the theory on a hemisphere; specifically, we have [166]

$$F_\partial \equiv -\frac{1}{2} \lim_{r\to\infty} \ln\Big(\frac{|Z_{HS^4}|^2}{Z_{S^4}}\Big)\,, \tag{3.86}$$

where $r = R/\epsilon$ is the quotient of the radius R of the (hemi)sphere and a UV regulator ϵ.

Calculations of the partition function in theories with supersymmetry are often tractable using the technique of supersymmetric localization; see [124] for a review. In particular, the calculation of the partition function, in addition to generic half-BPS Wilson loop observables, for $\mathcal{N} = 2$ (or $\mathcal{N} = 4$) supersymmetric gauge theories on a background S^4 was first performed in [126]. Localization was later applied to compute 't Hooft loop observables [190] and $\frac{1}{8}$-BPS Wilson loop observables [191] in such theories, and generalizations to theories on ellipsoids appeared in [192], as reviewed in [193]. Analogous calculations were performed for $\mathcal{N} = 2$ theories on S^3 in [127], with exact evaluation of the partition function for three-dimensional quiver gauge theories appearing in [194–196]. Localization calculations on manifolds with boundary in two and three dimensions first appeared in [197]; in four dimensions, the first direct calculations appeared in [198], which considered Neumann and Dirichlet boundary conditions only, followed by [199], which considered more general boundary conditions for the Abelian theory. Earlier general considerations for the case with boundaries can be found in [166, 200, 201]. More recent results involving localization and supersymmetric boundaries and interfaces include [178, 187, 202, 203].

We will therefore endeavour in this section to compare our gravity results to the calculation of F_∂ using supersymmetric localization on the field theory side. In particular, we will restrict our attention to theories arising from D3-branes and NS5-branes only (i.e. with arbitrary linking numbers $\{K_i\}$, but $\{L_i\} = \emptyset$). In this case, the form of the partition function as a zero-dimensional matrix integral may be inferred by recalling the established results for the hemisphere with Neumann boundary conditions [187, 198] and three-dimensional quiver gauge theories [127, 194–196], and applying the gluing formula of [201]. Using S-duality, we can obtain results for general

D5-like boundary conditions.

In the following, we will denote

$$\mathrm{sh}(x) = 2\sinh \pi x\,, \qquad \mathrm{ch}(x) = 2\cosh \pi x\,. \tag{3.87}$$

The partition function of $U(N)$ $\mathcal{N}=4$ SYM on the hemisphere HS^4 with Neumann boundary conditions is then

$$\begin{aligned} &Z_{\text{Neum.}}[HS^4_{r=1}] \\ &\qquad = \frac{1}{N!}\int \left(\prod_{i=1}^{N} d\lambda_i\right) e^{-\frac{4\pi^2}{g^2_{\text{YM}}}\sum_{i=1}^{N}\lambda_i^2} \prod_{i<j}^{N} (\lambda_i-\lambda_j)\mathrm{sh}(\lambda_i-\lambda_j)\,, \end{aligned} \tag{3.88}$$

and the partition function for a 3D $\mathcal{N}=4$ $U(n_1)\times\ldots\times U(n_{N_5})$ quiver gauge theory with M_i fundamental hypermultiplets associated to the $U(n_i)$ factor, with hypermultiplet masses $m_{i,j}$ and Fayet-Iliopoulos (FI) parameters α_i, is

$$\begin{aligned} Z_{\alpha,m}[S^3_{r=1}] = \frac{1}{n_1!\ldots n_{N_5}!}\int &\left(\prod_{j=1}^{N_5}\prod_{\ell=1}^{n_j} d\lambda_{j,\ell} e^{2\pi i\alpha_j\lambda_{j,\ell}}\right) \\ &\prod_{j=1}^{N_5}\prod_{k<\ell}^{n_j}\mathrm{sh}^2\left(\lambda_{j,k}-\lambda_{j,\ell}\right) \prod_{j=1}^{N_5-1}\prod_{k=1}^{n_j}\prod_{\ell=1}^{n_{j+1}} \frac{1}{\mathrm{ch}(\lambda_{j,k}-\lambda_{j+1,\ell})} \\ &\prod_{j=1}^{N_5}\prod_{\ell=1}^{n_j}\prod_{k=1}^{M_j} \frac{1}{\mathrm{ch}(\lambda_{j,\ell}-m_{j,k})}\,. \end{aligned} \tag{3.89}$$

The hemisphere partition function for the $\mathcal{N}=4$ SYM theory coupled to a quiver gauge theory at the boundary is then obtained by integrating the integrand of $Z_{\text{Neum.}}[HS^4]$ against an appropriate "brane factor" with respect to the bulk zero modes $(\lambda_1,\ldots,\lambda_N)$; in this case, the brane factor coincides with the partition function of the boundary theory $Z_{\alpha,m}[S^3]$, where the masses in the terminal node of the quiver diagram are replaced by the bulk zero modes (as the restriction of the bulk vector multiplet gauges the boundary flavour symmetry). For example, in the case where the quiver gauge theory contains vanishing FI parameters and no fundamental hyper-

multiplets (as will arise in the present case), we recover the partition function

$$Z[HS^4] = \frac{1}{n_1! \dots n_{N_5}!} \int \left(\prod_{j=1}^{N_5} \prod_{\ell=1}^{n_j} d\lambda_{j,\ell} \right) e^{-\frac{4\pi^2}{g_{\rm YM}^2} \sum_{i=1}^{N} \lambda_{N_5,i}^2} \times \prod_{i<j}^{N} (\lambda_{N_5,i} - \lambda_{N_5,j}) \, \mathrm{sh}(\lambda_{N_5,i} - \lambda_{N_5,j}) \times \prod_{j=1}^{N_5-1} \prod_{k<\ell}^{n_j} \mathrm{sh}^2 (\lambda_{j,k} - \lambda_{j,\ell}) \prod_{j=1}^{N_5-1} \prod_{k=1}^{n_j} \prod_{\ell=1}^{n_{j+1}} \frac{1}{\mathrm{ch}(\lambda_{j,k} - \lambda_{j+1,\ell})} \,, \quad (3.90)$$

where we will let $n_{N_5} \equiv N$ for convenience. In the brane construction, there are n_j D3-branes stretched between the $j^{\rm th}$ and $(j+1)^{\rm th}$ NS5-brane, so that for a configuration satisfying the Gaiotto-Witten constraints, one has $0 < K_1 \leq \ldots \leq K_{N_5}$ where $K_i \equiv n_i - n_{i-1}$.

Since the calculation of F_∂ involves a subtraction of the partition function for the theory on the full S^4, we will need to know the partition function for $U(N)$ $\mathcal{N} = 4$ SYM on S^4. One has matrix integral partition function [126]

$$Z[S^4_{r=1}] = \frac{1}{N!} \int \left(\prod_{i=1}^{N} d\lambda_i \right) e^{-\frac{8\pi^2}{g_{\rm YM}^2} \sum_{i=1}^{N} \lambda_i^2} \prod_{i<j}^{N} (\lambda_i - \lambda_j)^2 \quad (3.91)$$

on S^4 with unit radius $r = 1$, where the measure factor $\frac{1}{N!} \prod_{i<j} (\lambda_i - \lambda_j)^2$ arises from reducing the integration over the full Lie algebra $\mathfrak{u}(N)$ to the Cartan subalgebra, and the exponential factor is the classical contribution to the partition function, coming from evaluating the on-shell action.[55] For S^4_r with arbitrary radius, the purely gauge-theoretic measure should be invariant, but the classical contribution has

$$S_{\rm E}^{\text{on-shell}}(r) \sim r^2 S_{\rm E}^{\text{on-shell}}(r = 1) \,. \quad (3.92)$$

[55] The one-loop and instanton corrections vanish in this highly symmetric situation.

The calculation can be found in Appendix B.6: it provides

$$Z[S^4_r] = (2\pi)^{N/2} \left(\frac{g_{\rm YM}}{4\pi r}\right)^{N^2} G_2(N+1)\,, \tag{3.93}$$

where

$$G_2(N+1) \equiv \prod_{k=1}^{N-1} k! \tag{3.94}$$

is the Barnes G-function. One then has

$$\ln Z[S^4_r] = -N^2 \ln r + \frac{N^2}{2} \ln\left(\frac{\lambda}{16\pi^2 N}\right) + \ln G_2(N+1) + \frac{N}{2} \ln 2\pi\,. \tag{3.95}$$

For the purposes of comparing to the gravity calculation, we will typically be interested in the large N behaviour of this expression, so we require the asymptotics of

$$\ln G_2(N+1) = \sum_{k=1}^{N-1} (N-k) \ln k = N \ln(N-1)! - \sum_{k=1}^{N-1} k \ln k\,. \tag{3.96}$$

The asymptotics of the first term are given by the Stirling formula

$$N \ln(N-1)! = N^2 \ln N - N^2 + \mathcal{O}(N \ln N)\,. \tag{3.97}$$

To find an asymptotic expression for the sum $\sum_{k=1}^{N-1} k \ln k$, we will use the Euler-Maclaurin formula

$$\begin{aligned}\sum_{k=a}^{b} f(k) \sim \int_a^b f(x)\,dx \\ + \frac{f(b)+f(a)}{2} + \sum_{k=1}^{\infty} \frac{B_{2k}}{(2k)!}\big(f^{2k-1}(b) - f^{(2k-1)}(a)\big)\,,\end{aligned} \tag{3.98}$$

whence

$$\sum_{k=1}^{N-1} k \ln k = \frac{N^2 \ln N}{2} - \frac{N^2}{4} + \mathcal{O}(N \ln N)\,. \tag{3.99}$$

It is straightforward to determine the higher order terms if needed. All

together, we have

$$\ln G_2(N+1) = \frac{N^2}{2}\ln N - \frac{3}{4}N^2 + \mathcal{O}(N\ln N)\,, \tag{3.100}$$

and so

$$\ln Z[S^4_r] = -N^2\ln r + \frac{N^2}{2}\ln\Big(\frac{\lambda}{16\pi^2}\Big) - \frac{3}{4}N^2 + \frac{N}{2}\ln 2\pi + \mathcal{O}(N\ln N)\,. \tag{3.101}$$

It is worth noting that, from the general theory of the structure of UV divergences in the partition function, we anticipate

$$\ln Z[S^4_r] = A_1 r^4 + A_2 r^2 + A\ln r + F_4\,; \tag{3.102}$$

here, A_1, A_2 can be tuned through the addition of local counterterms, as can F_4 (the local counterterm corresponds to the Euler density). Although these quantities are scheme-dependent, they will cancel out in the calculation of F_∂ as long as we are consistent. The coefficient A of the logarithmic divergence, however, is physically meaningful: it is proportional to the A-type anomaly a for the $\mathcal{N}=4$ SYM theory on S^4, with

$$\frac{\partial}{\partial\ln r}\ln Z[S^4_r] = -64\pi^2 a\,. \tag{3.103}$$

The general Weyl anomaly in four dimensions is

$$\langle T^\mu_\mu\rangle = aE - cW^2\,, \tag{3.104}$$

with E the Euler density and W^2 shorthand for a contraction of the Weyl tensor, and in the super-Yang-Mills theory,

$$\langle T^\mu_\mu\rangle = \frac{N^2}{64\pi^2}\left(E - W^2\right)\,. \tag{3.105}$$

We thus indeed recover $a = \frac{N^2}{64\pi^2}$, and therefore $A = -N^2$, which confirms the r-dependence.

3.5.1 Neumann boundary condition

As a warm-up to the case of general NS5-like boundary conditions, we can consider a pure Neumann boundary condition. This corresponds to N D3-branes ending on a single NS5-brane, associated with parameter values

$$N_{NS5} = \sqrt{g}d = 1\,, \qquad \hat{k} = \frac{1}{\sqrt{g}}k = N\,, \tag{3.106}$$

that is,

$$d = \sqrt{\frac{4\pi N}{\lambda}}\,, \qquad k = \sqrt{\frac{\lambda N}{4\pi}}\,. \tag{3.107}$$

The partition function for this theory (expressed as a matrix integral in [198]) on the unit hemisphere is

$$Z_{\text{Neum.}}[HS^4_{r=1}] = \frac{1}{N!}\int\left(\prod_{i=1}^{N} d\lambda_i\right) e^{-\frac{4\pi^2}{g^2_{\text{YM}}}\sum_{i=1}^{N}\lambda_i^2} \prod_{i<j}^{N}(\lambda_i-\lambda_j)\text{sh}(\lambda_i-\lambda_j)\,. \tag{3.108}$$

This is similar to the S^4 partition function (3.91), except one now has one-loop determinant

$$Z^{1-\text{loop}}_{\text{Neum.}} = \prod_{i<j}\frac{\text{sh}(\lambda_i-\lambda_j)}{\lambda_i-\lambda_j}\,, \tag{3.109}$$

where we have combined one-loop factors from an $\mathcal{N}=2$ vector multiplet and an adjoint $\mathcal{N}=2$ hypermultiplet to recover the full one-loop determinant for the $\mathcal{N}=4$ vector multiplet theory. Using the results of Appendix B.6, this yields

$$Z_{\text{Neum.}}[HS^4_{r=1}] = (2\pi)^{\frac{N^2}{2}}\left(\frac{g^2_{\text{YM}}}{8\pi^2}\right)^{\frac{N^2}{2}} e^{\frac{g^2_{\text{YM}}N(N+1)(N-1)}{48}} G_2(N+1)\,. \tag{3.110}$$

We thus have

$$\ln\left|Z_{\text{Neum.}}[HS^4_{r=1}]\right| = \frac{\lambda(N+1)(N-1)}{48} + \frac{N^2}{2}\ln\left(\frac{\lambda}{4\pi N}\right) + \ln G_2(N+1)\,. \quad (3.111)$$

We therefore find that F_∂ is given by

$$\begin{aligned} F_\partial^{\text{Neum.}} &= -\left(\ln|Z_{\text{Neum.}}[HS^4_r]|^2 - \ln Z_{S^4_r}\right) \\ &= -\frac{\lambda(N^2-1)}{48} - \frac{N^2}{4}\ln\left(\frac{\lambda}{N}\right) \\ &\quad + \frac{N}{4}\ln 2\pi - \frac{1}{2}\ln G_2(N+1)\,. \end{aligned} \quad (3.112)$$

Using the results above, we we can expand this for large N as

$$F_\partial^{\text{Neum.}} = \frac{N^2}{8}\Big(-\frac{\lambda}{6} - 2\ln(\lambda) + 3\Big) + \mathcal{O}(N\ln N)\,. \quad (3.113)$$

This may be compared to the gravity result

$$F_\partial^{\text{SUGRA}} = \frac{N^2}{8}\Big(-\frac{\lambda}{6} - 2\ln(\lambda) + 3\Big)\,. \quad (3.114)$$

Remarkably, at leading order in N, the exact expression for F_∂ agrees exactly with the supergravity result as a function of λ.

3.5.2 General NS5-like boundary conditions

We would like to evaluate the integral

$$Z[HS^4] = \lim_{\alpha_1,\ldots,\alpha_{N_5-1}\to 0} \frac{1}{n_1!\ldots n_{N_5}!} \int \left(\prod_{j=1}^{N_5}\prod_{\ell=1}^{n_j} d\lambda_{j,\ell}\right) e^{-\frac{4\pi^2}{g_{\rm YM}^2}\sum_{i=1}^{N}\lambda_{N_5,i}^2} \times \left(\prod_{j=1}^{N_5-1}\prod_{\ell=1}^{n_j} e^{2\pi i\alpha_j\lambda_{j,\ell}}\right)\prod_{i<j}^{N}(\lambda_{N_5,i}-\lambda_{N_5,j})\,\mathrm{sh}(\lambda_{N_5,i}-\lambda_{N_5,j}) \times \prod_{j=1}^{N_5-1}\prod_{k<\ell}^{n_j}\mathrm{sh}^2\left(\lambda_{j,k}-\lambda_{j,\ell}\right)\prod_{j=1}^{N_5-1}\prod_{k=1}^{n_j}\prod_{\ell=1}^{n_{j+1}}\frac{1}{\cosh(\lambda_{j,k}-\lambda_{j+1,\ell})}\,. \quad (3.115)$$

As detailed in Appendix B.6, this integral yields

$$Z[HS^4] = (2\pi)^{-\sum_{i=1}^{N_5-1}n_i}\left(\frac{g_{\rm YM}^2}{4\pi}\right)^{\frac{N^2}{2}} e^{\frac{g_{\rm YM}^2}{48}\sum_{c=1}^{N_5}K_c(K_c-1)(K_c+1)} \left(\prod_{c=1}^{N_5}G_2(K_c+1)\right)\prod_{c<d}^{N_5}\left[2^{-(K_d-K_c)K_c}\left(\frac{\pi}{2}\right)^{\epsilon_{cd}K_c} \left(((K_d-K_c)!!)^{K_c}\prod_{k=1}^{K_c-1}\left(\frac{K_d-K_c}{2}+k\right)^{K_c-k}\right)^2\right], \quad (3.116)$$

where $K_i \equiv n_i - n_{i-1}$ is the $i^{\rm th}$ linking number (satisfying $0 < K_1 \leq \ldots \leq K_{N_5}$), and

$$\epsilon_{cd} \equiv \frac{1-(-1)^{K_c-K_d}}{2}\,. \quad (3.117)$$

We thus find

$$\begin{aligned}
F_\partial &= -\ln\left|Z[HS^4]\right| + \frac{1}{2}\ln Z[S^4] \\
&= -\left(\frac{N(2N-1)}{4} - \sum_{p=1}^{N_5}(N_5-p)K_p\right)\ln(2\pi) - \frac{N^2}{4}\ln\left(\frac{\lambda}{4\pi^2 N}\right) \\
&\quad - \frac{\lambda}{48N}\left(\sum_{p=1}^{N_5}K_p^3 - N\right) - \sum_{p=1}^{N_5}\ln G_2(K_p+1) \\
&\quad + \frac{1}{2}\ln G_2(N+1) + \ln 2\sum_{p<q}^{N_5}K_p(K_q-K_p) \\
&\quad - \ln\left(\frac{\pi}{2}\right)\sum_{p<q}^{N_5}\epsilon_{pq}K_p - 2\sum_{p<q}^{N_5}K_p\ln\left((K_q-K_p)!!\right) \\
&\quad - 2\sum_{p<q}^{N_5}\sum_{k=1}^{K_p-1}(K_p-k)\ln\left(\frac{K_q-K_p}{2}+k\right).
\end{aligned} \tag{3.118}$$

Equation (3.118) is our exact expression for the boundary free energy, in the case with exclusively NS5-branes.

One particular case of interest is when we have N D3-branes ending on N_5 NS5-branes of equal linking number $K = N/N_5$. In this case,

$$\begin{aligned}
F_\partial = &-\left(\frac{N(N-N_5)}{2} + \frac{N}{4}\right)\ln(2\pi) - \frac{N^2}{4}\ln\left(\frac{\lambda}{4\pi^2 N}\right) \\
&- \frac{\lambda}{48}\left(\frac{N^2}{N_5^2} - 1\right) - N_5^2\ln G_2\left(\frac{N}{N_5}+1\right) + \frac{1}{2}\ln G_2(N+1)\,.
\end{aligned} \tag{3.119}$$

This is the exact version of the supergravity expression (3.80).

3.5.3 General D5-like boundary conditions

We can obtain F_∂ for a general D5-like boundary condition by applying an S-duality transformation to the above result, which simply amounts to replacing the NS5-brane linking numbers with D5-brane linking numbers,

and performing an S-transformation to the gauge coupling $\frac{\lambda}{4\pi N} \to \frac{4\pi N}{\lambda}$. We thus obtain

$$\begin{aligned} F_\partial &= -\ln|Z[HS^4]| + \frac{1}{2}\ln Z[S^4] \\ &= -\left(\frac{N(2N-1)}{4} - \sum_{p=1}^{N_5}(N_5-p)L_p\right)\ln(2\pi) - \frac{N^2}{4}\ln\left(\frac{4N}{\lambda}\right) \\ &\quad - \frac{\pi^2 N}{3\lambda}\left(\sum_{p=1}^{N_5} L_p^3 - N\right) - \sum_{p=1}^{N_5}\ln G_2(L_p+1) \\ &\quad + \frac{1}{2}\ln G_2(N+1) + \ln 2\sum_{p<q}^{N_5} L_p(L_q-L_p) \\ &\quad - \ln\left(\frac{\pi}{2}\right)\sum_{p<q}^{N_5}\epsilon_{pq}L_p - 2\sum_{p<q}^{N_5} L_p\ln\left((L_q-L_p)!!\right) \\ &\quad - 2\sum_{p<q}^{N_5}\sum_{k=1}^{L_p-1}(L_p-k)\ln\left(\frac{L_q-L_p}{2}+k\right). \end{aligned} \tag{3.120}$$

For N D3-branes ending on N_5 D5-branes of equal linking number $L = N/N_5$, we obtain

$$\begin{aligned} F_\partial = &-\left(\frac{N(N-N_5)}{2} + \frac{N}{4}\right)\ln(2\pi) - \frac{N^2}{4}\ln\left(\frac{4N}{\lambda}\right) \\ &- \frac{\pi^2 N^2}{3\lambda}\left(\frac{N^2}{N_5^2}-1\right) - N_5^2\ln G_2\left(\frac{N}{N_5}+1\right) + \frac{1}{2}\ln G_2(N+1)\,. \end{aligned} \tag{3.121}$$

This is the exact version of the supergravity expression (3.77).

Comparison with supergravity results

We now compare the localization result (3.118) with our supergravity results.

When the K_k (and their differences) are taken to be large in (3.118), then we can use the Euler-Maclaurin approximation for the last term to

find

$$\begin{aligned}
&-2\sum_{p<q}^{N_5}\sum_{k=0}^{K_p-1} k\ln\left(\frac{K_q+K_p}{2}-k\right)\\
&\quad\approx -2\sum_{p<q}^{N_5}\int_{k=0}^{K_p-1} dx\, x\ln\left(\frac{K_q+K_p}{2}-x\right)\\
&\quad= -\frac{1}{4}\sum_{p<q}^{N_5}\left((K_q+K_p)^2\ln(K_q+K_p)-(K_q-K_p)^2\ln(K_q-K_p)\right)\\
&\qquad-\sum_{p<q}^{N_5} K_p(K_p-K_q)\ln(K_q-K_p)\\
&\qquad+\frac{1}{2}\sum_{p<q}^{N_5} K_p(K_q+2(1+\ln 2)K_p)+O(N_5^2K\ln K)\,.
\end{aligned} \tag{3.122}$$

Meanwhile, using the Stirling approximation, we find

$$\ln(M!!)=\frac{M}{2}\ln M-\frac{M}{2}+O(\ln M)\,. \tag{3.123}$$

Thus,

$$\begin{aligned}
&-2\sum_{p<q}^{N_5} K_p\ln((K_q-K_p)!!)\\
&\qquad=-2\sum_{p<q}^{N_5} K_p\left(\frac{(K_q-K_p)}{2}\ln(K_q-K_p)-\frac{(K_q-K_p)}{2}\right)\\
&\qquad\qquad+O(N_5^2K\ln K)\,.
\end{aligned} \tag{3.124}$$

We thus find

$$\begin{aligned}
F_\partial = &-\left(\frac{N^2}{2}-\sum_{p<q}^{N_5}K_p\right)\ln(2\pi)-\frac{N^2}{4}\ln\left(\frac{\lambda}{4\pi^2N}\right)-\frac{\lambda}{48N}\sum_{p=1}^{N_5}K_p^3\\
&-\sum_{p=1}^{N_5}\left(\frac{K_p^2}{2}\ln K_p-\frac{3K_p^2}{4}\right)+\frac{1}{2}\left(\frac{N^2}{2}\ln N-\frac{3N^2}{4}\right)\\
&+\ln 2\sum_{p<q}^{N_5}K_p(K_q-K_p)-\ln\left(\frac{\pi}{2}\right)\sum_{p<q}^{N_5}\epsilon_{pq}K_p\\
&-2\sum_{p<q}^{N_5}K_p\left(\frac{(K_q-K_p)}{2}\ln(K_q-K_p)-\frac{(K_q-K_p)}{2}\right)\\
&-\frac{1}{4}\sum_{p<q}^{N_5}\left((K_q+K_p)^2\ln(K_q+K_p)-(K_q-K_p)^2\ln(K_q-K_p)\right)\\
&-\sum_{p<q}^{N_5}K_p(K_p-K_q)\ln(K_q-K_p)+\frac{1}{2}\sum_{p<q}^{N_5}K_p(K_q+2(1+\ln 2)K_p)\\
&+O(N_5^2K\ln K)\,.
\end{aligned}\tag{3.125}$$

Massaging this expression, we arrive at

$$\begin{aligned}
F_\partial = &\frac{N^2}{4}\left(\frac{3}{2}+\ln\left(\frac{4N^2}{\lambda}\right)\right)-\frac{\lambda}{48N}\sum_{p=1}^{N_5}K_p^3\\
&-\frac{1}{16}\sum_{p,q}^{N_5}\Big[(K_q+K_p)^2\ln\left((K_q+K_p)^2\right)\\
&-(K_q-K_p)^2\ln\left((K_q-K_p)^2\right)\Big]+O(N_5^2K\ln K)\,.
\end{aligned}\tag{3.126}$$

This limit exactly reproduces our result from the supergravity calculation. We can similarly check that the exact expression for general D5-brane boundary conditions reproduces the supergravity answer when the linking numbers and their differences are large.

Comparison for finite N

We can also compare the exact results with the supergravity results for finite N. We note that the $\log\lambda$ term agrees exactly between the supergravity and localization calculations, while the term of order λ in the NS5-brane supergravity expression (or $1/\lambda$ in the D5-brane expression) becomes exact under the replacement

$$\sum_A K_A^3 \to \sum_A (K_A^3 - K_A) \tag{3.127}$$

(or the same replacement with L_A for the D5-brane expression).

The remaining terms are λ-independent. It is straightforward to calculate these for all possible boundary conditions for small fixed values of the gauge group rank N and compare supergravity results with the exact results. For $N = 2$, $N = 3$, and $N = 8$, this λ-independent part of the spectrum of boundary F values is shown in Figure 3.5.

We see that the results agree reasonably well even for small values of N. As an example, for the $N = 8$ case, the λ-independent parts of the boundary F values for linking numbers

$$\begin{gathered}\big([1,1,1,1,1,1,1,1],[1,1,1,1,1,1,1,2],[1,1,1,1,2,2],[1,1,2,2,2],\\ [2,2,2,2],[1,1,1,1,1,3],[1,1,1,2,3],[1,2,2,3],[1,1,3,3],[2,3,3],\\ [1,1,1,1,4],[1,1,2,4],[2,2,4],[1,3,4],[4,4],[1,1,1,5],[1,2,5],\\ [3,5],[1,1,6],[2,6],[1,7],[8]\big)\end{gathered} \tag{3.128}$$

are (rounded to the nearest integer)

$$\begin{gathered}(101,89,81,75,71,76,69,65,61,59,63,\\ 58,55,52,47,50,47,43,39,37,30,24)\end{gathered} \tag{3.129}$$

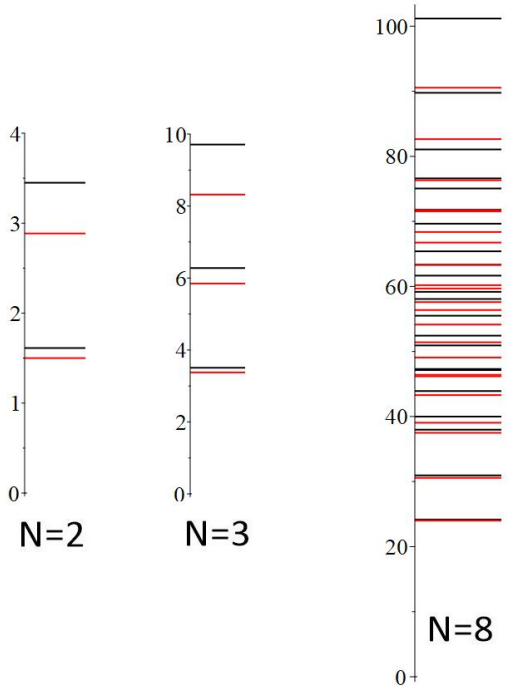

Figure 3.5: The λ-independent part of the spectrum of possible boundary F values for $U(N)$ $\mathcal{N}=4$ SYM theory with $N=2$, 3, 8. Black lines represent the exact values while red lines give the supergravity approximation.

using the exact results and

$$(90, 82, 76, 71, 68, 71, 66, 63, 59, 57, 60, \\ 56, 54, 51, 46, 49, 46, 43, 39, 37, 30, 24) \quad (3.130)$$

with the supergravity expressions.

3.6 Statistics of boundary F

In this section, we will use our results above to investigate the distribution of possible values for F_∂ for a given N, for various types of boundary conditions.

For fixed λ and N, there are infinitely many superconformal boundary conditions that one can impose, since we can couple in an arbitrarily complicated 3D SCFT. We expect that there is a lower bound, but no upper bound on the allowed value of F_∂, which can be thought of as a measure of the number of local boundary degrees of freedom.

For the class of theories corresponding to D3-branes ending on D5-branes only or NS5-branes only, we have only a finite set of possibilities, enumerated by partitions of N, the rank of the gauge group. In this case, we have upper and lower bounds for F_∂ that depend on N and λ, and we can investigate the distribution of F_∂ values for a given N and λ either using the supergravity expressions or the exact results from localization.

D5-brane boundary conditions

Defining $p_A = L_A/N$, our supergravity expression for F_∂ for the theories associated with D3-branes ending on D5-branes is

$$F_\partial^{\text{SUGRA}} = \frac{N^2}{4}\left(\frac{3}{2} + \ln\left(\frac{\lambda}{4\pi^2 N^2}\right)\right) - \frac{\pi^2 N^4}{3}\sum_A p_A^3 \\ - \frac{N^2}{16}\sum_{A,B}\Big[(p_A+p_B)^2 \ln\left((p_A+p_B)^2\right) \\ - (p_A-p_B)^2 \ln\left((p_A-p_B)^2\right)\Big], \quad (3.131)$$

where the positivity of L_i and the relation $\sum_A L_A = N$ give $p_A \geq 0$ and $\sum_A p_A = 1$. Thus $\{p_A\}$ satisfies the constraints of a probability distribution.

In Appendix B.7, we show that the minimum and maximum values of $F_\partial^{\text{SUGRA}}$ are obtained by considering the distribution $\{p_A\}$ with the minimum and maximum entropy respectively, i.e. where $\{p_A\} = \{1\}$ and $\{p_A\} = \{1/N, \ldots, 1/N\}$. This yields

$$N^2\left(-\frac{\pi^2 N^2}{3\lambda} - \frac{1}{4}\ln\left(\frac{16\pi^2 N^2}{\lambda}\right) + \frac{3}{8}\right) \leq F_\partial^{\text{SUGRA}} \leq N^2\left(\frac{1}{4}\ln\left(\frac{\lambda}{16\pi^2}\right) + \frac{3}{8} - \frac{\pi^2}{3\lambda}\right) . \quad (3.132)$$

Assuming that the same sets of linking numbers lead to the minimum and maximum values for F_∂ with the exact expression, we find a range of allowed values

$$F_\partial^- \leq F_\partial \leq F_\partial^+ \quad (3.133)$$

where F_∂^+ corresponds to the maximum entropy configuration and is given by (setting $L = 1$ in (3.121))

$$F_\partial^+ = -\frac{N}{4}\ln(2\pi) - \frac{N^2}{4}\ln\left(\frac{4N}{\lambda}\right) + \frac{1}{2}\ln G_2(N+1) , \quad (3.134)$$

and F_∂^- corresponds to the minimum entropy configuration and is given by (setting $L = N$ in (3.121))

$$F_\partial^- = -\left(\frac{N^2}{2} - \frac{N}{4}\right)\ln(2\pi) - \frac{N^2}{4}\ln\left(\frac{4N}{\lambda}\right) - \frac{\pi^2 N^2}{3\lambda}(N-1)(N+1) - \frac{1}{2}\ln G_2\left(N+1\right) . \quad (3.135)$$

Using the large N approximation to the Barnes G-function, we then find

that up to $\mathcal{O}(N \ln N)$ corrections we have a range of allowed values

$$N^2 \left(-\frac{\pi^2 N^2}{3\lambda} - \frac{1}{4} \ln \left(\frac{16\pi^2 N^2}{\lambda} \right) + \frac{3}{8} \right) \leq F_\partial^{D5} \leq N^2 \left(\frac{1}{4} \ln \left(\frac{\lambda}{4} \right) - \frac{3}{8} \right) . \quad (3.136)$$

We note that the upper bound is modified here compared to the supergravity result (3.138). We emphasize that we have not proven that the left and right sides here are actually the upper and lower bounds on F_∂; this will be true assuming that the same boundary conditions giving rise to the minimum and maximum for $F_\partial^{\rm SUGRA}$ also give rise to the minimum and maximum for F_∂.

We see that this allowed range covers primarily negative values, with the upper end of the range positive only for sufficiently large λ. We can understand the large negative values of boundary F that arise for boundary conditions associated with D3-branes ending on few D5-branes by the fact that the scalars are developing an expectation value, and this results in a large fraction of the N^2 fields becoming massive, with mass increasing as we approach the boundary. Thus, we lose degrees of freedom compared with the situation where the scalar vevs are vanishing. The quantity boundary F is in some sense a measure of the number of boundary degrees of freedom, but in this case, the negative value indicates that it is taking away from the bulk degrees of freedom.

NS5-brane boundary conditions

A similar analysis applies to the NS5-brane boundary conditions. Defining $p_A = K_A/N$, we have

$$F_\partial^{\rm SUGRA} = \frac{N^2}{4}\left(\frac{3}{2} + \ln\left(\frac{4}{\lambda}\right)\right) - \frac{\lambda N^2}{48}\sum_A p_A^3 - \frac{N^2}{16} - \frac{N^2}{16}\sum_{A,B}\Big[(p_A+p_B)^2\ln\left((p_A+p_B)^2\right) - (p_A-p_B)^2\ln\left((p_A-p_B)^2\right)\Big], \quad (3.137)$$

A similar argument to that for the D5-brane boundary conditions shows that $F_\partial^{\rm SUGRA}$ is again minimized/maximized on the minimum/maximum entropy distribution, yielding

$$N^2\left(-\frac{\lambda}{48} - \frac{1}{4}\ln\lambda + \frac{3}{8}\right) \le F_\partial^{\rm SUGRA} \le N^2\left(-\frac{\lambda}{48N^2} + \frac{1}{4}\ln\left(\frac{N^2}{\lambda}\right) + \frac{3}{8}\right). \quad (3.138)$$

Assuming that the same sets of linking numbers lead to the minimum and maximum values for F_∂ with the exact expression, we find a range of allowed values

$$F_\partial^- \le F_\partial \le F_\partial^+ \quad (3.139)$$

where F_∂^- corresponds to the "minimum entropy" configuration and is given by (setting $K = N$ in (3.119))

$$F_\partial^+ = -\left(\frac{N^2}{2} - \frac{N}{4}\right)\ln(2\pi) - \frac{N^2}{4}\ln\left(\frac{\lambda}{4\pi^2 N}\right) - \frac{\lambda}{48}(N-1)(N+1) - \frac{1}{2}\ln G_2\left(N+1\right), \quad (3.140)$$

and F_∂^+ corresponds to the "maximum entropy" configuration and is given

by (setting $K = 1$ in (3.119))

$$F_\partial^- = -\frac{N}{4}\ln(2\pi) - \frac{N^2}{4}\ln\left(\frac{\lambda}{4\pi^2 N}\right) + \frac{1}{2}\ln G_2(N+1)\,, \tag{3.141}$$

Using the large N approximation to the Barnes G-function, we then find that up to $\mathcal{O}(N\ln N)$ corrections, we have a range of allowed values

$$N^2\left(-\frac{\lambda}{48} - \frac{1}{4}\ln\lambda + \frac{3}{8}\right) \leq F_\partial^{NS5} \leq N^2\left(\frac{1}{4}\ln\left(\frac{4\pi^2N^2}{\lambda}\right) - \frac{3}{8}\right)\,. \tag{3.142}$$

As above, the upper bound is modified here compared to the supergravity result (3.138), which is expected since the linking numbers are not large in this case. We emphasize that we have not proven that the left and right sides here are actually the upper and lower bounds on F_∂; this will be true assuming that the same boundary conditions giving rise to the minimum and maximum for $F_\partial^{\rm SUGRA}$ also give rise to the minimum and maximum for F_∂.

We see that at least for small values of λ, the range of allowed boundary F values for these boundary conditions is positive, consistent with the fact that the scalar vevs are zero for these boundary conditions and the full set of massless bulk degrees of freedom remain.

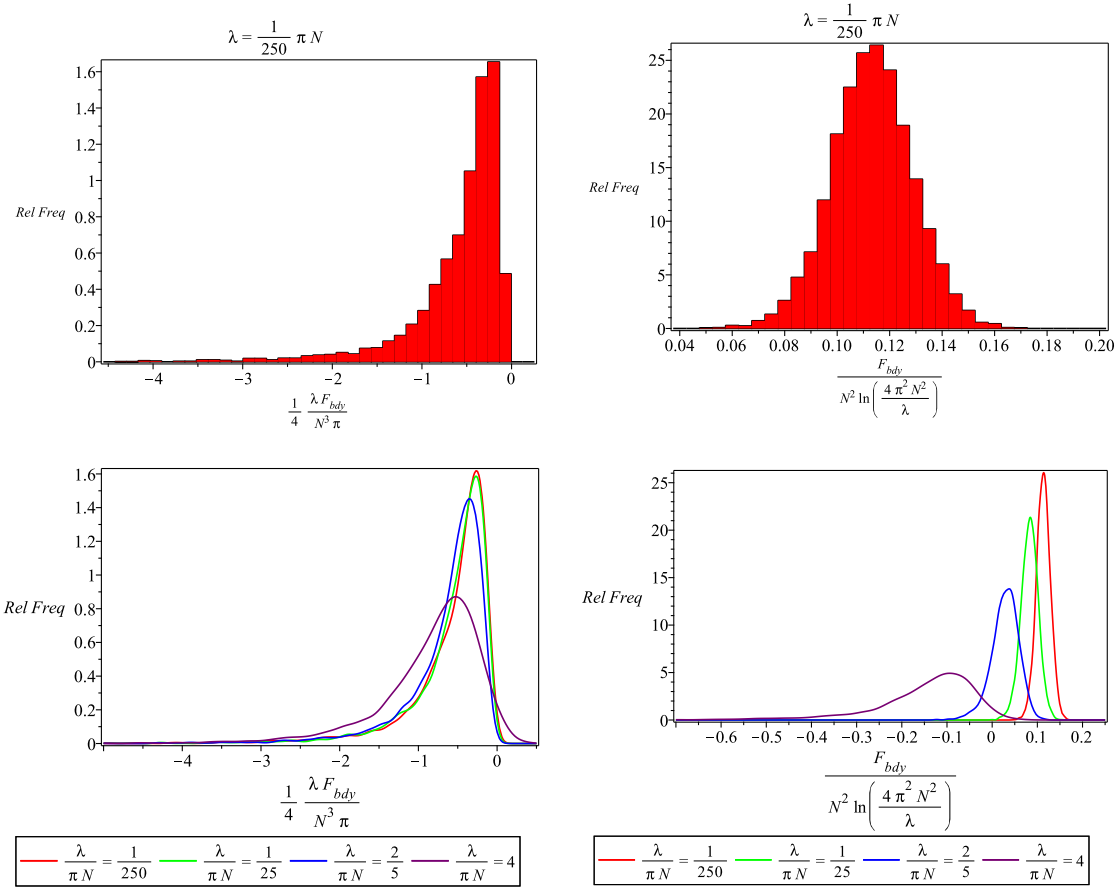

Figure 3.6: (Top Left) Histogram of values of $\frac{\lambda}{4\pi N}\frac{F_\partial}{N^2}$ for D5-like boundary conditions, with $N = 100$ and $\frac{\lambda}{4\pi N} = 10^{-3}$. (Bottom Left) Contours of histograms of $\frac{\lambda}{4\pi N}\frac{F_\partial}{N^2}$ (bins removed for clarity) for D5-like boundary conditions, with $N = 100$ and various values of λ up to the self-dual value $\lambda = 4\pi N$. (Top Right) Histogram of values of $\frac{1}{\ln(4\pi^2 N^2/\lambda)}\frac{F_\partial}{N^2}$ for NS5-like boundary conditions, with $N = 100$ and $\frac{\lambda}{4\pi N} = 10^{-3}$. (Bottom Right) Contours of histograms of $\frac{1}{\ln(4\pi^2 N^2/\lambda)}\frac{F_\partial}{N^2}$ (bins removed for clarity) for NS5-like boundary conditions, with $N = 100$ and various values of λ up to the self-dual value $\lambda = 4\pi N$. For each histogram, we uniformly sample 5000 partitions of the integer N, and compute F_∂ for the associated boundary conditions.

Distribution of boundary F values

It is also of interest to ask about the distribution of allowed F_∂ values for a given N and λ. In Figure 3.6, we display contour plots for histograms of allowed values (scaled by positive factors involving λ and N for convenience) for the case $N = 100$ with various values of λ. We display the results for D5-brane and NS5-brane boundary conditions with up to the self-dual value $\lambda = 4\pi N$ for the 't Hooft coupling; these confirm that, for λ below the self-dual value, F_∂ is predominantly negative for D5-brane boundary conditions, and predominantly positive for NS5-brane boundary conditions. These plots also implicitly reveal the behaviour of F_∂ for λ above the self-dual value; the distribution of F_∂ for D5-brane boundary conditions with such λ is identical to that for NS5-brane boundary conditions with the dual value of the 't Hooft coupling, and vice versa.

We also display similar plots for the case of fixed λ and increasing N in Figure 3.7. One notable feature of these plots is that, for fixed λ, the proportion of D5-like/NS5-like boundary conditions for which F_∂ is positive/negative appears to asymptote to zero for increasing N; this is illustrated further in Figure 3.8.

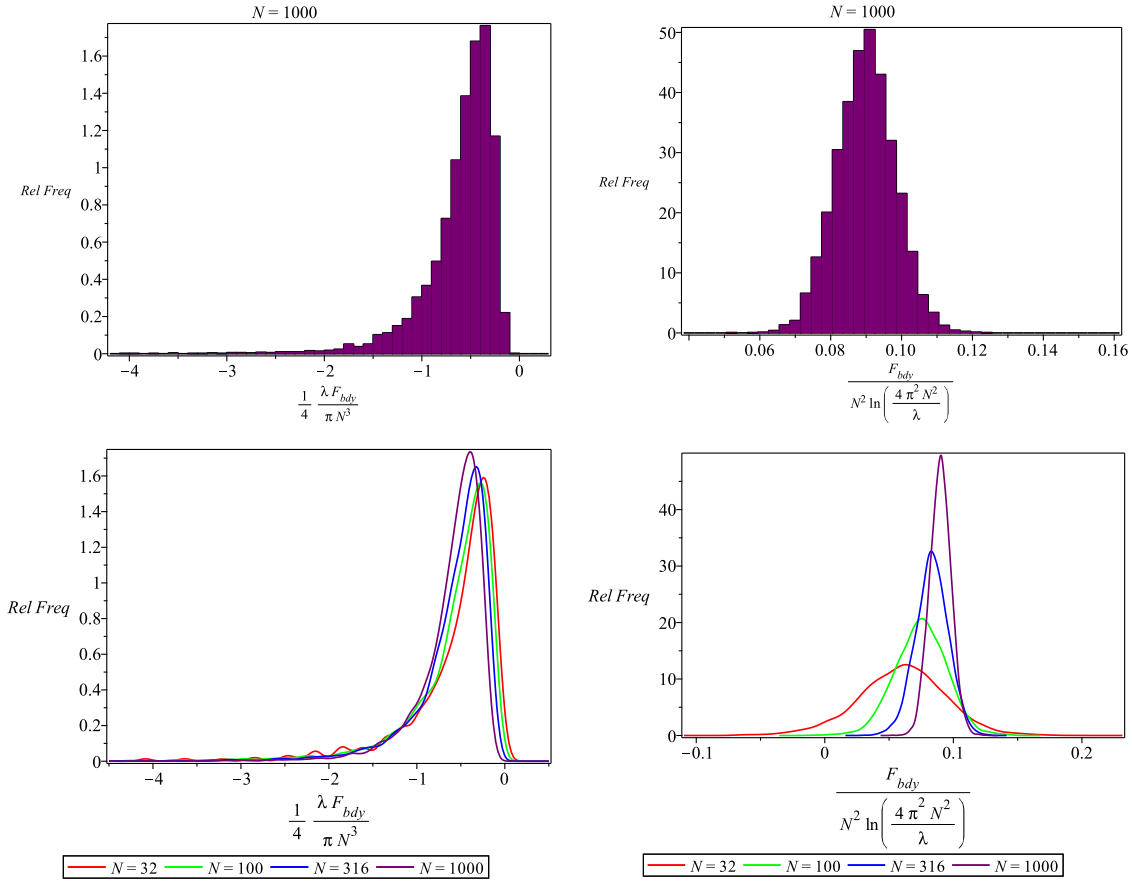

Figure 3.7: (Top Left) Histogram of values of $\frac{\lambda}{4\pi N}\frac{F_\partial}{N^2}$ for D5-like boundary conditions, with $\lambda = 20$ and $N = 10^3$. (Bottom Left) Contours of histograms of $\frac{\lambda}{4\pi N}\frac{F_\partial}{N^2}$ (bins removed for clarity) for D5-like boundary conditions, with $\lambda = 20$ and various values of N. (Top Right) Histogram of values of $\frac{1}{\ln(4\pi^2 N^2/\lambda)}\frac{F_\partial}{N^2}$ for NS5-like boundary conditions, with $\lambda = 20$ and $N = 10^3$. (Bottom Right) Contours of histograms of $\frac{1}{\ln(4\pi^2 N^2/\lambda)}\frac{F_\partial}{N^2}$ (bins removed for clarity) for NS5-like boundary conditions, with $\lambda = 20$ and various values of N. For each histogram, we uniformly sample 5000 partitions of the integer N, and compute F_∂ for the associated boundary conditions.

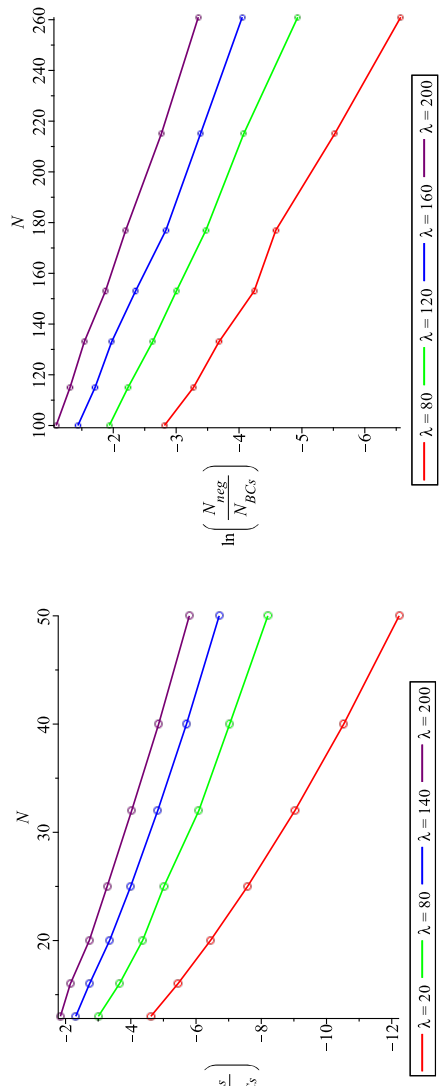

Figure 3.8: (Left) Logarithm of the proportion of D5-like boundary conditions giving rise to positive F_∂, for various values of λ and increasing N. Values are exact, as we include every possible such boundary condition. (Right) Logarithm of the proportion of NS5-like boundary conditions giving rise to negative F_∂, for various values of λ and increasing N. Each point is based on 5000 uniformly sampled partitions of the integer N.

Arbitrarily large boundary F for general boundary conditions

To conclude this section, we verify the claim that by considering general boundary conditions involving D5-branes and NS5-branes, we can make F_∂ arbitrarily large. This is expected, since the general boundary conditions can be understood as coupling in a SCFT to one of the theories with D5-branes or NS5-branes only, and we can take this SCFT to have arbitrarily many degrees of freedom. We are therefore motivated to verify this claim by considering such a boundary condition with a large number of boundary degrees of freedom; for simplicity, we consider the case of a single stack of many D5-branes and a single stack of many NS5-branes, with linking numbers

$$\tilde{L} = -1 \,, \qquad K = 1 \,, \tag{3.143}$$

and with N, N_{NS5} taken to be large independent parameters, with $N \ll N_{NS5}$. We then have

$$N_{D5} = N_{NS5} - N \,. \tag{3.144}$$

The supergravity parameters $\hat{l}, \hat{k}$ are given by

$$\begin{aligned} -1 &= \hat{l} - \frac{2}{\pi} N_{NS5} \arctan(g\hat{k}/\hat{l}) \,, \\ 1 &= \hat{k} + \frac{2}{\pi} (N_{NS5} - N) \arctan(g\hat{k}/\hat{l}) \,, \end{aligned} \tag{3.145}$$

which has perturbative solution

$$\begin{aligned} \hat{k} &= \frac{2\pi^2}{\lambda} \frac{N^2}{N_{NS5}^2} + O\left(\frac{N^3}{N_{NS5}^3}\right) \\ \hat{l} &= \frac{N}{N_{NS5}} + O\left(\frac{N^2}{N_{NS5}^2}\right) \,. \end{aligned} \tag{3.146}$$

Most of the terms appearing in the uncorrected F_∂ in the case of this boundary condition are suppressed by $\frac{N}{N_{NS5}}$, and will vanish in the limit $\frac{N}{N_{NS5}} \to 0$ with fixed λ and N; the terms which are not suppressed in this limit are the

constant contribution $\frac{3}{8}N^2$, the "cubic terms"

$$\begin{aligned} -\frac{1}{\pi}c^2 dlD\left[\frac{1}{2}-\frac{ik}{2l}\right] &\sim NN_{NS5}\ln 2\,, \\ -\frac{1}{\pi}d^2 ckD\left[\frac{1}{2}-\frac{il}{2k}\right] &\sim \frac{2\pi^2}{\lambda}N^2\ln(N_{NS5})\,, \end{aligned} \tag{3.147}$$

and the "quartic term"

$$-\frac{1}{2\pi^2}c^2d^2\left\{\mathcal{L}\left(\frac{(k+il)^2}{(k-il)^2}\right)+\mathcal{L}\left(\frac{(k+il)^2}{4ikl}\right)-\zeta(3)\right\} \sim N_{NS5}^2\ln(N_{NS5})\,. \tag{3.148}$$

Meanwhile, the anticipated corrections from the vicinity of the D5-branes and NS5-branes are $O(N_{NS5}^2)$ (see Appendix B.5). Consequently, the leading term in the uncorrected F_∂, which is $N_{NS5}^2\ln N_{NS5}$, should provide a good approximation to F_∂ when $N_{NS5}\gg N$. Since N_{NS5} can take arbitrarily large values, we see that F_∂ is unbounded from above.

3.7 Discussion

In this final section, we mention a few possible applications of our results.

RG ordering of BCFTs

We recall that F_∂ has been conjectured to decrease under boundary renormalization group flows. Assuming that this is true, our results provide very detailed information about which boundary RG flows are possible between the various BCFTs we consider. For cases where the endpoints of an RG flow are known, for example where we add supersymmetric mass terms or Fayet-Illiopoulos parameters to a UV theory, it would be interesting to verify the decrease of boundary F to provide support for the conjecture; this was done in [162] for the simple case considered there.

We note that for $N>7$, the ordering of boundary F for different theories depends on the bulk 't Hooft coupling parameter λ. Thus, if the boundary

F monotonicity conjecture is correct, we could have the interesting situation where some relevant perturbation of theory A flows to theory B for small values of λ while some relevant perturbation of theory B flows to theory A for large values of λ. Of course, it may also be the case that no RG flows are possible between theories whose boundary F values switch orderings as a function of λ.

Holographic interpretation

As we discussed in Section 3.3, the addition of a boundary to the $\mathcal{N} = 4$ theory corresponds to the addition of a certain type of "end-of-the-world" brane in the five-dimensional gravity picture. This corresponds in the higher-dimensional picture to a region where the internal space smoothly degenerates. In many holographic applications of BCFTs, the gravity side is described using a bottom-up approach, in which such an ETW brane is simply described by adding a boundary action with certain parameters to the bulk gravitational theory [79, 87]. The simplest such parameter is the tension of the ETW brane. An interesting question, one of the questions that motivated this work, is to understand the range of tension parameters in bottom-up models for which the qualitative physics can be reproduced in microscopic constructions.

As discussed in [87], there is a direct relationship between the tension parameter of a bottom up model and the boundary entropy, obtained by performing a holographic calculation of boundary F as a function of this tension. We provide this calculation in the four-dimensional case in Appendix B.8, with the result that

$$F = c_{\text{bulk}} \left(\frac{T}{1-T^2} + \frac{1}{2} \ln \frac{1+T}{1-T} \right) . \tag{3.149}$$

where we define $c_{\text{bulk}} = (L^3_{\text{AdS}}\pi/4G)$ and the tension is $3L_{\text{AdS}}T/(8\pi G)$. This provides a guide to choosing the tension parameter if one wishes to model the physics of our more detailed microscopic theories using a bottom-up model.

Generalizations

There is a significantly larger class of theories with the same symmetry as the theories considered in this chapter. The more general theories correspond to $\mathcal{N} = 4$ SYM theory with a supersymmetric planar defect, or to supersymmetric interfaces between $\mathcal{N} = 4$ SYM theories with different parameters. Type IIB supergravity solutions for these theories are also known, so it should be straightforward to use the methods of this chapter to calculate the defect/interface entropy for these theories.

Part III

Braneworlds

Chapter 4

Black Hole Microstate Cosmology

4.1 Introduction

The AdS/CFT correspondence is believed to provide a non-perturbative description of quantum gravity for spacetimes which are asymptotic to anti-de Sitter space. For a holographic CFT defined on a spatial sphere, typical pure states with large energy expectation value correspond to microstates of a large black hole in AdS. Simple observables in the CFT can be used to probe the exterior geometry of this black hole, revealing the usual AdS Schwarzschild metric with a horizon. However, what lies beyond the horizon for such states and how this is encoded in the CFT is still a significant open question.

Classically, a static (eternal) black hole solution can be extended to include a second full asymptotically AdS region. In this classical picture, the horizon is not distinguished by any local physics, so a conventional expectation is that black hole microstate geometries should include at least some of the behind-the-horizon region from the maximally extended geometry.[56] On the other hand, including the full second asymptotic region is tantamount to introducing the degrees of freedom of a second CFT, so it is very plausible that single-CFT microstate geometries have at most a part of the second

[56] Some authors have argued that quantum effects should modify these expectations: the "fuzzball" proposal [204–207] suggests that microstate geometries are actually horizonless, while proponents of the "firewall" scenario [59, 60] argued that consistency with unitarity and the equivalence principle imply that the geometry must end in some type of singularity at or just beyond the horizon. But many authors have given counter-arguments suggesting a more conventional picture.

asymptotic region in common with the maximally extended spacetime.

In this chapter, following [208] and [209], we will explore the possibility that for certain CFT states, the corresponding black hole geometry is captured by the Penrose diagram in Figure 4.1.[57] Here, the geometry on the right side is the AdS-Schwarzschild black hole exterior. On the left, instead of the full second asymptotic region that would be present in the maximally extended black hole geometry, we have a finite region terminating on an end-of-the-world (ETW) brane (shown in red in Figure 4.1). In the microscopic description, this brane could involve some branes from string/M-theory theory or could correspond to a place where the spacetime effectively ends due to a degeneration of the internal space (as in a "bubble of nothing" geometry [211]). In this note we mainly make use of a simple effective description of the ETW brane, which we describe in detail below.

In order to decode the physics of these microstate spacetimes from the microscopic CFT state, we need to understand the CFT description of physics behind the black hole horizon. This is a notoriously difficult problem; the present understanding is that decoding local physics behind the horizon requires looking at extremely complicated operators in the CFT and furthermore that the operators needed depend on the particular CFT state being considered [212–215].[58]

Fortunately, we will see that in many cases, entanglement entropy in the CFT can probe the geometry behind the horizon, and in particular can be used to inform us about the effective geometry of the ETW brane. To understand this, recall that for holographic theories, the entanglement entropy for a spatial region in the CFT corresponds to the area in the corresponding geometry of the minimal area extremal surface homologous to the region [42, 218]. In the geometry of Figure 4.1, we have extremal surfaces that remain outside the black hole horizon and extremal surfaces

[57] The recent paper [210] that appeared during the course of our work also considered black hole microstate geometries, describing a picture somewhat different from the one in Figure 4.1. However, [210] were discussing typical black hole microstates, while we are focusing on more specific states, so there is no conflict.

[58] For recent discussions of state dependence and bulk reconstruction of black hole interiors from the quantum error correction perspective, see [216, 217].

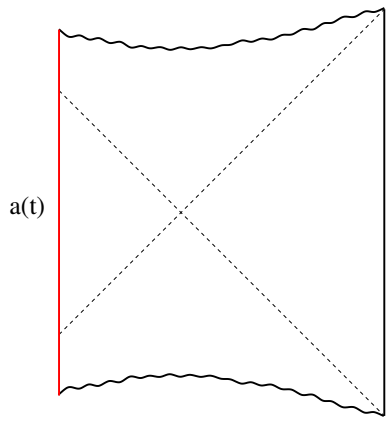

Figure 4.1: Penrose diagram for spacetimes associated with certain black hole microstates. The spacetime terminates on the left with an effective end-of-the-world brane (shown in red on the left) whose worldvolume geometry is a four-dimensional FRW big bang/big crunch cosmology. For certain brane trajectories, the physics of the left region would correspond to a Randall-Sundrum II cosmology, with gravity localized on the brane. If there are CFT states that realize this scenario, the CFT would provide a complete microscopic description of this cosmology.

that penetrate the horizon and end on the ETW brane, as shown in Figure 4.2. We find that if the black hole is sufficiently large, the behind-the-horizon region is not too large, and the CFT region is large enough, the extremal surfaces penetrating the horizon can have the minimal area for some window of boundary time $[-t_E, t_E]$, where t_E depends on the size of the region being considered. During this time, the entanglement entropy is time-dependent and directly probes the geometry of the ETW brane. This was observed for a simple case in [219].[59]

Our investigations were motivated by the work of [208] in the context of the SYK model, a simple toy model for AdS/CFT. Here, Kourkoulou and Maldacena argued that for states $e^{-\beta H}|B\rangle$ arising via Euclidean evolution of states $|B\rangle$ with limited entanglement, the corresponding AdS_2 black hole microstate take a form similar to that shown in Figure 4.1. This work was generalized to CFTs in [209], where the states $|B\rangle$ were taken to be conformally invariant boundary states of the CFT.[60] In that case, the corresponding geometries were deduced by making use of a simple ansatz discussed by Karch and Randall [78], and by Takayanagi [87] for how to holographically model conformally invariant boundary conditions in CFTs. The resulting geometries again take the form shown in Figure 4.1, with the trajectory of the ETW brane depending on properties of the CFT boundary state. We review the construction of these states and their corresponding geometries in Section 4.2, generalizing the calculations to higher dimensions. We make use of this particular set of geometries for our detailed calculations since they are simple to interpret holographically, but we expect that the qualitative picture of Figure 4.1 should hold in a more complete holographic treatment of Euclidean-time-evolved CFT boundary states, and perhaps for a more general class of states.

Our calculations of entanglement entropy for these states are described in detail in Section 4.3. As an example of the results, Figure 4.3 shows the

[59] Various other works have considered the entanglement entropy in black hole geometries with a time-dependent exterior, such as the Vaidya geometry (see, for example, [220]). In these cases, the entanglement entropy can also probe behind the horizon.

[60] The states $e^{-\beta H}|B\rangle$ in this case have been considered in the past by Cardy and collaborators [221], [222] as time-dependent states used to model quantum quenches.

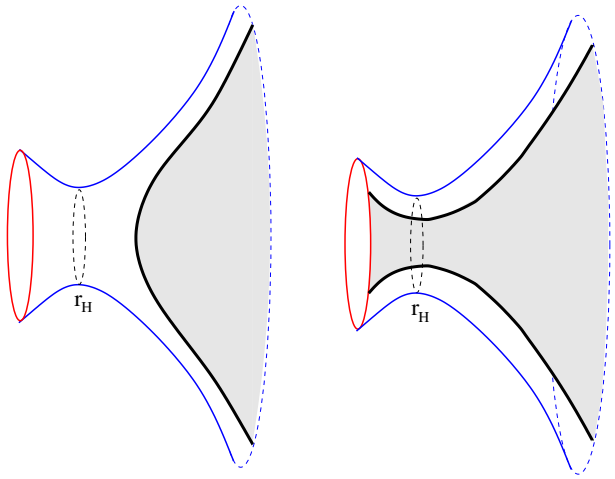

Figure 4.2: Two possibilities for extremal surfaces and associated entanglement wedges (shaded) for ball-shaped boundary regions. The extremal surface on the right has the topology of S^{d-2} times an interval, so is connected for $d > 2$.

entanglement entropy for ball-shaped regions in a particular five-dimensional black hole geometry with constant-tension ETW brane behind the horizon. For small subsystems or late times, the RT surfaces stay outside the horizon and the entanglement entropy is time-independent. However, for large enough subsystems, there is an interval of time where the minimal-area extremal surfaces probe behind the horizon and end on the ETW brane. Thus, the entanglement entropy gives a direct probe of behind-the-horizon physics.

The ansatz of Karch/Randall/Takayanagi, in which boundaries in the asymptotic region are extended into the bulk along a dynamical ETW brane of a fixed tension, is the simplest proposal that reproduces expected properties of boundary CFT entanglement entropy via a holographic calculation. For specific microstates of specific CFTs, the detailed microstate geometry is more complicated and the ETW brane will have a more specific microscopic description, but it is plausible that the qualitative picture is similar. Thus, our results for the behavior of entanglement entropy using the simple ansatz

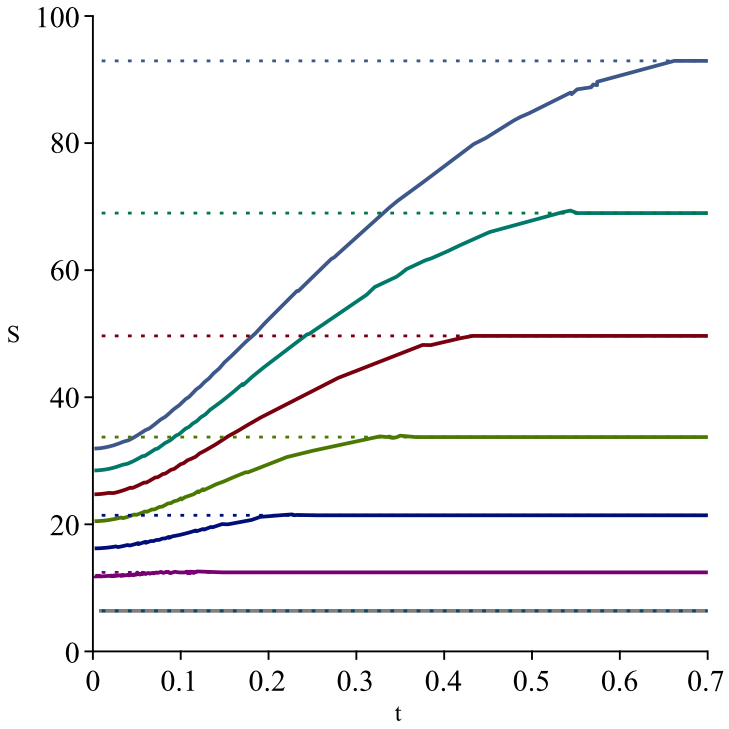

Figure 4.3: Time-dependence of subsystem entanglement entropy for a five-dimensional black hole microstate modeled by a constant tension ETW brane behind the horizon. Curves from bottom to top correspond to successively larger ball-shaped subsystems on the sphere. For large enough subsystems, the minimal area extremal surfaces probe behind the horizon for an interval of time.

can be viewed as a prediction for the qualitative behaviour of entanglement entropy in actual Euclidean-time-evolved boundary states of holographic CFTs. This can be tested by direct calculation for specific states; obtaining results similar to the ones we find based on the above described simple ansatz would provide a check that our general picture is viable.

As a warm-up for such a direct test, we perform an analogous calculation in a generalization of the SYK model, a coupled-cluster model which includes both all-to-all within-cluster interactions and spatially local between-cluster interactions. Here, the states we consider are analogs of those of [208] extended to include the physics of spatial locality, where in place of the boundary state $|B\rangle$, we have states which are eigenstates of a collection of spin operators formed from pairs of fermions. We numerically calculate the entanglement entropy as a function of time for subsets of various numbers of fermions (as a model for CFT spatial regions on varying size) for a single SYK cluster and for two coupled SYK clusters. We find that the dependence of entanglement entropy on time and on the fraction of the system being considered is qualitatively similar to our predictions for holographic CFT states (compare Figure 4.20 with Figure 4.3), but (as expected) without the sharp features observed in the holographic case. We also give analytical large-N arguments that apply to many clusters, where direct numerical calculation is not possible. These calculations are described in detail in Section 4.4.

It is noteworthy that imaginary time-evolved product states have also been considered in the condensed matter literature. For example, they were proposed as tools to efficiently sample from thermal distributions of spin chains. In that context, they were named minimally entangled typical thermal states (METTS), with the expectation that they would be only lightly entangled [223, 224]. Interestingly, we find that such states are generically highly entangled, unlike what was seen for simple gapped spin chains [223, 224]. One can argue that the low entanglement observed in the finite-size gapped spin chain occurs because of the strong microscopic-scale energy gap. To better understand the holographic and SYK results in some simple models, and with this quantum matter background in mind, we also

give some additional results for spin/qubit models in Appendices C.3 and C.4.

We also consider in Section 4.5 the calculation of holographic complexity [225–227] (both the action and volume versions). These provide additional probes of the behind-the-horizon physics, though their CFT interpretation is less clear. We find interesting differences in behavior between the action and volume versions. While both show the expected linear growth at late times, the volume-complexity increases smoothly from the time-symmetric point $t = 0$, while the action-complexity has a phase transition that separates the late-time growth from an earlier period where the action-complexity is constant.

In Section 4.6, we point out a Rindler analogue of our construction in 2+1 dimensions, where the maximally extended black hole geometry is replaced with empty AdS space divided into complementary Rindler wedges and the microstates are particular states of a CFT on a half-sphere with BCFT boundary conditions. Since the BTZ geometry is obtained as a quotient of pure AdS_3, we can unwind the compact direction and reuse the results of Section 4.3 to determine when knowledge of a boundary subsystem grants access to the region behind the Rindler horizon.

Black hole microstate cosmology

An interesting feature of the geometries we consider is that the geometry on the left side can be thought of as an asymptotically AdS spacetime (the second asymptotic region of the maximally extended geometry) cut off by a UV brane. This is reminiscent of the Randall-Sundrum II scenario for braneworld cosmology. In that case, we have gravity localized on the brane; that is, the physics on the brane can be described (in the case where the full spacetime is $d+1$-dimensional) over a large range of scales by d-dimensional gravity coupled to matter.[61]

Whether or not we have an effective four-dimensional description for

[61] Via another application of the AdS/CFT correspondence, some of the matter, dual to the gravitational physics in the partial second asymptotic region, should be described by a cutoff d-dimensional conformal field theory.

physics in the second asymptotic region will depend on the details of the microstate geometry, in particular on the size of the black hole relative to the AdS scale and to the ETW brane trajectory. These in turn depend on the details of the state we are considering. If there exist states for which the conditions for localized gravity are realized, the effective description of the physics beyond the black hole horizon would correspond to d-dimensional FRW cosmology, where the evolution of the scale factor corresponds to the evolution of the proper size of the ETW brane in the full geometry. This evolution corresponds to an expanding and contracting FRW spacetime which classically starts with a big bang and ends with a big crunch, though we expect that the early and late time physics does not have a good d-dimensional description.

Since the states we are describing are simply specific high-energy states in our original CFT, the original CFT should provide a complete microscopic description of this cosmological physics. A very optimistic scenario is that for the right choice of four-dimensional CFT (or other non-conformal holographic theory) and black hole microstate, the effective four-dimensional description of the dynamics of the ETW brane could match with the cosmology in our universe. In this case, the CFT itself could be supersymmetric[62]; the effective theory on the ETW brane will be related to the choice of state in the CFT and need not have unbroken supersymmetry. The small cosmological constant would be explained by having a large central charge in the CFT together with some properties of the CFT state we are considering.

Even if the relevant cosmologies turn out not to be realistic, it is intriguing that CFTs could provide a microscopic description of interesting cosmological spacetimes, since the usual applications of AdS/CFT describe spacetimes whose asymptotics are static.[63] Understanding how to generalize AdS/CFT to provide a non-perturbative formulation of quantum gravity in cosmological situations is among the most important open questions in the field, so it is very interesting to explore whether the scenario we describe

[62] Perhaps it could even be $\mathcal{N} = 4$ supersymmetric Yang-Mills theory.

[63] There have been many other approaches to describing cosmological physics using holography. For examples, see [228–233].

can be realized in microscopic examples.

In Section 4.7, we give a more detailed review of Randall-Sundrum II cosmology and the conditions for localizing gravity. We then explore whether these conditions can be met in the simple class of geometries with a constant tension ETW brane. Our analysis suggests that realizing the localized cosmology requires considering a black hole which is much larger than the AdS scale, and an ETW brane tension that is sufficiently large. Unfortunately, while the Lorentzian geometries corresponding to these parameters are sensible, our analysis in Section 4.2 suggests that for CFT states corresponding to these parameter values, a different branch of solutions for the dual gravity solution may be preferred. However, a more complete holographic treatment for the BCFT physics will be required in order to reach a more decisive conclusion.

Finally, in Section 4.8, we comment on various possible generalizations and future directions.

4.2 Microstates with behind-the-horizon geometry

In this section, we describe a specific class of CFT excited states which describe certain black hole microstates when the CFT is holographic. For these states, it is possible to plausibly describe the full black hole geometry, at least approximately. These states were suggested and studied in the context of the SYK model by [208], and later studied directly in the context of holographic CFTs in [209]. Simple specific examples of these states and the corresponding geometries have been discussed earlier, for example in [41, 219, 234]. The microstate geometries will be time-dependent and hence "non-equilibrium"; for a different construction of non-equilibrium microstates with geometry behind the horizon, see [235]. In this section, we will review and generalize those discussions, starting with the definition of the CFT states and then moving to the geometrical interpretation. We will make use of this specific construction in the remainder of the chapter in

order to have an example where we can do explicit calculations.

4.2.1 CFT states

The states we consider, suggested in [208], have two equivalent descriptions. First, consider the thermofield double state of two CFTs (on S^d) which we will call the left and right CFTs,

$$|\Psi^\beta_{\rm TFD}\rangle = \frac{1}{Z_\beta}\sum e^{\frac{-\beta E_i}{2}}|E_i\rangle_L \otimes |E_i\rangle_R \ . \tag{4.1}$$

For high enough temperatures, this corresponds to the maximally extended AdS-Schwarzschild black hole geometry. Now consider projecting this state onto some particular pure state $|B\rangle$ of the left CFT. This could be the result of measuring the state on the left. We will be more specific about the pure state $|B\rangle$ later on. The result is a pure state of the right CFT given by

$$|\hat{\Psi}^\beta_B\rangle = \frac{1}{Z_\beta}\sum e^{\frac{-\beta E_i}{2}}\langle B|E_i\rangle|E_i\rangle \ . \tag{4.2}$$

We can think of this state as the result of measuring the state of the left CFT. If this measurement corresponds to looking at the state of local (UV) degrees of freedom, we might expect that the effects on the corresponding geometry propagate inwards causally (forward and backward, since we will be considering time-symmetric states) from near the left boundary, so that the geometry retains a significant portion of the second asymptotic region. This motivates considering states $|B\rangle$ with no long-range entanglement.

We can also consider a closely related state $|\Psi^\beta_B\rangle$ obtained by complex conjugation of the coefficients in the superposition,

$$\begin{aligned} |\Psi^\beta_B\rangle &= \frac{1}{Z_\beta}\sum e^{\frac{-\beta E_i}{2}}\langle E_i|B\rangle|E_i\rangle \\ &= \frac{1}{Z_\beta}\sum e^{\frac{-\beta E_i}{2}}|E_i\rangle\langle E_i|B\rangle \\ &= \frac{1}{Z_\beta}e^{-\beta H/2}|B\rangle \ . \end{aligned} \tag{4.3}$$

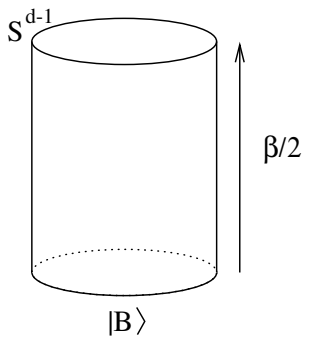

Figure 4.4: Path integral description of black hole microstates $|\Psi_B^\beta\rangle$.

We recall that the operation $|\hat{\Psi}_B^\beta\rangle \to |\Psi_B^\beta\rangle$ is anti-linear and anti-unitary and corresponds to the operation of time-reversal. For example, given any Hermitian $\mathcal{O}$ we have that

$$\langle \Psi_B^\beta(t)|\mathcal{O}|\Psi_B^\beta(t)\rangle = \langle \hat{\Psi}_B^\beta(-t)|\mathcal{O}|\hat{\Psi}_B^\beta(-t)\rangle \ . \tag{4.4}$$

In our case, we will consider states which are time-reversal symmetric, so the two definitions are equivalent.

We see from (4.3) that the states $|\Psi_B^\beta\rangle$ correspond to starting from a state $|B\rangle$ and having a finite amount of Euclidean evolution. These states are naturally defined by a Euclidean path integral as shown in Figure 4.4. Since the CFT path integral for holographic theories maps onto the gravity path integral, we will be able to make use of the AdS/CFT corresponence to deduce the corresponding geometries if we can choose states $|B\rangle$ for which we can understand a gravity prescription for dealing with the boundary condition at the initial Euclidean time.

Euclidean evolution of CFT boundary states

In the CFT context, a nice class of states to consider for the states $|B\rangle$ are certain *boundary states* of the CFT, as suggested in [208] and explored in detail in [209]. For any CFT, we can ask whether it is possible to define the theory on a manifold with boundary. In general, there will be a family

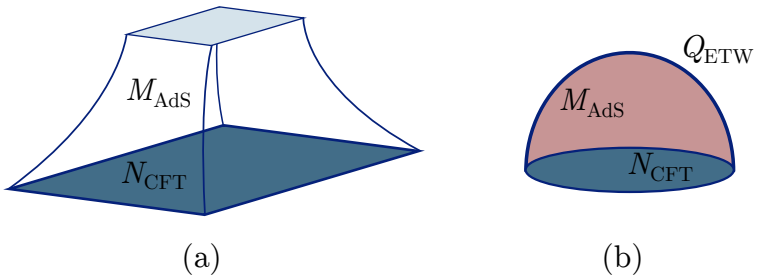

Figure 4.5: (a) The AdS/CFT correspondence, with an asymptotically AdS bulk M_{AdS} and an asymptotic boundary $N_{\text{CFT}} = \partial M_{\text{AdS}}$. (b) The AdS/BCFT correspondence. We add a boundary to the CFT, whose holographic "image" is the ETW brane Q.

of distinct theories corresponding to different allowed boundary conditions. Some of these boundary conditions are special in the sense that they preserve some of the conformal symmetry of the theory; specifically, the vacuum state of the CFT on a half space with such a boundary condition would preserve $SO(2, d-1)$ of the $SO(2, d)$ conformal symmetry.

For each of these allowed boundary conditions, we can associate a boundary state $|B\rangle$ for the CFT on S^{d-1} by saying that choosing this state in (4.3) is equivalent to the state obtained from the Euclidean path integral with our chosen boundary condition at $\tau = -\beta/2$. The boundary state itself (equal to $|\Psi_B^\beta\rangle$ in the limit $\beta \to 0$) is singular and has infinite energy. It also can be understood to have no long range entanglement, as we motivated above [236]. However, the Euclidean evolution suppresses the high-energy contributions to give a state with finite energy. The states $|\Psi_B^\beta\rangle$ are generally time-dependent and were considered by Cardy and collaborators in studying quantum quenches [221, 222, 237].

For our purposes, the boundary states are interesting since now the description of our states is completely in terms of a Euclidean path integral with a specific boundary condition for the CFT at $\tau = -\beta/2$.

4.2.2 Holographic model

In [78] and [87, 88], these boundary conditions were discussed in the context of AdS/CFT. These references proposed that the gravitational dual for a CFT with boundary should be some asymptotically AdS spacetime with a dynamical IR boundary that forms an extension of the CFT boundary into the bulk, as depicted in Figure 4.5. For simplicity, the physics of this boundary was modeled by an end-of-the-world brane with constant tension, and a Neumann boundary condition ensuring that no energy/momentum flows through the brane. A modified proposal for how to treat the boundary conditions was presented recently in [238], but for the cases we consider, the proposals are equivalent.

It is convenient to introduce a dimensionless tension parameter T defined so that the stress-energy tensor on the ETW brane is

$$8\pi G T_{ab} = (1-d) T g_{ab}/L_{\text{AdS}} \,, \tag{4.5}$$

where T can be positive or negative. The parameter T is related to properties of the boundary state; we will review the physical significance of this parameter in the CFT below. The gravitational action including bulk and boundary terms is then given as

$$\begin{aligned} I_{\text{bulk}} + I_{\text{ETW}} = \frac{1}{16\pi G}\int_{M_{\text{AdS}}} \mathrm{d}^{d+1}x\,\sqrt{-g}\,(R-2\Lambda) \\ + \frac{1}{8\pi G}\int_{Q_{\text{ETW}}} \mathrm{d}^{d}y\,\sqrt{-h}\,(K-(d-1)T/L_{\text{AdS}})\,, \end{aligned} \tag{4.6}$$

where $\Lambda = -d(d-1)/2L_{\text{AdS}}^2$. With this simple model, various expected properties of boundary CFT were shown to be reproduced via gravity calculations. In [87] and [88], the boundary conditions were taken as spatial boundary conditions for a CFT on an interval or strip, but we can apply the same model in our case with a past boundary in Euclidean time.

For general holographic BCFTs, we expect that the boundary action would be more complicated; it could include general terms involving intrinsic and extrinsic curvatures, sources for various bulk fields, and additional

fields localized to the boundary. However, for this chapter, we will focus on studying the simple one-parameter family of models as proposed in [78, 87].

Relation between tension and boundary entropy in 1+1 dimensions

The significance of the tension parameter T may be understood most simply for the case of 1+1 dimensional conformal field theories. In that case, each conformally invariant boundary condition may be characterized by a parameter g that can be understood as a boundary analogue of the central charge [81, 160]. We can define g by

$$g = \langle 0|B\rangle \tag{4.7}$$

which has the interpretation of the disk partition function, computed with the boundary conditions associated with $|B\rangle$. Along boundary RG flows (defined by deforming a BCFT by some boundary operator), the parameter g always decreases [84]. This parameter g also appears in the expression for the vacuum entanglement entropy for the CFT on a half line [239]. The entanglement entropy for an interval of length L including the boundary is given in general by

$$S(L) = \frac{c}{6}\log\left(\frac{L}{\epsilon}\right) + \log(g)\ . \tag{4.8}$$

Here, the second term is known as the *boundary entropy* and in general can have either sign.

Using the holographic prescription, Takayanagi computed both the disk partition function and the entanglement entropy for intervals on a half line, showing that in both cases, the holographic calculation matches with the CFT result if the tension parameter is related to the boundary entropy by

$$\log g = \frac{L_{\mathrm{AdS}}}{4G}\mathrm{arctanh}(T)\ . \tag{4.9}$$

Thus, larger values of the tension correspond to larger boundary entropy, or

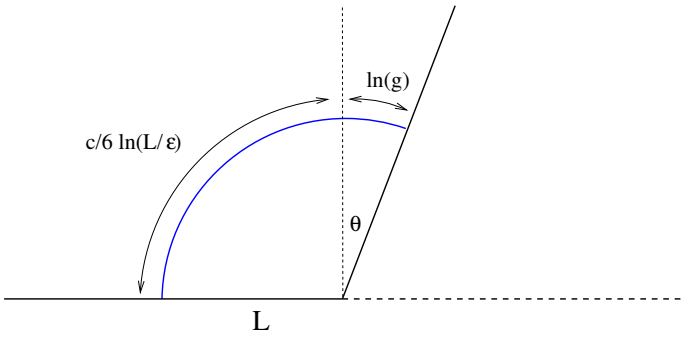

Figure 4.6: Calculation of entanglement entropy for an interval of length L including the boundary in the vacuum state of a holographic BCFT. The geometry is locally Poincaré-AdS, with the ETW brane at a constant angle $\theta = \arcsin(T)$. The boundary entropy is the $x > 0$ portion of the RT area.

more degrees of freedom associated with the boundary. We expect that this qualitative relationship also holds in higher dimensions.

Geometrically, the tension parameter T determines the angle at which the ETW brane intersects the boundary, via $T = \sin(\theta)$; this also holds in higher dimensions [88]. As an example, Figure 4.6 depicts the calculation of entanglement entropy for an interval including the boundary in the vacuum state of a holographic BCFT.

4.2.3 Microstate geometries from Euclidean-time-evolved boundary states

We now make use of the simple holographic BCFT recipe to deduce the microstate geometries associated with Euclidean-time-evolved boundary states

$$|\Psi\rangle = e^{-\tau_0 H}|B\rangle. \tag{4.10}$$

This was already carried out for 1+1 dimensional CFT states in [209]. We review their calculations and generalize to higher dimensions.

We are considering a CFT on a spatial S^{d-1} with the state prepared by a Euclidean path integral with boundary conditions in the Euclidean past at $\tau = -\tau_0$. We would like to work out a Lorentzian geometry dual to our state.

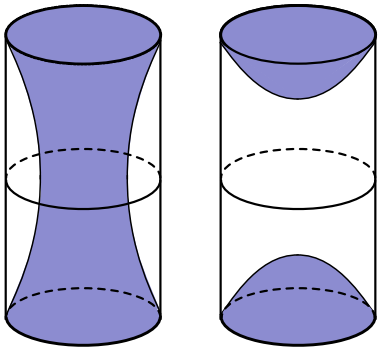

Figure 4.7: Euclidean gravity solutions corresponding to the CFT path integral for $\langle B|e^{-\beta H}|B\rangle$. The boundary geometry is a cylinder $S^d \times [-\tau_0, \tau_0]$. The phase with a connected ETW brane configuration (left), dominant for small τ_0, gives rise to a Lorentzian black hole geometry.

We start by noting that $t = 0$ correlators in our state $|\Psi_B^{\tau_0}\rangle$ may be computed via the Euclidean path integral on S^{d-1} times an interval of Euclidean time $\tau \in [-\tau_0, \tau_0]$, with operators inserted at $\tau = 0$. Holographically, this can be computed using the extrapolate dictionary as a limit of bulk correlators in a Euclidean geometry with boundary $S^{d-1} \times [-\tau_0, \tau_0]$ that is determined by extremizing the gravitational action with appropriate boundary terms for the ETW brane. This geometry is time-reversal symmetric. To find the Lorentzian geometry associated with our state, we take the $\tau = 0$ bulk slice as the initial data for our Lorentzian solution (which will also be time-reversal symmetric).

There are two possible configurations of the ETW brane in the Euclidean solution, depending on the values of T and τ_0, as shown in Figure 4.7. The configuration which dominates the gravitational path integral is the one with lower action. For some values of T we can have a transition between these solutions analogous to the Hawking-Page transition. Above a critical value $\tau_{\text{crit}}(T)$, the lower action configuration is a portion of Euclidean AdS, and the Lorentzian solution will be pure AdS with a small amount of quantum matter (as we have for the dual of a finite temperature CFT below the Hawking-Page transition). For $\tau_0 < \tau_{\text{crit}}(T)$, the Lorentzian solution corresponds to a part of the AdS-Schwarzschild geometry. For $T > 0$, this includes the full

exterior solution plus spacetime behind the horizon terminating with the ETW brane.

In Appendix C.1, we present a detailed derivation of the Euclidean and Lorentzian solutions corresponding to the Euclidean-time-evolved boundary states; here, we summarize the basic results.

Euclidean solutions

We begin by describing the Euclidean solutions for each of the phases. In each case, the boundary geometry is taken to be a sphere S^{d-1} with unit radius times an interval $[-\tau_0, \tau_0]$. For the case $d = 2$, our calculation is actually equivalent to a calculation in [88], who considered the Euclidean solutions associated with the path integral for a BCFT defined on an interval (i.e. with two boundaries) at finite temperature. In that case, the interval $[-\tau_0, \tau_0]$ represented the spatial direction, while the S^1 was the thermal circle.

Since the states we consider preserve spherical symmetry, the relevant geometries will also be spherically symmetric, and must therefore locally be described by the Euclidean AdS-Schwarzschild geometry,

$$ds^2 = f(r)d\tau^2 + \frac{dr^2}{f(r)} + r^2 d\Omega_{d-1}^2 \tag{4.11}$$

with

$$f(r) = \frac{r^2}{L_{\text{AdS}}^2} + 1 - \frac{r_H^{d-2}}{r^{d-2}}\left(\frac{r_H^2}{L_{\text{AdS}}^2} + 1\right) . \tag{4.12}$$

Here, the value of r_H will depend on which phase we are in and on the values of τ_0 and T. The periodicity of τ (for $r_H > 0$) is determined by smoothness at $r = r_H$ to be $\tau \sim \tau + \beta$ with

$$\beta = \frac{4\pi r_H L_{\text{AdS}}^2}{(d-2)L_{\text{AdS}}^2 + d r_H^2} . \tag{4.13}$$

This relates the inverse black hole temperature to r_H.

For convenience, we will set $L_{\text{AdS}} = 1$ in much of the following.

Black hole phase

We will mainly be interested in the "black hole" phase in which the ETW brane is connected and takes the form shown on the left in Figure 4.7. Describing the spherically symmetric brane embedding by $r(\tau)$ we find that the equations of motions for the brane imply that the trajectory obeys

$$\frac{dr}{d\tau} = \frac{f(r)}{Tr}\sqrt{f(r) - T^2 r^2} \ . \tag{4.14}$$

Solutions that are symmetric about $\tau = 0$ will have $\frac{dr}{d\tau} = 0$ for $\tau = 0$, with r equal to some minimum value r_0 determined in terms of T and r_H by

$$f(r_0) = T^2 r_0^2 \ . \tag{4.15}$$

This gives the maximum ETW brane radius in the Lorenzian solution. As we increase T, the ratio r_0/r_H increases monotonically from 1 at $T = 0$. In $d = 2$, we have simply

$$\frac{r_0}{r_H} = \frac{1}{\sqrt{1 - T^2}} \ , \tag{4.16}$$

while in higher dimensions, we will see below that this ratio reaches a finite maximum value.

The brane locus is then given by

$$\tau(r) = \int_{r_0}^{r} d\hat{r} \frac{T\hat{r}}{f(\hat{r})\sqrt{f(\hat{r}) - T^2\hat{r}^2}} \ . \tag{4.17}$$

A typical solution for $T > 0$ is depicted in Figure 4.8. On the left, the full disk represents the r, τ coordinates of the Euclidean Schwarzschild geometry, with r ranging from r_H at the center to infinity at the boundary. We have an S^{d-1} of radius r associated with each point. The ETW brane bounds a portion of the spacetime (shaded) that gives the Euclidean geometry associated with our state. This has a time-reflection symmetry about the horizontal axis. The invariant codimension one surface (blue dashed line) gives the $t = 0$ geometry (depicted on the right) for the associated Lorentzian solution. In this picture, the minimum radius sphere corresponds to the black

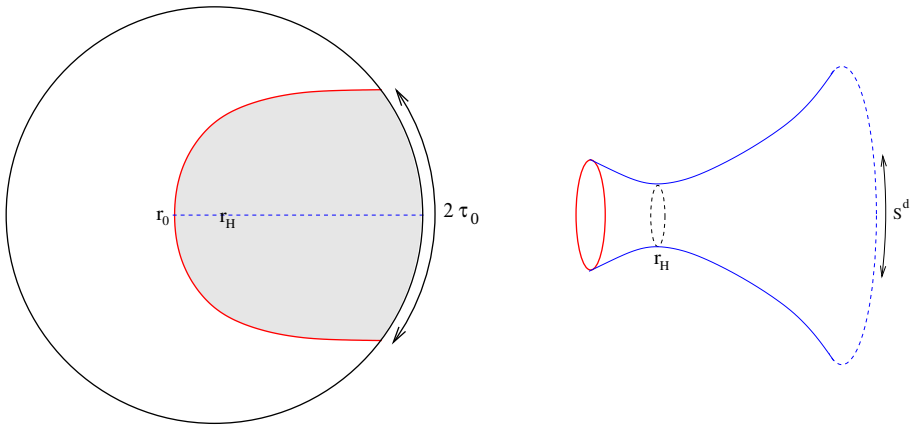

Figure 4.8: Euclidean geometry associated with a $T > 0$ state. Left: ETW brane trajectory on the (r, τ)-plane, with $r = r_H$ at the center and $r = \infty$ represented as the boundary of the disk. We have an S^{d-1} of radius r associated with each point. Right: spatial geometry fixed by time-reflection symmetry (blue dashed line on the left). This provides the initial data for the Lorentzian solution.

hole horizon, so we see that the ETW brane is behind the horizon. For $T < 0$, we obtain the same trajectories, but the geometry corresponds to the unshaded part, and the ETW brane from the initial data slice is outside the horizon.

For a given r_H and T, the Euclidean preparation time τ_0 associated with the solution corresponds to half the range of τ bounded by the ETW brane at the AdS boundary. This is given explicitly by

$$\tau_0 = \frac{2\pi r_H}{(d-2) + d r_H^2} - \int_{r_0}^{\infty} dr \frac{Tr}{f(r)\sqrt{f(r) - T^2 r^2}} \,. \tag{4.18}$$

For a specified tension T and preparation time τ_0, the temperature of the corresponding black hole is determined implicitly by this equation. There can be more than one pair r_H that gives the same τ_0 for fixed T, but in this case, the solution with smaller r_H is never the minimum action solution.

For $d = 2$, we find that for every value of T and r_H, the ETW brane trajectory meets the boundary of the (r, τ) disc at antipodal points, so the

black hole temperature is very simply related to the Euclidean preparation time,

$$\tau_0 = \frac{\beta}{4} = \frac{\pi}{2r_H} \ . \tag{4.19}$$

In this case, the ETW brane radius on the initial data slice is

$$r_0 = \frac{r_H}{\sqrt{1-T^2}} \ , \tag{4.20}$$

so the region behind the horizon can become arbitrarily large as we take $T \to 1$.

For $d > 2$ we find that Euclidean solutions in this phase exist only for a portion of the (τ_0, T)-plane, shown for $d = 4$ in Figure 4.9. In particular, for any r_H, there is a value $T_*(r_H)$ above which there are no Euclidean solutions with a connected ETW brane (corresponding to a Lorentzian black hole geometry). The values $T_*(r_H)$ converge to some finite $T_{\max}$ in the large r_H limit, giving an absolute maximum value for T above which no such solutions exist.

- For $d = 3$, we find $T_{\max} \approx 0.95635$. This leads to a maximum value of $\max_{r_H}\{r_0/r_H\} \approx 2.2708$ for the ratio of the ETW brane radius to the horizon radius.
- For $d = 4$, we find $T_{\max} \approx 0.79765$. This leads to a maximum value of $\max_{r_H}\{r_0/r_H\} \approx 1.2876$ for the ratio of the ETW brane radius to the horizon radius.

For $T > T_*(r_H)$, the corresponding Euclidean solutions are not sensible since the ETW brane overlaps itself, as shown on the left in Figure 4.10. In this case, the thermal AdS geometry (with disconnected ETW branes bounding the Euclidean past and future in the Euclidean solution) is apparently the only possibility.

Pure AdS phase

For any value of τ_0 and $T > 0$, we can also have a Euclidean solution where the ETW brane has two disconnected components as shown on the right

in Figure 4.7. The Euclidean geometry is a portion of pure Euclidean AdS (described by the metric in (4.11) with $f(r) = r^2 + 1$) bounded by the two branes. We can parameterize the brane embedding by $\tau(r)$ with $\tau(\infty) = \pm\tau_0$ for the upper and lower brane respectively. The equations determining the brane location are the same as in the previous case since the geometry takes the same form, so we find that the brane embedding is given by

$$\tau(r) - \tau_0 = \int_r^\infty d\hat{r} \frac{T\hat{r}}{f(\hat{r})\sqrt{f(\hat{r}) - T^2\hat{r}^2}} \,, \tag{4.21}$$

with $f(r) = r^2 + 1$. Integrating, we find (in any dimension)

$$\tau(r) - \tau_0 = \text{arcsinh}\left(\frac{T}{\sqrt{r^2+1}\sqrt{1-T^2}}\right) \tag{4.22}$$

The negative τ component of the ETW brane is obtained via $\tau \to -\tau$.

Comparison of the gravitational actions

In order to determine which type of solution leads to the classical geometry associated with our state for given (τ_0, T), we need to compare the gravitational action for solutions from the two phases. For $d = 2$, this calculation was carried out in [88] (Section 4) while studying the Hawking-Page type transition for BCFT on an interval. Our calculations in Appendix C.1 generalize this to arbitrary dimensions. In order to compare the actions, we need to regularize; in each case, we can integrate up to the r corresponding to $z = \epsilon$ in Fefferman-Graham coordinates and then take the limit $\epsilon \to 0$ after subtracting the actions for the two phases.

As examples, we find that for $d = 2$, we have

$$\lim_{\epsilon\to 0}(I_E^{\text{AdS}}(T, \tau_0, \epsilon) - I_E^{\text{BH}}(T, \tau_0, \epsilon)) \\ = \frac{1}{2G}\left[-\text{arctanh}(T) - \frac{\tau_0}{2} + \frac{\pi^2}{8\tau_0}\right] \,. \tag{4.23}$$

Thus, our states (for a CFT on a unit circle) correspond to bulk black holes

when

$$\tau_0 < -\text{arctanh}(T) + \sqrt{\frac{\pi^2}{4} + \text{arctanh}^2(T)} \,. \tag{4.24}$$

This phase boundary is shown in Figure 4.9. Our result agrees with the calculation of [88] (reinterpreted for our context).

For $d = 4$, the action difference is given in equation (C.25) in the appendix. The resulting phase boundary is shown in Figure 4.9; the critical τ_0 decreases from $\pi/6$ at $T = 0$ to 0 at $T = T_{\text{max}}$. We see that for $T > 0$, the black hole solutions typically have lower action when they exist.

It is somewhat surprising that the black hole phase never dominates (and doesn't even exist) for any value of T above T_{max}, since taking τ_0 sufficiently small would be expected to lead to a state of arbitrarily large energy, which should correspond to a black hole in the Lorentzian picture. One possible resolution to this puzzle is that among the possible conformally invariant boundary conditions for holographic CFTs, there may not exist examples that correspond to $T > T_*$ in our models. Our Euclidean gravity results could be seen as a prediction of some constraints on the possible boundary conditions for holographic CFTs (and specifically on a higher-dimensional analogue of boundary entropy).

Alternatively, the simple prescription of holographically modelling the CFT boundary by introducing a bulk ETW brane with some constant tension may not be adequate to model boundary conditions which naively correspond to larger values of T. For example, about T_*, solving the equations to determine the Euclidean trajectory naively gives a result that folds back on itself. But a more complete model of the ETW brane physics would presumably include interactions of the brane with itself that invalidate our naive analysis. For example, an effective repulsion could turn a naively unphysical solution into a physical one, as shown in Figure 4.10.

Lorentzian geometries

To find the Lorentzian geometries associated with our states, we use the $\tau = 0, \pi$ slice of the Euclidean geometry as initial data for Lorenztian evolution. The resulting geometry is a portion of the maximally extended black

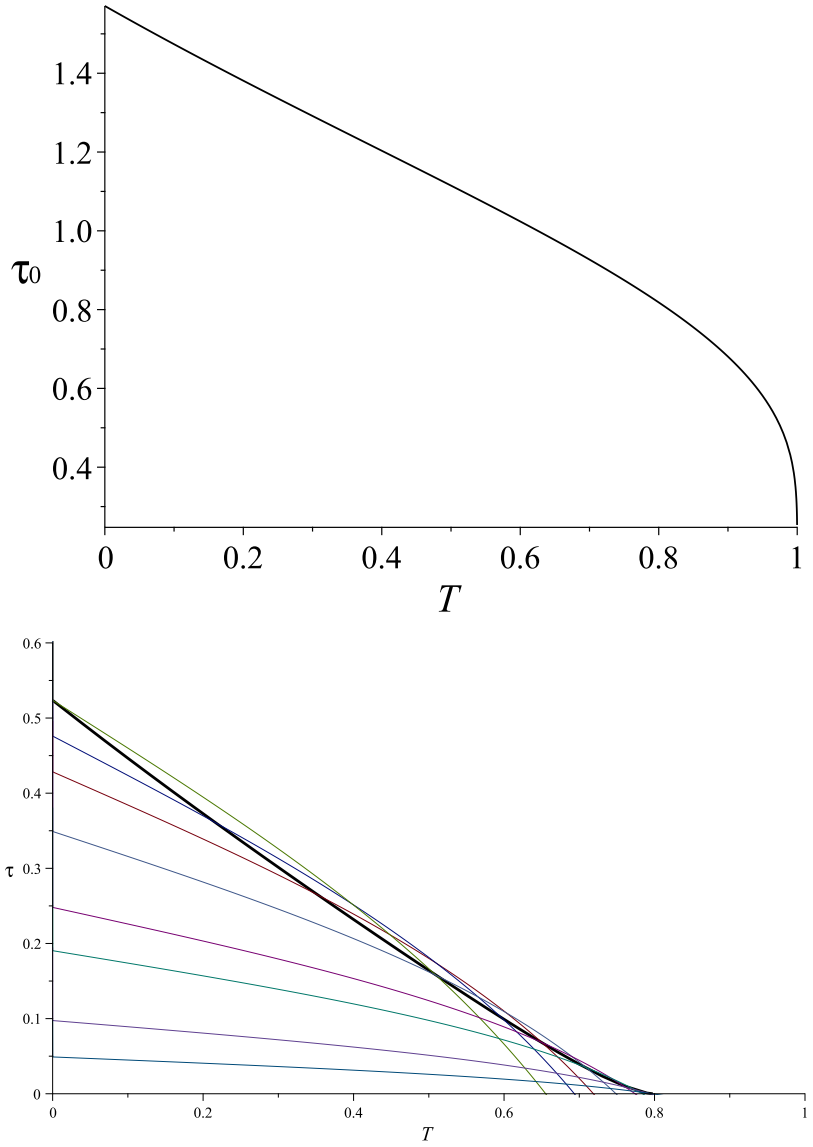

Figure 4.9: Critical value of τ_0 vs T for $d = 2$ (top) and $d = 4$ (bottom). The thick curve on the right shows the phase boundary below which the black hole phase dominates. The other curves on the right show $\tau_0(T)$ for fixed values of r_H, equal to 1, 1.25, 1.5, 2, 3, 4, 8, and 16 from top to bottom on the left. Where the curves overlap in the black hole phase region, the value of r_H for the physical solution is always the larger one.

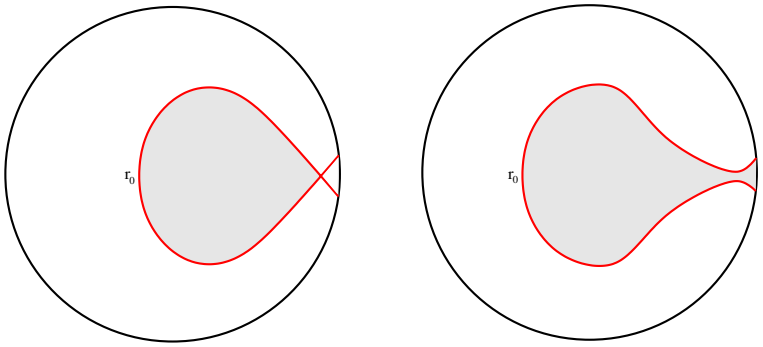

Figure 4.10: (Left) Euclidean ETW brane trajectories for dimension $d > 2$ and $T_*(r_H) < T < T_{\rm crit}$. The naive ETW brane trajectory overlaps itself. (Right) A possible alternative picture in a more complete holographic model with self-interactions of the ETW brane.

hole geometry, with one side truncated by a dynamical ETW brane. These Lorentzian geometries parallel earlier results on domain walls and thin shells in AdS [240–242].[64]

For $T > 0$, we will see that the brane emerges from the past singularity, expands into the second asymptic region and collapses again into the future singularity. For $T < 0$ we have an equivalent ETW brane trajectory but on the other side of the black hole, so that the brane emerges from the horizon, enters the right asymptotic region, and falls back into the horizon.

Using Schwarzschild coordinates to describe the portion of the ETW brane trajectory in one of the black hole exterior regions, the brane locus is given by the analytic continuation of the Euclidean trajectory,

$$t(r) = \int_{r_0}^{r} d\hat{r} \frac{T\hat{r}}{f(\hat{r})\sqrt{T^2\hat{r}^2 - f(\hat{r})}} \,. \tag{4.25}$$

For example, in $d = 2$, we obtain

$$\cosh(tr_H)\sqrt{\frac{r^2}{r_H^2} - 1} = \frac{T}{\sqrt{1-T^2}} \,. \tag{4.26}$$

[64] Indeed, the Neumann condition reduces to the thin shell junction condition where the extrinsic curvature on the "excised" side of the brane vanishes.

To understand the behaviour of the brane in the full spacetime, it is convenient to rewrite the equation in terms of the proper time λ on the brane, related to Schwarzschild time by

$$\frac{dt}{d\lambda} = \gamma = \sqrt{\frac{f(r)}{f(r)^2 - \dot{r}^2}} \ . \tag{4.27}$$

We then find that the coordinate-independent equation of motion for the brane relating the proper radius r to the proper time λ is simply

$$\dot{r}^2 + [f(r) - T^2 r^2] = 0 \ , \tag{4.28}$$

where now the dot indicates a derivative with respect to proper time. In terms of $L = \log(r)$, this becomes simply

$$\dot{L}^2 + V(L) = T^2 \tag{4.29}$$

where

$$V(L) = \frac{f(r)}{r^2} = 1 + e^{-2L} - e^{-d(L-L_H)}(1 + e^{-2L_H}) \ . \tag{4.30}$$

So the trajectory $L(\lambda)$ is that of a particle in a one-dimensional potential $V(L)$ with energy T^2. These potentials take the form shown in Figure 4.11.

Considering general values of T, we can have five classes of trajectories (two for $d = 2$), as shown in Figure 4.11. However, all of our time-symmetric Euclidean solutions in the black hole phase correspond to values $T < 1$ (corresponding to case (a) in Figure 4.11) for which the Lorentzian trajectory starts at $r = 0$, increases to $r = r_0$ and decreases back to $r = 0$. Thus, the brane emerges from the past singularity, reaches a maximum size r_0, and shrinks again to $r = 0$ at the future singularity.

Using the proper time parametrization, the worldvolume metric for the brane takes the close FRW form

$$ds_d^2 = -d\lambda^2 + r(\lambda)^2 d\Omega_{d-1}^2 \ , \tag{4.31}$$

where the scale factor $r(\lambda)$ is determined from equation (4.28). The entire

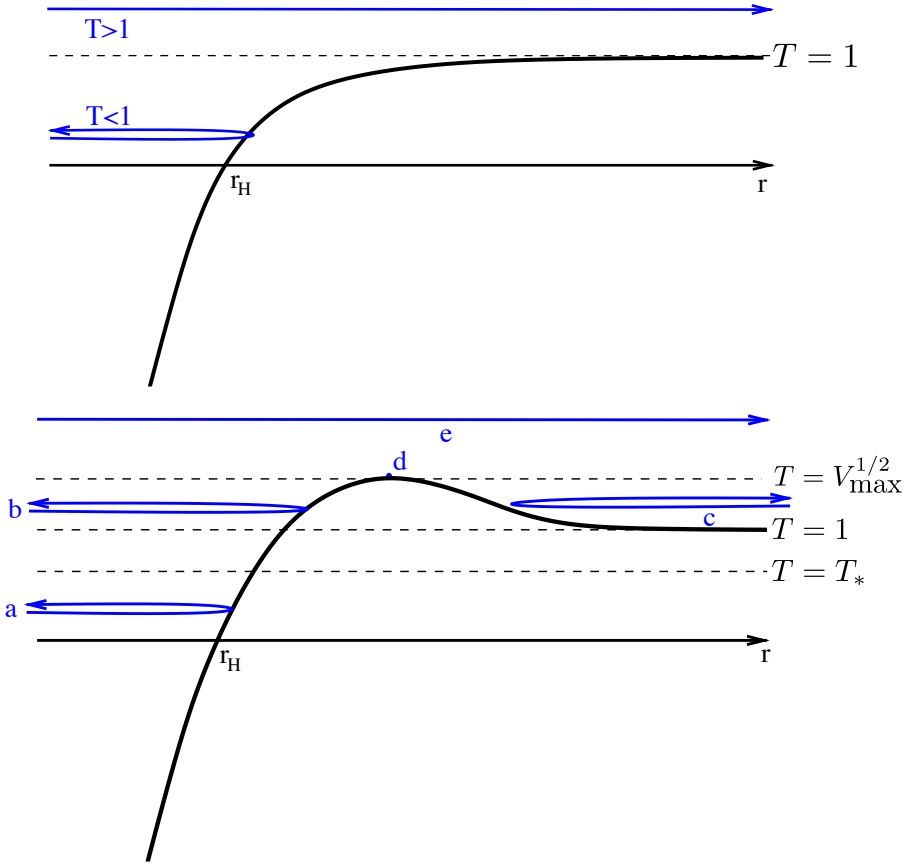

Figure 4.11: Effective potential $V(L)$ and types of Lorenzian ETW brane trajectories for $d = 2$ (top) and $d > 2$ (bottom).

trajectory covers some finite amount of proper time given by

$$\lambda_{\rm tot} = 2\int_0^{r_0} \frac{dr}{\sqrt{T^2 r^2 - f(r)}} \ . \tag{4.32}$$

For $d = 2$, the explicit scale factor in the worldvolume metric is

$$r(\lambda) = \frac{r_H}{1-T^2}\cos(\lambda\sqrt{1-T^2}) \tag{4.33}$$

and the total proper time for the evolution is

$$\lambda_{\rm tot}^{d=2} = \frac{\pi}{\sqrt{1-T^2}} \ . \tag{4.34}$$

For $d = 4$, the scale factor is

$$r(\lambda) = \frac{\left[\cos(2\sqrt{1-T^2}\lambda)\sqrt{1+4(1-T^2)r_H^2(1+r_H^2)}-1\right]^{\frac{1}{2}}}{\sqrt{2(1-T^2)}} \tag{4.35}$$

and the total proper time for the evolution is

$$\lambda_{\rm tot}^{d=4} = \frac{1}{\sqrt{1-T^2}}\arccos\left(\frac{1}{\sqrt{1+4(1-T^2)r_H^2(1+r_H^2)}}\right) \ . \tag{4.36}$$

The $d = 3$ results are given in terms of elliptic integrals.

We briefly discuss the remaining trajectories in Appendix C.1, in case they may be relevant to some other class of CFT states. In Section 4.7 we discuss the possibility that for certain parameter ranges, we can have gravity localized to the ETW brane, so that the FRW metrics here would represent cosmological solutions of an effective d-dimensional theory of gravity.

4.3 Probing behind the horizon with entanglement

In this section, we consider the holographic calculation of entanglement entropy for CFT states whose dual geometries are captured by Figure 4.1. We will continue to use the simple model of a spacetime terminating with an ETW brane, but we expect the same qualitative conclusions when the ETW brane is replaced by a more complete microscopic description. We begin by considering a general behind-the-horizon ETW brane trajectory $r(t)$ symmetric about $t = 0$ with maximum radius $r(0) = r_0$.

We will consider the entanglement entropy for ball-shaped regions on the sphere as a function of size and of CFT time. As depicted in Figure 4.2, we have extremal surfaces that stay outside the horizon, but we can also have extremal surfaces that enter the horizon and end on the ETW brane.[65] Depending on the value of time and the ball size, we can have transitions between which type of surface has least area. In the phase where the exterior surface has less area, the CFT entanglement entropy will be time-independent (at leading order in large N), while in the other phase, we will have time-dependence inherited from the time-dependent ETW brane trajectory. In our examples below, we will find that in favourable cases, the minimal area surface for sufficiently large balls goes behind the horizon during some time interval $[-t_0, t_0]$ which increases with the size of the ball.

We now turn to the details of the holographic calculation of entanglement entropy given some ETW brane trajectory $r(t)$. This was calculated for the $T = 0$ case in [219]. Similar methods were used in slightly more exotic geometries, and reaching different conclusions, in [243].

[65] We recall that the topological constraint on the extremal surfaces is that they are homologous to the boundary region under consideration. This means that the surface together with the boundary region form the boundary of some portion of a spatial slice of the bulk spacetime. The relevant regions in the two cases are shown as the shaded regions in Figure 4.2. In the case where the extremal surfaces go behind the horizon and terminate on the ETW brane, this region includes part of the ETW brane. We emphasize that this is not part of the extremal surface and its area should not be included in the holographic calculation of entanglement entropy.

Exterior extremal surfaces

First, consider the exterior extremal surfaces, working in Schwarzschild coordinates. Let θ_0 be the angular size of the ball, such that $\theta_0 = \pi/2$ corresponds to a hemisphere.

Since the exterior geometry is static, the extremal surface lives in a constant t slice, and we can parameterize it by $r(\theta)$. In terms of this, the area is calculated as

$$\text{Area}_{\text{ext}} = \omega_{d-2} \int d\theta \, r^{d-2} \sin^{d-2}\theta \sqrt{r^2 + \frac{1}{f(r)}(r')^2} \, . \tag{4.37}$$

where ω_{d-2} is the volume of a $(d-2)$-dimensional sphere.

Extremizing this action, we obtain equations of motion that can be solved numerically (or analytically in the $d = 2$ case — see below).

To obtain a finite result for entanglement entropy, we can regulate by integrating up to some fixed $r_{\max}$ corresponding to $z = \epsilon$ in Fefferman-Graham coordinates, subtracting off the vacuum entanglement entropy (calculated in the same way but with $f(r) = r^2 + 1$), and then taking $\epsilon \to 0$.

Interior extremal surfaces

To study extremal surfaces that pass through the horizon, it is convenient to work in a set of coordinates that cover the entire spacetime. In this case, we parameterize the surfaces by a time coordinate and a radial coordinate, which are both taken to be functions of an angle θ on the sphere.

The only new element here is that the extremal surfaces intersect the ETW brane, and we need to understand the appropriate boundary conditions here. Since we are extremizing area, our extremal surfaces must intersect the ETW brane normally, so that a variation of the intersection locus does not change the surface area to first order.

Criterion for seeing behind the horizon with entanglement

When the behind-the-horizon extremal surfaces have less area, the CFT entanglement is detecting a difference between our state and the thermal state. We expect that this is most likely to happen for $\theta = \pi/2$, where we are looking at the largest possible subsystem, and for $t = 0$, since at other times the state will become more thermalized.

For this case $\theta_0 = \pi/2$, $t = 0$, the behind-the-horizon extremal surface remains at $\theta = \pi/2$ and $t = 0$, extending all the way to the ETW brane on the far side of the horizon. This intersects the ETW brane normally by the time-reflection symmetry. In this case, we can calculate the regulared areas explicitly as

$$\begin{aligned}&\text{Area}_{\text{int}}(\theta = \pi/2, t = 0, r_0) \\ &\qquad = \omega_{d-2} \int_{r_H}^{r_{\max}} dr \frac{r^{d-2}}{\sqrt{f(r)}} + \omega_{d-2} \int_{r_H}^{r_0} dr \frac{r^{d-2}}{\sqrt{f(r)}} \,. \end{aligned} \tag{4.38}$$

When this area is greater than the area of the exterior extremal surface corresponding to $\theta = \pi/2$, we expect that the entanglement entropy will always be calculated in terms of the exterior surfaces. Thus, we have a basic condition

$$\text{Area}_{\text{ext}}(\pi/2) > \text{Area}_{\text{int}}(\theta = \pi/2, t = 0, r_0) \tag{4.39}$$

for when entanglement will tell us something about the geometry behind the horizon. This is more likely to be satisfied for smaller values of r_0 (ETW brane not too far past the horizon). It can fail to be satisfied even for $r_0 = r_H$ if the black hole is too small, so below some minimum value $r_H^{\min}$, all minimal area extremal surfaces probe outside the horizon.

For $d = 2$, we will see below that the constraint (4.39) gives explicitly (with factors of L_{AdS} restored)

$$(r_H^{\min})^{d=2} = \frac{2L_{\text{AdS}}}{\pi} \text{arcsinh}(1) \tag{4.40}$$

and that for larger r_H, the maximum brane radius must satisfy

$$\frac{r_0}{r_H} \leq \frac{1}{2}\left(\sinh\left(\frac{r_H\pi}{2L_{AdS}}\right) + \sinh^{-1}\left(\frac{r_H\pi}{2L_{AdS}}\right)\right) . \tag{4.41}$$

in order that we can see behind the horizon with entanglement.

4.3.1 Example: BCFT states for $d = 2$

In this section, we work out the explicit results for $d = 2$ where the CFT lives on a circle. We calculate the entanglement entropy $S(\Delta\theta, t)$ for an interval of angular size $\Delta\theta$ on the circle, as a function of CFT time t. We find that having access to a large enough subsystem of the CFT allows us to probe behaind the horizon, and thus renders the microstates distinguishable, in broad qualitative agreement with [244].

Exterior extremal surfaces

First consider the exterior surfaces, which we parameterize by $r(\theta)$. Since the integrand $\mathcal{L}$ in (4.37) does not depend explicitly on θ, the extremizing surfaces must satisfy

$$r'\frac{\delta\mathcal{L}}{\delta r'} - \mathcal{L} = \text{constant} \tag{4.42}$$

Calling this constant r_* (this represents the minimum value of r on the trajectory, where $r' = 0$), we get

$$r' = \pm\frac{r}{r_* L_{\text{AdS}}}\sqrt{(r^2 - r_H^2)(r^2 - r_*^2)} . \tag{4.43}$$

The solution, taking $\theta = 0$ to be the point where $r = r_*$, is given implicitly by

$$\theta = -\frac{L_{\text{AdS}}}{2r_H}\ln\left[\frac{-2r_H^2 r_*^2 + r_H^2 r^2 + r^2 r_*^2 - 2r_* r_H\sqrt{(r^2 - r_*^2)(r^2 - r_H^2)}}{r^2(r_*^2 - r_H^2)}\right] . \tag{4.44}$$

We will only need that

$$\theta(r=\infty) = \frac{L_{\rm AdS}}{2r_H} \ln\left(\frac{r_* + r_H}{r_* - r_H}\right) , \tag{4.45}$$

so that

$$\frac{r_*}{r_H} = \coth\left(\frac{r_H \Delta\theta}{2L_{\rm AdS}}\right) . \tag{4.46}$$

The area of such a surface, regulating by integrating only up to $r_{\rm max} = L_{\rm AdS}/\epsilon$ is

$$\text{Area}_{\rm ext}(\Delta\theta) = 2L_{\rm AdS} \ln\left(\frac{2L_{\rm AdS}}{\epsilon r_H} \sinh(r_H \Delta\theta/2L_{\rm AdS})\right) \tag{4.47}$$

where we have dropped terms of order ϵ. Using $c = 3L_{\rm AdS}/2G$, this gives an entropy $S = \text{Area}/4G$ of

$$S = \frac{c}{3} \ln\left(\frac{2L_{\rm AdS}}{\epsilon r_H} \sinh(r_H \Delta\theta/2L_{\rm AdS})\right) . \tag{4.48}$$

In terms of the CFT effective temperature β, we have $r_H/L_{\rm AdS} = 2\pi L_{\rm CFT}/\beta$, so the result in terms of CFT parameters is

$$S = \frac{c}{3} \ln\left(\frac{\beta}{\pi\epsilon L_{\rm CFT}} \sinh(\pi L_{\rm CFT} \Delta\theta/\beta)\right) . \tag{4.49}$$

where $L_{\rm CFT}$ is the size of the circle on which the CFT lives.

For comparison, the area of a disconnected surface with two parts extending from the interval boundaries to the horizon via the geodesic path at constant θ and t gives

$$\text{Area}_0 = 2\int_{r_H}^{r_{\rm max}} \frac{dr}{\sqrt{f(r)}} = 2L_{\rm AdS} \ln(2L_{\rm AdS}/\epsilon r_H) . \tag{4.50}$$

This shows that regardless of what happens behind the horizon, the entanglement entropy of an interval with size $\Delta\theta$ will be calculated by an extremal

surface outside the horizon if

$$\sinh(r_H \Delta\theta / 2L_{\rm AdS}) \leq 1 \ . \tag{4.51}$$

This will hold even for the largest interval $\Delta\theta = \pi$ if

$$r_H / L_{\rm AdS} \leq \frac{2}{\pi} \text{arcsinh}(1) \ . \tag{4.52}$$

Thus, we must have a sufficiently large black hole if the CFT entanglement entropy is going to have any chance of seeing behind the horizon.

Interior extremal surfaces

Now we consider the extremal surfaces that enter the horizon and end on the ETW brane. Here, it is most convenient to use coordinates for which the maximally extended black hole spacetime takes the form (with $L_{\rm AdS} = 1$)

$$ds^2_{\rm BTZ} = \frac{1}{\cos^2(y)} \left(-ds^2 + dy^2 + r_H^2 \cos^2(s)\, d\phi^2 \right) \tag{4.53}$$

where the coordinate ranges are $-\pi/2 \leq s, y \leq \pi/2$, with the horizons at $y = \pm s$. The coordinate transformations relating this to Schwarzschild coordinates are given in Appendix C.1. Using these, the ETW brane trajectory is found to be simply

$$y = -\arcsin(T) \ . \tag{4.54}$$

We find that the general spacelike geodesics in this geometry take the form

$$\sin(s_B - s_0) \sin(y) = \sin(s - s_0) \ , \tag{4.55}$$

where the geodesic passes through s_0 at $y = 0$ and ends on the AdS boundary ($y = \pi/2$) at s_B. The geodesics with fixed s_B and different s_0 all end on the same point at the AdS boundary, but different points on the ETW brane. However, requiring that the surface extremize area also with respect to variations of this boundary point on the ETW brane implies that the geodesic should be normal to the ETW brane worldvolume. This gives the

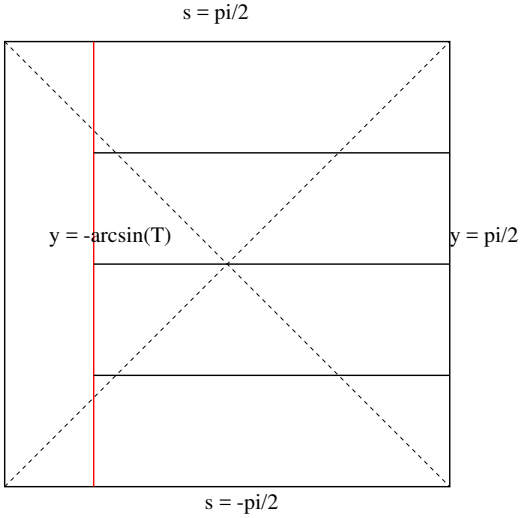

Figure 4.12: BTZ black hole in s, y coordinates, showing ETW brane (red) and various geodesics orthogonal to it. Geometry to the left of the ETW brane is excised.

very simple class of geodesics

$$s = s_0 \tag{4.56}$$

which sit at fixed θ and s. The black hole geometry together with these geodesics is depicted in Figure 4.12.

We can now evaluate the area of these extremal surfaces. We will evaluate the area up to the same regulator point $r_{\max} = L_{\text{AdS}}/\epsilon$. This gives a maximum y of

$$y_{\max} = \arctan\left(e^{-r_H t_B}\sqrt{\frac{r_{\max}/r_H - 1}{r_{\max}/r_H + 1}}\right) + \arctan\left(e^{r_H t_B}\sqrt{\frac{r_{\max}/r_H - 1}{r_{\max}/r_H + 1}}\right), \tag{4.57}$$

Note that this depends on the Schwarzschild time t_B. We have then

$$\text{Area}_{\text{int}}(\Delta\theta) \;=\; 2\int_{-\arcsin(T)}^{y_{\max}} \frac{dy}{\cos(y)}$$

$$= \quad 2L_{\text{AdS}} \ln\left(\frac{2L_{\text{AdS}}}{\epsilon r_H}\right) \tag{4.58}$$

$$+2L_{\text{AdS}} \ln\left(\cosh\left(\frac{t_B r_H}{L^2_{\text{AdS}}}\right)\sqrt{\frac{1+T}{1-T}}\right) . \tag{4.59}$$

where we have again restored factors of L_{AdS}. The regulated entanglement entropy is then

$$S = \frac{c}{3}\ln\left(\frac{2L_{\text{AdS}}}{\epsilon r_H}\cosh(t_B r_H/L^2_{\text{AdS}})\sqrt{\frac{1+T}{1-T}}\right) . \tag{4.60}$$

In terms of CFT parameters, this gives

$$S = \frac{c}{3}\ln\left(\frac{\beta}{\epsilon\pi L_{\text{CFT}}}\cosh(2\pi t_{\text{CFT}}/\beta)\sqrt{\frac{1+T}{1-T}}\right) . \tag{4.61}$$

This gives less area than the exterior surface (so that entanglement entropy will probe the interior) when

$$\sinh\left(\frac{r_H\Delta\theta}{2L_{\text{AdS}}}\right) \geq \cosh\left(\frac{t_B r_H}{L^2_{\text{AdS}}}\right)\sqrt{\frac{1+T}{1-T}} . \tag{4.62}$$

When this is satisfied, the entanglement entropy is given by the expression (4.60) and is time-dependent but independent of the interval size.[66] Otherwise, the entanglement entropy is time-independent but depends on the interval size and is given by (4.48).

The entanglement entropy as a function of interval size for various times is shown in Figure 4.14. The entanglement entropy as a function of time for various interval sizes is shown in Figure 4.13. The fact that the entanglement entropies are independent of angle when the minimal-area extremal surfaces probe behind the horizon is a special feature of the $d = 2$ case arising from

[66] If we express condition (4.62) in terms of the radius r of the ETW brane where we shoot out a normal geodesic, we obtain an even simpler condition

$$\sinh\left(\frac{r_H\Delta\theta}{2L_{\text{AdS}}}\right) \geq \frac{r_H}{(1-L_{\text{AdS}}T)r}.$$

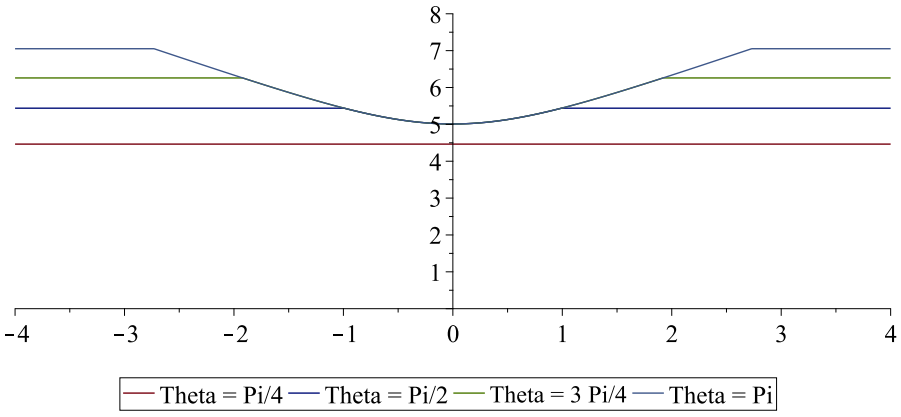

Figure 4.13: Regulated entanglement entropy as a function of time for various interval sizes for $T = 0.5$, $r_H = 2L_{\text{AdS}}$, $\epsilon = 0.01$. Plots from bottom to top show $\Delta\theta = \pi/4,\ \pi/2,\ 3\pi/4,\ \pi$.

the fact that these extremal surfaces have two disconnected parts, each at a constant angle. In higher dimensions, the corresponding surfaces are connected and we have non-trivial angular dependence for all angles.

4.3.2 Results for $d = 4$

As another explicit example, we consider the case of a (4+1)-dimensional black hole. In this case, the Lagrangian describing the extremal surfaces has an explicit angle dependence, and the surfaces must be found numerically.

Interior extremal surfaces

The metric for the (4+1)-dimensional Schwarzschild black hole in Schwarzschild coordinates is

$$ds^2 = -f(r)dt^2 + \frac{dr^2}{f(r)} + r^2 d\Omega_3^2 \tag{4.63}$$

where

$$f(r) = \frac{r^2}{L_{\text{AdS}}^2} + 1 - \frac{r_H^2}{r^2}\left(\frac{r_H^2}{L_{\text{AdS}}^2} + 1\right) . \tag{4.64}$$

Once again, we set $L_{\text{AdS}} = 1$ in the following.

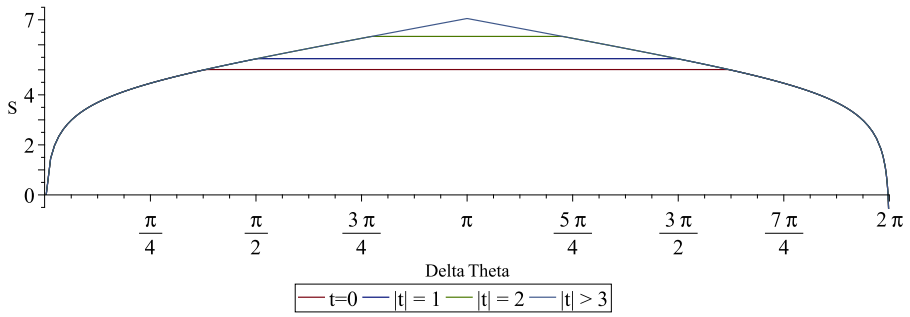

Figure 4.14: Regulated entanglement entropy as a function of interval size for various times for $T = 0.5$, $r_H = 2L_{\rm AdS}$, $\epsilon = 0.01$. Plots from bottom to top show successively later times starting at $t = 0$.

To switch to Kruskal-type coordinates (Y, S), we define

$$t = \frac{r_H}{2(2r_H^2+1)} \ln\left(\frac{Y+S}{Y-S}\right) , \quad g(r) = \frac{r_H}{2(2r_H^2+1)} \ln(Y^2 - S^2) , \tag{4.65}$$

where

$$\begin{aligned} g(r) &= \int^r \frac{dr}{f(r)} \\ &= \frac{r_H}{2(2r_H^2+1)} \log\left|\frac{r_H - r}{r_H + r}\right| + \frac{\sqrt{r_H^2+1}}{2r_H^2+1} \arctan\frac{r}{\sqrt{r_H^2+1}} + C . \end{aligned} \tag{4.66}$$

Then the metric is

$$\begin{aligned} ds^2 &= \frac{r_H^2 e^{-\frac{2(2r_H^2+1)}{r_H} g(r)}}{(2r_H^2+1)^2} f(r)[-dS^2 + dY^2] + r^2 d\Omega^2 \\ &= \frac{r_H^2}{(2r_H^2+1)^2} \frac{f(r)}{Y^2 - S^2}[-dS^2 + dY^2] + r^2 d\Omega^2 \end{aligned} \tag{4.67}$$

where r is defined implicitly as a function of $Y^2 - S^2$ by the second equation in (4.65). Note that the zero at $r = r_H$ in $f(r)$ cancels the pole in the exponential factor, leaving a function that is regular at the horizon.

Changing the constant C amounts to a rescaling of Y and S, so we can

make a choice $C = 0$. Then, the metric is

$$ds^2 = B(r)(-dS^2 + dY^2) + r^2 d\Omega^2 \tag{4.68}$$

with

$$B(r) = \frac{r_H^2}{(2r_H^2+1)^2}\frac{(r+r_H)^2(r^2+r_H^2+1)}{r^2} \times \exp\left[-\frac{2\sqrt{r_H^2+1}}{r_H}\arctan\left(\frac{r}{\sqrt{r_H^2+1}}\right)\right] \tag{4.69}$$

and r defined in terms of $Y^2 - S^2$ as

$$Y^2 - S^2 = \left(\frac{r-r_H}{r+r_H}\right) e^{\frac{2\sqrt{r_H^2+1}}{r_H}\arctan\left(\frac{r}{\sqrt{r_H^2+1}}\right)} \equiv F(r)\ . \tag{4.70}$$

We would like to extremize the action

$$\begin{aligned} S &= 4\pi \int dY\ r^2 \sin^2\theta \sqrt{B(r)\left(1-\left(\frac{dS}{dY}\right)^2\right) + r^2\left(\frac{d\theta}{dY}\right)^2} \\ &\equiv 4\pi \int dY\ \mathcal{L} \end{aligned} \tag{4.71}$$

for surfaces described by $S(Y)$, $\theta(Y)$, $r(Y)$ with

$$Y^2 - S^2 - F(r) = 0\ . \tag{4.72}$$

Introducing a Lagrange multiplier $4\pi\Lambda$ for the constraint, this gives equations

$$\begin{aligned} \frac{d}{dY}\frac{\delta\mathcal{L}}{\delta S'} + 2\Lambda S &= 0 \\ \frac{d}{dY}\frac{\delta\mathcal{L}}{\delta\theta'} - \frac{\delta\mathcal{L}}{\delta\theta} &= 0 \\ \frac{\delta\mathcal{L}}{\delta r} - \Lambda\frac{dF}{dr} &= 0\ , \end{aligned} \tag{4.73}$$

where primes denote derivatives with respect to Y. Eliminating Λ, and using (4.72) to get an equation for r', we get

$$\begin{aligned} \frac{d}{dY}\frac{\delta\mathcal{L}}{\delta S'} + \frac{2S}{dF/dr}\frac{\delta\mathcal{L}}{\delta r} &= 0 \\ \frac{d}{dY}\frac{\delta\mathcal{L}}{\delta\theta'} - \frac{\delta\mathcal{L}}{\delta\theta} &= 0 \\ r' + \frac{2}{dF/dr}(SS' - Y) &= 0\,. \end{aligned} \tag{4.74}$$

These differential equations can be solved numerically, along with the equation for the surface area, $\text{Area}_{\text{int}} = A$ with

$$A' = 4\pi r^2 \sin^2\theta \sqrt{B(r)\left(1 - \left(\frac{dS}{dY}\right)^2\right) + r^2\left(\frac{d\theta}{dY}\right)^2}\,, \tag{4.75}$$

to determine the functions $(S(Y), \theta(Y), r(Y), A(Y))$. For initial conditions, we should again enforce normality of the extremal surface to the brane. One can use the brane equation of motion

$$\dot{r}^2 + [f(r) - r^2T^2] = 0 \tag{4.76}$$

to determine the brane trajectory, and select some collection of initial coordinates $(t_{\text{br}}, r_{\text{br}}, \theta_{\text{br}})$ on the brane. The Kruskal coordinate transformation in equation (4.65) is then used to find the corresponding $S_{\text{br}}, Y_{\text{br}}$, and we take initial conditions

$$S(Y_{\text{br}}) = S_{\text{br}}\,, \quad \theta(Y_{\text{br}}) = \theta_{\text{br}}\,, \quad r(Y_{\text{br}}) = r_{\text{br}}\,, \tag{4.77}$$

$$A(Y_{\text{br}}) = 0\,, \quad S'(Y_{\text{br}}) = \frac{\sqrt{1 - \frac{f(r_{\text{br}})}{r_{\text{br}}^2T^2}}Y_{\text{br}} - S_{\text{br}}}{\sqrt{1 - \frac{f(r_{\text{br}})}{r_{\text{br}}^2T^2}}S_{\text{br}} - Y_{\text{br}}}\,. \tag{4.78}$$

Provided that this extremal surface does not fall into the singularity, one can integrate up to some cutoff radius $r = r_{\text{max}}$ near the AdS-Schwarzschild boundary; the result of this computation is a cutoff surface area A_{int}, a

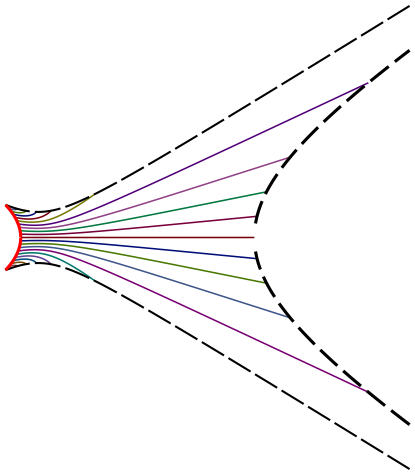

Figure 4.15: Radial profiles of extremal surfaces in Kruskal coordinates (S, Y). Those surfaces emitted from the brane at sufficiently late or early times fall into the singularity.

boundary subregion size θ_B, and a boundary Schwarzschild time t_B.

Exterior extremal surfaces

The exterior extremal surface was computed in Schwarzschild coordinates; again, the geometry is static, so the surface lives in a constant t slice, and one has action

$$S = 4\pi \int d\lambda \, r^2 \sin^2\theta \sqrt{\frac{(r')^2}{f(r)} + r^2(\theta')^2} \equiv 4\pi \int d\lambda \, \mathcal{L} \, . \tag{4.79}$$

There is of course a reparametrization invariance; it is numerically desirable to consider the gauge

$$M(\lambda) \equiv \frac{(r')^2}{f(r)} + r^2(\theta')^2 = 1 \, . \tag{4.80}$$

Substituting this constraint into the equations of motion, one arrives at

$$2r'f(r)\cos\theta\sqrt{1-\frac{(r')^2}{f}}+r''rf(r)\sin\theta \\ +\Big(3f(r)-\frac{r}{2}\frac{df}{dr}\Big)(r')^2\sin\theta-3f(r)^2\sin\theta=0\,, \quad (4.81)$$

which can be integrated together with our constraint equation, and the equation for the surface area, $A_{\text{ext}} = A$ with

$$A' = 4\pi r^2\sin^2\theta\,, \quad (4.82)$$

to determine the functions $(r(\lambda), \theta(\lambda), A(\lambda))$ given some initial conditions[67] $r(0) = r_*, \theta(0) = 0, A(0) = 0$. We can again integrate up to some radius $r_{\max}$ to find a cutoff area A_{ext} and a boundary angle θ_B.

Regularization of the surface area

To understand the divergences appearing in the entanglement entropy, it is helpful to work out an explicit expression for the regularized entanglement entropy in the case of vacuum AdS. In this case, the area associated with extremal surfaces in the vacuum geometry may be calculated most easily by working in Poincaré coordinates where the extremal surfaces are hemispheres with some radius $R(\theta_B)$. Making the appropriate change of coordinates and integrating the area up to the value of z that corresponds to $r = r_{\max}$ gives

$$A_{\text{vac}}(\theta_B) = 2\pi[r_{\max}^2\sin^2\theta_B - \ln(2r_{\max}\sin\theta_B) - \frac{1}{2}\cos(2\theta_B)] + \mathcal{O}(r_{\max}^{-2}) \quad (4.83)$$

In performing numerical calculations, the divergent part of this can be subtracted from the cutoff areas of the extremal surfaces in the black hole geometry to give a finite result in the limit $r_{\max} \to \infty$.

The results of this computation are found in Figures 4.16 and 4.17. The

[67] The boundary angle θ_B turns out to be a smooth function of r_*; we can invert this function $\theta_B(r_*)$ to find the appropriate initial condition r_* given some boundary angle θ_B, allowing us to compare interior and exterior surface areas with fixed θ_B.

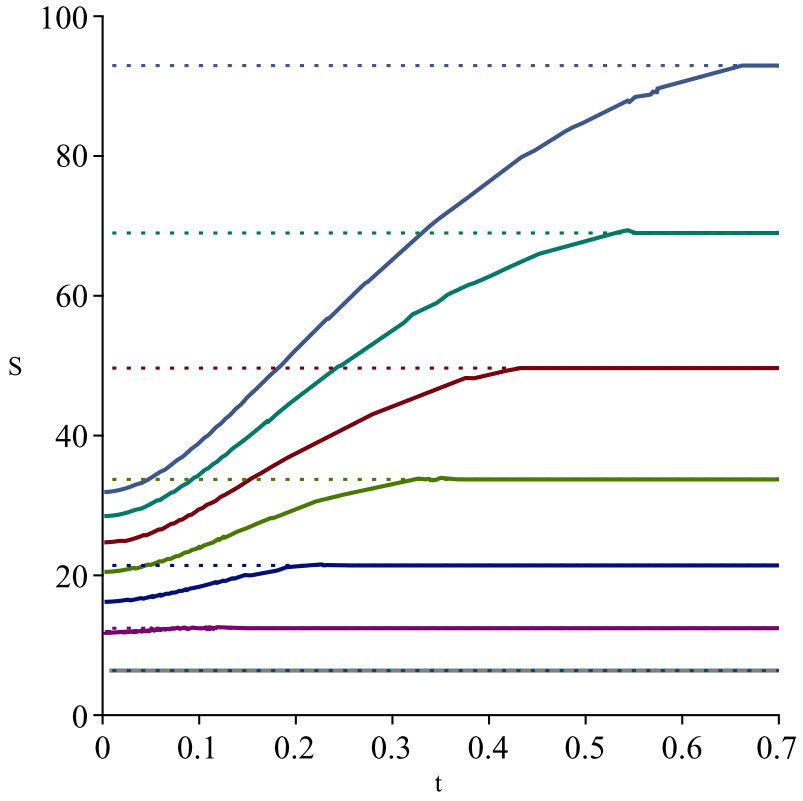

Figure 4.16: Regulated entanglement entropy as a function of time for $T = 0.5$, $r_H = 3L_{\text{AdS}}$, $r_{\text{max}} = 100$. Plots from bottom to top show $\Delta\theta = 1.0, 1.2, 1.4, 1.6, 1.8, 2.0, 2.2$.

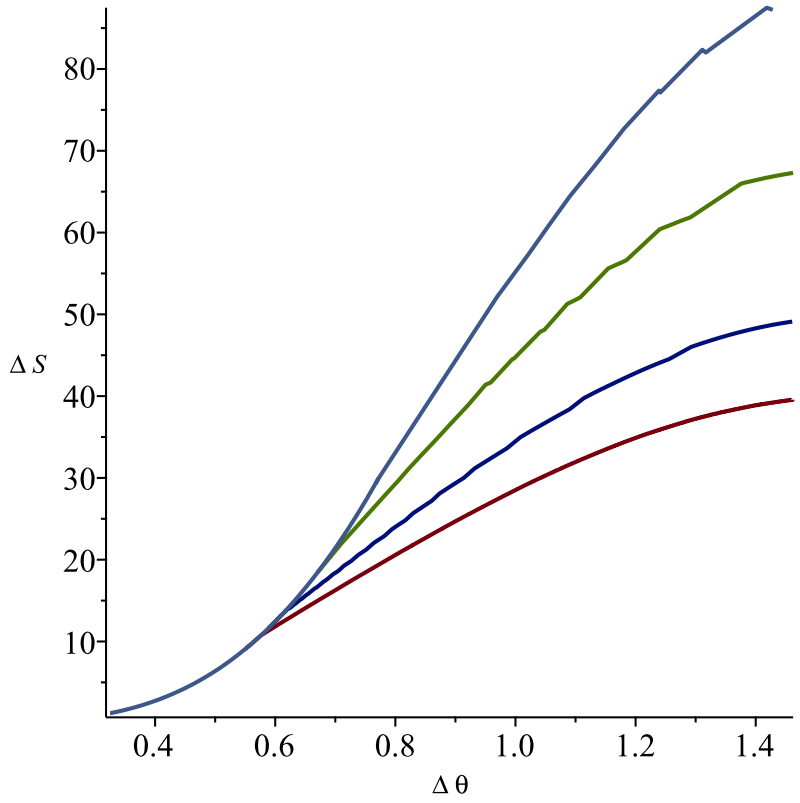

Figure 4.17: Regulated entanglement entropy as a function of subregion size for $T = 0.5$, $r_H = 3L_{\text{AdS}}$, $r_{\text{max}} = 100$. Plots from bottom to top show $t/L_{\text{AdS}} = 0,\ 0.1,\ 0.2,\ 0.3$.

results are qualitatively similar to the case of $d = 2$ dimensions; in particular, for a boundary subregion of sufficiently large size, the entanglement entropy has a period of time dependence, during which the extremal surface probes the brane geometry. However, whereas in $d = 2$ the entanglement entropy was independent of the size of the boundary subregion whilst the minimal area surface was probing the brane, this is visibly no longer the case in $d = 4$. This property was unique to $d = 2$, where the area of the interior extremal surface was independent of the size of the subtended boundary region.

4.4 Entanglement entropy: SYK model calculation

Here we study a coupled-cluster generalization [245] of the single SYK cluster consider in [208]. The first step is to define the analog of boundary states for this model, which now include both spatial and internal degrees of freedom, and generalize the analysis of [208]. We also present entanglement data obtained from exact diagonalization of a single cluster and two coupled clusters which corroborate the holographic entanglement calculations above.

Consider LN Majorana fermions $\chi_{r,a}$ with $r = 1, \cdots, L$ and $a = 1, \cdots, N$ with N even. The basic anti-commutator is

$$\{\chi_{r,a}, \chi_{r',a'}\} = \delta_{r,r'}\delta_{a,a'} \, . \tag{4.84}$$

The Majorana fermions are arranged in the Hamiltonian into L clusters of N Majoranas each, with the clusters having only nearest neighbor interactions. The Hamiltonian is

$$H = \sum_{r=1}^{L} \sum_{a<b<c<d} J_{abcd}\chi_{r,a}\chi_{r,b}\chi_{r,c}\chi_{r,d} + \sum_{r=1}^{L} \sum_{a<b,c<d} \tilde{J}_{abcd}\chi_{r,a}\chi_{r,b}\chi_{r+1,c}\chi_{r+1,d} \, , \tag{4.85}$$

assuming periodic boundary conditions. The couplings are Gaussian random

variables with zero mean and variances

$$\overline{J^2_{abcd}} = \frac{6J_0^2}{N^3} , \qquad \overline{\tilde{J}^2_{abcd}} = \frac{J_1^2}{N^3} . \tag{4.86}$$

The bare Euclidean 2-point function is

$$\langle \chi_{r,a}(\tau)\chi_{r',a'}(0)\rangle = \frac{1}{2}\,\mathrm{sgn}(\tau)\delta_{r,r'}\delta_{a,a'} . \tag{4.87}$$

The dressing is the usual melonic large N analysis, but here extended to the coupled chain [245]. For our present purpose, the key point of this analysis is that the system possesses an emergent $O(N)^L$ symmetry at large N. Essentially, one can apply an independent $O(N)$ transformation acting on the a index of $\chi_{r,a}$ at every site of the chain. This occurs because, ignoring a possible spin glass or localized phase, the J and $\tilde{J}$ couplings can be treated as dynamical fields with a particular two-point function, at large N.

A complete basis for the Hilbert space can be obtained as follows. For each pair of Majorana operators in a cluster, $\chi_{r,2k-1}$ and $\chi_{r,2k}$, define the complex fermion

$$c_{r,k} = \frac{\chi_{r,2k-1} + i\chi_{r,2k}}{\sqrt{2}} . \tag{4.88}$$

These fermions obey the usual algebra, $\{c_{r,k}, c^\dagger_{r',k'}\} = \delta_{r,r'}\delta_{k,k'}$. It is convenient to label the Hilbert space using the spin-like operator $\hat{s}_{r,k} = 1 - 2c^\dagger_{r,k}c_{r,k} = \pm 1$. In terms of the Majoranas, it is

$$\hat{s}_{r,k} = 1 - 2c^\dagger_{r,k}c_{r,k} = -2i\chi_{r,2k-1}\chi_{r,2k} . \tag{4.89}$$

The mutual eigenbasis of all the $\hat{s}_{r,k}$ operators forms a complete basis denoted $|s\rangle$ and obeying

$$\hat{s}_{r,k}|s\rangle = s_{r,k}|s\rangle . \tag{4.90}$$

Note that the transformations which flip a particular even numbered χ, such as taking $\chi_{r,2k}$, to $-\chi_{r,2k}$, also flips the eigenvalue of $\hat{s}_{s,k}$.

Now consider the imaginary time evolved $|s\rangle$ basis,

$$|s,\beta\rangle = e^{-\beta H/2}|s\rangle \,. \tag{4.91}$$

Let $Q_{r,k}$ denote the unitary which sends $\chi_{r,2k}$ to $-\chi_{r,2k}$. The idea of the analysis in [208] is, roughly speaking, that the Hamiltonian is invariant under $Q_{r,k}$ at large N, so that when computing correlation functions one can use the relation

$$Q_{r,k}e^{-\beta H/2}|s\rangle \sim e^{-\beta H/2}Q_{r,k}|s\rangle \,, \tag{4.92}$$

though it is not literally true for fixed J and $\tilde{J}$.

The goal is to analyze various physical properties in the states $|s,\beta\rangle$. The most basic object is the two-point function,

$$G_{r,a}(\tau;s,\beta) = \frac{\langle s,\beta|\chi_{r,a}(\tau)\chi_{r,a}(0)|s,\beta\rangle}{\langle s,\beta|s,\beta\rangle} \,. \tag{4.93}$$

Since each $\chi_{r,a}$ is mapped to $\pm\chi_{r,a}$ by $Q_{r,k}$, it follows from equation (4.92) that $G_{r,a}(\tau;s,\beta)$ is actually independent of s, at least to leading order at large N. Hence, even though the states $|s,\beta\rangle$ are not translation invariant in general, the two-point function in state $|s,\beta\rangle$ is approximately translation invariant.

To determine the value of $G_{r,a}(\tau;s,\beta)$, first observe that the leading large N part of $\langle s,\beta|s,\beta\rangle$ is also independent of s by virtue of equation (4.92). Summing over s gives

$$\sum_s \langle s,\beta|s,\beta\rangle = \mathrm{Tr}(e^{-\beta H}) = Z(\beta) \,, \tag{4.94}$$

so since each term is approximately equal, it must be that

$$\langle s,\beta|s,\beta\rangle \approx \frac{Z(\beta)}{\mathcal{D}} \,, \tag{4.95}$$

with $\mathcal{D}$ the Hilbert space dimension. This in turn implies that $G_{r,a}(\tau;s,\beta)$ must be given by the thermal answer at inverse temperature β independent of s.

One property of particular interest is the entanglement entropy of subregions in the state $|s,\beta\rangle$. The n-th Rényi entropy of a subset A of Majorana fermions in the normalized state

$$\sigma(s,\beta) = \frac{|s,\beta\rangle\langle s,\beta|}{\langle s,\beta|s,\beta\rangle} \tag{4.96}$$

is

$$e^{-(n-1)S_n(A)} = \mathrm{Tr}\left(\Pi_n^A \sigma(s,\beta)^{\otimes n}\right) . \tag{4.97}$$

Here Π_n^A is a shift operator acting on the n copies which swaps fermions from the set A between the copies. It is defined for a single pair of Majoranas below. Crucially, it is invariant under the $Q_{r,k}$ transformation provided it is enacted in every copy (replica) simultaneously. Hence at the level of rigor we have been observing, it follows that the large N part of the Renyi entropy of a collection A in state $|s,\beta\rangle$ is independent of s.

The value of $S_n(A)$ is less clear. The same trick, summing over s, which showed that $G_{r,a}(\tau;s,\beta)$ was thermal does not work here because there are two copies of the state appearing. While the thermal Renyi entropy is one natural candidate, this cannot be true for all collections since the state is pure. At a minimum, non-thermality must occur when A exceeds half the total system. However, it is certainly consistent to lose thermality for smaller sets, as this occurs in holographic calculations. To say more requires a detailed calculation of the Renyi entropy using the replicated path integral, which we defer to future work.

Note that, in the numerical data reported below, the entanglement entropy of subsystems is computed by first grouping fermions into pairs and performing a Jordan-Wigner transformation to a spin basis. The definition of entanglement in the spin basis is trivial, and moreover, one can show that the precise location of the Jordan-Wigner string does not effect the entropy calculation. This is because given two different strings, meaning two different mappings of fermion states to spin states, the two final sets of spin states are related by a local unitary. Hence as long a fixed fermion pairing is chosen to define the spins, the choice of string is actually irrelevant since

entanglement entropy is invariant under local unitary transformations.

4.4.1 Data for a single SYK cluster

Here data is presented for a single SYK cluster, $L = 1$, for a variety of N and β. Turning first to the diagonal matrix elements of the thermal state, Figure 4.18 shows a histogram of $\langle s, \beta | s, \beta \rangle$ for all s for an $N = 28$ cluster. There is a clear concentration around the central value of $Z(\beta)/\mathcal{D}$ and some evidence of an emerging universal distribution at large β, although the data are also consistent with the distribution merely varying slowly with β.

Turning to the entanglement of subsets of the Majoranas, Figure 4.19 shows a histogram of the entanglement of the first site for various β and $N = 28$. As β increases, the distribution appears to peak near one, although the width does not dramatically decrease with increasing β. An analysis of the data for smaller values of N suggests that the distribution is also becoming sharper as N increases.

Next we consider the time evolution of entanglement, with Figure 4.20 showing the time evolution of entanglement for a single state s and $N = 32$ fermions. For small subsystems, the entanglement entropy is close to the thermal value (obtained by imaginary time evolution acting on a random Hilbert space state) even at zero time. The result is similar to the holographic results, where it was found that small subsystems look exactly thermal to leading order in large N. By contrast, larger systems deviate from thermality at early time but quickly thermalize. Unlike the holographic calculations, there is no sharp transition as subsystem size is increased, but such a transition is not expected at finite N.

To show that such imaginary time-evolved boundary states have a thermal character for systems beyond SYK at large-N, Appendices C.3 and C.4 contain simple spin systems where very rapid entanglement growth and other thermal properties of boundary states can be shown exactly.

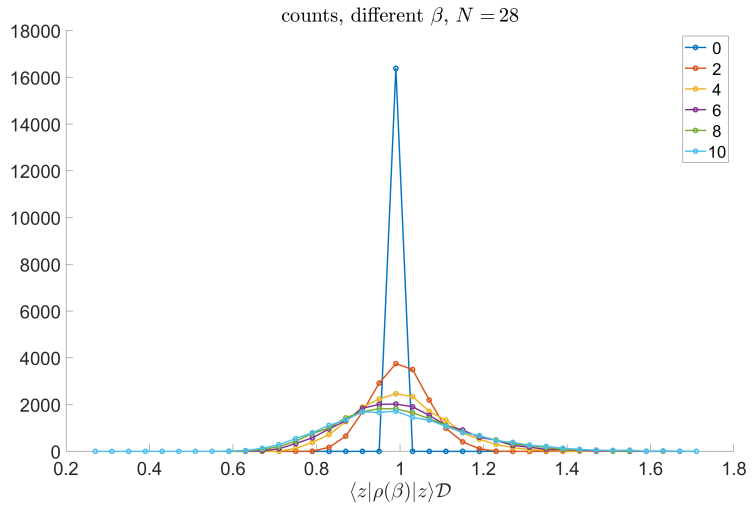

Figure 4.18: Histogram of $\langle s, \beta | s, \beta \rangle$ for $N = 28$ Majorana fermions in a single SYK cluster ($L = 1$). The different curves correspond to $\beta = 0, \cdots, 10$ in units with $J_0 = 1$. There is a strong concentration around the value predicted by the random model studied above.

4.4.2 Data for two coupled clusters

The single cluster analysis can be repeated for two coupled clusters, with the caveat that adding a second cluster reduces the number of fermions that can be studied in each cluster. Figures 4.21, 4.22, and 4.23 show data for two coupled SYK clusters, $L = 2$, with $N = 12$ Majoranas in each cluster. Some similar features to the single cluster case are visible, although the necessarily smaller sizes induce larger finite size effects.

In Figure 4.21 we see evidence that the diagonal matrix elements of the thermal density are beginning to concentrate near the value $Z(\beta)/\mathcal{D}$ predicted by the large-N analysis. However, the distribution is considerably wider. One possible explanation is that the much smaller value of N has led to much larger finite size effects. Figure 4.22 shows a histogram of the entanglement of one cluster normalized to its thermal value. A similar kind of concentration effect near the thermal value is seen as β is increased.

Finally, Figure 4.23 shows a thermofield double-like correlation averaged

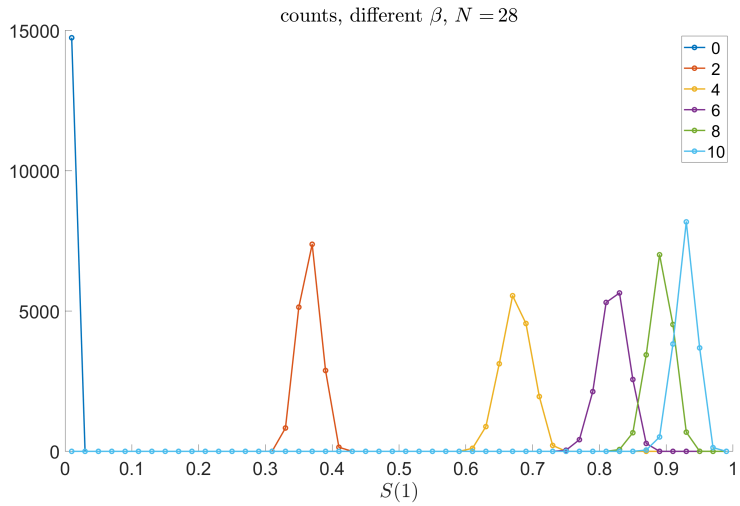

Figure 4.19: Histogram of the entropy of one pair of Majoranas for $N = 28$ Majorana fermions in a single SYK cluster ($L = 1$). The different curves correspond to $\beta = 0, \cdots, 10$ in units with $J_0 = 1$. As β varies, the entropy increases from zero and remains reasonably peaked. As the average approaches one, the distribution appears to become more peaked, possibly indicating convergence to a value independent of s at large β and large N.

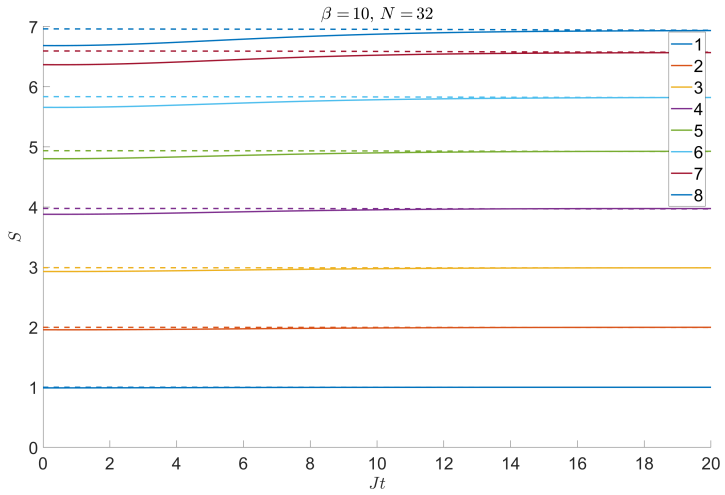

Figure 4.20: The solid lines are the entropies of different sized subsystems as a function of time for $N = 32$ Majoranas in a single SYK cluster ($L = 1$) with $\beta = 10$. The dashed lines show the same subsystem entropies in a random state which has been evolved in imaginary time as a proxy for the thermal entropy. After a short time of order β, all subsystem entropies have reached their late time thermal values.

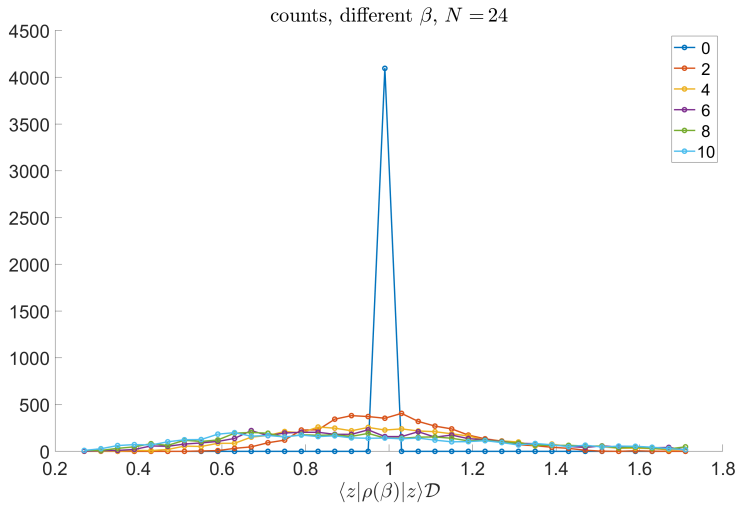

Figure 4.21: Histogram of $\langle s|\rho(\beta)|s\rangle\mathcal{D}$ for two coupled SYK clusters corresponding to $L = 2$ and $N = 12$. The different curves correspond to $\beta = 0, \cdots, 10$ in units with $J_0 = 1$.

over all the fermions. Those data also show signs of concentrating near the thermal value, albeit with significant width to the distribution. It is plausible that this broadening is a finite size effect coming from the rather small value of N on each cluster in the two cluster system.

We did not study time-evolution of entanglement for the two cluster system because the single cluster data is already a reasonable caricature of the holographic results and the numerics do not have enough spatial resolution to study in detail the dependence on spatially non-uniform boundary states. The above data for $L = 2$ indicate that the thermal behavior of boundary states expected at large-N is beginning to emerge for two coupled SYK clusters at quite modest N, but a definite conclusion is hard to make from the finite size numerical data.

In Appendix C.4 we exhibit a simple model with spatial locality where the thermality of simple correlators can be shown rigourously. Hence, evidence is accumulating that imaginary time evolved states across a broad class of models, including those with spatial locality, have a thermal character.

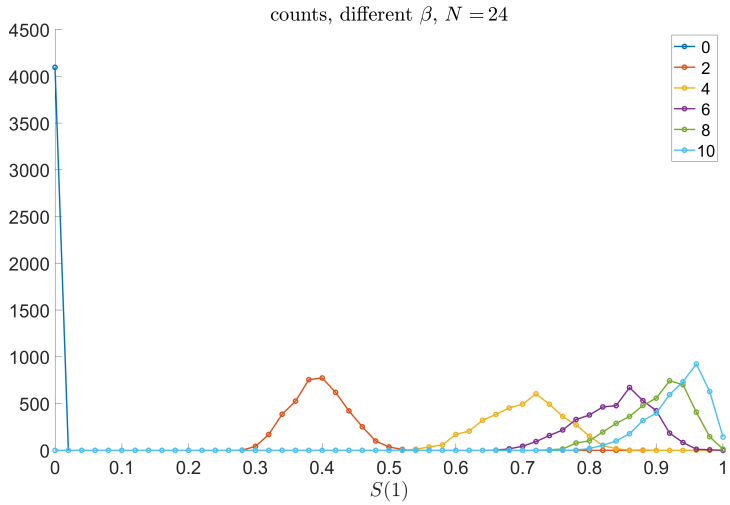

Figure 4.22: Histogram of the entropy of one cluster relative to thermal value for two coupled SYK clusters corresponding to $L = 2$ and $N = 12$. The different curves correspond to $\beta = 0, \cdots, 10$ in units with $J_0 = 1$.

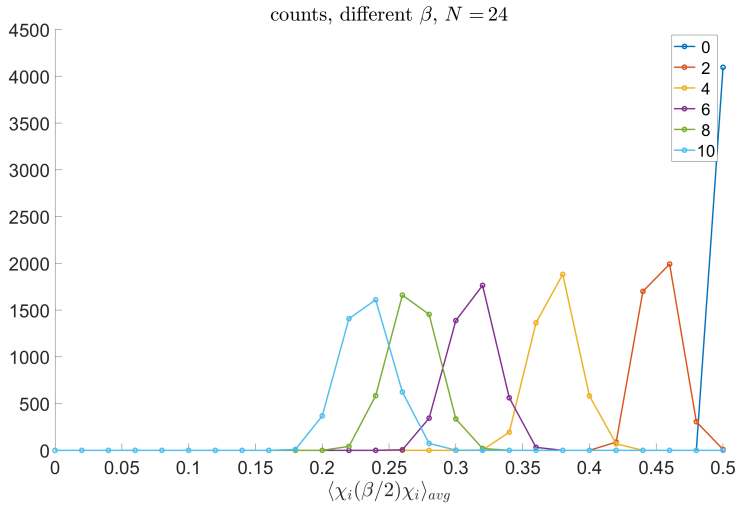

Figure 4.23: Histogram of TFD-like correlation averaged over fermions for two coupled SYK clusters corresponding to $L = 2$ and $N = 12$. The different curves correspond to $\beta = 0, \cdots, 10$ in units with $J_0 = 1$.

4.4.3 Swap operator for fermions

Given n fermion modes, the shift operator, Π_n, is defined by $\Pi_n a_i \Pi_n^{-1} = a_{i+1}$ for $i < n$ and $\Pi_n a_n \Pi_n^{-1} = (-1)^{n-1} a_1$. Its meaning is obtained from its relation to Renyi entropies. Given a fermion density matrix $\rho = (1-p) + (2p-1)a^\dagger a$, the n-th Renyi entropy of ρ is

$$e^{-(n-1)S_n} = (1-p)^n + p^n. \tag{4.98}$$

From the definition of Π_n it follows that the empty state and the full state are mapped to themselves with no phase factor by Π_n. The factor of $(-1)^{n-1}$ is needed to ensure that the full state does not acquire a phase, since

$$\Pi_n a_1^\dagger \cdots a_n^\dagger \Pi_n^{-1} = (-1)^{n-1} a_2^\dagger \cdots a_n^\dagger a_1^\dagger = a_1^\dagger \cdots a_n^\dagger. \tag{4.99}$$

Every other state in the a_i basis is mapped to an orthogonal state (obtained, up to a phase, by rearranging the occupation numbers). Hence the expectation value of Π_n in the n-copy state is

$$\mathrm{Tr}\left(\Pi_n \prod_{i=1}^{n} \rho(a_i)\right) = (1-p)^n + p^n, \tag{4.100}$$

the desired Renyi entropy.

Now suppose each a_i is written in terms of Majorana operators,

$$a_i = \frac{\chi_i + i\tilde{\chi}_i}{\sqrt{2}}, \tag{4.101}$$

and consider the transformation $\tilde{\chi}_i \to -\tilde{\chi}_i$. This transformation maps a_i to $a_i^\dagger$ and hence exchanges the empty and filled states. Moreover, it commutes with the transformation induced by Π_f, hence if the unitary Q implements the sign inversion, then $Q\Pi_n Q^{-1} = \Pi_n$. For example, with two copies, $n = 2$, the shift is

$$\Pi_2 = e^{-\frac{\pi}{2}(a_1^\dagger a_2 - a_2^\dagger a_1)}, \tag{4.102}$$

which enacts $\Pi_2 a_1 \Pi_2^{-1} = a_2$ and $\Pi_2 a_2 \Pi_2^{-1} = -a_1$. Its Majorana representa-

tion is

$$\Pi_2 = e^{-\frac{\pi}{2}(\chi_1\chi_2+\tilde{\chi}_1\tilde{\chi}_2)}, \tag{4.103}$$

which is manifestly invariant under a sign flip of all $\tilde{\chi}_i$.

The generalization to many modes in a single copy is straightforward. The conclusion remains the same: the swap operator is invariant under the transformation $\chi_{i,\alpha} \to -\chi_{i,\alpha}$ provided it acts on all copies simultaneously.

4.5 Holographic complexity

We have seen that the entanglement entropy for sufficiently large CFT subsystems can provide a probe of behind-the-horizon physics for our black hole microstates. In [225] and [227], a pair of additional probes capable of providing information behind the horizon were defined holographically and conjectured to provide a measure of the complexity of the CFT state.[68] The first, which we denote by $\mathcal{C}_V$, is proportional to the volume of the maximal-volume spacelike hypersurface ending on the boundary time slice at which the state is defined [225]. The second, which we denote by $\mathcal{C}_A$, is proportional to the gravitational action evaluated on the spacetime region formed by the union of all spacelike hypersurfaces ending on this boundary time slice (called the Wheeler-deWitt patch for this time slice) [227].

In this section, we explore the behaviour of both of these quantities as a function of time and the parameter T for our microstates in the case $d = 2$. We will see that while the late-time growth of both quantities is the same and matches the expectations for complexity, the time-dependence at early times is significantly different. This may provide some insight into the CFT interpretations for these two quantities.

[68] For a more detailed exposition of the definition and calculation of holographic complexity, see [246].

4.5.1 Calculation of $\mathcal{C}_V$ for $d = 2$

The volume-complexity for a CFT state defined on some boundary time slice is defined holographically as

$$\mathcal{C}_V = \frac{V}{Gl} \,, \tag{4.104}$$

where V is the volume of the maximal-volume co-dimension one bulk hypersurface anchored at the asymptotic CFT boundary on the time slice in question. Here, l is a length scale associated to the geometry in question, taken here to be L_{AdS}. We will generally set $L_{\text{AdS}} = 1$ and make use of the s, y coordinates defined in Appendix C.2.

Consider the boundary time slice corresponding to a particular time s_B at the boundary. The maximal volume bulk hypersurface anchored here will wrap the circle direction and have some profile $s(y)$ in the other two directions. For a surface described by such a parametrization, the volume is

$$V = 2\pi r_H \int dy \frac{\cos(s)}{\cos^2(y)} \sqrt{1 - \left(\frac{ds}{dy}\right)^2} \,. \tag{4.105}$$

Extremizing this gives

$$\frac{d^2 s}{dy^2} = \left(1 - \left(\frac{ds}{dy}\right)^2\right) \left(\tan(s) - 2\tan(y)\frac{ds}{dy}\right) \,. \tag{4.106}$$

Maximizing volume also requires that the slice intersects the ETW brane normally,

$$\left.\frac{ds}{dy}\right|_{y=y_{\text{br}}} = 0 \,. \tag{4.107}$$

We regulate the volume by integrating up to $r_{\max} = L/\epsilon$ in the Schwarzschild coordinates. We can subtract the regulated volume for pure AdS to obtain a result that is finite for $\epsilon \to 0$. This regulated volume for pure AdS (working

in Schwarzschild coordinates with $f(r) = r^2 + 1$) is

$$\begin{aligned} V_{\text{AdS}} &= \int_0^{\frac{1}{\epsilon}} dr\, 2\pi r \sqrt{\frac{1}{f(r)} - f(r)\left(\frac{dt}{dr}\right)^2} \\ &= 2\pi\left[\frac{1}{\epsilon} - 1 + \mathcal{O}(\epsilon)\right] . \end{aligned} \tag{4.108}$$

In the s, y coordinates, this maximum value corresponds to

$$\begin{aligned} y_{\text{max}} &= \arctan\left(e^{-r_H t}\sqrt{\frac{r_{\text{max}} - r_H}{r_{\text{max}} + r_H}}\right) + \arctan\left(e^{r_H t}\sqrt{\frac{r_{\text{max}} - r_H}{r_{\text{max}} + r_H}}\right) \\ &= \pi/2 - \epsilon\frac{r_H}{\cosh(t r_H)} + \mathcal{O}(\epsilon^2) \end{aligned} \tag{4.109}$$

The values of s at the boundary are related to the original Schwarzschild time by

$$t_B = \frac{1}{r_H}\ln(\tan(\pi/4 + s_B/2)) . \tag{4.110}$$

We find that there is a monotonic relationship between the intersection time s_{br} of the maximal volume slice with the ETW brane and the Schwarzschild time t_B of the maximal volume slice at the AdS boundary. A finite range $s_{\text{br}} \in [-s_*, s_*]$ with $s_* < \pi/2$ maps to the full range $t_B \in [-\infty, \infty]$ of Schwarzschild time. We have that $s_* \to 0$ as $T \to 1$ or equivalently as y_{br} (the brane location) approaches $-\pi/2$.

For $t = 0$, the maximal volume slice is just the $s = 0$ slice of the spacetime, and the subtracted volume is

$$\begin{aligned} V_{t=0} &= 2\pi r_H \int_{y_{\text{br}}}^{y_{\text{max}}} \frac{dy}{\cos^2 y} - V_{\text{AdS}} \\ &= \lim_{\epsilon\to 0}\left[2\pi r_H(\tan(y_{\text{max}}) - \tan(y_{\text{br}})) - V_{\text{AdS}}(r_{\text{max}})\right] \\ &= 2\pi(1 + r_H \tan|y_{\text{br}}|) \\ &= 2\pi(1 + \frac{r_H T}{\sqrt{1-T^2}}) . \end{aligned} \tag{4.111}$$

It is actually convenient to subtract off the 2π here and below, since the remaining volumes are all proportional to r_H. We will refer to this subtracted

volume as ΔV.

We can numerically find the maximal volume slices and evaluate ΔV for different values of $s_{\rm br}$ to understand how the volume depends on time. For each $s_{\rm br}$ we calculate t_B, the Schwarzschild time where the slice intersecting the ETW brane at $s_{\rm br}$ intersects the AdS boundary. The results for $\Delta V/r_H$ vs $t_B r_H$ are independent of r_H; these are plotted in Figure 4.24.

As a function of Schwarzschild time, the regulated volume increases smoothly to infinity as $t \to \infty$, with a linear increase in volume as a function of Schwarzschild time for late times. The slope is the same in all cases,

$$\frac{dV}{dt} \sim \pi r_H^2 \ . \tag{4.112}$$

Using this result to compute the late time rate of change of volume-complexity, one finds:

$$\lim_{t\to\infty} \frac{dC_V}{dt} = \frac{\pi r_H^2}{G} = 8\pi M \ , \tag{4.113}$$

where we have used the relation

$$r_H^2 = 8GM \tag{4.114}$$

between the horizon radius r_H and the black hole mass M for a non-rotating BTZ black hole.

The same slope can be obtained analytically as a lower bound by noting that in the future interior region, which can be described by Schwarzschild coordinates with[69]

$$ds^2 = -\frac{dt^2}{r_H^2 - t^2} + (r_H^2 - t^2)dr^2 + t^2 d\theta^2 \ , \tag{4.115}$$

with $t \in [-r_H, 0]$, there is an extremal volume surface Σ described by

$$t = -\frac{\sqrt{2}}{2} r_H \ . \tag{4.116}$$

[69] These are related to the u, v coordinates by $u = e^{r r_H}\sqrt{\frac{r_H+t}{r_H-t}}$, $v = e^{-r r_H}\sqrt{\frac{r_H+t}{r_H-t}}$.

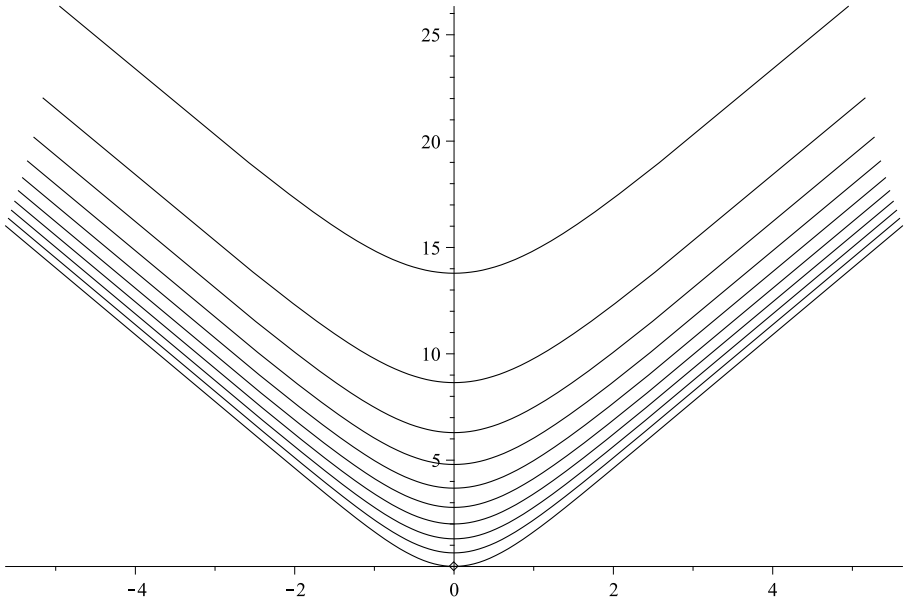

Figure 4.24: Volume $\Delta V/r_H$ of maximal slice vs Schwarzschild time $r_H t_B$ for $T = k/10$ with $k \in \{0, \ldots, 9\}$ from bottom to top.

This is a tube with constant radius $r_H/\sqrt{2}$. In the u, v coordinates, this is $uv = (2-\sqrt{2})/(2+\sqrt{2})$. From a time t_B at the AdS boundary, we can consider a surface which coincides with a future-directed lightlike surface $u = e^{r_H t_B}$ until the intersection with Σ and then along Σ until the intersection with the ETW brane. The part of this surface with $y > 0$ has volume

$$V = \pi r_H^2 t_B + \pi r_H \ln\left(\frac{1}{\sqrt{2}-1}\right) . \tag{4.117}$$

This gives a lower bound for the maximal volume, and has the same time derivative as our result above.

The late time growth of C_V is in line with earlier studies (e.g. [225, 247]) of holographic complexity for black hole states (e.g. evolution of the two-sided black hole with forward time-evolution on both sides), and has the same qualitative bulk explanation. We also see a monotonic increase for all $t > 0$, as would generically be expected for the evolution of complexity in a

generic state with less-than-maximal complexity.

4.5.2 Calculation of $\mathcal{C}_A$ for $d = 2$

The action-complexity for a CFT state defined on some boundary time slice is defined holographically as

$$\mathcal{C}_A = \frac{I_{\mathcal{W}}}{\pi\hbar} \,. \tag{4.118}$$

Here, $I_{\mathcal{W}}$ is the value of the gravitational action of the bulk theory when evaluated on some region $\mathcal{W}$. In particular, this region is the Wheeler-DeWitt patch anchored at the asymptotic boundary at the time slice in question. That is, $\mathcal{W}$ is the union of all the spatial slices anchored at this time slice. Again, in these calculations we will take $L_{\text{AdS}} = 1$.

As shown in Figure 4.25, the boundary of the region $\mathcal{W}$ is comprised of different surfaces depending upon which asymptotic time slice we choose. To avoid conflating this boundary time with the bulk Schwarzschild time coordinate, let us refer to the time on the asymptotic CFT boundary as t_B (and s_B for the boundary time in s, y coordinates). We find that there are three distinct phases depending on the time slice in question:

$$\begin{aligned} &\text{Phase (i):} && s_B < -\arcsin(T) \\ &\text{Phase (ii):} && -\arcsin(T) < s_B < \arcsin(T) \\ &\text{Phase (iii):} && s_B > \arcsin(T) \end{aligned} \tag{4.119}$$

As before, this s_B is related to the Schwarzschild boundary time, t_B, by

$$t_B = \frac{1}{r_H} \ln\left[\tan\left(\frac{\pi}{4} + \frac{s_B}{2}\right)\right] \,. \tag{4.120}$$

The Wheeler-DeWitt patches for each of these phases are depicted in the Penrose diagrams shown in Figure 4.25. One should note that, due to the symmetry of our system, the results for the negative boundary times are related to those for the positive times by $t_B \to -t_B$. Hence, we only explicitly list here the results for the distinctly different phases (ii) and (iii).

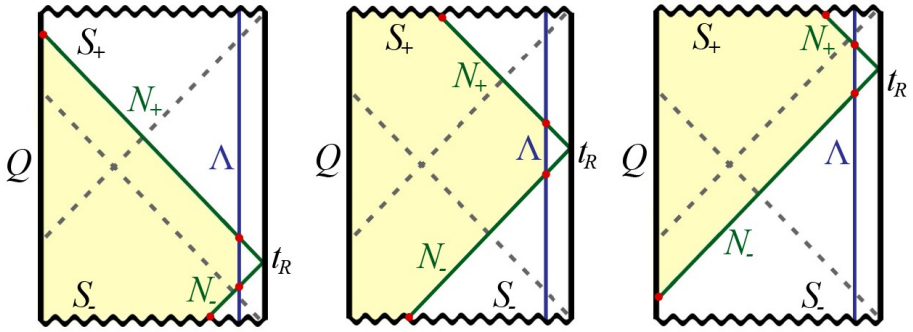

Figure 4.25: Penrose diagrams showing the Wheeler-DeWitt patch (shaded yellow) during each phase. Left-to-right: Phase (i), Phase (ii), Phase (iii). The surface Λ is used in calculations of the regulated action.

The details of our calculations in this section may be found in Appendix C.5; here, we describe the results. The action diverges as we integrate up to the asymptotic boundary, but we can define a finite quantity by subtracting off half of the action for the two-sided black hole at time $\tau = t_L + t_R = 0$ where t_L and t_R are the thermofield double's left and right boundary times respectively.[70] We will refer to this subtracted complexity as $\Delta\mathcal{C}_A$; results for the bare complexity with an explicit UV regulator may be found in the appendix.

In phase (ii), for times $|s_B| < \arcsin(T)$, we find the very simple result

$$\Delta\mathcal{C}_A(s_B) - \Delta\mathcal{C}_A(0) = 0\,. \tag{4.121}$$

We can understand this directly from the geometric argument shown in Figure 4.26.

The complexity during phase (iii), with the divergence subtracted in the same way as above, is found to simply be[71]

$$\Delta\mathcal{C}_A(s_B) - \Delta\mathcal{C}_A(0) = \frac{r_H}{4\pi G\hbar}\frac{\sin(s_B - s_*)}{\cos s_*}\ln\left(\frac{\sin(s_B - s_*)}{\cos s_B}\right) \tag{4.122}$$

[70] The asymptotic geometries are the same here, so the subtraction is unambiguous.
[71] We don't know if there is any reason for the "entropic" form of this result.

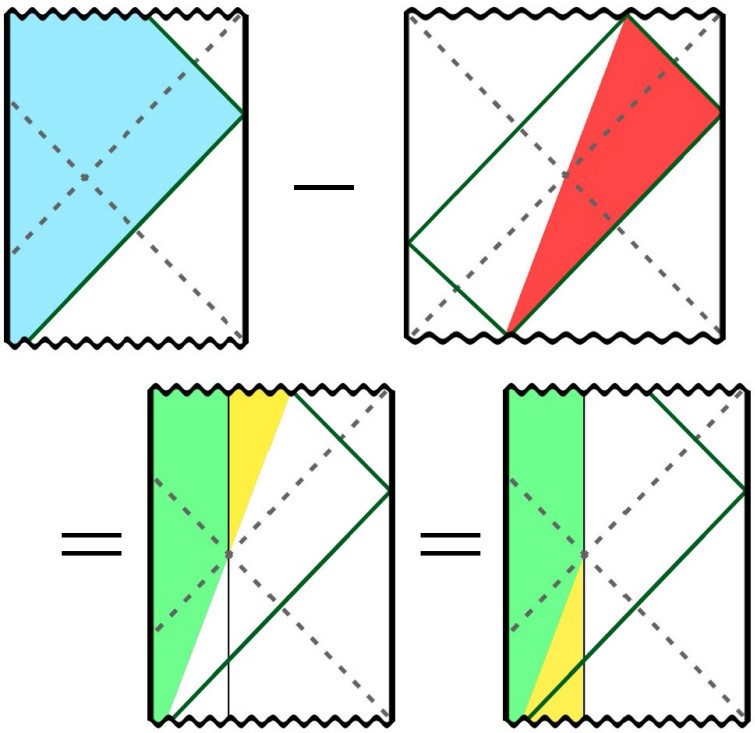

Figure 4.26: The geometric argument for why the complexity is constant during phase (ii). The half TFD Wheeler-DeWitt patch (red) is subtracted from the phase (ii) patch (blue). The remaining region is broken into two pieces (green and yellow) that are rearranged to become the entire region behind the horizon. This "proof" is independent of boundary time.

where $s_* = \arcsin(T)$ or equivalently[72]

$$\Delta\mathcal{C}_A(t_B) - \Delta\mathcal{C}_A(0) = \frac{r_H}{4\pi G\hbar} \ln\left|\sqrt{1-T^2}\sinh(r_H t_B) - T\right| \times \left(\tanh(r_H t_B) - \frac{T\,\mathrm{sech}(r_H t_B)}{\sqrt{1-T^2}}\right) . \quad (4.123)$$

In the $T \to 0$ limit this result is simply the complexity for the BTZ geometry without any additional spacetime behind the horizon. Figure 4.27 shows the regularized complexity for a range of ETW brane tensions. We

[72]The results here include the null boundary counterterms first proposed in [248].

see again the linear growth of complexity at late times, which takes the form

$$\lim_{t\to\infty} \frac{d\mathcal{C}_A}{dt} = \frac{2M}{\pi\hbar} \,. \tag{4.124}$$

We see that both $\mathcal{C}_V$ and $\mathcal{C}_A$ grow linearly at late times, but exhibit different behaviour at early times. The volume-complexity increases smoothly from the time-symmetric surface $t = 0$, but the action-complexity is constant until one of the null boundaries defining the Wheeler-DeWitt patch intersects the ETW brane. During the period that the action-complexity is constant, the entanglement entropy is increasing, indicating thermalisation without complexity increase. This is puzzling, but not impossible. Alternatively, it may be that the action tracks the complexity well over large time scales but not during this early-time regime.

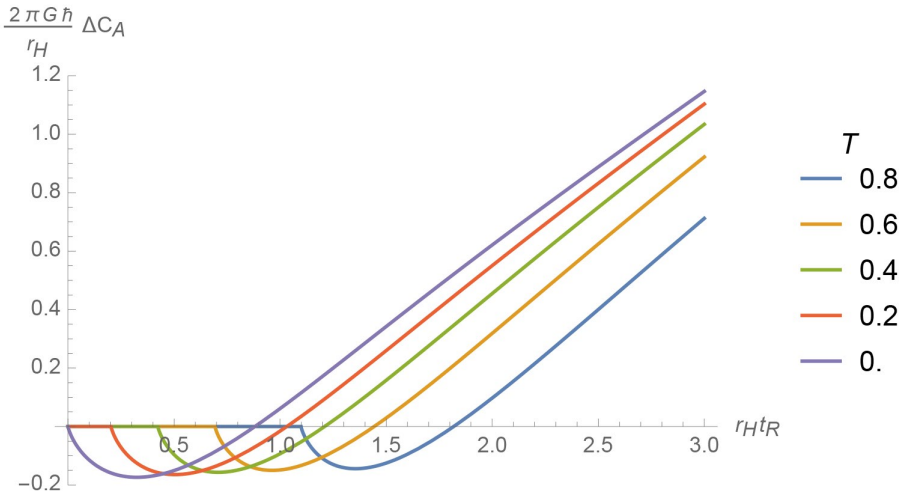

Figure 4.27: The regularized complexity during phases (ii) and (iii), as a function of boundary time, for a selection of different brane tensions, T.

4.6 Pure AdS analogue

There is a close analogy between the maximally extended AdS-Schwarzschild black hole spacetime and pure AdS space divided into complementary Rindler

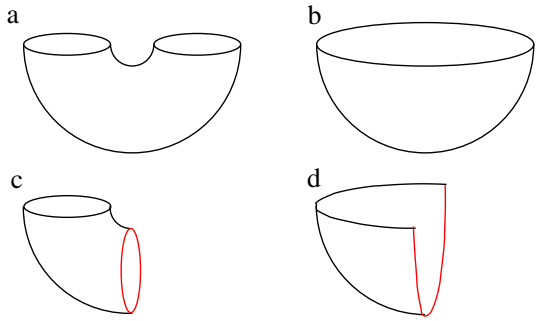

Figure 4.28: Euclidean path integral geometries defining (a) the thermofield double state of two CFTs, (b) the vacuum state of a single CFT, (c) a black hole microstate, and (d) a microstate for a half space. Red curves indicate BCFT boundary conditions.

wedges [249], where the two exterior regions correspond to the interiors of the two Rindler wedges, as shown in Figure 4.29. In this section, we extend this analogy to describe states of a CFT on a half-sphere that are analogous to the black hole microstates considered in the main part of the chapter. We specialize to 2+1 dimensions for simplicity.

In the black hole story, the full geometry is described by two entangled CFTs, each in a thermal state. Our microstates are pure states of just one of these CFTs. For pure AdS, the geometry is described by a state in which the CFT degrees of freedom on two halves of a circle are entangled. The analog of a black hole microstate is a pure state of the CFT on a half circle (i.e. an interval). To make this fully well-defined, we can place boundary conditions on the two ends of the interval, so that our CFT on a circle is replaced by a pair of BCFTs each on an interval. As discussed in [250], we can define an entangled state of this pair of BCFTs whose dual geometry is a good approximation to the geometry of the original CFT state (inside a Wheeler-deWitt patch). Now, the analog of one of our black hole microstates is a pure state of one of these BCFTs that we can define using a path integral, as shown in Figure 4.28.

The path integral in Figure 4.28(d) is equivalent via a conformal transformation to the path integral that defines the vacuum state of the BCFT

on an interval. For this state, the corresponding geometry was described in [87] and can be represented as a portion of the global AdS geometry ending on a static ETW brane, as shown in Figure 4.29. That figure also shows the Rindler wedges that are analogous to the two exterior regions in the maximally extended black hole geometry. We can see that (in the $T > 0$ case) the ETW brane emerges from the past Rindler horizon in the second asymptotic region, reaches some maximum distance from the horizon, and then falls back in.

Explicit geometry

To find the geometry associated with the BCFT vacuum state, it is simplest to consider a conformal frame where the interval on which the BCFT lives is $(-\infty, 0]$. In this case, we recall from Section 4.2 that in Poincaré coordinates

$$ds^2 = \frac{L^2}{z^2}(-dt^2 + dz^2 + dx^2) \ , \tag{4.125}$$

the vacuum geometry corresponds to the region $x/z < T/\sqrt{1-T^2}$ terminating with an ETW brane, as shown in Figure 4.6. Passing to global coordinates via the transformations

$$\begin{aligned} L/z &= \cosh(\rho)\cos(\tau) - \sinh(\rho)\sin(\theta) \\ x/z &= \sinh(\rho)\cos(\theta) \\ t/z &= \cosh(\rho)\sin(\tau) \ , \end{aligned} \tag{4.126}$$

the ETW brane locus becomes

$$\sinh(\rho)\cos(\theta) = \frac{T}{\sqrt{1-T^2}} \tag{4.127}$$

in coordinates where the metric is

$$ds^2 = L^2(-\cosh^2\rho d\tau^2 + d\rho^2 + \sinh^2\rho d\theta^2) \ . \tag{4.128}$$

Here, the brane is static in the global coordinates, extending to antipodal points at the boundary of AdS, as shown in Figure 4.29. In that figure, we see that from the point of view of one of the Rindler wedges, the brane falls into the horizon.

To make the analogy with the black hole more clear, we can now describe the ETW brane trajectory for $T > 0$ in a Rindler wedge, the analog of the second asymptotic region in the black hole case. Defining coordinates (χ, ζ, r) from the Poincaré coordinates by

$$\begin{aligned} t/L &= e^{\chi} \sinh(\zeta) \sqrt{1 - \frac{1}{r^2}} \\ x/L &= e^{\chi} \cosh(\zeta) \sqrt{1 - \frac{1}{r^2}} \\ z/L &= e^{\chi} \frac{1}{r} \ , \end{aligned} \tag{4.129}$$

the Rindler wedge corresponding to the second asymptotic region takes the form of a Schwarzschild metric with non-compact horizon [251],

$$ds^2 = L^2(-(r^2-1)d\zeta^2 + \frac{dr^2}{r^2-1} + r^2 d\chi^2) \ , \tag{4.130}$$

and the brane locus is simply

$$\sqrt{r^2-1}\cosh(t) = \frac{T}{\sqrt{1-T^2}} \ . \tag{4.131}$$

Note that this is precisely the same as the result (4.26) (setting $r_H = 1$). The reason is that the black hole geometry we considered previously is simply obtained from the present case by periodically identifying the χ direction. Thus, as in that case, for each time t, the ETW brane sits at a constant r in the Schwarzschild picture, with $r(t)$ reaching a maximum at $t = 0$.

Entanglement calculations

In analogy to the earlier result for BTZ black holes, the entanglement entropy of sufficiently large intervals in the BCFT can provide information

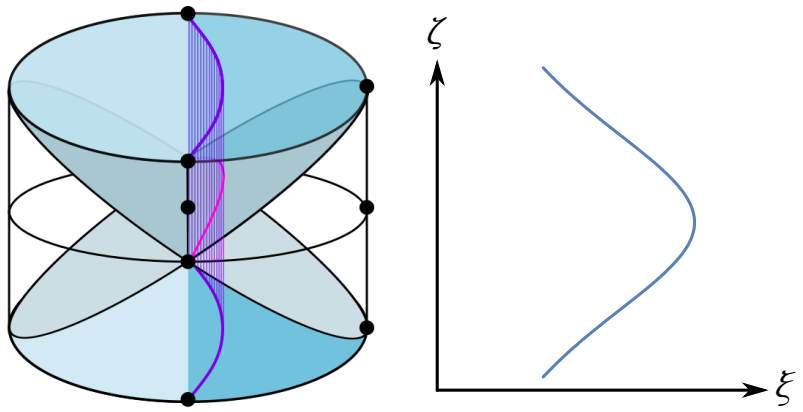

Figure 4.29: (Left) The ETW brane in global AdS. For $T > 0$ we have the geometry on the left of the brane. For $T > 0$, we have the geometry on the right of the brane. Diagonal planar surfaces are Rindler horizons dividing the spacetime into complementary Rindler wedges plus past and future regions. (Right) Dependence of the radial position parameter $\xi = \sqrt{r^2 - 1}$ on Schwarzschild time ζ.

about the geometry behind the Rindler horizon.

Using the standard CFT time in a conformal frame where we have a fixed distance between the two boundaries, the entanglement entropy for a connected boundary region is time-independent. However, to provide the closest analogy with our earlier calculations, we can instead consider the entanglement entropy of an interval of fixed width in the Schwarzschild spatial coordinate χ, as shown in Figure 4.30.

We have seen that the geometry and the brane trajectory in the present case is mathematically identical to the black hole case for $r_H = 1$ except that the χ coordinate is now non-compact. The compactness of θ did not enter into the previous calculations of entanglement entropy, so all the calculations in Section 4.3 apply here as well, and we can immediately jump to the result, that the entangling surface will probe behind the horizon when

$$\sinh\left(\frac{\Delta\chi}{2}\right) \geq \cosh(\zeta_0)\sqrt{\frac{1+T}{1-T}}\,. \tag{4.132}$$

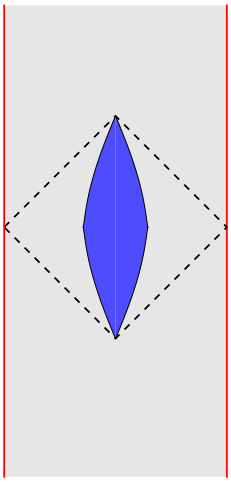

Figure 4.30: Interval of fixed width in Schwarzschild time (blue shaded region) in the BCFT worldvolume geometry.

Since χ is noncompact now, we have that for any time ζ_0 and any T, we can always choose a large enough interval $\Delta\chi$ so that the entangling surface probes behind the horizon. The explicit expressions for entanglement entropy in the two phases are the same as those in Section 4.3.1 (with $r_H = 1$).

Thus, if we unwrap the compact direction of the BTZ black hole, the ETW branes will be dual to boundary states on a spatial interval of pure AdS_3. Our BTZ entanglement calculations carry over, implying that control of a suitably large boundary subregion should allow an observer to probe behind the Rindler horizon.

4.7 Effective cosmological description?

We have seen in Section 4.2 that the worldvolume geometry of our ETW brane takes the form of a d-dimensional FRW spacetime. For the simple model with a constant tension ETW brane, the explicit metric was given in (4.35) for the case of a (3+1)-dimensional ETW brane. Generally speaking, the physics on this brane does not provide a model of d-dimensional cosmology, since the gravitational physics is higher-dimensional. However, there is

a vast literature on braneworld cosmology (see [77] for a review) exploring scenarios where the physics of a d-dimensional brane embedded in a higher-dimensional spacetime does have an effective description as d-dimensional gravity coupled to matter. This requires gravity to "localize" to the brane, such that over a large range of distance scales gravitational interactions between matter on the brane are well-described by d-dimensional rather than higher-dimensional gravity. In [72], such localization was shown to occur for a brane which cuts off the UV region of an anti-de Sitter spacetime; this is known as the Randall-Sundrum II (RSII) braneworld scenario. In our geometries, the brane cuts off the UV in an asymptotically AdS spacetime (the AdS-Schwarzschild black hole). While this is globally different from pure AdS, it is expected that for appropriate values of L_{AdS}, r_H, and the ETW brane trajectory, the physics should be sufficiently similar to the pure AdS case that gravity localization still occurs and we still have an effective d-dimensional description. Since our brane worldvolume is that of a cosmological FRW spacetime, our model would then provide a microscopic description of d-dimensional braneworld cosmology.

Gravity localization in the Randall-Sundrum II model

In this section, we will review the basic mechanism of gravity localization (see [252] for a pedagogical introduction) and try to understand the requirements on the parameters in our model in order that an effective lower-dimensional description exists. In the Randall-Sundrum II model [72] we have an infinite extra dimension, but the bulk metric (for $d = 4$) is now a warped product of the form

$$ds_5^2 = dz^2 + e^{-2A(z)} g_{\mu\nu}(x) dx^\mu dx^\nu \,, \qquad -\infty < z < \infty \,, \tag{4.133}$$

with a 3-brane placed at $z = 0$ and $\mathbb{Z}_2$-symmetry imposed in this coordinate. In the original RSII model, one has warp factor $A(z) \sim |z|/\ell$; the bulk spacetime is then simply a slice of AdS_5 which is cut off in the UV by a 3-brane (referred to as a UV or Planck brane), with $\mathbb{Z}_2$-symmetry imposed about the brane. Tuning the brane tension against the bulk cosmological

constant allows for a Poincaré-invariant brane metric $g_{\mu\nu}(x) = \eta_{\mu\nu}$. Randall and Sundrum found that, within this set-up, one reproduces 4-dimensional Einstein gravity on the brane for distances much larger than the AdS radius $L_{\rm AdS}$; for example, the gravitational potential on the brane is [253]

$$V(r) \approx \frac{GM}{r}\Big(1 + \frac{2L^2_{\rm AdS}}{3r^2}\Big)\,. \tag{4.134}$$

The reason for the localization is that the warp factor suppresses metric perturbations far from the brane, with $L_{\rm AdS}$ the length scale on which this suppression occurs. Formally, one considers separable metric perturbations of the form $h_{\mu\nu} = \epsilon_{\mu\nu}\psi(z)\phi(x^\mu)$, with $\phi(x^\mu)$ an eigenstate of the 4-dimensional wave operator $\Box_4\phi = m^2\phi$; the linearized Einstein equations then reduce to an analogue Schrödinger problem for $\psi(z)$, where the Schrödinger "energy" determines the particle mass in the four-dimensional description. The analysis reveals a massless 'zero mode' wavefunction which localizes at the brane and exactly reproduces the 4-dimensional Newtonian potential; the continuum of massive Kaluza-Klein modes provide corrections, but they are suppressed at the position of the brane due to a peak in the potential.

The localization phenomenon has been interpreted in the context of AdS/CFT [73–76, 254–256], by the observation that the RSII model in a $(d+1)$-dimensional AdS bulk (and its curved-brane descendents in $(d+1)$-dimensional AAdS spacetimes) should be equivalent to a d-dimensional CFT with some UV cutoff coupled to dynamical gravity on the brane.[73]

Locally localized gravity

Based on these results, it is natural to ask whether gravity localization extends to cases where we have an approximately AdS bulk cut off by a UV brane which is approximately Minkowski. In fact, there are some complications; for example, as noted by Karch and Randall in [79], in the case of a

[73] This doesn't provide a full microscopic description of the theory since the dynamical gravity is added in "by hand" to the cutoff CFT. In contrast, the CFT in our discussion corresponds to the asymptotic region on the far side of the black hole; this is an ordinary CFT with no dynamical gravity and thus can provide a microscopic description.

brane with AdS_4 worldvolume in global AdS_5, one no longer has a normalizable zero mode. This is because only part of the UV region of global AdS is excised by the introduction of an AdS_4 UV brane; a graviton at the brane can still tunnel toward the true boundary of AdS, where the warp factor blows up, so this geometry does not trap gravity at the brane. However, Karch and Randall showed that if we are close enough to the Minkowski situation, the time scale for this tunneling is long, so that four-dimensional Einstein gravity still provides a good approximation over sufficiently short time scales. This supports the more general idea that localization of gravity should be a "local" phenomenon, which should not depend upon the behaviour of the warp factor far from some region of interest.

Branes in AdS Schwarzschild

The question relevant for us is whether one retains gravity localization when the bulk is modified through the introduction of a black hole, and the brane worldvolume is allowed to be dynamical. The first question has been previously investigated [257–263]. Based on the work of Karch and Randall, one expects that if the brane is taken far enough from the black hole horizon, so that the nearby spacetime is approximately AdS, then the local character of gravity localization should allow for effective Einstein gravity on the brane, up to $\mathcal{O}(r_H/r_{\rm br})$ corrections (where $r_{\rm br}$ is the position of the brane). The detailed analysis performed in [261, 262] for the case of an Einstein static (ES) braneworld (with $r_{\rm br} = \text{const}$) in AdS Schwarzschild supports this conclusion. Our FRW branes are not static, but we expect similar qualitative behaviour during the period when the effective Hubble parameter is small compared with the AdS scale $H \equiv \dot{r}/r \ll 1/L_{\rm AdS}$.

Implications for the constant-tension brane scenario

Let is now apply these constraints to the geometries arising in the simple model with a constant tension ETW brane. We have seen that obtaining an effective four-dimensional description requires $r_{\rm br} \gg r_H$ and $H \ll L_{\rm AdS}$. In our set-up, the maximum proper radial size of the brane, in the case of

critical tension $T = 1$, is given for $d = 4$ by $r_0 = r_H\sqrt{1 + \frac{r_H^2}{L_{\rm AdS}^2}}$; thus, in order to have some regime for which $r_{\rm br} \gg r_H$, we must consider a large black hole $r_H \gg L_{\rm AdS}$, and almost-critical tension $T \approx 1$. The requirement that $H \ll L_{\rm AdS}$ will be satisfied for most of the evolution as long as the total proper time (4.36) is large in AdS units. Again, this requires that T is very close to 1.

Unfortunately, we recall that while the Lorentzian solutions for any value $T < 1$ (and even larger values for $d > 2$) look physically reasonable, the corresponding Euclidean solutions for $d > 2$ appear to make sense only for $T < T_* < 1$ since otherwise the ETW brane overlaps itself in the Euclidean picture (see Figure 4.10). The requirement $T < T_*$ would rule out a viable model with an effective four dimensional description since this required $r < 1.2876\, r_H$. On the other hand, we had reason to question the validity of the simple holographic treatment in these cases.

To summarize, in the simplest toy model for how to treat the BCFT boundary conditions holographically, it does not seem possible to realize microstates for which the effective description of the ETW brane physics corresponds to a four-dimensional cosmology. However, it remains very interesting to understand whether this scenario for cosmology can be realized with more general effective actions that would correspond to a more complete treatment of the holographic BCFT physics.

4.8 Discussion

In this final section, we discuss a few possible generalizations and future directions.

For the specific examples in this chapter, we have mainly considered geometries obtained by assuming the very simple holographic ansatz for how to model CFT boundary conditions holographically. In that model, the ETW brane is filling in for some more detailed microscopic physics. This could involve branes or orientifold planes of string/M-theory, or geometrical features such as the degeneration of an internal manifold. Depending on the

particular situation, a more realistic model might include additional terms in the brane action or couplings to additional bulk fields. As a particular example, scalar operators in a BCFT can have one-point functions growing as $1/y^{2\Delta}$ as the distance y to the boundary decreases. This would correspond to having some extra scalar fields in the bulk, sourced by the ETW brane.[74] In our context, this would lead to matter outside the black hole that falls into the horizon. Thus, the explicit geometries we have utilized should be viewed as simple examples that may elucidate the basic physics of more precise holographic duals for Euclidean-time-evolved boundary states. It will be interesting to flesh out the AdS/CFT correspondence for BCFTs more fully and explore the microstate geometries emerging from more general bulk effective actions. It will also be interesting to understand better the constraints on boundary conditions/boundary states for a given holographic CFT that lead to a fully geometrical bulk description.

Within the context of any particular choice of bulk effective action (e.g. the constant tension ETW brane model we used here), it is also interesting to understand which parameter values can be realized in some microscopic theory. For example, if there are microscopic models that realize (at least approximately) the simple ansatz, which values of the parameter T arise from legitimate boundary conditions for a holographic CFT. For (1+1)-dimensional CFTs, this is related to the question of which boundary entropies are possible. Some constraints have been discussed previously [267], but these do not apply for holographic models. An interesting result is that for the monster CFT, only positive values (or perhaps extremely small negative values) of $\ln(g)$ (proportional to $\operatorname{arctanh}(T)$ in the holographic case) are allowed [268]. If this extended to holographic theories, it would imply that only the case with an ETW brane behind the horizon is physical.

Another interesting generalization would be to consider states constructed in a similar way, but with boundary conditions that do not preserve conformal invariance. For example, we can have boundary conditions that correspond to boundary RG flows from one conformally invariant boundary

[74] Some particular top-down examples of complete geometries dual to supersymmetric BCFT states have already been understood: see [264–266].

condition to another. These may be represented by a more general class of ETW brane actions, and give rise to a wider variety of geometries. Finally, we can consider similar constructions in holographic theories which are not conformal, for example in holographic RG flow theories or in holographic theories derived from low-energy Dp-brane actions. For all these cases, we expect that the basic idea of probing behind-the-horizon physics via time-dependence of subsystem entanglement remains valid.

It would be very interesting to perform direct entanglement entropy calculations for Euclidean-time-evolved boundary states in specific CFTs, to see whether the results are qualitatively similar to those in our model calculation, and to generate microscopic examples of black hole microstates for which we can learn about the behind-the-horizon physics directly. Naively, this will be challenging in strongly coupled holographic CFTs, but perhaps even calculations for tractable non-holographic theories (such as large c symmetric orbifold CFTs)[75] will be enlightening. It may also be possible to perform direct calculations in holographic CFTs by assuming something about the structure of holographic BCFT correlators, similar to the calculations in [269, 270].

Finally, with a larger toolbox for studying holographic duals of Euclidean-time-evolved boundary states, it will be interesting to see if it is possible to realize any examples where gravity is localized on the ETW brane, or more generally, that the physics of the spacetime causally disconnected from the asymptotic boundary is effectively described by four-dimensional cosmology. This would be very interesting whether or not such a cosmology can be made realistic, since there currently aren't any known complete, non-perturbative quantum descriptions of four-dimensional big bang cosmology, as far as we are aware. In our case, the CFT and the specific microstate would provide the complete description and allow (in principle) a calculation of the initial conditions for cosmology that should be used as inputs for the effective field theory description (also to be determined from the CFT/state) that would be valid at intermediate times.[76] Of course, these calculations would require

[75] We thank Volker Schomerus for this suggestion.

[76] If our approach can be realized, it would be similar in some ways to the Hartle and

a much better understanding of how black hole behind-the-horizon physics is encoded in a CFT.

One of the major challenges in coming up with candidates for quantum gravity theories capable of describing cosmology is that it is not even clear what the very basic mathematical framework could be. Usual examples of holography making use of conventional quantum systems describe spacetimes with some fixed asymptotic behavior. This is normally assumed to be incompatible with cosmological physics, so various qualitative ideas have been put forward for how to come up with something more general (see e.g. [43, 228, 231, 272–274] for a variety of perspectives). However, to date, none of these has led to a complete model, or even a precise mathematical structure that could generalize the usual state-in-a-Hilbert-space of ordinary quantum mechanics. A likely possibility is that we have simply not yet stumbled across the right idea. But it is worth considering the alternative, that cosmology is somehow described by a conventional quantum system, just like the rest of physics. If this quantum system is related to gravity in the usual holographic way, we would need to understand how our cosmological observations could be compatible with fixed asymptotic behavior for the global spacetime. One of the most attractive features of our suggestion is that it gives a possible way to realize this, and thus, to describe cosmology with ordinary quantum mechanics.

Hawking's 'no boundary' approach to cosmology [271], except that our Euclidean path integral is for a non-gravitational boundary theory, and the path integral itself is defined using a boundary. So one might call it the "boundary-boundary-no-boundary" approach.

Chapter 5

Bottom-Up Holographic Models for Cosmology

5.1 Introduction

An important open question in theoretical physics is how to formulate a non-perturbative quantum mechanical description of gravity in cosmological backgrounds. Given the theoretical successes of the AdS/CFT correspondence over the past two decades [29], an especially appealing prospect is the possibility of embedding cosmological physics in AdS/CFT, though the viability of this approach for "realistic" cosmologies remains unclear at present. A number of differing holographic approaches to cosmology appear in the literature; an incomplete catalogue of these includes [228, 230–233, 275].

The class of holographic models that we will be interested in here originated with [2], and has subsequently been further studied in [276–278]. In the model considered in these papers, a Euclidean boundary conformal field theory (BCFT) path integral is used to prepare a state of a holographic CFT; via a simple effective or "bottom-up" model for AdS/BCFT introduced in [78, 87, 88], this state is understood to correspond to an AdS black hole terminating on an end-of-the-world (ETW) brane behind the horizon. The worldvolume of this ETW brane is a recollapsing (negative cosmological constant) FRW universe. Under appropriate conditions, when the ETW brane propagates far outside the black hole horizon in the second asymptotic region, the effective theory on the ETW brane would be expected to exhibit gravity localization via the Karch/Randall/Sundrum mechanism [72, 79]; the upshot is that gravitational physics on a cosmological background is

encoded in a particular state, prepared by a Euclidean path integral, in a holographic theory. See Figure 5.1 for a visualization of this logic; references [2, 277, 278] should be consulted for additional details.

The simple model analyzed in the references mentioned above has proven interesting and suggestive, but not entirely satisfactory: the properties required for the solution to exhibit gravity localization cannot actually be realized within the parameter space.[77] In particular, analytically continuing the Lorentzian solutions where gravity localization is expected to Euclidean signature, we find that the corresponding Euclidean solutions involve self-intersecting ETW branes, whose holographic interpretation is not clear; see Figure 5.2.

An approach to circumventing this issue was proposed by Van Raamsdonk in [278]. It was suggested that the previous bottom-up models could be modified by adding an additional "interface brane" separating two regions of asymptotically AdS spacetime in the bulk, generally with differing AdS lengths $L^{(1)}_{\text{AdS}}$ and $L^{(2)}_{\text{AdS}}$, as shown in Figure 5.3. A practical rationale for this proposition is to avoid the self-intersection problem mentioned above, which arises because the Euclidean gravity solutions require a periodically identified coordinate $z \sim z + \beta$ to avoid developing a singularity at the coordinate horizon; in the case with both an ETW brane and an interface brane, the region between these branes no longer includes a coordinate horizon, and therefore need not have any periodically identified coordinate.

A somewhat more sophisticated motivation was also given in [278], making use of an effect observed in [279]. To understand the second motivation, one should note that, by performing a different analytic continuation of the bulk Euclidean solutions with a single ETW brane, corresponding to Wick rotating one of the transverse coordinates suppressed in Figures 5.1, 5.2, and 5.3 (which we assume to have $\mathbb{R}^{d-1}$ planar symmetry for a $(d+1)$-dimensional bulk), one obtains a static Lorentzian solution with an ETW

[77] The exception to this point is [276], in which it was found that an ETW brane propagating in a charged black hole background could enjoy the desired properties for cosmology. It is not clear how to make sense of this set-up as an analytic continuation of Euclidean AdS/CFT, since it appears that the gauge field component A^0 should be imaginary in the Euclidean signature solution.

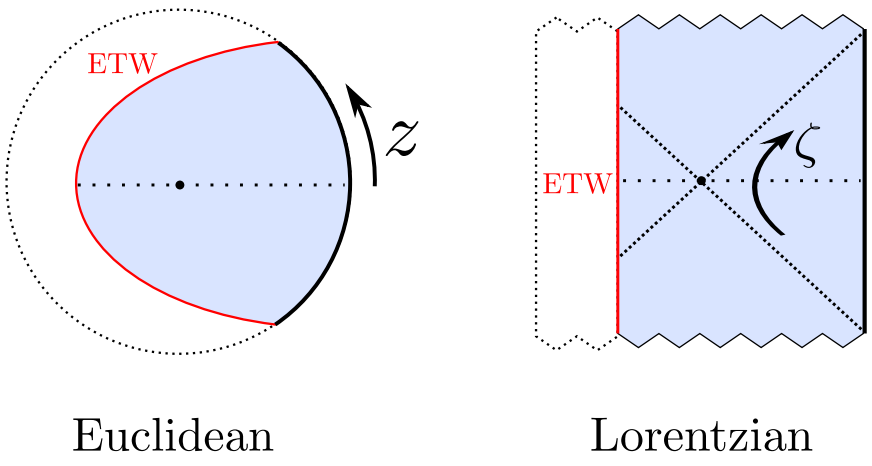

Figure 5.1: An approach to holographic cosmology proposed in [2]. We begin on the left with a Euclidean BCFT path integral (bold black line), with some choice of boundary condition imposed in the past and future Euclidean time. The transverse directions suppressed in this figure could be taken to have S^d or $\mathbb{R}^d$ symmetry, so that the Euclidean CFT path integral is on a cylinder or a strip respectively. Cutting open this path integral at the moment of time symmetry, we obtain some state $|\Psi\rangle$ of the holographic CFT. In the bulk, we have a Euclidean asymptotically AdS spacetime (blue) terminating on an ETW brane (red). We may then analytically continue to Lorentzian time to obtain the leading geometry encoding the evolution of $|\Psi\rangle$, shown on the right. The ETW brane stays behind the horizon of an AdS black hole; it is a "big bang/big crunch" cosmology (with spherical or flat spatial sections). The construction is time-symmetric throughout, with the moment of time symmetry illustrated as a dotted line. Here, z indicates the Euclidean coordinate analytically continued to the Lorentzian time ζ.

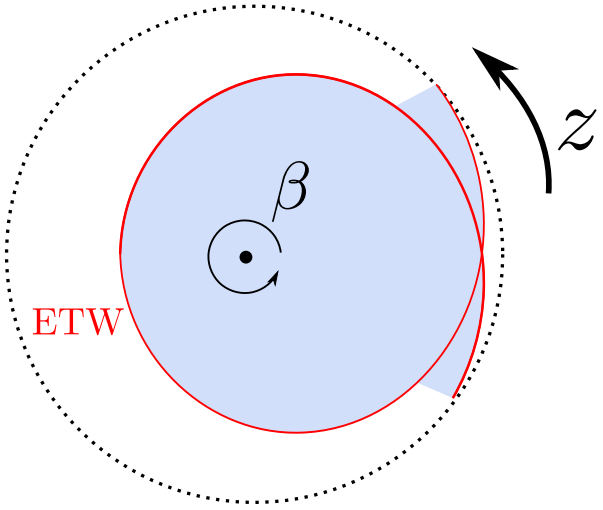

Figure 5.2: Pathological Euclidean gravity solution with a self-intersecting ETW brane (red). The trajectory of the ETW brane in the Euclidean asymptotically AdS spacetime (blue) can be determined from the equations of motion; the fact that this trajectory self-intersects arises from the coordinate periodicity $z \sim z + \beta$ which must be imposed to ensure smoothness at the coordinate horizon (central dot).

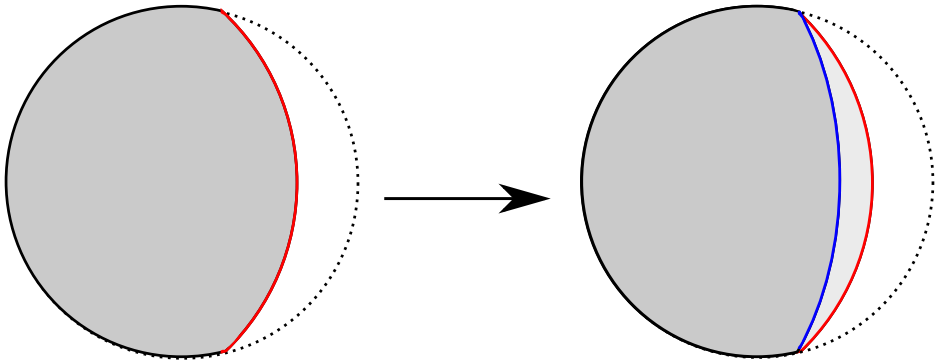

Figure 5.3: Two putative bulk duals of holographic BCFT. Here, ETW branes are shown in red, and interface branes in blue; the shaded region is an asymptotically AdS Euclidean spacetime. The premise of this work is to move from the model depicted on the left to that depicted on the right, i.e. to introduce an additional interface brane.

brane whose worldvolume is an asymptotically AdS traversable wormhole; see Figure 5.4. Consequently, the effective description of the cosmology is related by "double analytic continuation" to an effective theory involving a cutoff CFT on a traversable wormhole background; from this perspective, the non-existence of the solutions relevant for cosmology appears to be related to a no-go result for such traversable wormholes in the absence of large amounts of negative energy [280]. However, in a simple bottom-up model for the holographic dual of a conformal interface between two CFTs (also shown in Figure 5.4), the authors of [279] found that one could produce an anomalously large negative Casimir energy in one of the two CFTs in a particular critical limit of the tension of a bulk interface brane. From this interface CFT starting point, the model that we are concerned with in this chapter would correspond to "coupling one of the CFTs to gravity" by introducing an ETW "Planck brane" in the bulk. In this case, one might hope that a similar "negative energy enhancement" effect could allow for a means of negating the hypotheses of the aforementioned no-go result.

The purpose of this work is to investigate this possibility, generalizing the model of [2] by adding an interface brane. We begin by considering the case where this interface brane is governed by a single tension parameter; in this case, we argue that there are no consistent solutions in the region of parameter space where we expect to recover gravity localization in the cosmology, suggesting that this model has no significant advantage over the previous model. In particular, putative solutions do not have an ETW brane and an interface brane which join properly; for example, they may instead intersect. We then generalize the model further by incorporating Einstein-Hilbert terms on the ETW brane,[78] arguing that solutions with the desirable properties should exist in this case. We comment on the nature of the relevant region of parameter space from the perspective of physics in the effective theory on the ETW brane, but leave further commentary about the physicality of this region, and an exploration of the parameter space more

[78] This is referred to as a "DGP term" in [281], after an analogous construction by Dvali, Gabadadze and Porrati [282], though of course the present model has an asymptotically AdS bulk.

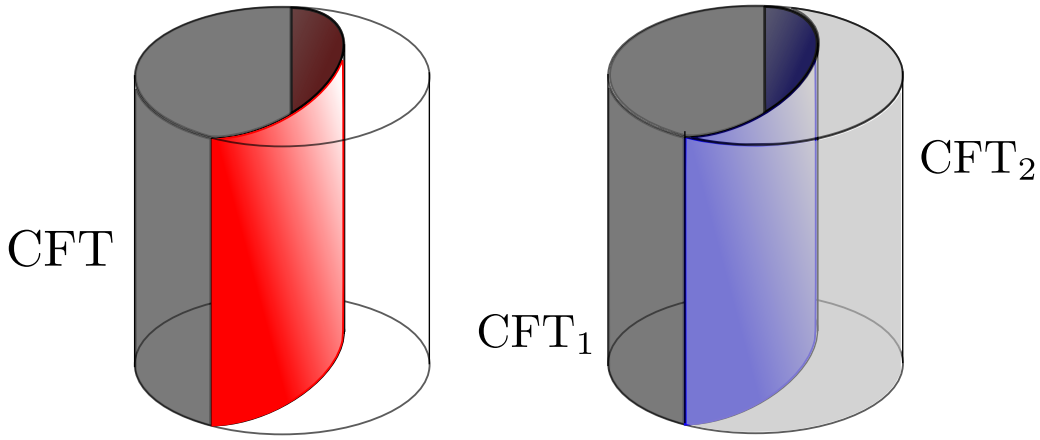

Figure 5.4: Holographic duals of (left) boundary CFT and (right) interface CFT. The ETW brane is illustrated in red, and the interface brane in blue. We can interpret these diagrams as either representing Euclidean spacetimes, or the Lorentzian spacetimes obtained by Wick rotating a coordinate of one of the transverse directions suppressed in Figures 5.1, 5.2, and 5.3, which is the vertical direction here. In Lorentzian signature, the intrinsic geometry of the ETW/interface brane is a traversable asymptotically AdS wormhole.

broadly, to future work.

The outline of this chapter is as follows. In Section 5.2, we attempt to briefly review the relevant results already appearing in the literature. We follow this in Section 5.3 with an analysis of the model with an additional interface brane of constant tension, and then further augment this model in Section 5.4 with an Einstein-Hilbert term on the ETW brane. We briefly conclude in Section 5.5.

Note: As this work was nearing completion, we were alerted to the existence of similar work by Seamus Fallows and Simon Ross [283]. These authors graciously agreed to coordinate in submitting pre-prints.

5.2 Review of bottom-up holographic solutions for boundary/interface CFT

To keep our presentation self-contained, we will review the relevant holographic models and solutions in this section, and briefly recapitulate some important results in this and the following section. The models discussed in this section follow a prescription for AdS/BCFT involving ETW/interface branes which originated in [78, 87, 88], and the solutions we discuss in this section appear in [2, 278, 279, 284]; the purpose of this section is to summarize the pertinent information from the latter references, and to establish notation. The gravity solutions discussed in Section 5.2.1 and 5.2.2 correspond to those in the first and second panels of Figure 5.4 respectively: they are Euclidean asymptotically AdS_{d+1} spacetimes, with either an ETW brane or an interface brane, and preserving a transverse $\mathbb{R}^{d-1}$ symmetry.

5.2.1 Solutions with an ETW brane

We begin by considering a class of models for the gravitational dual of a holographic BCFT, determined by the Euclidean gravitational action

$$\begin{aligned} S &= S_{\text{bulk}} + S_{\text{ETW}}^{\text{matter}} \\ S_{\text{bulk}} &= \frac{1}{16\pi G_{\text{bulk}}} \int_{\mathcal{M}} d^{d+1}x\sqrt{g}\ (R - 2\Lambda) \\ &\qquad + \frac{1}{8\pi G_{\text{bulk}}} \int_{\text{ETW}} d^d y\sqrt{h}\, K\,, \end{aligned} \tag{5.1}$$

where we take the brane matter action to be[79]

$$S_{\text{ETW}}^{\text{matter}} = \frac{(1-d)\lambda}{8\pi G_{\text{bulk}}} \int_{\text{ETW}} d^d y\sqrt{h}\,. \tag{5.2}$$

[79] In this chapter, we use the symbols λ and κ for the ETW brane and interface brane tensions respectively rather than T as in the previous chapter, in order to differentiate between these two types of branes.

The cosmological constant Λ is related to the AdS length L_{AdS} by

$$\Lambda = -\frac{d(d-1)}{2L_{\text{AdS}}^2} \,. \tag{5.3}$$

Here and throughout, we will take λ to lie in the interval $\left(0, \frac{1}{L_{\text{AdS}}}\right)$.

The bulk equation of motion is simply the Einstein equation with cosmological constant Λ; meanwhile, the ETW brane trajectory is given by the equation of motion (see Appendix D.1)

$$K_{ab} = \lambda h_{ab} \,. \tag{5.4}$$

In [2], Euclidean solutions with a S^{d-1} spherical symmetry were considered; here, we will instead consider Euclidean solutions with a $\mathbb{R}^{d-1}$ symmetry, though the two cases are completely analogous. The appropriate bulk ansatz is then the *Euclidean AdS soliton* solution

$$ds^2 = L_{\text{AdS}}^2 f(r) dz^2 + \frac{dr^2}{f(r)} + r^2 dx_\mu dx^\mu \,, \qquad f(r) = \frac{r^2}{L_{\text{AdS}}^2} - \frac{\mu}{r^{d-2}} \,. \tag{5.5}$$

The radial coordinate r ranges from the coordinate horizon value $r_H = (\mu L_{\text{AdS}}^2)^{1/d}$ to infinity. In order to avoid a conical singulariy, the z coordinate must be taken to be periodic, with period[80]

$$\beta = \frac{4\pi L_{\text{AdS}}}{dr_H} \,. \tag{5.6}$$

The ETW brane has trajectory $z = z^{\text{ETW}}(r)$ in this (Euclidean) background, determined by the equation of motion (see Appendix D.1)

$$\left(\frac{dz^{\text{ETW}}}{dr}\right)^2 = \frac{\lambda^2 r^2}{L_{\text{AdS}}^2 f(r)^2} \frac{1}{f(r) - \lambda^2 r^2} \,. \tag{5.7}$$

[80] In the solutions of interest to us here, this coordinate horizon is kept in our solution, rather than being excised by the ETW brane, so this periodicity must be enforced.

In particular, the ETW brane attains a minimum radius at $r_0^{\rm ETW}$ with

$$f(r_0^{\rm ETW}) = \lambda^2 (r_0^{\rm ETW})^2 \,, \qquad r_0^{\rm ETW} = \frac{r_H}{\left(1-\lambda^2 L_{\rm AdS}^2\right)^{1/d}} \,. \tag{5.8}$$

We will also denote the z-coordinate distance traversed by the ETW brane from its minimum radius to infinity by

$$\Delta z^{\rm ETW} \equiv \int_{r_0^{\rm ETW}}^{\infty} dr \, \frac{dz^{\rm ETW}}{dr} \,. \tag{5.9}$$

Despite the appearance that $r_0^{\rm ETW}$ can be made arbitrarily large by sending $\lambda \to L_{\rm AdS}^{-1}$, one must recall that the z coordinate is periodic, and such solutions have the ETW brane self-intersecting at finite r in the case $d > 2$,[81] as shown in Figure 5.2. This places an upper bound $\lambda \leq \lambda_*(r_H)$ on allowed values of the tension parameter λ with sensible Euclidean solutions. Explicitly, this upper bound can be found by demanding $2\Delta z^{\rm ETW} = \beta$, that is, by enforcing

$$\beta = 2\int_{r_0^{\rm ETW}}^{\infty} dr \, \frac{\lambda_* r}{L_{\rm AdS} f(r)} \frac{1}{\sqrt{f(r) - \lambda_*^2 r^2}} \,. \tag{5.10}$$

A maximal upper bound can be found from $\lambda_{\rm max} = \max_{r_H}\{\lambda_*(r_H)\}$. For example, we find

- $d = 3$: $\lambda_{\rm max} L_{\rm AdS} \approx 0.95635$ and $\frac{r_0^{\rm ETW}}{r_H} \lesssim 2.2708$
- $d = 4$: $\lambda_{\rm max} L_{\rm AdS} \approx 0.79765$ and $\frac{r_0^{\rm ETW}}{r_H} \lesssim 1.2876$.

Lorentzian picture and cosmology

In the Lorentzian picture with $z \to i\zeta$, the ETW brane analytically continues to a spatially flat FRW universe; it is worth noting a few features of the intrinsic geometry of these solutions.

[81] For $d = 2$, the ETW brane always spans coordinate range $2\Delta z^{\rm ETW} = \frac{\beta}{2}$, so the desired limit can be realized.

In terms of the proper time s on the brane defined by

$$1 = L_{\rm AdS}^2 f \left(\frac{d\zeta}{ds}\right)^2 - \frac{1}{f}\left(\frac{dr}{ds}\right)^2 , \tag{5.11}$$

the metric on the ETW brane is the FRW metric

$$ds_d^2 = -ds^2 + r(s)^2 dx_\mu dx^\mu , \qquad \left(\frac{dr}{ds}\right)^2 = \lambda^2 r^2 - f(r) . \tag{5.12}$$

Comparing to the usual Friedmann equation for a flat universe

$$\frac{1}{r^2}\left(\frac{dr}{ds}\right)^2 = \frac{8\pi G\rho}{3} , \tag{5.13}$$

we infer that our cosmology is effectively sourced by a negative vacuum energy

$$\frac{8\pi G\rho_\Lambda}{3} = -\frac{1}{L_{\rm AdS}^2}\left(1 - \lambda^2 L_{\rm AdS}^2\right) \tag{5.14}$$

and a "dark radiation" term

$$\frac{8\pi G\rho_{\rm rad}}{3} = \frac{\mu}{r^d} . \tag{5.15}$$

We may also note that the total proper time elapsed on the brane is finite, given by

$$s_{\rm tot} = 2\int_0^{r_0^{\rm ETW}} \frac{dr}{\sqrt{\lambda^2 r^2 - f(r)}} . \tag{5.16}$$

That is, the spacetime is geodesically incomplete, beginning with a "big bang" and ending with a "big crunch". We thus have that the model introduced here necessarily describes a recollapsing FRW universe with radiation and a negative cosmological constant.

It was suggested in [2] that locally localized gravity on the ETW brane may be expected in a region which exhibits "quasistatic" cosmological evolution, and for which the brane remains far outside of the bulk black hole horizon

$$|H| \ll \frac{1}{L_{\rm AdS}} , \qquad r \gg r_H , \tag{5.17}$$

where H is the Hubble parameter. Note that we have for the Lorentzian solution

$$|H|L_{\rm AdS} = \sqrt{-(1-\lambda^2 L_{\rm AdS}^2) + \frac{r_H^d}{r^d}}\,, \qquad \frac{r}{r_H} < \left(1-\lambda^2 L_{\rm AdS}^2\right)^{-1/d}\,, \quad (5.18)$$

so both conditions require $\lambda L \to 1$, and therefore lead to self-intersecting solutions in Euclidean signature.

5.2.2 Solutions with an interface brane

Analogous to the boundary case in the previous subsection, one may consider a class of models for the gravitational dual of holographic interface conformal field theory (ICFT), determined by the Euclidean gravitational action

$$\begin{aligned} S &= S_{\rm bulk} + S_{\rm interface}^{\rm matter} \\ S_{\rm bulk} &= \frac{1}{16\pi G_{\rm bulk}} \sum_{i=1}^{2} \int_{\mathcal{M}_i} d^{d+1}x\sqrt{g}\ (R - 2\Lambda_i) \\ &\quad + \frac{1}{8\pi G_{\rm bulk}} \int_{\rm interface} d^d y \sqrt{h}\ [K]\ , \end{aligned} \quad (5.19)$$

where we take the brane matter action to be

$$S_{\rm interface}^{\rm matter} = \frac{(1-d)\kappa}{8\pi G_{\rm bulk}} \int_{\rm interface} d^d y\sqrt{h}\,. \quad (5.20)$$

Here and in the following, the brackets represent the discontinuity $[X] = X_1 - X_2$ across the interface brane separating regions $\mathcal{M}_1$ and $\mathcal{M}_2$. We are also permitting two different cosmological constants Λ_i, related to the AdS lengths L_i as in equation (5.3). Here, κ lies within the interval

$$\kappa \in (\kappa_-, \kappa_+)\ , \qquad \kappa_- = \left|\frac{1}{L_1} - \frac{1}{L_2}\right|\,, \qquad \kappa_+ = \frac{1}{L_1} + \frac{1}{L_2}\,. \quad (5.21)$$

The bulk equations of motion are simply the Einstein equations with the appropriate cosmological constants, while the interface brane trajectory is

determined by the junction conditions (see Appendix D.1)

$$[h_{ab}] = 0\,, \qquad [K_{ab}] = \kappa h_{ab}\,. \tag{5.22}$$

We again assume the Euclidean solutions have a $\mathbb{R}^{d-1}$ symmetry; the bulk solutions therefore involve the gluing together of two pieces of the AdS soliton geometry, described by the metric

$$ds^2 = L_i^2 f_i(r_i) dz_i^2 + \frac{dr_i^2}{f_i(r_i)} + r_i^2 dx_\mu dx^\mu\,, \qquad f_i(r_i) = \frac{r_i^2}{L_i^2} - \frac{\mu_i}{r_i^{d-2}}\,, \tag{5.23}$$

where L_i is the AdS radius related to the central charge of the i^{th} CFT (which we call CFT_i). One may choose coordinates so that the x^μ agree across the interface joining these two regions; this is our rationale for neglecting a subscript on these coordinates. We may also choose the radial coordinates so that $r_1 = r_2 = r$ on the interface, so we will sometimes drop the subscript of r_i for quantities on the interface brane. The trajectory of the interface $z_i^{\text{int}}(r)$ in each region is determined by equations (4.1) - (4.4) of [279], which are analogous to (5.7) from the ETW brane case. These solutions are analyzed extensively in [279, 284], and we will try to reiterate only the necessary features.

It will be useful to introduce the parameters

$$u = \frac{L_2}{L_1}\,, \qquad \mu = \frac{\mu_2}{\mu_1}\,, \qquad e = \frac{\kappa - \kappa_-}{\kappa_+ - \kappa_-}\,. \tag{5.24}$$

The full interface solution is then completely specified by the parameters (L_1, μ_1, u, μ, e).

Periodicity of z_i coordinates in interface solutions

In contrast to the boundary case in the previous subsection, the coordinate z_i need only be taken periodic, with period β_i given by equation (5.6), if the region $\mathcal{M}_i$ includes the coordinate value $r_i = r_H^{(i)} = (\mu_i L_i^2)^{1/d}$; if not, then the z_i coordinate need not be periodic, and in fact the region can be "multiply wound" from the perspective of this naive periodicity.

To clarify what we mean by "multiply wound", we can first define the quantity Δz_i^{int} to be equal to the z_i-coordinate distance traversed by the interface brane from its minimum radius r_i to infinity; in equations, we may define

$$\Delta z_i^{\text{int}} \equiv \int_{r_0^{\text{int}}}^{\infty} dr_i \, \frac{dz_i^{\text{int}}}{dr_i} \, , \tag{5.25}$$

where r_0^{int} is the minimum value of both the r_1 and r_2 coordinates on the interface brane, and $\frac{dz_i^{\text{int}}}{dr_i}$ is given by the equation of motion (4.4) in [279]. Explicitly, one finds[82]

$$\begin{aligned} \Delta z_1^{\text{int}} &= -\frac{1}{L_1} \int_{r_0^{\text{int}}}^{\infty} \frac{dr}{f_1 \sqrt{V_{\text{eff}}}} \left(\frac{1}{2\kappa r}(f_1 - f_2) + \frac{1}{2}\kappa r \right) \, , \\ V_{\text{eff}} &= f_1 - \left(\frac{f_2 - f_1 - \kappa^2 r^2}{2\kappa r} \right)^2 \, , \end{aligned} \tag{5.26}$$

and an analogous expression for Δz_2^{int}.

Importantly, Δz_i^{int} can be either positive or negative, depending on the data specifying our solution; the former case corresponds to a situation where the i^{th} gravity region contains the coordinate horizon, whereas the latter case corresponds to a situation where it does not. See Figure 5.5 for an illustration of this.

One may then define the quantity $R_i = R_i(u, \mu, e)$ to be the fraction of the span of the asymptotic z_i coordinate in the pure AdS soliton solution (with period β_i) that is covered by the patch associated with CFT_i in the interface solution. We then have two different cases:

- If Δz_i^{int} is positive, then $R_i = \frac{2\Delta z_i^{\text{int}}}{\beta_i}$.
- If Δz_i^{int} is negative, then $R_i = 1 - \frac{2|\Delta z_i^{\text{int}}|}{\beta_i} = 1 + \frac{2\Delta z_i^{\text{int}}}{\beta_i}$.

The multiply wound case corresponds to a situation where Δz_i^{int} is positive (so that the coordinate horizon is not included), and we have $R_i > 1$.

[82] The notation V_{eff} is based on the analysis of [279], which reduces the dynamics of the interface brane to that of a particle moving an an effective potential. We keep the notation here for consistency.

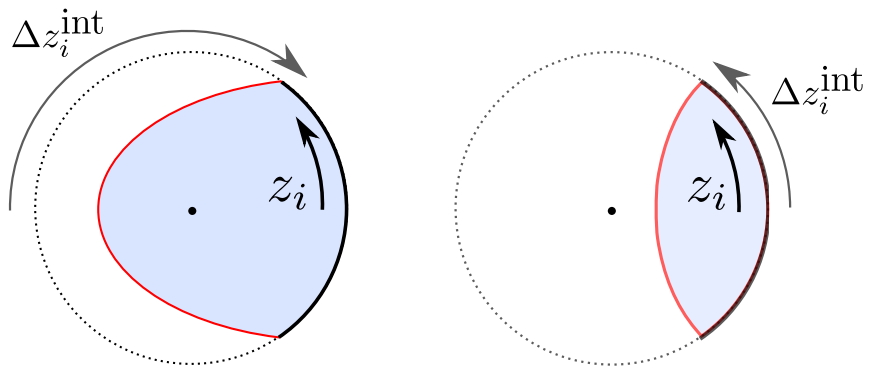

Figure 5.5: (Left) In the case that $\Delta z_i^{\text{int}} < 0$, the i^{th} gravity region includes the horizon. (Right) In the case that $\Delta z_i^{\text{int}} > 0$, the i^{th} gravity region does not include the horizon.

Throughout this work, as a matter of convention, we would like to choose $\mathcal{M}_1$ to be the bulk region which excludes $r = r_H$; in this case, Δz_1^{int} is positive and $R_1 = \frac{2\Delta z_1^{\text{int}}}{\beta_1}$, while the similarly defined Δz_2^{int} is negative and $R_2 = 1 + \frac{2\Delta z_2^{\text{int}}}{\beta_2}$. The condition for this to be the case can be readily derived from checking the sign of the expression (5.26) for Δz_1^{int}; one finds that the condition is

$$\mu < \frac{1}{u^2} - \kappa^2 L_1^2 \,, \tag{5.27}$$

which we will assume henceforth.

Negative energy enhancement: motivation

The above Euclidean interface solutions, analytically continued to Lorentzian signature in one of the transverse planar directions, are anticipated to provide a simple holographic description of two CFTs on $\mathbb{R}^{d-2,1}$ times an interval of width w_i, coupled at their endpoints via a conformal interface (see the right panel of Figure 5.4). Due to the symmetries of this theory, the energy-momentum tensor must take the form

$$T_{\mu\nu}^{(i)} = \eta_{\mu\nu} \frac{F_i}{w_i^d} \,, \qquad T_{zz}^{(i)} = -\frac{(d-1)F_i}{w_i^d} \,, \qquad T_{\mu z}^{(i)} = 0 \,, \tag{5.28}$$

where z is the CFT interval direction. Here, F_i is a characteristic scale for the vacuum state energy in CFT_i. Following [279], one may then define

$$E_i = (F_i/F_\beta)^{1/d} \tag{5.29}$$

to be the ratio of the scale of the energy density for CFT_i on the strip of width w_i (in the interface case) to that of the same CFT on a periodic direction of length $\beta = w_i$. One expects that this quantity should be a function of the dimensionless ratio

$$x = \frac{w_2}{w_1} \tag{5.30}$$

of the widths for the two CFTs. It is useful to note that this ratio is given in terms of bulk quantities by

$$x = \frac{R_2\beta_2}{R_1\beta_1}\,. \tag{5.31}$$

The authors of [279] observed that a particularly interesting regime in the parameter space occurred for[83]

$$\boxed{x \text{ fixed}\,, \qquad u < 1\,, \qquad e \to 0}\,, \tag{5.32}$$

where the requirement that x remains fixed can be understood as a particular way of taking the limit $\mu \to 0$, as we will see below. In this limit, E_1 increases without bound, suggesting that CFT_1 can exhibit an arbitrarily large negative Casimir energy provided that a family of interfaces realizing this limit can be considered. Interestingly, this effect is only observed in CFT_1 when $u < 1$, i.e. when the central charge of CFT_2 is smaller than that of CFT_1. We will henceforth refer to the limit in (5.32) as the "negative energy enhancement" or NEE limit.

In the bulk, this effect can be attributed to the fact that $\mu \to 0$ cor-

[83] We note that this limit eventually implies the condition (5.27), so we need not worry about the latter being satisfied when we are interested in the limit. On the other hand, if we are interested in fixed small $e > 0$, we should check that (5.27) is still satisfied.

responds to the limit in which the black hole mass associated to region 1 becomes much larger than that associated to region 2; this results directly in a similar hierarchy for the energy density in the two CFT regions. We can then think of the NEE limit as taking the lengths L_1, L_2 to be held fixed (as is natural since these correspond to the central charges of the two CFTs), taking the black hole mass μ_1 associated with region 1 to be much larger than μ_2, and adjusting the interface brane tension as $e \to 0$ to maintain a fixed value of x in the limit. This relies crucially on the possibility of having a multiply wound region 1, since maintaining fixed x while $\beta_1 \to 0$ requires $R_1 \to \infty$.

We may also observe that the limit $e \to 0$ amounts to shifting the brane out toward the asymptotic region associated to CFT_1. This can be seen by noting that the Poincaré angle between the normal to the AdS boundary and the brane in each region is given by [279]

$$\begin{aligned} \theta_1 &= \arcsin\left[\frac{1}{2}\left(\kappa L_1 + \frac{1}{\kappa L_1} - \frac{L_1}{\kappa L_2^2}\right)\right] \overset{e\to 0}{\to} -\frac{\pi}{2}\,, \\ \theta_2 &= \arcsin\left[\frac{1}{2}\left(\kappa L_2 + \frac{1}{\kappa L_2} - \frac{L_2}{\kappa L_1^2}\right)\right] \overset{e\to 0}{\to} \frac{\pi}{2}\,. \end{aligned} \tag{5.33}$$

We will now provide some important technical details underlying the above result.

Negative energy enhancement: details

Since the NEE limit involves fixing $u < 1$, we will collect here some important expressions pertaining to this regime. Defining

$$\begin{aligned}
\alpha_0 &= \frac{1}{2}\frac{u^2(1-\mu)^2}{(1-u+2eu)\sqrt{(1-\mu u)^2+4ue\mu(1-u+ue)}+2u(1+\mu)(1-e)(1+eu)-(1+u)(1+\mu u)} \\
\alpha_1 &= \frac{1}{2}\frac{u(\mu-1)}{(1-u)(1-2e)-2e^2u} \\
\alpha_2 &= -\frac{(1-u)(1-2e)-2e^2u}{\sqrt{e(1-e)(1+eu)(1-u+eu)}}\,,
\end{aligned}$$

it was found in [279] that

$$R_1 = -\frac{1}{4\pi}\frac{\alpha_2}{\alpha_0^{1/d}}\mathcal{I}_d\left(\frac{\alpha_1}{\alpha_0},\frac{1}{\alpha_0},\frac{\alpha_1^2\alpha_2^2}{4\alpha_0^2}\right)+\Theta\left[\mu-(1-2e)\left(\frac{2}{u}-1+2e\right)\right] \qquad (\text{for } u<1) \tag{5.34}$$

where $\Theta(\cdot)$ is a step function and

$$\mathcal{I}_d(a,b,c) = \int_1^\infty \frac{dy}{y^{1/d}}\frac{(y-a)}{(y-b)\sqrt{(y-1)(y+c)}}\,. \tag{5.35}$$

Meanwhile, defining

$$\begin{aligned}
\hat{\alpha}_0 &= \frac{1}{2u^2}\frac{(1-\frac{1}{\mu})^2}{\left(\frac{1}{u}-1+2e\right)\sqrt{\left(1-\frac{1}{\mu}\frac{1}{u}\right)^2+\frac{4e}{\mu}\left(\frac{1}{u}-1+e\right)}+2\left(1+\frac{1}{\mu}\right)(1-e)\left(\frac{1}{u}+e\right)-\left(1+\frac{1}{u}\right)\left(1+\frac{1}{\mu}\frac{1}{u}\right)} \\
\hat{\alpha}_1 &= \frac{1}{2u^2}\frac{\left(1-\frac{1}{\mu}\right)}{\left(\frac{1}{u}-1\right)\left(\frac{1}{u}+2e\right)+2e^2} \\
\hat{\alpha}_2 &= \frac{\left(\frac{1}{u}-1\right)\left(\frac{1}{u}+2e\right)+2e^2}{\sqrt{e(1-e)\left(\frac{1}{u}+e\right)\left(\frac{1}{u}-1+e\right)}}\,,
\end{aligned} \tag{5.36}$$

one has

$$R_2 = -\frac{1}{4\pi}\frac{\hat{\alpha}_2}{\hat{\alpha}_0^{1/d}}\mathcal{I}_d\left(\frac{\hat{\alpha}_1}{\hat{\alpha}_0},\frac{1}{\hat{\alpha}_0},\frac{\hat{\alpha}_1^2\hat{\alpha}_2^2}{4\hat{\alpha}_0^2}\right)+\Theta\left[\frac{1}{\mu}-(1+2eu)(2u-1-2eu)\right] \qquad (\text{for } u<1)\,. \tag{5.37}$$

Moreover, the minimum radius of the interface brane is

$$\left(r_0^{\text{int}}\right)^d = \mu_2 L_2^2\hat{\alpha}_0 \qquad (\text{for } u<1)\,. \tag{5.38}$$

Assuming $u<1$ and $\mu<\frac{1}{u}$ (both of which are prerequisites for the NEE limit), it was found that

$$\begin{aligned}
&\alpha_0\to\tfrac{1-\mu u}{4e}\,,\quad \alpha_1\to\tfrac{1}{2}\tfrac{u(\mu-1)}{1-u}\,,\quad \alpha_2\to-\sqrt{\tfrac{1-u}{e}}\,, && (u<1\,,\ \mu<\tfrac{1}{u}\,,\ e\to 0)\\
&\hat{\alpha}_0\to\tfrac{1-\mu u}{4e\mu u^2}\,,\quad \hat{\alpha}_1\to\tfrac{1}{2\mu}\tfrac{\mu-1}{1-u}\,,\quad \hat{\alpha}_2\to\tfrac{1}{u}\sqrt{\tfrac{1-u}{e}}\,. && (u<1\,,\ \mu<\tfrac{1}{u}\,,\ e\to 0)
\end{aligned}$$

Thus, defining

$$\mathcal{I}_0 = \frac{4^{1/d}}{4\pi}\int_1^\infty \frac{dy}{y^{1/d}\sqrt{y(y-1)}} = \frac{4^{1/d}}{4\pi}\frac{\Gamma\left(\frac{1}{2}\right)\Gamma\left(\frac{1}{d}\right)}{\Gamma\left(\frac{1}{2}+\frac{1}{d}\right)}\,, \tag{5.39}$$

it was found that

$$\begin{aligned} R_1 &= \frac{2\Delta z_1}{\beta_1} \sim \frac{\mathcal{I}_0}{e^{\frac{1}{2}-\frac{1}{d}}}\frac{\sqrt{1-u}}{(1-\mu u)^{1/d}} && (u<1\,,\ \mu<\frac{1}{u}\,,\ e\to 0)\\ R_2 &= 1+\frac{2\Delta z_2}{\beta_2} \sim 1-\mu^{1/d}u^{2/d-1}\frac{\mathcal{I}_0}{e^{1/2-1/d}}\frac{\sqrt{1-u}}{(1-\mu u)^{1/d}}\,. && (u<1\,,\ \mu<\frac{1}{u}\,,\ e\to 0) \end{aligned} \tag{5.40}$$

Moreover, in this limit, the minimum radius goes as

$$r_0^{\text{int}} \sim r_H^{(2)}\left(\frac{1-u\mu}{4e\mu u^2}\right)^{1/d} = r_H^{(1)}\left(\frac{1-u\mu}{4e}\right)^{1/d}\,. \qquad (u<1\,,\ \mu<\frac{1}{u}\,,\ e\to 0) \tag{5.41}$$

So far, we have been considering limits with a general fixed value of μ; eventually, we would like to instead consider the NEE limit in which we instead fix x. Indeed, it is clear from the expression for R_2 that we cannot consistently take $u < 1$ and $\mu < \frac{1}{u}$ fixed and send $e \to 0$; doing so would result in a negative value of R_2, taking the result beyond its regime of validity. It is therefore more convenient to express the results in terms of the ratio x defined in (5.30), which is related to $\mu(x)$ at leading order by

$$\mu(x) = \frac{e^{\frac{d}{2}-1}}{u^2}\left(\frac{u}{(1+x)\mathcal{I}_0\sqrt{1-u}}\right)^d . \tag{5.42}$$

The NEE limit properly involves fixing $u < 1$ and x, and sending $e \to 0$, which will also send $\mu \to 0$ as a result of this equation. The authors of [279] then found

$$E_1 \sim \frac{1}{e^{\frac{1}{2}-\frac{1}{d}}}\mathcal{I}_0\sqrt{1-u} \quad \text{and} \quad E_2 \sim \frac{x}{1+x} . \qquad \text{(NEE)} \tag{5.43}$$

This limit is the most physical from the CFT perspective, since one would typically like to keep the dimensions of the strip on which the CFTs are defined fixed while varying a parameter related to properties of the conformal interface.

5.3 Bottom-up model with constant tension branes

In the previous section, we reviewed a model of holographic BCFT and its application to cosmology, as well as a model for holographic interfaces exhibiting an interesting "negative energy enhancement" effect in an appropriate limit. In this section, we would like to combine these two models, considering a gravitational bulk with both an ETW brane and an interface brane; see Figure 5.6. The motivation for this is to see whether, in this augmented model, it is possible to obtain well-behaved Euclidean solutions, without intersecting or self-intersecting branes, so that conditions analo-

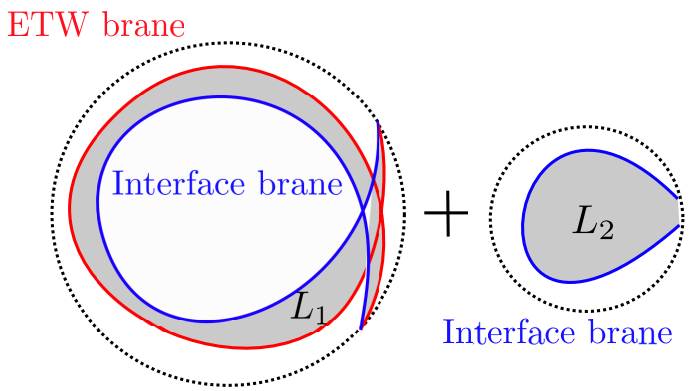

Figure 5.6: Two Euclidean AdS soliton regions of a holographic interface solution. Here, z_i is the angular direction and r_i is the radial direction, with $i = 1$ on the left and $i = 2$ on the right; planar directions are suppressed. In this figure, region 1 is "multiply wound" in the z_1 direction, while region 2 (which includes the horizon $r_2 = r_H$) is not.

gous to those of (5.17) hold for the ETW brane cosmology arising in the Lorentzian continuation.

We might expect that an effective description of the physics in this combined model should involve a non-gravitational CFT joined at an interface to a CFT coupled to gravity;[84] the background for the latter is the geometry of the ETW brane in the bulk picture, which can be interpreted as a traversable wormhole.[85] It has been argued that large quantities of negative null energy would be required to support such traversable wormholes [280]; as pointed out in [278], it is therefore natural to look for bulk solutions with both an ETW brane and an interface brane in the critical interface tension or NEE limit considered in the previous section. We will argue in this section that it is not possible to find such solutions in that limit in

[84] This is the usual Karch/Randall/Sundrum mechanism [72]: given a holographic CFT, we anticipate that introducing a "UV" or "Planck" brane in the bulk has the effect of introducing a cutoff to the CFT and coupling to dynamical gravity. Here, we anticipate that introducing an ETW brane in region 1 has this effect on CFT_1, while region 2 is not cut off and CFT_2 therefore does not couple to gravity directly. See [278] for a discussion of this.

[85] We are here thinking about the Lorentzian picture where we Wick rotate one of the x^μ coordinates.

the present model, prompting a modification to the model explored in the following section.

Before preceding to elucidate this result, it is worth taking a moment to comment on the anticipated effect of adding an interface brane to our model, beyond what we have already mentioned. Introducing this additional ingredient into our model allows us to describe a larger class of holographic duals of boundary states, with different boundary spectra, each of which will give rise to different effective theories on the brane. The geometry of the region between the interface and ETW branes is intimately related to the physics of the BCFT boundary degrees of freedom, including the number of these degrees of freedom; this can be understood as an example of generalized wedge holography [285], where we have a bulk dual of a BCFT involving two "wedges" of AdS separated by an interface brane (see also [4] for a microscopic version of this phenomenon). In particular, as in the previous section, we are typically interested in the case $u < 1$, so that, despite considering a BCFT with central charge c_2, we have a holographic dual including a spacetime region which we expect to be described by a CFT with larger central charge $c_1 > c_2$; this suggests that the corresponding BCFT is defined by permitting many degrees of freedom localized near the boundary, and we anticipate that, as a result, the effective theory on the brane will also have more degrees of freedom than the non-gravitating CFT in the effective picture.

One could nominally be concerned that adding an interface brane could disrupt the condition for gravity localization, namely an ETW brane far in the UV; for example, one could worry that the interface brane may localize gravity in this set-up. However, we do not expect that the interface brane should interfere with the gravity localization condition, particularly in a region where the ETW brane is much further in the UV than the interface brane. While it is true that interface branes can also exhibit gravity localization (as in the original Randall-Sundrum II model [72]), we have in our case a situation where the interface brane is not situated at a local maximum of the warp factor, and we therefore do not expect it to support a localized bound state of the $(d+1)$-dimensional graviton. Moreover, following the in-

tuition of [79], we can observe that the ETW brane localization phenomenon should be a consequence of local physics, rather than depending on global features of the bulk spacetime; provided we are interested in a region where the ETW brane and interface brane are significantly separated, we should be able to recover locally localized gravity. Just as in [79], we expect to find a massive, normalizable Kaluza-Klein mode whose wavefunction localizes to the ETW brane, but whose precise profile depends on the details of the IR physics, including the location and geometry of the interface brane.

5.3.1 Non-existence of solutions

The Euclidean action for the theory considered in this section is obtained by straightforwardly combining those for the two models considered in the previous section, found in (5.1) and (5.19), and is given in Appendix D.1. We assume without loss of generality that the ETW brane is added to region 1, so that in the effective description, CFT_1 is coupled to gravity via the Randall/Sundrum mechanism while CFT_2 is not.

We again consider Euclidean solutions with $\mathbb{R}^{d-1}$ symmetry (or $\mathbb{R}^{d-2,1}$ symmetry upon Wick rotating one of the x^μ coordinates); these are again pieces of the Euclidean AdS soliton geometry, which we will continue to parametrize as in (5.23). The interface brane trajectory in the two regions is given by the same equation of motion for $z_i^{\mathrm{int}}(r)$ as in Section 5.2.2, and $\Delta z_i^{\mathrm{int}}$ still denotes the z_i-coordinate distance traversed by the interface brane from its minimum radius $r_i = r_0^{\mathrm{int}}$ to infinity, as in (5.25); $z_1^{\mathrm{ETW}}(r_1)$ and $\Delta z_1^{\mathrm{ETW}}$ are analogous quantities for the ETW brane, following the definitions in (5.7) and (5.9). We will assume $z_1^{\mathrm{int}}(r_0^{\mathrm{int}}) = 0$ without loss of generality, a choice for the zero of the coordinate z_1; solutions where the ETW brane and interface brane join properly at infinity must therefore have $z_1^{\mathrm{ETW}}(r_0^{\mathrm{ETW}}) = 0$ by symmetry, so we will assume this in the following.

As in the previous section, we will be interested in the case that region 1 does not include the coordinate horizon $r_1 = r_H^{(1)}$ while region 2 does include the coordinate horizon $r_2 = r_H^{(2)}$; this permits region 1 to be multiply wound, which is what we expect to be required to obtain the negative energy

enhancement effect in CFT_1. Recall that this implies $\Delta z_1 > 0$, and therefore $R_1 = \frac{2\Delta z_1}{\beta_1} > 0$.

Conditions for existence of solutions

It is clear that solutions of the desired type, parametrized by (L_1, μ_1, u, μ, e) and the ETW brane tension λ (and with $z_1^{\mathrm{int}}(r_0^{\mathrm{int}}) = z_1^{\mathrm{ETW}}(r_0^{\mathrm{ETW}}) = 0$ as mentioned above), will exist if and only if the following conditions are satisfied:

1. $R_2(u, \mu, e) > 0$;
2. $\Delta z_1^{\mathrm{int}} = \Delta z_1^{\mathrm{ETW}}$;
3. $r_0^{\mathrm{ETW}} > r_0^{\mathrm{int}}$ and $|z_1^{\mathrm{int}}(r_1)| > |z_1^{\mathrm{ETW}}(r_1)|$ for all $r_1 > r_0^{\mathrm{ETW}}$.

The first condition ensures that the interface solution on its own would be well-defined[86] (the width of CFT_2 is non-negative), the second that the ETW brane and interface brane join properly (they subtend the same z_1-coordinate length), and the third that the ETW brane always sits at a larger value of the radial coordinate than the interface brane in region 1.

In particular, to demonstrate the *non-existence* of solutions for a given set of parameters (L_1, μ_1, u, μ, e) and *any* λ, it is sufficient to show that one of the following two conditions is not satisfied:

(C1) $R_2(u, \mu, e) > 0$

(C2) For $\lambda = \lambda_0$ with λ_0 defined by $f_1(r_0^{\mathrm{int}}) = \lambda_0^2 (r_0^{\mathrm{int}})^2$, one has

$$\frac{\Delta z_1^{\mathrm{ETW}}}{\Delta z_1^{\mathrm{int}}} < 1 \,. \tag{5.44}$$

The latter condition requires a brief explanation. Here, λ_0 is the value of the ETW brane tension λ for which the minimum radius r_0^{ETW} of the ETW brane would coincide with that of the interface brane, r_0^{int}. We know from (5.8) that r_0^{ETW} monotonically increases over $(r_H^{(1)}, \infty)$ as a function of

[86] The requirement $R_1 > 0$ is already enforced by our assumption $\Delta z_1 > 0$.

$\lambda L_1 \in (0,1)$, and as shown in Appendix D.2, we have $\Delta z_1^{\rm ETW}$ monotonically increasing from zero to infinity over the same range of ETW brane tensions. Consequently, condition (C2) above is equivalent to the existence of a tension $\lambda L_1 \in (\lambda_0 L_1, 1)$ such that

$$r_0^{\rm ETW} > r_0^{\rm int}\,, \qquad \Delta z_1^{\rm ETW} = \Delta z_1^{\rm int}\,. \tag{5.45}$$

In the following, we will show that these two conditions cannot simultaneously be satisfied in the NEE limit.

No solutions in the NEE limit

We can begin by determining when (C2) can be satisfied. Recalling the limiting behaviour of (5.40) and (5.41)

$$\Delta z_1^{\rm int} \sim \frac{2\pi L_1}{d r_H^{(1)}} \frac{\mathcal{I}_0}{e^{\frac{1}{2}-\frac{1}{d}}} \frac{\sqrt{1-u}}{(1-\mu u)^{1/d}}\,, \qquad r_0^{\rm int} \sim \frac{r_H^{(1)}(1-u\mu)^{1/d}}{(4e)^{1/d}}\,, \tag{5.46}$$

we have from the definition of λ_0

$$\lambda_0 = \frac{1}{L_1}\left(1 - \frac{2e}{(1-\mu u)}\right) + O(e^2)\,. \tag{5.47}$$

In the limit $e \to 0$,

$$\Delta z_1^{\rm ETW}(\lambda = \lambda_0) \sim \frac{2\pi L_1}{d r_H^{(1)}} \left(\frac{1-\mu u}{e}\right)^{\frac{1}{2}-\frac{1}{d}} \mathcal{I}_0\,, \tag{5.48}$$

and thus

$$\frac{\Delta z_1^{\rm ETW}(\lambda = \lambda_0)}{\Delta z_1^{\rm int}} \sim \sqrt{\frac{1-\mu u}{1-u}}\,. \tag{5.49}$$

Assuming fixed $u < 1$, we thus have two possibilities. If $\mu < 1$, then this quantity will be greater than one, so that (C2) is not satisfied in the limit, while if $1 < \mu < \frac{1}{u}$, then this quantity will be less than one, so (C2) is satisfied and a solution may exist.

On the other hand, we have already seen in (5.40) that

$$R_2 \sim 1 - \mu^{1/d} u^{2/d-1} \frac{\mathcal{I}_0}{e^{\frac{1}{2}-\frac{1}{d}}} \frac{\sqrt{1-u}}{(1-\mu u)^{1/d}} \, ; \tag{5.50}$$

for fixed $u < 1$, we see that requiring $R_2 > 0$ in the $e \to 0$ limit requires $\mu \to 0$. Thus, the condition $\mu \to 0$ imposed by (C1) is inconsistent with $\mu > 1$ imposed by (C2).

Solutions for $u < 1$

While we have shown that it is not possible to obtain solutions with an ETW brane and an interface brane that join properly in the NEE limit, it is certainly the case that well-behaved solutions exist elsewhere in the parameter space. The reason that we are not concerned with these solutions here is that they are not expected to be relevant for cosmology, on the basis of arguments we have previously mentioned regarding the effective description of the bulk physics of this model; without the NEE limit, we expect the background for the gravitational CFT to have a 4D curvature scale L_4 of order L_{Planck} (the cutoff scale for the gravitational CFT) rather than some hierarchically larger length scale.[87] Nonetheless, we briefly comment here about the larger parameter space.

A convenient feature for an investigation of this parameter space is that both conditions (C1) and (C2) can be expressed in terms of inequalities which depend only on the parameters (u, μ, e). From (5.37), we recall that,

[87] As observed in equation (4.10) of [278], the boundary central charge $c_{3\text{D}} = L_4^2/G_4$ in our set-up, which is the bulk description of a holographic BCFT, is equal (up to $O(1)$ factors) to the coefficient F of the energy density for the gravitational CFT in an expression analogous to (5.28), i.e. in $T_{00} \sim F/w^4$. One would expect that the typical value for F is roughly equal to the number of degrees of freedom in the gravitational CFT, which is not expected to be large in general, implying that we should generically expect $L_4 \sim L_{\text{Planck}}$ unless we consider something like the NEE limit. We thank Mark Van Raamsdonk for emphasizing this point.

if $u < 1$, the first condition yields the inequality

$$R_2(u,\mu,e) = R_1\left(\frac{1}{u},\frac{1}{\mu},e\right) = 1 - \frac{1}{4\pi}\frac{\hat{\alpha}_2}{\hat{\alpha}_0^{1/d}}\mathcal{I}_d\left(\frac{\hat{\alpha}_1}{\hat{\alpha}_0},\frac{1}{\hat{\alpha}_0},\frac{\hat{\alpha}_1^2\hat{\alpha}_2^2}{4\hat{\alpha}_0^2}\right) > 0 \qquad (u<1)\,. \tag{5.51}$$

On the other hand, recalling from (5.38) that

$$\frac{(r_0^{\rm int})^d}{\mu_1 L_1^2} = \mu u^2 \hat{\alpha}_0 \qquad (u<1)\,, \tag{5.52}$$

and from (5.8) that

$$\lambda = \frac{\sqrt{f_1(r_0^{\rm ETW})}}{r_0^{\rm ETW}} = \frac{1}{L_1}\sqrt{1-\frac{\mu_1 L_1^2}{(r_0^{\rm ETW})^d}}\,, \qquad r_0^{\rm ETW} = \left(\frac{\mu_1 L_1^2}{1-L_1^2\lambda^2}\right)^{1/d}\,, \tag{5.53}$$

we see that when the tension takes the value λ_0 for which $r_0^{\rm ETW} = r_0^{\rm int} = r_0$, we have

$$\begin{aligned}\Delta z^{\rm ETW} &= \int_{r_0}^{\infty} dr\,\frac{r\lambda_0}{L_1 f_1(r)}\frac{1}{\sqrt{f_1(r)-r^2\lambda_0^2}} \\ &= \frac{L_1\sqrt{\mu u^2\hat{\alpha}_0-1}}{dr_0}\mathcal{I}_d\left(0,\frac{1}{\mu u^2\hat{\alpha}_0},0\right)\,.\end{aligned} \tag{5.54}$$

We therefore have

$$\frac{\Delta z_{\rm ETW}(\lambda=\lambda_0)}{\Delta z_{\rm int}} = -2\left(\frac{\alpha_0}{\mu u^2\hat{\alpha}_0}\right)^{1/d}\sqrt{\mu u^2\hat{\alpha}_0-1}\,\frac{\mathcal{I}_d(0,\frac{1}{\mu u^2\hat{\alpha}_0},0)}{\alpha_2\mathcal{I}_d\left(\frac{\alpha_1}{\alpha_0},\frac{1}{\alpha_0},\frac{\alpha_1^2\alpha_2^2}{4\alpha_0^2}\right)}\,. \tag{5.55}$$

It follows that we can express the conditions introduced above as

(C1) $1 - \frac{1}{4\pi}\frac{\hat{\alpha}_2}{\hat{\alpha}_0^{1/d}}\mathcal{I}_d\left(\frac{\hat{\alpha}_1}{\hat{\alpha}_0},\frac{1}{\hat{\alpha}_0},\frac{\hat{\alpha}_1^2\hat{\alpha}_2^2}{4\hat{\alpha}_0^2}\right) > 0$

(C2) $-2\left(\frac{\alpha_0}{\mu u^2\hat{\alpha}_0}\right)^{1/d}\sqrt{\mu u^2\hat{\alpha}_0-1}\,\frac{\mathcal{I}_d(0,\frac{1}{\mu u^2\hat{\alpha}_0},0)}{\alpha_2\mathcal{I}_d\left(\frac{\alpha_1}{\alpha_0},\frac{1}{\alpha_0},\frac{\alpha_1^2\alpha_2^2}{4\alpha_0^2}\right)} < 1.$

These expressions are a convenient reformulation of (C1) and (C2) for the

purposes of verifying their compatibility within the parameter space.

As a preliminary for determining where such well-behaved solutions could exist in the parameter space, our goal in the remainder of this section will be to indicate a portion of the parameter space where these solutions cannot occur. We will restrict our attention to the region satisfying:

- $u < 1$
- $\mu < \min\{\frac{1}{u}, \frac{1}{u^2} - \kappa^2 L_1^2\}$;

however, one could ultimately explore the parameter space more broadly. We note that, together, these conditions imply $0 < e < \frac{1}{2}$. We therefore assume here that

$$\boxed{0 < u < 1\,, \quad 0 < e < \frac{1}{2}\,, \quad \mu < \min\Big\{\frac{1}{u}, \frac{1}{u^2}\left(1 - (1 - u + 2eu)^2\right)\Big\}}\,. \tag{5.56}$$

We will denote

$$\begin{aligned} c_1(u,\mu,e) &= \frac{1}{4\pi}\frac{\hat{\alpha}_2}{\hat{\alpha}_0^{1/d}}\mathcal{I}_d\left(\frac{\hat{\alpha}_1}{\hat{\alpha}_0}, \frac{1}{\hat{\alpha}_0}, \frac{\hat{\alpha}_1^2\hat{\alpha}_2^2}{4\hat{\alpha}_0^2}\right)\,, \\ c_2(u,\mu,e) &= -2\left(\frac{\alpha_0}{\mu u^2\hat{\alpha}_0}\right)^{1/d}\sqrt{\mu u^2\hat{\alpha}_0 - 1}\,\frac{\mathcal{I}_d(0, \frac{1}{\mu u^2\hat{\alpha}_0}, 0)}{\alpha_2\mathcal{I}_d\left(\frac{\alpha_1}{\alpha_0}, \frac{1}{\alpha_0}, \frac{\alpha_1^2\alpha_2^2}{4\alpha_0^2}\right)}\,, \end{aligned} \tag{5.57}$$

so that the condition (C_i) corresponds to the inequality $c_i(u,\mu,e) < 1$.

We observe (but will not attempt to prove here) that, for fixed (e,u), the function $c_1(u,\mu,e)$ is monotonically decreasing in μ, while $c_2(u,\mu,e)$ is monotonically increasing in μ. Assuming that this is true, then a pair of parameters (u,e) may be ruled out, meaning that they do not permit a well-behaved solution, if the solution $\mu = \mu_0$ to the equation $c_1(u,\mu,e) = 1$ (which we may obtain numerically) yields $c_2(u,\mu_0,e) > 1$. Using this approach, we construct the plot shown in Figure 5.7. The shaded portion of the plot corresponds to a region of the parameter space which has been ruled out, meaning that it does not contain any well-behaved solutions; the unshaded portion may or may not contain solutions (further investigation would be needed to determine this). This plot already confirms the conclusion of

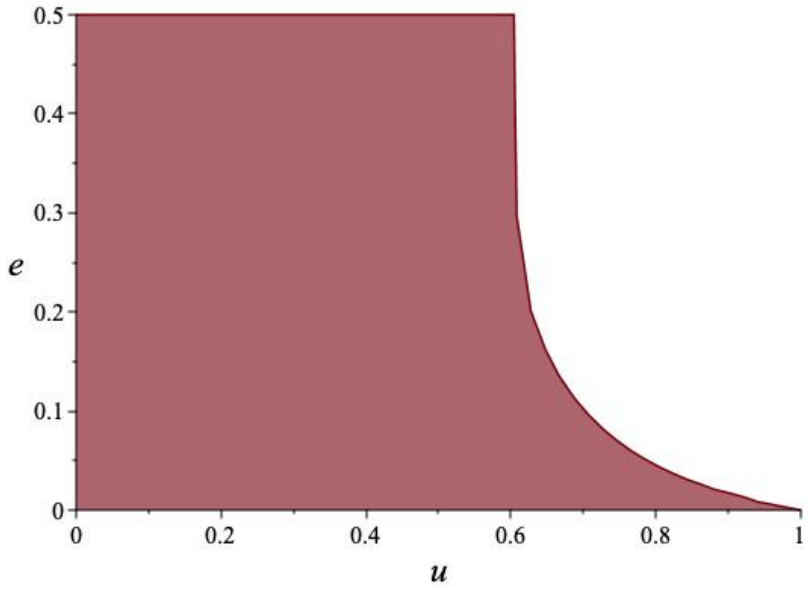

Figure 5.7: Plot of "ruled out" region of the (u, e)-plane. Here, the region shaded in red is part of the parameter space where we *do not* expect solutions to occur, as conditions (C1) and (C2) cannot be simultaneously satisfied. The remaining unshaded region in the upper right corner may or may not have solutions (our procedure for ruling out regions of the parameter space was not exhaustive).

Section 5.3 that solutions cannot exist in the NEE limit, which requires $e \to 0$ for fixed $u < 1$.

5.4 Bottom-up model with Einstein-Hilbert term on the ETW brane

We will now consider a generalization of the model considered above, where an Einstein-Hilbert term is added to the ETW brane.[88] In particular, we modify the ETW brane contribution to the action of the previous section to

[88] We do not add an Einstein-Hilbert term to the interface brane, as this complicates the analysis, though we provide the relevant equations in Appendix D.1.

become

$$S_{\rm ETW} = \frac{1}{16\pi G_{\rm ETW}} \int_{\rm ETW} d^d y \sqrt{h}\, R^{(d)} + S_{\rm ETW}^{\rm matter}\,, \tag{5.58}$$

where the matter contributions are from constant tension terms as before, and where we will introduce the constant γ defined by

$$\frac{1}{G_{\rm ETW}} = \frac{\gamma}{G_{\rm bulk}}\,. \tag{5.59}$$

Again, for the solutions with the desired symmetry, the bulk consists of two AdS soliton regions; the equations of motion for the ETW brane can be found in Appendix D.1.2.

While there may be various constraints on the model parameters, including γ, required to ensure that the bulk theory is a reasonable holographic dual of a BCFT, a good starting point is to consider those theories for which the corresponding effective theory enjoys a positive-sign Einstein-Hilbert term. Ideally, one will also have a suppression of the higher curvature terms in the effective theory. We should therefore clarify the action for the effective theories describing the physics of the above models. We can do so following the general recipe outlined in [281].

As derived in [286] (see also [281]), the contribution induced by integrating the bulk action (including the Gibbons-Hawking-York term) on-shell is given by

$$\begin{aligned} S_{\rm induced} = \frac{1}{16\pi G_{\rm bulk}} \int d^d x \sqrt{-h} \Bigg[& \frac{2(d-1)}{L_1} + \frac{L_1}{(d-2)} R^{(d)} \\ & + \frac{L_1^3}{(d-4)(d-2)^2} \left(R_{ab} R^{ab} - \frac{d}{4(d-1)} R^2 \right) + \dots \Bigg]\,. \end{aligned} \tag{5.60}$$

Higher order terms would be expected to depend in detail on the IR physics, including the dynamics of the interface brane. In fact, we are interested in the case $d = 4$, so the last term shown will be modified; we anticipate that the numerical coefficient will be replaced by an order one number, and an additional "non-local" term of the schematic form "$R^2 L_1^3 \ln(R L_1^2)$" will

occur. The full effective action, including the terms from $S_{\rm ETW}$, is therefore

$$\begin{aligned} S_{\rm eff} = \frac{1}{16\pi G_{\rm bulk}} \int d^d x \sqrt{-h} \Bigg[& \frac{2(d-1)}{L_1} \left(1 - \lambda L_1\right) \\ & + \frac{L_1}{(d-2)} \left(\frac{(d-2)\gamma}{L_1} + 1 \right) R^{(d)} + \dots \Bigg] . \end{aligned} \tag{5.61}$$

Canonically normalizing the Einstein-Hilbert term, we should define an effective Newton constant

$$\frac{1}{G_{\rm eff}} = \frac{1}{G_{\rm bulk}} \frac{L_1}{(d-2)} \left(\frac{(d-2)\gamma}{L_1} + 1 \right) , \tag{5.62}$$

obtaining

$$\begin{aligned} S_{\rm eff} = \frac{1}{16\pi G_{\rm eff}} \int d^d x \sqrt{-h} \Bigg[& R^{(d)} \\ & + \frac{2(d-1)(d-2)}{L_1^2} \frac{\left(1 - \lambda L_1\right)}{\frac{(d-2)\gamma}{L_1} + 1} + \dots \Bigg] . \end{aligned} \tag{5.63}$$

In particular, the cosmological constant for the effective theory is then

$$2\Lambda = -\frac{2(d-1)(d-2)}{L_1^2} \frac{\left(1 - \lambda L_1\right)}{(d-2)\frac{\gamma}{L_1} + 1} , \tag{5.64}$$

and we must also scale the higher order terms suitably, by replacing $G_{\rm bulk} \to G_{\rm eff} \frac{L_1}{(d-2)} \left(\frac{(d-2)\gamma}{L_1} + 1 \right)$.

As in the previous section, we would now like to establish the existence of solutions with non-intersecting branes in the NEE limit. We begin by considering the special case of a trivial interface, before permitting an interface with non-zero tension.

5.4.1 Trivial interface

We will begin by considering the case with only an ETW brane and no interface brane.[89] In this case, we must demand the z coordinate to have the appropriate periodicity β. While one might hope that the addition of an extra parameter as compared to the model of Section 5.2.1 could permit solutions with the property $r_0^{\rm ETW}/r_H \gg 1$, we will see that this does not occur.

We will be interested in the limit where $L\lambda \to 1$, which we recognize as the critical tension limit where $r_0^{\rm ETW} \to \infty$ due to (5.8) (note that the expression for $r_0^{\rm ETW}$ in terms of λ is unchanged from the pure tension case); to investigate this limit, we will consider the tension

$$\lambda L = 1 - \epsilon \tag{5.65}$$

with $\epsilon > 0$ small. At leading order, we find

$$\frac{2\Delta z^{\rm ETW}}{\beta} = \left(\frac{2}{\epsilon}\right)^{1/2-1/d} \mathcal{I}_0 \sqrt{\frac{(d-2)\gamma}{L} + 1}\,, \tag{5.66}$$

taking all parameters other than ϵ to be fixed. To avoid self-intersections, this ratio should be smaller than one; this would appear to be possible provided that we take $\gamma \to -\frac{L}{(d-2)}$ sufficiently quickly, namely

$$\left|\frac{(d-2)\gamma}{L} + 1\right| = O(\epsilon^{1-2/d})\,. \tag{5.67}$$

In particular, we should saturate these asymptotics to avoid sending $\Delta z^{\rm ETW}/\beta$ to zero.

Note that, in this case, the cosmological constant for the effective theory (5.64) will be vanishing in the limit, while our expectation is that the coefficients for the higher curvature terms will blow up, due to the rescaling of coefficients required to obtain the canonically normalized effective

[89] We are free to drop the subscript on bulk quantities in this subsection, since we have a single region of the AdS soliton.

action. We are most interested in an effective theory where the higher curvature terms remain under control, so the trivial interface does not appear desirable for our purposes.

5.4.2 Non-zero tension interface

We would now like to consider the case where we restore the interface, but leave the interface brane action as a pure tension term, and take the NEE limit. To this end, we again consider near-critical ETW brane tension

$$\lambda L_1 = 1 - \epsilon \,, \tag{5.68}$$

with $\epsilon > 0$ small. Note that we require (at leading order) $\epsilon < \frac{2e}{1-\mu u}$ to ensure that the minimum ETW brane radius is larger than that of the interface brane, using the expression (5.8) for r_0^{ETW} and (5.41) for r_0^{int} in the NEE limit. We then obtain

$$\Delta z_1^{\text{ETW}} \sim \frac{2\pi L_1}{d r_H^{(1)}} \left(\frac{2}{\epsilon}\right)^{1/2-1/d} \mathcal{I}_0 \sqrt{\frac{(d-2)\gamma}{L_1} + 1} \,, \tag{5.69}$$

and thus

$$\frac{\Delta z_1^{\text{ETW}}}{\Delta z_1^{\text{int}}} \sim \left(\frac{2}{1-\mu u}\frac{e}{\epsilon}\right)^{1/2-1/d} \sqrt{\frac{1-\mu u}{1-u}} \sqrt{\frac{(d-2)\gamma}{L_1} + 1} \,. \tag{5.70}$$

Since we would like to require that this approaches one in the limit, and we have in the limit

$$\left(\frac{2}{1-\mu u}\frac{e}{\epsilon}\right)^{1/2-1/d} \sqrt{\frac{1-\mu u}{1-u}} > 1 \,, \tag{5.71}$$

we see that this is still a requirement that γ be negative in the limit; however, it is less stringent than in the case of a trivial interface. In particular, if we take ϵ to scale proportionally to e (while keeping $\epsilon < \frac{2e}{1-\mu u}$ throughout), and recall that $\mu \to 0$ is required to ensure $R_2(u, \mu, e) > 0$, then we see that this bound always requires $\frac{(d-2)\gamma}{L_1} + 1$ to approach a positive constant, rather

than zero, in the limit.

Specifically, if we take $\epsilon \sim \frac{2ec}{1-\mu u}$ with fixed $0 < c < 1$, then we require

$$\lim_{\text{NEE}} \left(\frac{(d-2)\gamma}{L_1} + 1 \right) = c^{1-2/d} (1-u) \ . \tag{5.72}$$

In particular, we see that the limiting value of γ lies within the range

$$-1 < \frac{(d-2)\gamma}{L_1} < -u \, . \tag{5.73}$$

The fact that the quantity appearing in (5.72), which appeared as a scaling factor in the denominator of terms in the properly normalized effective action (5.63), is now a positive constant in the limit implies that the coefficients for the higher curvature terms will remain finite. Consequently, for a weakly curved ETW brane, it seems plausible that the physics should be well-described by pure Einstein gravity with small corrections. The cosmological constant for the effective theory again vanishes in the limit. We expect that the curvature length scale of the ETW brane should become parametrically larger than the $(d+1)$-dimensional AdS scale in the limit, with the ratio diverging in the strict limit.

Here we have shown that it is possible to indicate a limit for which one can obtain a solution with properly joining branes, for which the minimum radius of the ETW brane is larger than that of the interface brane. This limit can be interpreted as taking the NEE limit while tuning the ETW brane tension so that the brane propagates close to the asymptotic AdS boundary, and tuning the Einstein-Hilbert or DGP term so that the ETW and interface branes join properly; it is given by

$$\boxed{\mu \to 0 \, , \ e \to 0 \, , \ 1 - \lambda L_1 \sim 2ec \, , \ \left(\frac{(d-2)\gamma}{L_1} + 1 \right) \sim c^{1-2/d} (1-u)} , \tag{5.74}$$

where we keep $0 < u < 1$ and $0 < c < 1$ fixed. Here, one must take μ to simply vanish sufficiently quickly so that R_2 remains positive in the limit, meaning that $\mu = O(e^{\frac{d}{2}-1})$. Note that we have yet to establish that the

ETW brane stays outside of the interface brane, i.e. that the branes do not intersect, in order to verify that the desired solutions indeed exist. We verify this property in Appendix D.3.[90]

We note in passing that, for the limit considered here, the coupling for the Einstein-Hilbert term in the action for the effective theory satisfies

$$\frac{1}{16\pi G_{\text{eff}}} \sim \frac{c^{1-2/d}}{16\pi G_{\text{bulk}}} \frac{L_1 - L_2}{(d-2)} \,, \tag{5.75}$$

so the effective coupling in the limit is controlled by the positive difference between the central charges of the two CFTs.

5.5 Conclusions

In this work, we have pursued the suggestion of [278] that adding an interface brane to the existing bottom-up holographic models in [2, 277, 278] could permit solutions capable of realizing localized gravity on an ETW brane via the Karch/Randall/Sundrum mechanism, making such solutions "cosmologically viable". We provide evidence to affirm this suggestion, with an important caveat: one also needs to include additional local geometrical terms in the ETW brane action, such as an Einstein-Hilbert term. In particular, just adding a constant tension interface brane (with no Einstein-Hilbert term on the ETW brane) was not sufficient, and just adding an Einstein-Hilbert term to the ETW brane (with no interface brane) was also not sufficient.

With both ingredients, we found that solutions appear in the region of parameter space, the "NEE limit", associated with cosmologically viable solutions; this represents an important proof-of-concept for these models. Solutions in this limit require a "wrong sign" Einstein-Hilbert term on the ETW brane, as indicated in (5.74) and (5.73), but correspond to a "correct sign" Einstein-Hilbert term in the action describing the physics of the effective theory. While the latter is the most important criterion for ensur-

[90] In particular, we verify that it holds for $d \geq 4$, including the case $d = 4$ we are especially interested in.

ing a physically reasonable model (given that the effective theory is where the cosmology lives), one may still wonder whether there may be other important constraints on the parameters involved in this model arising from the requirement that the bulk physics represents a valid holographic dual of a BCFT. Indeed, it has been suggested that such negative values of the "DGP coupling" parameter may be problematic for holographic models of this type; for example, it was noted in Appendix B of [281] that such models may permit the formation of "Ryu-Takayanagi bubbles" on the brane whose associated generalized entropy may be negative, an evident pathology.[91] We leave the interesting question of better understanding these possible additional constraints to future work.

[91] We thank Dominik Neuenfeld for emphasizing this and related points.

Chapter 6

Finding $\mathbf{AdS}_5 \times S^5$ in (2+1)-Dimensional Superconformal Field Theory Physics

6.1 Introduction

End-of-the-world (ETW) branes arise in many applications of string theory, from model building, to cosmology[92] [2, 276–278], to recent studies of black hole evaporation [5, 281, 287–291].

A particularly interesting case occurs when an ETW brane cuts off the asymptotic region of an asymptotically AdS spacetime [72]. In this case, gravity can localize on the ETW brane such that over a significant range of scales, gravity on the brane appears to be four-dimensional. Such ETW branes can have a microscopic description when the brane intersects the asymptotic boundary of AdS. As explained by Karch and Randall [78, 79] (see also [87]), in this case the full system can be dual to a boundary conformal field theory (BCFT). The localization of gravity can arise in the situation where there are many more boundary degrees of freedom than bulk degrees of freedom.

Often, such ETW branes are considered in bottom-up models where the brane is described as a codimension-one boundary hypersurface with some simple action. In this case, gravity localization can occur when this brane

[92] See [77] for a review of braneworld cosmology.

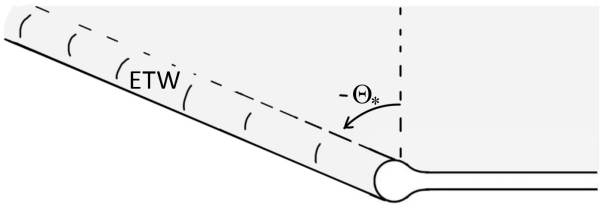

Figure 6.1: Schematic of geometries dual to $\mathcal{N} = 4$ SYM theory on half of $\mathbb{R}^{1,3}$ coupled to a 3D SCFT at the boundary. The geometry contains a region that approximates a range $\Theta \in (\Theta_*, \pi/2)$ of Poincaré $AdS_5 \times S^5$, and an end-of-the-world brane region where the S^5 smoothly degenerates. When the 3D boundary SCFT has many more local degrees of freedom than the $\mathcal{N} = 4$ theory, the internal space typically grows to a large volume before pinching off.

intersects the boundary at a large angle, so that it removes a region $\Theta < \Theta_* = -\pi/2 + \epsilon$ of AdS, where Θ is the polar angle in Poincaré coordinates formed by the radial direction and the field theory direction perpendicular to the CFT boundary. The limit $\epsilon \to 0$ corresponds to the tension of the brane increasing to a critical value.

There are also fully microscopic models which realize ETW brane physics, e.g. [174, 175]. In these cases, the ETW brane often corresponds to a region of a higher-dimensional geometry where the internal space degenerates smoothly. In [292], examples were provided of such microscopic models where gravity is localized to the ETW brane. In this chapter, we further study these models, showing that the bulk geometry away from the ETW brane can include a region $\Theta > \Theta_* = -\pi/2 + \epsilon$ of Poincaré AdS with arbitrarily small ϵ. That is, we can push the ETW brane arbitrarily far towards the missing asymptotic boundary.

We further show that there exist solutions with two ETW branes such that the dual contains a region well-approximated by the $-\pi/2 + \epsilon < \Theta < \pi/2 - \epsilon$ wedge of AdS, again with arbitrarily small ϵ.

In the first case, we conclude that the physics of the missing half of the bulk CFT can be reproduced by a set of boundary degrees of freedom. In the second case, the physics of a higher-dimensional CFT can be reproduced

by a carefully chosen lower dimensional theory. This is reminiscent of the "deconstructing dimensions" story [293].

The microscopic set-up

In the microscopic set-ups we consider, the BCFT is $U(N)$ $\mathcal{N} = 4$ supersymmetric Yang-Mills theory on $\mathbb{R}^{1,2} \times \mathbb{R}^+$ with boundary physics preserving half supersymmetry and an $OSp(4|4)$ superconformal symmetry. This boundary physics can generally be understood as a set of boundary degrees of freedom coupled to the $\mathcal{N} = 4$ fields in some way. These theories arise in string theory from the low-energy limit of D3-branes ending on stacks of D5-branes and NS5-branes, with additional D3-branes stretched between the five-branes. In many cases, the boundary physics can be considered independently and describes a three-dimensional superconformal theory with $OSp(4|4)$ symmetry.

The vacuum states of these field theories on a half-space are dual to known solutions of type IIB supergravity. These solutions have an asymptotically $\mathrm{AdS}_5 \times S^5$ asymptotic region whose boundary geometry is half of $\mathbb{R}^{1,3}$. The full geometry has a part that is well approximated by a portion $\Theta > \Theta_*$ of Poincaré $\mathrm{AdS}_5 \times S^5$, where $\Theta \in (-\pi/2, \pi/2)$ is the angle in Poincaré coordinates that labels different AdS_4 slices and $\Theta = \pi/2$ corresponds to the asymptotic region that is present.[93] The remaining part of the geometry can be understood as a geometrical "end-of-the-world brane": this is a region of the ten-dimensional geometry where the internal space smoothly degenerates, so that we have a spacetime boundary from the five-dimensional point of view. This ETW brane emerges from the CFT boundary where the SCFT lives. Such geometries are illustrated schematically in Figure 6.1.

For a fixed set of parameters in the $\mathcal{N} = 4$ theory, different choices of the boundary physics (i.e. the choice of 3D SCFT and how this is coupled to the $\mathcal{N} = 4$ theory) give supergravity solutions with the same asymptotically

[93] Here, we assume that Θ_* is the smallest such angle for which this is true, given some criterion for how closely the geometry should match $\mathrm{AdS}_5 \times S^5$.

$\mathrm{AdS}_5 \times S^5$ region but a different behavior for the ETW brane, and in particular, a different brane angle Θ_*. The main goal of this chapter is to show that by choosing the boundary physics appropriately, we can find examples with Θ_* arbitrarily close to $-\pi/2$. In other words, with the right choice of boundary degrees of freedom, we can, to an arbitrarily good approximation, reproduce the physics of the missing half of the $\mathcal{N} = 4$ theory.

At the level of type IIB supergravity, it is trivial to exhibit families of such solutions that recover all of Poincaré $\mathrm{AdS}_5 \times S^5$ in a limit. However, the flux quantization conditions of the full type IIB string theory imply that the parameters present in the supergravity solutions cannot be varied continuously, but instead correspond to discrete solutions of a family of non-linear equations. These parameters correspond to the discrete data used to specify the choice of boundary SCFT to which we couple the $\mathcal{N} = 4$ theory. The non-linear constraints on the supergravity parameters are complicated enough that it is not possible to find a general solution analytically. Nevertheless, we are able to exhibit the existence of sequences of such solutions with the behavior that $\Theta_* \to -\pi/2$.

On the field theory side, the theories that give $\Theta_* \sim -\pi/2$ correspond to boundary theories with many degrees of freedom. These arise from string theory brane constructions where we have D3-branes ending on stacks of D5-branes and NS5-branes where both N_{D5} and N_{NS5} are taken large. The SCFTs describing these boundary degrees of freedom correspond to the IR limit of quiver gauge theories where the quiver generally has many nodes; we provide some explicit examples below.

Three-dimensional duals to arbitrarily large wedges of $\mathbf{AdS}_5 \times S^5$

For a give choice of boundary physics, we can also consider introducing a second boundary with the same physics (arising from an equivalent configuration of branes) so that supersymmetry is preserved. This theory, now on a strip, will flow to some SCFT in the infrared. The gravity dual for this theory will correspond to a wedge $-|\Theta_*| < \Theta < |\Theta_*|$ of $\mathrm{AdS}_5 \times S^5$ with ETW branes on either side. Such solutions were considered in [294] and pro-

vide a microscopic example of the "wedge holography" discussed in [285]. Our results in this chapter show that the wedge can actually be arbitrarily large, i.e. with an angle that is arbitrarily close to π. Thus, we can have a $(2+1)$-dimensional theory whose dual geometry contains an arbitrarily large wedge of $\mathrm{AdS}_5 \times S^5$.

End-of-the-world brane geometries

The ETW branes in these constructions have a ten-dimensional geometry that was compared by Bachas and Lavdas [292] to a bagpipe. Here, the "bag" is a small perturbation to the $\mathrm{AdS}_4 \rtimes M_6$ geometry dual to the decoupled 3D SCFT, where M_6 is a compact internal space. When the SCFT is coupled to the higher-dimensional $\mathcal{N} = 4$ SYM theory, the previously compact internal space M_6 is perturbed to include a narrow semi-infinite "pipe" with the geometry of S^5 times a non-compact direction [292]. The perturbation is small since the $\mathcal{N} = 4$ theory has many fewer local degrees of freedom than the SCFT.

The curvature scale of the internal space M_6 is generally of the same order of magnitude as the scale $L^{(4)}_{\mathrm{AdS}}$ describing the non-compact AdS_4 geometry of the ETW brane, and these are both much larger than the AdS_5 scale $L^{(5)}_{\mathrm{AdS}}$. The lack of scale separation between the AdS_4 scale and the curvature radius of the M_6 has been noted in the past [292, 295]; we provide a direct argument for it in Appendix E.1.

Outline

In the remainder of the chapter, we review in Section 6.2 the field theories that we consider and their gravity duals in type IIB supergravity. In Section 6.3, we derive conditions on the parameters describing the boundary SCFT such that the dual theories include a region that is well-approximated by a region $\Theta > -\pi/2 + \epsilon$ of $\mathrm{AdS}_5 \times S^5$ to an accuracy δ. In Sections 6.4 and 6.5, we find explicit examples of sequences of theories (with fixed g_{YM} and N for the $\mathcal{N} = 4$ theory) that satisfy our conditions with parameters ϵ and δ both approaching zero. In Section 6.6, we describe 3D SCFTs whose duals

include arbitrarily large wedges of $\mathrm{AdS}_5 \times S^5$ ($|\Theta| < \pi/2 - \epsilon$ with arbitrarily small ϵ). We end with a brief discussion in Section 6.7.

6.2 Background

The field theories we consider and the corresponding supergravity solutions were reviewed in detail in Sections 3.2 and 3.3. We refer the reader to those sections, or to the earlier references [89, 90] for a discussion of theories with half-maximal supersymmetry $\mathcal{N} = 4$ on a half-space and [172–175] for a discussion of the supergravity solutions. Here, we summarize only the basic information that we will use.

The set of supergravity solutions that we discuss take the form of $\mathrm{AdS}_4 \times S^2 \times S^2$ fibred over a two-dimensional space Σ that we can take to be the positive quadrant of a plane. Explicitly, the metric takes the form

$$ds^2 = f_4^2 ds^2_{\mathrm{AdS}_4} + f_1^2 ds^2_{S_1^2} + f_2^2 ds^2_{S_2^2} + 4\rho^2 (dr^2 + r^2 d\theta^2) \,, \tag{6.1}$$

where $\theta \in [0, \pi/2]$ and $ds^2_{\mathrm{AdS}_4}$ and $ds^2_{S_i^2}$ are metrics for AdS_4 and two-spheres with unit radius. Here, f_i and ρ are functions of r and θ which are given explicitly in terms of a pair of harmonic functions h_1, h_2 on Σ.

The general expressions for the harmonic functions corresponding to vacua of $\mathcal{N} = 4$ SYM on a half space with various choices for the boundary physics are given as

$$\begin{aligned} h_1 &= \frac{\pi \ell_s^2}{2} \frac{r \cos\theta}{\sqrt{g}} + \frac{\ell_s^2}{4} \sum_A \frac{c_A}{\sqrt{g}} \ln \left(\frac{(r\cos\theta + l_A)^2 + r^2 \sin^2\theta}{(r\cos\theta - l_A)^2 + r^2 \sin^2\theta} \right) \\ h_2 &= \frac{\pi \ell_s^2}{2} \sqrt{g} r \sin\theta \\ &\quad + \frac{\ell_s^2}{4} \sum_B d_B \sqrt{g} \ln \left(\frac{r^2 \cos^2\theta + (r\sin\theta + k_B)^2}{r^2 \cos^2\theta + (r\sin\theta - k_B)^2} \right) \,. \end{aligned} \tag{6.2}$$

Here, the sets $\{l_A\}$ and $\{k_B\}$ represent the locations of poles on the x-axis and y-axis respectively. These correspond to throats in the ETW brane region of the geometry that are sources of D5-brane flux and NS5-brane

flux respectively. The parameters c_A and d_B control the amount of D5 and NS5-brane flux emerging from these throats.

In string theory, the five-brane flux is quantized; this gives the constraints that

$$N_{D5}^{(A)} \equiv \frac{1}{\sqrt{g}} c_A \in \mathbb{N}^+ , \qquad N_{NS5}^{(B)} \equiv \sqrt{g} d_B \in \mathbb{N}^+ . \tag{6.3}$$

The throats also have D3-brane flux, and there are additional constraints related to the quantization of this. These are

$$\begin{aligned} N_{D3}^{A} &= \sqrt{g} l_A + \frac{2}{\pi} \sum_{B=1} N_{NS5}^{(B)} \arctan \frac{l_A}{k_B} \in \mathbb{N}^+ , \\ \hat{N}_{D3}^{B} &= \frac{k_B}{\sqrt{g}} + \frac{2}{\pi} \sum_{A=1} N_{D5}^{(A)} \arctan \frac{k_B}{l_A} \in \mathbb{N}^+ . \end{aligned} \tag{6.4}$$

Here, the integer parameters N_{D3}^A and $\hat{N}_{D3}^B$ can roughly be thought of as the number of units of D3-brane charge per D5-brane associated with the l_A throat or NS5-brane associated with the k_B throat respectively.

The parameters $(N_{D5}^{(A)}, N_{NS5}^{(B)}, N_{D3}^A, \hat{N}_{D3}^B)$ are directly related to the parameters specifying the field theory. The connection is described most easily by referring to the string theory brane constructions from which the field theory arises. It is convenient to define

$$\begin{aligned} (L_i) &= (N_{D3}^A \text{ with multiplicity } N_{D5}^A) \\ (K_i) &= (\hat{N}_{D3}^B \text{ with multiplicity } N_{D5}^B) , \end{aligned}$$

where both sets are ordered from left to right. Then, in the set-up of Figure 6.2, K_i is the net number of D3-branes ending from the right on the i^{th} NS5-brane *plus* the number of D5-branes to the left of this NS5-brane, and L_i is the net number of D3-branes ending from the right on the i^{th} D5-brane *plus* the number of NS5-branes to the left of this D5-brane.[94]

[94] It is sometimes convenient to order the 5-branes such that all NS5-branes occur to the left of all D5-branes; in this case, L_i is the net number of D3-branes ending on the i^{th} D5-brane plus the *total* number of NS5-branes, while K_i is simply the net number of D3-branes ending on the i^{th} NS5-brane.

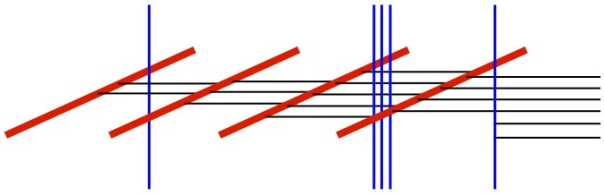

Figure 6.2: Cartoon of D-brane configuration giving rise to a supersymmetric boundary condition of $\mathcal{N} = 4$ SYM; here, D3-branes are black, D5-branes are blue, and NS5-branes are red. This configuration corresponds to linking numbers $L = (1, 3, 3, 3, 6)$ and $K = (2, 2, 3, 3)$. Removing the semi-infinite D3-branes on the right, we have a brane configuration that gives rise to a 3D SCFT in the infrared.

6.3 Obtaining a large $\mathbf{AdS}_5 \times S^5$ region

The solutions dual to $OSp(4|4)$-preserving BCFTs we consider can be thought of as having two general geometrical regions with distinct features:

- *Region I:* An asymptotically $\mathrm{AdS}_5 \times S^5$ region occurring at large values of the radial coordinate $r \gg l_A, k_B$ on Σ, where $O(l_A/r)$, $O(k_b/r)$ corrections due to the 5-brane throats are small; and
- *Region II:* An "end-of-the-world" brane region at $r \lesssim l_A, k_B$ where the geometry caps off smoothly except at the locations of the 5-brane throats.

We are interested in considering whether certain allowed choices for the supergravity parameters are able to produce a geometry where region (I) is large and approximates pure $\mathrm{AdS}_5 \times S^5$; by "large", we mean that the $\mathrm{AdS}_5 \times S^5$ region extends to Poincaré angle $\Theta_* \approx -\pi/2$.

Conditions for a large $\mathbf{AdS}_5 \times S^5$ region

Consider the harmonic functions (6.2) that determine the metric and other fields. Expanding these in $1/r$, we can write

$$\begin{aligned} h_1 &= h_1^{\rm AdS} + \frac{\ell_s^2}{\sqrt{g}}\Big[\frac{1}{2}\frac{\sum_A c_A l_A - \sum_B d_B k_B}{r}\cos\theta \\ &\qquad + \sum_{n=1}^{\infty}\sum_A c_A \left(\frac{l_A}{r}\right)^{2n+1}\frac{\cos((2n+1)\theta)}{2n+1}\Big] \\ h_2 &= h_2^{\rm AdS} + \ell_s^2\sqrt{g}\Big[-\frac{1}{2}\frac{\sum_A c_A l_A - \sum_B d_B k_B}{r}\sin\theta \\ &\qquad + \sum_{n=1}^{\infty}\sum_B d_B \left(-\frac{k_B}{r}\right)^{2n+1}\frac{\sin((2n+1)\theta)}{2n+1}\Big]\,, \end{aligned} \tag{6.5}$$

where

$$h_1^{\rm AdS} = \frac{L_{\rm AdS}^2}{4}\frac{1}{\sqrt{g}}\cos\theta(\frac{r}{r_0}+\frac{r_0}{r})\,, \qquad h_2^{\rm AdS} = \frac{L_{\rm AdS}^2}{4}\sqrt{g}\sin\theta(\frac{r}{r_0}+\frac{r_0}{r}) \tag{6.6}$$

are the harmonic functions that give pure $\mathrm{AdS}_5 \times S^5$, with AdS length $L_{\rm AdS}$ given by

$$L_{\rm AdS}^4 = 4\pi\ell_s^4(\sum_A c_A l_A + \sum_B d_B k_B) = 4\pi\ell_s^4 N\,, \qquad r_0 = \frac{L_{\rm AdS}^2}{2\pi\ell_s^2}\,. \tag{6.7}$$

For the pure $\mathrm{AdS}_5 \times S^5$ solution, the plane $r = r_0$ is an AdS_4 slice perpendicular to the boundary that divides the space in half.

We note that for $r \leq r_0$, the first term in square brackets will be small compared to the terms in $h^{\rm AdS}$ if and only if

$$\Delta \equiv \big|\sum_A c_A l_A - \sum_B d_B k_B\big| \ll N\,. \tag{6.8}$$

The ratio Δ/N gives the fractional size of the corrections (which do not have a significant dependence on r for $r < r_0$).

The remaining corrections, involving higher powers of $1/r$, become larger (relative to the leading terms) for smaller r. It is straightforward to check

that these corrections will be small relative to the leading terms provided that $r \gg l_A$ and $r \gg k_B$. For example, when this is true, we have

$$\frac{\ell_s^2}{\sqrt{g}} \sum_A c_A \frac{l_A^{2n+1}}{r^{2n+1}} \ll \frac{\ell_s^2}{\sqrt{g}} \sum_A c_A l_A \frac{1}{r} \sim \frac{\ell_s^2}{\sqrt{g}} \frac{N}{r} \approx \frac{L_{\rm AdS}^2}{\sqrt{g}} \frac{r_0}{r} \,, \tag{6.9}$$

where the term on the right is the leading term in $h_1^{\rm AdS}$ in the $r < r_0$ region.

To summarize, we expect that provided the condition (6.8) holds, the solutions will be well-approximated by pure $\mathrm{AdS}_5 \times S^5$ in a region $r > r_*$ where the coordinate r is much larger than any of the l_A or k_B. For $h_i = h_i^{\rm AdS}$, the coordinate r is related to the Poincaré angle Θ by [296]

$$\frac{r}{r_0} = \tan\left(\frac{\Theta}{2} + \frac{\pi}{4}\right) \tag{6.10}$$

so the geometry includes a region well-approximated by the $\Theta > \Theta_*$ region of Poincaré AdS, where

$$\Theta_* = -\frac{\pi}{2} + 2\tan^{-1}\frac{r_*}{r_0} \,. \tag{6.11}$$

In particular, having Θ_* close to $-\pi/2$ requires $r_* \ll r_0$, which requires

$$k_A, l_A \ll \sqrt{N} \,. \tag{6.12}$$

Thus, we have arrived at the two conditions (6.8) and (6.12). In Appendix E.2, we provide a more detailed justification that these give solutions with small Θ_*.

Satisfying the conditions within string theory

In the context of type IIB supergravity, it is trivial to find solutions satisfying the constraints (6.8) and (6.12) for a given fixed N. We are free to take the individual l_A and k_B as small as we like, and then choose c_A and d_B so that

$$N = \sum_A c_A l_A + \sum_B d_B k_B \,. \tag{6.13}$$

and (6.8) is satisfied.

However, in string theory, the solutions obey flux quantization conditions (6.3) and (6.4). Below, we will investigate, for fixed $(g, L_{\rm AdS})$ (or equivalently fixed parameters $(g_{\rm YM}, N)$ in the $\mathcal{N} = 4$ theory), the space of parameters $\{l_A, k_B, c_A, d_B\}$ that satisfy both the quantization conditions and the constraints (6.8) and (6.12). We will demonstrate discrete families of solutions for which we obtain an arbitrarily large region[95] of $\mathrm{AdS}_5 \times S^5$, approximated arbitrarily well, within the family.

6.4 Solutions with single D5-pole and NS5-pole

It is not possible to obtain a large $\mathrm{AdS}_5 \times S^5$ region when we have a boundary condition corresponding to a D-brane configuration with only D5-branes or only NS5-branes, since this manifestly violates (6.8) in our constraints. Thus, the simplest possibility is a solution with a single D5-brane throat and a single NS5-brane throat. We consider this case in the present section.

We fix the parameters N and g. Then, in terms of the integer parameters N_{D5}, N_{NS5}, the relation (6.7) and the constraint (6.4) demands that l, k satisfy

$$\begin{aligned} N &= \frac{k}{\sqrt{g}} N_{NS5} + l\sqrt{g} N_{D5} \\ N_{D3} &\equiv \sqrt{g} l + \frac{2}{\pi} N_{NS5} \arctan\left(\frac{l}{k}\right) \in \mathbb{N}^+ \\ \hat{N}_{D3} &\equiv \frac{k}{\sqrt{g}} + \frac{2}{\pi} N_{D5} \arctan\left(\frac{k}{l}\right) \in \mathbb{N}^+ \,, \end{aligned} \tag{6.14}$$

In Appendix E.3, we show that the allowed (l, k) are in one-to-one correspondence with positive parameters $(N_{D5}, N_{NS5}, N_{D3}, \hat{N}_{D3})$ such that

$$G \equiv \gcd(N_{D5}, N_{NS5}) \mid N \,, \tag{6.15}$$

[95] That is, for any $\epsilon > 0$ there exists a solution within the family for which $r_* \ll \epsilon r_0$.

and

$$N_{D5}N_{D3} + N_{NS5}\hat{N}_{D3} = N + N_{D5}N_{NS5}\,. \tag{6.16}$$

The latter equation always has at least one solution with positive integers $(N_{D3}, \hat{N}_{D3})$ provided that (6.15) is satisfied.

In this section, we will understand the space of quadruples of parameters $(N_{D5}, N_{NS5}, N_{D3}, \hat{N}_{D3})$ which can realize constraints (6.8) and (6.12), and therefore give rise to supergravity solutions with a large region of $\mathrm{AdS}_5 \times S^5$.

The main results of this section are as follows:

- If we would like a solution that is well approximated by $\mathrm{AdS}_5 \times S^5$ to an accuracy $\delta \ll 1$ in some range $r > \epsilon r_0$ (meaning that $\frac{|cl-dk|}{r_0^2} \sim \delta^2$), it is necessary that $\gcd(N_{D5}, N_{NS5}) \mid N$ and

$$\begin{aligned} N_{NS5} &\gtrapprox \frac{1}{2\epsilon}\sqrt{gN} \\ N_{D5} &\gtrapprox \frac{1}{2\epsilon}\frac{\sqrt{N}}{\sqrt{g}}\,. \end{aligned} \tag{6.17}$$

- When these are satisfied, the additional condition

$$\frac{\pi}{8G}\left(\left(\frac{gN_{D5}}{N_{NS5}}\right) + \left(\frac{gN_{D5}}{N_{NS5}}\right)^{-1}\right) < \delta^2 \tag{6.18}$$

  is sufficient to ensure the existence of suitable $(N_{D3}, \hat{N}_{D3})$ to give a solution with the desired properties. In particular, if we choose N_{D5}, N_{NS5} such that $\gcd(N_{D5}, N_{NS5}) = N$ and $gN_{D5}/N_{NS5} = \mathcal{O}(1)$, the approximation accuracy δ will be of order $1/\sqrt{N}$.

- We explicitly construct sequences of solutions labeled by a parameter $n \in \mathbb{Z}^+$ with

$$\lim_{n\to\infty} \max\{l(n), k(n)\} = 0\,, \qquad \lim_{n\to\infty} |c(n)l(n) - d(n)k(n)| = 0\,, \tag{6.19}$$

  thus obtaining an arbitrarily good approximation to an arbitrarily large $\mathrm{AdS}_5 \times S^5$ region for large n. For example, in the case of self-

dual coupling $g = 1$, this occurs for the choice

$$\begin{aligned} N_{D5}(n) &= nN\,, & N_{NS5}(n) &= nN + 2\,, \\ N_{D3}(n) &= \frac{N}{2}(n-1) + 1\,, & \hat{N}_{D3}(n) &= \frac{N}{2}(n+1) \end{aligned} \tag{6.20}$$

(or exchanging $N_{D5} \leftrightarrow N_{NS5}$ and $N_{D3} \leftrightarrow \hat{N}_{D3}$ in these expressions), where $n \in \mathbb{N}^+$ is an integer parameter (and we must also require that n is odd if N is odd). More generally, we construct such families for any string coupling g and any choice of relative scaling $zN_{D5} \sim N_{NS5}, z \in \mathbb{R}^+$.

6.4.1 Necessary conditions for solutions with large $\mathbf{AdS}_5 \times S^5$ region

Suppose we would like a solution that is well-approximated by $\mathrm{AdS}_5 \times S^5$ to an accuracy δ in some range $r > \epsilon r_0$. Then according to the conditions (6.8) and (6.12) we require that

$$l < \epsilon\sqrt{N} \tag{6.21}$$

$$k < \epsilon\sqrt{N} \tag{6.22}$$

$$\tfrac{1}{\sqrt{N}} \left| \tfrac{kN_{NS5}}{\sqrt{g}} - lN_{D5}\sqrt{g} \right|^{\frac{1}{2}} < \delta\,. \tag{6.23}$$

Recalling that

$$\frac{k}{\sqrt{g}} N_{NS5} + l\sqrt{g}N_{D5} = N\,, \tag{6.24}$$

we may combine (6.23) and (6.24) to find that

$$\begin{aligned} \frac{N}{2}(1-\delta^2) &< \frac{k}{\sqrt{g}} N_{NS5} < \frac{N}{2}(1+\delta^2) \\ \frac{N}{2}(1-\delta^2) &< l\sqrt{g}N_{D5} < \frac{N}{2}(1+\delta^2)\,. \end{aligned} \tag{6.25}$$

Combining these with (6.21) and (6.22), we see that

$$N_{NS5} > \sqrt{gN}\frac{1}{2\epsilon}\left(1-\delta^2\right)$$

$$N_{D5} > \sqrt{\frac{N}{g}} \frac{1}{2\epsilon} \left(1 - \delta^2\right) \ . \tag{6.26}$$

Consequently, we see that *both* N_{D5} and N_{NS5} must be sufficiently large for (6.8) and (6.12) to simultaneously be satisfied, in addition to the previous requirement $G \mid N$. Notably, this implies that if we would like to construct a family of solutions which can achieve an arbitrarily large $\mathrm{AdS}_5 \times S^5$ region, then we will need to take both N_{D5} and N_{NS5} to be increasingly large within this family.

6.4.2 Sufficient conditions for solutions with large $\mathbf{AdS}_5 \times S^5$ region

Given N_{D5}, N_{NS5} satisfying $G \mid N$ and (6.26), we will now investigate the additional conditions which guarantee a choice of (l, k) in the range (6.25) for which N_{D3} and $\hat{N}_{D3}$ are integers.

For N_{D5} and N_{NS5} satisfying constraints (6.26) and $G \mid N$, we have from (6.25) that

$$\frac{k}{l} \in g \frac{N_{D5}}{N_{NS5}} [1 - 2\delta^2, 1 + 2\delta^2] \ . \tag{6.27}$$

Using (6.14) together with (6.25) and (6.27), we have that

$$\begin{aligned} N_{D3} &\approx N_{D3}^{(0)} = \frac{N}{2N_{D5}} + \frac{2}{\pi} N_{NS5} \arctan\left(\frac{N_{NS5}}{gN_{D5}}\right) \\ \hat{N}_{D3} &\approx \hat{N}_{D3}^{(0)} = \frac{N}{2N_{NS5}} + \frac{2}{\pi} N_{D5} \arctan\left(\frac{gN_{D5}}{N_{NS5}}\right) \ . \end{aligned} \tag{6.28}$$

More precisely, taking into account the allowed range of l and k/l, L must lie in a range of values with half width

$$\Delta N_{D3} = 2\delta^2 \left[\frac{N}{4N_{D5}} + \frac{2}{\pi} \frac{gN_{D5}}{1 + \left(\frac{gN_{D5}}{N_{NS5}}\right)^2} \right] \ . \tag{6.29}$$

We can show that the second term here is larger when (6.26) is satisfied, so

we can take the range as

$$\Delta N_{D3} \approx 2\delta^2 \left[\frac{2}{\pi} \frac{g N_{D5}}{1 + \left(\frac{g N_{D5}}{N_{NS5}}\right)^2} \right] . \tag{6.30}$$

We need the range $[N_{D3}^{(0)} - \Delta N_{D3}, N_{D3}^{(0)} + \Delta N_{D3}]$ to be large enough to contain an integer value. More specifically, we need a value for which $\hat{N}_{D3} - N_{D5} = (N - N_{D3}N_{D5})/N_{NS5}$ is also an integer. This requires that $G \mid N$, in which case, a range of N_{D3} of length N_{NS5}/G will lead to at least one integer value of $\hat{N}_{D3}$.

Thus, for fixed g and N, and some chosen N_{D5} and N_{NS5} satisfying the constraints (6.26) and that $G \mid N$, we will get a solution provided that the range (6.29) is at least N_{NS5}/G; that is, it should be sufficient that

$$\frac{1}{G} < \delta^2 \left[\frac{8}{\pi} \frac{\left(\frac{g N_{D5}}{N_{NS5}}\right)}{1 + \left(\frac{g N_{D5}}{N_{NS5}}\right)^2} \right] , \tag{6.31}$$

or

$$\frac{\pi}{8G} \left(\left(\frac{g N_{D5}}{N_{NS5}}\right) + \left(\frac{g N_{D5}}{N_{NS5}}\right)^{-1} \right) < \delta^2 . \tag{6.32}$$

Since the term in brackets is larger than or equal to 2 and $G < N$, we expect that our sufficient condition can be satisfied provided that δ is at least $1/\sqrt{N}$. However, we will see below that for fixed N, arbitrarily small values of ϵ and δ are possible for carefully chosen parameters.

6.4.3 One-parameter families with arbitrarily large $\mathbf{AdS}_5 \times S^5$ region

For simplicity, we will begin with the case of self-dual coupling $g = 1$. We consider a sequence of parameters labeled by $n \in \mathbb{N}^+$ (and further imposing that n is odd for odd N to satisfy (6.15)), defining

$$N_{D5} = nN , \quad N_{NS5} = nN + 2 , \tag{6.33}$$

and

$$N_{D3} = \frac{N}{2}(n-1)+1\,, \quad \hat{N}_{D3} = \frac{N}{2}(n+1)\,, \tag{6.34}$$

or alternatively, using the same expressions but with $N_{D5} \leftrightarrow N_{NS5}$ and $N_{D3} \leftrightarrow \hat{N}_{D3}$. In this case, we can check that (6.15) and (6.16) are satisfied, so our results in Appendix E.3 show that there will be a unique choice (l,k) satisfying (6.14).

For large n, we can write this solution perturbatively as

$$\begin{aligned} l &= \frac{1}{2n} - \frac{1}{2n^2}\left(\frac{\pi}{4}+\frac{1}{N}\right) + \mathcal{O}(n^{-3}) \\ k &= \frac{1}{2n} + \frac{1}{2n^2}\left(\frac{\pi}{4}-\frac{1}{N}\right) + \mathcal{O}(n^{-3})\,. \end{aligned} \tag{6.35}$$

From these, we find that

$$|cl-dk| = \frac{1}{n}\left(1+\frac{\pi N}{4}\right) + \mathcal{O}(n^{-2})\,. \tag{6.36}$$

so we can indeed make $\max\{l,k\}$ and $|cl-dk|$ arbitrarily small within this particular class of solutions, by choosing sufficiently large n. Thus, we can have an arbitrarily large region of $\mathrm{AdS}_5 \times S^5$ arbitrarily well-approximated by our solution.

To emphasize that these choices of parameters indeed give rise to a large $\mathrm{AdS}_5 \times S^5$ region, we show in Figures 6.3 and 6.4 the metric functions obtained for particular choices of these parameters, as well as the metric functions of $\mathrm{AdS}_5 \times S^5$ for reference. We find that these metric functions agree to good approximation for r above some r_* which becomes small as the parameter n is taken to be large.

General construction of one-parameter families

Next, we consider a more general case where the string coupling takes the form

$$g = m\cot\left(\frac{\pi}{2}\frac{a}{b}\right)\,, \tag{6.37}$$

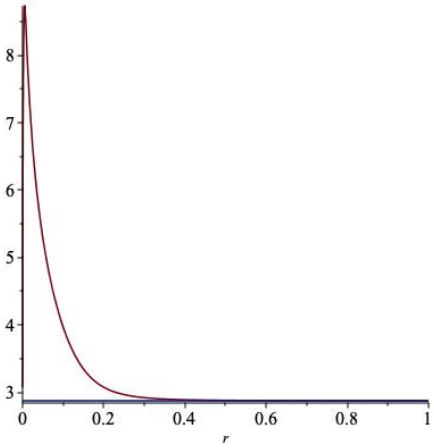

(a) $\ln f_1^2\left(r, \frac{\pi}{4}\right)$ versus r

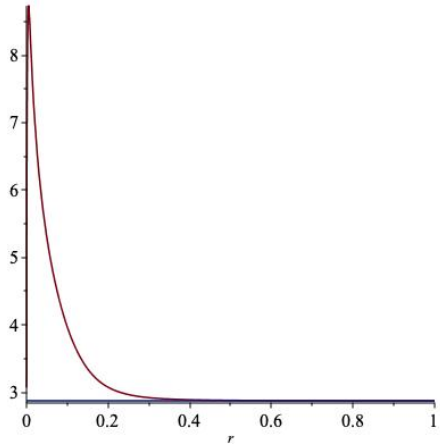

(b) $\ln f_2^2\left(r, \frac{\pi}{4}\right)$ versus r

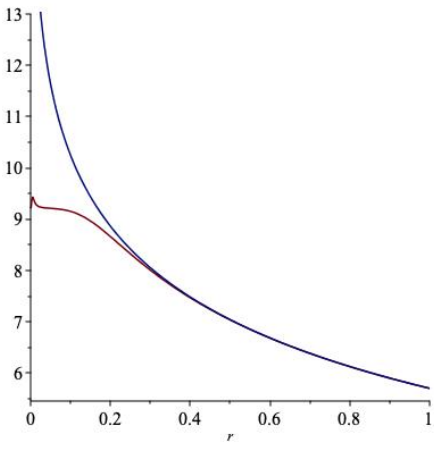

(c) $\ln f_4^2\left(r, \frac{\pi}{4}\right)$ versus r

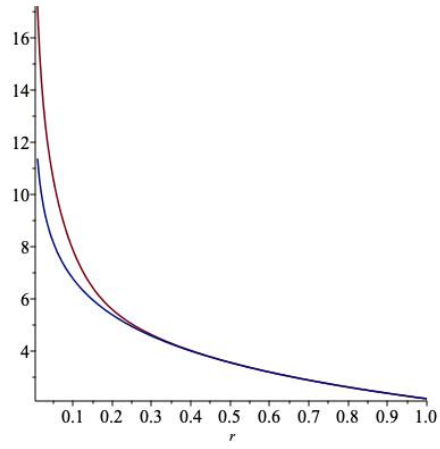

(d) $\ln \rho^2\left(r, \frac{\pi}{4}\right)$ versus r

Figure 6.3: In these figures, we are taking $g = 1, \ell_s = 1, N = 100$. The metric functions shown in red are for the case $(c, d, l, k) = (10^4, 10^4+2, 4.96\times 10^{-3}, 5.04 \times 10^{-3})$ (namely $n = 100$ in our family of solutions), while the metric functions shown in blue are for pure $AdS_5 \times S^5$. Note that in this case $r_0 \approx 5.64$.

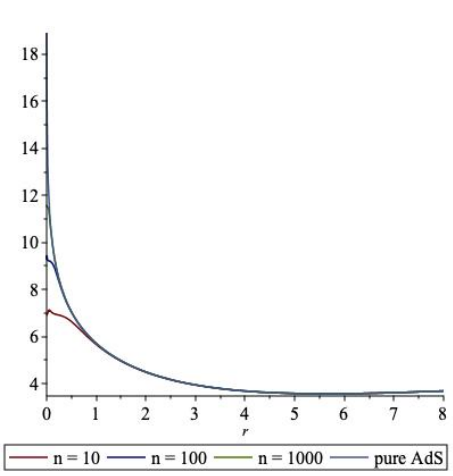

(a) $\ln\left(f_4^2\left(r,\frac{\pi}{4}\right)\right)$ versus r on $r \in (0,8)$

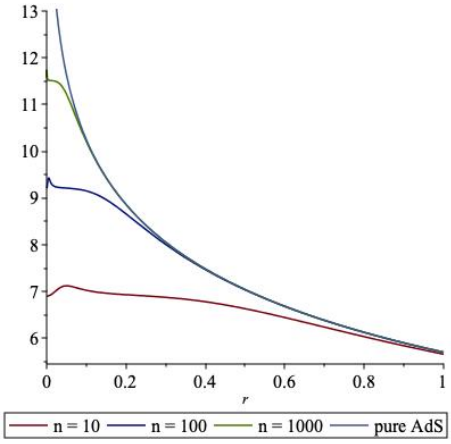

(b) Close-up: $\ln\left(f_4^2\left(r,\frac{\pi}{4}\right)\right)$ versus r on $r \in (0,1)$

Figure 6.4: In these figures, we are taking $g = 1, \ell_s = 1, N = 100$. The metric functions shown correspond to the indicated values of n in the family of solutions above, as well as the case of pure $AdS_5 \times S^5$.

where $m \in \mathbb{Z}^+$ and $a < b$ are relatively prime. The set of such string couplings is dense in $[0, \infty)$. Taking (α, δ) to be any solution to the Diophantine equation[96]

$$(b-a)\alpha - b\delta = N\,, \tag{6.38}$$

we define a sequence[97]

$$\begin{aligned} N_{D5}(n) &= bn + \alpha \\ N_{NS5}(n) &= m(bn+\alpha) - b \\ N_{D3}(n) &= amn - a + m(\alpha - \delta) \\ \hat{N}_{D3}(n) &= (b-a)n + \delta\,. \end{aligned} \tag{6.39}$$

We can also consider a similar sequence with the replacements $N_{D5} \leftrightarrow N_{NS5}, N_{D3} \leftrightarrow \hat{N}_{D3}, g \leftrightarrow 1/g$. This choice is motivated in Appendix E.4.

[96] A simple explicit case is to take $b = a+1$ (so that $g = m\tan(\pi/2b)$), $\alpha = N$, and $\delta = 0$.

[97] Note that different choices for (α, δ) lead to the same sequence with a redefinition of n.

For these choices, it is straightforward to check that (6.16) is satisfied. Also, constraint $\sqrt{g}N_{D5}l + \frac{1}{\sqrt{g}}N_{NS5}k = N$ implies that both l and k are at most $O\left(n^{-1}\right)$, so these go to zero in the limit $n \to \infty$. Finally, we need to verify that $|cl - dk|$ also vanishes in this limit.

From the definitions of $N_{D3}(n)$, $N_{NS5}(n)$, and g, we see that

$$\frac{N_{D3}(n)}{N_{NS5}(n)} = \frac{a}{b} + O\left(n^{-1}\right) = \frac{2}{\pi}\arctan(m/g) + O\left(n^{-1}\right) \tag{6.40}$$

The equations (6.14) yield

$$\frac{N_{D3}(n)}{N_{NS5}(n)} = \frac{2}{\pi}\arctan(l/k) + O\left(n^{-2}\right) \ . \tag{6.41}$$

Thus, we have

$$l/k = m/g + O\left(n^{-1}\right) \ . \tag{6.42}$$

It follows that

$$|cl - dk| = \left|\, (\sqrt{g}bn)\left(\frac{km}{g} + O\left(n^{-2}\right)\right) - \left(\frac{1}{\sqrt{g}}bmn\right)k\right| = O\left(n^{-1}\right) \ , \tag{6.43}$$

as desired. Thus, an arbitrarily large region of $\mathrm{AdS}_5 \times S^5$ becomes arbitrarily well approximated for solutions corresponding to large enough n.

The construction so far applies to a particular dense set of string couplings of the form (6.37), and leads to a scaling of parameters

$$N_{D5} \sim mN_{NS5} \ , \tag{6.44}$$

where m is an integer. In Appendix E.4, we generalize the construction to arbitrary real string coupling and find families of solutions that exhibit a more general scaling $N_{NS5} \sim zN_{D5}$ for arbitrary $z > 0$.

For general z, conditions (6.8) and (6.12) then fix the scaling for the linking numbers to be

$$\frac{N_{D3}}{N_{NS5}} \sim \frac{2}{\pi}\arctan(z/g) \ , \qquad \frac{\hat{N}_{D3}}{N_{D5}} \sim \frac{2}{\pi}\arctan(g/z) \ . \tag{6.45}$$

6.4.4 Field theory interpretation for solution families approaching $\mathbf{AdS}_5 \times S^5$

We would now like to understand from the field theory perspective what boundary physics for the $\mathcal{N} = 4$ SYM theory gives rise to the solutions with arbitrarily large regions of $\mathrm{AdS}_5 \times S^5$ (Θ_* arbitrarily close to $-\pi/2$). In each case, we are coupling the $\mathcal{N} = 4$ SYM theory on a half space to a particular 3D SCFT[98] that can be understood as arising from the low-energy physics of a particular brane configuration in string theory, or as the IR limit of a quiver gauge theory.

To understand the brane construction corresponding to the parameters $(N_{D5}, N_{NS5}, N_{D3}, \hat{N}_{D3})$, we note that the parameters L_i introduced in Section 6.2 are simply N_{D3} with multiplicity N_{D5}, while the parameters K_i are $\hat{N}_{D3}$ with multiplicity N_{NS5}. From the relation between these parameters and the brane configuration, we can check that this set corresponds to having N_{NS5} NS5-branes which we can initially think of as being separated along a direction x^3 (the direction in which the D3-branes are semi-infinite), with a stack of N_{D5} D5-branes between the N_{D3}^{th} and $(N_{D3}+1)^{\text{th}}$ NS5-brane from the left. We additionally have n_i D3-branes stretched between the i^{th} and $(i+1)^{\text{th}}$ NS5, where

$$n_i = \begin{cases} i\hat{N}_{D3} & i \leq N_{D3} \\ i\hat{N}_{D3} - N_{D5}(i - N_{D3}) & i > N_{D3} \end{cases} . \tag{6.46}$$

To the right of the final NS5-brane, we have the N semi-infinite D3-branes.

Stripping off the semi-infinite D3-branes gives a brane set-up whose low-energy physics is a SCFT that corresponds to the IR limit of the quiver

[98] We recall that the general $OSp(4|4)$-invariant boundary condition of this theory can be specified by a triple $(\rho, H, \mathcal{B})$ [89, 90]; here, $\rho : \mathfrak{su}(2) \to \mathfrak{g}$ is a homomorphism into the Lie algebra of the gauge group (in our case $U(N)$) which specifies the "Nahm pole" boundary condition for the scalars in the bulk 4D hypermultiplet, H is the residual symmetry group at the field theory boundary, and $\mathcal{B}$ is the 3D SCFT coupled at the boundary. For the boundary conditions in the one-parameter families that we are currently considering, we are imposing a simple Dirichlet boundary condition on the bulk hypermultiplet (and a Neumann condition on the 4D vector multiplet), and there is no reduction in gauge symmetry; our boundary conditions are then entirely specified by the SCFT $\mathcal{B}$.

gauge theory shown in Figure 6.5. Such a quiver consists of $N_{NS5}-1$ nodes, with N_{D5} fundamental hypermultiplets coupled to the N_{D3}^{th} node. For nodes to the left of the N_{D3}^{th} node, the gauge group rank increases in increments of $\hat{N}_{D3}$ as we read the quiver from left to right; for nodes to the right, the gauge group rank decreases in increments of $N_{D5}-\hat{N}_{D3}$.

So far, this construction is completely general within boundary conditions involving a single D5-brane throat and a single NS5-brane throat; we now restrict to boundary conditions within the families considered in this section. For the one-parameter family introduced at the beginning of Section 6.4.3 (with $g=1$ and $z=1$), we see that the corresponding quiver is approximately "left-right symmetric" for large n; given that our family has $\frac{N_{D3}}{N_{NS5}} \approx \frac{1}{2}$ for large n, the hypermultiplets are coupled to a single node which is roughly in the middle of the quiver, after which the gauge group rank decreases in increments of $N_{D5}-\hat{N}_{D3}$, where $\frac{N_{D5}-\hat{N}_{D3}}{\hat{N}_{D3}} \approx 1$ for large n. More generally, we find that, if we parametrize the quiver by its length $N_{NS5}-1 \approx N_{NS5}$, then we will have $N_{D5} \approx \frac{1}{z}N_{NS5}$ fundamental hypermultiplets coupled to a node whose placement in the quiver grows proportionally to the length of the quiver to enforce the ratio $\frac{N_{D3}}{N_{NS5}} \approx \frac{2}{\pi}\arctan(z/g)$. In particular, we note that in the case of small coupling $g \ll z$, the fundamental hypermultiplets will be roughly at the right end of the quiver, while in the case of large coupling $g \gg z$ they will be at the left end.

The fact that all the hypermultiplets are attached to the same gauge group factor (or that the D5-branes in the brane construction come in a single stack) is an artifact of our simplifying assumption that the harmonic functions leading to the supergravity solution have only a single D5-brane pole and a single NS5-brane pole. We expect that there are many other choices with additional poles that lead to more general quivers but still give $\Theta_* \to -\pi/2$ in a limit. In Appendix E.5, we will verify that such cases can be obtained by small deformations of the boundary conditions in this section. In particular, we construct examples where we couple in additional hypermultiplets to an additional node of the quiver; this corresponds to adding in additional D5 and NS5-brane poles. We also consider deforming our single-pole boundary conditions by coupling the corresponding quivers

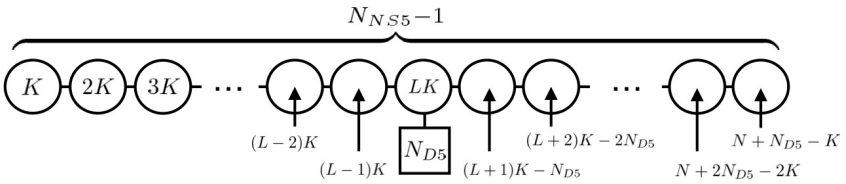

Figure 6.5: General form of a quiver gauge theory which corresponds to the field theory boundary conditions determined by the data $(N_{D5}, N_{NS5}, N_{D3}, \hat{N}_{D3})$, where we take $N_{D3} = L$ and $\hat{N}_{D3} = K$.

to an additional small quiver at the left endpoint. In both of these contexts, we find more general sequences of solutions that still yield $\Theta_* \to -\pi/2$. We will consider a further generalization with multiple D5-brane poles in the following section.

6.5 Solutions with multiple poles

In this section, we consider a more general case where we still have only a single NS5-brane pole in h_2 at location $y = k$ with multiplicity N_{NS5}, but we allow arbitrary numbers of D5-brane poles in h_1 at (possibly coincident) locations $x = l_i$.

These poles will correspond to some linking numbers K with multiplicity N_{NS5} and N_{D5} linking numbers $\{L_i\}$, such that

$$N_{NS5}\hat{N}_{D3} + \sum_i L_i = N + N_{NS5}N_{D5} \ . \tag{6.47}$$

Given linking numbers satisfying this, the corresponding pole locations k and $\hat{l}_i$ must satisfy

$$\begin{aligned} L_i &= \sqrt{g}\hat{l}_i + \frac{2}{\pi}N_{NS5}\arctan\frac{l_i}{k} \\ \hat{N}_{D3} &= \frac{k}{\sqrt{g}} + \frac{2}{\pi}\sum_i \arctan\frac{k}{l_i} \ . \end{aligned} \tag{6.48}$$

We can determine k and l_i as follows. Defining

$$F_k(x) = \sqrt{g}x + \frac{2}{\pi}N_{NS5}\arctan\frac{x}{k} \tag{6.49}$$

and noting that for any k, F_k is a monotonic map from $[0,\infty)$ to $[0,\infty)$, we have that

$$l_i = F_k^{-1}(l_i)\ . \tag{6.50}$$

The actual value of k is determined by solving[99]

$$N = \frac{k}{\sqrt{g}}N_{NS5} + \sqrt{g}\sum_i F_k^{-1}(L_i)\ . \tag{6.51}$$

To see which linking numbers satisfy our conditions for having a Θ_* close to $-\pi/2$, we note that the requirements that

$$\sqrt{g}\sum_i l_i + \frac{k}{\sqrt{g}}N_{NS5} = N \tag{6.52}$$

(which follows from the first three equations of this section) and our condition

$$|\sqrt{g}\sum_i l_i - \frac{k}{\sqrt{g}}N_{NS5}| \ll N \tag{6.53}$$

require that both terms in each expression are close to $N/2$ so

$$\sqrt{g}\sum_i l_i \approx \frac{N}{2} \tag{6.54}$$

and

$$k \approx k^{(0)} \equiv \frac{\sqrt{g}N}{2N_{NS5}}\ . \tag{6.55}$$

In order that $k \ll \sqrt{N}$, the latter condition implies

$$N_{NS5} \gg \sqrt{gN}\ . \tag{6.56}$$

[99] We note that each term on the right is monotonically increasing with k, and the entire right side increases monotonically from a value less than N for $k = 0$ to infinity for $k = \infty$, so there will be a unique solution.

Then the l_i are approximately related to L_i by

$$l_i \approx l_i^{(0)} \equiv F^{-1}_{k^{(0)}}(L_i) \, . \tag{6.57}$$

The condition $l_i \ll \sqrt{N}$ gives that

$$F^{-1}_{k^{(0)}}(L_i) \ll \sqrt{N} \, . \tag{6.58}$$

From the condition (6.54), we have

$$\sqrt{g} \sum_i F^{-1}_{k^{(0)}}(L_i) \approx \frac{N}{2} \, . \tag{6.59}$$

Since each $l_i = F^{-1}_{k^{(0)}}(L_i)$ in the sum is required to be much less than $\sqrt{N}$ but also greater than or equal to $F^{-1}_{k^{(0)}}(1) \sim \pi\sqrt{g}N/(4N_{NS5}^2)$, we note that the number of D5-brane poles (including multiplicity) must satisfy

$$\frac{1}{2}\sqrt{\frac{N}{g}} \ll N_{D5} < \frac{2N_{NS5}^2}{\pi g} \, . \tag{6.60}$$

Our choice of the L_i must be such that

$$\hat{N}_{D3} = N_{D5} + \frac{N - \sum_i L_i}{N_{NS5}} \tag{6.61}$$

is an integer. To see when this is possible, we note that for $L_i \ll N_{NS5}$, F is linear and

$$l_i = F^{-1}_{k^{(0)}}(L_i) \approx \frac{\pi}{4}\frac{\sqrt{g}N}{N_{NS5}^2} L_i \, . \tag{6.62}$$

Thus, adding an additional pole with $L = 1$ or varying one of the L_i by 1 leads to a change in the left side of (6.59) of

$$\frac{\pi}{4}\frac{gN}{N_{NS5}^2} \ll 1 \, . \tag{6.63}$$

Given any set of L_i, changing the sum by an amount less than N_{NS5} will be enough to give an integer $\hat{N}_{D3}$. If we add or change the L_i in the linear

regime of F, the change in $\sqrt{g}\sum_i l_i$ will be less than

$$\frac{\pi}{4}\frac{gN}{N_{NS5}}\,. \tag{6.64}$$

We can satisfy (6.59) for integer $\hat{N}_{D3}$ provided that this quantity is much less than $N/2$, so we have the additional condition

$$N_{NS5} \gg g\,. \tag{6.65}$$

So far, we have assumed that $k = k^{(0)}$. The actual value of k corresponding to our chosen L_i and $\hat{N}_{D3}$ is determined by

$$\frac{k}{\sqrt{g}}N_{NS5} + \sqrt{g}\sum_i F_k^{-1}(L_i) - N = 0\,. \tag{6.66}$$

We need to check that for this actual value, $|k/\sqrt{g}N_{NS5} - N/2| \ll N$ so that (6.53) is still satisfied. Since

$$|\frac{k^{(0)}}{\sqrt{g}}N_{NS5} + \sqrt{g}\sum_i F_{k^{(0)}}^{-1}(L_i) - N| \ll N\,, \tag{6.67}$$

we know that the function

$$G(k) = \frac{k}{\sqrt{g}}N_{NS5} + \sqrt{g}\sum_i F_k^{-1}(L_i) \tag{6.68}$$

varies by an amount much less than N as k is varied from $k^{(0)}$ to its actual value. This gives

$$\delta k \ll \frac{N}{G'(k)}\,, \tag{6.69}$$

so $kN_{NS5}/\sqrt{g}$ will change by an amount much less than N provided that the right side here is less than $\sqrt{g}N/N_{NS5}$, or $G'(k) > N_{NS5}/\sqrt{g}$. This is clearly true, since the k derivative of the first term in G is $N_{NS5}/\sqrt{g}$ and the k derivative of the second term is positive.

To summarize, given N and g, the following procedure will yield a set of linking numbers that satisfy our conditions:

- Choose some N_{NS5} satisfying $N_{NS5} \gg \sqrt{gN}$ and $N_{NS5} \gg g$ and N_{D5} satisfying (6.60).
- Choose a set $\{L_i\}$ of N_{D5} L_i such that (6.58) and (6.59) are satisfied and
$$\hat{N}_{D3} = N_{D5} + \frac{N - \sum_i L_i}{N_{NS5}} \tag{6.70}$$
is an integer. This will be possible provided the conditions on N_{NS5} and N_{D5} are satisfied.
- Once the linking numbers are fixed in this way, the precise k and l_i are determined by the procedure described at the beginning of this subsection.

For this more general class of SCFTs, the corresponding quiver gauge theory will have fundamental matter distributed among the nodes of the quiver, with the number of distinct L_i determining the number of nodes with fundamental matter.

If we require that $l_i < \epsilon\sqrt{N}$ to satisfy (6.58), we get

$$\max\{L_i\} \approx F_{k^{(0)}}(\epsilon\sqrt{N}) = \epsilon\sqrt{gN} + \frac{2}{\pi} N_{NS5} \arctan\left(\frac{2\epsilon N_{NS5}}{\sqrt{gN}}\right) . \tag{6.71}$$

If $N_{NS5} \gg \sqrt{gN}/\epsilon$, we get $\max\{L_i\} \approx N_{NS5}$. As there are N_{NS5} nodes in the quiver, it seems possible in some cases to have matter uniformly distributed throughout the quiver, with order one fundamentals per node.

6.6 Microscopic wedge holography

In this section we describe a generalization of the previous construction in which we have two ETW branes bounding an arbitrarily large wedge $\Theta \in (-\Theta_*, \Theta_*)$ of $\mathrm{AdS}_5 \times S^5$. In this case, only an $\mathbb{R}^{1,2}$ of the original asymptotic region $\mathbb{R}^{1,3}$ of $\mathrm{AdS}_5 \times S^5$ remains, and the dual theory is a three-dimensional SCFT.

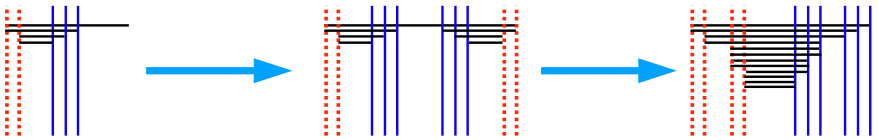

Figure 6.6: Illustration of procedure used to define families of solutions realizing arbitrarily large wedges of $AdS_5 \times S^5$; here, D3-branes are black, D5-branes are blue, and NS5-branes are red. To pass from the second to the third configuration, we rearrange the five-branes so that all NS5-branes are to the left of all D5-branes, while D3-branes between these five-branes are created or annihilated to maintain fixed linking numbers. The third configuration is convenient for defining the quantities $N_3^{(A)}$, $\hat{N}_3^{(B)}$ in (6.73): they represent the net number of D3-branes ending on branes in the A^{th} D5-brane stack or the B^{th} NS5-brane stack respectively.

6.6.1 A 3D dual to an arbitrarily large wedge of $AdS_5 \times S^5$.

We have seen that for an appropriate choice of 3D SCFT coupled to $\mathcal{N} = 4$ SYM theory on a half space, the ETW brane region of the dual geometry can be pushed to a Poincaré angle that is arbitrarily close to $-\pi/2$. We next consider the situation where we introduce another such boundary parallel to the first so that the $\mathcal{N} = 4$ theory now lives on a strip. We can choose this second boundary SCFT to preserve the same set of supersymmetries as the first one. The brane construction of this SCFT involves the same set of branes as for the first SCFT, with the same orientations, but arranged in the opposite order in the spatial direction in which the D3-branes have a boundary;[100] see Figure 6.6.

We expect the dual of this theory to have two ETW branes, bounding a wedge of $AdS_5 \times S^5$ whose asymptotic region has the geometry $\mathbb{R}^{1,2}$ times an interval. The solutions of [172–175] are not general enough to describe this, since they correspond to theories with a 3D superconformal symmetry, while the interval in our construction introduces a scale. However, we expect that the IR limit of the theory on a strip will be a certain superconformal theory; this is the theory whose brane construction combines that of the original

[100] More generally, we could consider two different SCFTs which nevertheless preserve the same supersymmetries.

BCFT with that of the second SCFT, so that the initial semi-infinite D3-branes now connect the brane configurations describing the two SCFTs. The gravity dual of this IR SCFT is a wedge of $AdS_5 \times S^5$ with two ETW branes. Such wedge geometries can be described explicitly as particular cases of the solutions in [172–175] and were considered previously in [175, 294]. These geometries are microscopic realizations of the "wedge holography" discussed in [285].

The new element in our work is that we can, by the choices described in the previous section, arrange for the wedge of $AdS_5 \times S^5$ between the ETW branes to be arbitrarily large.

To verify this, we note that, making the change of coordinates $z = r_0 e^w = r_0 e^{x+iy}$ so that the positive quadrant is mapped to the strip $0 \leq \Im(w) \leq \pi/2$, the single boundary geometries correspond to harmonic functions

$$\begin{aligned} h_1 &= \frac{\pi \ell_s^2}{2\sqrt{g}} r_0 e^x \cos y + \frac{\ell_s^2}{4\sqrt{g}} \sum_A c_A \ln\left(\frac{\cosh(x+\alpha_A)+\cos(y)}{\cosh(x+\alpha_A)-\cos(y)}\right) \\ h_2 &= \frac{\pi \ell_s^2 \sqrt{g}}{2} r_0 e^x \sin y + \frac{\ell_s^2 \sqrt{g}}{4} \sum_B d_B \ln\left(\frac{\cosh(x+\beta_B)+\sin(y)}{\cosh(x+\beta_B)-\sin(y)}\right) , \end{aligned}$$

where we have defined $\alpha_A = -\ln(l_A/r_0)$ and $\beta_A = -\ln(k_A/r_0)$.

The pole of h_1 at $-\alpha$ and the pole of h_2 at $i\pi/2 - \beta$ lie at large negative values of x for the single-pole cases of interest. The corresponding solution with two ETW branes is given by

$$\begin{aligned} h_1 &= \frac{\ell_s^2}{4} \sum_{a=1}^{2} N_5^{(a)} \ln\left(\frac{\cosh(x-\delta_a)+\cos(y)}{\cosh(x-\delta_a)-\cos(y)}\right) \\ h_2 &= \frac{\ell_s^2}{4} \sum_{b=1}^{2} \hat{N}_5^{(b)} \ln\left(\frac{\cosh(x-\hat{\delta}_b)+\sin(y)}{\cosh(x-\hat{\delta}_b)-\sin(y)}\right) , \end{aligned}$$

where $N_5^{(1)} = N_5^{(2)} = N_{D5}$ and $\hat{N}_5^{(1)} = \hat{N}_5^{(2)} = N_{NS5}$ are the number of D5-branes and NS5-branes in the initial boundary condition, and now we have poles of h_1 at $\delta_{1/2}$ and of h_2 at $i\pi/2 + \hat{\delta}_{1/2}$ whose leading order behaviour is given by

$$\delta_1 \sim -\delta_2 \sim \alpha \,, \qquad \hat{\delta}_1 \sim -\hat{\delta}_2 \sim \beta \,. \tag{6.72}$$

Solutions corresponding to more general 3D SCFTs are obtained by allowing the poles to be at more general locations.

To demonstrate this claim, we will proceed by analyzing the D-brane constructions for these theories. We must first revisit the families of boundary conditions from the previous section, choosing for convenience a string coupling g in the boundary case to be of the form $g = m \cot\left(\frac{\pi}{2}\frac{a}{b}\right)$, as we have done above, and defining the parameters $(N_{D5}, N_{NS5}, N_{D3}, \hat{N}_{D3})$ using (6.39). As in [175], when we pass to the dual of the 3D theory, we may consistently set $g = 1$ (while the dilaton is left arbitrary).

The doubled theory is described in the language of [175] by parameters[101]

$$\begin{aligned}
&N_5^{(1)} = N_5^{(2)} = N_{D5}\ , \\
&\hat{N}_5^{(1)} = \hat{N}_5^{(2)} = N_{NS5}\ , \\
&N_3^{(1)} = 2N_{NS5} - N_{D3}\ , \quad N_3^{(2)} = N_{D3}\ , \\
&\hat{N}_3^{(1)} = \hat{N}_{D3}\ , \quad \hat{N}_3^{(2)} = 2N_{D5} - \hat{N}_{D3}\ ,
\end{aligned} \tag{6.73}$$

where the supergravity parameters $\delta_a, \hat{\delta}_b$ are related to the D3-brane charges by

$$\begin{aligned}
N_3^{(a)} &= \frac{2}{\pi}\sum_{b=1}^{2} \hat{N}_5^{(b)} \tan^{-1}\left(e^{\delta_a - \hat{\delta}_b}\right) \\
\hat{N}_3^{(b)} &= \frac{2}{\pi}\sum_{a=1}^{2} N_5^{(a)} \tan^{-1}\left(e^{\delta_a - \hat{\delta}_b}\right)\ .
\end{aligned} \tag{6.74}$$

These latter equations yield at leading order in n

$$\begin{aligned}
e^{\delta_1 - \hat{\delta}_1} &= \frac{g}{m}\ , \qquad e^{\delta_1 - \hat{\delta}_2} = \frac{4mb^2n^2}{\pi N}\ , \\
e^{\delta_2 - \hat{\delta}_1} &= \frac{\pi N}{4mb^2n^2}\ , \qquad e^{\delta_2 - \hat{\delta}_2} = \frac{m}{g}\ ,
\end{aligned} \tag{6.75}$$

[101] Our notation is actually slightly different from that of [175]: the $N_3^{(i)}$ and $\hat{N}_3^{(i)}$ are both defined to be positive quantities, and differ from the conventions of that reference by factors of $N_5^{(i)}$ and $\hat{N}_5^{(i)}$ respectively.

so that without loss of generality we may take leading order behaviour

$$e^{\delta_1} = \frac{g}{m} e^{\hat{\delta}_1} = e^{-\delta_2} = \frac{g}{m} e^{-\hat{\delta}_2} = \frac{2\sqrt{g}bn}{\sqrt{\pi N}} \,. \tag{6.76}$$

Comparing with the supergravity parameters from the boundary case

$$\frac{l}{r_0} \sim \frac{\sqrt{\pi N}}{2\sqrt{g}bn} \,, \qquad \frac{k}{r_0} \sim \frac{\sqrt{g\pi N}}{2mbn} \,, \tag{6.77}$$

we find the leading behaviour of the poles $\delta_{1/2}$ and $\hat{\delta}_{1/2}$ mentioned above.

One can consider h_1, h_2 at leading order, and show that they give rise to an $\mathrm{AdS}_5 \times S^5$ region when $|x| \ll \ln n$. Indeed, we find in this region

$$\begin{aligned} h_1 &\sim \frac{L^2_{\mathrm{AdS}}}{2\sqrt{g}} \cosh x \cos y \,, \\ h_2 &\sim \frac{\sqrt{g} L^2_{\mathrm{AdS}}}{2} \cosh x \sin y \,, \end{aligned} \tag{6.78}$$

where $L^2_{\mathrm{AdS}} = \sqrt{4\pi N}\ell_s^2$. We recognize these as corresponding to pure $\mathrm{AdS}_5 \times S^5$. As n is increased, the curvature scale of the $\mathrm{AdS}_5 \times S^5$ region approaches a constant value, while the size of this region increases.

In Figure 6.7, we show the metric functions for such solutions (as well as those of $\mathrm{AdS}_5 \times S^5$ for comparison) in the vicinity of the locally $\mathrm{AdS}_5 \times S^5$ bridge between the two ETW branes, for various increasing values of n. We see that for increasing n, the bridge connecting the two ETW brane regions corresponds to an increasingly large wedge of $\mathrm{AdS}_5 \times S^5$.

6.6.2 Multi-wedge geometries

We have given a specific class of constructions describing arbitrarily large wedges of $\mathrm{AdS}_5 \times S^5$ as the dual of a 3D SCFT. For concreteness, we focused on the case obtained by doubling a brane configuration considered earlier in the context of boundary conditions for the 4D $\mathcal{N} = 4$ theory. More generally, we may consider 3D SCFTs which descend from linear quivers arising from "gluing" together several large sub-quivers of the type discussed

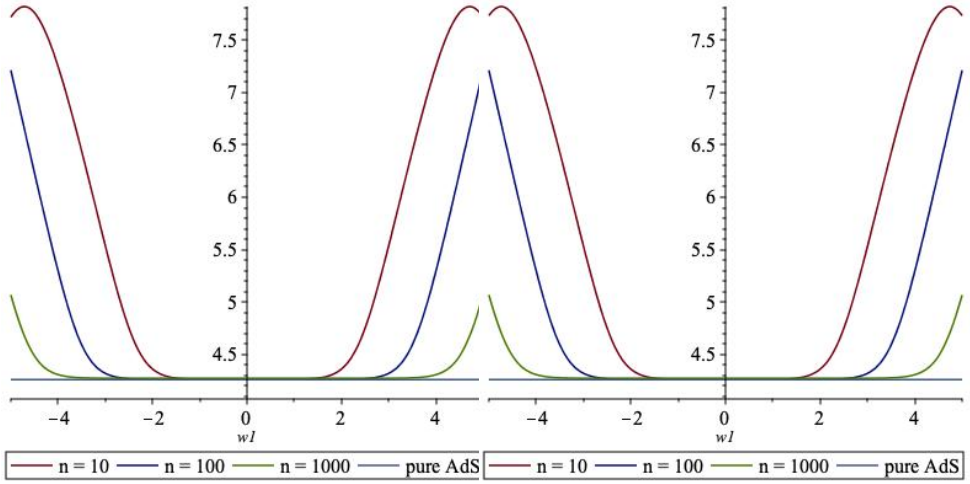

(a) $\ln f_1^2$ versus w_1

(b) $\ln f_2^2$ versus w_1

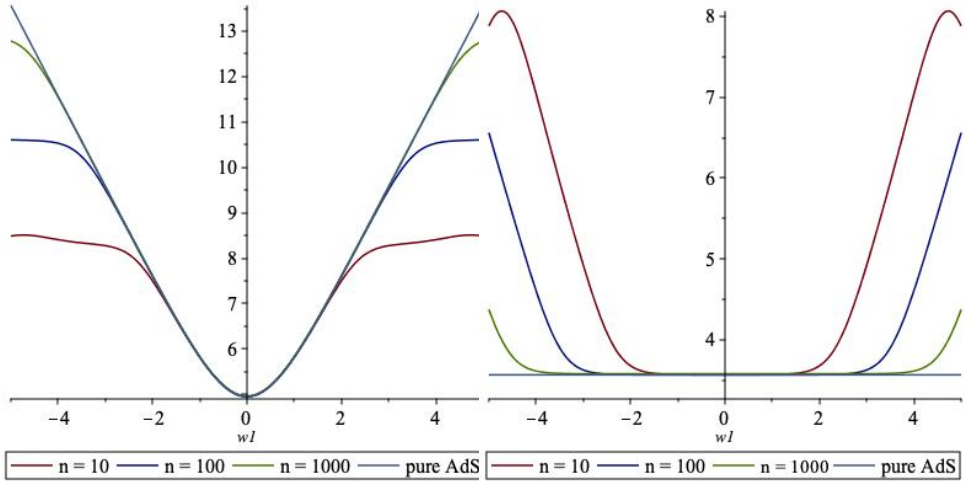

(c) $\ln f_4^2$ versus w_1

(d) $\ln \rho^2$ versus w_1

Figure 6.7: In these figures, we are taking $g = 1, \ell_s = 2, N = 100$. The metric functions shown are for $N_5 = 2nN, \hat{N}_5 = 2(nN+2), \hat{N}_3^{(1)} = \frac{N}{2}(n+1)$ with the values of n given, while the metric functions shown in light blue are for pure $AdS_5 \times S^5$ (with L_{AdS} fixed by N). We are displaying the metric functions with respect to complex coordinates $(w, \bar{w}) = (w_1 + iw_2, w_1 - iw_2) = \left(\ln\left(re^{i\theta}/r_0\right), \ln\left(re^{-i\theta}/r_0\right)\right)$, and setting $\theta = \pi/4$ in the figures. Note that the Jacobian of this coordinate change modifies ρ^2 from the expression provided.

in Section 6.4.4 by coupling the first and last nodes of consecutive subquivers with bifundamental matter to some additional $U(m_A)$ nodes with small m_A. This procedure is in the spirit of the "quantum gate" solutions described by Bachas and Lavdas in [294], but the result here is a spacetime description involving multiple wedges of $\mathrm{AdS}_5 \times S^5$ separated by interface branes.

This "multi-wedge" construction suggests further generalizations for holographic theories realizing the same $OSp(4|4)$ symmetry as the 3D SCFTs, including the $OSp(4|4)$-preserving BCFTs and 3D SCFTs descending from circular quiver gauge theories. In the former case, the holographic description involves a large $\mathrm{AdS}_5 \times S^5$ region in the vicinity of the asymptotic boundary, but this region is connected to an additional multi-wedge region by an interface brane. In the latter case, we again obtain a multi-wedge geometry whose boundary is only an $\mathbb{R}^{1,2}$ subset of the asymptotic $\mathbb{R}^{1,3}$ of $\mathrm{AdS}_5 \times S^5$, but in this case, the first and last $\mathrm{AdS}_5 \times S^5$ wedges are connected by another interface brane, so that we have non-contractible loops in the internal space which traverse all of the wedges. We leave a more detailed analysis of multi-wedge solutions to Appendix E.6.

6.7 Discussion

We have provided a number of microscopic constructions of 4D BCFTs enjoying a holographic description with an arbitrarily large $\mathrm{AdS}_5 \times S^5$ region terminating on an ETW brane, as well as 3D SCFTs which correspond to an arbitrarily large $\mathrm{AdS}_5 \times S^5$ wedge. While the possibility of realizing similar features by considering limits of the supergravity solutions provided in [174, 175, 297] has been discussed previously (e.g. in [175, 292, 294, 297]), we have provided an important check that the required limits can indeed be realized in string theory, where the various charges are subject to quantization requirements, and we have characterized the appropriate boundary conditions explicitly in terms of the corresponding field theory data.

The simplest such BCFT boundary conditions arise in string theory from

a single stack of N_{D5} D5-branes and N_{NS5} NS5-branes; choosing N_{D5}, N_{NS5} sufficiently large with $gN_{D5}/N_{NS5} = O(1)$ ensures a large $\mathrm{AdS}_5 \times S^5$ region, and a judicious choice of these parameters and the linking numbers L, K can make this region arbitrarily large. While these "single-pole" boundary conditions are especially easy to analyze, we have indicated several generalizations involving multiple five-brane throats in the ETW brane region, including small perturbations to the single-pole boundary conditions, boundary conditions which redistribute the fundamental matter throughout the defining quiver diagram, and boundary conditions involving extended quivers which give rise to "multi-wedge" duals. By invoking similar D-brane constructions to generate supersymmetric boundary conditions for the 4D $\mathcal{N} = 4$ SYM theory or 3D SCFTs describing the IR physics of linear or circular quiver gauge theories, we are able to produce holographic duals for these theories in type IIB supergravity that possess similar local features, including one or more $\mathrm{AdS}_5 \times S^5$ wedges. This suggests a precise sense in which the physics of these degrees of freedom can be associated to the wedge. In all of our examples, such wedges are necessarily accompanied by a large ETW brane region.

There are a number of further directions which remain interesting to explore. While we have studied a large class of solutions with large $\mathrm{AdS}_5 \times S^5$ regions, it would be desirable to provide a general characterization of theories which possess this feature. It is also interesting to understand if there is a relationship between our work and the "dimensional (de)construction" story [293, 298]. In this context, it is shown that certain quiver gauge theories may admit a low-energy effective description with emergent extra dimensions; for example, this may occur in superconformal theories moved onto the Higgs branch, with the spectrum of massive vectors obtained via the Higgs mechanism organizing precisely into the Kaluza-Klein modes of the higher-dimensional theory. Our results also suggest a relationship between 3D and 4D supersymmetric theories, in the sense that the physics of large wedges of $\mathrm{AdS}_5 \times S^5$ can either be described by degrees of freedom in the 4D $\mathcal{N} = 4$ SYM theory or in a suitably chosen 3D SCFT capturing the low-energy behaviour of a quiver gauge theory.

Part IV

Black Holes

Chapter 7

Information Radiation in BCFT Models of Black Holes

7.1 Introduction

Within the context of holographic models of quantum gravity, the formation and evaporation of black holes is a manifestly unitary process in the sense that the underlying quantum system evolves through conventional Schrödinger evolution with a Hermitian Hamiltonian. However, in the gravity picture, the physics of the black hole interior and the mechanism through which information about the microstate of the black hole emerges in the Hawking radiation are still not fully understood.

A crucial piece of physics to understand is the evolution of the density matrix for the black hole radiation. Hawking's original calculation [56] suggests that the entropy of this density matrix continues to increase throughout the black hole's evaporation. But unitary evolution predicts that this entropy should begin decreasing at the "Page time" when the black hole's (macroscopic) entropy has been reduced to half of its original value [57, 58] and the remaining black hole becomes maximally entangled with the radiation system. The specific increasing and then decreasing behavior of the entropy of the radiation system as a function of time is known as the Page curve. Understanding how this curve comes about from the gravity picture is a key challenge.

A further mystery appeared in the work [59–61, 299, 300], in which the authors argued that assuming a unitary picture of black hole evaporation leads to the conclusion that there cannot be a smooth region of spacetime

behind the horizon of an evaporating black hole past the Page time. The argument was based on an apparent inconsistency between having maximal entanglement between the black hole and its early Hawking radiation after the Page time and having entanglement between field theory degrees of freedom on either side of the black hole horizon, as required by smoothness. The proposed alternative is that the old black hole develops a "firewall" at its horizon.

A fascinating suggestion [45] to avoid this firewall conclusion, making use of the general idea that the connectivity of spacetime is related to quantum entanglement between underlying degrees of freedom [44, 301], is that the entanglement between the black hole and its early radiation past the Page time is actually responsible for the existence of a smooth geometry behind the black hole horizon, in the same way that the entanglement between two conformal field theories (CFTs) in the thermofield double state gives rise to a smooth wormhole geometry connecting the two black hole exteriors.[102] In this picture, the behind-the-horizon degrees of freedom are the radiation degrees of freedom, so there is no contradiction that both are entangled with outside-the-horizon modes of the black hole.

Very recently, a series of papers [9, 63, 64] have provided more detailed insight into how the black hole radiation can be seen to have an entropy described by a Page curve yet avoid the firewall paradox by the mechanism of [45] (see also [303]). The examples in these papers make use of an auxiliary radiation system coupled to a system that would otherwise describe an equilibrium black hole.[103] The new insights come by making use of the quantum version [145, 149] of the Ryu-Takayanagi formula [42, 305], which gives the gravity interpretation of entanglement entropies for subsystems of a holographic quantum system.[104] Importantly, the prescription for calcu-

[102] It was suggested in [302] that this analogy could be made precise by coupling a holographic CFT to an auxiliary "radiation" system consisting of another copy of the holographic CFT. In this case, an initial pure-state black hole described by the first CFT would evolve to an entangled state of the two CFTs which could be dual to a two-sided black hole. In this case, the radiation system manifestly describes the region behind the horizon of the original black hole.

[103] See [304] for an early application of this idea.

[104] For a subsystem A of a holographic system, the quantum Ryu-Takayanagi (RT) surface

lating these entropies in the gravity picture requires the identification of a "quantum extremal surface" on which the functional (7.1) is evaluated to calculate the entanglement entropy. A central observation of [9, 63, 64] is that during the evaporation of a black hole, the quantum extremal surface that computes the entanglement entropy of the radiation system can jump, leading to a first-order transition in the entanglement entropy that provides the necessary switch from increasing to decreasing behavior.

Further insights in [9, 63, 64] make use of the notion of the "entanglement wedge" of a subsystem of a holographic system, which is the portion of the full spacetime that is dual to or reconstructible from the density matrix for the subsystem, and is understood to be the bulk region enclosed by the quantum extremal surface [146, 148, 306–310]. In the examples of [9, 63, 64], it is seen that after the transition in the quantum extremal surface, the entanglement wedge of the radiation system actually includes a portion of the black hole interior. Thus, the underlying degrees of freedom for this interior region after the transition are understood to be the degrees of freedom of the radiation system, in accord with the proposal of [45].

Summary and outline

In this chapter, our first motivation is to further elucidate the observations of [9, 63, 64] by studying the evolution of black holes in a new class of models where the evolution of entanglement entropy and the entanglement wedge can be studied very explicitly through direct holographic calculations. Our models are similar to and motivated by the one in [9] in that they have a holographic description in one higher dimension than the original black hole of interest, and the full dynamics of entanglement entropy for the basic degrees of freedom is captured geometrically through the behaviour

$\tilde{A}$ in the dual gravitational picture is a bulk surface which is homologous to A and has the minimum value of the functional

$$S_{\rm grav}(A) = \frac{\text{Area}(\tilde{A})}{4G} + S_{\rm bulk}(\Sigma_A) \tag{7.1}$$

among extrema of this functional. Here $S_{\rm bulk}(\Sigma_A)$ is the entanglement entropy of bulk fields in the bulk region Σ_A enclosed by $\tilde{A}$.

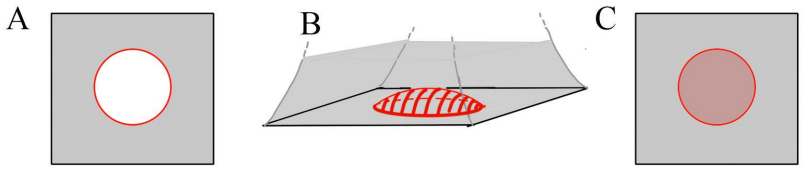

Figure 7.1: Basic set-up. (A) Our thermal system, dual to a bulk black hole, is the red boundary. It interacts with a bulk CFT which can serve as an auxiliary system into which the black hole can radiate. (B) The higher-dimensional bulk picture. The red surface is a dynamical "end-of-the-world" (ETW) brane whose tension is monotonically related to the number of local degrees of freedom in the boundary system. For large tension, this ETW brane moves close to the boundary and behaves like a Randall-Sundrum Planck brane. (C) The Planck brane picture suggests an effective lower-dimensional description where a part of the CFT in the central region is replaced with a cutoff CFT coupled to gravity, similar to the set-up in [9].

of classical Hubeny-Rangamani-Takayanagi (HRT) surfaces. However, our systems are described somewhat more explicitly than the one in [9] and have an additional parameter that controls the Page time for the black hole.

Our specific construction, described in Section 7.2, starts with a d-dimensional holographic system on S^{d-1} in a high-energy state, or a thermofield double state with a second copy of the holographic system. These holographically describe one-sided or two-sided black holes in spacetimes that are asymptotically AdS if the theory that we start with is a CFT. The black holes are in equilibrium with their Hawking radiation, which reflects off the boundary of the spacetime. In order to have the black holes evaporate, we couple our holographic system to an auxiliary system as in [9, 63, 64, 302, 304]. Our auxiliary system is a CFT in one higher dimension living on a space whose boundary is S^{d-1} (or two copies of this), such that our original degrees of freedom provide boundary degrees of freedom for this higher-dimensional CFT. We can take the higher-dimensional CFT to be holographic, such that the full system is a holographic boundary conformal field theory (BCFT) (or flows to one in the IR). We show in Section 7.2 that the Page time for the black hole is proportional to the ratio $c_{\text{bdy}}/c_{\text{bulk}}$ of

the local number of boundary degrees of freedom to the local number of degrees of freedom in the bulk CFT. In the limit where c_{bdy} is large and c_{bulk} is fixed, the Page time that we calculate from CFT considerations matches the Page time obtained in the gravity picture in AdS with absorbing boundary conditions [311].

For our explicit calculations, we consider various states of the BCFT constructed via Euclidean path integrals, so that the dual gravity geometries can be understood explicitly. For these states, we will consider the computation of entanglement entropy for the auxiliary system, considering a spatial region defined by the points at distance greater than a from the boundary system. We calculate the entanglement entropy for this system as a function of time and of the distance a. We perform the calculation holographically by finding the HRT surface in a dual $(d+1)$-dimensional gravitational system. We make use of a bottom-up holographic prescription for studying the dual BCFTs in which the CFT boundary extends into the bulk as a dynamical end-of-the-world brane whose tension is directly related to c_{bdy}. We also reproduce the results of these holographic calculations through direct calculations in our BCFT system, making use of standard assumptions about holographic CFTs.

As hoped, our calculations show a first order phase transition of the entanglement entropy at the Page time after which the entropy of the radiation stops increasing; a sample result for the transition time is shown in Figure (7.2). In the higher-dimensional gravity picture, we find that after the transition, the entanglement wedge of the radiation system includes a portion of the black hole interior.

A new qualitative result of the present chapter is that the phase transition described in the previous paragraph can occur even when the black hole is not evaporating, but simply coupled to an open radiation system which is in thermal equilibrium with the black hole. In this case, we find that while the energy density is static everywhere, the entanglement entropy for subsets of the radiation system still shows interesting dynamics, increasing with time until a phase transition after which it is constant. Again, the entanglement wedge of the radiation system includes a portion of the black

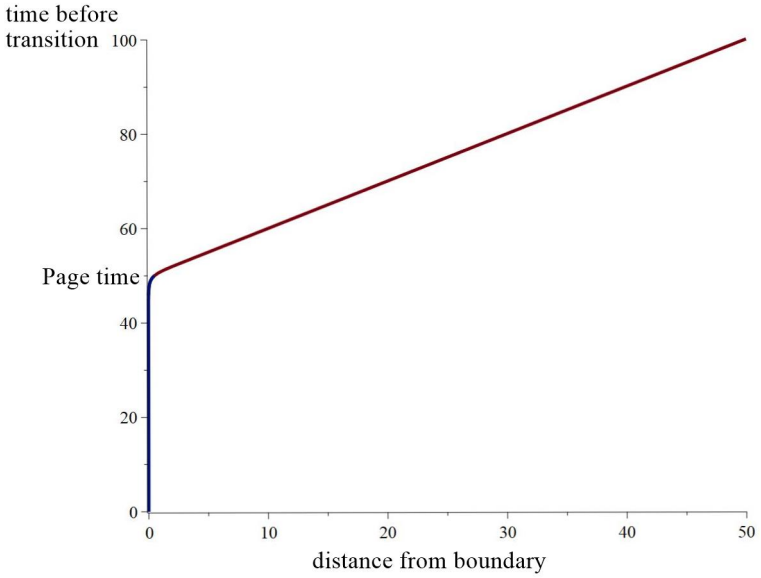

Figure 7.2: Time at which the subsystem of the radiation system greater than some distance from the BCFT boundary exhibits a transition in its entanglement entropy, for the case $c_{\text{bdy}}/c_{\text{bulk}} \sim 50$. After the transition, the entanglement wedge of this subset of the radiation system includes a portion of the black hole interior. After a time equal to the Page time plus the light travel time from the boundary to our subsystem, there is enough information in the subsystem to reconstruct part of the black hole.

hole interior after the transition. This static case is the focus of Section 7.3.

In Section 7.4, we consider more general states for which the initial radiation system is not in equilibrium with the black hole and the energy density is time-dependent. These more closely model evaporating black holes. Our detailed results are again in line with the expectations of [9, 63, 64] and confirm some of the qualitative predictions of [9].

We end in Section 7.5 with a discussion. There, we describe some directions for future work and describe further holographic constructions of evaporating black hole systems. We also point out that the transition in extremal surfaces described in this chapter and in [9, 63, 64] is closely related to a similar transition [2] that can occur when looking at the entanglement entropy for subsystems of a CFT on S^{d-1} in a high-energy state dual to a single-sided black hole. For the CFT states described in [2], we can have a transition as the subsystem size is increased, after which the entanglement wedge of the subsystem includes part of the geometry behind the black hole horizon. Remarkably, in the case of 3D gravity, the CFT calculations that exhibit this transition are precisely the same CFT calculations that show the entanglement wedge transition in the present chapter.

Note added: While this manuscript was in preparation, the paper [312] appeared, which has some overlap with Section 7.3 of this chapter.

7.2 Basic set-up

A schematic of our basic set-up is shown in Figure 7.1(A). We imagine starting with a holographic system on S^{d-1} whose high-energy states or high-temperature thermal states describe black holes in a dual gravitational picture. In these systems, the black hole is in equilibrium with its Hawking radiation, which reflects off the boundary of the spacetime.

Next, following [9, 63, 64, 302] we augment our holographic model with additional degrees of freedom which will serve as an auxiliary radiation system, allowing the black hole to evaporate. As in [9, 64], our auxiliary degrees of freedom will take the form of a higher-dimensional CFT living on a space with boundary S^{d-1}, such that the original system now serves as a set of

boundary degrees of freedom for the higher-dimensional CFT. We will denote by $c_{\rm bulk}$ the number of local bulk CFT degrees of freedom and by $c_{\rm bdy}$ the local number of boundary degrees of freedom. We have in mind that $c_{\rm bdy} \gg c_{\rm bulk} \gg 1$. This will allow the full system to be holographic, but as we show below, will give a parametrically large evaporation time.

Holographic models of this type can arise in string theory by considering branes ending on other branes. For example, we can have a stack of n D3-branes in directions (0123) ending on various D5- and NS5-branes at some locations in the 3 direction [89, 90]. The low-energy physics is $\mathcal{N} = 4$ SYM theory on a half-space with some boundary conditions. We can have an additional N D3-branes of finite extent in the 3 direction which are stretched between some of the five-branes. Without the original n D3-branes, these can give rise to a 3D CFT in the infrared. In the full set-up, this 3D CFT is coupled to the $\mathcal{N} = 4$ theory at its boundary. Here, in this set-up, we have $c_{\rm bdy}/c_{\rm bulk} = N^2/n^2$.

Evaporation time in the CFT picture

Now, suppose we have some initial energy M in the boundary degrees of freedom such that the energy corresponds to a temperature above the Hawking-Page transition for that system. The relation between temperature, energy, and entropy is

$$E \sim c_{\rm bdy} R^{d-1} T^d \,, \qquad\qquad S \sim c_{\rm bdy} R^{d-1} T^{d-1} \,, \tag{7.2}$$

for a boundary system of size R. If this system is coupled to a higher-dimensional CFT with $c_{\rm bulk}$ local degrees of freedom, we expect that the energy will be radiated away at a rate

$$\frac{dE}{dt} \sim -e c_{\rm bulk} R^{d-1} T^{d+1} \,, \tag{7.3}$$

where we are using a Boltzmann law, with emissivity e that presumably depends on the nature of the coupling. The factor of $c_{\rm bulk}$ can be understood from a weak-coupling picture where we have $c_{\rm bulk}$ light fields that can carry

away the energy.

Using these results, we have that

$$\frac{dT}{dt} = -\hat{e}\frac{c_{\rm bulk}}{c_{\rm bdy}}T^2 \ , \tag{7.4}$$

where $\hat{e}$ is defined to absorb any numerical coefficients we are ignoring. Solving, we have

$$T = \frac{1}{\frac{1}{T_0} + \hat{e}\frac{c_{\rm bulk}}{c_{\rm bdy}}t} \ . \tag{7.5}$$

The Page time is when half the (macroscopic) entropy of the black hole has been radiated. This corresponds to a temperature

$$T_{\rm Page} = \frac{1}{2^{\frac{1}{d-1}}}T_0 \ . \tag{7.6}$$

Ignoring $O(1)$ factors, we find that

$$t_{\rm Page} \sim \frac{c_{\rm bdy}}{c_{\rm bulk}}\frac{1}{\hat{e}T_0} \tag{7.7}$$

or

$$t_{\rm Page}/R \sim \frac{c_{\rm bdy}^{1+\frac{1}{d}}}{\hat{e}c_{\rm bulk}}\frac{1}{(MR)^{\frac{1}{d}}} \ . \tag{7.8}$$

Since the initial energy is of order $c_{\rm bdy}$, it is also illustrative to write $MR = xc_{\rm bdy}$, so that

$$t_{\rm Page}/R \sim \frac{c_{\rm bdy}}{\hat{e}c_{\rm bulk}}\frac{1}{x^{\frac{1}{d}}} \ . \tag{7.9}$$

We see that the Page time is proportional to $\frac{c_{\rm bdy}}{c_{\rm bulk}}$; we can make the black hole evaporation take a long time by choosing $c_{\rm bdy} \gg c_{\rm bulk}$.

Evaporation time for a black hole with absorbing boundary conditions

We can compare this to the calculation in [311] of Page (see also [313]), who considers perfectly absorbing boundary conditions for a large black hole in

AdS. Using those results, one finds a Page time

$$t_{\rm Page} \sim \frac{L_{\rm AdS}^{d+1-\frac{2}{d}}}{G^{1+\frac{1}{d}}} \frac{1}{M^{\frac{1}{d}}} \tag{7.10}$$

where we have omitted some numerical factors. An energy of $1/R$ in the field theory corresponds to energy $1/L_{\rm AdS}$ on the gravity side, while field theory entropy $c_{\rm bdy} R^{d-1} T^{d-1}$ corresponds on the gravity side to $r_H^{d-1}/G = T^{d-1} L_{\rm AdS}^{2d-2}/G$, so we can relate

$$c_{\rm bdy} R^{d-1} = \frac{L_{\rm AdS}^{2d-2}}{G} \ . \tag{7.11}$$

Rewriting (7.10) in terms of field theory parameters, we get

$$t_{\rm Page}/R \sim \frac{c_{\rm bdy}^{1+\frac{1}{d}}}{(MR)^{\frac{1}{d}}} \tag{7.12}$$

Comparing with the expression (7.8) above, we see that the expressions have the same dependence on $c_{\rm bdy}$ and M; to match the gravity calculation, we should take $c_{\rm bulk}\hat{e}$ to be of order 1, at least in terms of scaling with $c_{\rm bdy}$. In order that the full system is holographic, we want to take $c_{\rm bdy} \gg c_{\rm bulk} \gg 1$.

7.2.1 Holographic duals of BCFTs

In this section, we briefly review the gravitational dual description of holographic BCFTs and explain how the dual of a BCFT with large $c_{\rm bdy} \gg c_{\rm bulk}$ can give rise to the physics of a Planck brane whose geometry is the geometry of the black hole we are studying.

In their vacuum state, BCFTs preserve the conformal invariance of a CFT in one lower dimension. Thus, the gravity dual of a d-dimensional CFT with boundary in its vacuum state will generally correspond to a spacetime that is a warped product of AdS_d with some internal space, but which has an asyptotically AdS_{d+1} region with boundary geometry equal to the half space. For various supersymmetric examples, gravitational dual solu-

tions corresponding to the vacuum state are known explicitly [264, 265]. For example, there is a family of half-supersymmetric solutions to type IIB supergravity that correspond to the vacua of $\mathcal{N} = 4$ SYM theory living on half-space with the various boundary conditions preserving half of the supersymmetry (e.g. [172–175]).

In general it is difficult to work with the fully microscopic examples and to find full solutions of the ten or eleven-dimensional supergravity equations that would correspond to various BCFT states. Thus, rather than employing this top-down approach, we will consider bottom-up models of BCFT duals, introduced in [78, 87, 88].[105] Here, the bulk dual of a d-dimensional CFT with boundary is taken to be a $(d+1)$-dimensional gravitational theory on a space which has a dynamical boundary extending from the CFT boundary into the bulk. Just as we can consider various possibilities for the bulk gravitational effective action, we can choose various terms for the boundary effective action. We expect that for appropriate choices of the bulk and boundary effective actions, we can accurately capture the physics of various holographic CFTs.[106] In this chapter, we consider the simple situation where the "end-of-the-world" (ETW) brane couples only to the bulk metric field; its action is taken to include a boundary cosmological constant (interpreted as the brane tension) and a Gibbons-Hawking-York term involving the trace of the extrinsic curvature. The details of the action and equation of motion, and all the solutions that we will require in this chapter may be found in [2].

The work of [87] established a connection between the tension of the ETW brane and the boundary entropy (or higher-dimensional generalizations), which can be understood as a measure of the number of degrees of freedom associated with the boundary. One simple calculation that indicates this relation is the holographic calculation of entanglement entropy for a region of the BCFT that is the interior of a half-sphere centred on the

[105] Note that other bottom-up constructions for the bulk dual of a BCFT have been proposed, e.g. [314].

[106] We note that in the top-down models, there is generally not an explicit ETW brane; instead, the spacetime can "end" by a smooth degeneration of the internal space; the ETW brane in the bottom-up model models this higher-dimensional behavior.

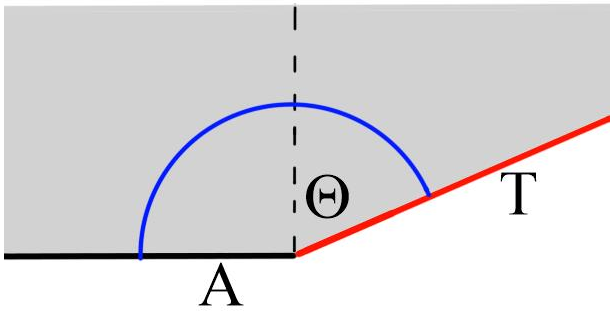

Figure 7.3: An ETW brane with tension parameter T enters the bulk at coordinate angle Θ in Fefferman-Graham coordinates. Larger T gives a larger angle Θ. Shown in blue is the RT surface computing the entanglement entropy of the subsystem A which includes the boundary. The area to the right of the dashed line is proportional to the boundary entropy.

boundary. Holographically, this is computed via the area of an extremal surface anchored to the half-sphere which extends into the bulk and ends on the ETW brane. For larger tension of the ETW brane, this brane enters the bulk at a larger coordinate angle from the vertical in Fefferman-Graham coordinates for the asymptotic region, as shown in Figure 7.3. As a result, the area of the extremal surface becomes larger, indicating a larger boundary entropy.

In our application, we would like to consider the case where the number of local boundary degrees of freedom is large compared with the number of local bulk degrees of freedom. In this case, there is an independent way to motivate the ETW brane picture. Since we are considering the bulk CFT degrees of freedom to be much fewer than the boundary degrees of freedom, we expect that in some sense, they act as a small perturbation. Over short time scales (much shorter than the Page time), the physics of the boundary degrees of freedom is not significantly affected by the bulk CFT degrees of freedom. We can think of the d-dimensional geometry of the ETW brane as the usual holographic dual of the $(d-1)$-dimensional boundary system in its state at a particular time. The $(d+1)$-dimensional system dual to the bulk CFT-degrees of freedom couples to this system, and this corresponds to

adding in the bulk (d+1)-dimensional geometry coupled to the d-dimensional brane. Over long time scales, the bulk CFT degrees of freedom can have a significant impact (e.g. when the black hole evaporates). Thus, over long time scales, the full geometry of the ETW brane can be affected significantly by its coupling to the bulk gravity modes, so it is important to consider the full $(d+1)$-dimensional system when understanding the long-time dynamics of the system.

The Randall-Sundrum Planck brane and the effective gravity picture

As we have reviewed above, a large number of boundary degrees of freedom corresponds to a large tension for the ETW brane and in this case, the ETW brane enters the bulk at a very large angle to the AdS boundary. For the case of a single sphere-topology boundary, the resulting dual gravity solutions have ETW branes that stay close to the boundary in some sense (e.g. they correspond to a cutoff surface in a complete AdS spacetime for which light signals can propagate out to the AdS boundary and back in small proper time). In this and similar cases, the ETW brane behaves as a "Planck brane" in the Randall-Sundrum sense [72], cutting off a portion of the asymptotic region of the geometry so that this part of the spacetime now terminates with a dynamical brane.[107] This point of view suggests a third description of the physics of our situation: from the CFT point of view, the addition of a Planck brane to a region of the bulk corresponds to cutting off the CFT in some spatial region and coupling to gravity in this region. The cutoff goes to infinity at the boundary of the region. This picture corresponds to the "2D gravity with holographic matter" picture of [9]. This latter picture most closely aligns with the model in [64]. The three pictures are summarized in Figure 7.1. Note that it is this last picture (Figure 7.1(C)) where the coupling between the black hole system and the radiation system is strictly at the boundary of the gravitational system.

[107] It is interesting that BCFTs can provide a microscopic realization of Randall-Sundrum models; this idea manifested itself in a different way in the recent work [2, 315].

7.3 Two-dimensional models: static case

In this section, we will consider a very simple system that already exhibits all of the key features of the entanglement dynamics described in [9, 63, 64]. The system we consider is not an evaporating black hole, but one where the auxiliary radiation system has the same initial temperature as the black hole, so that the two systems are in equilibrium. The system we look at has a static energy density (in a particular conformal frame), but the entanglement entropy for various subsystems still evolves with time and the entanglement wedge exhibits a phase transition similar to the ones discussed in [9, 63, 64].

Specifically, we consider a $(1+1)$-dimensional BCFT which is in the thermofield double state with a second copy of this system. This can be constructed via a path integral on a quarter-cylinder $y \leq 0$, $0 \leq \phi \leq \pi$, where ϕ is the Euclidean time direction, and the boundary of each CFT is at $y = 0$. This is shown in Figure 7.4(a).

To understand the gravity dual, we use the bottom-up prescription where the boundary system leads to a bulk ETW brane. For $(1+1)$-dimensional CFTs, it is convenient to define

$$c_{\text{bdy}} = 6 \ln g \,, \tag{7.13}$$

where $\ln g$ is the usual boundary entropy. Then, defining

$$F = \frac{c_{\text{bdy}}}{c_{\text{bulk}}} \,, \tag{7.14}$$

the tension parameter T (defined explicitly in [2]) for the ETW brane is related to F and to the angle Θ in Figure 7.3 by

$$T = \tanh F = \sin \Theta \,. \tag{7.15}$$

The dual Euclidean solution corresponding to our state is a portion of Euclidean AdS, which we may describe using metric (setting $L_{\text{AdS}} = 1$)

$$ds^2 = (\rho^2 + 1) dy^2 + \frac{d\rho^2}{\rho^2 + 1} + \rho^2 d\phi^2 \,. \tag{7.16}$$

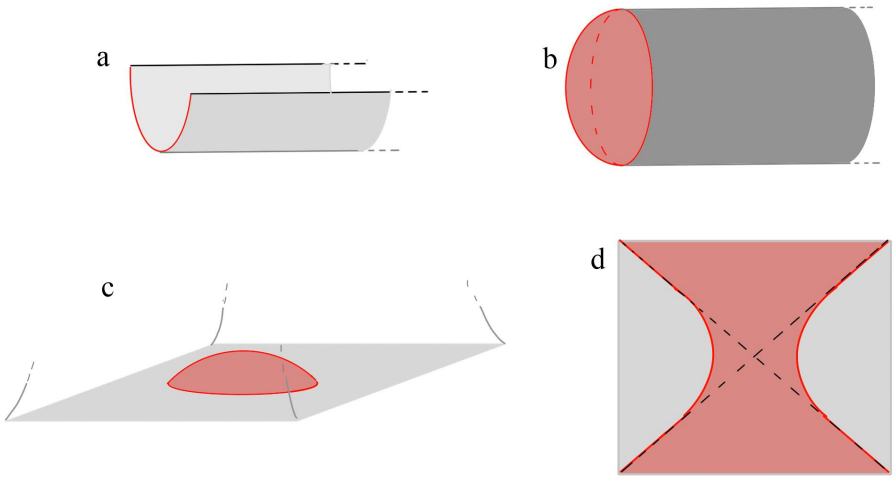

Figure 7.4: (a) BCFT path integral defining the thermofield double state of two $(1+1)$-dimensional BCFTs. (b) Euclidean geometry dual to the BCFT thermofield double. The red surface is an ETW brane. (c) The same geometry represented as part of Euclidean Poincaré AdS. (d) Lorentzian geometry of the original state, viewed along the z-axis. Dashed lines represent horizons on the ETW brane, corresponding to the horizons of the two-sided black hole represented by the boundary system.

The specific solution we need was already constructed in [2, 88]. The bulk Euclidean solution terminates on an end-of-the-world (ETW) brane with locus

$$y(\rho) = -\text{arcsinh}\left(\frac{\tan\Theta}{\sqrt{\rho^2+1}}\right) , \tag{7.17}$$

where Θ is related to the brane tension and the number of boundary degrees of freedom by (7.15). The Euclidean geometry is depicted in Figure 7.4(b). The Lorentzian geometry dual to our state is obtained by taking the geometry of the $\phi = 0, \pi$ slice of the Euclidean solution as our initial data.

To analyze the extremal surfaces in the Lorentzian version of this geometry, it will be convenient to change to Poincaré coordinates, via the transformations

$$y = \ln(r) \qquad \rho = \tan(\theta) \tag{7.18}$$

which bring us to spherical Poincaré coordinates and

$$z = r\cos\theta \qquad x = r\sin\theta\cos\phi \qquad \tau = r\sin\theta\sin\phi\ . \tag{7.19}$$

which bring us to the usual Cartesian Poincaré coordinates in which the metric is

$$ds^2 = \frac{1}{z^2}(dz^2 + dx^2 + d\tau^2)\ . \tag{7.20}$$

In these coordinates, the CFT boundary is at $x^2 + \tau^2 = 1$, while the ETW brane is the surface

$$x^2 + \tau^2 + (z + \tan\Theta)^2 = \sec^2\Theta\ , \tag{7.21}$$

as shown in Figure 7.4(c). We obtain the Lorentzian solution by analytic continuation $\tau \to it$. This gives

$$ds^2 = \frac{1}{z^2}(dz^2 + dx^2 - dt^2)\ , \tag{7.22}$$

with CFT boundary at $x^2 - t^2 = 1$, and ETW brane at

$$x^2 - t^2 + (z + \tan\Theta)^2 = \sec^2\Theta\ . \tag{7.23}$$

This is shown in Figure 7.4(d).

Horizons on the ETW brane

Let's now understand the causal structure of the ETW brane geometry to map out the horizons of the black hole that it contains. Consider the ETW brane in the Lorentzian picture, where it is described as the surface (7.23) in the metric (7.22). We would like to find the future horizon for this surface, i.e. the boundary of the set of points from which it is possible to reach the right ETW brane boundary on a causal curve. The lightlike curves on the ETW brane satisfy

$$x(t)^2 - t^2 + (z(t) + \tan\Theta)^2 = \sec^2\Theta \tag{7.24}$$

and

$$\left(\frac{dx}{dt}\right)^2 + \left(\frac{dz}{dt}\right)^2 = 1 \ . \tag{7.25}$$

We find that they are given by

$$x(t) = vt \pm \frac{\sqrt{1-v^2}}{\cos\Theta} \ , \qquad z(t) = |\sqrt{1-v^2}t \pm v\sec\Theta| - \tan\Theta \tag{7.26}$$

for $|v| < 1$. The right and left boundaries of the ETW brane are described by $x = \pm\sqrt{t^2+1}$. The future horizons are the lightlike curves that asymptote to this for $t \to \infty$. These are the trajectories

$$x = \pm t \qquad z = \frac{1-\sin\Theta}{\cos\Theta} \ . \tag{7.27}$$

Thus, independent of Θ, we have horizons on the ETW brane located at $x = \pm t$ and these lie at constant z. The black hole interior can be identified with the region $|x| < t$, or alternatively $z > \frac{1-\sin\Theta}{\cos\Theta}$.

Extremal surfaces

We would now like to investigate the HRT surfaces which calculate the entanglement entropy associated with the spacetime region spacelike separated

from the interval $[-x_0, x_0]$ at $t = t_0$ (equivalently, the union of intervals $[\pm x_0, \pm\infty)$ at $t = t_0$).

In general, there are two possibilities for this HRT surface. First, we have the connected surfaces described by the semicircle

$$t = t_0 \,, \qquad z^2 + x^2 = x_0^2 \,. \tag{7.28}$$

We can also have disconnected surfaces that end on the ETW brane. We need to compare the areas to find out which one is the minimal area extremal surface that computes the entanglement entropy.

It will be somewhat simpler to perform our calculations in the Euclidean picture and then analytically continue the results to the Lorentzian case. That is, we will look at geodesics in the Euclidean geometry, evaluate their length and the length difference between the two cases, and find the phase boundary for transitions between the two surfaces. The Lorentzian version of all of these things can be obtained by analytic continuation.[108]

To find the areas, we note that the area of a geodesic semicircle of coordinate radius R from the point $z = R$ of maximum z to some $z_{\min}$ is

$$\begin{aligned} A(R, z_{\min}) &= \operatorname{arccoth}\left(\frac{1}{\sqrt{1 - \frac{z_{\min}^2}{R^2}}}\right) \\ &= \frac{1}{2}\ln\left(\frac{1 + \sqrt{1 - z_{\min}^2/R^2}}{1 - \sqrt{1 - z_{\min}^2/R^2}}\right) \,. \end{aligned} \tag{7.29}$$

For $z_{\min} = \epsilon$ with infinitesimal ϵ, this reduces to $\ln(2R/\epsilon)$.

From this, the area of the connected extremal surface is

$$A_c = 2\ln\left(\frac{2x_0}{\epsilon}\right) \,. \tag{7.30}$$

For the disconnected surface, each part is the arc of a circle which lies at constant θ, intersecting the ETW brane orthogonally and intersecting one

[108] We have checked that this matches with direct Lorentzian calculations.

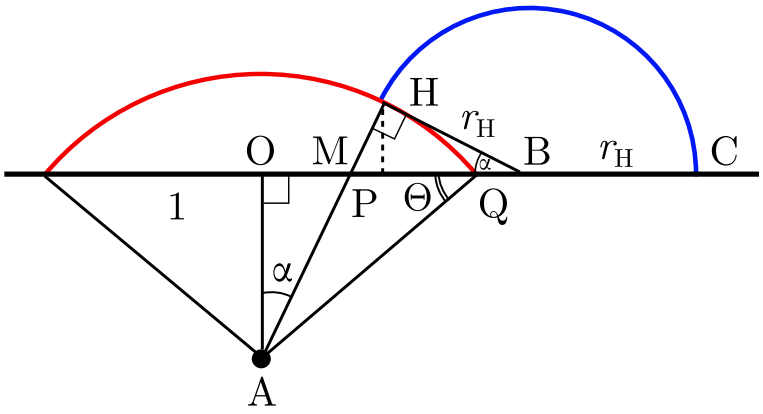

Figure 7.5: Geometry of the ETW brane and half of the disconnected RT surface in the plane of the RT surface. We have $OQ = 1$ and $OA = \tan\Theta$. Thus, $AQ = AH = \sec\Theta$. Also $HB \perp AH$ so $AH^2 + HB^2 = OA^2 + OB^2$. This gives $\boxed{r_H = (r^2-1)/(2r)}$. Now $OM = OA\tan\alpha = \tan\Theta\tan\alpha$ and $AM = OA\sec\alpha = \tan\Theta\sec\alpha$. So $HM = HA - MA = \sec\Theta - \tan\Theta\sec\alpha$. Finally, $HM/HB = \tan\alpha$ gives $\boxed{r_H = \sec\Theta\cot\alpha - \tan\Theta\csc\alpha}$, while $HP = HB\sin\alpha$ gives $\boxed{z = r_H\sin\alpha}$. The boxed equations allow us to express z and r_H in terms of r.

of the the points $(\pm x_0, \tau_0)$.[109] This is shown in Figure 7.5.

Using basic geometry (see Figure 7.5), we find that the extremal surface has coordinate radius

$$r_H = \frac{r^2-1}{2r} \tag{7.31}$$

and intersects the ETW brane at z coordinate

$$z_{\rm br} = \frac{\cos\Theta}{\frac{r^2+1}{r^2-1} + \sin\Theta} \tag{7.32}$$

where $r^2 = x_0^2 + \tau_0^2$.

From (7.29), we find that the area of the disconnected surface (including

[109] In the Lorentzian picture, the disconnected RT surfaces lie at constant x/t and are related by a boost to the circle arc from the point $(x = \sqrt{x_0^2 - t_0^2}, t = 0)$ to the ETW brane.

both parts) is

$$A_d = 2\ln\left(\frac{r^2-1}{\epsilon}\frac{1+\sin\Theta}{\cos\Theta}\right) \tag{7.33}$$

The difference in areas between the two possible extremal surfaces is

$$A_d - A_c = 2\ln\left(\frac{x_0^2+\tau_0^2-1}{2x_0}\frac{1+\sin\Theta}{\cos\Theta}\right) . \tag{7.34}$$

From this, we see that there will be a transition when

$$\tau_0^2 + \left(x_0 - \frac{1-\sin\Theta}{\cos\Theta}\right)^2 = \frac{2}{1+\sin\Theta} . \tag{7.35}$$

In the Lorentzian picture, this gives the trajectory of the phase boundary as

$$\left(x_0 - \frac{1-\sin\Theta}{\cos\Theta}\right)^2 = t^2 + \frac{2}{1+\sin\Theta} . \tag{7.36}$$

We can now map back to the original conformal frame (corresponding to Figure 7.4(a)) where the energy density is time-independent.

Using the coordinate transformations

$$x = e^y \cos\phi \qquad \tau = e^y \sin\phi \tag{7.37}$$

we have that the phase boundary in Euclidean coordinates is

$$e^F \sinh y = \cos\phi . \tag{7.38}$$

Here, ϕ is the Euclidean time, so in Lorentzian coordinates (where η is the time coordinate), this phase boundary becomes

$$e^F \sinh y = \cosh\eta . \tag{7.39}$$

Finally, if we consider an interval $[y_0, \infty)$ (together with the equivalent interval in the other BCFT), we find that the entanglement wedge for this subsystem makes a transition to include geometry behind the black hole

horizon when

$$\eta = \text{arccosh}(e^F \sinh y_0) \sim F + y_0 \tag{7.40}$$

where the last relation holds for large y_0 and F. Thus, for intervals that include most of the radiation system (when y_0 is some small order 1 number), we see a transition at the Page time after which the black hole interior can be reconstructed from the radiation system. For large y_0 the time is increased by an amount which is the time taken for the radiation to reach y_0. The behavior of the transition time is shown in Figure 7.2. In this frame, the entanglement entropy is constant after the transition, since each part of the disconnected extremal surface in this case is just a boosted version of the extremal surface for earlier times. Thus, the entanglement entropy increases from the initial time and then remains constant after the transition. Using the results above, the precise expression for the entropy as a function of time is[110]

$$S = \begin{cases} \frac{c_{\text{bulk}}}{3} \ln\left(\frac{2}{\epsilon}\cosh\eta\right) & \eta < \text{arccosh}(e^F \sinh y_0) \\ 2\ln g + \frac{c_{\text{bulk}}}{3}\ln\left(\frac{2}{\epsilon}\sinh y_0\right) & \eta > \text{arccosh}(e^F \sinh y_0) \end{cases}, \tag{7.41}$$

so we have an approximately linear increase before the transition and a constant entropy afterwards.

Let's understand the physics of this phase transition in the behavior of the entanglement. We have that the energy density in both BCFTs is completely time-independent. However, the entanglement entropy for the union of regions $x > x_0$ in the two CFTs increases with time, then undergoes a first order phase transition after which it is constant. The entanglement wedge initially does not include the black hole system, but after the transition includes a portion of the interior of the black hole.

Thus, while everything is static from an energy point of view, the state is evolving in such a way that information about the black hole interior eventually becomes accessible in the auxiliary radiation system.

To understand this better, it is helpful to recall that for a free field

[110] Here, we use that the cutoff surface $\rho = 1/\epsilon$ maps to the cutoff surface $z = \epsilon r$ in the Poincaré coordinates. We use this cutoff surface in the equations (7.30) and (7.33) to calculate the entanglement entropies in the original y-coordinates.

theory in the thermofield double state, each mode in one copy of the system is purified by the corresponding mode in the other copy of the system. In our present case, we expect similarly that the boundary system is initially purified to a large extent by the other copy of the boundary system, while the bulk system is purified by the other copy of the bulk system.[111] However, as we evolve forward in time, the entanglement structure evolves, and the information initially contained within the boundary system (describing our black hole initial state) leaks out into the bulk degrees of freedom, eventually leading to the transition we observe.

7.3.1 Entanglement wedge after the transition

We would now like to understand where the boundary of the entanglement wedge lies on the ETW brane after the transition.

Consider a point (x_0, τ_0) on the Euclidean transition surface (7.35). Just after the transition to a disconnected minimal area extremal surface, the part of the surface originating at (x_0, τ_0) will end on the ETW brane at a point $(x_{\rm br}, \tau_{\rm br}) = \lambda(x_0, \tau_0)$. From Figure 7.5 we see that the distance $r_{\rm br} = \sqrt{x_{\rm br}^2 + \tau_{\rm br}^2}$ from the origin for this point will satisfy

$$r = r_{\rm br} + r_H + \sqrt{r_H^2 - z_{\rm br}^2}\,. \tag{7.42}$$

This gives

$$r_{\rm br} = \frac{2r}{r^2(1+\sin\Theta) + (1-\sin\Theta)}\,, \tag{7.43}$$

so we have

$$\begin{aligned} \lambda &= \frac{r_{\rm br}}{r} = \frac{2}{(x_0^2+\tau_0^2)(1+\sin\Theta) + (1-\sin\Theta)} \\ &= \frac{1}{x_0\cos\Theta + 1}\,, \end{aligned}$$

[111] Here, we are describing the situation relative to the vacuum case. Of course, there is always an infinite entanglement entropy between the boundary system of one CFT and the bulk of that CFT.

where we have used (7.35) in the last line. Thus, we have

$$x_{\rm br} = \frac{x_0}{x_0 \cos\Theta + 1} \qquad \tau_{\rm br} = \frac{\tau_0}{x_0 \cos\Theta + 1} \ . \tag{7.44}$$

Inverting these relations and plugging the resulting expressions for x_0 and τ_0 in (7.35), we find that the points $(x_{\rm br}, \tau_{\rm br})$ lie on a curve

$$(1 + (1 - \sin\Theta)^2)x_{\rm br}^2 + 2\tan\Theta(1 - \sin\Theta)x_{\rm br} + \tau_{\rm br}^2 = 1 \ . \tag{7.45}$$

For the Lorentzian version of the problem, this becomes

$$(1 + (1 - \sin\Theta)^2)x_{\rm br}^2 + 2\tan\Theta(1 - \sin\Theta)x_{\rm br} = t_{\rm br}^2 + 1 \ . \tag{7.46}$$

Note that $x_0 > \sqrt{t_0^2 + 1} > t_0$, so from (7.44), we see that we will also have $x_{\rm br} > t_{\rm br}$. Thus, while the curve (7.46) crosses the horizon, the part beyond the horizon isn't relevant to us. The extremal surface always ends at a point on the brane that is outside the horizon.

Let's now calculate the proper distance to the horizon from the intersection point $(x_{\rm br}, t_{\rm br}, z_{\rm br})$ on the ETW brane. We can consider a plane containing the origin and the point (x_0, t_0) and extending directly inward in the z direction; in this plane, the geometry is as in Figure 7.5, where the outermost point is at distance $r = \sqrt{x_0^2 - t_0^2}$.

This is the proper distance along the red curve in Figure 7.5 from H to the top of the red arc, which lies at

$$z_{\rm max} = \sec\Theta - \tan\Theta \ . \tag{7.47}$$

The distance is

$$d = \int_{z_{\rm br}}^{z_{\rm max}} \frac{dz}{z}\sqrt{dz^2 + dr^2} \tag{7.48}$$

Using

$$r^2 + (z + \tan\theta)^2 = \sec^2\theta \ , \tag{7.49}$$

we find that the result is

$$d = \frac{1}{\cos\Theta} \ln\left(\frac{r+1}{r-1}\right) . \tag{7.50}$$

In the y_0 coordinates and in terms of F, this is

$$d = \cosh(F) \ln\left(\frac{1+e^{-y_0}}{1-e^{-y_0}}\right) \tag{7.51}$$

We see that for large y_0, the location of the HRT surface intersection with the ETW brane after the transition is very close to the horizon.

Finally, we can look at the trajectory of the intersection point as a function of time after the transition. For the interval with left boundary y_0 in the y-coordinates, the initial intersection point is at

$$x_{\rm br} = \frac{\sec\Theta}{1+\frac{2}{(1+\sin\Theta)(e^{2y_0}-1)}} \tag{7.52}$$

on the curve (7.46) and the later trajectory follows the curve

$$x_{\rm br}^2 - t_{\rm br}^2 = e^{2y_0}(1 - x_{\rm br}\cos\Theta)^2 . \tag{7.53}$$

At late times, independent of y_0, this approaches the point

$$x = t = \sec\Theta = \cosh(F) \tag{7.54}$$

on the horizon.

The outgoing lightlike curve along the ETW brane from this point is $x = t$, while the ingoing lightlike curve along the ETW brane from this point is simply $x = \sec\Theta$ for all t (using the result (7.26)). We note that the corresponding lightlike curve $x = -\sec\Theta$ on the other side of the black hole does not intersect this curve, but the ingoing lightlike curve from any closer point does intersect this curve. Thus, the points $t = \pm x = \sec\Theta$ are a distinguished pair of points on the horizon for which the ingoing lightlike curves barely meet at the future singularity. The late-time intersection between the entanglement wedge for the radiation system and the black hole

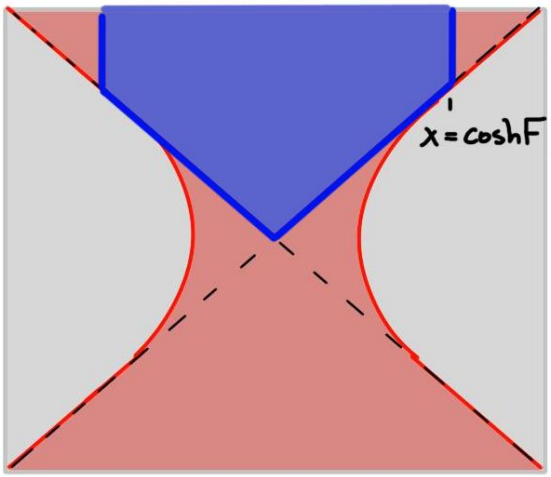

Figure 7.6: The blue shaded region is the portion of the black hole interior that is included in the late-time entanglement wedge of the radiation subsystem $|x| > a$ (in Poincaré coordinates), for any a.

geometry is shown in Figure 7.6.

7.3.2 CFT calculation

The calculations of the previous section relied on holographic calculations of the entanglement entropy in a bottom-up holographic model where the number of boundary degrees of freedom in our BCFT is related to the tension of an ETW brane. While bottom-up models in AdS/CFT are widely studied and known to produce qualitative results that agree with those in systems that can be studied using a top-down approach, one might worry about whether our results correctly capture the physics of genuine holographic CFTs.

In this section, we will attempt to alleviate these concerns by reproducing our results for the entanglement entropies using direct CFT calculations, invoking standard assumptions about the properties of holographic CFTs.

Recall that entanglement entropy can be calculated from Rényi entropies

using the replica trick:

$$S_A = \lim_{n\to 1} S_A^{(n)} = \lim_{n\to 1} \frac{1}{1-n} \log \mathrm{Tr}[\rho_A^n].$$

The operator ρ_A^n can be related to the partition function of the n-fold branched cover, or *replica manifold*, of the original geometry. This, in turn, can be calculated for 2D CFTs by introducing certain *twist operators* Φ_n at the entangling points of A [239]. The partition function is given by a correlator of these twists. For $A = [z_1, z_2]$ for instance, we have

$$\mathrm{Tr}[\rho_A^n] = \langle \Phi_n(z_1)\Phi_{-n}(z_2)\rangle \,.$$

In holographic theories, these correlation functions are dominated by the identity block in some channel. A change in dominance will lead to a phase transition in entanglement entropy. In an ordinary two-dimensional holographic CFT, this exchange causes a sudden shift from the disconnected to the connected entanglement wedge for two disjoint intervals. In a holographic BCFT, this exchange can occur for a *two-point* correlator of twists, corresponding to the entanglement entropy of a single interval. This is analogous to the four-point result in a CFT since the two-point function in a BCFT has the same symmetries as the four-point function, and can be evaluated using the method of images.

Consider a BCFT with central charge c and boundary condition b on the upper half-plane (UHP), $\{\Im(z) \geq 0\}$. We can perform a global transformation to the complement of the disk of radius R via

$$w = R\left(\frac{1}{z - i/2} - i\right) \,. \tag{7.55}$$

For simplicity, we also define $\vartheta \equiv w + iR$. We then have

$$z = \frac{R}{\vartheta} + \frac{i}{2} \,, \quad \Im[z(w)] = \frac{|w|^2 - R^2}{2|\vartheta|^2} \,, \quad w'(z) = -\frac{1}{R}\vartheta^2 \,. \tag{7.56}$$

Since we have performed a global transformation, the energy density van-

ishes:

$$\langle T(w)\rangle = \frac{c}{12}\{z;w\} = \frac{c}{12}\frac{z'''z' - (3/2)(z'')^2}{(z')^2} = 0\,. \tag{7.57}$$

Consider a two-point function of twist operators, $\Phi_n(w_1), \Phi_{-n}(w_2)$, introducing an n-fold branched cover with branch cut from w_1 to w_2. The twists are primary by definition, so the correlation function transforms as

$$\begin{aligned}\langle \Phi_n(w_1)\Phi_{-n}(w_2)\rangle_{\overline{\text{disk}}} &= |w'(z_1)w'(z_1)|^{-d_n}\langle \Phi_n(z_1)\Phi_{-n}(z_2)\rangle_{\text{UHP}} \\ &= \left|\frac{(\vartheta_1\vartheta_2)^2}{R^2}\right|^{-d_n}\langle \Phi_n(z(w_1))\Phi_{-n}(z(w_2))\rangle_{\text{UHP}}\,.\end{aligned} \tag{7.58}$$

For holographic BCFTs, the correlator of twists on the UHP can be evaluated [316], using vacuum block dominance and an appropriate sparsity condition on the density of states, in a similar vein to [219]. Using this correlator and the replica trick, the entanglement entropy of the interval $A = (-\infty, w_1]\cup[w_2,\infty)$ is calculated by

$$\begin{aligned}S_A &= \lim_{n\to 1}\frac{1}{1-n}\log\langle \Phi_n(w_1)\Phi_{-n}(w_2)\rangle_{\overline{\text{disk}}} \\ &= \frac{c}{6}\Bigg[2\log\left|\frac{\vartheta_1\vartheta_2}{R}\right| + \min\Bigg\{\frac{12}{c}g^b \\ &\qquad + \log\left|\frac{(|w_1|^2-R^2)(|w_2|^2-R^2)}{(\vartheta_1\vartheta_2\epsilon)^2}\right|, \log\left|\frac{Rw_{12}}{\vartheta_1\vartheta_2\epsilon}\right|^2\Bigg\}\Bigg]\,,\end{aligned}$$

where $g^b := -\log\langle 0|b\rangle$ is the boundary entropy, and F is given by (7.14). We note the relations

$$e^F = \frac{1+T}{\sqrt{1-T^2}} = \frac{1+\sin\Theta}{\cos\Theta}\,, \quad 1 - e^{-2F} = \frac{2\sin\Theta}{1+\sin\Theta}\,, \tag{7.59}$$

which we will use momentarily. Note that the UV regulator ϵ is chosen in the physical conformal frame, namely the complement of the disk.

We now specialize to the symmetric interval A at some fixed time $\Im(w) = \tau_0$, with $w_{1,2} = \pm x_0 + i\tau_0$. Exponentiating (7.59), a phase transition occurs

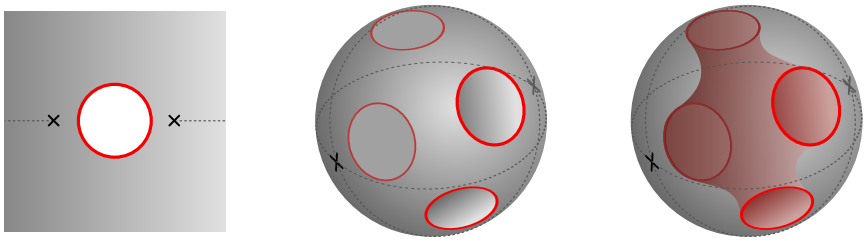

Figure 7.7: Replica calculation of entanglement entropy.

at

$$\left(x_0^2 - e^{-F}R\right)^2 + \tau_0^2 = R^2(1 - e^{-2F}) \tag{7.60}$$

$$\Longrightarrow \quad \left(x_0^2 - \frac{\cos\Theta}{1+\sin\Theta}R\right)^2 + \tau_0^2 = \frac{2R\sin\Theta}{1+\sin\Theta}\,, \tag{7.61}$$

using (7.59). In Lorentzian signature $\tau_0^2 \to -t_0^2$, we obtain

$$\left(x_0^2 - \frac{\cos\Theta}{1+\sin\Theta}R\right)^2 = t_0^2 + \frac{2R\sin\Theta}{1+\sin\Theta}\,. \tag{7.62}$$

These phase boundaries precisely match (7.35) and (7.36) for $R = 1$.

7.3.3 Holographic replica calculation

It is interesting to consider a replica version of the same calculation.[112] In calculating the entanglement entropy, we want to evaluate the Rényi entropies by calculating the BCFT partition function on a replica manifold obtained by gluing n copies of the Euclidean space shown in Figure 7.7 across the cut. The topology of the replica manifold is a sphere with n boundaries, as shown in the second figure. Considering a larger and smaller portion of the radiation system corresponds to enlarging or shrinking the size of the boundaries relative to the size of the sphere.

[112] The observations of this section relating the entanglement wedge phase transition and the appearance of connected boundary saddles were directly inspired by similar observations in the JT-gravity context [66]; related observations were made independently by [65].

Now we can consider performing this path-integral calculation holographically, using the bottom-up approach where the boundaries extend into the bulk as ETW branes. In the case of a smaller portion of the radiation system, the holes in the second picture will be small, and we will have a set of disconnected ETW branes of disk topology that "cap off" the boundary holes. On the other hand, as we consider a larger portion of the radiation system, the circles become large in the second picture, and we expect that the dominant saddle in the gravitational calculation will correspond to the topology shown in the picture on the right where we have a single connected ETW brane with multiple boundary components.

It seems immediately plausible that the transition to this new bulk topology is directly related to the transition of HRT surfaces in our original calculation, since the two calculations must agree. However, it also appears at first slightly confusing: the CFT calculation correctly reproduces the disconnected bulk HRT surface from the disconnected contribution to the twist correlation function alone, while this bulk saddle is a complicated connected geometry involving both twist operators. To align the CFT and bulk pictures, note that the same issue appears when calculating the entanglement entropy of two (or multiple) intervals in the vacuum of a 2D CFT [219]. There, the higher Rényi entropies are also computed by a connected bulk geometry [317], but the entanglement entropy is a sum of disconnected contributions. This is consistent because the semi-classical Virasoro block describing the connected geometry reduces to the identity exchange in the limit $n \to 1$. Despite the slightly different setting, the same ideas and kinematics describe the BCFT Rényi calculation [316].

Thus, taking into account the second HRT surface that correctly sees the decreasing branch of entanglement entropy corresponds in the gravity version of the replica calculation to including non-trivial topologies. Had we stuck with the original topology (as we would do if treating gravity perturbatively) it seems that we would get an answer which misses the transition, and is perhaps more akin to Hawking's original calculation.

7.4 2D evaporating and single sided examples

In this section, we continue focusing on two-dimensional models, but generalize the simple example of the previous section to a case where we have a pure state of a single-sided black hole, and to cases with a dynamical energy density (as in the example of [9]) that more closely models the physics of a genuine evaporating black hole.[113]

7.4.1 Single-sided case

It is straightforward to come up with BCFT examples of single-sided black holes. For example, Figure 7.8(a) shows a path integral defining the state of a BCFT with some boundary system (fat red line) with many degrees of freedom. Here, instead of evolving the full BCFT from $\tau = -\infty$ to define the vacuum state of this system, we only evolve the boundary system from some finite past Euclidean time, as for the SYK states in [208]. For prior Euclidean times, we have a different boundary condition (thin red line) that we take to be associated with a small number of boundary degrees of freedom. At the transition between these two boundaries we have an appropriate boundary condition changing operator.

This construction should place the boundary system in a high-energy state, while the bulk CFT degrees of freedom should be in a lower-energy state (through they are also affected by the change of boundary conditions in the Euclidean past). In this case, the dual gravity solution will involve ETW branes with different tensions, and some junction between branes dual to the boundary-condition changing operator. This may simply be a codimension-two surface, or something smoother, as depicted in Figure 7.8(b).

It would be interesting to analyze this example in detail. For now, we point out that we can understand the physics of a very similar example using the results of the previous section. Figure 7.8(c) shows almost the same

[113] Of course, there are many examples that we can obtain from the previous case via local conformal transformations which would have non-trivial evolution of the energy density and may look more like an evaporating black hole. However, in this section, we focus on examples that are not conformally related to the one in the previous section.

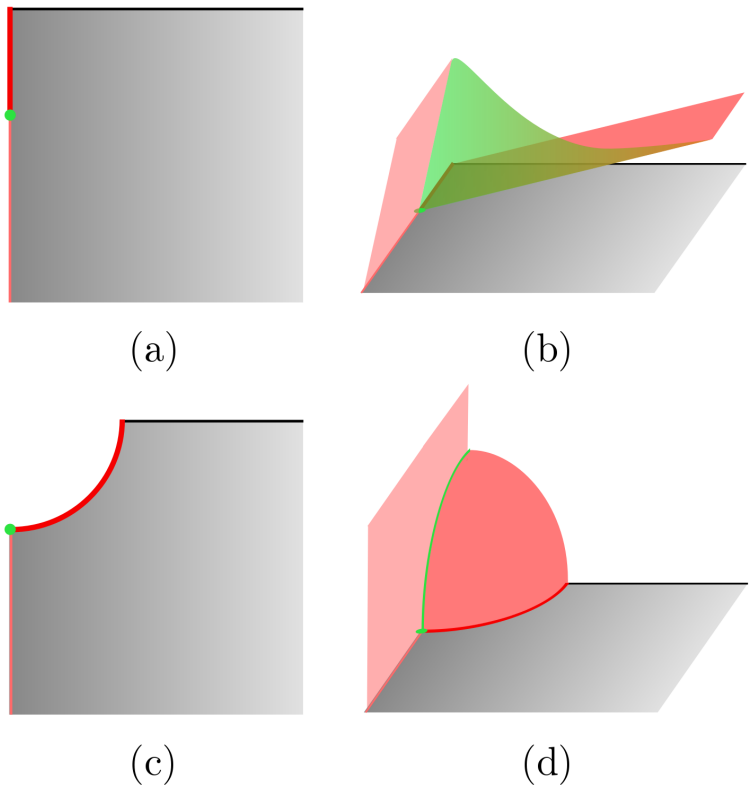

Figure 7.8: BCFT models for single-sided black holes.

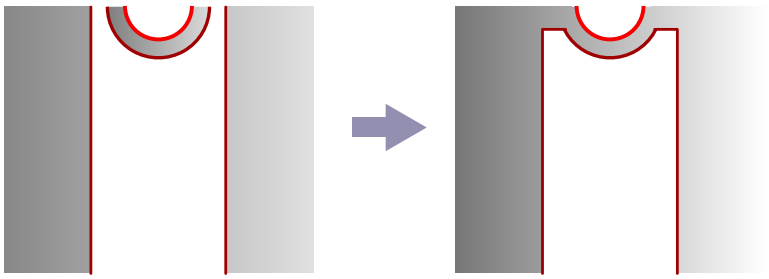

Figure 7.9: 2D model for an evaporating black hole.

set-up, but with a different geometry for the path-integral. This picture is similar to a $\mathbb{Z}_2$ identification of our set-up from the previous section. If we choose the lower boundary condition to correspond to a $T = 0$ ETW brane in the bulk and we choose the boundary-condition changing operator appropriately (so that the equation of motion at the codimension-two brane gives a constraint that the two-types of ETW branes should meet orthogonally), then the dual geometry for this set-up will be precisely a $\mathbb{Z}_2$ identification of the bulk geometries from the previous section, with a zero-tension ETW brane at the $\mathbb{Z}_2$ fixed point, as shown in Figure 7.8(d). In this case, all of our calculations and qualitative conclusions go through almost unchanged. The only significant difference is that the connected RT surface from the previous section is now replaced by its Z_2 identification, which ends on the $T = 0$ brane.

7.4.2 Dynamical case

We can also modify our two-sided example in order to introduce time evolution of the energy density more characteristic of an evaporating black hole. We would like to have a situation where our auxiliary system starts out in a state that is closer to the vacuum state, so that the energy in the initial black hole state will radiate into this system.

A simple construction (similar to that discussed in [9]) is shown in Figure 7.9. The left picture shows a state of four quantum systems. The outer systems are BCFTs with some boundary condition (denoted by a dark red

boundary) that we imagine has a small boundary entropy. The path integrals shown place these systems into their vacuum state. The remaining part of the path integral constructs a thermofield double state of two systems, each of which is a BCFT living on a small interval with different boundary conditions on the two ends. The dark red boundary condition is the same as before, but the semicircular boundary (shown bright red) corresponds to a boundary system with many degrees of freedom as in the example of the previous section.

In order to make the two-sided black hole evaporate, we consider a modified system where we glue the systems together as shown on the right side of Figure (7.9). In the final path integral, shown on the right, we are describing a state of the same system that we considered in the earlier part of this section. However, since our Euclidean path integral is in some sense a small modification of the picture on the left, we expect that far away from the black hole, the local physics of the reservoir system will be similar to the vacuum. In this case, the energy in the (bright red) boundary degrees of freedom will gradually leak out into the reservoir system. The dual gravitational picture will be that of an evaporating black hole.

In studying the dual system explicitly using the bottom-up approach, we will now have two types of branes, one with a larger tension corresponding to the bright red boundary condition, and one with a smaller tension corresponding to the dark red boundary condition. The latter is what [9] refer to as the Cardy brane. We expect that the behaviour of this system should match the qualitative picture described in [9], but now it should be possible to study everything quantitatively. Since the branes only couple to the metric and we are in three dimensions, the local geometry of the holographic dual will be that of AdS, and the dynamics of the system will be reflected in the trajectories of the ETW branes.

Phase boundaries on the annulus

In order to study situations like the previous section, we can apply the methods of [318, 319] who were making use of a similar Euclidean set-up

(without the middle boundary) to study local quenches in a holographic CFT. For any specific shape of the boundaries in (7.9), it is possible to map the doubled picture describing the full CFT path integral conformally to an annulus, where the circular boundary maps to the inner edge of the annulus and the other boundaries (shown in dark red) together map to the outer boundary of the annulus. We can also map the annulus to a finite cylinder, so we see that the physics will be related to the physics of the thermofield double state of a pair of CFTs on a finite interval with different boundary conditions on the two ends.

We can again start with the global AdS metric (7.16) in which we know the ETW trajectories explicitly. Here, though, we consider a finite segment of the boundary cylinder, with a boundary condition corresponding to tension T at $y = -L$ and a boundary condition corresponding to tension $T = 0$ (or some other tension) at $y = 0$. Changing to Poincaré coordinates as in Section 7.3, the CFT region becomes an annulus with inner radius $R = e^{-L}$ and outer radius 1, centred at the origin. Also as in that section, the location of the ETW brane corresponding to the inner boundary is

$$x^2 + \tau^2 + (z + R\tan\Theta)^2 = R^2 \sec^2\Theta\,, \qquad \Theta = \arcsin(T)\,, \tag{7.63}$$

while that corresponding to the outer boundary is

$$x^2 + \tau^2 + z^2 = 1\,. \tag{7.64}$$

For sufficiently large L, the two BCFT boundaries are far apart and the phase boundaries for the transition between connected and disconnected HRT surfaces are those found previously for the case of a single boundary; the phase boundary for the transition between a connected surface and a disconnected surface ending on the inner ETW brane has locus

$$\Big(x - \frac{R(1-\sin\Theta)}{\cos\Theta}\Big)^2 + \tau^2 = \frac{2R^2}{1+\sin\Theta}\,, \tag{7.65}$$

while that for the outer ETW brane is

$$(x+1)^2+\tau^2=2\,. \tag{7.66}$$

(These are the phase boundaries in the region $x>0$; the $x<0$ phase boundaries are given by symmetry about $\tau=0$.) As L is decreased to some critical value

$$L_{\rm c}\equiv-\ln\Big(\frac{(-1+\sqrt{2})\cos\Theta}{(1-\sin\Theta)+\sqrt{2(1-\sin\Theta)}}\Big)\,, \tag{7.67}$$

the phase boundaries will osculate within the annulus at $\tau=0$; for smaller L, a direct transition between disconnected HRT surfaces ending on the higher tension brane and surfaces ending on the lower tension brane can occur (see Figure 7.10). The phase boundary between these disconnected phases is given by

$$x^2+\tau^2=R\Big(\frac{(1-\sin\Theta)+R\cos\Theta}{R(1-\sin\Theta)+\cos\Theta}\Big)\equiv\ell^2\,. \tag{7.68}$$

We can now map to a new conformal frame with the desired dynamical Cardy brane; the phase boundaries should simply be pushed forward using the appropriate conformal transformation, then analytically continued to Lorentzian signature. Note [318] that, starting from Poincaré coordinates

$$ds^2=\frac{d\eta^2+d\zeta d\bar{\zeta}}{\eta^2}\,, \tag{7.69}$$

a map $\zeta=f(w)$ corresponds to a coordinate transformation

$$\begin{aligned}\zeta &= f(w)-\frac{2z^2(f')^2(\bar{f}'')}{4|f'|^2+z^2|f''|^2}\\ \eta &= \frac{4z|f'|^3}{4|f'|^2+z^2|f''|^2}\end{aligned}$$

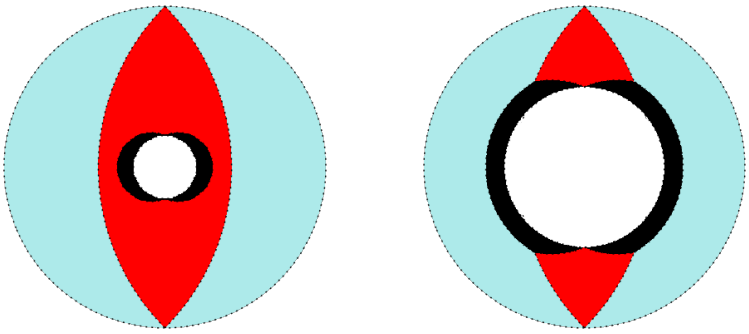

Figure 7.10: Phase diagram for annulus with supercritical and subcritical L respectively. The point (x, y) belongs to one of three regions, depending on whether the RT surface anchored at points $\{(x, y), (-x, y)\}$ is connected (red), disconnected and ending on the inner ETW brane (black), or disconnected and ending on the outer ETW brane (light blue).

in the dual asymptotically AdS geometry, which gives a metric

$$ds^2 = \frac{1}{z^2}\big(dz^2 + dwd\bar{w} + z^2(T(w)dw^2 + \bar{T}(\bar{w})d\bar{w}^2) + z^4 T(w)\bar{T}(\bar{w})dwd\bar{w}\big)\,, \quad (7.70)$$

where the holographic stress tensors (corresponding to the stress tensors in the CFT state) are given by

$$T(w) = \frac{3(f'')^2 - 2f'f'''}{4(f')^2}\,, \qquad \bar{T}(\bar{w}) = \frac{3(\bar{f}'')^2 - 2\bar{f}'\bar{f}'''}{4(\bar{f}')^2}\,. \quad (7.71)$$

Conformal mapping

As a specific example, we can take the "single joining quench" geometry of [318] and add to it another boundary centered at the origin; this second boundary is taken to be the image of the inner boundary of the annulus

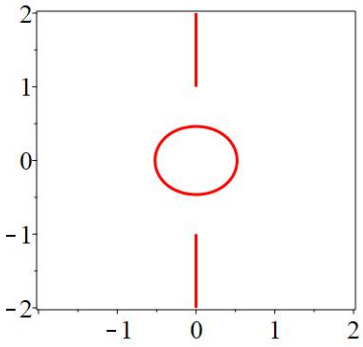

Figure 7.11: Example path integral geometry generating a BCFT state corresponding to a two-sided black hole system with dynamical energy density.

under the conformal transformation

$$w(\zeta) = \frac{2\zeta}{1-\zeta^2}\,, \tag{7.72}$$

which takes us from the unit disk (with complex coordinate $\zeta = x + i\tau$) to the single joining quench geometry (with coordinate $w = \hat{x} + i\hat{\tau}$). An example of the resulting path integral geometry is shown in Figure 7.11.

We note a few important features of such a map. Firstly, the symmetry $x \to -x$ translates to a symmetry $\hat{x} \to -\hat{x}$, and likewise symmetry $\tau \to -\tau$ translates to symmetry $\hat{\tau} \to -\hat{\tau}$. Secondly, the outer annular boundary $|\zeta| = 1$ maps to the intersection of the slits $i[1,\infty)$ and $-i[1,\infty)$, while the inner boundary maps to

$$\hat{x}^2 + \hat{\tau}^2 = \frac{1}{2\cosh^2(L)}\Big(1 + \sqrt{1 + \frac{4\hat{x}^2}{\tanh^2(L)}}\Big)\,. \tag{7.73}$$

Finally, we note that the energy density with respect to Euclidean time $\hat{\tau}$ is

defined by

$$\begin{aligned} T(w) + \bar{T}(\bar{w}) &= \frac{3}{4(1+w^2)^2} + \frac{3}{4(1+\bar{w}^2)^2} \\ &= \frac{3}{2}\Big(\frac{\hat{\tau}^4 - 2(3\hat{x}^2+1)\hat{\tau}^2 + (\hat{x}^2+1)^2}{((1+\hat{x}^2-\hat{\tau}^2)^2 + 4\hat{x}^2\hat{\tau}^2)^2}\Big)\,; \end{aligned} \tag{7.74}$$

the Lorentzian analogue decays as we move away from the boundary which represents the black hole.

In the new coordinates, the phase boundary between connected HRT surfaces and disconnected surfaces ending on the outer ETW brane is $\hat{x}^2+\hat{\tau}^2 = 1$, while the phase boundary between connected surfaces and disconnected surfaces ending on the inner ETW brane is

$$\Big(\alpha(\hat{x}^2+\hat{\tau}^2) - \beta\hat{x} - \sin\Theta\Big)^2 = (\hat{x}^2+\hat{\tau}^2+1)^2 - 4\hat{\tau}^2\,, \tag{7.75}$$

with

$$\begin{aligned} \alpha &= \frac{(1+R^2)^2(1+\sin\Theta) - 4R^2}{4R^2} = \cosh^2(L)(1+\sin\Theta) - 1\,, \\ \beta &= \frac{(1+R^2)}{R}\cos\Theta = 2\cosh(L)\cos\Theta\,. \end{aligned} \tag{7.76}$$

If a transition between the two disconnected phases is present, the phase boundary has locus

$$\hat{x}^2+\hat{\tau}^2 = \frac{2\ell^2}{(1+\ell^2)^2}\Big(1+\sqrt{1+\frac{4\hat{x}^2(1+\ell^2)^2}{(1-\ell^2)^2}}\Big) \tag{7.77}$$

See Figure 7.12. We can analytically continue $\hat{t} = -i\hat{\tau}$ to determine the BCFT boundaries and phase boundaries in Lorentzian signature. For $L > L_{\rm c}$, the phase boundaries now meet at the point

$$\hat{x}_0 = \frac{\alpha - \sin\Theta}{2+\beta}\,, \qquad \hat{t}_0 = \sqrt{\hat{x}_0^2 - 1}\,. \tag{7.78}$$

For $|\hat{t}| < \hat{t}_0$ we have three distinct phases, while for $|\hat{t}| > \hat{t}_0$ we just have the two disconnected phases. For $L < L_{\rm c}$, we just have the two disconnected

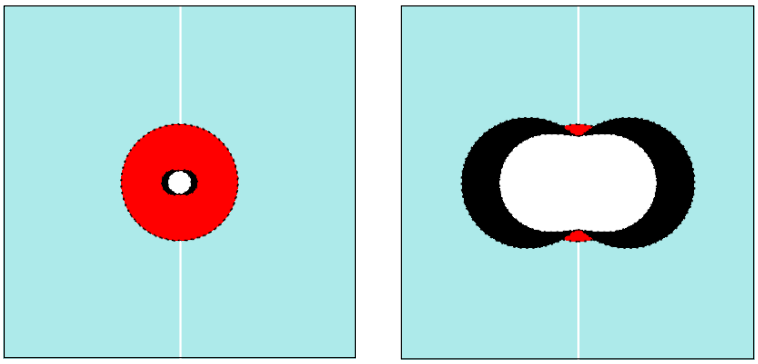

Figure 7.12: Phase diagram for Euclidean modified (two-boundary) single joining quench geometry with supercritical and subcritical L respectively. As before, the point (x, y) belongs to one of three regions, depending on whether the RT surface anchored at points $\{(x, y), (-x, y)\}$ is connected (red), disconnected and ending on the inner ETW brane (black), or disconnected and ending on the outer ETW brane (light blue).

phases (see Figure 7.13).

One can now determine the time-dependence of the entanglement entropy along any desired trajectory. Recall from previous sections that, on the annulus, the HRT surfaces for symmetrically situated intervals (with inner endpoints $(\pm x, \tau)$) are circular arcs, and the corresponding entanglement entropy is given by

$$S(x,\tau) = \begin{cases} \ln\left(\frac{2x}{\tilde{\epsilon}(x,\tau)}\right), & \text{connected} \\ \ln\left(\frac{(x^2+\tau^2-R^2)(1+\sin\Theta)}{\tilde{\epsilon}(x,\tau)R\cos\Theta}\right), & \text{disconnected } T>0 \\ \ln\left(\frac{1-x^2-\tau^2}{\tilde{\epsilon}(x,\tau)}\right), & \text{disconnected } T=0\,, \end{cases} \tag{7.79}$$

where we have recalled [319] that the UV regulator ϵ in the physical set-up requires a position dependent regulator $\tilde{\epsilon}(x, \tau) = |\zeta'(w)|\epsilon$ in the annular set-up. It is a simple matter to apply the appropriate conformal transformation and Wick rotate to Lorentzian signature, whence we recover the expression for the entanglement entropy of symmetrically situated intervals in the Lorentzian modified local quench geometry.

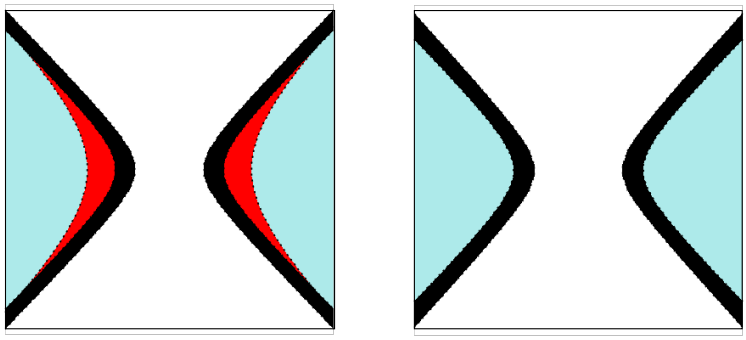

Figure 7.13: Phase diagram for Lorentzian modified (two boundary) single joining quench geometry with supercritical and subcritical L respectively. We have simply analytically continued the phase boundaries from the Euclidean case.

7.5 Discussion

In this section we present a few additional observations and some directions for future work.

7.5.1 A connection to behind-the-horizon physics of black hole microstates

There is an interesting connection between the transitions in entanglement entropy that we have observed in this chapter and another type of transition for entanglement entropy pointed out in [2]. In that paper, the authors (including some of the present authors) considered black hole microstates for a holographic CFT on S^d defined via a Euclidean path integral on a finite cylinder, with a boundary at time τ_0 in the Euclidean past. This corresponds to the evolution of a boundary state $|B\rangle$ by Euclidean time τ_0. In the 2D CFT case for small enough τ_0, this state corresponds to a single-sided black hole at inverse temperature $\beta = \tau_0/4$, with a time-dependent ETW brane behind the horizon providing an inner boundary for the black hole.

For these states, the entanglement entropy for an interval can exhibit a phase transition as the interval size is increased, such that after the tran-

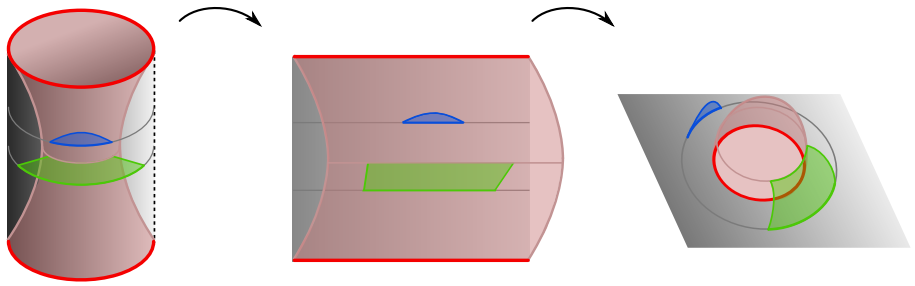

Figure 7.14: BTZ black hole microstates have the same brane profile and hence entanglement entropy as the planar black hole dual to a global quench. The quench geometry is obtained from a local conformal transformation of the excised disk, so the transition in entanglement entropy for the static case described above, and the BTZ microstates in [2], are controlled by the same CFT correlator.

sition, the entanglement wedge of the interval includes a region behind the black hole horizon (terminating on the ETW brane). This is somewhat reminiscent of the entanglement wedge transition discussed in this chapter, but it turns out that there is a precise connection between the two.

If we unwrap the circle on which the CFT lives, we obtain a planar black hole dual (above the Hawking-Page transition [236]) to the global quench geometry [237]. The holographic results for entanglement entropy in this situation are the same as in the compact case, since the gravity dual for the compact case is just a periodic identification of the gravity dual for the non-compact case.

The CFT calculation of entanglement entropy in the non-compact case is carried out via a correlation function of twist operators on an infinite strip. But a local conformal transformation maps this calculation to exactly the CFT calculation in Section 7.3.2 used to deduce the phase transition in this chapter.

We visualize this connection in Figure 7.14. In the single-sided microstates, there is a transition in the extremal surfaces as the boundary region is increased (blue and green regions in Figure 7.14). In the CFT, this can be calculated by a correlator of twists in the large-c limit and simple spectral constraints [316]. Remarkably, this is essentially the same correlator

governing the transition in entanglement wedge, as a function of subsystem size, as the static 2D case described in Section 7.3.

7.5.2 CFT constructions for duals of higher-dimensional evaporating black holes

In future work, it would be interesting to study explicitly some higher-dimensional analogues of the constructions considered in this chapter. We describe a few specific constructions in this final section. For these higher-dimensional examples, a detailed study will likely require some numerics as the bulk geometry will no longer be locally AdS. However, as the geometries depend on only two variables, such a study should be quite feasible.

BCFT microstate construction

Figure 7.15 shows on the left a Euclidean path integral for a high-energy CFT state obtained by placing some boundary conditions in the Euclidean past (at the red sphere). This corresponds to a black hole with some time-dependent behind-the-horizon physics, as described in [2]. We have in mind that the red boundary corresponds to a boundary condition with a large boundary entropy, so that the holographic description involves a brane with large tension.

Now we couple this system to a bulk CFT as shown on the right. Here, we need to introduce an additional boundary component (shown in green) into the Euclidean path integral. Two possible choices for the topology of this boundary component are shown. We have in mind that this boundary has a small boundary entropy, perhaps corresponding to a $T = 0$ brane. This set-up is the precise higher-dimensional analog of the single-sided set-up of Section 7.4.1.

In the dual holographic theory, using the bottom-up approach, we will have a bulk $(d+1)$-dimensional gravity action, but also two different types of d-dimensional ETW branes corresponding to the two different boundary conditions. Finally, there will be another $(d-1)$-dimensional brane that serves as the interface between the two types of d-dimensional branes. This

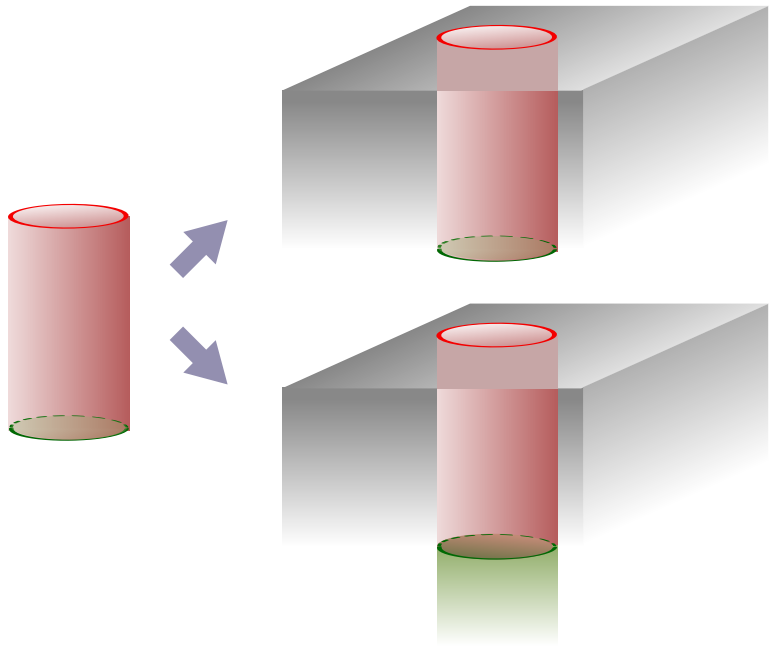

Figure 7.15: Higher dimensional construction based on BCFT microstates.

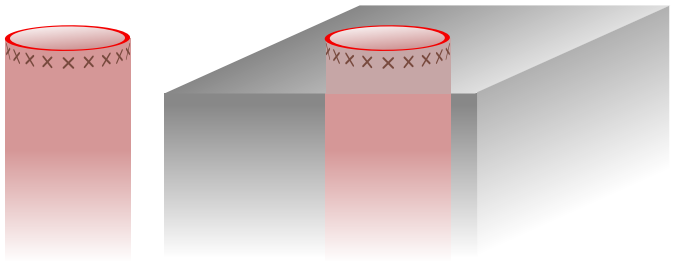

Figure 7.16: Higher-dimensional construction based on CFT-Vaidya states.

can have its own tension parameter independent of the others.

Vaidya-type construction

Another interesting case makes use of the set-up of [270]. Figure 7.16 shows on the left a Euclidean path integral for a CFT state dual to a shell of matter that collapses to form a black hole. We have insertions of many operators at some small time in the Euclidean past. Alternatively, we could consider a smooth source for some operator, again localized around some particular time $\tau = -\epsilon$. We can take a limit where $\tau \to 0$ but the sources/insertions are chosen such that we end up with a finite energy state.

Now we couple this system to a bulk CFT as shown on the right. Without the sources, this path-integral would give the vacuum state of the BCFT. We expect that the sources mainly excite boundary degrees of freedom, so the bulk part of the CFT is still nearly in the vacuum state. In this case, we expect that the state is dual to a shell that collapses to form a black hole but then evaporates.

Part V

Conclusions

Chapter 8

The Unreasonable Effectiveness of Branes

A central goal of modern research in theoretical physics is to formulate a consistent quantum theory of gravity capable of serving as a complete mathematical description of the universe which we inhabit. The motivation for this goal is far greater than the mere aesthetic appeal of fitting all known physical phenomena into a unified framework; rather, it is expected that detailed knowledge of this complete theory is necessary to understand the physics of the *big bang* and of *black holes*, both of which exhibit strong spacetime curvature. In the case of cosmology, we are faced with the exciting prospect that near-term precision measurements will reveal features of the early universe which are sensitive to physics at very high energies, pointing the way toward the correct framework for reality (see e.g. [320]). Even in the absence of data capable of distinguishing between *UV complete* (or valid-at-all-energy-scales) theories of quantum gravity, simply formulating a consistent quantum mechanical description of cosmology or black holes appears surprisingly challenging; establishing the existence of metastable string theory compactifications with a positive *cosmological constant*, which many believe should feature in our universe, is a source of active research and some controversy [321–324], while reconciling black hole evaporation with the *unitarity* (or information-preserving nature) of quantum mechanics, and thereby resolving the *black hole information paradox* [50, 56], has dominated research in quantum gravity for decades.

One of the driving forces behind many contemporary developments in quantum gravity research has been the advent of the *AdS/CFT correspon-*

dence [29], an equivalence or *duality* between theories of quantum gravity in spacetimes with negative cosmological constant (such as *anti-de Sitter* or *AdS* space) and lower-dimensional, non-gravitating quantum systems (such as *conformal field theories* or *CFTs*). The fundamental insights furnished by AdS/CFT have been innumerable, but some recent highlights include the revelation that tools from *quantum information theory* should play a central role in understanding the emergence of gravitational physics (e.g. [42, 44, 144, 146, 301, 308, 309, 325, 326]), and a partial resolution of the black hole information problem [9, 63–67].

In this thesis, we have used a version of the AdS/CFT correspondence, applicable to *boundary conformal field theories (BCFTs)*, to address a wide range of different physical questions. This iteration of the correspondence has allowed us to use calculations in classical gravity to learn about the space of boundary conditions for a particular widely-studied supersymmetric gauge theory known as the $\mathcal{N} = 4$ *supersymmetric Yang-Mills (SYM)* theory. It has also permitted us to introduce new dynamical objects, known as *end-of-the-world (ETW) branes*, in the gravitational bulk, such that the standard tools of AdS/CFT may be used to analyze the interesting time-dependent physics of these objects.

We began in Chapter 3 by studying the space of half-supersymmetric boundary conditions of the $\mathcal{N} = 4$ SYM theory with gauge group $U(N)$. These boundary conditions define theories which correspond to the low-energy effective description of a stack of N D3-branes ending on stacks of D5-branes and/or NS5-branes in type IIB string theory. We made use of the Ryu-Takayanagi formula to perform a holographic computation of a quantity called boundary F, which can be thought of as characterizing the number of boundary-localized degrees of freedom in a BCFT, for all half-supersymmetric boundary conditions. We also computed the same quantity exactly, using results from supersymmetric localization, for a subset of these boundary conditions corresponding to the physics of D3-branes ending on D5-branes only or NS5-branes only. We found precise agreement at leading order in large N, for all values of the 't Hooft coupling λ, perhaps suggesting a non-renormalization theorem governing the α' corrections.

In Chapter 4, we considered a class of high-energy states of a holographic CFT prepared by the Euclidean evolution of CFT boundary states. Using the ansatz of [78, 87, 88], such states were seen to correspond to black hole microstates including part of the behind-the-horizon region, with the second asymptotic region cut off by an ETW brane. We investigated the time-dependence of the entanglement entropy in these states using the RT formula, observing that this was able to probe behind-the-horizon physics for sufficiently large CFT subsystems in some cases, due to the possibility for RT surfaces to penetrate the horizon and end on the ETW brane. We also provided a direct check of the qualitative behaviour of the entanglement entropy by computing this quantity for analogous states in the SYK model, and we computed the holographic complexity as a function of time for these states using both the action-complexity and volume-complexity conjectures. Observing that the intrinsic geometry of the ETW brane is a big bang/big crunch cosmology, we proposed that this model could provide an approach to realizing cosmological physics within AdS/CFT, though we found no regime within our simple model allowing both brane-localized gravity and a sensible Euclidean path integral construction.

To further investigate the plausibility of our toy model for holographic cosmology, we considered generalizations of this model in Chapter 5, augmenting the previous model with an additional interface brane and modifications to the gravitational action. We observed that bulk solutions with a viable cosmological interpretation existed only in the presence of both modifications, for example in the case with both an interface brane and an Einstein-Hilbert term added to the ETW brane action. Even in this case, the required regime of the parameter space enforced a negative value for the ETW brane Einstein-Hilbert term, though the Einstein-Hilbert term for the effective theory on the braneworld obtained by integrating out the holographic direction remains positive.

To pursue the possibility of brane-localized gravity in string theory, we returned in Chapter 6 to the half-supersymmetric boundary conditions for $\mathcal{N} = 4$ SYM, in order to identify limits of the dual supergravity solutions, satisfying certain quantization conditions required in string theory, in which

the ETW brane region could be moved arbitrarily close to the "missing" AdS boundary, thereby recovering a large region of $\mathrm{AdS}_5 \times S^5$. We identified simple families of such boundary conditions with this property. Likewise, we considered families of 3D superconformal field theories, preserving the same supersymmetry algebra as the half-supersymmetric $\mathcal{N} = 4$ SYM BCFTs, and identified families of these 3D SCFTs whose dual solutions could produce arbitrarily large $\mathrm{AdS}_5 \times S^5$ wedges, a microscopic realization of wedge holography.

Finally, in Chapter 7, we considered a simple holographic model for an evaporating black hole inspired by [9], wherein a coupled black hole-radiation system was modelled by a BCFT with a large number of boundary degrees of freedom. We used the RT formula to explicitly quantify the information emitted by the black hole in this model, observing that its time-dependence was consistent with unitary quantum mechanical evolution, exhibiting a characteristic phase transition between RT surfaces as predicted by [287]. These observations confirmed that a portion of the black hole interior lies within the entanglement wedge of the radiation system following the phase transition, providing a doubly-holographic justification for the island rule for gravitational entropy.

It is perhaps mildly surprising how many new insights into deep questions regarding quantum gravitational physics are apparently enabled by applications of the AdS/BCFT correspondence; in this thesis, we have examined a few such applications highlighting the "unreasonable effectiveness of branes". It appears that these models provide us with a useful and tractable picture of the physics of holographic BCFTs, and that their further application may continue to yield insights into the nature of quantum gravity.

Bibliography

[1] M. V. Raamsdonk and C. Waddell, *Holographic and localization calculations of boundary F for $\mathcal{N} = 4$ SUSY Yang-Mills theory*, *JHEP* **02** (2021) 222, [2010.14520].

[2] S. Cooper, M. Rozali, B. Swingle, M. Van Raamsdonk, C. Waddell and D. Wakeham, *Black Hole Microstate Cosmology*, *JHEP* **07** (2019) 065, [1810.10601].

[3] C. Waddell, *Bottom-up holographic models for cosmology*, *JHEP* **09** (2022) 176, [2203.03096].

[4] M. Van Raamsdonk and C. Waddell, *Finding $AdS^5 \times S^5$ in 2+1 dimensional SCFT physics*, *JHEP* **11** (2021) 145, [2109.04479].

[5] M. Rozali, J. Sully, M. Van Raamsdonk, C. Waddell and D. Wakeham, *Information radiation in BCFT models of black holes*, *JHEP* **05** (2020) 004, [1910.12836].

[6] W. Reeves, M. Rozali, P. Simidzija, J. Sully, C. Waddell and D. Wakeham, *Looking for (and not finding) a bulk brane*, *JHEP* **12** (2021) 002, [2108.10345].

[7] S. Antonini, P. Simidzija, B. Swingle, M. Van Raamsdonk and C. Waddell, *Accelerating cosmology from $\Lambda < 0$ gravitational effective field theory*, 2212.00050.

[8] M. Van Raamsdonk and C. Waddell, *Possible hints of decreasing dark energy from supernova data*, 2305.04946.

[9] A. Almheiri, R. Mahajan, J. Maldacena and Y. Zhao, *The Page curve of Hawking radiation from semiclassical geometry*, 1908.10996.

[10] J. F. Donoghue, *Introduction to the effective field theory description of gravity*, in *Advanced School on Effective Theories*, 6, 1995. gr-qc/9512024.

[11] C. P. Burgess, *Quantum gravity in everyday life: General relativity as an effective field theory*, *Living Rev. Rel.* **7** (2004) 5–56, [gr-qc/0311082].

[12] S. Weinberg, *ULTRAVIOLET DIVERGENCES IN QUANTUM THEORIES OF GRAVITATION*, pp. 790–831. 1980.

[13] S. Weinberg, *The Cosmological Constant Problem*, *Rev. Mod. Phys.* **61** (1989) 1–23.

[14] J. J. Atick, G. W. Moore and A. Sen, *CATOPTRIC TADPOLES*, *Nucl. Phys. B* **307** (1988) 221–273.

[15] S. Mandelstam, *The n loop string amplitude: Explicit formulas, finiteness and absence of ambiguities*, *Phys. Lett. B* **277** (1992) 82–88.

[16] E. D'Hoker and D. H. Phong, *Momentum analyticity and finiteness of the one loop superstring amplitude*, *Phys. Rev. Lett.* **70** (1993) 3692–3695, [hep-th/9302003].

[17] N. Berkovits, *Multiloop amplitudes and vanishing theorems using the pure spinor formalism for the superstring*, *JHEP* **09** (2004) 047, [hep-th/0406055].

[18] T. Yoneya, *Quantum gravity and the zero slope limit of the generalized Virasoro model*, *Lett. Nuovo Cim.* **8** (1973) 951–955.

[19] T. Yoneya, *Connection of Dual Models to Electrodynamics and Gravidynamics*, *Prog. Theor. Phys.* **51** (1974) 1907–1920.

[20] J. Scherk and J. H. Schwarz, *Dual Models and the Geometry of Space-Time*, *Phys. Lett. B* **52** (1974) 347–350.

[21] T. Kaluza, *Zum Unitätsproblem der Physik*, *Sitzungsber. Preuss. Akad. Wiss. Berlin (Math. Phys.)* **1921** (1921) 966–972, [1803.08616].

[22] O. Klein, *Quantum Theory and Five-Dimensional Theory of Relativity. (In German and English)*, *Z. Phys.* **37** (1926) 895–906.

[23] J. Polchinski, *Dirichlet Branes and Ramond-Ramond charges*, *Phys. Rev. Lett.* **75** (1995) 4724–4727, [hep-th/9510017].

[24] J. D. Bekenstein, *Black holes and the second law*, *Lett. Nuovo Cim.* **4** (1972) 737–740.

[25] J. D. Bekenstein, *Black holes and entropy*, *Phys. Rev. D* **7** (1973) 2333–2346.

[26] J. D. Bekenstein, *Entropy bounds and black hole remnants*, *Phys. Rev. D* **49** (1994) 1912–1921, [gr-qc/9307035].

[27] G. 't Hooft, *Dimensional reduction in quantum gravity*, *Conf. Proc. C* **930308** (1993) 284–296, [gr-qc/9310026].

[28] L. Susskind, *The World as a hologram*, *J. Math. Phys.* **36** (1995) 6377–6396, [hep-th/9409089].

[29] J. M. Maldacena, *The Large N limit of superconformal field theories and supergravity*, *Adv. Theor. Math. Phys.* **2** (1998) 231–252, [hep-th/9711200].

[30] S. S. Gubser, I. R. Klebanov and A. M. Polyakov, *Gauge theory correlators from noncritical string theory*, *Phys. Lett. B* **428** (1998) 105–114, [hep-th/9802109].

[31] E. Witten, *Anti-de Sitter space and holography*, *Adv. Theor. Math. Phys.* **2** (1998) 253–291, [hep-th/9802150].

[32] I. Heemskerk, J. Penedones, J. Polchinski and J. Sully, *Holography from Conformal Field Theory*, *JHEP* **10** (2009) 079, [0907.0151].

[33] I. Heemskerk and J. Sully, *More Holography from Conformal Field Theory*, *JHEP* **09** (2010) 099, [1006.0976].

[34] S. El-Showk and K. Papadodimas, *Emergent Spacetime and Holographic CFTs*, *JHEP* **10** (2012) 106, [1101.4163].

[35] A. L. Fitzpatrick and J. Kaplan, *AdS Field Theory from Conformal Field Theory*, *JHEP* **02** (2013) 054, [1208.0337].

[36] X. O. Camanho, J. D. Edelstein, J. Maldacena and A. Zhiboedov, *Causality Constraints on Corrections to the Graviton Three-Point Coupling*, *JHEP* **02** (2016) 020, [1407.5597].

[37] N. Afkhami-Jeddi, T. Hartman, S. Kundu and A. Tajdini, *Einstein gravity 3-point functions from conformal field theory*, *JHEP* **12** (2017) 049, [1610.09378].

[38] S. Caron-Huot, D. Mazac, L. Rastelli and D. Simmons-Duffin, *AdS Bulk Locality from Sharp CFT Bounds*, 2106.10274.

[39] J. McGreevy, *Holographic duality with a view toward many-body physics*, *Adv. High Energy Phys.* **2010** (2010) 723105, [0909.0518].

[40] S. A. Hartnoll, A. Lucas and S. Sachdev, *Holographic quantum matter*, 1612.07324.

[41] J. M. Maldacena, *Eternal black holes in anti-de Sitter*, *JHEP* **04** (2003) 021, [hep-th/0106112].

[42] S. Ryu and T. Takayanagi, *Holographic derivation of entanglement entropy from AdS/CFT*, *Phys. Rev. Lett.* **96** (2006) 181602, [hep-th/0603001].

[43] M. Van Raamsdonk, *Comments on quantum gravity and entanglement*, 0907.2939.

[44] M. Van Raamsdonk, *Building up spacetime with quantum entanglement*, *Gen. Rel. Grav.* **42** (2010) 2323–2329, [1005.3035].

[45] J. Maldacena and L. Susskind, *Cool horizons for entangled black holes*, *Fortsch. Phys.* **61** (2013) 781–811, [1306.0533].

[46] J. M. Bardeen, B. Carter and S. W. Hawking, *The Four laws of black hole mechanics*, *Commun. Math. Phys.* **31** (1973) 161–170.

[47] W. Israel, *Event horizons in static vacuum space-times*, *Phys. Rev.* **164** (Dec, 1967) 1776–1779.

[48] W. Israel, *Event horizons in static electrovac space-times*, *Commun. Math. Phys.* **8** (1968) 245–260.

[49] B. Carter, *Axisymmetric black hole has only two degrees of freedom*, *Phys. Rev. Lett.* **26** (Feb, 1971) 331–333.

[50] S. W. Hawking, *Particle Creation by Black Holes*, *Commun. Math. Phys.* **43** (1975) 199–220.

[51] G. W. Gibbons and S. W. Hawking, *Action Integrals and Partition Functions in Quantum Gravity*, *Phys. Rev. D* **15** (1977) 2752–2756.

[52] A. Almheiri, T. Hartman, J. Maldacena, E. Shaghoulian and A. Tajdini, *The entropy of Hawking radiation*, *Rev. Mod. Phys.* **93** (2021) 035002, [2006.06872].

[53] A. Strominger and C. Vafa, *Microscopic origin of the Bekenstein-Hawking entropy*, *Phys. Lett. B* **379** (1996) 99–104, [hep-th/9601029].

[54] I. Mandal and A. Sen, *Black Hole Microstate Counting and its Macroscopic Counterpart*, *Class. Quant. Grav.* **27** (2010) 214003, [1008.3801].

[55] E. Witten, *Anti-de Sitter space, thermal phase transition, and confinement in gauge theories*, *Adv. Theor. Math. Phys.* **2** (1998) 505–532, [hep-th/9803131].

[56] S. W. Hawking, *Breakdown of Predictability in Gravitational Collapse*, *Phys. Rev.* **D14** (1976) 2460–2473.

[57] D. N. Page, *Average entropy of a subsystem*, *Phys. Rev. Lett.* **71** (1993) 1291–1294, [gr-qc/9305007].

[58] D. N. Page, *Information in black hole radiation*, *Phys. Rev. Lett.* **71** (1993) 3743–3746, [hep-th/9306083].

[59] A. Almheiri, D. Marolf, J. Polchinski and J. Sully, *Black Holes: Complementarity or Firewalls?*, *JHEP* **02** (2013) 062, [1207.3123].

[60] A. Almheiri, D. Marolf, J. Polchinski, D. Stanford and J. Sully, *An Apologia for Firewalls*, *JHEP* **09** (2013) 018, [1304.6483].

[61] S. D. Mathur, *The Information paradox: A Pedagogical introduction*, *Class. Quant. Grav.* **26** (2009) 224001, [0909.1038].

[62] S. L. Braunstein, H.-J. Sommers and K. Zyczkowski, *Entangled black holes as ciphers of hidden information*, 0907.0739.

[63] G. Penington, *Entanglement Wedge Reconstruction and the Information Paradox*, 1905.08255.

[64] A. Almheiri, N. Engelhardt, D. Marolf and H. Maxfield, *The entropy of bulk quantum fields and the entanglement wedge of an evaporating black hole*, 1905.08762.

[65] G. Penington, S. H. Shenker, D. Stanford and Z. Yang, *Replica wormholes and the black hole interior*, 1911.11977.

[66] A. Almheiri, T. Hartman, J. Maldacena, E. Shaghoulian and A. Tajdini, *Replica Wormholes and the Entropy of Hawking Radiation*, 1911.12333.

[67] C. Akers, N. Engelhardt, D. Harlow, G. Penington and S. Vardhan, *The black hole interior from non-isometric codes and complexity*, 2207.06536.

[68] V. Balasubramanian, A. Lawrence, J. M. Magan and M. Sasieta, *Microscopic origin of the entropy of black holes in general relativity*, 2212.02447.

[69] V. Balasubramanian, A. Lawrence, J. M. Magan and M. Sasieta, *Microscopic origin of the entropy of astrophysical black holes*, 2212.08623.

[70] N. Arkani-Hamed, S. Dimopoulos and G. R. Dvali, *The Hierarchy problem and new dimensions at a millimeter*, *Phys. Lett. B* **429** (1998) 263–272, [hep-ph/9803315].

[71] L. Randall and R. Sundrum, *A Large mass hierarchy from a small extra dimension*, *Phys. Rev. Lett.* **83** (1999) 3370–3373, [hep-ph/9905221].

[72] L. Randall and R. Sundrum, *An Alternative to compactification*, *Phys. Rev. Lett.* **83** (1999) 4690–4693, [hep-th/9906064].

[73] S. S. Gubser, *AdS / CFT and gravity*, *Phys. Rev.* **D63** (2001) 084017, [hep-th/9912001].

[74] H. L. Verlinde, *Holography and compactification*, *Nucl. Phys.* **B580** (2000) 264–274, [hep-th/9906182].

[75] S. W. Hawking, T. Hertog and H. S. Reall, *Brane new world*, *Phys. Rev.* **D62** (2000) 043501, [hep-th/0003052].

[76] S. de Haro, K. Skenderis and S. N. Solodukhin, *Gravity in warped compactifications and the holographic stress tensor*, *Class. Quant. Grav.* **18** (2001) 3171–3180, [hep-th/0011230].

[77] R. Maartens and K. Koyama, *Brane-World Gravity*, *Living Rev. Rel.* **13** (2010) 5, [1004.3962].

[78] A. Karch and L. Randall, *Open and closed string interpretation of SUSY CFT's on branes with boundaries*, *JHEP* **06** (2001) 063, [hep-th/0105132].

[79] A. Karch and L. Randall, *Locally localized gravity*, *JHEP* **05** (2001) 008, [hep-th/0011156].

[80] J. L. Cardy, *Conformal Invariance and Surface Critical Behavior*, *Nucl. Phys. B* **240** (1984) 514–532.

[81] J. L. Cardy, *Boundary Conditions, Fusion Rules and the Verlinde Formula*, *Nucl. Phys.* **B324** (1989) 581–596.

[82] I. Affleck and A. W. W. Ludwig, *Universal noninteger 'ground state degeneracy' in critical quantum systems*, *Phys. Rev. Lett.* **67** (1991) 161–164.

[83] I. Affleck, *Boundary condition changing operators in conformal field theory and condensed matter physics*, *Nucl. Phys. B Proc. Suppl.* **58** (1997) 35–41, [hep-th/9611064].

[84] D. Friedan and A. Konechny, *On the boundary entropy of one-dimensional quantum systems at low temperature*, *Phys. Rev. Lett.* **93** (2004) 030402, [hep-th/0312197].

[85] I. Affleck, *Conformal field theory approach to the Kondo effect*, *Acta Phys. Polon. B* **26** (1995) 1869–1932, [cond-mat/9512099].

[86] A. Recknagel and V. Schomerus, *Boundary Conformal Field Theory and the Worldsheet Approach to D-Branes*. Cambridge Monographs on Mathematical Physics. Cambridge University Press, 11, 2013, 10.1017/CBO9780511806476.

[87] T. Takayanagi, *Holographic Dual of BCFT*, *Phys. Rev. Lett.* **107** (2011) 101602, [1105.5165].

[88] M. Fujita, T. Takayanagi and E. Tonni, *Aspects of AdS/BCFT*, *JHEP* **11** (2011) 043, [1108.5152].

[89] D. Gaiotto and E. Witten, *Supersymmetric Boundary Conditions in N=4 Super Yang-Mills Theory*, *J. Statist. Phys.* **135** (2009) 789–855, [0804.2902].

[90] D. Gaiotto and E. Witten, *S-Duality of Boundary Conditions In N=4 Super Yang-Mills Theory*, *Adv. Theor. Math. Phys.* **13** (2009) 721–896, [0807.3720].

[91] S. W. Hawking and G. F. R. Ellis, *The Large Scale Structure of Space-Time*. Cambridge Monographs on Mathematical Physics. Cambridge University Press, 2, 2011, 10.1017/CBO9780511524646.

[92] K. Skenderis, *Lecture notes on holographic renormalization*, *Class. Quant. Grav.* **19** (2002) 5849–5876, [hep-th/0209067].

[93] M. Van Raamsdonk, *Lectures on Gravity and Entanglement*, in *Theoretical Advanced Study Institute in Elementary Particle Physics: New Frontiers in Fields and Strings*, pp. 297–351, 2017. 1609.00026. DOI.

[94] L. Fidkowski, V. Hubeny, M. Kleban and S. Shenker, *The Black hole singularity in AdS / CFT*, *JHEP* **02** (2004) 014, [hep-th/0306170].

[95] K. Becker, M. Becker and J. H. Schwarz, *String theory and M-theory: A modern introduction*. Cambridge University Press, 12, 2006, 10.1017/CBO9780511816086.

[96] M. Ammon and J. Erdmenger, *Gauge/gravity duality: Foundations and applications*. Cambridge University Press, Cambridge, 4, 2015.

[97] J. H. Schwarz and P. C. West, *Symmetries and Transformations of Chiral N=2 D=10 Supergravity*, *Phys. Lett. B* **126** (1983) 301–304.

[98] J. H. Schwarz, *Covariant Field Equations of Chiral N=2 D=10 Supergravity*, *Nucl. Phys. B* **226** (1983) 269.

[99] P. S. Howe and P. C. West, *The Complete N=2, D=10 Supergravity*, *Nucl. Phys. B* **238** (1984) 181–220.

[100] M. Schottenloher, ed., *A mathematical introduction to conformal field theory*, vol. 759. 2008, 10.1007/978-3-540-68628-6.

[101] P. Di Francesco, P. Mathieu and D. Senechal, *Conformal Field Theory*. Graduate Texts in Contemporary Physics. Springer-Verlag, New York, 1997, 10.1007/978-1-4612-2256-9.

[102] J. Polchinski, *String theory. Vol. 1: An introduction to the bosonic string*. Cambridge Monographs on Mathematical Physics. Cambridge University Press, 12, 2007, 10.1017/CBO9780511816079.

[103] D. Simmons-Duffin, *The Conformal Bootstrap*, in *Theoretical Advanced Study Institute in Elementary Particle Physics: New Frontiers in Fields and Strings*, pp. 1–74, 2017. 1602.07982. DOI.

[104] S. Rychkov, *EPFL Lectures on Conformal Field Theory in D>= 3 Dimensions*. SpringerBriefs in Physics. 1, 2016, 10.1007/978-3-319-43626-5.

[105] T. Hartman, "Lecture notes on black holes and quantum information." http://www.hartmanhep.net/topics2021/, 2021.

[106] D. McAvity and H. Osborn, *Conformal field theories near a boundary in general dimensions*, *Nucl. Phys. B* **455** (1995) 522–576, [cond-mat/9505127].

[107] O. Aharony, S. S. Gubser, J. M. Maldacena, H. Ooguri and Y. Oz, *Large N field theories, string theory and gravity*, *Phys. Rept.* **323** (2000) 183–386, [hep-th/9905111].

[108] J. Polchinski, *String theory. Vol. 2: Superstring theory and beyond*. Cambridge Monographs on Mathematical Physics. Cambridge University Press, 12, 2007, 10.1017/CBO9780511618123.

[109] J. Wess and J. Bagger, *Supersymmetry and supergravity*. Princeton University Press, Princeton, NJ, USA, 1992.

[110] P. LaBelle, *Supersymmetry Demystified*. McGraw Hill Professional, 2010.

[111] M. Bertolini, "Lectures on supersymmetry." `https://people.sissa.it/~bertmat/teaching.htm`.

[112] E. D'Hoker and D. Z. Freedman, *Supersymmetric gauge theories and the AdS / CFT correspondence*, in *Theoretical Advanced Study Institute in Elementary Particle Physics (TASI 2001): Strings, Branes and EXTRA Dimensions*, pp. 3–158, 1, 2002. `hep-th/0201253`.

[113] S. J. Gates, M. T. Grisaru, M. Rocek and W. Siegel, *Superspace Or One Thousand and One Lessons in Supersymmetry*, vol. 58 of *Frontiers in Physics*. 1983.

[114] A. Van Proeyen, *Tools for supersymmetry*, *Ann. U. Craiova Phys.* **9** (1999) 1–48, [`hep-th/9910030`].

[115] O. Aharony, A. Hanany, K. A. Intriligator, N. Seiberg and M. J. Strassler, *Aspects of N=2 supersymmetric gauge theories in three-dimensions*, *Nucl. Phys. B* **499** (1997) 67–99, [`hep-th/9703110`].

[116] N. Seiberg and E. Witten, *Gauge dynamics and compactification to three-dimensions*, in *Conference on the Mathematical Beauty of Physics (In Memory of C. Itzykson)*, pp. 333–366, 6, 1996. `hep-th/9607163`.

[117] W. Nahm, *Supersymmetries and their Representations*, *Nucl. Phys. B* **135** (1978) 149.

[118] S. Minwalla, *Restrictions imposed by superconformal invariance on quantum field theories*, *Adv. Theor. Math. Phys.* **2** (1998) 783–851, [`hep-th/9712074`].

[119] C. Cordova, T. T. Dumitrescu and K. Intriligator, *Multiplets of Superconformal Symmetry in Diverse Dimensions*, *JHEP* **03** (2019) 163, [`1612.00809`].

[120] L. Eberhardt, *Superconformal symmetry and representations*, *J. Phys. A* **54** (2021) 063002, [2006.13280].

[121] L. Brink, J. H. Schwarz and J. Scherk, *Supersymmetric Yang-Mills Theories*, *Nucl. Phys. B* **121** (1977) 77–92.

[122] W. Skiba, *Correlators of short multitrace operators in N=4 supersymmetric Yang-Mills*, *Phys. Rev. D* **60** (1999) 105038, [hep-th/9907088].

[123] S. Cremonesi, *An Introduction to Localisation and Supersymmetry in Curved Space*, *PoS* **Modave2013** (2013) 002.

[124] V. Pestun et al., *Localization techniques in quantum field theories*, *J. Phys. A* **50** (2017) 440301, [1608.02952].

[125] G. Festuccia and N. Seiberg, *Rigid Supersymmetric Theories in Curved Superspace*, *JHEP* **06** (2011) 114, [1105.0689].

[126] V. Pestun, *Localization of gauge theory on a four-sphere and supersymmetric Wilson loops*, *Commun. Math. Phys.* **313** (2012) 71–129, [0712.2824].

[127] A. Kapustin, B. Willett and I. Yaakov, *Exact Results for Wilson Loops in Superconformal Chern-Simons Theories with Matter*, *JHEP* **03** (2010) 089, [0909.4559].

[128] T. Hartman, "Lecture notes on quantum gravity and black holes." http://www.hartmanhep.net/topics2015/, 2015.

[129] D. Harlow, *Jerusalem Lectures on Black Holes and Quantum Information*, *Rev. Mod. Phys.* **88** (2016) 015002, [1409.1231].

[130] D. Harlow, *TASI Lectures on the Emergence of Bulk Physics in AdS/CFT*, *PoS* **TASI2017** (2018) 002, [1802.01040].

[131] J. Kaplan, "Lectures on ads/cft from the bottom up." https://sites.krieger.jhu.edu/jared-kaplan/files/2016/05/AdSCFTCourseNotesCurrentPublic.pdf, 2016.

[132] K. Skenderis and B. C. van Rees, *Real-time gauge/gravity duality: Prescription, Renormalization and Examples*, *JHEP* **05** (2009) 085, [0812.2909].

[133] D. Marolf, *States and boundary terms: Subtleties of Lorentzian AdS / CFT*, *JHEP* **05** (2005) 042, [hep-th/0412032].

[134] D. Harlow and D. Stanford, *Operator Dictionaries and Wave Functions in AdS/CFT and dS/CFT*, 1104.2621.

[135] L. Apolo, A. Belin, S. Bintanja, A. Castro and C. A. Keller, *CFTs dual to quantum gravity with strongly coupled matter*, 2212.07436.

[136] J. Penedones, *Writing CFT correlation functions as AdS scattering amplitudes*, *JHEP* **03** (2011) 025, [1011.1485].

[137] A. L. Fitzpatrick, J. Kaplan, J. Penedones, S. Raju and B. C. van Rees, *A Natural Language for AdS/CFT Correlators*, *JHEP* **11** (2011) 095, [1107.1499].

[138] M. F. Paulos, *Towards Feynman rules for Mellin amplitudes*, *JHEP* **10** (2011) 074, [1107.1504].

[139] A. L. Fitzpatrick and J. Kaplan, *Analyticity and the Holographic S-Matrix*, *JHEP* **10** (2012) 127, [1111.6972].

[140] O. Aharony, J. Marsano, S. Minwalla, K. Papadodimas and M. Van Raamsdonk, *The Hagedorn - deconfinement phase transition in weakly coupled large N gauge theories*, *Adv. Theor. Math. Phys.* **8** (2004) 603–696, [hep-th/0310285].

[141] S. W. Hawking and D. N. Page, *Thermodynamics of Black Holes in anti-De Sitter Space*, *Commun. Math. Phys.* **87** (1983) 577.

[142] J. B. Hartle and S. W. Hawking, *Path Integral Derivation of Black Hole Radiance*, *Phys. Rev. D* **13** (1976) 2188–2203.

[143] T. Faulkner, T. Hartman, M. Headrick, M. Rangamani and B. Swingle, *Snowmass white paper: Quantum information in quantum field theory and quantum gravity*, in *Snowmass 2021*, 3, 2022. 2203.07117.

[144] A. Lewkowycz and J. Maldacena, *Generalized gravitational entropy*, *JHEP* **08** (2013) 090, [1304.4926].

[145] T. Faulkner, A. Lewkowycz and J. Maldacena, *Quantum corrections to holographic entanglement entropy*, *JHEP* **11** (2013) 074, [1307.2892].

[146] D. L. Jafferis, A. Lewkowycz, J. Maldacena and S. J. Suh, *Relative entropy equals bulk relative entropy*, *JHEP* **06** (2016) 004, [1512.06431].

[147] V. E. Hubeny, M. Rangamani and T. Takayanagi, *A Covariant holographic entanglement entropy proposal*, *JHEP* **07** (2007) 062, [0705.0016].

[148] A. C. Wall, *Maximin Surfaces, and the Strong Subadditivity of the Covariant Holographic Entanglement Entropy*, *Class. Quant. Grav.* **31** (2014) 225007, [1211.3494].

[149] N. Engelhardt and A. C. Wall, *Quantum Extremal Surfaces: Holographic Entanglement Entropy beyond the Classical Regime*, *JHEP* **01** (2015) 073, [1408.3203].

[150] N. Engelhardt, "Quantum information in ads/cft." https://sites.google.com/colorado.edu/tasi-2021-wiki/lecture-topics/quantum-information-in-adscft, 2021.

[151] X. Dong, *Holographic Entanglement Entropy for General Higher Derivative Gravity*, *JHEP* **01** (2014) 044, [1310.5713].

[152] A. Hamilton, D. N. Kabat, G. Lifschytz and D. A. Lowe, *Holographic representation of local bulk operators*, *Phys. Rev. D* **74** (2006) 066009, [hep-th/0606141].

[153] A. Zamolodchikov, *Irreversibility of the Flux of the Renormalization Group in a 2D Field Theory*, *JETP Lett.* **43** (1986) 730–732.

[154] D. L. Jafferis, I. R. Klebanov, S. S. Pufu and B. R. Safdi, *Towards the F-Theorem: N=2 Field Theories on the Three-Sphere*, *JHEP* **06** (2011) 102, [1103.1181].

[155] H. Casini and M. Huerta, *On the RG running of the entanglement entropy of a circle*, *Phys. Rev. D* **85** (2012) 125016, [1202.5650].

[156] J. L. Cardy, *Is There a c Theorem in Four-Dimensions?*, *Phys. Lett. B* **215** (1988) 749–752.

[157] Z. Komargodski and A. Schwimmer, *On Renormalization Group Flows in Four Dimensions*, *JHEP* **12** (2011) 099, [1107.3987].

[158] S. Giombi and I. R. Klebanov, *Interpolating between a and F*, *JHEP* **03** (2015) 117, [1409.1937].

[159] I. R. Klebanov, S. S. Pufu and B. R. Safdi, *F-Theorem without Supersymmetry*, *JHEP* **10** (2011) 038, [1105.4598].

[160] I. Affleck and A. W. W. Ludwig, *Universal noninteger 'ground state degeneracy' in critical quantum systems*, *Phys. Rev. Lett.* **67** (1991) 161–164.

[161] K. Jensen and A. O'Bannon, *Holography, Entanglement Entropy, and Conformal Field Theories with Boundaries or Defects*, *Phys. Rev. D* **88** (2013) 106006, [1309.4523].

[162] J. Estes, K. Jensen, A. O'Bannon, E. Tsatis and T. Wrase, *On Holographic Defect Entropy*, *JHEP* **05** (2014) 084, [1403.6475].

[163] P. Liendo, L. Rastelli and B. C. van Rees, *The Bootstrap Program for Boundary CFT_d*, *JHEP* **07** (2013) 113, [1210.4258].

[164] D. Mazáč, L. Rastelli and X. Zhou, *An analytic approach to $BCFT_d$*, *JHEP* **12** (2019) 004, [1812.09314].

[165] M. Nozaki, T. Takayanagi and T. Ugajin, *Central Charges for BCFTs and Holography*, *JHEP* **06** (2012) 066, [1205.1573].

[166] D. Gaiotto, *Boundary F-maximization*, 1403.8052.

[167] N. Kobayashi, T. Nishioka, Y. Sato and K. Watanabe, *Towards a C-theorem in defect CFT*, *JHEP* **01** (2019) 039, [1810.06995].

[168] S. Giombi and H. Khanchandani, *CFT in AdS and boundary RG flows*, 2007.04955.

[169] H. Casini, I. Salazar Landea and G. Torroba, *The g-theorem and quantum information theory*, *JHEP* **10** (2016) 140, [1607.00390].

[170] K. Jensen and A. O'Bannon, *Constraint on Defect and Boundary Renormalization Group Flows*, *Phys. Rev. Lett.* **116** (2016) 091601, [1509.02160].

[171] H. Casini, I. Salazar Landea and G. Torroba, *Irreversibility in quantum field theories with boundaries*, *JHEP* **04** (2019) 166, [1812.08183].

[172] E. D'Hoker, J. Estes and M. Gutperle, *Exact half-BPS Type IIB interface solutions. I. Local solution and supersymmetric Janus*, *JHEP* **06** (2007) 021, [0705.0022].

[173] E. D'Hoker, J. Estes and M. Gutperle, *Exact half-BPS Type IIB interface solutions. II. Flux solutions and multi-Janus*, *JHEP* **06** (2007) 022, [0705.0024].

[174] O. Aharony, L. Berdichevsky, M. Berkooz and I. Shamir, *Near-horizon solutions for D3-branes ending on 5-branes*, *Phys. Rev.* **D84** (2011) 126003, [1106.1870].

[175] B. Assel, C. Bachas, J. Estes and J. Gomis, *Holographic Duals of D=3 N=4 Superconformal Field Theories*, *JHEP* **08** (2011) 087, [1106.4253].

[176] B. Assel, J. Estes and M. Yamazaki, *Large N Free Energy of 3d N=4 SCFTs and AdS_4/CFT_3*, *JHEP* **09** (2012) 074, [1206.2920].

[177] J. Estes, D. Krym, A. O'Bannon, B. Robinson and R. Rodgers, *Wilson Surface Central Charge from Holographic Entanglement Entropy*, *JHEP* **05** (2019) 032, [1812.00923].

[178] K. Goto, L. Nagano, T. Nishioka and T. Okuda, *Janus interface entropy and Calabi's diastasis in four-dimensional $\mathcal{N} = 2$ superconformal field theories*, 2005.10833.

[179] H. Casini, M. Huerta and R. C. Myers, *Towards a derivation of holographic entanglement entropy*, *JHEP* **05** (2011) 036, [1102.0440].

[180] R. C. Myers and A. Sinha, *Seeing a c-theorem with holography*, *Phys. Rev. D* **82** (2010) 046006, [1006.1263].

[181] R. C. Myers and A. Sinha, *Holographic c-theorems in arbitrary dimensions*, *JHEP* **01** (2011) 125, [1011.5819].

[182] T. Kawano, Y. Nakaguchi and T. Nishioka, *Holographic Interpolation between a and F*, *JHEP* **12** (2014) 161, [1410.5973].

[183] P. Calabrese and J. Cardy, *Entanglement entropy and conformal field theory*, *J. Phys. A* **42** (2009) 504005, [0905.4013].

[184] D. V. Fursaev and S. N. Solodukhin, *Anomalies, entropy and boundaries*, *Phys. Rev. D* **93** (2016) 084021, [1601.06418].

[185] C. P. Herzog, K.-W. Huang and K. Jensen, *Universal Entanglement and Boundary Geometry in Conformal Field Theory*, *JHEP* **01** (2016) 162, [1510.00021].

[186] S. Yamaguchi, *Holographic RG flow on the defect and g theorem*, *JHEP* **10** (2002) 002, [hep-th/0207171].

[187] Y. Wang, *Taming Defects in $\mathcal{N} = 4$ Super-Yang-Mills*, 2003.11016.

[188] N. R. Constable, R. C. Myers and O. Tafjord, *The Noncommutative bion core*, *Phys. Rev. D* **61** (2000) 106009, [hep-th/9911136].

[189] A. Hanany and E. Witten, *Type IIB superstrings, BPS monopoles, and three-dimensional gauge dynamics*, *Nucl. Phys. B* **492** (1997) 152–190, [hep-th/9611230].

[190] J. Gomis, T. Okuda and V. Pestun, *Exact Results for 't Hooft Loops in Gauge Theories on S^4*, *JHEP* **05** (2012) 141, [1105.2568].

[191] V. Pestun, *Localization of the four-dimensional N=4 SYM to a two-sphere and 1/8 BPS Wilson loops*, *JHEP* **12** (2012) 067, [0906.0638].

[192] N. Hama and K. Hosomichi, *Seiberg-Witten Theories on Ellipsoids*, *JHEP* **09** (2012) 033, [1206.6359].

[193] K. Hosomichi, *$\mathcal{N} = 2$ SUSY gauge theories on S^4*, *J. Phys. A* **50** (2017) 443010, [1608.02962].

[194] A. Kapustin, B. Willett and I. Yaakov, *Nonperturbative Tests of Three-Dimensional Dualities*, *JHEP* **10** (2010) 013, [1003.5694].

[195] S. Benvenuti and S. Pasquetti, *3D-partition functions on the sphere: exact evaluation and mirror symmetry*, *JHEP* **05** (2012) 099, [1105.2551].

[196] T. Nishioka, Y. Tachikawa and M. Yamazaki, *3d Partition Function as Overlap of Wavefunctions*, *JHEP* **08** (2011) 003, [1105.4390].

[197] S. Sugishita and S. Terashima, *Exact Results in Supersymmetric Field Theories on Manifolds with Boundaries*, *JHEP* **11** (2013) 021, [1308.1973].

[198] E. Gava, K. Narain, M. Muteeb and V. Giraldo-Rivera, *$N = 2$ gauge theories on the hemisphere HS^4*, *Nucl. Phys. B* **920** (2017) 256–297, [1611.04804].

[199] R. Kumar Gupta, C. P. Herzog and I. Jeon, *Duality and Transport for Supersymmetric Graphene from the Hemisphere Partition Function*, *JHEP* **05** (2020) 023, [1912.09225].

[200] N. Drukker, D. Gaiotto and J. Gomis, *The Virtue of Defects in 4D Gauge Theories and 2D CFTs*, *JHEP* **06** (2011) 025, [1003.1112].

[201] M. Dedushenko, *Gluing II: Boundary Localization and Gluing Formulas*, 1807.04278.

[202] S. Komatsu and Y. Wang, *Non-perturbative Defect One-Point Functions in Planar $\mathcal{N} = 4$ Super-Yang-Mills*, 2004.09514.

[203] M. Dedushenko and D. Gaiotto, *Algebras, traces, and boundary correlators in $\mathcal{N} = 4$ SYM*, 2009.11197.

[204] O. Lunin and S. D. Mathur, *AdS / CFT duality and the black hole information paradox*, *Nucl. Phys.* **B623** (2002) 342–394, [hep-th/0109154].

[205] O. Lunin and S. D. Mathur, *Statistical interpretation of Bekenstein entropy for systems with a stretched horizon*, *Phys. Rev. Lett.* **88** (2002) 211303, [hep-th/0202072].

[206] S. D. Mathur, *The Fuzzball proposal for black holes: An Elementary review*, *Fortsch. Phys.* **53** (2005) 793–827, [hep-th/0502050].

[207] K. Skenderis and M. Taylor, *The fuzzball proposal for black holes*, *Phys. Rept.* **467** (2008) 117–171, [0804.0552].

[208] I. Kourkoulou and J. Maldacena, *Pure states in the SYK model and nearly-AdS_2 gravity*, 1707.02325.

[209] A. Almheiri, A. Mousatov and M. Shyani, *Escaping the Interiors of Pure Boundary-State Black Holes*, 1803.04434.

[210] J. De Boer, S. F. Lokhande, E. Verlinde, R. Van Breukelen and K. Papadodimas, *On the interior geometry of a typical black hole microstate*, 1804.10580.

[211] E. Witten, *Instability of the Kaluza-Klein Vacuum*, *Nucl. Phys.* **B195** (1982) 481–492.

[212] K. Papadodimas and S. Raju, *An Infalling Observer in AdS/CFT*, *JHEP* **10** (2013) 212, [1211.6767].

[213] K. Papadodimas and S. Raju, *State-Dependent Bulk-Boundary Maps and Black Hole Complementarity*, *Phys. Rev.* **D89** (2014) 086010, [1310.6335].

[214] D. Harlow, *Aspects of the Papadodimas-Raju Proposal for the Black Hole Interior*, *JHEP* **11** (2014) 055, [1405.1995].

[215] K. Papadodimas and S. Raju, *Remarks on the necessity and implications of state-dependence in the black hole interior*, *Phys. Rev.* **D93** (2016) 084049, [1503.08825].

[216] P. Hayden and G. Penington, *Learning the Alpha-bits of Black Holes*, 1807.06041.

[217] A. Almheiri, *Holographic Quantum Error Correction and the Projected Black Hole Interior*, 1810.02055.

[218] M. Rangamani and T. Takayanagi, *Holographic Entanglement Entropy*, *Lect. Notes Phys.* **931** (2017) pp.1–246, [1609.01287].

[219] T. Hartman and J. Maldacena, *Time Evolution of Entanglement Entropy from Black Hole Interiors*, *JHEP* **05** (2013) 014, [1303.1080].

[220] J. Abajo-Arrastia, J. Aparicio and E. Lopez, *Holographic Evolution of Entanglement Entropy*, *JHEP* **11** (2010) 149, [1006.4090].

[221] J. Cardy, *Quantum Quenches to a Critical Point in One Dimension: some further results*, *J. Stat. Mech.* **1602** (2016) 023103, [1507.07266].

[222] J. Cardy, *Bulk Renormalization Group Flows and Boundary States in Conformal Field Theories*, *SciPost Phys.* **3** (2017) 011, [1706.01568].

[223] S. R. White, *Minimally entangled typical quantum states at finite temperature*, *Phys. Rev. Lett.* **102** (May, 2009) 190601.

[224] E. M. Stoudenmire and S. R. White, *Minimally entangled typical thermal state algorithms*, *New Journal of Physics* **12** (May, 2010) 055026, [1002.1305].

[225] L. Susskind, *Computational Complexity and Black Hole Horizons*, *Fortsch. Phys.* **64** (2016) 44–48, [1403.5695].

[226] D. Stanford and L. Susskind, *Complexity and Shock Wave Geometries*, *Phys. Rev.* **D90** (2014) 126007, [1406.2678].

[227] A. R. Brown, D. A. Roberts, L. Susskind, B. Swingle and Y. Zhao, *Holographic Complexity Equals Bulk Action?*, *Phys. Rev. Lett.* **116** (2016) 191301, [1509.07876].

[228] T. Banks and W. Fischler, *An Holographic cosmology*, hep-th/0111142.

[229] T. Banks and W. Fischler, *The Holographic Space-Time Model of Cosmology*, 1806.01749.

[230] A. Strominger, *The dS / CFT correspondence*, *JHEP* **10** (2001) 034, [hep-th/0106113].

[231] M. Alishahiha, A. Karch, E. Silverstein and D. Tong, *The dS/dS correspondence*, *AIP Conf. Proc.* **743** (2005) 393–409, [hep-th/0407125].

[232] B. Freivogel, V. E. Hubeny, A. Maloney, R. C. Myers, M. Rangamani and S. Shenker, *Inflation in AdS/CFT*, *JHEP* **03** (2006) 007, [hep-th/0510046].

[233] P. McFadden and K. Skenderis, *Holography for Cosmology*, *Phys. Rev.* **D81** (2010) 021301, [0907.5542].

[234] J. Louko and D. Marolf, *Single exterior black holes and the ads / cft conjecture*, *Phys. Rev.* **D59** (1999) 066002, [hep-th/9808081].

[235] K. Papadodimas, *A class of non-equilibrium states and the black hole interior*, 1708.06328.

[236] M. Miyaji, S. Ryu, T. Takayanagi and X. Wen, *Boundary States as Holographic Duals of Trivial Spacetimes*, *JHEP* **05** (2015) 152, [1412.6226].

[237] P. Calabrese and J. Cardy, *Quantum quenches in 1+1 dimensional conformal field theories*, *J. Stat. Mech.* **1606** (2016) 064003, [1603.02889].

[238] R.-X. Miao, C.-S. Chu and W.-Z. Guo, *New proposal for a holographic boundary conformal field theory*, *Phys. Rev.* **D96** (2017) 046005, [1701.04275].

[239] P. Calabrese and J. L. Cardy, *Entanglement entropy and quantum field theory*, *J. Stat. Mech.* **0406** (2004) P06002, [hep-th/0405152].

[240] P. Kraus, *Dynamics of anti-de Sitter domain walls*, *JHEP* **12** (1999) 011, [hep-th/9910149].

[241] L. Fidkowski, V. Hubeny, M. Kleban and S. Shenker, *The black hole singularity in AdS/CFT*, *JHEP* **02** (2004) 014, [hep-th/0306170].

[242] B. Freivogel, V. E. Hubeny, A. Maloney, R. C. Myers, M. Rangamani and S. Shenker, *Inflation in AdS/CFT*, *JHEP* **03** (2006) 007.

[243] I. Bah, A. Faraggi, L. A. Pando Zayas and C. A. Terrero-Escalante, *Holographic entanglement entropy and phase transitions at finite temperature*, *Int. J. Mod. Phys.* **A24** (2009) 2703–2728, [0710.5483].

[244] N. Bao and H. Ooguri, *Distinguishability of black hole microstates*, *Phys. Rev.* **D96** (2017) 066017, [1705.07943].

[245] Y. Gu, X.-L. Qi and D. Stanford, *Local criticality, diffusion and chaos in generalized Sachdev-Ye-Kitaev models*, *Journal of High Energy Physics* **5** (May, 2017) 125, [1609.07832].

[246] D. Carmi, R. C. Myers and P. Rath, *Comments on Holographic Complexity*, *JHEP* **03** (2017) 118, [1612.00433].

[247] D. Carmi, S. Chapman, H. Marrochio, R. C. Myers and S. Sugishita, *On the Time Dependence of Holographic Complexity*, *JHEP* **11** (2017) 188, [1709.10184].

[248] L. Lehner, R. C. Myers, E. Poisson and R. D. Sorkin, *Gravitational action with null boundaries*, *Phys. Rev.* **D94** (2016) 084046, [1609.00207].

[249] B. Czech, J. L. Karczmarek, F. Nogueira and M. Van Raamsdonk, *Rindler Quantum Gravity*, *Class. Quant. Grav.* **29** (2012) 235025, [1206.1323].

[250] M. Van Raamsdonk, *Building up spacetime with quantum entanglement II: It from BC-bit*, 1809.01197.

[251] R. Emparan, *AdS / CFT duals of topological black holes and the entropy of zero energy states*, *JHEP* **06** (1999) 036, [hep-th/9906040].

[252] P. D. Mannheim, *Brane-Localized Gravity*. World Scientific, 2005.

[253] J. Garriga and T. Tanaka, *Gravity in the brane world*, *Phys. Rev. Lett.* **84** (2000) 2778–2781, [hep-th/9911055].

[254] S. B. Giddings, E. Katz and L. Randall, *Linearized gravity in brane backgrounds*, *JHEP* **03** (2000) 023, [hep-th/0002091].

[255] S. B. Giddings and E. Katz, *Effective theories and black hole production in warped compactifications*, *J. Math. Phys.* **42** (2001) 3082–3102, [hep-th/0009176].

[256] N. S. Deger and A. Kaya, *AdS / CFT and Randall-Sundrum model without a brane*, *JHEP* **05** (2001) 030, [hep-th/0010141].

[257] P. Singh and N. Dadhich, *Localization of gravity in brane world cosmologies*, *Mod. Phys. Lett.* **A18** (2003) 983–992, [hep-th/0204190].

[258] P. Singh and N. Dadhich, *Localized gravity on FRW branes*, hep-th/0208080.

[259] C. Csaki, J. Erlich, T. J. Hollowood and Y. Shirman, *Universal aspects of gravity localized on thick branes*, *Nucl. Phys.* **B581** (2000) 309–338, [hep-th/0001033].

[260] E. Kiritsis and F. Nitti, *On massless 4D gravitons from asymptotically AdS(5) space-times*, *Nucl. Phys.* **B772** (2007) 67–102, [hep-th/0611344].

[261] S. S. Seahra, C. Clarkson and R. Maartens, *Delocalization of brane gravity by a bulk black hole*, *Class. Quant. Grav.* **22** (2005) L91–L102, [gr-qc/0504023].

[262] C. Clarkson and S. S. Seahra, *Braneworld resonances*, *Class. Quant. Grav.* **22** (2005) 3653–3688, [gr-qc/0505145].

[263] A. Hebecker and J. March-Russell, *Randall-Sundrum II cosmology, AdS / CFT, and the bulk black hole*, *Nucl. Phys.* **B608** (2001) 375–393, [hep-ph/0103214].

[264] M. Chiodaroli, E. D'Hoker and M. Gutperle, *Simple Holographic Duals to Boundary CFTs*, *JHEP* **02** (2012) 005, [1111.6912].

[265] M. Chiodaroli, E. D'Hoker and M. Gutperle, *Holographic duals of Boundary CFTs*, *JHEP* **07** (2012) 177, [1205.5303].

[266] M. Gutperle and J. Samani, *Holographic RG-flows and Boundary CFTs*, *Phys. Rev.* **D86** (2012) 106007, [1207.7325].

[267] D. Friedan, A. Konechny and C. Schmidt-Colinet, *Lower bound on the entropy of boundaries and junctions in 1+1d quantum critical systems*, *Phys. Rev. Lett.* **109** (2012) 140401, [1206.5395].

[268] D. Friedan, A. Konechny and C. Schmidt-Colinet, *Precise lower bound on Monster brane boundary entropy*, *JHEP* **07** (2013) 099, [1305.2122].

[269] T. Hartman, C. A. Keller and B. Stoica, *Universal Spectrum of 2d Conformal Field Theory in the Large c Limit*, *JHEP* **09** (2014) 118, [1405.5137].

[270] T. Anous, T. Hartman, A. Rovai and J. Sonner, *Black Hole Collapse in the 1/c Expansion*, *JHEP* **07** (2016) 123, [1603.04856].

[271] J. B. Hartle and S. W. Hawking, *Wave Function of the Universe*, *Phys. Rev.* **D28** (1983) 2960–2975.

[272] Y. Nomura, N. Salzetta, F. Sanches and S. J. Weinberg, *Toward a Holographic Theory for General Spacetimes*, *Phys. Rev.* **D95** (2017) 086002, [1611.02702].

[273] S. B. Giddings, *Quantum-first gravity*, 1803.04973.

[274] Y. Ito, J. Nishimura and A. Tsuchiya, *Power-law expansion of the Universe from the bosonic Lorentzian type IIB matrix model*, *JHEP* **11** (2015) 070, [1506.04795].

[275] T. Hertog and G. T. Horowitz, *Towards a big crunch dual*, *JHEP* **07** (2004) 073, [hep-th/0406134].

[276] S. Antonini and B. Swingle, *Cosmology at the end of the world*, *Nature Phys.* **16** (2020) 881–886, [1907.06667].

[277] M. Van Raamsdonk, *Comments on wormholes, ensembles, and cosmology*, *JHEP* **12** (2021) 156, [2008.02259].

[278] M. Van Raamsdonk, *Cosmology from confinement?*, 2102.05057.

[279] A. May, P. Simidzija and M. Van Raamsdonk, *Negative energy enhancement in layered holographic conformal field theories*, 2103.14046.

[280] B. Freivogel, V. Godet, E. Morvan, J. F. Pedraza and A. Rotundo, *Lessons on eternal traversable wormholes in AdS*, *JHEP* **07** (2019) 122, [1903.05732].

[281] H. Z. Chen, R. C. Myers, D. Neuenfeld, I. A. Reyes and J. Sandor, *Quantum Extremal Islands Made Easy, Part I: Entanglement on the Brane*, *JHEP* **10** (2020) 166, [2006.04851].

[282] G. R. Dvali, G. Gabadadze and M. Porrati, *4-D gravity on a brane in 5-D Minkowski space*, *Phys. Lett. B* **485** (2000) 208–214, [hep-th/0005016].

[283] S. Fallows and S. F. Ross, *Constraints on cosmologies inside black holes*, 2203.02523.

[284] P. Simidzija and M. Van Raamsdonk, *Holo-ween*, *JHEP* **12** (2020) 028, [2006.13943].

[285] I. Akal, Y. Kusuki, T. Takayanagi and Z. Wei, *Codimension two holography for wedges*, *Phys. Rev. D* **102** (2020) 126007, [2007.06800].

[286] S. de Haro, S. N. Solodukhin and K. Skenderis, *Holographic reconstruction of space-time and renormalization in the AdS / CFT correspondence*, *Commun. Math. Phys.* **217** (2001) 595–622, [hep-th/0002230].

[287] A. Almheiri, R. Mahajan, J. Maldacena and Y. Zhao, *The Page curve of Hawking radiation from semiclassical geometry*, *JHEP* **03** (2020) 149, [1908.10996].

[288] H. Z. Chen, R. C. Myers, D. Neuenfeld, I. A. Reyes and J. Sandor, *Quantum Extremal Islands Made Easy, Part II: Black Holes on the Brane*, *JHEP* **12** (2020) 025, [2010.00018].

[289] H. Geng and A. Karch, *Massive islands*, *JHEP* **09** (2020) 121, [2006.02438].

[290] H. Geng, A. Karch, C. Perez-Pardavila, S. Raju, L. Randall, M. Riojas et al., *Information Transfer with a Gravitating Bath*, 2012.04671.

[291] C. F. Uhlemann, *Islands and Page curves in 4d from Type IIB*, 2105.00008.

[292] C. Bachas and I. Lavdas, *Massive Anti-de Sitter Gravity from String Theory*, *JHEP* **11** (2018) 003, [1807.00591].

[293] N. Arkani-Hamed, A. G. Cohen and H. Georgi, *(De)constructing dimensions*, *Phys. Rev. Lett.* **86** (2001) 4757–4761, [hep-th/0104005].

[294] C. Bachas and I. Lavdas, *Quantum Gates to other Universes*, *Fortsch. Phys.* **66** (2018) 1700096, [1711.11372].

[295] C. Bachas and J. Estes, *Spin-2 spectrum of defect theories*, *JHEP* **06** (2011) 005, [1103.2800].

[296] M. Van Raamsdonk and C. Waddell, *Holographic and localization calculations of boundary F for $\mathcal{N}$ = 4 SUSY Yang-Mills theory*, *JHEP* **02** (2021) 222, [2010.14520].

[297] B. Assel, C. Bachas, J. Estes and J. Gomis, *IIB Duals of D=3 N=4 Circular Quivers*, *JHEP* **12** (2012) 044, [1210.2590].

[298] N. Arkani-Hamed, A. G. Cohen, D. B. Kaplan, A. Karch and L. Motl, *Deconstructing (2,0) and little string theories*, *JHEP* **01** (2003) 083, [hep-th/0110146].

[299] D. Marolf and J. Polchinski, *Gauge/Gravity Duality and the Black Hole Interior*, *Phys. Rev. Lett.* **111** (2013) 171301, [1307.4706].

[300] S. L. Braunstein, S. Pirandola and K. Życzkowski, *Better Late than Never: Information Retrieval from Black Holes*, *Phys. Rev. Lett.* **110** (2013) 101301, [0907.1190].

[301] J. M. Maldacena, *Eternal black holes in anti-de Sitter*, *JHEP* **04** (2003) 021, [hep-th/0106112].

[302] M. Van Raamsdonk, *Evaporating Firewalls*, *JHEP* **11** (2014) 038, [1307.1796].

[303] C. Akers, N. Engelhardt and D. Harlow, *Simple holographic models of black hole evaporation*, 1910.00972.

[304] J. V. Rocha, *Evaporation of large black holes in AdS: Coupling to the evaporon*, *JHEP* **08** (2008) 075, [0804.0055].

[305] V. E. Hubeny, M. Rangamani and T. Takayanagi, *A Covariant holographic entanglement entropy proposal*, *JHEP* **07** (2007) 062, [0705.0016].

[306] B. Czech, J. L. Karczmarek, F. Nogueira and M. Van Raamsdonk, *The Gravity Dual of a Density Matrix*, *Class. Quant. Grav.* **29** (2012) 155009, [1204.1330].

[307] M. Headrick, V. E. Hubeny, A. Lawrence and M. Rangamani, *Causality & holographic entanglement entropy*, *JHEP* **12** (2014) 162, [1408.6300].

[308] A. Almheiri, X. Dong and D. Harlow, *Bulk Locality and Quantum Error Correction in AdS/CFT*, *JHEP* **04** (2015) 163, [1411.7041].

[309] X. Dong, D. Harlow and A. C. Wall, *Reconstruction of Bulk Operators within the Entanglement Wedge in Gauge-Gravity Duality*, *Phys. Rev. Lett.* **117** (2016) 021601, [1601.05416].

[310] T. Faulkner and A. Lewkowycz, *Bulk locality from modular flow*, *JHEP* **07** (2017) 151, [1704.05464].

[311] D. N. Page, *Finite upper bound for the Hawking decay time of an arbitrarily large black hole in anti–de Sitter spacetime*, *Phys. Rev.* **D97** (2018) 024004, [1507.02682].

[312] A. Almheiri, R. Mahajan and J. Maldacena, *Islands outside the horizon*, 1910.11077.

[313] Y. C. Ong, *Hawking Evaporation Time Scale of Topological Black Holes in Anti-de Sitter Spacetime*, *Nucl. Phys.* **B903** (2016) 387–399, [1507.07845].

[314] A. Faraji Astaneh and S. N. Solodukhin, *Holographic calculation of boundary terms in conformal anomaly*, *Phys. Lett.* **B769** (2017) 25–33, [1702.00566].

[315] S. Antonini and B. Swingle, *Cosmology at the end of the world*, 1907.06667.

[316] J. Sully, M. Van Raamsdonk and D. Wakeham, "In preparation.".

[317] T. Faulkner, *The Entanglement Renyi Entropies of Disjoint Intervals in AdS/CFT*, 1303.7221.

[318] T. Shimaji, T. Takayanagi and Z. Wei, *Holographic Quantum Circuits from Splitting/Joining Local Quenches*, *JHEP* **03** (2019) 165, [1812.01176].

[319] P. Caputa, T. Numasawa, T. Shimaji, T. Takayanagi and Z. Wei, *Double Local Quenches in 2D CFTs and Gravitational Force*, *JHEP* **09** (2019) 018, [1905.08265].

[320] R. Flauger, V. Gorbenko, A. Joyce, L. McAllister, G. Shiu and E. Silverstein, *Snowmass White Paper: Cosmology at the Theory Frontier*, in *2022 Snowmass Summer Study*, 3, 2022. 2203.07629.

[321] G. Obied, H. Ooguri, L. Spodyneiko and C. Vafa, *De Sitter Space and the Swampland*, 1806.08362.

[322] H. Ooguri, E. Palti, G. Shiu and C. Vafa, *Distance and de Sitter Conjectures on the Swampland*, *Phys. Lett. B* **788** (2019) 180–184, [1810.05506].

[323] S. K. Garg and C. Krishnan, *Bounds on Slow Roll and the de Sitter Swampland*, *JHEP* **11** (2019) 075, [1807.05193].

[324] U. H. Danielsson and T. Van Riet, *What if string theory has no de Sitter vacua?*, *Int. J. Mod. Phys. D* **27** (2018) 1830007, [1804.01120].

[325] T. Faulkner, M. Guica, T. Hartman, R. C. Myers and M. Van Raamsdonk, *Gravitation from Entanglement in Holographic CFTs*, *JHEP* **03** (2014) 051, [1312.7856].

[326] D. Harlow, *The Ryu–Takayanagi Formula from Quantum Error Correction*, *Commun. Math. Phys.* **354** (2017) 865–912, [1607.03901].

[327] D. Marolf, *Chern-Simons terms and the three notions of charge*, in *International Conference on Quantization, Gauge Theory, and Strings: Conference Dedicated to the Memory of Professor Efim Fradkin*, pp. 312–320, 6, 2000. hep-th/0006117.

[328] H. Araki, *Gibbs states of a one dimensional quantum lattice*, *Comm. Math. Phys.* **14** (1969) 120–157.

[329] R.-G. Cai, S.-M. Ruan, S.-J. Wang, R.-Q. Yang and R.-H. Peng, *Action growth for AdS black holes*, *JHEP* **09** (2016) 161, [1606.08307].

[330] E. Poisson, *A relativist's toolkit: the mathematics of black-hole mechanics*. Cambridge university press, 2004.

[331] G. Hayward, *Gravitational action for space-times with nonsmooth boundaries*, *Phys. Rev.* **D47** (1993) 3275–3280.

[332] A. Reynolds and S. F. Ross, *Divergences in Holographic Complexity*, *Class. Quant. Grav.* **34** (2017) 105004, [1612.05439].

[333] K. Parattu, S. Chakraborty, B. R. Majhi and T. Padmanabhan, *A Boundary Term for the Gravitational Action with Null Boundaries*, *Gen. Rel. Grav.* **48** (2016) 94, [1501.01053].

[334] J. Polchinski and E. Silverstein, *Dual Purpose Landscaping Tools: Small Extra Dimensions in AdS/CFT*, 0908.0756.

[335] D. Tsimpis, *Supersymmetric AdS vacua and separation of scales*, *JHEP* **08** (2012) 142, [1206.5900].

[336] F. F. Gautason, M. Schillo, T. Van Riet and M. Williams, *Remarks on scale separation in flux vacua*, *JHEP* **03** (2016) 061, [1512.00457].

[337] L. F. Alday and E. Perlmutter, *Growing Extra Dimensions in AdS/CFT*, *JHEP* **08** (2019) 084, [1906.01477].

Appendix A

Appendices for Chapter 2

A.1 Path integral methods

Path integral methods offer a useful approach to calculations in quantum mechanics and quantum field theory. They play a particularly central role in the AdS/CFT correspondence, since one of the most useful and explicit tools for studying holographic systems makes use of the equivalence of path integrals on two sides of the duality, the GKPW dictionary of (2.100). We provide a brief introduction to how the path integral will be used in this thesis; more detailed information can be found in Appendix A of [102] and Chapters 4 - 6 of [128]. As in the rest of this thesis, we set $\hbar = 1$ throughout.

States and amplitudes

In quantum field theory, a transition amplitude between two field eigenstates $|\phi_1\rangle$, $|\phi_2\rangle$ is obtained by evolving the first state and then projecting onto the second state; an important result is that this is equivalent to a (Lorentzian) path integral

$$\langle \phi_2 | e^{-iHT} | \phi_1 \rangle = \int_{\phi(t=0)=\phi_1}^{\phi(t=T)=\phi_2} \mathcal{D}\phi(t)\, e^{iS_L[\phi(t)]} \,. \tag{A.1}$$

In principle, ϕ may denote a collection of fields. We are implicitly assuming a fixed, static background of the form $\mathbb{R} \times \Sigma_{d-1}$, though generalizations can be made to curved backgrounds.

Similarly, an amplitude with Euclidean evolution by $\beta = iT$ is equivalent

to a Euclidean path integral

$$\langle \phi_2 | e^{-\beta H} | \phi_1 \rangle = \int_{\phi(\tau=0)=\phi_1}^{\phi(\tau=\beta)=\phi_2} \mathcal{D}\phi(\tau)\, e^{-S_E[\phi(\tau)]} \,. \tag{A.2}$$

The latter often has better convergence properties, since the exponential is damped rather than oscillatory off-shell; under sufficient assumptions, including the requirement that the Hamiltonian is bounded from below, one anticipates that these should be related by analytic continuation. We will work exclusively with the Euclidean path integral in the following.

We may define a state of a Lorentzian theory by *slicing* the Euclidean path integral. This means that we perform the Euclidean path integral on a manifold-with-boundary $\mathcal{M}$ whose boundary $\partial\mathcal{M}$ is the surface Σ_{d-1} on which we would like to quantize the Lorentzian theory, leaving the boundary condition open. Formally, this procedure defines a wavefunctional $\Psi[\phi_0]$, which should correspond to a state $|\Psi\rangle$ in the Hilbert space such that $\Psi[\phi_0] = \langle \phi_0 | \Psi \rangle$, via

$$\Psi[\phi_0] = \int^{\phi(\partial\mathcal{M})=\phi_0} \mathcal{D}\phi\, e^{-S_E[\phi]} \,. \tag{A.3}$$

Though $\mathcal{M}$ could be arbitrary, we are typically interested in the case that the Euclidean manifold is Σ_{d-1} times a Euclidean "time" direction, so that we have the interpretation of a state being *prepared* by Euclidean time evolution. The simplest example of such a state prepared by a Euclidean path integral is the (non-normalized) vacuum state, which arises from the semi-infinite path integral (without boundary in the Euclidean past).

Correlation functions and operator insertions

Euclidean correlation functions of local operators are computed via the Euclidean path integral with *operator insertions*

$$\langle O(x_1) \dots O(x_n) \rangle = \int \mathcal{D}\phi\, e^{-S_E[\phi]} O(x_1) \dots O(x_n) \,, \tag{A.4}$$

where $O(x)$ are any local operators built from the fundamental fields ϕ and their derivatives. As is clear from the path integral construction, we

may interpret these correlators as vacuum expectation values of products of operators ordered relative to the choice of quantization. In the operator language, this ordering is important; as an example, if we consider a two-point vacuum correlator

$$\begin{aligned}\langle 0|O_1(\tau_1,x_1)O_2(\tau_2,x_2)|0\rangle \\ = \langle 0|e^{H\tau_1}O_1(0,x_1)e^{-H(\tau_1-\tau_2)}O_2(0,x_2)e^{-H\tau_2}|0\rangle\,, \end{aligned} \quad \text{(A.5)}$$

then having non-time-ordered operators $\tau_1 < \tau_2$ would result in the action of $e^{-H(\tau_1-\tau_2)}$ on the state to its right being ill-defined, assuming that the spectrum of H is unbounded from above.

More general vacuum correlation functions of local operators, including Lorentzian time-ordered or out-of-time-order correlation functions, may be constructed using path integrals whose time-contour includes both Euclidean and Lorentzian sections; these are sometimes called *Schwinger-Keldysh contours*. However, for the purposes of this thesis, Lorentzian correlators of interest will be related to Euclidean correlators directly by analytic continuation $\tau = it$, which is expected to hold under certain technical assumptions.[114]

Operator insertions may also be used in state preparation by a Euclidean path integral. In this construction, the wavefunctional $\Psi[\phi_0]$ is defined by

$$\Psi[\phi_0] = \int^{\phi(\partial\mathcal{M})=\phi_0} \mathcal{D}\phi\, e^{-S_E[\phi]} O_1(x_1)\dots O_n(x_n)\,, \quad \text{(A.6)}$$

where we have inserted operators at specific locations $x_1,\dots,x_n \in \mathcal{M}$.

Operators, density matrices, and the partition function

Euclidean path integrals with two open cuts formally define operators on the Hilbert space. An important example is the un-normalized *thermal density matrix* $\hat{\rho}_\beta = e^{-\beta H}$, which is defined by performing the path integral over

[114] This is the content of the *Osterwalder-Schrader reconstruction theorem.*

Euclidean time β

$$\langle \phi_2 | \hat{\rho}_\beta | \phi_1 \rangle \equiv \int_{\phi(0)=\phi_1}^{\phi(\beta)=\phi_2} \mathcal{D}\phi \, e^{-S_E[\phi]} \, . \tag{A.7}$$

Since the *thermal partition function* $Z(\beta)$ may be computed by taking the trace of this operator, which in the path integral corresponds to identifying the $\tau = 0$ and $\tau = \beta$ surfaces and "sewing them together" by integrating over field configurations on this surface, we deduce that the partition function is calculated by performing the path integral on $S^1_\beta \times \Sigma_{d-1}$

$$Z(\beta) = \int \mathcal{D}\phi_0 \langle \phi_0 | \hat{\rho}_\beta | \phi_0 \rangle = \int_{S^1_\beta \times \Sigma_{d-1}} \mathcal{D}\phi \, e^{-S_E[\phi]} \, . \tag{A.8}$$

Here, S^1_β is a circle of circumference β, sometimes called the *thermal circle*.

More generally, we may define operators on the Hilbert space by Euclidean path integrals with two open cuts that also contain local operator insertions. As for the thermal density matrix, we may also compute traces of these operators by performing the path integral with a periodic identification of the Euclidean time direction.

The thermofield double

Implicit in the above discussion is a notion of conjugation for states in the Hilbert space. This is implemented by an anti-linear map Θ, which can be thought of as a CPT map, relating bras and kets. When visualizing the path integral, the action of this map can be thought of as reversing the orientation of a given boundary condition. For example, we often implicitly illustrate kets as path integrals with a free upper boundary condition, and bras as path integrals with a free lower boundary condition; the inner products then corresponds to "sewing" together these two path integrals at the boundaries with the open boundary conditions.

With this in mind, we claim that the un-normalized *thermofield double*

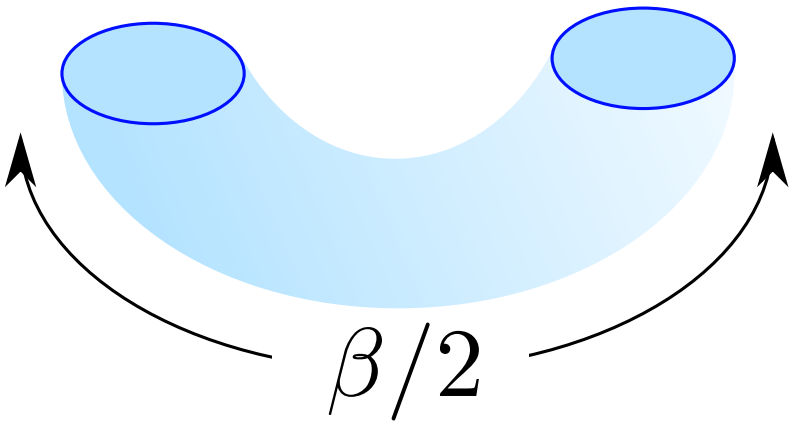

Figure A.1: Path integral construction for the thermofield double state on two copies of S^1.

state on two copies of Σ_{d-1}, namely the state

$$|\mathrm{TFD}_\beta\rangle_{12} \equiv \sum_n e^{-\beta E_n/2}|n\rangle_1|n\rangle_2\,, \tag{A.9}$$

is defined by the path integral shown in Figure A.1, corresponding to an evolution by Euclidean time $\beta/2$ followed by the action of CPT on one of the two boundaries. We can verify this identification by evalutating the inner product with a general field eigenstate tensor product

$$\begin{aligned}(\langle\phi_1|_1 \otimes \langle\phi_2|_2)\,|\text{path integral}\rangle_{12} &= \langle\phi_2|e^{-\beta H/2}|\phi_1^*\rangle \\ &= \sum_n \langle\phi_2|n\rangle\langle n|\phi_1^*\rangle e^{-\beta E_n/2} \\ &= (\langle\phi_1|_1 \otimes \langle\phi_2|_2)\,|\mathrm{TFD}_\beta\rangle_{12}\,,\end{aligned} \tag{A.10}$$

which confirms that the two states are equivalent.

A.2 A CFT primer

In this section, we will clarify some definitions relevant to classical and quantum field theories, and particularly to conformal field theories. We aim

only for internal consistency, and our terminology will necessarily disagree with that found in other references. We will be more pedantic in this section than elsewhere, in order to clearly state and motivate the definition and properties of conformal field theory in the main text. We implicitly work in Euclidean signature for concreteness, though the extension to Lorentzian signature is generally trivial. This section draws on material from [100, 101, 103–105].

Classical field theory: For our purposes, a *classical field theory* will be specified by a Riemannian manifold (M, g), a list of fundamental fields $\{\Phi\}$, and an action functional S which depends on the fields and their derivatives. In practice, one might want to demand that the action S satisfy certain physical assumptions. Under favourable circumstances, one can use these ingredients to define a *statistical field theory* (i.e. a Euclidean quantum field theory) via the path integral.

Diffeomorphism: A *diffeomorphism* is a differentiable bijection $f : M \to N$ between manifolds M, N whose inverse is also differentiable. One can state the definition of a diffeomorphism with any chosen degree of differentiability, making it the natural isomorphism between manifolds with that degree of differentiability.

Coordinate transformation: Given a manifold M with overlapping subsets $U, U' \subseteq M$ and associated coordinate charts $\phi : U \to \mathbb{R}^d$ and $\phi' : U' \to \mathbb{R}^d$, one can define a *coordinate transformation* as the map

$$\phi' \circ \phi^{-1}|_{\phi(U\cap U')} : \phi(U \cap U') \to \phi'(U \cap U') \,. \tag{A.11}$$

In pedestrian terms, this is the map between coordinates in one coordinate chart and another coordinate chart with overlapping domain.

In the following, we will often use the notation

$$x^\mu \to x'^\mu(x) \,, \tag{A.12}$$

or simply $x \to x'(x)$, to denote a coordinate transformation; the x^μ and x'^μ of course denote the coordinates of $\phi(p)$ and $\phi'(p)$ for a given point $p \in M$ in terms of the standard basis of $\mathbb{R}^d$. We recall that tensor components transform under coordinate transformations with suitable factors of the Jacobian $\frac{\partial x'^\mu}{\partial x^\nu}$ or its inverse $\frac{\partial x^\mu}{\partial x'^\nu}$. We often denote the transformed field with a prime, so that for example a vector field transforms under a coordinate transformation as

$$V^\mu(x) \to V'^\mu(x') = \frac{\partial x'^\mu}{\partial x^\nu} V^\nu(x) \,. \tag{A.13}$$

For compactness, we will frequently suppress Lorentz indices in the remainder of this subsection, and denote by $R(x, x')$ the appropriate product of Jacobians required for a coordinate transformation of a tensor $O(x)$ with a given index structure, writing

$$O'(x') = R(x, x')O(x) \,. \tag{A.14}$$

In a statistical field theory, observables like correlation functions should be invariant under coordinate transformations, meaning that

$$\langle O'(x'_1) \dots O'(x'_n) \rangle_{g'} = R(x_1, x'_1) \dots R(x_n, x'_n) \langle O(x_1) \dots O(x_n) \rangle_g \,. \tag{A.15}$$

The underlying metric $ds^2 = g_{\mu\nu} dx^\mu dx^\nu = g'_{\mu\nu} dx'^\mu dx'^\nu$ is of course fixed.

Strictly speaking, a diffeomorphism is not a coordinate transformation; the two objects have different definitions, and in particular the definition of a diffeomorphism entails two possibly different manifolds (which could have different geometry in the Riemannian case). A diffeomorphism can in principle be used to define a coordinate transformation, since a diffeomorphism $f : M \to N$ composed with a coordinate chart $\phi : W \to \mathbb{R}^d$ with $W \subseteq N$ naturally defines a coordinate chart on the manifold M via the pullback $\phi \circ f : f^{-1}(W) \to \mathbb{R}^d$. On the other hand, a change of coordinates is locally defined with respect to a single coordinate chart, and there is no general procedure for reconstructing a diffeomorphism from a manifold M to itself

given a change of coordinates on M.

Nonetheless, given a coordinate chart $\phi : U \to \mathbb{R}^d$ with $U \subseteq M$, new coordinate charts $\phi' : U \to \mathbb{R}^d$ with the same image $\phi(U) = \phi'(U)$ are in one-to-one correspondence with diffeomorphisms $f : U \to U$ via

$$\phi' = \phi \circ f \,. \tag{A.16}$$

One can think of this diffeomorphism as actively implementing the change of coordinates; for example, the coordinate change $x' = (x+y)/\sqrt{2}, y' = (x-y)/\sqrt{2}$ on $\mathbb{R}^2$ can be implemented in this way by a diffeomorphism which rotates the plane clockwise by 45°. This correspondence is the rationale for referring to coordinate transformations and diffeomorphisms of $\mathbb{R}^d$ interchangeably.

Isometry: Given two Riemannian manifolds (M, g) and (N, h), an *isometry* is a diffeomorphism $f : M \to N$ such that $g = f^*h$, where f^* denotes the pullback. In local coordinates, the definition of an isometry implies

$$g_{\mu\nu}(x) = \frac{\partial x'^{\rho}}{\partial x^{\mu}} \frac{\partial x'^{\sigma}}{\partial x^{\nu}} h_{\rho\sigma}(x') \,. \tag{A.17}$$

We are often interested in considering the isometries from a manifold (M, g) to itself, namely those diffeomorphisms $f : M \to M$ satisfying $g = f^*g$. Defining a coordinate transformation via $\phi' = \phi \circ f$, this condition becomes

$$g_{\mu\nu}(x) = \frac{\partial x'^{\rho}}{\partial x^{\mu}} \frac{\partial x'^{\sigma}}{\partial x^{\nu}} g_{\rho\sigma}(x') \,, \tag{A.18}$$

or, multiplying by the inverse Jacobians, using that g transforms as a tensor, and relabelling x' as x,

$$g'_{\mu\nu}(x) = g_{\mu\nu}(x) \,. \tag{A.19}$$

An important example is the group of isometries from the Euclidean plane $\mathbb{R}^d$ to itself, which form the d-dimensional Euclidean group.

Symmetry: We will take the term *symmetry* to refer to a transforma-

tion of the dynamical fields in a theory, rather than the coordinates or any background fields (like the metric or other sources) that might be present, under which the action is invariant. This may include spacetime symmetries, which may reflect isometries of the manifold; however, we can always express symmetries, including spacetime symmetries, as pure field transformations, and whether or not a transformation is a symmetry is always dependent on the theory, not just the structure of the base space. For example, we could always ensure that the isometries of the base manifold are not realized as symmetries of the theory by adding position-dependent sources to the action.

When the coordinate transformation $x \to x'$ induced by an isometry from a manifold to itself is a genuine symmetry of a theory, then the correlators in the statistical field theory satisfy

$$\langle O'(x_1) \dots O'(x_n) \rangle_g = \langle O(x_1) \dots O(x_n) \rangle_g \, ; \tag{A.20}$$

this expression is more than a statement about covariance under coordinate transformations, instead representing a non-trivial equality between distinct correlators in the theory. Of course, the path integral measure must also be invariant under the symmetry for this equality to hold.

Conformal isometry: Given two Riemannian manifolds (M, g) and (N, h), a *conformal isometry* (sometimes called a *conformal diffeomorphism*) is a diffeomorphism $f : M \to N$ such that $\Omega^2 g = f^* h$, with $\Omega : M \to \mathbb{R}_+$. The function Ω is sometimes called a conformal factor. In local coordinates, this implies

$$\Omega^2(x) g_{\mu\nu}(x) = \frac{\partial x'^{\rho}}{\partial x^{\mu}} \frac{\partial x'^{\sigma}}{\partial x^{\nu}} h_{\mu\nu}(x') \, . \tag{A.21}$$

We are often interested in considering conformal isometries from a manifold (M, g) to itself, namely those diffeomorphisms $f : M \to M$ satisfying $\Omega^2 g = f^* g$. With analogous manipulations to the case of isometries, one

can write

$$g'_{\mu\nu}(x) = \omega^{-2}(x) g_{\mu\nu}(x) \,, \qquad \omega^2(x') = \Omega^2(x) \,. \tag{A.22}$$

An important example is the group of conformal isometries from the Euclidean plane $\mathbb{R}^d$ to itself, which form the Euclidean conformal group $SO(1, d+1)$.

Weyl transformation: In field theory, a *Weyl transformation* is a position-dependent rescaling of the fields, including the metric, which *does not* change the coordinates. One typically chooses a spacetime-dependent Weyl factor $\Omega(x)$, and posits that the various fundamental fields are *primaries* of scaling dimension Δ, meaning that they transform under a Weyl transformation as

$$\phi(x) \to \Omega(x)^{-\Delta} \phi(x) \,. \tag{A.23}$$

One is often interested in geometrical Weyl transformations, where the background metric transforms as $g_{\mu\nu}(x) \to \Omega^2(x) g_{\mu\nu}(x)$; evidently, such a transformation naïvely changes the geometry, but preserves angles.

Although a Weyl transformation does not meet our definition of a symmetry when it changes the background metric, it may be the case that the action (and path integral measure) are invariant under such transformations; in this case, we have a non-trivial relation between correlators on the two different backgrounds related by the Weyl transformation

$$\langle O_1(x_1) \dots O_n(x_n) \rangle_{\Omega^2 g} = \Omega^{-\Delta_1}(x_1) \dots \Omega^{-\Delta_n}(x_n) \langle O_1(x_1) \dots O_n(x_n) \rangle_g \,. \tag{A.24}$$

Conformal transformation: We define a *conformal transformation* in a field theory to be a conformal isometry, which results in a pointwise rescaling $g_{\mu\nu} \to \omega^{-2} g_{\mu\nu}$, composed with a Weyl rescaling with Weyl factor ω to pointwise restore the original metric. Conformal transformations are consequently transformations on a theory with a fixed background, which act on

primary fields of conformal dimension Δ and general tensor structure as

$$O'(x') = \omega(x)^{-\Delta} R(x, x') O(x) \,, \quad \omega(x) = \left| \frac{\partial x'}{\partial x} \right|^{1/d} . \tag{A.25}$$

Note that a conformal isometry generally has Jacobian $\frac{\partial x'^{\mu}}{\partial x^{\nu}} = \omega(x) S^{\mu}_{\nu}(x)$ with $S^{\mu}_{\nu} \in SO(d)$.

A *(classical) conformal field theory* is a theory whose action is invariant under conformal transformations, namely a theory with conformal symmetry. The correlators of primary fields in the corresponding statistical field theory satisfy

$$\langle O'(x_1) \dots O'(x_n) \rangle_g = \langle O(x_1) \dots O(x_n) \rangle_g \,, \tag{A.26}$$

where $O'(x')$ for a conformal transformation is defined as above.

Given that a field theory is necessarily invariant under conformal isometries, since these are merely diffeomorphisms, conformal invariance can also be viewed as a statement about invariance under a restricted class of Weyl transformations, namely those which can arise from conformal isometries of a given manifold. This implies that a conformally invariant theory has a non-trivial relationship between correlators on two different backgrounds,

$$\langle O(x_1) \dots O(x_n) \rangle_{\Omega^2 g} = \langle O'(x'_1) \dots O'(x'_n) \rangle_g \,, \quad \Omega = |\partial x' / \partial x|^{1/d} \,. \tag{A.27}$$

Appendix B

Appendices for Chapter 3

B.1 AdS/CFT correspondence: conventions

We here establish various formulae relevant to type IIB string theory. The Planck scale and string scale are related by

$$\ell_p = g^{\frac{1}{4}} \ell_s \ , \tag{B.1}$$

where g is the string coupling and ℓ_s is defined in terms of the string tension $\frac{1}{2\pi\alpha'}$ by

$$\alpha' = \ell_s^2 \ . \tag{B.2}$$

The ten-dimensional Newton constant is defined as

$$G = 8\pi^6 g^2 \ell_s^8 \ . \tag{B.3}$$

In the AdS/CFT correspondence relating $U(N)$ $\mathcal{N} = 4$ SYM theory to type IIB string theory on $\mathrm{AdS}_5 \times S^5$, we have that the AdS radius in string frame is related to the rank of the gauge group by

$$(L_{\mathrm{AdS}}^{(\mathrm{SF})})^4 = 4\pi g N \ell_s^4 \ . \tag{B.4}$$

If we make the transformation $g_{\mu\nu} \to e^{-\Phi/2} g_{\mu\nu}$ to Einstein frame, including the asymptotic value of the dilaton $g = e^{\Phi_\infty}$ in Φ, this becomes

$$L_{\mathrm{AdS}}^4 = 4\pi N \ell_s^4 \ . \tag{B.5}$$

In this case, we should use $G = 8\pi^6 \ell_s^8$ for the Newton constant. The string coupling (equal to the asymptotic value of e^{Φ} where Φ is the dilaton) is

related to the Yang-Mills coupling by

$$4\pi g = g_{YM}^2 \ . \tag{B.6}$$

The 't Hooft coupling is

$$\lambda = g_{YM}^2 N \ . \tag{B.7}$$

To evaluate the number of units of quantized 3-form flux through a sphere, we use

$$N_{D5} = \frac{1}{4\pi^2 \ell_s^2} \int_{S^3} F_3 \tag{B.8}$$

and

$$N_{NS5} = \frac{1}{4\pi^2 \ell_s^2} \int_{S^3} H_3 \tag{B.9}$$

where F_3 and H_3 are the R-R and NS-NS three-form field strengths. In the absence of three-form fields, the number of units of five-form flux through a five-sphere is given by

$$N_{D3} = \frac{1}{16\pi^4 \ell_s^4} \int_{S^5} F_5 \ . \tag{B.10}$$

The analysis of five-form fluxes and their relation to D3-brane charges is more subtle when three-form fields are present (as they are in the solutions we consider). See [174, 327] or [175] for a detailed discussion.

B.2 Supergravity solutions: form fields

In this appendix, we review for completeness the gauge fields in the supergravity solutions, following the conventions of [175].

The form fields are again expressed in terms of the harmonic functions h_i together with the harmonic duals h_i^D defined so that

$$\begin{aligned} \mathcal{A}_1 &= \frac{1}{2}(h_1^D + i h_1) \\ \mathcal{A}_2 &= \frac{1}{2}(h_2 - i h_2^D) \end{aligned}$$

are holomorphic. The ambiguity in choosing h_i^D corresponds to gauge freedom in defining the potentials for the form fields.

The NS-NS 3-form field strength H_3 and the R-R 3-form field strength F_3 take the form

$$H_3 = \omega^{45} \wedge db_1 \qquad\qquad F_3 = \omega^{67} \wedge db_2 \tag{B.11}$$

where ω^{45} and ω^{67} are volume forms on the first and second unit-radius S^2s. The real functions b_i are defined in terms of the harmonic functions by

$$b_1 = 2h_2^D + 2h_1^2 h_2 \frac{X}{N_1} , \qquad b_2 = -2h_1^D + 2h_1 h_2^2 \frac{X}{N_2} , \tag{B.12}$$

where

$$X \equiv i \left(\partial_w h_1 \partial_{\bar{w}} h_2 - \partial_w h_2 \partial_{\bar{w}} h_1\right) . \tag{B.13}$$

The fiveform field strength can be expressed as

$$F_5 = -4 f_4^4 \omega^{0123} \wedge \mathcal{F} + 4 f_1^2 f_2^2 \omega^{45} \wedge \omega^{67} \wedge (*_2 \mathcal{F}) . \tag{B.14}$$

Here, ω^{0123} is the volume form on the unit-radius AdS_4, $\mathcal{F}$ is a one-form on Σ, and $*_2$ denotes Poincar'e duality with respect to the metric on Σ.

We have that

$$f_4^4 \mathcal{F} = dj_1 \tag{B.15}$$

where

$$\begin{aligned} j_1 &= 3\mathcal{C} + 3\bar{\mathcal{C}} - 3\mathcal{D} + \frac{h_1 h_2 X}{W} \\ \partial_w \mathcal{C} &= \mathcal{A}_1 \partial_w \mathcal{A}_2 - \mathcal{A}_2 \partial_w \mathcal{A}_1 \\ \mathcal{D} &= \bar{\mathcal{A}}_1 \mathcal{A}_2 + \mathcal{A}_1 \bar{\mathcal{A}}_2 . \end{aligned}$$

So far, we have assumed that the R-R zero-form potential vanishes, but more general solutions with non-vanishing axion can be obtained using the $SL(2,\mathbb{R})$ symmetry of type IIB supergravity.

B.3 Regularization of the area integrals

In this appendix we explain in detail the regularization procedure used in computing boundary F via the RT formula. Given the metric dual to one of the BCFTs, we can redefine coordinates to place the metric in Fefferman-Graham form

$$ds^2 = \frac{L^2}{z^2}(dz^2 + dx_\perp^2 - dt^2 + d\vec{x}^2) + d\Omega_5^2 + \mathcal{O}(z^2) \tag{B.16}$$

where the correction terms do not involve dz. We then compute the area of the $z > \epsilon$ portion of the RT surface for a half-ball region of radius R centered on the BCFT boundary, and subtract half the area of the RT surface for a ball of radius R in $\mathcal{N} = 4$ SYM theory.

Regulated area in the BCFT duals

To calculate the regulated area of the extremal surface corresponding to a half ball in one of our BCFT duals, we need to understand where the cutoff surface $z = \epsilon$ lies in the coordinates we are using. Representing the AdS_4 metric as

$$\begin{aligned} ds^2_{\mathrm{AdS}_4} &= \frac{1}{u^2}(-dt^2 + du^2 + d\vec{x}^2) \\ &= \frac{1}{\rho^2 \cos^2\theta_P}(-dt^2 + d\rho^2 + \rho^2 d\theta_P^2 + \rho^2 \sin^2\theta_P d\phi^2)\,, \end{aligned} \tag{B.17}$$

we will have that the cutoff surface lies at some $u_{min}(r, \theta)$. In the full metric, this AdS_4 slice enters as

$$ds^2 = f_4^2(\frac{1}{u^2}(-dt^2 + du^2 + d\vec{x}^2)) + \dots \tag{B.18}$$

Converting to Fefferman-Graham coordinates, this will become asymptotically

$$ds^2 = \frac{L^2}{z^2}(dz^2 + dx_\perp^2 - dt^2 + d\vec{x}^2) + \dots \tag{B.19}$$

where z and $x_\perp$ are determined in terms of the other coordinates, and $L_{\rm AdS}$ is the asymptotic AdS curvature scale that will be determined in terms of the parameters appearing in the metric. Thus, asymptotically, we must have that

$$\frac{f_4^2}{u^2} = \frac{L_{\rm AdS}^2}{z^2} \ . \tag{B.20}$$

This allows us to fix the cutoff surface as

$$u_{min}(r,\theta) = \frac{\epsilon}{L_{\rm AdS}} f_4(r,\theta) \ . \tag{B.21}$$

The locus of the extremal surface in each AdS_4 slice is $\rho^2 = u^2+x^2+y^2 = R^2$, and the two-dimensional area of the portion of this surface inside the cutoff is

$$\int_0^{\cos^{-1}(\frac{u_{min}}{R})} d\theta \frac{2\pi \sin\theta}{\cos^2\theta} = 2\pi \left(\frac{R}{u_{min}} - 1\right) \ . \tag{B.22}$$

Using this, we find that the regulated eight-dimensional area of the extremal surface is given by

$$\begin{aligned} \text{Area} &= 128\pi^3 \int_0^{u_{min}(r,\theta)=R} r dr d\theta \rho^2 f_1^2 f_2^2 f_4^2 \left(\frac{R}{u_{min}(r,\theta)} - 1\right) \\ &= -1024\pi^3 \int_0^{f_4(r,\theta)=RL_{\rm AdS}/\epsilon} r dr d\theta \, h_1 h_2 \\ &\qquad \times \partial_w \partial_{\bar{w}} (h_1 h_2) \left(\frac{RL_{\rm AdS}}{\epsilon f_4(r,\theta)} - 1\right) \ . \end{aligned} \tag{B.23}$$

From this expression, we need to subtract off half the area of the extremal surface corresponding to a ball in the parent $\mathcal{N} = 4$ SYM theory. The area to be subtracted off can be expressed in a similar way to (B.23) by taking h_1 and h_2 to be the expressions (3.30) relevant to pure AdS. Since we would like to subtract off half of the regulated area of the extremal surface in pure AdS, we can keep only the part for $x_\perp \leq 0$ in Fefferman-Graham coordinates, which translates to the part with $r \geq r_0$ in the coordinates we are using.

Thus, the regulated half-hemisphere area is

$$\frac{1}{2}\text{Area}_{\text{AdS}} = -1024\pi^3 \int_{r_0}^{f_4^{\text{AdS}}(r,\theta)\leq RL_{\text{AdS}}/\epsilon} r dr d\theta \, h_1^{\text{AdS}} h_2^{\text{AdS}} \times \partial_w \partial_{\bar{w}} (h_1^{\text{AdS}} h_2^{\text{AdS}}) \left(\frac{RL_{\text{AdS}}}{\epsilon f_4^{\text{AdS}}(r,\theta)} - 1 \right) . \quad \text{(B.24)}$$

Details of the subtraction

In order to evaluate the integrals, it is convenient to split the integration domain into a part with $r \in [0, \Lambda]$ and an asymptotic part $\{r \geq \Lambda, f_4(r,\theta) \leq RL_{\text{AdS}}/\epsilon\}$, for some large Λ that we will take to infinity as $\epsilon \to 0$.

For the first part,

$$-1024\pi^3 \int_0^{\Lambda} dr \int_0^{\frac{\pi}{2}} d\theta \, r h_1 h_2 \partial_w \partial_{\bar{w}} (h_1 h_2) \left(\frac{RL_{\text{AdS}}}{\epsilon f_4(r,\theta)} - 1 \right) , \quad \text{(B.25)}$$

the first term does not contribute to the final result since it gives an R/ϵ term that is eliminated by the derivative in the definition (3.4,3.7,3.8) of boundary F. Thus, this part of the integral gives a contribution to boundary F of

$$F_1 = -\frac{256\pi^3}{G} \int_0^{\Lambda} dr \int_0^{\frac{\pi}{2}} d\theta \, r h_1 h_2 \partial_w \partial_{\bar{w}} (h_1 h_2) . \quad \text{(B.26)}$$

From this, we subtract off the corresponding integral for pure AdS, so we have a contribution

$$F_2 = \frac{256\pi^3}{G} \int_{r_0}^{\Lambda} dr \int_0^{\frac{\pi}{2}} d\theta \, r h_1^{\text{AdS}} h_2^{\text{AdS}} \partial_w \partial_{\bar{w}} (h_1^{\text{AdS}} h_2^{\text{AdS}}) . \quad \text{(B.27)}$$

To evaluate the asymptotic part of the integral (i.e the region with $r > \Lambda$), we use that the asymptotic form of f_4 in the general solution is

$$f_4(r,\theta) = Ar + B(\theta)\frac{1}{r} + \mathcal{O}(1/r^2) , \quad \text{(B.28)}$$

while the asymptotic form of the integrand is

$$I(r,\theta) = I_1(\theta) r + I_2(\theta)\frac{1}{r} + \mathcal{O}(1/r^2)\,. \tag{B.29}$$

Then the integral in the asymptotic region takes the form

$$\int_0^{\frac{\pi}{2}} d\theta \int_{\Lambda}^{\frac{RL_{\rm AdS}}{\epsilon A} - \frac{B(\theta)\epsilon}{RL_{\rm AdS}} + \dots} dr \left[I_1(\theta) r + I_2(\theta)\frac{1}{r} + \dots \right] \times \left[\frac{RL_{\rm AdS}}{\epsilon A r} - 1 + \dots \right], \tag{B.30}$$

where the omitted terms give contributions that vanish in the limit $\epsilon \to 0$ and $\Lambda \to \infty$. Evaluating the integral for the remaining terms gives

$$\int_0^{\frac{\pi}{2}} d\theta \left[\frac{R^2 L_{\rm AdS}^2}{2\epsilon^2 A^2} I_1(\theta) - \frac{RL_{\rm AdS}\Lambda}{\epsilon} I_1(\theta) + \frac{1}{2} I_1(\theta)\Lambda^2 - I_2(\theta) \ln\left(\frac{RL_{\rm AdS}}{\epsilon A \Lambda}\right) + \dots \right]. \tag{B.31}$$

Now, we can check that A, $I_1(\theta)$ and $\int d\theta I_2(\theta)$ all give the same results for the general solution and for the pure AdS case with the corresponding $L_{\rm AdS}$ and r_0. Thus, when we perform the subtraction, there are no terms that contribute from this $r > \Lambda$ region in the limits $\epsilon \to 0$ and $\Lambda \to \infty$.

To summarize, our final result is that boundary F is given by the $\Lambda \to \infty$ limit of the sum of the two contributions (B.26) and (B.27),

$$F_\partial = -\lim_{\Lambda\to\infty} \frac{256\pi^3}{G} \Big\{ \int_0^{\Lambda} dr \int_0^{\frac{\pi}{2}} d\theta r h_1 h_2 \partial_w \partial_{\bar{w}} (h_1 h_2) - \int_{r_0}^{\Lambda} dr \int_0^{\frac{\pi}{2}} d\theta r h_1^{AdS} h_2^{AdS} \partial_w \partial_{\bar{w}} (h_1^{AdS} h_2^{AdS}) \Big\}. \tag{B.32}$$

B.4 Verification of field theory constraints for linking numbers

In this appendix, we show that for any linking numbers defined in terms of supergravity parameters as in (3.44), the field theory constraints on linking numbers that (3.21) are positive are automatically satisfied.

For this appendix, we define M_n to be the number of D5-branes with linking number $\tilde{L} = n - N_{NS5}$, where $1 \leq n < N_{NS5}$. We will also let the indices on the linking numbers $\{\tilde{L}_i, K_i\}$ refer to the i^{th} 5-brane, rather than the i^{th} 5-brane stack.

We will prove that for linking numbers violating the inequalities

$$\sum_{n=1}^{j-1}(j-n)M_n < \sum_{i=1}^{j} K_i \,, \qquad j \in \{1, 2, \ldots, N_{NS5}\} \,, \tag{B.33}$$

i.e. for which not all of the quantities (3.21) are positive, there is no set of supergravity parameters that can give rise to these linking numbers via (3.44).

We see immediately that if we define index subset

$$\mathcal{I} \equiv \{i \,:\, \tilde{L}_i > 0\} \,, \tag{B.34}$$

then violating the final inequality

$$\sum_{n=1}^{N_{NS5}-1}(N_{NS5}-n)M_n < \sum_{i=1}^{N_{NS5}} K_i \,, \tag{B.35}$$

which can be written as

$$-\sum_{i\notin\mathcal{I}} \tilde{L}_i < \sum_i K_i \,, \tag{B.36}$$

implies

$$N = \sum_{i\in\mathcal{I}} \tilde{L}_i + \sum_{i\notin\mathcal{I}} \tilde{L}_i + \sum_i K_i \leq \sum_{i\in\mathcal{I}} \tilde{L}_i \,, \tag{B.37}$$

and therefore

$$N = \left(\sum_{i\notin\mathcal{I}} \hat{l}_i + \sum_i \hat{k}_i\right) + \sum_{i\in\mathcal{I}} \hat{l}_i > \sum_{i\in\mathcal{I}} \hat{l}_i \geq \sum_{i\in\mathcal{I}} \tilde{L}_i \geq N\,, \tag{B.38}$$

a contradiction, implying that the system of equations has no solution. Here, we have used that $\hat{l}_i, \hat{k}_i > 0$ and

$$\tilde{L}_i = \hat{l}_i - \frac{2}{\pi}\sum_j \arctan\left(\frac{g\hat{k}_j}{\hat{l}_i}\right) \leq \hat{l}_i\,. \tag{B.39}$$

We would like to check that violating the other inequalities similarly leads to a system with no solutions. We restrict to the case that $K_1 > 0$, i.e. the first of the inequalities in (B.33) is always satisfied; this is because we are interested in configurations which will correspond to theories with boundaries rather than interfaces. Moreover, we may restrict to the case that the last of the inequalities is satisfied, since we have already shown that violating this inequality leads to an insoluble system. To this end, let us fix arbitrary $N_{NS5} \geq 3$; our task is to show that violating the inequality in (B.33) indexed by $j \in \{2, \ldots, N_{NS5} - 1\}$ leads to a contradiction in our system of equations defining the supergravity parameters. This system is constituted by the relations

$$\begin{aligned} \hat{k}_i &= K_i - \frac{2}{\pi}\sum_j \arctan\left(\frac{g\hat{k}_i}{\hat{l}_j}\right)\,, \\ \hat{l}_i &= \tilde{L}_i + \frac{2}{\pi}\sum_j \arctan\left(\frac{g\hat{k}_j}{\hat{l}_i}\right)\,, \end{aligned} \tag{B.40}$$

which in particular furnish inequalities

$$K_i > \frac{2}{\pi}\sum_j \arctan\left(\frac{g\hat{k}_i}{\hat{l}_j}\right)\,, \qquad \tilde{L}_i > -\frac{2}{\pi}\sum_j \arctan\left(\frac{g\hat{k}_j}{\hat{l}_i}\right)\,. \tag{B.41}$$

First, suppose that we violate the inequality indexed by $j = 2$; that is,

suppose

$$K_1 + K_2 \leq M_1 \,. \tag{B.42}$$

We may assume $M_1 > 0$ without loss of generality, so that $\tilde{L}_1 = \ldots = \tilde{L}_{M_1} = -(N_{NS5} - 1)$, and in particular $N_{D5} > 0$; otherwise, $M_1 \leq 0$ and $K_1 + K_2 \leq M_1$ would imply $K_2 < 0$, which is incompatible with (B.40) and the assumption that $\hat{k}_A, \hat{l}_A$ are positive. But since

$$\frac{\pi}{2} K_i > \sum_j \arctan\left(\frac{g\hat{k}_i}{\hat{l}_j}\right) \,, \qquad \frac{\pi}{2}\tilde{L}_1 > -\sum_B \arctan\left(\frac{g\hat{k}_j}{\hat{l}_i}\right) \tag{B.43}$$

by (B.40), we find

$$\begin{aligned} \sum_{j=1}^{M_1} \sum_{i\geq 3} \arctan\left(\frac{g\hat{k}_i}{\hat{l}_j}\right) &> \sum_{j=1}^{M_1} \left(-\frac{\pi}{2}\tilde{L}_j - \arctan\left(\frac{g\hat{k}_1}{\hat{l}_j}\right) - \arctan\left(\frac{g\hat{k}_2}{\hat{l}_j}\right)\right) \\ &> \frac{\pi}{2}\left((N_{NS5} - 1)M_1 - K_1 - K_2\right) \\ &\geq \frac{\pi}{2}(N_{NS5} - 2)M_1 \,, \end{aligned} \tag{B.44}$$

contradicting the bound $\arctan(x) < \frac{\pi}{2}$.

More generally, suppose that we violate the inequality indexed by $j \in \{2, \ldots, N_{NS5} - 1\}$; that is, suppose that we have

$$\sum_{i=1}^{j} K_i \leq \sum_{n=1}^{j-1} (j - n) M_n \,. \tag{B.45}$$

We may assume that at least one of $M_1, \ldots, M_{j-1}$ is positive (since otherwise

at least one of the K_i would be negative). Then, letting $M \equiv M_1 + \ldots + M_{j-1}$,

$$\begin{aligned}\sum_{i>j}\sum_{m=1}^{M} \arctan\left(\frac{g\hat{k}_i}{\hat{l}_m}\right) &> -\frac{\pi}{2}\sum_{m=1}^{M}\tilde{L}_m - \sum_{i=1}^{j}\sum_{m=1}^{M}\arctan\left(\frac{g\hat{k}_i}{\hat{l}_m}\right) \\ &> \frac{\pi}{2}\left(\sum_{n=1}^{j-1}(N_{NS5}-n)M_n - \sum_{i=1}^{j}K_i\right) \\ &\geq \frac{\pi}{2}(N_{NS5}-j)\sum_{n=1}^{j-1}M_n = \frac{\pi}{2}(N_{NS5}-j)M\,,\end{aligned} \tag{B.46}$$

again contradicting $\arctan(x) < \frac{\pi}{2}$. This demonstrates our original claim.

B.5 Corrections to the supergravity approximation

In this appendix, we estimate the size of the corrections to the supergravity result, following the procedure outlined at the end of Section 3.4.

B.5.1 Estimating the corrections

Recall that our solutions are generated by the harmonic functions in (3.36), determined by positive real constants l_A, k_B. These can be combined to define *Einstein frame* metric functions and dilaton field, using (3.26), (3.27), (3.28) in Section 3.3.1; to transform to the *string frame*, we should multiply all of the metric functions by $e^{\phi} \equiv e^{\Phi/2}$. We begin by determining the string frame Ricci curvature and dilaton field in the vicinity of a D5-brane or NS5-brane stack. It will be useful to define

$$\begin{aligned}\gamma_C &\equiv \pi + 2\sum_B \frac{d_B k_B}{l_C^2 + k_B^2} = \frac{\pi}{c_C}\frac{d}{dl_C}N_{D3}^{(C)} \\ \delta_D &\equiv \pi + 2\sum_A \frac{c_A l_A}{k_D^2 + l_A^2} = \frac{\pi}{d_D}\frac{d}{dk_D}N_{D3}^{(D)}\,;\end{aligned} \tag{B.47}$$

note that in the case with only D5-branes one has $\gamma_C = \pi$, and in the case with only NS5-branes one has $\delta_D = \pi$.

First, we consider the vicinity of the D5-stack at $(x, y) = (l_C, 0)$, and let L_0 denote the distance in the first quadrant Σ from l_C to the nearest 5-brane stack (or the origin), namely

$$L_0 \equiv \min_{A,B\neq C}\{|l_A - l_C|, \sqrt{k_B^2 + l_C^2}, l_C\}\,. \tag{B.48}$$

Using polar coordinates $(x, y) = (l_C + r\cos\theta, r\sin\theta)$, we therefore have the expansion

$$\begin{aligned} h_1 &= \frac{\pi\ell_s^2}{2}\frac{1}{\sqrt{g}}\Big[-\frac{c_C}{2\pi}\ln(r^2/4l_C^2) + \left(l_C + \sum_{A\neq C}\frac{c_A}{2\pi}\ln\left(\frac{(l_C+l_A)^2}{(l_C-l_A)^2}\right)\right) \\ &\qquad + r\cos\theta\left(1 + \frac{c_C}{2\pi l_C} - \frac{2}{\pi}\sum_A \frac{c_A l_A}{(l_C^2 - l_A^2)}\right) + \mathcal{O}(r^2/L_0^2)\Big] \\ h_2 &= \frac{\pi\ell_s^2}{2}\sqrt{g}\Bigg[r\sin\theta\left(1 + \frac{2}{\pi}\sum_B \frac{d_B k_B}{(l_C^2 + k_B^2)}\right) \\ &\qquad + r^2\sin\theta\cos\theta\left(-\frac{4l_C}{\pi}\sum_B \frac{d_B k_B}{(l_C^2 + k_B^2)^2}\right) + \mathcal{O}(r^3/L_0^3)\Bigg]\,. \end{aligned} \tag{B.49}$$

We therefore have string frame metric functions given at leading order in r/L_0 by

$$\begin{aligned} \rho^2 &= \frac{\sqrt{2g}\gamma_C\ell_{\rm s}^2}{4}\frac{1}{r\ln(4l_C^2/r^2)^{1/2}}\,, \quad f_4^2 = \frac{\sqrt{2g}\gamma_C\ell_{\rm s}^2}{2}\,r\ln(4l_C^2/r^2)^{1/2}\,, \\ f_1^2 &= \frac{\sqrt{2g}\gamma_C\ell_{\rm s}^2}{2}\,r\ln(4l_C^2/r^2)^{1/2}\,, \quad f_2^2 = \sqrt{2g}\gamma_C\ell_{\rm s}^2\frac{r\sin^2\theta}{\ln(4l_C^2/r^2)^{1/2}}\,, \end{aligned} \tag{B.50}$$

and dilaton

$$e^{2\phi} = \frac{\sqrt{2}g\gamma_C}{c_C}\frac{r}{\sqrt{\ln(4l_C^2/r^2)}}\,. \tag{B.51}$$

We thereby deduce string frame Ricci scalar at leading order

$$\alpha' R = -\frac{6}{\gamma_C r}\sqrt{\frac{2}{g}\ln(4l_C^2/r^2)}\,. \tag{B.52}$$

We can perform a similar analysis near an NS5-brane stack at $(x, y) = (0, k_D)$, for which we find dilaton and Ricci scalar

$$e^{2\phi} = \frac{g d_D}{\sqrt{2}\delta_D} \frac{\ln(4k_D^2/r^2)^{1/2}}{r} , \qquad \alpha' R = \frac{6}{\sqrt{g} d_D} \tag{B.53}$$

at leading order.

The above expressions tell us the minimum radius $r_{\max}$ past which the correction terms appearing in the effective action should be suppressed. Evidently, for the D5-brane stacks, the divergence of the string frame curvature implies that we are only justified in ignoring corrections in the region $r \gg r_{\max}$ with

$$r_{\max} \sim \frac{1}{\sqrt{g}\gamma_C} \sqrt{W(g l_C^2 \gamma_C^2)} , \tag{B.54}$$

where $W(\cdot)$ denotes the Lambert W-function, and we suppress order one numerical factors. The contribution to F_∂ from the complementary region is

$$\int_{0<r<r_{\max}} r dr d\theta \, \hat{h}_1 \hat{h}_2 \partial\bar{\partial}(\hat{h}_1 \hat{h}_2) \sim c_C^2 \gamma_C^2 r_{\max}^2 \ln(4 l_C^2 / r_{\max}^2) . \tag{B.55}$$

For the NS5-brane stacks, we see that the curvature corrections will be suppressed provided we take $N_{NS5}^{(D)} \gg 1$, but will be large *throughout* the region $r \ll L_0$ otherwise; evaluating the contribution to F_∂ from a region within $r_{\max} \sim L_0$ gives

$$\int_{0<r<r_{\max}} r dr d\theta \, \hat{h}_1 \hat{h}_2 \partial\bar{\partial}(\hat{h}_1 \hat{h}_2) \sim d_D^2 \delta_D^2 L_0^2 \ln(4 k_D^2 / L_0^2) . \tag{B.56}$$

Meanwhile, the string loop corrections are small outside the region

$$r_{\max} \sim \frac{g d_D}{\delta_D} \sqrt{W\left(\frac{\delta_D^2 k_D^2}{g^2 d_D^2}\right)} , \tag{B.57}$$

and the contribution to boundary F from the complementary region is

$$\int_{0<r<r_{\max}} r dr d\theta \, \hat{h}_1 \hat{h}_2 \partial\bar{\partial}(\hat{h}_1 \hat{h}_2) \sim d_D^2 \delta_D^2 r_{\max}^2 \ln(4 k_D^2 / r_{\max}^2) . \tag{B.58}$$

In cases of interest, we can compare these contributions for each stack to those appearing in our classical SUGRA calculation of F_∂; if there are terms in F_∂ which dominate all of the naïve estimates of the corrections from near the five-brane stacks, then these terms should provide a reliable approximation to F_∂.

B.5.2 Examples

Here we will consider some examples to illustrate the procedure of comparing the anticipated corrections to the terms appearing in the uncorrected expression for F_∂. To recover a classical supergravity dual in the asymptotic region, we should always consider the limit $N \to \infty$ and $\lambda \gg 1$.

Single stack of D5-branes

Suppose we have a single stack of N_5 D5-branes, each with linking number $\tilde{L} = N/N_5$; here N_5 is $\Omega(N^0)$ and $O(N)$. The anticipated correction in the vicinity of this stack is of order

$$O\left(N_5^2 \cdot W\left(\pi^2\tilde{L}^2\right) \cdot \ln\left(\frac{4\pi^2\tilde{L}^2}{W\left(\pi^2\tilde{L}^2\right)}\right)\right) = \begin{cases} O(N_5^2) & \tilde{L} \sim 1 \\ O\left((N_5 \ln \tilde{L})^2\right) & \tilde{L} \gg 1 \end{cases}, \quad \text{(B.59)}$$

while our uncorrected expression for F_∂ is

$$F_\partial = \frac{N^2}{8}\left[3 - \frac{8\pi^2}{3\lambda}\frac{N^2}{N_5^2} - 2\ln\left(\frac{16\pi^2}{\lambda}\frac{N^2}{N_5^2}\right)\right]. \quad \text{(B.60)}$$

When N is taken to be large, we see that the α'-corrections are expected to be suppressed relative to all terms appearing in the uncorrected F_∂ unless we have $\tilde{L} \sim 1$, in which case the corrections become comparable. Note that $\tilde{L} = 1$ corresponds to the Dirichlet boundary condition for the gauge theory, which we refer to as a "maximum entropy" boundary condition in Section 3.6; in that section we will see that the exact evaluation of F_∂ for this boundary condition does indeed demonstrate that F_∂ receives corrections at leading order.

Single stack of NS5-branes

We now consider the case with a single stack of N_5 NS5-branes, each with linking number $K = N/N_5$; again, N_5 is $\Omega(N^0)$ and $O(N)$. The expected α'-correction is of order $O(N^2)$ if $N_5 \sim 1$, and should be subleading if $N_5 \gg 1$. The expected string loop correction is of order

$$O\left(N_5^4 \cdot W(\pi^2 K^2/N_5^2) \cdot \ln\left(\frac{4\pi^2 K^2}{N_5^2 \cdot W\left(\pi^2 K^2/N_5^2\right)}\right)\right) = \begin{cases} O\left(\left(N_5^2 \ln\left(K^2/N_5^2\right)\right)^2\right) & K \gg N_5 \\ O(N_5^4) & K \sim N_5 \\ O(N^2) & K \ll N_5 \end{cases} . \tag{B.61}$$

Meanwhile, the uncorrected expression is

$$F = \frac{N^2}{8}\left[3 - \frac{\lambda}{6N_5^2} - 2\ln\left(\frac{\lambda}{N_5^2}\right)\right] . \tag{B.62}$$

When N is taken to be large, we see that the α'-corrections and string loop corrections are both expected to be suppressed relative to the leading term in F_∂, which is order $O(N^2 \ln N_5)$, provided that we take $N_5 \gg 1$. Moreover, they will also be suppressed relative to the second leading term, which is $O(N^2)$, provided that we take $1 \ll N_5 \ll K$. However, they will not be suppressed relative to the third term, which is order $O(K^2)$, unless $N_5 = o(\sqrt{K})$. Note that $N_5 = N$ is referred to as a "maximum entropy" boundary condition in Section 3.6; in that section, we see that the exact evaluation of F_∂ for this boundary condition demonstrates that the leading $O(N^2 \ln N)$ term is uncorrected while the next-to-leading $O(N^2)$ term is corrected, as we have predicted here.

Single stack of D5-branes and single stack of NS5-branes

We will focus here on a specific choice of boundary configuration involving one stack of D5-branes and one stack of NS5-branes, where we fix

$$\tilde{L} = -1 \,, \qquad K = 1 \,, \tag{B.63}$$

and take N, N_{NS5} to be large independent parameters, with $N \ll N_{NS5}$. We have

$$N_{D5} = N_{NS5} - N \,. \tag{B.64}$$

This is the situation considered in Section 3.6 to illustrate the unboundedness of F_∂; it is a natural boundary condition to consider in order to understand a situation where the number of boundary degrees of freedom is taken to be much larger than the number of bulk degrees of freedom. Given that the supergravity parameters are given at leading order by

$$\hat{l} = \frac{N}{N_{NS5}} + O\left(\frac{N^2}{N_{NS5}^2}\right) \,, \qquad \hat{k} = \frac{2\pi^2}{\lambda}\frac{N^2}{N_{NS5}^2} + O\left(\frac{N^3}{N_{NS5}^3}\right) \,, \tag{B.65}$$

we find

$$\gamma = \frac{\pi N_{NS5}}{N} + O(1) \,, \qquad \delta = \frac{\lambda}{2\pi}\frac{N_{NS5}^2}{N^2} + O\left(\frac{N_{NS5}}{N}\right) \,, \tag{B.66}$$

and thus an α'-correction of order

$$(N_{NS5} - N)^2 W(\gamma^2\hat{l}^2) \ln\left(\frac{4\gamma^2\hat{l}^2}{W(\gamma^2\hat{l}^2)}\right) = O\left(N_{NS5}^2\right) \tag{B.67}$$

from the vicinity of the D5-brane stack, and a string loop correction of order

$$N_{NS5}^4 W\left(\frac{\delta^2\hat{k}^2}{N_{NS5}^2}\right) \ln\left(\frac{4\delta^2\hat{k}^2}{N_{NS5}^2 W\left(\frac{\delta^2\hat{k}^2}{N_{NS5}^2}\right)}\right) = O\left(N_{NS5}^2\right) \tag{B.68}$$

from the vicinity of the NS5-brane stack. We stated in Section 3.6 that the leading contribution to the uncorrected F_∂ was $O(N_{NS5}^2 \ln N_{NS5})$ while the

next largest contribution is of order $O(N_{NS5})$; consequently, we expect only the leading large N_{NS5} term in the uncorrected expression to be reliable.

B.6 Localization integrals

In Section 3.5, we need to evaluate integrals of the form

$$\begin{aligned} I_1(a,b,s,N) &= \frac{1}{N!}\int \prod_{i=1}^{N} \frac{d\lambda_i}{\sqrt{2\pi}} e^{-\frac{1}{2s}\sum_{i=1}^{N}\lambda_i^2} \\ &\qquad \times \prod_{i<j}^{N} 2\sinh\left(\frac{a}{2}(\lambda_i-\lambda_j)\right)\, 2\sinh\left(\frac{b}{2}(\lambda_i-\lambda_j)\right) \\ I_2(b,s,N) &= \frac{1}{N!}\int \prod_{i=1}^{N} \frac{d\lambda_i}{\sqrt{2\pi}} e^{-\frac{1}{2s}\sum_{i=1}^{N}\lambda_i^2} \\ &\qquad \times \prod_{i<j}^{N} 2(\lambda_i-\lambda_j)\sinh\left(\frac{b}{2}(\lambda_i-\lambda_j)\right) \\ I_3(s,N) &= \frac{1}{N!}\int \prod_{i=1}^{N} \frac{d\lambda_i}{\sqrt{2\pi}} e^{-\frac{1}{2s}\sum_{i=1}^{N}\lambda_i^2} \prod_{i<j}^{N}(\lambda_i-\lambda_j)^2 \,. \end{aligned} \tag{B.69}$$

Noting that

$$\begin{aligned} I_2(b,s,N) &= \lim_{a\to 0} a^{-\frac{N(N-1)}{2}} I_1(a,b,s,N)\,, \\ I_3(s,N) &= \lim_{b\to 0} b^{-\frac{N(N-1)}{2}} I_2(b,s,N)\,, \end{aligned} \tag{B.70}$$

we see it is sufficient to calculate $I_1(a,b,s,N)$, and take the appropriate limits to recover $I_2(b,s,N)$ and $I_3(s,N)$. Using the identity

$$\prod_{i<j}^{N} 2\sinh\left(\frac{\lambda_i-\lambda_j}{2}\right) = \sum_{\sigma\in S_N}(-1)^{\sigma}\prod_{j=1}^{N}\exp\left(\left(\frac{N+1}{2}-\sigma_j\right)\lambda_j\right)\,, \tag{B.71}$$

we may write

$$I_1(a,b,s,N) = \frac{1}{N!}\int \prod_{i=1}^{N} \frac{d\lambda_i}{\sqrt{2\pi}} e^{-\frac{1}{2s}\sum_{i=1}^{N}\lambda_i^2} \sum_{\sigma,\hat{\sigma}\in S_N} (-1)^{\sigma+\hat{\sigma}} \exp\left(\sum_{j=1}^{N}\Big[a\Big(\frac{N+1}{2}-\sigma_j\Big)+b\Big(\frac{N+1}{2}-\hat{\sigma}_j\Big)\Big]\right) . \quad \text{(B.72)}$$

Recalling the Gaussian integration

$$\int \frac{d\lambda}{\sqrt{2\pi}} e^{-\frac{1}{2s}\lambda^2} e^{b\lambda} = \sqrt{s} e^{sb^2/2} , \quad \text{(B.73)}$$

we obtain

$$\begin{aligned} I_1(a,b,s,N) &= \frac{s^{\frac{N}{2}}}{N!} \sum_{\sigma,\hat{\sigma}\in S_N} (-1)^{\sigma+\hat{\sigma}} e^{\frac{s}{2}\sum_{j=1}^{N}\left[a\left(\frac{N+1}{2}-\sigma_j\right)+b\left(\frac{N+1}{2}-\hat{\sigma}_j\right)\right]^2} \\ &= s^{\frac{N}{2}} \sum_{\sigma'\in S_N} (-1)^{\sigma'} e^{\frac{s}{2}\sum_{j=1}^{N}\left[a\left(\frac{N+1}{2}-\sigma'_j\right)+b\left(\frac{N+1}{2}-j\right)\right]^2} , \end{aligned} \quad \text{(B.74)}$$

where σ' denotes the relative permutation between σ and $\hat{\sigma}$. We therefore find

$$I_1(a,b,s,N) = s^{\frac{N}{2}} e^{-\frac{s(a+b)^2N(N+1)^2}{8}} e^{\frac{s(a^2+b^2)N(N+1)(2N+1)}{12}} \sum_{\sigma'\in S_N} (-1)^{\sigma'} \prod_{j=1}^{N} e^{sabj\sigma'_j} . \quad \text{(B.75)}$$

Noting

$$\sum_{\sigma}(-1)^{\sigma}\prod_{j=1}^{N} e^{sabj\sigma_j} = e^{\frac{sabN(N+1)^2}{4}} \prod_{i<j}^{N} 2\sinh\left(\frac{sab(j-i)}{2}\right) , \quad \text{(B.76)}$$

where we have used our earlier identity (B.71) with $\lambda_j \to -sabj$, we find

$$\begin{aligned} I_1(a,b,s,N) &= s^{\frac{N}{2}} e^{\frac{s(a^2+b^2)N(N+1)(N-1)}{24}} \prod_{i<j} 2\sinh\left(\frac{sab(j-i)}{2}\right) \\ &= s^{\frac{N}{2}} e^{\frac{s(a^2+b^2)N(N+1)(N-1)}{24}} \prod_{j=1}^{N-1} \left(2\sinh\left(\frac{sabj}{2}\right)\right)^{N-j} . \end{aligned} \tag{B.77}$$

We therefore also deduce

$$I_2(b,s,N) = s^{\frac{N^2}{2}} b^{\frac{N(N-1)}{2}} e^{\frac{sb^2N(N+1)(N-1)}{24}} G_2(N+1) , \tag{B.78}$$

and

$$I_3(s,N) = s^{\frac{N^2}{2}} G_2(N+1) , \tag{B.79}$$

where one recalls the definition of the Barnes G-function

$$\prod_{k=1}^{N-1} k! \equiv G_2(N+1) . \tag{B.80}$$

We can extract the partition function of $\mathcal{N}=4$ $U(N)$ SYM on S^4 from

$$Z[S^4] = (2\pi)^{\frac{N}{2}} I_3\left(\frac{g_{\rm YM}^2}{16\pi^2}, N\right) , \tag{B.81}$$

and the partition function of $\mathcal{N}=4$ $U(N)$ SYM on HS^4 with Neumann boundary conditions from

$$Z_{\rm Neum.}[HS^4] = (2\pi)^{\frac{N}{2}} \lim_{b\to 2\pi} I_2\left(b, \frac{g_{\rm YM}^2}{8\pi^2}, N\right) . \tag{B.82}$$

B.6.1 General NS5-like localization integrals

We also need to evaluate integrals of the form

$$Z[HS^4] = \frac{1}{n_1! \dots n_{N_5}!} \int \left(\prod_{j=1}^{N_5} \prod_{\ell=1}^{n_j} d\lambda_{j,\ell} \right) \left(\prod_{j=1}^{N_5-1} \prod_{\ell=1}^{n_j} e^{2\pi i \alpha_j \lambda_{j,\ell}} \right) \\ e^{-\frac{4\pi^2}{g_{\rm YM}^2} \sum_{i=1}^{N} \lambda_{N_5,i}^2} \prod_{i<j}^{N} (\lambda_{N_5,i} - \lambda_{N_5,j}) \, \mathrm{sh}(\lambda_{N_5,i} - \lambda_{N_5,j}) \\ \prod_{j=1}^{N_5-1} \prod_{k<\ell}^{n_j} \mathrm{sh}^2 (\lambda_{j,k} - \lambda_{j,\ell}) \prod_{j=1}^{N_5-1} \prod_{k=1}^{n_j} \prod_{\ell=1}^{n_{j+1}} \frac{1}{\mathrm{ch}(\lambda_{j,k} - \lambda_{j+1,\ell})} \,, \quad \text{(B.83)}$$

where we recall the notation

$$\mathrm{sh}(x) \equiv 2 \sinh \pi x \,, \qquad \mathrm{ch}(x) \equiv 2 \cosh \pi x \,. \quad \text{(B.84)}$$

We are ultimately interested in taking the limit $\alpha_i \to 0$. It will be convenient to introduce the function

$$h_s(\alpha) \equiv \sum_{n=0}^{\infty} (-1)^{ns} e^{-(2n+1)\pi\alpha} = \begin{cases} \frac{1}{\mathrm{ch}(\alpha)} & 2 \nmid s \\ \frac{1}{\mathrm{sh}(\alpha)} & 2 \mid s \end{cases} . \quad \text{(B.85)}$$

We let $n_0 \equiv 0, n_{m+1} \equiv N$ for notational ease. Additionally, we denote the index sets

$$S_a \equiv \{ n_{a-1} + 1, n_{a-1} + 2, \dots, n_a \} \,. \quad \text{(B.86)}$$

We will begin by showing that the integral

$$\mathcal{I}_{n_1,\ldots,n_{s+1}}(\alpha_1,\ldots,\alpha_s) \equiv \int \left(\prod_{j=1}^{n_s} d\lambda_{s,j}\right) e^{2\pi i \sum_{j=1}^{s} \alpha_j \sum_{k\in S_j} \lambda_{s,k}} \prod_{a=1}^{s} \prod_{\substack{k,\ell\in S_a \\ k<\ell}} \mathrm{sh}^2(\lambda_{s,k}-\lambda_{s,\ell}) \prod_{a<b}^{s} \prod_{k\in S_a} \prod_{\ell\in S_b} \mathrm{sh}(\lambda_{s,k}-\lambda_{s,\ell}) \prod_{k=1}^{n_s} \prod_{\ell=1}^{n_{s+1}} \frac{1}{\mathrm{ch}(\lambda_{s,k}-\lambda_{s+1,\ell})} \quad \text{(B.87)}$$

is given by

$$\mathcal{I}_{n_1,\ldots,n_{s+1}}(\alpha_1,\ldots,\alpha_s) = \frac{i^{-n_s(n_{s+1}-n_s)}}{(n_{s+1}-n_s)!} \tilde{H}^s_{n_1,\ldots,n_{s+1}}(\alpha_1,\ldots,\alpha_s) \sum_{\sigma\in S_{n_{s+1}}} \frac{\prod_{a=1}^{s} e^{2\pi i\alpha_a \sum_{\ell=1}^{n_a} \lambda_{s+1,\sigma(\ell)}}}{\prod_{a<b}^{s+1} \prod_{k\in S_a} \prod_{\ell\in S_b} \mathrm{sh}(\lambda_{s+1,\sigma(k)}-\lambda_{s+1,\sigma(\ell)})} , \quad \text{(B.88)}$$

where we have the recursive relation

$$\tilde{H}^s_{n_1,\ldots,n_{s+1}}(\alpha_1,\ldots,\alpha_s) = h_{n_1+n_s+n_{s+1}}(\alpha_1+\ldots+\alpha_s)^{n_1} \times \tilde{H}^{s-1}_{n_2-n_1,\ldots,n_{s+1}-n_1}(\alpha_2,\ldots,\alpha_s) , \quad \text{(B.89)}$$

with $\tilde{H}^1_{n_1,n_2}(\alpha_1) = h_{n_2}(\alpha_1)^{n_1}$.

Proof. We can verify this claim inductively. To begin, we determine

$$\mathcal{I}_{n_1,n_2}(\alpha_1) \equiv \int \left(\prod_{\ell=1}^{n_1} d\lambda_{1,\ell} e^{2\pi i\alpha_1\lambda_{1,\ell}}\right) \prod_{k<\ell}^{n_1} \mathrm{sh}^2(\lambda_{1,k}-\lambda_{1,\ell}) \prod_{k=1}^{n_1} \prod_{\ell=1}^{n_2} \frac{1}{\mathrm{ch}(\lambda_{1,k}-\lambda_{2,\ell})} . \quad \text{(B.90)}$$

First, we integrate out the variable $\lambda_{1,1}$. Specifically, we would like to eval-

uate

$$\int d\lambda_{1,1} e^{2\pi i \alpha_1 \lambda_{1,1}} \prod_{i=2}^{n_1} \mathrm{sh}^2(\lambda_{1,1} - \lambda_{1,i}) \prod_{j=1}^{n_2} \frac{1}{\mathrm{ch}(\lambda_{1,1} - \lambda_{2,j})} \,. \tag{B.91}$$

Noting that the integrand is suppressed in the upper half plane for large $|\lambda_1|$ (when $\alpha_1 > 0$), we may close the integration contour in the upper half plane and apply the residue theorem. The poles occur at $\lambda_{1,1} = \lambda_{2,j} + (n + 1/2)i$ for $j \in \{1, \ldots, n_2\}, n \in \mathbb{N}$, and the contribution to the integral from such a pole is given by

$$i^{-(n_2-1)}(-1)^{(n_1-1)-nn_2} \times \frac{e^{2\pi i \alpha_1 (\lambda_{2,j} + (n+1/2)i)} \prod_{i=2}^{n_1} \mathrm{ch}^2(\lambda_{2,j} - \lambda_{1,i})}{\prod_{\ell \neq j}^{n_2} \mathrm{sh}(\lambda_{2,j} - \lambda_{2,\ell})} \,. \tag{B.92}$$

Consequently, summing over all of the poles, we find the full integral

$$i^{-(n_2-1)+2(n_1-1)} h_{n_2}(\alpha_1) \sum_{j_1=1}^{n_2} \frac{e^{2\pi i \alpha_1 \lambda_{2,j_1}} \prod_{i=2}^{n_1} \mathrm{ch}^2(\lambda_{1,i} - \lambda_{2,j_1})}{\prod_{\ell \neq j_1}^{n_2} \mathrm{sh}(\lambda_{2,j_1} - \lambda_{2,\ell})} \,, \tag{B.93}$$

and substituting this into $\mathcal{I}_1$ gives

$$\begin{aligned} &\frac{i^{-(n_2-1)+2(n_1-1)}}{n_1!} h_{n_2}(\alpha_1) \sum_{j_1=1}^{n_2} \frac{e^{2\pi i \alpha_1 \lambda_{2,j_1}}}{\prod_{\ell \neq j_1} \mathrm{sh}(\lambda_{2,j_1} - \lambda_{2,\ell})} \\ &\qquad \int \left(\prod_{\ell=2}^{n_1} d\lambda_{1,\ell} e^{2\pi i \alpha_1 \lambda_{1,\ell}} \right) \prod_{1<k<\ell}^{n_1} \mathrm{sh}^2(\lambda_{1,k} - \lambda_{1,\ell}) \\ &\qquad\qquad \prod_{k=2}^{n_1} \left(\mathrm{ch}(\lambda_{1,k} - \lambda_{2,j_1}) \prod_{\ell \neq j_1}^{n_2} \frac{1}{\mathrm{ch}(\lambda_{1,k} - \lambda_{2,\ell})} \right) \,. \end{aligned} \tag{B.94}$$

Applying this approach to each successive integration, we find after inte-

grating out all of the $\lambda_{1,i}$ variables that $\mathcal{I}_{n_1,n_2}(\alpha_1)$ is given by

$$\frac{i^{-n_1(n_2-n_1)}(-1)^{n_1(n_1-1)/2}}{n_1!}[h_{n_2}(\alpha_1)]^{n_1} \sum_{j_1\neq\ldots\neq j_{n_1}}^{n_2} \frac{e^{2\pi i\alpha_1\sum_{\ell=1}^{n_1}\lambda_{2,j_\ell}}\prod_{a<b}^{n_1}\mathrm{sh}(\lambda_{2,j_b}-\lambda_{2,j_a})}{\prod_{\ell\neq j_1}^{n_2}\mathrm{sh}(\lambda_{2,j_1}-\lambda_{2,\ell})\ldots\prod_{\ell\neq j_1,\ldots,j_{n_1}}^{n_2}\mathrm{sh}(\lambda_{2,j_{n_1}}-\lambda_{2,\ell})}$$
$$= \frac{i^{-n_1(n_2-n_1)}}{n_1!(n_2-n_1)!}[h_{n_2}(\alpha_1)]^{n_1} \sum_{\sigma\in S_{n_2}} \frac{e^{2\pi i\alpha_1\sum_{\ell=1}^{n_1}\lambda_{2,\sigma(\ell)}}}{\prod_{k=1}^{n_1}\prod_{\ell=n_1+1}^{n_2}\mathrm{sh}(\lambda_{2,\sigma(k)}-\lambda_{2,\sigma(\ell)})}\,, \quad \text{(B.95)}$$

which indeed is of the desired form.

Now suppose that the claim holds for $\mathcal{I}_{n_1,\ldots,n_s}(\alpha_1,\ldots,\alpha_{s-1})$. To determine $\mathcal{I}_{n_1,\ldots,n_{s+1}}(\alpha_1,\ldots,\alpha_s)$, we may again apply the residue theorem to perform the first n_1 integrals

$$\int\left(\prod_{\ell=1}^{n_1}d\lambda_{s,\ell}\right)e^{2\pi i(\alpha_1+\ldots+\alpha_s)\sum_{\ell=1}^{n_1}\lambda_{s,\ell}}\prod_{k<\ell}^{n_1}\mathrm{sh}^2\left(\lambda_{s,k}-\lambda_{s,\ell}\right) \prod_{j=1}^{s}\prod_{a\in S_0}\prod_{b\in S_j}\mathrm{sh}\left(\lambda_{s,a}-\lambda_{s,b}\right)\prod_{k\in S_0}\prod_{\ell=1}^{n_{s+1}}\frac{1}{\mathrm{ch}(\lambda_{s,k}-\lambda_{s+1,\ell})}\,, \quad \text{(B.96)}$$

which gives

$$i^{-n_1(n_{s+1}-n_s)+n_1(n_1-1)}[h_{n_1+n_s+n_{s+1}}(\alpha_1+\ldots+\alpha_s)]^{n_1} \sum_{j_1\neq\ldots\neq j_{n_1}}^{n_{s+1}}\Big[e^{2\pi i(\alpha_1+\ldots+\alpha_s)\sum_{k=1}^{n_1}\lambda_{s+1,j_k}}\prod_{k<\ell}^{n_1}\mathrm{sh}(\lambda_{s+1,j_\ell}-\lambda_{s+1,j_k}) \prod_{k=1}^{n_1}\prod_{b=n_1+1}^{n_s}\mathrm{ch}(\lambda_{s,b}-\lambda_{s+1,j_k})\Big]$$
$$\Big[\prod_{\ell\neq j_1}^{n_{s+1}}\mathrm{sh}(\lambda_{s+1,j_1}-\lambda_{s+1,\ell})\ldots\prod_{\ell\neq j_1,\ldots,j_{n_1}}^{n_{s+1}}\mathrm{sh}(\lambda_{s+1,j_{n_1}}-\lambda_{s+1,\ell})\Big]^{-1}\,. \quad \text{(B.97)}$$

Substituting this into $\mathcal{I}_{n_1,\ldots,n_{s+1}}(\alpha_1,\ldots,\alpha_s)$ gives

$$
\begin{aligned}
&i^{-n_1(n_{s+1}-n_s)}[h_{n_1+n_s+n_{s+1}}(\alpha_1+\ldots+\alpha_s)]^{n_1}\\
&\sum_{j_1\neq\ldots\neq j_{n_1}}^{n_{s+1}}\frac{e^{2\pi i(\alpha_1+\ldots+\alpha_s)\sum_{k=1}^{n_1}\lambda_{s+1,j_k}}\prod_{k<\ell}^{n_1}\mathrm{sh}(\lambda_{s+1,j_k}-\lambda_{s+1,j_\ell})}{\prod_{\ell\neq j_1}^{n_{s+1}}\mathrm{sh}(\lambda_{s+1,j_1}-\lambda_{s+1,\ell})\ldots\prod_{\ell\neq j_1,\ldots,j_{n_1}}^{n_{s+1}}\mathrm{sh}(\lambda_{s+1,j_{n_1}}-\lambda_{s+1,\ell})}\\
&\qquad\int\left(\prod_{\ell=n_1+1}^{n_s}d\lambda_{s,\ell}\right)e^{2\pi i\alpha_2\sum_{\ell=n_1+1}^{n_2}\lambda_{s,\ell}}\ldots e^{2\pi i\alpha_s\sum_{\ell=n_1+1}^{n_s}\lambda_{s,\ell}}\\
&\qquad\prod_{a=1}^{s-1}\prod_{n_a<k<\ell}^{n_{a+1}}\mathrm{sh}^2\left(\lambda_{s,k}-\lambda_{s,\ell}\right)\prod_{1<a<b}^{s}\prod_{i\in S_a}\prod_{j\in S_b}\mathrm{sh}\left(\lambda_{s,i}-\lambda_{s,j}\right)\\
&\qquad\qquad\prod_{k=n_1+1}^{n_s}\prod_{\ell\neq j_1,\ldots,j_{n_1}}^{n_{s+1}}\frac{1}{\mathrm{ch}(\lambda_{s,k}-\lambda_{s+1,\ell})}\,.
\end{aligned}
\tag{B.98}
$$

Evidently, the integral appearing in this expression is simply

$$
\mathcal{I}_{n_2-n_1,n_3-n_1,\ldots,n_{s+1}-n_1}(\alpha_2,\ldots,\alpha_s)\,,
\tag{B.99}
$$

which by inductive hypothesis is

$$
\begin{aligned}
&i^{-(n_s-n_1)(n_{s+1}-n_s)}\tilde{H}^{s-1}_{n_2-n_1,\ldots,n_{s+1}-n_1}(\alpha_2,\ldots,\alpha_s)\\
&\qquad\sum_{j_{n_1+1}\neq\ldots\neq j_{n_s}}\frac{\prod_{a=2}^{s}e^{2\pi i\alpha_a\sum_{\ell=n_1+1}^{n_a}\lambda_{s+1,j_\ell}}}{\prod_{1<a<b}^{s+1}\prod_{k\in S_a}\prod_{\ell\in S_b}\mathrm{sh}(\lambda_{s+1,j_k}-\lambda_{s+1,j_\ell})}\,.
\end{aligned}
\tag{B.100}
$$

Thus, we have

$$
\begin{aligned}
\mathcal{I}_{n_1,\ldots,n_{s+1}}(\alpha_1,\ldots,\alpha_s) &= i^{-n_s(n_{s+1}-n_s)}[h_{n_1+n_s+n_{s+1}}(\alpha_1+\ldots+\alpha_s)]^{n_1}\\
&\tilde{H}^{s-1}_{n_2-n_1,\ldots,n_{s+1}-n_1}(\alpha_2,\ldots,\alpha_s)\\
&\sum_{j_1\neq\ldots\neq j_{n_s}}^{n_{s+1}}\frac{\prod_{a=1}^{s}e^{2\pi i\alpha_a\sum_{k=1}^{n_a}\lambda_{s+1,j_k}}\prod_{k<\ell}^{n_1}\mathrm{sh}(\lambda_{s+1,j_k}-\lambda_{s+1,j_\ell})}{\prod_{\ell\neq j_1}^{n_{s+1}}\mathrm{sh}(\lambda_{s+1,j_1}-\lambda_{s+1,\ell})\ldots\prod_{\ell\neq j_1,\ldots,j_{n_1}}^{n_{s+1}}\mathrm{sh}(\lambda_{s+1,j_{n_1}}-\lambda_{s+1,\ell})}\\
&\qquad\frac{1}{\prod_{1<a<b}^{s+1}\prod_{k\in S_a}\prod_{\ell\in S_b}\mathrm{sh}(\lambda_{s+1,j_k}-\lambda_{s+1,j_\ell})}
\end{aligned}
\tag{B.101}
$$

that is,

$$\mathcal{I}_{n_1,\ldots,n_{s+1}}(\alpha_1,\ldots,\alpha_s) = \frac{i^{-n_s(n_{s+1}-n_s)}}{(n_{s+1}-n_s)!}\tilde{H}^s_{n_1,\ldots,n_s}(\alpha_1,\ldots,\alpha_s) \sum_{\sigma\in S_{n_{s+1}}} \frac{\prod_{a=1}^s e^{2\pi i\alpha_a\sum_{k=1}^{n_a}\lambda_{s+1,\sigma(k)}}}{\prod_{a<b}^{s+1}\prod_{k\in S_a}\prod_{\ell\in S_b}\mathrm{sh}(\lambda_{s+1,\sigma(k)}-\lambda_{s+1,\sigma(\ell)})}\,, \quad \text{(B.102)}$$

which verifies the claim. □

We now claim that performing the integral

$$\mathcal{I}_s \equiv \frac{1}{n_1!\ldots n_s!}\int\left(\prod_{a=1}^s\prod_{\ell=1}^{n_a} d\lambda_{a,\ell}e^{2\pi i\alpha_a\lambda_{a,\ell}}\right) \prod_{a=1}^s\prod_{k<\ell}^{n_a}\mathrm{sh}^2\left(\lambda_{a,k}-\lambda_{a,\ell}\right)\prod_{a=1}^s\prod_{k=1}^{n_a}\prod_{\ell=1}^{n_{a+1}}\frac{1}{\mathrm{ch}(\lambda_{a,k}-\lambda_{a+1,\ell})} \quad \text{(B.103)}$$

yields

$$\mathcal{I}_s = \frac{i^{-\sum_{\ell=0}^{s-1}(n_{\ell+1}-n_\ell)(n_{s+1}-n_{\ell+1})}}{\prod_{\ell=0}^s(n_{\ell+1}-n_\ell)!}H_{(n_1,\ldots,n_{s+1})}(\alpha_1,\ldots,\alpha_s) \sum_{\sigma\in S_{n_{s+1}}}\frac{\prod_{a=1}^s e^{2\pi i\alpha_a\sum_{\ell=1}^{n_a}\lambda_{s+1,\sigma(\ell)}}}{\prod_{a<b}^{s+1}\prod_{i\in S_a}\prod_{j\in S_b}\mathrm{sh}(\lambda_{s+1,\sigma(i)}-\lambda_{s+1,\sigma(j)})}\,, \quad \text{(B.104)}$$

where $H_{(n_1,\ldots,n_{s+1})}(\alpha_1,\ldots,\alpha_s)$ is an expression involving the $h_n(\alpha)$, given recursively by

$$H_{(n_1,\ldots,n_{s+1})}(\alpha_1,\ldots,\alpha_s) = H_{(n_1,\ldots,n_s)}(\alpha_1,\ldots,\alpha_{s-1})\tilde{H}^s_{n_1,\ldots,n_{s+1}}(\alpha_1,\ldots,\alpha_s)\,, \quad \text{(B.105)}$$

and $H_{(n_1,n_2)}(\alpha_1) = h_{n_2}(\alpha_1)^{n_1}$.

Proof. We can inductively verify our expression for $\mathcal{I}_s$, using our previous inductive result. We have already checked the base case above. Now suppose

that the claim holds for $\mathcal{I}_{s-1}$. We have by induction hypothesis

$$\mathcal{I}_s = \frac{1}{n_s!}\int\left(\prod_{\ell=1}^{n_s} d\lambda_{s,\ell} e^{2\pi i\alpha_s\lambda_{s,\ell}}\right) \prod_{k<\ell}^{n_s}\mathrm{sh}^2\left(\lambda_{s,k}-\lambda_{s,\ell}\right)\prod_{k=1}^{n_s}\prod_{\ell=1}^{n_{s+1}}\frac{1}{\mathrm{ch}(\lambda_{s,k}-\lambda_{s+1,\ell})} \frac{i^{-\sum_{\ell=0}^{s-2}(n_{\ell+1}-n_\ell)(n_s-n_{\ell+1})}}{\prod_{\ell=0}^{s-1}(n_{\ell+1}-n_\ell)!} H_{(n_1,\ldots,n_s)}(\alpha_1,\ldots,\alpha_{s-1}) \sum_{\sigma\in S_{n_s}}\frac{e^{2\pi i\alpha_1\sum_{\ell=1}^{n_1}\lambda_{s,\sigma(\ell)}}\ldots e^{2\pi i\alpha_{s-1}\sum_{\ell=1}^{n_{s-1}}\lambda_{s,\sigma(\ell)}}}{\prod_{a<b}^{s}\prod_{i\in S_a}\prod_{j\in S_b}\mathrm{sh}(\lambda_{s,\sigma(i)}-\lambda_{s,\sigma(j)})}\,, \quad \text{(B.106)}$$

that is,

$$\mathcal{I}_s = \frac{i^{-\sum_{\ell=0}^{s-2}(n_{\ell+1}-n_\ell)(n_s-n_{\ell+1})}H_{(n_1,\ldots,n_s)}(\alpha_1,\ldots,\alpha_{s-1})}{\prod_{\ell=0}^{s-1}(n_{\ell+1}-n_\ell)!} \int\left(\prod_{\ell=1}^{n_s}d\lambda_{s,\ell}\right)e^{2\pi i\alpha_1\sum_{\ell=1}^{n_1}\lambda_{s,\ell}}\ldots e^{2\pi i\alpha_s\sum_{\ell=1}^{n_s}\lambda_{s,\ell}} \prod_{i=0}^{s-1}\prod_{n_i<k<\ell}^{n_{i+1}}\mathrm{sh}^2\left(\lambda_{s,k}-\lambda_{s,\ell}\right)\prod_{a<b}^{s}\prod_{i\in S_a}\prod_{j\in S_b}\mathrm{sh}\left(\lambda_{s,i}-\lambda_{s,j}\right) \prod_{k=1}^{n_s}\prod_{\ell=1}^{n_{s+1}}\frac{1}{\mathrm{ch}(\lambda_{s,k}-\lambda_{s+1,\ell})}\,. \quad \text{(B.107)}$$

But the integral appearing in this expression is of the form encountered in our previous claim, and is thus given by

$$\mathcal{I}_{n_1,\ldots,n_{s+1}}(\alpha_1,\ldots,\alpha_s) = \frac{i^{-n_s(n_{s+1}-n_s)}}{(n_{s+1}-n_s)!}\tilde{H}^s_{n_1,\ldots,n_{s+1}}(\alpha_1,\ldots,\alpha_s) \sum_{\sigma\in S_{n_{s+1}}}\frac{\prod_{a=1}^{s}e^{2\pi i\alpha_a\sum_{\ell=1}^{n_a}\lambda_{s+1,\sigma(\ell)}}}{\prod_{a<b}^{s+1}\prod_{k\in S_a}\prod_{\ell\in S_b}\mathrm{sh}(\lambda_{s+1,\sigma(k)}-\lambda_{s+1,\sigma(\ell)})}\,, \quad \text{(B.108)}$$

so

$$\mathcal{I}_s = \frac{i^{-n_s(n_{s+1}-n_s)-\sum_{\ell=0}^{s-2}(n_{\ell+1}-n_\ell)(n_s-n_{\ell+1})} H_{(n_1,\ldots,n_s)}(\alpha_1,\ldots,\alpha_{s-1})}{\prod_{\ell=0}^{s}(n_{\ell+1}-n_\ell)!} \tilde{H}^s_{n_1,\ldots,n_{s+1}}(\alpha_1,\ldots,\alpha_s) \sum_{\sigma\in S_{n_{s+1}}} \frac{\prod_{a=1}^{s} e^{2\pi i\alpha_a \sum_{\ell=1}^{n_a}\lambda_{s+1,\sigma(\ell)}}}{\prod_{a<b}^{s+1}\prod_{k\in S_a}\prod_{\ell\in S_b}\mathrm{sh}(\lambda_{s+1,\sigma(k)}-\lambda_{s+1,\sigma(\ell)})} . \quad \text{(B.109)}$$

We note that

$$\begin{aligned} &n_s(n_{s+1}-n_s)+\sum_{\ell=0}^{s-2}(n_{\ell+1}-n_\ell)(n_s-n_{\ell+1}) \\ &\quad = (n_s-n_{s-1})(n_{s+1}-n_s)+\sum_{\ell=0}^{s-2}(n_{\ell+1}-n_\ell)(n_{s+1}-n_{\ell+1}) , \end{aligned} \quad \text{(B.110)}$$

so

$$\mathcal{I}_s = \frac{i^{-\sum_{\ell=0}^{s-1}(n_{\ell+1}-n_\ell)(n_s-n_{\ell+1})} H_{(n_1,\ldots,n_{s+1})}(\alpha_1,\ldots,\alpha_s)}{\prod_{\ell=0}^{s}(n_{\ell+1}-n_\ell)!} \sum_{\sigma\in S_{n_{s+1}}} \frac{\prod_{a=1}^{s} e^{2\pi i\alpha_a \sum_{\ell=1}^{n_a}\lambda_{s+1,\sigma(\ell)}}}{\prod_{a<b}^{s+1}\prod_{k\in S_a}\prod_{\ell\in S_b}\mathrm{sh}(\lambda_{s+1,\sigma(k)}-\lambda_{s+1,\sigma(\ell)})} , \quad \text{(B.111)}$$

as desired. □

Using the above claim to perform all of the integrals except those with respect to the bulk zero modes, the partition function from the beginning

of this subsection is

$$Z[HS^4] = \frac{i^{-\sum_{\ell=0}^{N_5-2}(n_{\ell+1}-n_\ell)(n_{N_5}-n_{\ell+1})}}{\prod_{\ell=0}^{N_5-1}(n_{\ell+1}-n_\ell)!} \lim_{\alpha_1,\ldots,\alpha_{N_5-1}\to 0} H_{(n_1,\ldots,n_{N_5})}(\alpha_1,\ldots,\alpha_{N_5-1}) \int \left(\prod_{i=1}^{N} d\lambda_i\right) e^{-\frac{4\pi^2}{g_{\rm YM}^2}\sum_{i=1}^{N}\lambda_i^2} \prod_{a=1}^{N_5-1} e^{2\pi i\alpha_a \sum_{\ell=1}^{n_a}\lambda_\ell} \prod_{i<j}^{N}(\lambda_i-\lambda_j) \prod_{a=1}^{N_5} \prod_{\substack{i,j\in S_a \\ i<j}} \mathrm{sh}(\lambda_i-\lambda_j)\,. \quad \text{(B.112)}$$

We may as well take $\alpha_1 = \ldots = \alpha_{N_5-1}$ before taking the limit. We may therefore write

$$Z[HS^4] = \frac{i^{-\sum_{\ell=0}^{N_5-2}(n_{\ell+1}-n_\ell)(n_{N_5}-n_{\ell+1})}}{\prod_{\ell=0}^{N_5-1}(n_{\ell+1}-n_\ell)!} \lim_{\alpha,a\to 0}\lim_{b\to 2\pi} a^{-N(N-1)/2} H_{(n_1,\ldots,n_{N_5})}(\alpha) \int \left(\prod_{i=1}^{N} d\lambda_i\right) e^{-\frac{1}{2s}\sum_{i=1}^{N}\lambda_i^2} \prod_{c=1}^{N_5-1} e^{2\pi i\alpha_c \sum_{\ell=1}^{n_c}\lambda_\ell} \prod_{i<j}^{N} \mathrm{sh}\left(\frac{a(\lambda_i-\lambda_j)}{2\pi}\right) \prod_{c=1}^{N_5} \prod_{\substack{i,j\in S_c \\ i<j}} \mathrm{sh}\left(\frac{b(\lambda_i-\lambda_j)}{2\pi}\right)\,, \quad \text{(B.113)}$$

where we let $s \equiv \frac{g_{\rm YM}^2}{8\pi^2}$ and $H_{(n_1,\ldots,n_{N_5})}(\alpha) \equiv H_{(n_1,\ldots,n_{N_5})}(\alpha,\ldots,\alpha)$. Again using the identity (B.71), we may express

$$\mathcal{I} \equiv \int \left(\prod_{i=1}^{N} d\lambda_i\right) e^{-\frac{1}{2s}\sum_{i=1}^{N}\lambda_i^2} \prod_{c=1}^{N_5-1} e^{2\pi i\alpha_c \sum_{\ell=1}^{n_c}\lambda_\ell} \prod_{i<j}^{N} \mathrm{sh}\left(\frac{a(\lambda_i-\lambda_j)}{2\pi}\right) \prod_{c=1}^{N_5} \prod_{\substack{i,j\in S_c \\ i<j}} \mathrm{sh}\left(\frac{b(\lambda_i-\lambda_j)}{2\pi}\right) \quad \text{(B.114)}$$

as

$$\mathcal{I} = \int \left(\prod_{i=1}^{N} d\lambda_i\right) e^{-\frac{1}{2s}\sum_{i=1}^{N}\lambda_i^2} \prod_{c=1}^{N_5-1} e^{2\pi i\alpha_c \sum_{\ell=1}^{n_c}\lambda_\ell} \left(\sum_{\sigma\in S_N}(-1)^\sigma \prod_{j=1}^{N} e^{a\left(\frac{N+1}{2}-\sigma_j\right)\lambda_j}\right) \prod_{c=1}^{N_5}\left(\sum_{\sigma_c\in S_{n_c-n_{c-1}}}(-1)^{\sigma_c}\prod_{j\in S_c} e^{b\left(\frac{n_c-n_{c-1}+1}{2}-\sigma_{c,j-n_{c-1}}\right)\lambda_j}\right) . \quad \text{(B.115)}$$

Performing the Gaussian integrals, one finds

$$\mathcal{I} = (2\pi s)^{N/2}\sum_{\sigma\in S_N}(-1)^\sigma \sum_{\sigma_1,\ldots,\sigma_{m+1}}(-1)^{\sigma_1+\ldots+\sigma_m} \prod_{c=1}^{N_5}\left(\prod_{j\in S_c} e^{\frac{s}{2}\left[a\left(\frac{N+1}{2}-\sigma_j\right)+b\left(\frac{n_c-n_{c-1}+1}{2}-\sigma_{c,j-n_{c-1}}\right)+2\pi i(N_5-c)\alpha\right]^2}\right) , \quad \text{(B.116)}$$

and thus, defining $\ell_c \equiv n_c - n_{c-1}$ (the linking numbers in the case with only NS5-branes),

$$\mathcal{I} = (2\pi s)^{N/2} e^{\frac{sa^2N(N-1)(N+1)}{24}} e^{\frac{sb^2}{24}\sum_{c=1}^{N_5}\ell_c(\ell_c-1)(\ell_c+1)-2\pi^2 s\alpha^2\sum_{c=1}^{N_5}(N_5-c)^2\ell_c} e^{\pi i(N+1)s\alpha a\sum_{c=1}^{N_5}(N_5-c)\ell_c} \sum_{\sigma_1,\ldots,\sigma_{N_5}}(-1)^{\sigma_1+\ldots+\sigma_{N_5}} \sum_{\sigma\in S_N}(-1)^\sigma\prod_{j=1}^{N} e^{-\mu_j\sigma_j} , \quad \text{(B.117)}$$

where

$$\mu_j \equiv sab\left(\frac{\ell_c+1}{2}-\sigma_{c,j-n_{c-1}}\right)+2\pi isa\alpha(N_5-c) , \quad j\in S_c . \quad \text{(B.118)}$$

That is, using the identity (B.71) above, the Gaussian integral gives

$$\mathcal{I} = (2\pi s)^{N/2} e^{\frac{sa^2 N(N-1)(N+1)}{24}} e^{\frac{sb^2}{24}\sum_{c=1}^{N_5}\ell_c(\ell_c-1)(\ell_c+1)-2\pi^2 s\alpha^2\sum_{c=1}^{N_5}(N_5-c)^2\ell_c} \sum_{\sigma_1,\ldots,\sigma_{N_5}} (-1)^{\sigma_1+\ldots+\sigma_{N_5}} \prod_{i<j}^{N} \mathrm{sh}\left(\frac{\mu_i-\mu_j}{2\pi}\right) . \quad \text{(B.119)}$$

We therefore have

$$\begin{aligned} Z[HS^4] = {} & \frac{i^{-\sum_{\ell=0}^{N_5-2}(n_{\ell+1}-n_\ell)(n_{N_5}-n_{\ell+1})}}{\prod_{\ell=0}^{N_5-1}(n_{\ell+1}-n_\ell)!} \\ & \lim_{\alpha,a\to 0}\lim_{b\to 2\pi} a^{-N(N-1)/2} H_{(n_1,\ldots,n_{N_5})}(\alpha)(2\pi s)^{N/2} \\ & e^{\frac{sa^2N(N-1)(N+1)}{24}+\frac{sb^2}{24}\sum_{c=1}^{N_5}\ell_c(\ell_c-1)(\ell_c+1)-2\pi^2 s\alpha^2\sum_{c=1}^{N_5}(N_5-c)^2\ell_c} \\ & \sum_{\sigma_1,\ldots,\sigma_{N_5}} (-1)^{\sigma_1+\ldots+\sigma_{N_5}} \left(\prod_{c=1}^{N_5}\prod_{\substack{i,j\in S_c\\ i<j}} \mathrm{sh}\left(\frac{sab(\sigma_{c,j-n_{c-1}}-\sigma_{c,i-n_{c-1}})}{2\pi}\right)\right) \\ & \prod_{c<d}^{N_5}\prod_{i\in S_c}\prod_{j\in S_d} \mathrm{sh}\Big[\frac{sab(\sigma_{d,j-n_{d-1}}-\sigma_{c,i-n_{c-1}})}{2\pi} \\ & + \frac{sab(\ell_c-\ell_d)}{4\pi} + isa\alpha(d-c)\Big] . \end{aligned} \quad \text{(B.120)}$$

Taking the $a \to 0$ and $b \to 2\pi$ limits gives

$$Z[HS^4] = i^{-\sum_{\ell=0}^{N_5-2}(n_{\ell+1}-n_\ell)(n_{N_5}-n_{\ell+1})} \left(\frac{g_{\mathrm{YM}}^2}{4\pi}\right)^{\frac{N^2}{2}} e^{\frac{g_{\mathrm{YM}}^2}{48}\sum_{c=1}^{N_5}\ell_c(\ell_c-1)(\ell_c+1)} \prod_{c=1}^{N_5} G_2(\ell_c+1) \lim_{\alpha\to 0} H_{(n_1,\ldots,n_{N_5})}(\alpha) e^{-2\pi^2 s\alpha^2\sum_{c=1}^{N_5}(N_5-c)^2\ell_c} \left(\prod_{c<d}^{N_5}\prod_{i=1}^{\ell_c}\prod_{j=1}^{\ell_d}\left((j-i)+\frac{(\ell_c-\ell_d)}{2}+i\alpha(d-c)\right)\right) . \quad \text{(B.121)}$$

Now, we claim that

$$\begin{aligned}\lim_{\alpha\to 0}\tilde{H}^s_{n_1,\ldots,n_{s+1}}(\alpha) &\prod_{d=1}^{s}\prod_{i=1}^{(n_c-n_{c-1})}\prod_{j=1}^{(n_{s+1}-n_s)} \times\left((j-i)-\frac{(n_{s+1}-n_s)-(n_c-n_{c-1})}{2}+i\alpha(s+1-c)\right)\\ &= 2^{-n_s}\prod_{c=1}^{s}\left[((\ell_{s+1}-\ell_c)!!)^{\ell_c}\prod_{k=1}^{\ell_c-1}\left(\frac{\ell_{s+1}-\ell_c}{2}+k\right)^{\ell_c-k}\right]^2 \\ &\times \prod_{\substack{c\in\{1,\ldots,s\}\\(\ell_c-\ell_{s+1})\equiv 0 \,(\mathrm{mod}\ 2)}}\left(\frac{i}{\pi}\right)^{\ell_c}(-1)^{\frac{\ell_c}{2}(\ell_{s+1}-1)}2^{-(\ell_{s+1}-\ell_c)\ell_c} \\ &\times \prod_{\substack{c\in\{1,\ldots,s\}\\(\ell_c-\ell_{s+1})\equiv 1 \,(\mathrm{mod}\ 2)}}(-1)^{\frac{\ell_c\ell_{s+1}}{2}}2^{-(\ell_{s+1}-\ell_c+1)\ell_c} .\end{aligned} \quad \text{(B.122)}$$

Proof. We may verify this by induction. The base case $s = 1$ is straightforward to verify individually for the cases $\ell_1 - \ell_2$ even and odd.

Now suppose that the claim holds for some $s = p - 1$; then by induction

hypothesis, we have

$$\begin{aligned}
&\lim_{\alpha\to 0} \tilde{H}^p_{n_1,\dots,n_{p+1}}(\alpha) \prod_{c=1}^{p} \prod_{i=1}^{(n_c-n_{c-1})} \prod_{j=1}^{(n_{p+1}-n_p)} \\
&\quad \times \left((j-i) + \frac{(n_c-n_{c-1})-(n_{p+1}-n_p)}{2} + i\alpha(p+1-c) \right) \\
&\quad = \lim_{\alpha\to 0} h_{n_1+n_p+n_{p+1}}(p\alpha)^{n_1} \prod_{i=1}^{\ell_1} \prod_{j=1}^{\ell_{p+1}} \left((j-i) + \frac{\ell_1-\ell_{p+1}}{2} + i\alpha p \right) \\
&\qquad \times 2^{-(n_p-n_1)} \prod_{c=2}^{p} \left[((\ell_{p+1}-\ell_c)!!)^{\ell_c} \prod_{k=1}^{\ell_c-1} \left(\frac{\ell_{p+1}-\ell_c}{2} + k \right)^{\ell_c-k} \right]^2 \\
&\qquad \times \prod_{\substack{c\in\{2,\dots,p\} \\ (\ell_c-\ell_{p+1})\equiv 0 \pmod 2}} \left(\frac{i}{\pi} \right)^{\ell_c} (-1)^{\frac{\ell_c}{2}(\ell_{p+1}-1)} 2^{-(\ell_{p+1}-\ell_c)\ell_c} \\
&\qquad \times \prod_{\substack{c\in\{2,\dots,p\} \\ (\ell_c-\ell_{p+1})\equiv 1 \pmod 2}} (-1)^{\frac{\ell_c\ell_{p+1}}{2}} 2^{-(\ell_{p+1}-\ell_c+1)\ell_c} \,.
\end{aligned} \tag{B.123}$$

If $n_1+n_p+n_{p+1}$ is odd, then $\ell_1-\ell_{p+1} = n_1+n_p-n_{p+1}$ is odd, so

$$\begin{aligned}
&\lim_{\alpha\to 0} h_{n_1+n_p+n_{p+1}}(p\alpha)^{n_1} \prod_{i=1}^{\ell_1} \prod_{j=1}^{\ell_{p+1}} \left((j-i) + \frac{\ell_1-\ell_{p+1}}{2} + i\alpha p \right) \\
&\quad = 2^{-n_1} (-1)^{\frac{\ell_1}{2}(\ell_{p+1}-\ell_1+1)} \left(\left(\frac{1}{2}\right) \times \left(\frac{3}{2}\right) \times \dots \times \left(\frac{\ell_{p+1}-\ell_1}{2}\right) \right)^{2\ell_1} \\
&\qquad \times (-1)^{\frac{\ell_1}{2}(\ell_1-1)} \prod_{k=1}^{\ell_1-1} \left(\frac{\ell_{p+1}-\ell_1}{2} + k \right)^{2(\ell_1-k)} \,,
\end{aligned} \tag{B.124}$$

and thus

$$\begin{aligned}
&\lim_{\alpha\to 0} \tilde{H}^p_{n_1,\ldots,n_{p+1}}(\alpha) \prod_{c=1}^{p} \prod_{i=1}^{(n_c-n_{c-1})} \prod_{j=1}^{(n_{p+1}-n_p)} \\
&\quad \times \left((j-i) + \frac{(n_c-n_{c-1})-(n_{p+1}-n_p)}{2} + i\alpha(p+1-c) \right) \\
&\quad = 2^{-n_p} \prod_{c=1}^{p} \left[((\ell_{p+1}-\ell_c)!!)^{\ell_c} \prod_{k=1}^{\ell_c-1} \left(\frac{\ell_{p+1}-\ell_c}{2} + k \right)^{\ell_c-k} \right]^2 \\
&\qquad \times \prod_{\substack{c\in\{1,\ldots,p\} \\ (\ell_c-\ell_{p+1})\equiv 0 \,(\mathrm{mod}\ 2)}} \left(\frac{i}{\pi} \right)^{\ell_c} (-1)^{\frac{\ell_c}{2}(\ell_{p+1}-1)} 2^{-(\ell_{p+1}-\ell_c)\ell_c} \\
&\qquad \times \prod_{\substack{c\in\{1,\ldots,p\} \\ (\ell_c-\ell_{p+1})\equiv 1 \,(\mathrm{mod}\ 2)}} (-1)^{\frac{\ell_c\ell_{p+1}}{2}} 2^{-(\ell_{p+1}-\ell_c+1)\ell_c} ,
\end{aligned} \tag{B.125}$$

which is of the desired form. On the other hand, if $n_1 + n_p + n_{p+1}$ is even, then

$$\begin{aligned}
&\lim_{\alpha\to 0} h_{n_1+n_p+n_{p+1}}(p\alpha)^{n_1} \prod_{i=1}^{\ell_1} \prod_{j=1}^{\ell_{p+1}} \left((j-i) + \frac{\ell_1-\ell_{p+1}}{2} + i\alpha p \right) \\
&\quad = \left(\frac{i}{2\pi} \right)^{-n_1} (-1)^{\frac{\ell_1}{2}(\ell_{p+1}-\ell_1)} \left(1 \times 2 \times \ldots \times \left(\frac{\ell_{p+1}-\ell_1}{2} \right) \right)^{2\ell_1} \\
&\qquad \times (-1)^{\frac{\ell_1}{2}(\ell_1-1)} \prod_{k=1}^{\ell_1-1} \left(\frac{\ell_{p+1}-\ell_1}{2} + k \right)^{2(\ell_1-k)} ,
\end{aligned} \tag{B.126}$$

and thus

$$\begin{aligned}
&\lim_{\alpha\to 0} \tilde{H}^{p}_{n_1,\ldots,n_{p+1}}(\alpha) \prod_{c=1}^{p} \prod_{i=1}^{(n_c-n_{c-1})} \prod_{j=1}^{(n_{p+1}-n_p)} \\
&\quad \times \left((j-i) + \frac{(n_c - n_{c-1}) - (n_{p+1} - n_p)}{2} + i\alpha(p+1-c) \right) \\
&\quad = 2^{-n_p} \prod_{c=1}^{p} \left[((\ell_{p+1} - \ell_c)!!)^{\ell_c} \prod_{k=1}^{\ell_c - 1} \left(\frac{\ell_{p+1} - \ell_c}{2} + k \right)^{\ell_c - k} \right]^2 \\
&\qquad \times \prod_{\substack{c \in \{1,\ldots,p\} \\ (\ell_c - \ell_{p+1}) \equiv 0 \,(\mathrm{mod}\ 2)}} \left(\frac{i}{\pi} \right)^{\ell_c} (-1)^{\frac{\ell_c}{2}(\ell_{p+1}-1)} 2^{-(\ell_{p+1}-\ell_c)\ell_c} \\
&\qquad \times \prod_{\substack{c \in \{1,\ldots,p\} \\ (\ell_c - \ell_{p+1}) \equiv 1 \,(\mathrm{mod}\ 2)}} (-1)^{\frac{\ell_c \ell_{p+1}}{2}} 2^{-(\ell_{p+1}-\ell_c+1)\ell_c} ,
\end{aligned} \tag{B.127}$$

again of the desired form. This establishes the claim. □

We can use the above claim in an inductive argument to establish

$$\begin{aligned}
&\lim_{\alpha\to 0} H_{(n_1,\ldots,n_{N_5})}(\alpha) \left(\prod_{c<d}^{N_5} \prod_{i=1}^{\ell_c} \prod_{j=1}^{\ell_d} \left((j-i) + \frac{(\ell_c - \ell_d)}{2} + i\alpha(d-c) \right) \right) \\
&\quad = 2^{-\sum_{i=1}^{N_5-1} n_i} \prod_{c<d} \left[((\ell_d - \ell_c)!!)^{\ell_c} \prod_{k=1}^{\ell_c - 1} \left(\frac{\ell_d - \ell_c}{2} + k \right)^{\ell_c - k} \right]^2 \\
&\qquad \times \prod_{\{c<d : \ell_{cd} \equiv 0 \,(\mathrm{mod}\ 2)\}} \left(\frac{i}{\pi} \right)^{\ell_c} (-1)^{\frac{\ell_c}{2}(\ell_d - 1)} 2^{-(\ell_d - \ell_c)\ell_c} \\
&\qquad \times \prod_{\{c<d : \ell_{cd} \equiv 1 \,(\mathrm{mod}\ 2)\}} (-1)^{\frac{\ell_c \ell_d}{2}} 2^{-(\ell_d - \ell_c + 1)\ell_c}
\end{aligned} \tag{B.128}$$

Indeed, the base case $N_5 = 2$ coincides with the base case of the previous claim. Now, suppose that the claim holds for some N_5. Then we have by

induction hypothesis

$$\begin{aligned}
&\lim_{\alpha\to 0} H_{(n_1,\ldots,n_{N_5+1})}(\alpha)\left(\prod_{c<d}^{N_5+1}\prod_{i=1}^{\ell_c}\prod_{j=1}^{\ell_d}\left((j-i)+\frac{(\ell_c-\ell_d)}{2}+i\alpha(d-c)\right)\right)\\
&\quad= 2^{-\sum_{i=1}^{N_5-1} n_i}\prod_{c<d}\left[((\ell_d-\ell_c)!!)^{\ell_c}\prod_{k=1}^{\ell_c-1}\left(\frac{\ell_d-\ell_c}{2}+k\right)^{\ell_c-k}\right]^2\\
&\qquad\times\prod_{\{c<d:\ell_{cd}\equiv 0\,(\mathrm{mod}\,2)\}}\left(\frac{i}{\pi}\right)^{\ell_c}(-1)^{\frac{\ell_c}{2}(\ell_d-1)}2^{-(\ell_d-\ell_c)\ell_c}\\
&\qquad\times\prod_{\{c<d:\ell_{cd}\equiv 1\,(\mathrm{mod}\,2)\}}(-1)^{\frac{\ell_c\ell_d}{2}}2^{-(\ell_d-\ell_c+1)\ell_c}\\
&\qquad\times\lim_{\alpha\to 0}\tilde{H}^{N_5}_{n_1,\ldots,n_{N_5+1}}(\alpha)\\
&\qquad\times\prod_{c=1}^{N_5}\prod_{i=1}^{\ell_c}\prod_{j=1}^{\ell_{N_5+1}}\left((j-i)+\frac{\ell_d-\ell_c}{2}+i\alpha(N_5+1-c)\right)\,,
\end{aligned}\tag{B.129}$$

so the previous claim provides the desired result. We may therefore deduce

$$\begin{aligned}
Z[HS^4] &= i^{-\sum_{\ell=0}^{N_5-2}(n_{\ell+1}-n_\ell)(n_{N_5}-n_{\ell+1})}\left(\frac{g_{\mathrm{YM}}^2}{4\pi}\right)^{\frac{N^2}{2}}e^{\frac{g_{\mathrm{YM}}^2}{48}\sum_{c=1}^{N_5}\ell_c(\ell_c-1)(\ell_c+1)}\\
&\quad\times\left(\prod_{c=1}^{N_5}G_2(\ell_c+1)\right)2^{-\sum_{i=1}^{N_5-1}n_i}\\
&\quad\times\prod_{c<d}^{N_5}\left[((\ell_d-\ell_c)!!)^{\ell_c}\prod_{k=1}^{\ell_c-1}\left(\frac{\ell_d-\ell_c}{2}+k\right)^{\ell_c-k}\right]^2\\
&\quad\times\prod_{\{c<d:\ell_{cd}\equiv 0\,(\mathrm{mod}\,2)\}}\left(\frac{i}{\pi}\right)^{\ell_c}(-1)^{\frac{\ell_c}{2}(\ell_d-1)}2^{-(\ell_d-\ell_c)\ell_c}\\
&\quad\times\prod_{\{c<d:\ell_{cd}\equiv 1\,(\mathrm{mod}\,2)\}}(-1)^{\frac{\ell_c\ell_d}{2}}2^{-(\ell_d-\ell_c+1)\ell_c}\,.
\end{aligned}\tag{B.130}$$

If we denote

$$\epsilon_{cd} \equiv \begin{cases} 0 & \ell_{cd} \equiv 0 \,(\mathrm{mod}\ 2) \\ 1 & \ell_{cd} \equiv 1 \,(\mathrm{mod}\ 2) \end{cases}, \tag{B.131}$$

then we can write

$$\begin{aligned} Z[HS^4] = i^{-\sum_{\ell=0}^{N_5-2}(n_{\ell+1}-n_\ell)(n_{N_5}-n_{\ell+1})} \left(\frac{g_{\mathrm{YM}}^2}{4\pi}\right)^{\frac{N^2}{2}} e^{\frac{g_{\mathrm{YM}}^2}{48}\sum_{c=1}^{N_5}\ell_c(\ell_c-1)(\ell_c+1)} \\ \times \left(\prod_{c=1}^{N_5} G_2(\ell_c+1)\right) 2^{-\sum_{i=1}^{N_5-1} n_i} \\ \times \prod_{c<d}^{N_5}\left[\left(((\ell_d-\ell_c)!!)^{\ell_c}\prod_{k=1}^{\ell_c-1}\left(\frac{\ell_d-\ell_c}{2}+k\right)^{\ell_c-k}\right)^2\right. \\ \left. \times (-1)^{\frac{\ell_c\ell_d}{2}}\pi^{-(1-\epsilon_{cd})\ell_c}2^{-(\ell_d-\ell_c+\epsilon_{cd})\ell_c}\right], \end{aligned} \tag{B.132}$$

that is,

$$\begin{aligned} Z[HS^4] = (2\pi)^{-\sum_{i=1}^{N_5-1} n_i}\left(\frac{g_{\mathrm{YM}}^2}{4\pi}\right)^{\frac{N^2}{2}} \\ e^{\frac{g_{\mathrm{YM}}^2}{48}\sum_{c=1}^{N_5}\ell_c(\ell_c-1)(\ell_c+1)}\left(\prod_{c=1}^{N_5} G_2(\ell_c+1)\right) \\ \prod_{c<d}^{N_5}\left[2^{-(\ell_d-\ell_c)\ell_c}\left(\frac{\pi}{2}\right)^{\epsilon_{cd}\ell_c}\right. \\ \left.\left(((\ell_d-\ell_c)!!)^{\ell_c}\prod_{k=1}^{\ell_c-1}\left(\frac{\ell_d-\ell_c}{2}+k\right)^{\ell_c-k}\right)^2\right]. \end{aligned} \tag{B.133}$$

B.7 Statistics of boundary F: details

To understand the behaviour of $F_\partial^{\mathrm{SUGRA}}$, which is easier to analyze analytically than F_∂ and provides a good approximation for large N and suitable linking numbers, we will momentarily consider the contribution to the λ-

independent term in $F_\partial^{\rm SUGRA}$, proportional to

$$F_0(p_A) \equiv \sum_{A,B} \Big[(p_A+p_B)^2 \ln\left((p_A+p_B)^2\right) - (p_A-p_B)^2 \ln\left((p_A-p_B)^2\right) \Big] , \quad \text{(B.134)}$$

where $p_A = L_A/N$ for D5-branes or $p_A = K_A/N$ for NS5-branes. Using concavity of the logarithm, we find inequality

$$\begin{aligned} F_0(p_A) &\geq \sum_{A,B} \Big[(p_A+p_B)^2 \ln\left((p_A+p_B)^2\right) - (p_A-p_B)^2 \ln\left((p_A+p_B)^2\right) \Big] \\ &= 8 \sum_{A,B} p_A p_B \ln(p_A+p_B) \\ &\geq 8 \sum_{A,B} p_A p_B \left(\ln 2 + \frac{1}{2}\ln p_A + \frac{1}{2}\ln p_B \right) \\ &= 8\ln 2 + 8\sum_A p_A \ln p_A = 8\ln 2 - 8S(p_A) , \end{aligned} \quad \text{(B.135)}$$

where $S(p_A)$ is the classical entropy of the probability distribution. The smallest possible value for the right hand side of our inequality is $8\ln(2/N)$, realized on the maximum entropy distribution

$$p_1 = \ldots = p_N = \frac{1}{N} . \quad \text{(B.136)}$$

And in fact, for this particular distribution, the inequality is saturated and one finds

$$F_0\left(p_1 = \ldots = p_N = \frac{1}{N}\right) = 8\ln(2/N) . \quad \text{(B.137)}$$

We may therefore deduce that $F_0(p_A)$ is minimized for the maximum entropy probability distribution.

On the other hand, we note that if $p_1, p_2 \leq \frac{1}{2}$, then

$$0 \geq \Big[(p_1+p_2)^2 \ln\left((p_1+p_2)^2\right) - (p_1-p_2)^2 \ln\left((p_1-p_2)^2\right) \Big] , \quad \text{(B.138)}$$

while if $\frac{1}{2} \leq p_1 \leq 1$ and $0 < p_2 \leq 1 - p_1$ then

$$8p_1p_2 \ln(4p_1^2) \geq 2\Big[(p_1+p_2)^2 \ln\left((p_1+p_2)^2\right) - (p_1-p_2)^2 \ln\left((p_1-p_2)^2\right)\Big] + 4p_2^2 \ln(4p_2^2)\,. \quad \text{(B.139)}$$

Consequently, one finds that if the distribution $\{p_A\}$ has $p_1, \ldots, p_N \leq \frac{1}{2}$, then

$$F_0(p_A) \leq 0\,, \quad \text{(B.140)}$$

whereas if $p_1 \geq \frac{1}{2}$ and $p_2, \ldots, p_N \leq \frac{1}{2}$, then

$$\begin{aligned} F_0(p_A) &\leq 4p_1^2 \ln(4p_1^2) + 2\sum_{A>1}\Big[(p_1+p_A)^2 \ln\left((p_1+p_A)^2\right) \\ &\quad - (p_1-p_A)^2 \ln\left((p_1-p_A)^2\right)\Big] + 4\sum_{A>1} p_A^2 \ln(4p_A^2) \\ &\quad + 2\sum_{B>A>1}\Big[(p_A+p_B)^2 \ln\left((p_A+p_B)^2\right) \\ &\quad - (p_A-p_B)^2 \ln\left((p_A-p_B)^2\right)\Big] \\ &\leq 4p_1^2 \ln(4p_1^2) + 4\sum_{A>1} p_A^2 \ln(4p_A^2) \\ &\quad + 2\sum_{A>1}\Big[(p_1+p_A)^2 \ln\left((p_1+p_A)^2\right) \\ &\quad - (p_1-p_A)^2 \ln\left((p_1-p_A)^2\right)\Big] \\ &\leq 4p_1^2 \ln(4p_1^2) + 8p_1(1-p_1)\ln(4p_1^2) = 4p_1(2-p_1)\ln(4p_1^2)\,. \end{aligned} \quad \text{(B.141)}$$

The right hand side of this inequality is a monotonically increasing function, so it is maximized at $p_1 = 1$, where it is equal to $4 \ln 4$. In fact, the minimum entropy distribution

$$p_1 = 1\,, \qquad p_2 = \ldots = p_N = 0 \quad \text{(B.142)}$$

saturates this inequality, and one can see that

$$F_0\left(p_1 = 1, p_2 = \ldots = p_N = 0\right) = 4 \ln 4\,. \quad \text{(B.143)}$$

Thus, $F_0(p_A)$ is maximized for the minimum entropy probability distribution.

We can apply these considerations to determine for which boundary conditions consisting of D5-branes only or NS5-branes only $F_\partial^{\text{SUGRA}}$ will be maximized or minimized. For D5-brane boundary conditions, we found

$$F_\partial^{\text{SUGRA}} = \frac{N^2}{4}\left(\frac{3}{2} + \ln\left(\frac{\lambda}{4\pi^2 N^2}\right)\right) - \frac{\pi^2 N^4}{3\lambda}\sum_A p_A^3 - \frac{N^2}{16}F_0(p_A)\,. \quad \text{(B.144)}$$

The term in parentheses is independent of the choice of boundary condition, while the remaining terms are both minimized (maximized) on the minimum (maximum) entropy probability distributions. Thus, we can conclude that $F_\partial^{\text{SUGRA}}$ is minimized (maximized) on the minimum (maximum) entropy probability distributions. Similarly, for NS5-brane boundary conditions, we found

$$F_\partial^{\text{SUGRA}} = \frac{N^2}{4}\left(\frac{3}{2} + \ln\left(\frac{4}{\lambda}\right)\right) - \frac{\lambda N^2}{48}\sum_A p_A^3 - \frac{N^2}{16}F_0(p_A)\,, \quad \text{(B.145)}$$

so $F_\partial^{\text{SUGRA}}$ is again minimized (maximized) on the minimum (maximum) entropy probability distributions.

B.8 Calculation of boundary F in a bottom-up model

In this appendix, we will compute the boundary F in a bottom-up holographic model of a BCFT where the boundary in the CFT gives rise to an end-of-the-world (ETW) brane with tension T. Here, the vacuum solution may be described as a portion of pure AdS spacetime described by $x/z < \frac{T}{\sqrt{1-T^2}}$ in Fefferman-Graham coordinates, with an ETW brane at $x/z = \frac{T}{\sqrt{1-T^2}}$ [87]. Defining $z = w\cos(\theta)$ and $x = w\sin(\theta)$, we can write the metric as

$$ds^2 = \frac{L_{\text{AdS}}^2 d\theta^2}{\cos^2(\theta)} + \frac{L_{\text{AdS}}^2}{w^2\cos^2\theta}(dw^2 - dt^2 + dx_\perp^2)\,, \quad \text{(B.146)}$$

and the ETW now appears at $\theta = \arcsin(T)$. The extremal surface corresponds to the hemisphere $w = R$; using the result (B.22), we have that the regulated area of the extremal surface is

$$L^3_{\rm AdS} \int_{-\pi/2+\arcsin(\epsilon/R)}^{\arcsin(T)} \frac{d\theta}{\cos^3\theta} 2\pi \left(\frac{R\cos(\theta)}{\epsilon} - 1 \right) \tag{B.147}$$

From this, we need to subtract off half the regulated area of the hemispherical surface in pure AdS corresponding to a boundary ball of radius R. This area is

$$\begin{aligned} \text{Area}_{\rm AdS} &= L^3_{\rm AdS} \int_0^{\cos^{-1}\frac{\epsilon}{R}} d\theta \frac{4\pi \sin^2\theta}{\cos^3\theta} \\ &= L^3_{\rm AdS} \left(\frac{2\pi R^2}{\epsilon^2} - 2\pi \ln\frac{2R}{\epsilon} - \pi + \mathcal{O}(\epsilon^2) \right) . \end{aligned} \tag{B.148}$$

Using these results and applying the definitions (3.4,3.7,3.8), we find that

$$F_\partial = \frac{L^3_{\rm AdS}\pi}{4G} \left(\frac{T}{1-T^2} + \frac{1}{2}\ln\frac{1+T}{1-T} \right) . \tag{B.149}$$

This gives a monotonic relation between boundary F and the tension parameter T, where F_∂ is an odd function of T and where $F_\partial \to \pm\infty$ for $T \to \pm 1$.

Appendix C

Appendices for Chapter 4

C.1 Derivation of the microstate solutions

In this appendix, we provide details of the calculations in Section 4.2 for the geometries associated with Euclidean-time-evolved boundary states using the simple holographic prescription with a constant-tension ETW brane.

Action and equations of motion

The physics of the bulk spacetime and ETW brane can be encoded in an action $S = S_{\text{bulk}} + S_{\text{ETW}}$. The first term S_{bulk} is the usual Einstein-Hilbert term, regularised by a Gibbons-Hawking term at the asymptotic boundary:

$$S_{\text{bulk}} = \frac{1}{16\pi G}\int_{N_{AdS}} \mathrm{d}^{d+1}x\,\sqrt{-g}(R-2\Lambda) + S_{\text{bulk}}^{\text{matter}} + S_{\text{GHY}}. \tag{C.1}$$

The action on the ETW brane Q is a Gibbons-Hawking term, but for a dynamical boundary metric,

$$S_{\text{ETW}} = \frac{1}{8\pi G}\int_{Q_{\text{ETW}}} \mathrm{d}^{d-1}y\,\sqrt{-h}K + S_{\text{ETW}}^{\text{matter}}, \tag{C.2}$$

where y^a are intrinsic coordinates on the brane, h_{ab} is the intrinsic brane metric, and K_{ab} is the extrinsic curvature. The extrinsic curvature is roughly the derivative the intrinsic metric in the normal direction n_μ.

More precisely,

$$K_{ab} = n_{\mu;\nu}e_a^\mu e_b^\nu, \quad K = K_{ab}h^{ab} \quad e_a^\mu = \frac{\partial x^\mu}{\partial y^a}. \tag{C.3}$$

Stress-energy on the brane is defined as the variational derivative of the

brane matter action with respect to the intrinsic metric:

$$T^{\rm ETW}_{ab} = \frac{2}{\sqrt{-h}} \frac{\delta S^{\rm matter}_{\rm ETW}}{\delta h^{ab}}. \tag{C.4}$$

Varying with respect to $g^{\mu\nu}$ and h^{ab} [88], we obtain Einstein's equation in the bulk and the Neumann condition on the brane:

$$R_{\mu\nu} - \frac{1}{2} R g_{\mu\nu} = 8\pi G T^{\rm bulk}_{\mu\nu} - \Lambda g_{\mu\nu} \tag{C.5}$$

$$K_{ab} - K h_{ab} = 8\pi G T^{\rm ETW}_{ab}. \tag{C.6}$$

We will focus on *constant tension* branes, with

$$8\pi G T^{\rm ETW}_{ab} = (1-d) T h_{ab} \ , \tag{C.7}$$

where the prefactor on the right hand side is chosen for convenience.

Comparison of the gravitational actions: details

To establish the critical value $\tau_*(T)$ for τ_0 below which the black hole phase dominates the path-integral, we need to compare the gravitational action for solutions from the two phases. For $d = 2$, this calculation was carried out in [88] (Section 4) while studying the Hawking-Page type transition for BCFT on an interval. We now generalize this to arbitrary dimensions.

The Euclidean gravitational action is the sum of bulk and boundary contributions,

$$S_E = -\frac{1}{16\pi G} \int d^{d+1}x \sqrt{g}(R - 2\Lambda) - \frac{1}{8\pi G} \int d^d x \sqrt{h}(K - (d-1)T) \ . \tag{C.8}$$

For the solitions we consider, the bulk and boundary equations of motion (C.5), (C.7) imply that

$$R - 2\Lambda = -2d \tag{C.9}$$

and

$$(K - (d-1)T) = T \ . \tag{C.10}$$

For geometries of Schwarzschild form, we have

$$\sqrt{g} = r^{d-1} \,, \tag{C.11}$$

and with the ETW brane parameterized by $\tau(r)$ given by (4.17) or (4.21) we get

$$\begin{aligned} \sqrt{h} &= r^{d-1}\sqrt{f(r)\left(\frac{dr}{d\tau}\right)^2 + \frac{1}{f(r)}} \\ &= \frac{r^{d-1}}{\sqrt{f(r) - T^2 r^2}} \\ &= \pm\frac{1}{T} r^{d-2} f(r) \frac{d\tau}{dr} \,, \end{aligned}$$

where we have the $+$ or $-$ depending on whether τ is an increasing or decreasing function of r.

To regulate the actions, we integrate in each case up to $r_{\max}$ corresponding to $z = \epsilon$ in Fefferman-Graham coordinates.

Pure AdS phase: For the pure AdS phase (where $f(r) = r^2 + 1$), the bulk action gives

$$\frac{\omega_{d-1}}{8\pi G} \int_0^{r_{max}} dr d \cdot r^{d-1}(2\tau(r)) \tag{C.12}$$

where ω_{d-1} is the volume of a unit $d-1$ sphere and

$$\tau(r) = \tau_0 + \text{arcsinh}\left(\frac{T}{(r^2+1)\sqrt{1-T^2}}\right) \,. \tag{C.13}$$

Each component of the boundary action gives

$$\frac{\omega_{d-1}}{8\pi G} \int_0^{r_{max}} dr r^{d-2} f(r) \frac{d\tau}{dr} \,. \tag{C.14}$$

Combining these, we have

$$\begin{aligned} S_E^{AdS} &= \frac{\omega_{d-1}}{4\pi G} \int_0^{r_{max}} dr \left[d r^{d-1} \tau(r) + r^{d-2} f(r) \frac{d\tau}{dr} \right] \\ &= \frac{\omega_{d-1}}{4\pi G} \left\{ r_{max}^d \tau(r_{max}) + \int_0^{r_{max}} dr r^{d-2} \frac{d\tau}{dr} \right\} \end{aligned}$$

where $d\tau/dr$ can be read off from (4.21).

Black hole phase: For the black hole phase, we can write the bulk action as the full action for the Euclidean black hole up to $r = \hat{r}_{max}$ (generally not the same as r_{max} – see below) minus the action for the excised part. This gives

$$\frac{\omega_{d-1}}{8\pi G}\int_{r_H}^{r_M} drd\cdot r^{d-1}\beta - \int_{r_0}^{\hat{r}_{max}} drd\cdot r^{d-1}2\tau(r) \tag{C.15}$$

where $\tau(r)$ is given in (4.17). The brane action gives

$$-\frac{\omega_{d-1}}{4\pi G}\int_{r_0}^{\hat{r}_{max}} r^{d-2}f(r)\frac{d\tau}{dr}\ , \tag{C.16}$$

where in this case,

$$f(r) = r^2 + 1 - \frac{r_H^{d-2}}{r^{d-2}}(1+r_H^2) \tag{C.17}$$

Combining everything, we get

$$\begin{aligned} S_E^{BH} &= \frac{\omega_{d-1}}{4\pi G}\int_{r_H}^{\hat{r}_{max}} drd\cdot r^{d-1}\frac{\beta}{2} - \int_{r_0}^{\hat{r}_{max}} dr(d\cdot r^{d-1}\tau(r) + r^{d-2}f(r)\frac{d\tau}{dr}) \\ &= \frac{\omega_{d-1}}{4\pi G}\left\{\frac{\beta}{2}r^d\Big|_{r_H}^{\hat{r}_{max}} - r^d\tau(r)\Big|_{r_0}^{\hat{r}_{max}} - \int_{r_0}^{\hat{r}_{max}} dr(r^{d-2}f(r) - r^d)\frac{d\tau}{dr}\right\} \end{aligned}$$

where τ and $d\tau/dr$ can be read off from (4.17).

Cutoff surface: In order to compare the actions, we choose both r_{max} and $\hat{r}_{max}$ to each correspond to the surface $z = \epsilon$ in Fefferman-Graham coordinates. In each case, the z coordinate is related to the r coordinate by

$$\frac{dz}{z} = \frac{dr}{\sqrt{f(r)}} \tag{C.18}$$

with the integration constant fixed by demanding that $r \sim 1/z$ at leading

order for small z. For the pure AdS case, this gives in any dimension

$$r_{max} = \frac{1}{\epsilon} - \frac{\epsilon}{4} \tag{C.19}$$

while for the Euclidean black hole case, we get for example

$$\hat{r}^{d=2}_{max} = \frac{1}{\epsilon} + \frac{\pi^2 \epsilon}{16\tau_0^2} + \mathcal{O}(\epsilon^3) \tag{C.20}$$

for $d = 2$ and

$$\hat{r}^{d=4}_{max} = \frac{1}{\epsilon} - \frac{\epsilon}{4} + \frac{1}{8} r_H^2 (1 + r_H^2)\epsilon^3 + \mathcal{O}(\epsilon^5) \tag{C.21}$$

for $d = 4$.

Action difference: We can now evaluate the difference

$$S_E^{AdS}(T, \tau_0, \epsilon) - S_E^{BH}(T, \tau_0, \epsilon) \tag{C.22}$$

and take the limit $\epsilon \to 0$ in order to determine which solution has smaller action and gives rise to the classical geometry associated with the state.

As examples, we find that for $d = 2$, we have

$$\lim_{\epsilon \to 0} (S_E^{AdS}(T, \tau_0, \epsilon) - S_E^{BH}(T, \tau_0, \epsilon)) = \frac{1}{2G} \left[-\text{arctanh}(T) - \frac{\tau_0}{2} + \frac{\pi^2}{8\tau_0} \right] . \tag{C.23}$$

Thus, our states correspond to bulk black holes when

$$\tau_0 < -\text{arctanh}(T) + \sqrt{\frac{\pi^2}{4} + \text{arctanh}^2(T)} \, . \tag{C.24}$$

Here, we assume that the CFT is defined on a circle of length 2π. This critical value of τ_0 decreases monotonically from $\tau_*(-1) = \infty$ to $\tau_*(0) = \pi/2$ to $\tau_*(1) = 0$, as shown in Figure 4.9. This result agrees with the calculation of [88] (reinterpreted for our context).

For $d = 4$, it is most convenient to parameterize the action difference in terms of r_H and T since there can be more than one solution in the black

hole phase with the same T and τ_0. We find that

$$\begin{aligned}\Delta S(r_H,T) &\equiv \frac{4\pi G}{\omega_3}\lim_{\epsilon\to 0}(S_E^{AdS}(T,r_H,r_{max}(\epsilon)) - S_E^{BH}(T,r_H,\hat{r}_{max}(\epsilon))) \\ &= -\left[\frac{1}{2}r_H^2(1+r_H^2)\tau_0(r_H) - \frac{\pi r_H^5}{1+2r_H^2} + \frac{Tr_0(r_H,T)}{\sqrt{1-T^2}} - I_4(rH,T)\right] \\ &\qquad + \left[\frac{T}{1-T^2} + \text{arctanh}(T)\right] , \quad \text{(C.25)}\end{aligned}$$

where (taking $f(r) = r^2+1-r_H^2/r^2(1+r_H^2)$ in the formulae below), $r_0(r_H,T)$ is defined as above by

$$f(r_0) = T^2 r_0^2 , \quad \text{(C.26)}$$

and $\tau_0(r_H,T)$ is defined as

$$\tau_0(rH,T) = \int_{r_0}^{\infty} dr \frac{Tr}{f(r)\sqrt{f(r)-T^2r^2}} \quad \text{(C.27)}$$

and

$$I_4(rH,T) = \int_{r0(r_H,T)}^{\infty} dr \left\{ \frac{Tr(r^2 - r_H^2(1+r_H^2))}{f(r)\sqrt{f(r)-T^2r^2}} - \frac{T}{\sqrt{1-T^2}} \right\} . \quad \text{(C.28)}$$

Evaluating $\Delta S(r_H,T)$ for $T \geq 0$, we find that for $T < T_c \approx 0.37505$, the difference ΔS is positive for $r_H > r_H^*(T)$ where $r_H^*(T)$ increases monotonically from $r_H^* = 1$ at $T = 0$ to $r_H^* = \infty$ at $T = T_c$. The corresponding value of τ_0 decreases from $\pi/6$ at $T = 0$ to 0 at $T = T_c$, as shown in figure 4.9. We note that in cases where there are two solutions in the black hole phase with the same τ_0, the lowest action solution is always either the one with larger r_H or the corresponding pure AdS phase solution.

Lorentzian geometries: general T

In this subsection, we discuss the Lorentzian solutions corresponding to general values of the parameter T. We recall that in terms of the proper time and the variable $L = \log(r)$ (where r is the proper radius of the brane),

the equation for the brane trajectory is

$$\dot{L}^2 + V(L) = T^2 \tag{C.29}$$

where

$$V(L) = \frac{f(r)}{r^2} = 1 + e^{-2L} - e^{-d(L-L_H)}(1 + e^{-2L_H}) \,. \tag{C.30}$$

So the trajectory $L(\lambda)$ is that of a particle in a one-dimensional potential $V(L)$ with energy T^2. These potentials were displayed in Figure 4.11.

For $d = 2$, the potential is monotonically increasing and asymptotes to 1. The Lorentzian trajectories for $|T| < 1$ all correspond to time-symmetric configurations where the brane emerges from the past singularity at $r = 0$, reaches a maximum size $r_0 = r_H/\sqrt{1 - T^2}$, and shrinks again to $r = 0$ at the future singularity. These all have analytic continuations to Euclidean solutions as discussed above. For $T > 1$, there are no time-symmetric trajectories; the ETW brane size either increases from $r = 0$ to $r = \infty$ or shrinks from $r = \infty$ to $r = 0$. These do not come from analytically continued time-symmetric geometries, and we expect that they do not correspond to the types of states we have been disucussing.

For $d > 2$, the potential is monotonically increasing to some value $T^2_{\text{crit}} > 1$, where

$$T_{\text{crit}} = 1 + \left(\frac{2}{d}\right)^{\frac{2}{d-2}} \left(1 - \frac{2}{d}\right) \frac{1}{r_H^2 (1 + r_H^2)^{\frac{2}{d-2}}} \tag{C.31}$$

We have five classes of trajectories, as shown on the right in Figure 4.11. The corresponding spacetimes are shown in Figure C.1.

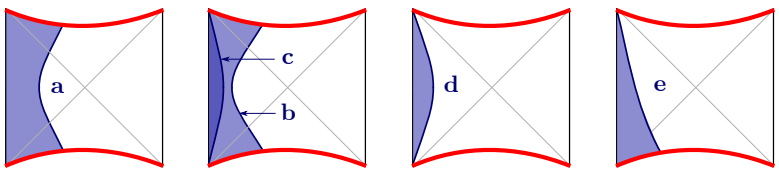

Figure C.1: Lorentzian ETW branes for various values of T.

Case a: $0 < T < T_*$

For this case, we have time-symmetric solutions which have analytic continuations to good Euclidean solutions corresponding to some finite positive Euclidean preparation time. These are the geometries that are most plausibly providing a holographic picture of the microstate geometries for some legitimate CFT states. The Lorentzian geometry takes the form in Figure 4.1. The brane emerges from the past singularity, expands and enters the second asymptotic region and then shrinks, eventually falling into the future horizon. The maximum radius of the ETW brane is r_0 (the minimal radius in the Euclidean solution), realized at the time-symmetric point $t = 0$. The entire trajectory covers some finite amount of proper time given by

$$\lambda_{\text{tot}} = 2 \int_0^{r_0} \frac{dr}{\sqrt{T^2 r^2 - f(r)}} \,. \tag{C.32}$$

For $d = 2$, this gives

$$\lambda_{\text{tot}}^{d=2} = \frac{\pi L_{\text{AdS}}}{\sqrt{1 - T^2}} \tag{C.33}$$

while for $d = 4$, we get

$$\lambda_{\text{tot}}^{d=4} = \frac{L_{\text{AdS}}}{\sqrt{1 - T^2}} \arccos\left(\frac{1}{\sqrt{(1 - T^2)(2r_H^2 + 1)^2 + T^2}} \right) \,. \tag{C.34}$$

The $d = 3$ result is given in terms of elliptic integrals.

Case b: $1 < T < T_{\text{crit}}$**, small** r **branch**

For this case, we have Lorentzian trajectories that are qualitatively similar to the previous case, but we recall that here the corresponding Euclidean solutions are not sensible (at least without some improvement of the model). It is possible that these Lorentzian solutions still correspond to some CFT states, but we do not have a clear argument for this.

Case c: $1 < T < T_{\text{crit}}$**, large** r **branch**

For these solutions the ETW brane starts and ends at infinite size, shrinking to a minimum size at the time-symmetric point. We have an infinitely large portion of the second asymptotic region both in the past and

the future, so it is unlikely these geometries correspond to pure states of a single CFT.

Case d: $T = T_{\text{crit}}$

In this case, we have Lorentzian brane trajectories at a constant radius, and the ETW brane geometry is the Einstein static universe. Here, the solutions retain the isometry present in the maximally extended black hole geometry and the physics of the CFT is time-independent. The Euclidean solutions in this case also have the brane at a constant radius, so the trajectory does not intersect the Euclidean boundary and does not seem likely to correspond to the class of states we have been discussing. However, it is interesting that the spacetime picture we have been discussing is similar to the proposal of [210] for the geometries dual to typical states, so perhaps the Lorentzian geometries in this case can serve as a model of the typical states. It is interesting that we are constrained to have the brane at one specific radius,

$$\frac{r}{r_H} = \left(\frac{d}{2}\right)^{\frac{1}{d-2}} (1 + r_H^2)^{\frac{1}{d-2}} \ . \tag{C.35}$$

Case e: $T > T_{\text{crit}}$

For these case, there are no time-symmetric ETW brane trajectories, and we have an infinitely large portion of the second asymptotic region either in the past or the future, so it seems unlikely that these geometries correspond to pure states of a single CFT.

C.2 Coordinate systems for $d = 2$

In this appendix, we give the coordinate transformations relating $s - y$ coordinates in (4.53) which cover the full maximally extended black hole geometry to the Schwarzschild coordinates.

We first go to Kruskal-type coordinates by defining

$$r = r_H \frac{1 - uv}{1 + uv} \qquad t = \frac{1}{2r_H} \ln\left(-\frac{u}{v}\right) \ . \tag{C.36}$$

In these coordinates, the metric becomes (here, we have set $L_{\text{AdS}} = 1$)

$$ds^2 = -\frac{4dudv}{(1+uv)^2} + r_H^2 \frac{(1-uv)^2}{(1+uv)^2} d\phi^2 \,. \tag{C.37}$$

These coordinates cover the whole extended spacetime. The two boundaries are at $uv = -1$, the singularities are at $uv = 1$, and the horizons are at $uv = 0$. The relation to Schwarzschild coordinates in the second asymptotic region is given by (C.36) with the replacement $u \leftrightarrow v$. To obtain the metric (4.53), we further define

$$u = \tan(\alpha) \qquad v = \tan(\beta) \qquad s = \beta + \alpha \qquad y = \alpha - \beta \,. \tag{C.38}$$

From (4.25), the Lorentzian ETW brane trajectory in Schwarzschild coordinates for the second asymptotic region is given (in the case for $0 < T < 1$) by

$$t = \frac{1}{r_H} \text{arctanh} \left(\frac{\sqrt{r_H^2 - r^2(1-T^2)}}{T r_H} \right) \,. \tag{C.39}$$

In the u, v coordinates, we find that this becomes (setting $L = 1$),

$$T = \frac{v-u}{\sqrt{1+u^2}\sqrt{1+v^2}} \,. \tag{C.40}$$

In the s, y coordinates we get simply

$$y = -\arcsin(T) \,. \tag{C.41}$$

C.3 Imaginary time entanglement growth

Imaginary time evolution can generate extremely rapid entanglement growth even if the Hamiltonian doesn't couple different degrees of freedom. This fact severely restricts any conceivable bound on entanglement growth under imaginary time dynamics.

Consider a decoupled Hamiltonian on N spins of the form

$$H = \sum_{r=1}^{N} \Delta \frac{1 - \sigma_r^z}{2}. \tag{C.42}$$

Spin up is identified with 0 and spin down with 1. The system is divided into two pieces, left L and right R, with $N/2$ spins each.

Now define two states as follows. State one is the all down state, the highest energy state of H,

$$|\psi_1\rangle = |1 \cdots 1\rangle. \tag{C.43}$$

State two is an entangled Bell-type state obtained as an equal superposition of all states $|\psi_i\rangle_L \otimes |\psi_i\rangle_R$ where $|\psi_i\rangle$ is a product state with $S^z = 0$ (we assume $N/2$ is even). There are approximately $2^{N/2}$ such states (a significant fraction of the full left or right Hilbert space). Note that energy of state one is $N\Delta$ and the energy of state two is $N\Delta/2$.

The example is based on the superposition

$$|\psi\rangle = \sqrt{1-\epsilon}|\psi_1\rangle + \sqrt{\epsilon}|\psi_2\rangle, \tag{C.44}$$

which can be prepared using a low depth quantum circuit. The entropy of L or R in this pure state is $N\epsilon/2$, so if ϵ is very small, then the entropy is very small. Now consider the imaginary time evolved state

$$e^{-\beta H/2}|\psi\rangle. \tag{C.45}$$

Up to an overall normalization, the effect is to exponentially re-weight states one and two in the superposition,

$$e^{-\beta H/2}|\psi\rangle \propto \sqrt{1-\epsilon}|\psi_1\rangle + \sqrt{\epsilon}e^{\beta N\Delta/2}|\psi_2\rangle. \tag{C.46}$$

The normalized state is

$$\frac{e^{-\beta H/2}|\psi\rangle}{\|e^{-\beta H/2}|\psi\rangle\|} = \sqrt{\frac{1-\epsilon}{1+(e^{N\beta\Delta/2}-1)\epsilon}}|\psi_1\rangle + \sqrt{\frac{\epsilon e^{N\beta\Delta/2}}{1+(e^{N\beta\Delta/2}-1)\epsilon}}|\psi_2\rangle. \tag{C.47}$$

Hence the entropy as a function of β is

$$S = \frac{N}{2}\frac{\epsilon e^{N\beta\Delta/2}}{1+(e^{N\beta\Delta/2}-1)\epsilon}. \tag{C.48}$$

This formula yields extremely rapid entanglement growth; for example, if $\epsilon \sim 1/N$ so that the initial entanglement is of order a single bit, then the imaginary time evolution can generate N bits of entanglement in an imaginary time of order $\frac{\ln N}{N\Delta}$.

If the ground state is also added to the superposition, then the entanglement depends on the relative size of the coefficients in the superposition. If the coefficients are roughly the same size, then the ground state will grow large much more rapidly than the middle energy states. In this case the entanglement may not ever become very large.

C.4 Boundary states in a solvable model

By considering a simple model with a completely classical Hamiltonian, it is possible to rigorously establish some claims analogous to those made at large N for the coupled SYK clusters.

Consider a classical Hamiltonian on N qubits,

$$H_c = \sum_{r,r'} J_{r,r'}\sigma_r^z\sigma_{r'}^z, \tag{C.49}$$

where classical means that the Hamiltonian is diagonal in a local product basis. One could add additional terms which are diagonal in the σ_r^z basis without changing the subsequent story.

Now consider a generic product state $|x\rangle$ in the σ_r^x basis. It obeys $\sigma_r^x|x\rangle =$

$x_r|x\rangle$ with $x_r = \pm 1$. When expanding in the z basis, these states are

$$|x\rangle = \frac{1}{\sqrt{2^n}} \sum_z \left(\prod_r z_r^{\frac{1-x_r}{2}} \right) |z\rangle. \tag{C.50}$$

Define the imaginary time-evolved states

$$|x, \beta\rangle = e^{-\beta H_c/2}|x\rangle. \tag{C.51}$$

The norm of these states is independent of x:

$$\langle x, \beta | x, \beta\rangle = \sum_z \left(\prod_r z_r^{\frac{1-x_r}{2}} \right)^2 \langle z|e^{-\beta H_c}|z\rangle = Z_c(\beta), \tag{C.52}$$

where Z_c is the partition function associated with H_c. Similarly, one can show that any moment of H_c in the state $|x, \beta\rangle$ is independent of x. More generally, any observable that is diagonal in the σ_r^z basis has an expectation value in the state $|x, \beta\rangle$ that is independent of x and given by the corresponding value in the classical statistical problem with weight $e^{-\beta\langle z|H_c|z\rangle}$.

Moreover, every state $|x, \beta\rangle$ is related to every other state $|x', \beta\rangle$ by a local unitary transformation. More precisely, we have

$$|x', \beta\rangle = \prod_{r=1}^{N} (\sigma_r^z)^{\frac{1-x_r x_r'}{2}} |x, \beta\rangle. \tag{C.53}$$

This shows that every state $|x, \beta\rangle$ has the same entanglement for every spatial subregion independent of x. In particular, even though the states $|x, \beta\rangle$ need not be translation invariant, all the entanglement entropies are if the Hamiltonian H_c is.

Finally, by tuning βH_c to a classical statistical critical point or into an ordered phases, it follows that imaginary time evolution can generate long-range correlations after only a "finite depth" imaginary time evolution. This is in stark contrast to the situation with real time dynamics, in which long-range correlations must be established slowly starting from a short-range correlated state due to causality restrictions. In fact, in one dimension

Araki has established an imaginary time analog of the Lieb-Robinson bound in which operators are allowed to expand exponentially fast [328].

C.5 Details of the Action-Complexity Calculation

As can be seen in figure 4.25, the Wheeler-DeWitt patch during each phase is defined by two null hypersurfaces, N_+ and N_-, anchored at the asymptotic boundary. Whether these null surfaces intersect the future/past singularity (S_+/S_-), or the ETW brane (Q), determines which phase is being considered. The problem of calculating the gravitational action on a region with boundaries is a well studied one (see [248] for a comprehensive review), and generically we will have terms corresponding to: the enclosed region, the region's boundaries, and the joints where boundaries meet non-smoothly. Here we breakdown each of these terms and state the results before and after the null boundary counterterm is included.

The first term that one must consider is the Einstein-Hilbert action evaluated on the Wheeler-DeWitt patch. In the s, y coordinates this amounts to computing:

$$\begin{aligned} S_{\text{EH}} &= \frac{1}{16\pi G}\int_{\mathcal{W}} d^{d+1}x\sqrt{-g}(R-2\Lambda) \\ &= -\frac{r_H}{4\pi G}\int_{\mathcal{W}} ds\ dy\ d\theta\ \sec^3(y)\cos(s) \end{aligned} \tag{C.54}$$

This term diverges during all phases, since we are integrating all the way out to the asymptotic boundary. As such, a regulator surface Λ is introduced to classify the divergence. In the the s, y coordinates Λ is the hypersurface defined by:

$$\Lambda: \quad y = \pi/2 - \delta \tag{C.55}$$

In the limit $\delta \to 0$ we simply recover our asymptotic boundary. Another common cutoff method is to set the Schwarzschild radius to some maximum value, i.e.:

$$\Lambda: \quad r = \frac{L_{\text{AdS}}}{\delta'} \tag{C.56}$$

Working with $L_{\text{AdS}} = 1$, one can convert back and forth between the two cutoff schemes via the relation:

$$\delta' = \frac{\sin(\delta)}{r_h \operatorname{sech}(r_H t_R)} \tag{C.57}$$

One may then ask what the contribution to the action is from this boundary Λ itself. In general, a non-null boundary, $\mathcal{B}$, contributes a Gibbons-Hawking-York (GHY) term to the action:

$$S_{\text{GHY}} = \frac{1}{8\pi G} \int_{\mathcal{B}} d^d x \sqrt{|h|} K \tag{C.58}$$

Here, we must be careful to choose the orientation of each hypersurface consistently so that the relative sign of each action contribution is correct. For the hypersurface Λ, a unit one-form normal is chosen to be:

$$\mathbf{n}_\Lambda = \frac{1}{\sin(\delta)} dy \tag{C.59}$$

Using this the extrinsic curvature is then calculated to be:

$$K_\Lambda = 2\cos(\delta) \tag{C.60}$$

Solving for the induce metric on Λ then putting this all into (C.58) gives the action contribution:

$$\begin{aligned} S_\Lambda &= \frac{r_H}{4\pi G} \frac{\cot(\delta)}{\sin(\delta)} \int_\Lambda ds\ d\theta\ \cos(s) \\ &= \frac{r_H}{\delta G} \operatorname{sech}(r_H t_R) + O(\delta) \end{aligned} \tag{C.61}$$

This term is present during all three phases.

Next we will consider the contribution due to the ETW brane. The integration limits will be different depending on the phase, however the form of the action is always the same:

$$S_Q = \frac{1}{8\pi G} \int_Q d^d x \sqrt{|h|} (K_Q - T) \tag{C.62}$$

This corresponds to the GHY term for the hypersurface plus a matter action. Here, a simplistic matter action for the brane is considered, with the matter Lagrangian being assumed to be a constant parametrised by the brane tension T (this follows the approach outlined in [88]) The unit normal one-form for Q is chosen to be:

$$\mathbf{n}_Q = -\frac{1}{\sqrt{1-T^2}}dy \tag{C.63}$$

Solving for the extrinsic curvature and induced metric we find:

$$S_Q = \frac{r_H}{8\pi G}\frac{T}{1-T^2}\int_Q ds\ d\theta\ \cos(s) \tag{C.64}$$

The only remaining non-null hypersurfaces to consider are the past and future singularities at $s = \pm\frac{\pi}{2}$. Calculating the contribution here slightly tricky: the induced metric on $S_\pm$ vanishes and the extrinsic curvature $K_\pm$ diverges. However, if we instead considers a hypersurfaces at $s =$ constant then we can compute the integrate explicitly. When doing this, one finds that in the limit $s \to \pm\frac{\pi}{2}$ the measure and extrinsic curvature actually combine to give a finite, regulator independent, integrand. The unit normal one-forms to the singularities are chosen to be:

$$\mathbf{t}_\pm = \sec(y)ds \tag{C.65}$$

The measure for a constant s surface is

$$\sqrt{|h|} = r_H \cos(s)\sec^2(y) \tag{C.66}$$

and the extrinsic curvature is:

$$K_\pm = \pm\tan(s)\cos(y) \tag{C.67}$$

Note that the sign difference here is due to the orientation of $S_\pm$. Combining this together, and taking the limit $s \to \pm\frac{\pi}{2}$, we write our GHY term for each

singularity respectively as:

$$S_{S_\pm} = \frac{r_H}{8\pi G}\int_{S_\pm} dy\ d\theta\ \sec(y) \tag{C.68}$$

This corresponds to a total contribution during phase ii of:

$$\text{Phase ii:}\ \ S_{S_+} + S_{S_-} = \frac{r_H}{2G}\operatorname{arctanh}(T) \tag{C.69}$$

During phase iii the contribution is

$$\text{Phase iii:}\ \ S_{S_+} = \frac{r_H}{4G}\left(r_H t_R + \operatorname{arctanh}(T)\right) \tag{C.70}$$

Notice that this calculation did not take into account any nonclassical effects. One might expect the divergences coming from the introduction of higher order curvature terms not to cancel away here. These stringy corrections have not been considered here, however in principle on could introduce a regulator surface in the same manner done for the asymptotic boundary in order to classify these divergences.[115]

We now move onto the discussion of the null hypersurfaces N_+ and N_-. These surfaces are defined by the equations:

$$\begin{aligned} N_+ :\ s &= -y + 2\arctan\left(e^{r_H t_R}\right) \\ N_- :\ s &= +y - 2\operatorname{arccot}\left(e^{r_H t_R}\right) \end{aligned} \tag{C.71}$$

The null normal one-forms for these surfaces are chosen to be:[116]

$$\mathbf{k}_\pm = \alpha_\pm(\pm ds + dy) \tag{C.72}$$

Here, α_+ and α_- are normalisation constants. We also endow each null hypersurface with coordinates $(\lambda_\pm, \theta)$, where θ is the angular BTZ coordinate

[115] Some related calculations can be found in [329], wherein the Gauss-Bonnet-AdS black hole is considered.

[116] For brevity, we omit the derivations of these quantities. A thorough examination of null hypersurfaces can be found in [330].

and $\lambda_\pm$ is given by:

$$\lambda_\pm = \frac{1}{\alpha_\pm}\tan(y) \tag{C.73}$$

Altogether, this constitutes an affine parametrization for the null hypersurfaces. I.e., they solve the affine geodesic equation:

$$\begin{aligned} k_{\alpha;\beta}k^\beta &= \kappa k_\alpha \\ &= 0 \end{aligned} \tag{C.74}$$

Thus, we see that for this parametrization the constant $\kappa = 0$. The boundary term for a null hypersurface is typically given by:

$$S_{N_\pm} = -\frac{1}{8\pi G}\int_{N_\pm} d\lambda d^{d-1}\theta\sqrt{\gamma}\kappa \tag{C.75}$$

However, since we have chosen an affine parametrization this contribution vanishes.

Next we consider the joints between each of these boundary surfaces. In principle we have joints where $N_\pm$ intersect $S_\pm$, Q and Λ, as well as non-null joints (of the type proposed in [331]) at $S_\pm \cap Q$. However, one finds that the joint terms at $S_\pm \cap Q$ and at $N_\pm \cap S_\pm$ all vanish. The only non-zero joint terms are from intersections of the null surfaces with the regulator surface and the ETW brane. These are joints betwen null and timelike hypersurfaces and so correspond to action contributions of the form:

$$\begin{aligned} S_{\text{joints}} &= \frac{1}{8\pi G}\int_\Sigma d^{d-1}x\sqrt{\sigma}a \\ a &= \epsilon \ln|\mathbf{k}\cdot\mathbf{n}| \\ \epsilon &= -\operatorname{sign}(\mathbf{k}\cdot\mathbf{n})\operatorname{sign}(\mathbf{k}\cdot\hat{t}) \end{aligned} \tag{C.76}$$

Here $\mathbf{k}$ and $\mathbf{n}$ are the normal one-forms to the null and timelike surfaces respectively, and $\hat{t}$ is some auxiliary unit vector tangent to the timelike hypersurface. Σ is the co-dimension two hypersurface that is the intersection between the two boundaries. Computing the contributions for $N_\pm \cap \Lambda$, one

finds that in all phases we have:

$$S_{N_+\cap\Lambda} + S_{N_-\cap\Lambda} = \frac{r_H}{4G}\left\{\frac{2\,\mathrm{sech}(r_H t_R)}{\delta}\ln\left(\frac{1}{\sqrt{\alpha_+\alpha_-}\delta}\right) + \tanh(r_h t_R)\ln\left(\frac{\alpha_-}{\alpha_+}\right) + O(\delta)\right\} \quad \text{(C.77)}$$

Similarly, one can compute the action contribution for the intersections $N_\pm \cap Q$. These turn out to be:

$$S_{N_\pm\cap Q} = -\frac{r_H}{4G}\ln(\alpha_\pm\sqrt{1-T^2})\left(\pm\tanh(r_H t_R) + \frac{T}{\sqrt{1-T^2}}\,\mathrm{sech}(r_h t_R)\right) \quad \text{(C.78)}$$

Where the term for $N_+ \cap Q$ is only present during phase i and the term for $N_+ \cap Q$ only appears in phase iii.

Unfortunately, if we were to combine together all of the terms above we would find that the resulting action is dependent on α_+ and α_-. This isn't ideal as the quantity we find is not invariant under different choices of the parametrization of each null surface. Recently, it has been suggested that a counterterm be introduced to the gravitational action in order to cancel this dependence on α_+ and α_-:[117]

$$\begin{aligned} S_{\text{counter}} &= -\frac{1}{8\pi G}\int_{\mathcal{B}} d\lambda\; d^{d-1}\theta\sqrt{\gamma}\Theta\ln|L\Theta| \\ \Theta &= \frac{1}{\sqrt{\gamma}}\frac{\partial\gamma}{\partial\lambda} \end{aligned} \quad \text{(C.79)}$$

Where we introduce such a term for each null boundary $\mathcal{B}$. Here, γ corresponds to the null hypersurface's metric. Just as the complexity=volume conjecture was only defined up to some relative length scale, this counterterm depends on an arbitrary length scale L. For the purposes of this analysis, we will simply choose to set $L = L_{\text{AdS}} = 1$.[118] For N_+ the counterterm takes

[117] This counterterm was first proposed in [248] and has since been discussed throughout the literature. Some more thorough exploration of this counterterm can be found in [332] and [333].

[118] Some easy to interpret graphs are provided in appendices of [247] that show the effects of changing the value of this length scale.

the form:

$$\begin{aligned} S_{N_+} &= -\frac{r_H}{4G}\alpha_+ \operatorname{sech}(r_H t_R) \\ &\quad \int_{N_+} d\lambda \, \ln\left|\frac{\alpha_+ \operatorname{sech}(r_H t_R)}{\alpha_+ \operatorname{sech}(r_H t_R)\lambda - \tanh(r_H t_R)}\right| \\ &= \frac{r_H}{4G}\operatorname{sech}(r_H t_R)\left(\sinh(r_H t_R) - \alpha_+\lambda\right) \\ &\quad \left(1 + \ln\left|\frac{\alpha_+}{\sinh(r_H t_R) - \alpha_+\lambda}\right|\right)\Bigg|_{\lambda_i}^{\lambda_f} \end{aligned} \tag{C.80}$$

where $\lambda_i = N_+ \cap \Lambda$ during every phase, and $\lambda_f = N_+ \cap Q$ during phase i or $N_+ \cap S_+$ otherwise. Similarly, the counterterm for N_- can be calculated using:

$$\begin{aligned} S_{N_-} &= -\frac{r_H}{8G}\alpha_- \operatorname{sech}(r_H t_R) \\ &\quad \int_{N_-} d\lambda \, \ln\left|\frac{\alpha_- \operatorname{sech}(r_H t_R)}{\alpha_- \operatorname{sech}(r_H t_R)\lambda + \tanh(r_H t_R)}\right| \\ &= -\frac{r_H}{4G}\operatorname{sech}(r_H t_R)\left(\sinh(r_H t_R) + \alpha_-\lambda\right) \\ &\quad \left(1 + \ln\left|\frac{\alpha_-}{\sinh(r_H t_R) + \alpha_-\lambda}\right|\right)\Bigg|_{\lambda_i}^{\lambda_f} \end{aligned} \tag{C.81}$$

with $\lambda_i = N_- \cap \Lambda$ during each phase, and λ_f being $N_- \cap Q$ during phase iii or $N_- \cap S_-$ otherwise. Both of these integrals result in many terms, so we will refrain from including them here.

With all of the individual contributions to the action in place, all that remains is to combine them all together in accordance with the phases depicted in figure 4.25 and use equation (4.118) to calculate the complexity. In doing this, many, many terms cancel, resulting in the simple expressions stated in equations (4.121) and (4.123) (the phase iii result is stated with the divergence already subtracted).

Appendix D

Appendices for Chapter 5

D.1 Brane trajectories

Throughout this appendix, we will be interested in a codimension-1 surface parametrized by $(z, r, x^\mu) = (Z(r), r, x^\mu)$ in the AdS soliton geometry

$$ds^2_{d+1} = L^2 f(r) dz^2 + \frac{dr^2}{f(r)} + r^2 dx_\mu dx^\mu \,. \tag{D.1}$$

This may be either an interface brane or an ETW brane; the calculation of intrinsic geometrical quantities and the extrinsic curvature with respect to one side will be identical in both cases, so we will not distinguish between these cases until we come to the equations of motion. We also suppress the coordinate subscripts that would differentiate between the regions $\mathcal{M}_1$ and $\mathcal{M}_2$ in the interface case. We could allow $dx_\mu dx^\mu = \eta_{\mu\nu} dx^\mu dx^\nu$ to denote the metric on either flat Euclidean or Minkowski space; the choice of signature will not affect any of the expressions we derive.

Geometrical quantities

We have tangent vector

$$e^\mu_r = (Z'(r), 1, \vec{0}) \,, \tag{D.2}$$

and the rest of the tangent vectors on the brane are just unit vectors spanning the x^μ directions. The induced metric h_{ab} on the ETW brane is of course

$$ds^2_d = \frac{L^2}{c(r)^2} dr^2 + r^2 dx_\mu dx^\mu \,, \qquad c(r) \equiv \sqrt{\frac{L^2 f(r)}{1 + L^2 f(r)^2 (Z'(r))^2}} \,. \tag{D.3}$$

The spacelike unit normal vector to the brane with the correct orientation (pointing out of the region) is given by

$$n_\mu = c(r)(-1, Z'(r), \vec{0}) \,. \tag{D.4}$$

We can now compute the extrinsic curvature

$$K_{ab} = e^\mu_a e^\nu_b \nabla_\mu n_\nu \,, \tag{D.5}$$

using that

$$\begin{aligned} \nabla_\mu n_\nu = \frac{L^2 c f f' Z'}{2} dz^2 + \left(\frac{cf'}{2f} - c'\right) dz\, dr + \frac{cf'}{2f} dr\, dz \\ + \left(\frac{cf'Z'}{2f} + c'Z' + cZ''\right) dr^2 + rcfZ' dx_\mu dx^\mu \,. \end{aligned} \tag{D.6}$$

We find

$$\begin{aligned} K_{rr} &= e^r_r e^r_r \nabla_r n_r + e^z_r e^r_r \nabla_z n_r + e^r_r e^z_r \nabla_r n_z + e^z_r e^z_r \nabla_z n_z \\ &= c\left(Z'' + \frac{f'Z'}{2f}(L^2 f^2 (Z')^2 + 3)\right) \\ K_{ii} &= rcfZ'\eta_{ii} \,, \end{aligned} \tag{D.7}$$

with all other components vanishing; here, the i appearing in K_{ii} is an (unsummed) $(d-1)$-dimensional Lorentz index. In particular, the scalar extrinsic curvature is

$$K = h^{ab} K_{ab} = \frac{c^3}{L^2}\left(Z'' + \frac{f'Z'}{2f}(L^2 f^2 (Z')^2 + 3)\right) + \frac{(d-1)}{r} cfZ' \,. \tag{D.8}$$

In some cases, it may be useful to phrase our analysis in terms of derivatives with respect to a proper length coordinate s along the brane in the (z, r)-plane; that is, we take this to be the coordinate appearing in our intrinsic parametrization of the brane, which then has metric

$$ds_d^2 = ds^2 + r(s)^2 dx_\mu dx^\mu \,. \tag{D.9}$$

Such a coordinate is defined by

$$L^2 f(r) \left(\frac{dz}{ds}\right)^2 + \frac{1}{f(r)} \left(\frac{dr}{ds}\right)^2 = 1 \,. \tag{D.10}$$

We then express the normal vector as $n_\mu = L(-\dot{r}, \dot{z}, \vec{0})$, so the non-vanishing components of the extrinsic curvature may be written as

$$\begin{aligned} K_{ss} &= \frac{L}{2} \frac{dz}{ds} f'(r) \left(3 - L^2 f(r) \left(\frac{dz}{ds}\right)^2\right) \\ K_{ii} &= Lrf(r) \frac{dz}{ds} \eta_{ii} \,. \end{aligned} \tag{D.11}$$

We note that reversing the orientation of the normal vector used in the definition of the extrinsic curvature has the effect of reversing its sign; this is especially important to note when deducing the interface equation of motion.

We will also be interested in features of the intrinsic geometry of the brane, namely the components of the Ricci tensor and the Ricci scalar. We find non-vanishing components

$$R^{(d)}_{rr} = -\frac{(d-1)}{r} \frac{c'(r)}{c(r)} \,, \qquad R^{(d)}_{ii} = -\frac{c(r)^2}{L^2} \left((d-2) + r\frac{c'(r)}{c(r)}\right) \eta_{ii} \,, \tag{D.12}$$

or, in the proper length coordinates,

$$\begin{aligned} R^{(d)}_{ss} &= -(d-1) \frac{r''(s)}{r(s)} \,, \\ R_{ii} &= -r(s)^2 \left(\frac{r''(s)}{r(s)} + (d-2)\frac{r'(s)^2}{r(s)^2}\right) \eta_{ii} \,. \end{aligned} \tag{D.13}$$

The Ricci scalars are

$$\begin{aligned} R^{(d)} &= -(d-1) \frac{c(r)^2}{r^2 L^2} \left((d-2) + 2r\frac{c'(r)}{c(r)}\right) \\ &= -(d-1) \left(2\frac{r''(s)}{r(s)} + (d-2)\frac{r'(s)^2}{r(s)^2}\right) \,. \end{aligned} \tag{D.14}$$

D.1.1 Constant tension branes

We will first consider the case with two branes of constant tension: an interface brane which divides the bulk into regions 1 and 2, and an ETW brane which we add to region 1.

Suppose we have the Euclidean gravitational action

$$\begin{aligned} S &= S_{\text{bulk}} + S^{\text{matter}}_{\text{interface}} + S^{\text{matter}}_{\text{ETW}} \\ S_{\text{bulk}} &= \frac{1}{16\pi G_{\text{bulk}}} \sum_{i=1}^{2} \int_{\mathcal{M}_i} d^{d+1}x\sqrt{g}\ (R - 2\Lambda_i) \\ &\quad + \frac{1}{8\pi G_{\text{bulk}}} \int_{\text{interface}} d^d y\sqrt{h}\ [K] \\ &\quad + \frac{1}{8\pi G_{\text{bulk}}} \int_{\text{ETW}} d^d y\sqrt{h}\, K\,, \end{aligned} \tag{D.15}$$

where we take the brane matter actions to be

$$\begin{aligned} S^{\text{matter}}_{\text{interface}} &= \frac{(1-d)\kappa}{8\pi G_{\text{bulk}}} \int_{\text{interface}} d^d y\sqrt{h}\,, \\ S^{\text{matter}}_{\text{ETW}} &= \frac{(1-d)\lambda}{8\pi G_{\text{bulk}}} \int_{\text{ETW}} d^d y\sqrt{h}\,. \end{aligned} \tag{D.16}$$

Here and in the following, the brackets represent the discontinuity $[X] = X_1 - X_2$ across the interface brane. We are also permitting two different cosmological constants Λ_i, related to the AdS lengths L_i by

$$\Lambda_i = -\frac{d(d-1)}{2L_i}\,. \tag{D.17}$$

The interface brane trajectory is then determined by the junction conditions

$$[h_{ab}] = 0\,, \quad [K_{ab} - K h_{ab}] = 8\pi G_{\text{bulk}} T^{\text{interface}}_{ab} = (1-d)\kappa h_{ab}\,, \tag{D.18}$$

where we use

$$T^{\text{interface}}_{ab} = \frac{2}{\sqrt{h}} \frac{\delta S^{\text{matter}}_{\text{interface}}}{\delta h^{ab}} = \frac{(1-d)\kappa}{8\pi G_{\text{bulk}}} h_{ab}\,. \tag{D.19}$$

It can be convenient to rewrite the second junction condition as

$$[K_{ab}] = \kappa h_{ab} \,. \tag{D.20}$$

Meanwhile, the ETW brane trajectory is determined by the equations of motion

$$K_{ab} - K h_{ab} = 8\pi G_{\rm N} T^{\rm ETW}_{ab} = (1-d)\lambda h_{ab} \,, \tag{D.21}$$

where we use

$$T^{\rm ETW}_{ab} = \frac{2}{\sqrt{h}} \frac{\delta S^{\rm matter}_{\rm ETW}}{\delta h^{ab}} = \frac{(1-d)\lambda}{8\pi G_{\rm bulk}} h_{ab} \,. \tag{D.22}$$

We can choose to write this equation as

$$K_{ab} = \lambda h_{ab} \,. \tag{D.23}$$

Details of the interface solutions can be found in [279]; the upshot is that the first junction condition implies that the r coordinates of the interface brane agree on both sides of the interface, while the second junction condition yields

$$L_1 f_1 \frac{dz_1}{ds} + L_2 f_2 \frac{dz_2}{ds} = \kappa r \,. \tag{D.24}$$

Using the relations

$$L_i^2 f_i \left(\frac{dz_i}{ds}\right)^2 + \frac{1}{f_i}\left(\frac{dr}{ds}\right)^2 = 1 \,, \tag{D.25}$$

we can rephrase this in terms of r-derivatives as

$$\begin{aligned} L_1 \frac{dz_1}{dr} &= -\frac{1}{f_1\sqrt{V_{\rm eff}}}\left(\frac{1}{2\kappa r}(f_1 - f_2) + \frac{1}{2}\kappa r\right) \\ L_2 \frac{dz_2}{dr} &= \frac{1}{f_2\sqrt{V_{\rm eff}}}\left(\frac{1}{2\kappa r}(f_2 - f_1) + \frac{1}{2}\kappa r\right) \,, \end{aligned} \tag{D.26}$$

where

$$V_{\rm eff}(r) = f_1 - \left(\frac{f_2 - f_1 - \kappa^2 r^2}{2\kappa r}\right)^2 \,. \tag{D.27}$$

For the ETW brane, we obtain the rr-component equation of motion

$$c_1(r) f_1(r) \frac{dz_1}{dr} = r\lambda \,. \tag{D.28}$$

Isolating $z_1'(r)$, we obtain

$$\frac{dz_1}{dr} = \frac{r\lambda}{L_1 f_1(r)} \frac{1}{\sqrt{f_1(r) - r^2\lambda^2}} \,. \tag{D.29}$$

Substituting this into any of the other equations of motion, we verify that these equations are also satisfied. These equations are similar to those obtained in the [2], though here we consider $(d-1)$-dimensional planar rather than spherical symmetry.

D.1.2 Branes with an Einstein-Hilbert term

We would now like to generalize the set-up of the previous subsection by introducing Einstein-Hilbert terms on the branes. In particular, we will now modify the brane actions to

$$\begin{aligned} S_{\text{interface}} &= \frac{1}{16\pi G_{\text{interface}}} \int_{\text{interface}} d^d y \sqrt{h}\, R^{(d)} + S^{\text{matter}}_{\text{interface}} \\ S_{\text{ETW}} &= \frac{1}{16\pi G_{\text{ETW}}} \int_{\text{ETW}} d^d y \sqrt{h}\, R^{(d)} + S^{\text{matter}}_{\text{ETW}} \,, \end{aligned} \tag{D.30}$$

where we will introduce the constants α, γ defined by

$$\frac{1}{G_{\text{interface}}} = \frac{\alpha}{G_{\text{bulk}}} \,, \qquad \frac{1}{G_{\text{ETW}}} = \frac{\gamma}{G_{\text{bulk}}} \,. \tag{D.31}$$

The Israel junction conditions at the interface then yield

$$[h_{ab}] = 0 \,, \qquad [K_{ab} - K h_{ab}] = 8\pi G_{\text{bulk}} T_{ab} \,, \quad T_{ab} \equiv \frac{2}{\sqrt{h}} \frac{\delta S_{\text{interface}}}{\delta h^{ab}} \,. \tag{D.32}$$

Notably, this can be interpreted as saying that the junction conditions are unaffected by the presence of the Einstein-Hilbert term on the brane except through the modification of the energy-momentum tensor (see Section 2.4

of [281]), which is now

$$T_{ab} = \frac{(1-d)\kappa}{8\pi G_{\text{bulk}}} h_{ab} - \frac{1}{8\pi G_{\text{interface}}} \left(R^{(d)}_{ab} - \frac{1}{2} R^{(d)} h_{ab} \right) . \tag{D.33}$$

All together, we have

$$[K_{ab}] = \kappa h_{ab} - \alpha \left(R^{(d)}_{ab} - \frac{1}{2(d-1)} R^{(d)} h_{ab} \right) . \tag{D.34}$$

On the other hand, the equation of motion for the ETW brane is

$$K_{ab} - K h_{ab} = (1-d)\lambda h_{ab} - \gamma \left(R^{(d)}_{ab} - \frac{1}{2} R^{(d)} h_{ab} \right) , \tag{D.35}$$

which we may also write as

$$K_{ab} = \lambda h_{ab} - \gamma \left(R^{(d)}_{ab} - \frac{1}{2(d-1)} R^{(d)} h_{ab} \right) . \tag{D.36}$$

Interface brane

As in the constant tension case, the first junction condition for the interface brane again implies that the r coordinate of the interface brane agrees on both sides of the interface brane. Now the second junction condition yields, in terms of the proper length parametrization,

$$L_1 f_1 \frac{dz_1}{ds} + L_2 f_2 \frac{dz_2}{ds} = \left(\kappa + \frac{\alpha(d-2)}{2r^2} \left(\frac{dr}{ds} \right)^2 \right) r . \tag{D.37}$$

As before, we can combine this with the expressions (D.25) to determine the derivatives of z_1, z_2 with respect to r; we find

$$\left(\frac{dr}{ds} \right)^2 = f_2 - y(r)^2 , \tag{D.38}$$

where $y(r)$ is a root of the equation

$$\alpha^2(d-2)^2y^4 - 4\alpha(d-2)ry^3 - 2(d-2)\alpha\left(\alpha(d-2)f_2 + 2\kappa r^2\right)y^2 + 4r\left(\alpha(d-2)f_2 + 2\kappa r^2\right)y + \alpha^2(d-2)^2f_2^2 + 4\alpha(d-2)f_2\kappa r^2 + 4\kappa^2r^4 - 4(f_1 - f_2)r^2 = 0\,. \quad \text{(D.39)}$$

ETW brane

For the ETW brane, we find the ii-component equation of motion

$$f_1(r)z_1'(r) = \frac{\lambda r}{c_1(r)} + \frac{\gamma(d-2)}{2L_1^2}\frac{c_1(r)}{r}\,. \quad \text{(D.40)}$$

and the rr-component

$$(d-2)rc_1(r)f_1(r)z_1'(r) + \frac{c_1(r)^3}{L_1^2}\left(z_1''(r) + \frac{f_1'(r)z_1'(r)}{2f_1(r)}(L_1^2f_1^2(r)z_1'(r)^2 + 3)\right)r^2 = (d-1)\lambda r^2 + \gamma\frac{(d-2)}{c_1(r)^2}L_1^2\left(\frac{(d-3)}{2} + r\frac{c_1'(r)}{c_1(r)}\right)\,. \quad \text{(D.41)}$$

Isolating the derivative $z_1'(r)$ in the first equation, we find

$$z_1'(r) = \frac{1}{\sqrt{2}L_1f_1(r)\sqrt{f_1(r) - r^2\lambda^2}}\left[(d-2)\gamma\lambda f_1(r) + 2\lambda^2r^2 - f_1(r) + \frac{f_1(r)}{r}\sqrt{(d-2)^2\gamma^2f_1(r) + (2(d-2)\gamma\lambda + 1)\,r^2}\right]^{1/2}\,. \quad \text{(D.42)}$$

D.2 Monotonicity of $\Delta z_1^{\rm ETW}(\lambda)$

We have the derivative

$$\begin{aligned}\frac{d}{d\lambda}\Delta z_1^{\rm ETW}(\lambda) &= \lim_{\epsilon\to 0}\frac{d}{d\lambda}\int_{r_0(\lambda)+\epsilon}^{\infty} dr \frac{r\lambda}{Lf(r)}\frac{1}{\sqrt{f(r)-r^2\lambda^2}} \\ &= \lim_{\epsilon\to 0}\Bigg[-\frac{dr_0(\lambda)}{d\lambda}\Big[\frac{r\lambda}{Lf(r)}\frac{1}{\sqrt{f(r)-r^2\lambda^2}}\Big]_{r=r_0(\lambda)+\epsilon} \\ &\qquad + \frac{1}{L}\int_{r_0(\lambda)+\epsilon}^{\infty} dr\, \frac{r}{(f(r)-r^2\lambda^2)^{3/2}}\Bigg],\end{aligned} \tag{D.43}$$

where we have introduced an IR regulator so that the terms in the derivative as per the Leibniz integral rule are finite, and we are dropping the subscripts 1 and 2 for convenience in this appendix (all quantities involve the ETW brane, which propagates in region 1 only). The first term goes as

$$\begin{aligned}&-\frac{dr_0(\lambda)}{d\lambda}\Big[\frac{r\lambda}{Lf(r)}\frac{1}{\sqrt{f(r)-r^2\lambda^2}}\Big]_{r=r_0(\lambda)+\epsilon} \\ &\qquad = -\frac{2}{d^{3/2}}\frac{L^2}{(1-L^2\lambda^2)^{3/2}}\frac{1}{\sqrt{r_0(\lambda)\epsilon}} + O(\sqrt{\epsilon})\,,\end{aligned} \tag{D.44}$$

while the second goes as

$$\begin{aligned}&\frac{1}{L}\int_{r_0(\lambda)+\epsilon}^{\infty} dr\, \frac{r}{(f(r)-r^2\lambda^2)^{3/2}} \\ &\qquad = \frac{L^2}{r_0(\lambda)(1-L^2\lambda^2)^{3/2}}\Big[\frac{2}{d^{3/2}}\sqrt{\frac{r_0(\lambda)}{\epsilon}} - \frac{2\sqrt{\pi}\Gamma(\frac{1}{d}+1)}{\Gamma(\frac{1}{d}-\frac{1}{2})}\Big]\,,\end{aligned} \tag{D.45}$$

where we use

$$\int \frac{dy}{y^2}\frac{1}{(1-y^{-d})^{3/2}} = -\frac{1}{y}{}_2F_1\left(\frac{3}{2},\frac{1}{d};1+\frac{1}{d};y^{-d}\right) \tag{D.46}$$

and

$$ {}_2F_1\left(\frac{3}{2},\frac{1}{d};1+\frac{1}{d};\left(1+\frac{\epsilon}{r_0}\right)^{-d}\right) = \frac{2}{d^{3/2}}\sqrt{\frac{r_0}{\epsilon}} - \frac{2\sqrt{\pi}\Gamma(\frac{1}{d}+1)}{\Gamma(\frac{1}{d}-\frac{1}{2})} + O(\sqrt{\epsilon})\,. \quad \text{(D.47)} $$

We therefore obtain (for $d > 2$)

$$ \frac{d}{d\lambda}\Delta z_1^{\rm ETW}(\lambda) = -\frac{2\sqrt{\pi}\Gamma(\frac{1}{d}+1)}{\Gamma(\frac{1}{d}-\frac{1}{2})}\frac{L^2}{r_0(\lambda)(1-L^2\lambda^2)^{3/2}}\,, \quad \text{(D.48)} $$

which is manifestly positive, as desired.

D.3 Confirmation of ETW/interface non-intersection

In general, suppose that we have verified that, for a fixed set of parameters (L_1, μ_1, u, μ, e) and λ, one has

$$ R_2(u,\mu,e) > 0 \quad \text{and} \quad r_0^{\rm ETW} > r_0^{\rm int} \quad \text{and} \quad \frac{\Delta z_1^{\rm ETW}(\lambda)}{\Delta z_1^{\rm int}} = 1\,. \quad \text{(D.49)} $$

This does not yet constitute a demonstration that the solution is well-behaved, because the ETW and interface branes may intersect at some finite r_1. We would like to verify that this does not occur for the solutions in the limit identified in Section 5.4.

In general, to verify that there are no intersections for some set of parameters, it suffices to show that

$$ (z_1^{\rm ETW})'(r_1) > (z_1^{\rm int})'(r_1) \qquad \text{for all } r_0^{\rm ETW} < r_1 < \infty\,. \quad \text{(D.50)} $$

Indeed, if by contradiction we had that the above inequality held and that

$z_1^{\rm int}(\tilde{r}_1) = z_1^{\rm ETW}(\tilde{r}_1) = \tilde{z}$ at some finite $\tilde{r}_1 > r_0^{\rm ETW}$, then we would obtain

$$\begin{aligned} 0 &= (\Delta z_1^{\rm int} - \tilde{z}) - (\Delta z_1^{\rm ETW} - \tilde{z}) \\ &= \int_{\tilde{r}_1}^{\infty} dr_1 \, \big((Z_1^{\rm int})'(r_1) - (Z_1^{\rm ETW})'(r_1) \big) < 0 \,, \end{aligned} \tag{D.51}$$

which is absurd.

To show that (D.50) holds, it suffices to show that there is no $r_1 \in (r_0^{\rm ETW}, \infty)$ such that $(z_1^{\rm ETW})'(r_1) = (z_1^{\rm int})'(r_1)$; the fact that the inequality manifestly holds at $r_1 = r_0^{\rm ETW}$ (where we are comparing a finite quantity to a formally infinite quantity), together with continuity, then implies that the inequality must hold for all finite $r_1 > r_0^{\rm ETW}$.

It is straightforward to find all solutions to the equation $(z_1^{\rm ETW})'(r_1) = (z_1^{\rm int})'(r_1)$ for the models considered in Section 5.4; letting $y = r_1^d$, we obtain a quartic equation with non-trivial solutions

$$\begin{aligned} \frac{y}{\mu_1 L_1^2} = \Bigg[& \pm (1 - (1-2e)u) \sqrt{a_1} \\ & + u^2 \big((d-2)\gamma \, (\mu - 2e(1-e)(1+\mu)) - (1-\mu)\,(1-2e)\, L_1 \big) \\ & + u \big(- (d-2)\gamma (1-2e)(1+\mu) + L_1(1-\mu) \big) + (d-2)\gamma \Bigg] \\ & \times \Bigg[- 4L_1(1-\lambda L_1)(1-u)^2 \\ & + 8e(1-u)\,(L_1 + (d-2)\gamma - 2uL_1(1-\lambda L_1)) \\ & - 8e^2 \Bigg((d-2)\gamma - 3u\,(L_1 + (d-2)\gamma) \\ & + u^2 \left(3L_1 \left(1 - \frac{2}{3}\lambda L_1 \right) + (d-2)\gamma \right) \Bigg) \\ & - 16ue^3 \left((d-2)\gamma - u\,(L_1 + (d-2)\gamma) \right) - 8(d-2)\gamma u^2 e^4 \Bigg]^{-1} \end{aligned} \tag{D.52}$$

$$\begin{aligned}\frac{y}{\mu_1 L_1^2} = \Bigg[& \pm \left(1-(1-2e)u\right)\sqrt{a_2} \\ & + u^2\big((d-2)\gamma\left(\mu - 2e(1-e)(1+\mu)\right) + (1-\mu)\left(1-2e\right)L_1\big) \\ & + u\big(-(d-2)\gamma(1-2e)(1+\mu) - L_1(1-\mu)\big) + (d-2)\gamma\Bigg] \\ & \times \Bigg[4L_1(1+\lambda L_1)(1-u)^2 \\ & + 8e(1-u)\left(-L_1 + (d-2)\gamma + 2uL_1(1+\lambda L_1)\right) \\ & - 8e^2\Bigg((d-2)\gamma - 3u\left(-L_1+(d-2)\gamma\right) \\ & + u^2\left(-3L_1\left(1+\frac{2}{3}\lambda L_1\right) + (d-2)\gamma\right)\Bigg) \\ & - 16ue^3\left((d-2)\gamma - u\left(-L_1+(d-2)\gamma\right)\right) - 8(d-2)\gamma u^2 e^4\Bigg]^{-1}, \end{aligned} \tag{D.53}$$

where

$$\begin{aligned} a_1 = {} & (d-2)^2\gamma^2\left(1+\mu u^2(\mu-4e(1-e)) - 2\mu u(1-2e)\right) \\ & + 2(d-2)(1-\mu)uL_1\gamma\left(1-u(1-e-(1-\mu)\lambda L_1)\right) \\ & + u^2(1-\mu)^2L_1^2 \\ a_2 = {} & (d-2)^2\gamma^2\left(1+\mu u^2(\mu-4e(1-e)) - 2\mu u(1-2e)\right) \\ & - 2(d-2)(1-\mu)uL_1\gamma\left(1-u(1-e+(1-\mu)\lambda L_1)\right) \\ & + u^2(1-\mu)^2L_1^2\,. \end{aligned} \tag{D.54}$$

We are interested in taking the limit identified in Section 5.4, namely

$$1-\lambda L_1 = \epsilon \sim \frac{2ec}{1-\mu u}\,, \qquad \frac{(d-2)\gamma}{L_1} + 1 \sim c^{1-2/d}(1-u)\,. \tag{D.55}$$

We also need to take the limit $\mu \to 0$ sufficiently quickly, so that $\mu = O(e^{\frac{d}{2}-1})$. In particular, we focus on the case $d \geq 4$, so that μ vanishes at least linearly in e.

We note that one has in the limit

$$(d-2)\gamma + uL_1 \sim (c^{1-2/d}-1)(1-u)L_1 < 0\,. \tag{D.56}$$

We therefore find that the leading order contributions to the solutions are

$$\begin{aligned}
\frac{y}{\mu_1 L_1^2} &= \frac{(d-2)\gamma + uL_1}{4ecL_1(1-u)(c^{-2/d}-1)} \\
\frac{y}{\mu_1 L_1^2} &= -\frac{(d-2)\gamma}{4}\frac{u^2}{(1-u)}\frac{1}{(d-2)\gamma + uL_1} \\
\frac{y}{\mu_1 L_1^2} &= \frac{1}{8(1-u)}\Bigg[-\sqrt{\left((d-2)\frac{\gamma}{L_1}-u\right)^2 + 4(d-2)\frac{\gamma}{L_1}u^2} \\
&\qquad - u + (d-2)\frac{\gamma}{L_1}\Bigg] \\
\frac{y}{\mu_1 L_1^2} &= \frac{1}{8(1-u)}\Bigg[\sqrt{\left((d-2)\frac{\gamma}{L_1}-u\right)^2 + 4(d-2)\frac{\gamma}{L_1}u^2} \\
&\qquad - u + (d-2)\frac{\gamma}{L_1}\Bigg]\,.
\end{aligned} \tag{D.57}$$

It is straightforward to see that all of these quantities are negative, with the first diverging and the last three converging to finite quantities, so we cannot have any intersections at finite r_1 in this case.

Appendix E

Appendices for Chapter 6

E.1 Size of the internal space in the ETW brane region

The fact that the compact spherical directions in the "bag" or "ETW brane" region of the geometries of interest in Chapter 6 cannot be suppressed relative to the AdS_4 scale has already been noted by Bachas and Lavdas in [292] (following previous related comments by Bachas and Estes in [295]). As remarked by these authors, this property is related to the issue of scale separation in the context of flux compactifications (see e.g. [334–336]). More generally, it is a broad prediction that in holographic theories with supersymmetry, the R-symmetry is geometrized at the AdS scale (see e.g. [337]). For the sake of completeness, we will here provide a direct argument for these assertions in the context of the supergravity solutions considered in this note, based on the formulation of the reduced BPS equations by D'Hoker, Estes, and Gutperle in [172, 173]. Our conclusions will apply to the solutions dual to the 3D $\mathcal{N} = 4$ SCFTs of Gaiotto-Witten [89, 90], first studied in [175], as well as the boundary and interface solutions studied in [174].

Our goal is to show that it is not possible to simultaneously have $f_1^2/f_4^2 \ll 1$ and $f_2^2/f_4^2 \ll 1$ in *any* region of the spacetime unless that region is locally $AdS_5 \times S^5$; the conclusion is therefore that at least one of the S^2 factors of the internal space remains large relative to the AdS_4 scale in the ETW brane region.

In the following, we will be relying on the conventions of [172], introducing only the ingredients necessary. We may write the complex axion/dilaton

P and connection Q one-forms as

$$P = p_a e^a \,, \qquad Q = q_a e^a \,, \tag{E.1}$$

and the anti-symmetric five-form and three-form tensors $F_{(5)}$ and G as

$$F_{(5)} = f_a \left(-e^{0123a} + \varepsilon^a_{\ b} e^{4567b} \right) \,, \quad G = g_a e^{45a} + i h_a e^{67a} \,, \tag{E.2}$$

where the e are wedge products of the appropriate vielbeins; the indices a, b are summed over the Riemann surface Σ directions. It is demonstrated in [172] that, for solutions with 16 supersymmetries, one can always apply an $SU(1,1)$ S-duality transformation to a frame where the axion field vanishes and the dilaton is real; this corresponds to the reality conditions

$$\bar{p}_a = p_a \,, \quad \bar{g}_a = g_a \,, \quad \bar{h}_a = h_a \,, \quad q_a = 0 \,. \tag{E.3}$$

The metric functions f_1, f_2, f_4 may be expressed in terms of a (Grassmann-even) spinor degree of freedom (equation (6.18) of [172])

$$\xi = \begin{pmatrix} \alpha \\ \beta \end{pmatrix} \,, \qquad \xi^* = \begin{pmatrix} \bar{\alpha} \\ \bar{\beta} \end{pmatrix} \,, \qquad \alpha, \beta \in \mathbb{C} \,, \tag{E.4}$$

in terms of which we have (equation (6.26) of [172])

$$\begin{aligned} f_4 &= \xi^\dagger \xi = \alpha\bar{\alpha} + \beta\bar{\beta} \\ f_1 &= -\nu \xi^\dagger \sigma^1 \xi = -\nu \left(\alpha\bar{\beta} + \beta\bar{\alpha} \right) \\ f_2 &= -\xi^\dagger \sigma^2 \xi = i \left(\beta\bar{\alpha} - \alpha\bar{\beta} \right) \,, \end{aligned} \tag{E.5}$$

where $\nu \in \{\pm 1\}$ (the sign will be irrelevant when we compare ratios of metric functions f_1^2, f_2^2 and f_4^2).

Suppose there is some neighbourhood of a point $(w, \bar{w})$ in the interior of our geometry where $f_1^2/f_4^2 \ll 1$ and $f_2^2/f_4^2 \ll 1$; we will restrict to considering this neighbourhood for the remainder of the subsection. In this case, we must have either $|\alpha| \ll |\beta|$ or $|\beta| \ll |\alpha|$ throughout the neighbourhood.

Indeed, using polar coordinates

$$\alpha = ae^{i\theta_1}\,, \qquad \beta = be^{i\theta_2}\,, \tag{E.6}$$

we have

$$\begin{aligned} \left|\frac{f_1}{f_4}\right| &= \frac{2ab}{a^2+b^2}\big|\cos\left(\theta_1-\theta_2\right)\big| \\ \left|\frac{f_2}{f_4}\right| &= \frac{2ab}{a^2+b^2}\big|\sin\left(\theta_1-\theta_2\right)\big|\,, \end{aligned} \tag{E.7}$$

and since

$$\min_{\theta_1,\theta_2}\max\{\big|\cos\left(\theta_1-\theta_2\right)\big|,\big|\sin\left(\theta_1-\theta_2\right)\big|\} = \frac{1}{\sqrt{2}}\,, \tag{E.8}$$

we must have $\frac{2ab}{a^2+b^2} \ll 1$, which requires $a \ll b$ or $b \ll a$.

On the other hand, the dilatino BPS equation (equation (6.28) of [172]) gives

$$4p_z\alpha + (g_z - ih_z)\,\beta = 0\,, \quad 4p_z\beta - (g_z + ih_z)\,\alpha = 0\,, \tag{E.9}$$

with $z, \bar{z}$ frame indices. These two equations together imply either that $p_z = g_z = h_z = 0$ or

$$\left|\frac{\alpha}{\beta}\right| = \left|\frac{4p_z}{g_z+ih_z}\right| = \left|\frac{4p_z}{g_z-ih_z}\right| = \left|\frac{\beta}{\alpha}\right|\,, \tag{E.10}$$

with the latter contradicting the conclusion that $|\alpha| \ll |\beta|$ or $|\beta| \ll |\alpha|$. We therefore must have that the special condition $p_z = g_z = h_z = 0$ holds throughout the neighbourhood we are considering.[119] But as shown in Section 6.9 of [172], that condition alone necessarily implies that the geometry is pure $\mathrm{AdS}_5 \times S^5$, with (subject to a particular choice of normalization)

$$\alpha = e^{-\nu w/2}\,, \qquad \beta = ie^{\nu w/2}\,, \tag{E.11}$$

[119] Note that we could have avoided this condition by requiring that *one of* f_1^2/f_4^2 or f_2^2/f_4^2 *but not both* was small; in this case, we would not necessarily require that $|\alpha| \ll |\beta|$ or $|\beta| \ll |\alpha|$, but could instead have that $\alpha\bar{\beta}$ was almost pure real or pure imaginary.

and metric functions

$$f_1 = 2\sin y\,, \qquad f_2 = -2\cos y\,, \qquad f_4 = 2\cosh x\,, \tag{E.12}$$

where $w = x + iy$ is a complex coordinate on the strip Σ. (We should note that the argument provided applies to the case where p_z, g_z, h_z are presumed to vanish everywhere, but the nature of the argument is local, and can be repeated to demonstrate that the geometry within the neighbourhood we are considering must be $\mathrm{AdS}_5 \times S^5$.) In particular, this can be consistent with our assumption $|\alpha| \ll |\beta|$ or $|\beta| \ll |\alpha|$ near the asymptotic boundary $x \to \pm\infty$, where the metric function f_4^2 diverges. We have therefore shown that the only case in which one can simultaneously have $f_1^2/f_4^2 \ll 1$ and $f_2^2/f_4^2 \ll 1$ is when the geometry is locally $\mathrm{AdS}_5 \times S^5$; as a corollary, we clearly cannot have the scale of the internal S^2 dimensions be small compared to the curvature scale of the non-compact dimensions.

E.2 Justification of condition (6.8)

In general, the *region I* introduced in Section 6.3 is only asymptotically $\mathrm{AdS}_5 \times S^5$, and may deviate from pure $\mathrm{AdS}_5 \times S^5$ significantly before the $O(l_A/r)$, $O(k_B/r)$ corrections become large. For example, considering the large-r asymptotics of the metric functions for our general solution, we find

$$\rho^2 = \frac{L_{\mathrm{AdS}}^2}{4}\frac{1}{r^2}\Bigg[1 - \frac{1}{r^2}\left(2\cos^2\theta - 1\right)\Big(\frac{1}{\pi}\sum_A c_A l_A\left(1 - \frac{l_A^2}{r_0^2}\right) - \frac{1}{\pi}\sum_B d_B k_B\left(1 - \frac{k_B^2}{r_0^2}\right)\Big) + o(r^{-2})\Bigg] \tag{E.13}$$

$$f_1^2 = L_{\rm AdS}^2 \cos^2\theta \Bigg[1 + \frac{1}{r^2}\Bigg(\frac{1}{\pi}\sum_A c_A l_A \Big(\big(2\cos^2\theta + 1\big) + \frac{l_A^2}{r_0^2}\big(2\cos^2\theta - 1\big)\Big) - \frac{1}{\pi}\sum_B d_B k_B \Big(\big(2\cos^2\theta + 1\big) + \frac{k_B^2}{r_0^2}\big(2\cos^2\theta - 1\big)\Big)\Bigg) + o(r^{-2})\Bigg] \quad \text{(E.14)}$$

$$f_2^2 = L_{\rm AdS}^2 \sin^2\theta \Bigg[1 + \frac{1}{r^2}\Bigg(\frac{1}{\pi}\sum_A c_A l_A \Big(\big(2\cos^2\theta - 3\big) + \frac{l_A^2}{r_0^2}\big(2\cos^2\theta - 1\big)\Big) - \frac{1}{\pi}\sum_B d_B k_B \Big(\big(2\cos^2\theta - 3\big) + \frac{k_B^2}{r_0^2}\big(2\cos^2\theta - 1\big)\Big)\Bigg) + o(r^{-2})\Bigg] \quad \text{(E.15)}$$

$$f_4^2 = \frac{L_{\rm AdS}^2 (r^2 + r_0^2)^2}{4 r_0^2 r^2} - \frac{L_{\rm AdS}^2 r^2}{4 r_0^2}\Bigg[\frac{1}{r^2}\big(2\cos^2\theta - 1\big)\Bigg(\frac{1}{\pi}\sum_A c_A l_A \left(1 + \frac{l_A^2}{r_0^2}\right) - \frac{1}{\pi}\sum_B d_B k_B \left(1 + \frac{k_B^2}{r_0^2}\right)\Bigg) + o(r^{-2})\Bigg]. \quad \text{(E.16)}$$

Evidently, if we would like the terms subleading in large r to be suppressed for any $r \ll r_0$, then in addition to (6.12), we require

$$\Big|\sum_A c_A l_A - \sum_B d_B k_B\Big| \ll r_*^2 \,. \quad \text{(E.17)}$$

We claim that conditions (6.12) and (E.17) are sufficient to ensure a large region of approximately pure $\mathrm{AdS}_5 \times S^5$.

To further motivate this fact, let us fix N from the beginning, and recall that $r_0^2 \equiv \frac{N}{\pi}$. Suppose we would like to have a geometry well-approximated

by pure $\mathrm{AdS}_5 \times S^5$ down to some radial coordinate $r_* \ll r_0$. Our approach will be to write down the metric functions in the limit $\frac{l_A}{r}, \frac{k_B}{r} \to 0$ with $\sum_A c_A l_A$ and $\sum_B d_B k_B$ held fixed, and to understand how these functions depend on the quantity $\Big|\sum_A c_A l_A - \sum_B d_B k_B\Big|$. In particular, letting

$$\sum_A c_A l_A = \frac{\pi}{2} r_0^2 \,(1+\varepsilon)\ , \qquad \sum_B d_B k_B = \frac{\pi}{2} r_0^2 \,(1-\varepsilon)\ , \tag{E.18}$$

we find that when $\frac{l_A}{r}, \frac{k_B}{r} \to 0$ in a way that keeps N and ε fixed, we have

$$\begin{aligned}
\left(\frac{\pi}{2}\right)^{-1} h_1(r,\theta) &= r\cos\theta + \frac{r_0^2 \cos\theta}{r}\,(1+\varepsilon) \\
\left(\frac{\pi}{2}\right)^{-1} h_2(r,\theta) &= r\sin\theta + \frac{r_0^2 \sin\theta}{r}\,(1-\varepsilon) \\
\left(\frac{\pi}{2}\right)^{-2} W(r,\theta) &= -\frac{2r_0^2 \sin\theta\cos\theta}{r^2}
\end{aligned} \tag{E.19}$$

and

$$\begin{aligned}
\left(\frac{\pi}{2}\right)^{-4} N_1(r,\theta) = \frac{\sin\theta\cos\theta}{2}\,&\big(r^2 + r_0^2(1+\varepsilon)\big) \\
&\times \Big[1 + \frac{r_0^2}{r^2}\big(3 + \varepsilon(1-4\cos^2\theta)\big) \\
&+ \frac{r_0^4}{r^4}(1+\varepsilon)\big(3 - \varepsilon(1-4\cos^2\theta)\big) + \frac{r_0^6}{r^6}(1+\varepsilon)^2(1-\varepsilon)\Big]
\end{aligned} \tag{E.20}$$

$$\begin{aligned}
\left(\frac{\pi}{2}\right)^{-4} N_2(r,\theta) = \frac{\sin\theta\cos\theta}{2}\,&\big(r^2 + r_0^2(1-\varepsilon)\big) \\
&\times \Big[1 + \frac{r_0^2}{r^2}\big(3 + \varepsilon(3-4\cos^2\theta)\big) \\
&+ \frac{r_0^4}{r^4}(1-\varepsilon)\big(3 - \varepsilon(3-4\cos^2\theta)\big) + \frac{r_0^6}{r^6}(1-\varepsilon)^2(1+\varepsilon)\Big]\,.
\end{aligned} \tag{E.21}$$

We then find the metric functions

$$\rho^2(r,\theta) = \frac{L^2}{4r^2}\left(1+\frac{r_0^2}{r^2}(1-\varepsilon)\right)^{-3/4}\left(1+\frac{r_0^2}{r^2}(1+\varepsilon)\right)^{-3/4} \left[\left(\left(1+\frac{r_0^2}{r^2}(1-\varepsilon)\right)\left(1+\frac{r_0^2}{r^2}(1+\varepsilon)\right)^2 - 4\varepsilon\cos^2\theta\frac{r_0^2}{r^2}\left(1-\frac{r_0^2}{r^2}(1+\varepsilon)\right)\right)\right. \left.\times\left(1+\frac{r_0^2}{r^2}\left(3+\varepsilon(3-4\cos^2\theta)\right)+\frac{r_0^4}{r^4}\left(4\varepsilon(1-\varepsilon)+3(1-\varepsilon)^2\right)+\frac{r_0^6}{r^6}(1-\varepsilon)^2(1+\varepsilon)\right)\right]^{1/4} \tag{E.22}$$

$$f_1^2(r,\theta) = L^2\cos^2\theta\left(1+\frac{r_0^2}{r^2}(1-\varepsilon)\right)^{1/4}\left(1+\frac{r_0^2}{r^2}(1+\varepsilon)\right)^{5/4} \left[\left(\left(1+\frac{r_0^2}{r^2}(1-\varepsilon)\right)\left(1+\frac{r_0^2}{r^2}(1+\varepsilon)\right)^2 - 4\varepsilon\cos^2\theta\frac{r_0^2}{r^2}\left(1-\frac{r_0^2}{r^2}(1+\varepsilon)\right)\right)^{-3}\right. \left.\times\left(1+\frac{r_0^2}{r^2}\left(3+\varepsilon(3-4\cos^2\theta)\right)+\frac{r_0^4}{r^4}\left(4\varepsilon(1-\varepsilon)+3(1-\varepsilon)^2\right)+\frac{r_0^6}{r^6}(1-\varepsilon)^2(1+\varepsilon)\right)\right]^{1/4} \tag{E.23}$$

$$f_2^2(r,\theta) = L^2 \sin^2\theta \left(1+\frac{r_0^2}{r^2}(1-\varepsilon)\right)^{5/4} \left(1+\frac{r_0^2}{r^2}(1+\varepsilon)\right)^{1/4}$$
$$\left[\left(\left(1+\frac{r_0^2}{r^2}(1-\varepsilon)\right)\left(1+\frac{r_0^2}{r^2}(1+\varepsilon)\right)^2 - 4\varepsilon\cos^2\theta\frac{r_0^2}{r^2}\left(1-\frac{r_0^2}{r^2}(1+\varepsilon)\right)\right)\right. \tag{E.24}$$
$$\left.\times\left(1+\frac{r_0^2}{r^2}\left(3+\varepsilon(3-4\cos^2\theta)\right)+\frac{r_0^4}{r^4}\left(4\varepsilon(1-\varepsilon)+3(1-\varepsilon)^2\right)+\frac{r_0^6}{r^6}(1-\varepsilon)^2(1+\varepsilon)\right)^{-3}\right]^{1/4}$$

$$f_4^2(r,\theta) = \frac{L^2r^2}{4r_0^2}\left(1+\frac{r_0^2}{r^2}(1-\varepsilon)\right)^{1/4} \left(1+\frac{r_0^2}{r^2}(1+\varepsilon)\right)^{1/4}$$
$$\left[\left(\left(1+\frac{r_0^2}{r^2}(1-\varepsilon)\right)\left(1+\frac{r_0^2}{r^2}(1+\varepsilon)\right)^2 - 4\varepsilon\cos^2\theta\frac{r_0^2}{r^2}\left(1-\frac{r_0^2}{r^2}(1+\varepsilon)\right)\right)\right. \tag{E.25}$$
$$\left.\times\left(1+\frac{r_0^2}{r^2}\left(3+\varepsilon(3-4\cos^2\theta)\right)+\frac{r_0^4}{r^4}\left(4\varepsilon(1-\varepsilon)+3(1-\varepsilon)^2\right)+\frac{r_0^6}{r^6}(1-\varepsilon)^2(1+\varepsilon)\right)\right]^{1/4}.$$

Of course, in the limit $\varepsilon \to 0$, we recover the metric function for pure $\mathrm{AdS}_5 \times S^5$. One can demonstrate directly from the above expressions that these metric functions can be made uniformly close to those of pure $\mathrm{AdS}_5 \times S^5$ in $r \in [r_*, \infty)$ and $\theta \in [0, \frac{\pi}{2}]$ for sufficiently small ε; we have plotted some examples in Section 6.4.3.

E.3 Space of solutions for the single pole case

In this section, we will understand the space of solutions to the constraints (6.14). First, taking a linear combination of the last two equations in (6.14), one obtains

$$N_{D5}N_{D3} + N_{NS5}\hat{N}_{D3} = N + N_{D5}N_{NS5}\,, \tag{E.26}$$

so it is necessary that

$$G \equiv \gcd(N_{D5}, N_{NS5}) \mid N\,. \tag{E.27}$$

Choosing any N_{NS5} and N_{D5} satisfying this constraint, the linear diophantine equation (E.26) for $\hat{N}_{D3}$ and N_{D3} will always have multiple integer solutions of the form

$$N_{D3} = N_{D3}^{(0)} + m\frac{N_{NS5}}{\gcd(N_{D5}, N_{NS5})}, \quad \hat{N}_{D3} = \hat{N}_{D3}^{(0)} - m\frac{N_{D5}}{\gcd(N_{D5}, N_{NS5})}, \quad m \in \mathbb{Z}, \tag{E.28}$$

with $(N_{D3}^{(0)}, \hat{N}_{D3}^{(0)})$ some nominal solution.

There will be at least one solution for positive $\hat{N}_{D3}$ and N_{D3}, since for real m, (E.28) parameterizes a line that intersects the positive quadrant of the $(\hat{N}_{D3}, N_{D3})$ plane, and the equal spacing between the $(\hat{N}_{D3}, N_{D3})$ values for integer m is less than the length of the line segment in the positive quadrant:

$$\sqrt{N_{D5}^2 + N_{NS5}^2} < \sqrt{\left(N_{D5} + \frac{N}{N_{NS5}}\right)^2 + \left(N_{NS5} + \frac{N}{N_{D5}}\right)^2}\,. \tag{E.29}$$

The number of solutions for $(N_{D3}, \hat{N}_{D3})$ is evidently of order

$$\sqrt{\frac{\left(N_{D5}+\frac{N}{N_{NS5}}\right)^2+\left(N_{NS5}+\frac{N}{N_{D5}}\right)^2}{N_{D5}^2+N_{NS5}^2}}\,, \tag{E.30}$$

so for $N_{D5}, N_{NS5} \gg N$ we typically have only a single solution. The conditions that N_{D3} and $\hat{N}_{D3}$ are positive combined with (E.26) mean that any solution will satisfy

$$\hat{N}_{D3} < \frac{N}{N_{NS5}} + N_{D5} \qquad N_{D3} < \frac{N}{N_{D5}} + N_{NS5}\ . \tag{E.31}$$

Now, given any choice of (N_{D5}, N_{NS5}) satisfying (E.27) and positive $(N_{D3}, \hat{N}_{D3})$ satisfying (E.26), we will show that there is a unique positive (k, l) satisfying the constraints (6.14). We do so by combining these constraints to yield

$$\frac{\frac{\hat{N}_{D3}}{N_{D5}}+\frac{N_{D3}}{N_{NS5}}-1}{\frac{N_{NS5}}{gN_{D5}}\frac{k}{l}+1} - \frac{N_{D3}}{N_{NS5}} + 1 = \frac{2}{\pi}\arctan\frac{k}{l}\ . \tag{E.32}$$

The right side increases monotonically from 0 to 1 as k/l increases from 0 to ∞. The left side varies monotonically from $\hat{N}_{D3}/N_{D5} > 0$ at $k/l = 0$ to $1 - N_{D3}/N_{NS5}$ for large k/l. Thus, there is exactly one solution for k/l. Call this $k/l = m$.

We then have a unique solution (k, l) that is the intersection between the line $k = ml$ and the line

$$\frac{k}{\sqrt{g}}N_{NS5} + l\sqrt{g}N_{D5} = N\ . \tag{E.33}$$

In terms of m, the result is

$$\begin{aligned} k &= \frac{N}{\frac{N_{NS5}}{\sqrt{g}}+\frac{\sqrt{g}N_{D5}}{m}} \\ l &= \frac{N}{\frac{mN_{NS5}}{\sqrt{g}}+\sqrt{g}N_{D5}}\ . \end{aligned} \tag{E.34}$$

E.4 General families with single D5-pole/NS5-pole and arbitrarily large $\mathbf{AdS}_5 \times S^5$ region

We will here provide a significant generalization to the one-parameter family initially introduced in Section 6.4.3. Our construction of a one-parameter family analogous to the one appearing in that section occurs most simply when g is such that there exists $m \in \mathbb{N}^+$ with

$$\arctan(m/g) = \frac{\pi}{2}\frac{a}{b}\,, \qquad a, b \in \mathbb{N}^+\,, \quad \gcd(a,b) = 1\,, \quad \frac{a}{b} \in (0,1)\,. \tag{E.35}$$

That is, we have $g = \frac{m}{\tan\left(\frac{\pi}{2}\frac{a}{b}\right)}$, with m, a, b positive integers and $0 < \frac{a}{b} < 1$ in reduced form. In this case, we will take

$$\begin{aligned} N_{D5}(n) &= bf_n + \alpha\,, \qquad & N_{NS5}(n) &= bmf_n + \beta\,, \\ N_{D3}(n) &= amf_n + \gamma\,, \qquad & \hat{N}_{D3}(n) &= (b-a)f_n + \delta\,, \end{aligned} \tag{E.36}$$

where f_n is a sequence which we leave undetermined for now. We then see that

$$\begin{aligned} &N_{D5}(n)N_{D3}(n) + N_{NS5}(n)\hat{N}_{D3}(n) \\ &\quad = (bf_n + \alpha)\,(amf_n + \gamma) + (bmf_n + \beta)\,((b-a)f_n + \delta) \\ &\quad = N_{D5}(n)N_{NS5}(n) + ((a-b)m\alpha + b\gamma - a\beta + bm\delta)\,f_n \\ &\qquad\quad + \alpha\gamma + \beta\delta - \alpha\beta\,, \end{aligned} \tag{E.37}$$

so to ensure that (E.26) holds, we would like to ask whether or not it is possible to choose $\alpha, \beta, \gamma, \delta$ such that

$$\begin{aligned} 0 &= (a-b)m\alpha + b\gamma - a\beta + bm\delta \\ N &= \alpha\gamma + \beta\delta - \alpha\beta\,. \end{aligned} \tag{E.38}$$

In fact, these equations *are* solvable for any (a, b, m). In particular, substituting the former into the latter yields

$$N = \left(\frac{(b-a)}{b}\alpha - \delta\right)(m\alpha - \beta) \ . \tag{E.39}$$

If we take

$$\beta = m\alpha - b \,, \tag{E.40}$$

then this equation gives

$$(a-b)\alpha + b\delta = -N \,. \tag{E.41}$$

We know that $\gcd((a-b), b) = 1$, since a and b were chosen to be relatively prime, so this linear diophantine equation has an integer solution (α, δ). We may then define

$$\gamma \equiv \frac{a}{b}\beta - \frac{a-b}{b}m\alpha - m\delta = -a + m(\alpha - \delta) \,, \tag{E.42}$$

which is manifestly integral.

We thus define the sequence of parameters $N_{D5}(n)$, $N_{NS5}(n)$, $N_{D3}(n)$, $\hat{N}_{D3}(n)$ by this choice $(\alpha, \beta, \gamma, \delta)$, taking f_n to be any growing sequence. Since $\sqrt{g}N_{D5}l + \frac{1}{\sqrt{g}}N_{NS5}k = N$ implies that both l and k are at most $O\left(f_n^{-1}\right)$, the equations (6.14) yield

$$\begin{aligned} \frac{N_{D3}(n)}{N_{NS5}(n)} &= \frac{a}{b} + O\left(f_n^{-1}\right) = \frac{2}{\pi}\arctan(m/g) + O\left(f_n^{-1}\right) \\ &= \frac{2}{\pi}\arctan(l/k) + O\left(f_n^{-2}\right) \ , \end{aligned} \tag{E.43}$$

and thus

$$l/k = m/g + O\left(f_n^{-1}\right) \ . \tag{E.44}$$

It follows that

$$|cl - dk| = \left|\left(\sqrt{g}bf_n\right)\left(\frac{km}{g} + O\left(f_n^{-2}\right)\right) - \left(\frac{1}{\sqrt{g}}bmf_n\right)k\right| = O\left(f_n^{-1}\right) , \tag{E.45}$$

as desired.

Thus, in the case that the string coupling g satisfies (E.35), we are able to identify a one-parameter family with scaling

$$mN_{D5} \sim N_{NS5} \sim \frac{b}{a} N_{D3} \sim \frac{mb}{(b-a)} \hat{N}_{D3} \,. \tag{E.46}$$

It is notable that such g are dense in $\mathbb{R}^+$, since the map $\tan \frac{\pi}{2} (\cdot) : (0,1) \to (0,\infty)$ is a continuous bijection, implying that the image of a dense set in this function is dense. We should therefore be able to extend the above result by considering sequences of suitable rational approximations.

Indeed, suppose that we fix arbitrary g and take as ansatz the linear scaling

$$zN_{D5} \sim N_{NS5} \,, \tag{E.47}$$

with $z \in \mathbb{R}^+$ *any* fixed positive constant. In this case, requiring (E.17) to be satisfied implies

$$\sqrt{g} l \sim \frac{z}{\sqrt{g}} k \,, \tag{E.48}$$

and given the relationship between linking numbers and SUGRA parameters (and the assumption that l, k will be suppressed), this would appear to require

$$\frac{N_{D3}}{N_{NS5}} \sim \frac{2}{\pi} \arctan(z/g) \,, \qquad \frac{\hat{N}_{D3}}{N_{D5}} \sim \frac{2}{\pi} \arctan(g/z) \,. \tag{E.49}$$

We would like to construct a sequence of quadruples of parameters $\Big(N_{D5}(n), N_{NS5}(n), N_{D3}(n), \hat{N}_{D3}(n)\Big)$ exhibiting the scaling that we have suggested, subject to the requirement that these parameters must be positive integers. The most natural way to approach this is to take sequences of rationals $\frac{a_n}{b_n}, \frac{p_n}{q_n}$ in reduced form such that

$$\frac{a_n}{b_n} \to \frac{2}{\pi} \arctan(z/g) \,, \qquad \frac{p_n}{q_n} \to z \,, \tag{E.50}$$

and then define[120]

$$\begin{aligned}
N_{D5}(n) &= b_n q_n f_n + \alpha_n \,, & \alpha_n &= o(b_n q_n f_n) \\
N_{NS5}(n) &= b_n p_n f_n + \beta_n \,, & \beta_n &= o(b_n p_n f_n) \\
N_{D3}(n) &= a_n p_n f_n + \gamma_n \,, & \gamma_n &= o(a_n p_n f_n) \\
\hat{N}_{D3}(n) &= (b_n - a_n) q_n f_n + \delta_n \,, & \delta_n &= o\left((b_n - a_n) q_n f_n\right) \,,
\end{aligned} \tag{E.51}$$

where f_n is left undetermined for the time being. Equation (E.26) then implies

$$\begin{aligned}
&N_{D5}(n) N_{D3}(n) + N_{NS5}(n) \hat{N}_{D3}(n) \\
&\quad = (b_n q_n f_n + \alpha_n)(a_n p_n f_n + \gamma_n) \\
&\qquad + (b_n p_n f_n + \beta_n)((b_n - a_n) q_n f_n + \delta_n) \\
&\quad = N_{D5}(n) N_{NS5}(n) \\
&\qquad + ((a_n - b_n) p_n \alpha_n + b_n q_n \gamma_n - a_n q_n \beta_n + b_n p_n \delta_n) f_n \\
&\qquad + \alpha_n \gamma_n + \beta_n \delta_n - \alpha_n \beta_n \,.
\end{aligned} \tag{E.52}$$

For any fixed n, this is precisely the same as (E.37), which we found to be consistent with the requirement $N_{D5} N_{D3} + N_{NS5} \hat{N}_{D3} = N + N_{D5} N_{NS5}$ for suitably chosen $(\alpha, \beta, \gamma, \delta)$. Consequently, we may here find $(\alpha_n, \beta_n, \gamma_n, \delta_n)$ which make our definitions of the parameters consistent with this equation for each n; once we have defined (a_n, b_n, p_n, q_n) and $(\alpha_n, \beta_n, \gamma_n, \delta_n)$ in this way, we may then simply choose a sequence f_n which scales sufficiently quickly such that we recover the necessary asymptotics

$$\begin{aligned}
\alpha_n &= o(b_n q_n f_n) \,, & \beta_n &= o(b_n p_n f_n) \,, \\
\gamma_n &= o(a_n p_n f_n) \,, & \delta_n &= o\left((b_n - a_n) q_n f_n\right) \,.
\end{aligned} \tag{E.53}$$

The sequence of solutions that we have defined will then have the desired asymptotic suppression of $\max\{l, k\}$ and $|cl - dk|$, as can be shown in a manner identical to that discussed above.

[120] In this section, $o()$ refers to the standard "little o" notation.

E.5 Nearby solutions with multiple poles

It is reasonable to expect that the precise form of our boundary condition, and in particular the linear quiver from which our boundary condition descends, can be relaxed somewhat, and indeed we expect that the broad geometrical features of the holographic description, including the existence of a large $\mathrm{AdS}_5 \times S^5$ region, should be robust to certain "small" deformations of this quiver. As a concrete example, we may consider a family of solutions (the simplest family constructed earlier in Appendix E.4) with parameters of the form

$$N_{D5} = bn + \alpha\,, \quad N_{NS5} = bzn + \beta\,, \quad N_{D3} = azn + \gamma\,, \quad \hat{N}_{D3} = (b-a)n + \delta\,; \tag{E.54}$$

here, $\alpha, \beta, \gamma, \delta$ are constants chosen to satisfy $N = \alpha\gamma + \beta\delta - \alpha\beta$, and the constants a, b, z satisfy

$$\tan^{-1}(z/g) = \frac{\pi}{2}\frac{a}{b}\,, \quad a, b \in \mathbb{N}^+\,, \quad \gcd(a,b) = 1\,. \tag{E.55}$$

Each element of this sequence corresponds to a quiver of the form provided in Figure 6.5. We will now consider deforming these quivers for each n by coupling an additional $s(n)$ fundamental hypermultiplets to the $(N_{D3}+1)^{\text{th}}$ node of the quiver, where $s(n)$ may scale with n but we require $s(n) = o(n)$. In this deformation, we have two stacks of D5-branes and two stacks of NS5-branes with inequivalent linking numbers, described by the parameters

$$\begin{aligned} N^{(1)}_{D5} &= bn + \alpha\,, \quad N^{(1)}_{NS5} = azn + \gamma + 1\,, \\ N^{(2)}_{D5} &= s\,, \quad N^{(2)}_{NS5} = (b-a)zn + \beta - \gamma - 1\,, \end{aligned} \tag{E.56}$$

and

$$\begin{aligned} N^{1}_{D3} &= azn + \gamma\,, \quad \hat{N}^{1}_{D3} = (b-a)n + \delta\,, \\ N^{2}_{D3} &= azn + \gamma + 1\,, \quad \hat{N}^{2}_{D3} = (b-a)n + \delta + s\,. \end{aligned} \tag{E.57}$$

At leading order (namely at order $O(n)$), (6.4) gives the conditions

$$\begin{aligned}
\frac{\pi}{2}a &= a\tan^{-1}(l_1/k_1) + (b-a)\tan^{-1}(l_1/k_2) + o(n^0) \\
\frac{\pi}{2}a &= a\tan^{-1}(l_2/k_1) + (b-a)\tan^{-1}(l_2/k_2) + o(n^0) \\
\frac{\pi}{2}(b-a) &= b\tan^{-1}(k_1/l_1) + o(n^0) \\
\frac{\pi}{2}(b-a) &= b\tan^{-1}(k_2/l_1) + o(n^0)\,,
\end{aligned} \tag{E.58}$$

from which we can infer

$$\frac{g}{z} = \frac{k_1}{l_1} + o(n^0) = \frac{k_2}{l_1} + o(n^0) = \frac{k_1}{l_2} + o(n^0) = \frac{k_2}{l_2} + o(n^0) \tag{E.59}$$

and thus from (6.13)

$$\begin{aligned}
l_1 &= \frac{N}{\sqrt{g}b}\frac{1}{2n} + o(n^{-1})\,, \qquad & l_2 &= \frac{N}{\sqrt{g}b}\frac{1}{2n} + o(n^{-1})\,, \\
k_1 &= \frac{\sqrt{g}N}{zb}\frac{1}{2n} + o(n^{-1})\,, \qquad & k_2 &= \frac{\sqrt{g}N}{zb}\frac{1}{2n} + o(n^{-1})\,,
\end{aligned} \tag{E.60}$$

and

$$\Delta = \left|c_1 l_1 + c_2 l_2 - d_1 k_1 - d_2 k_2\right| = o(n^0)\,. \tag{E.61}$$

Since $\max\{l_A, k_B\}$ and Δ are again suppressed for large n, we find that we recover the desired geometrical features in this limit. In particular, while we now have two D5-brane throats and two NS5-brane throats, the total D5-brane and NS5-brane charges are approximately the same as before, and the separation between each pair of 5-brane throats in this case is subleading in n,

$$\frac{l_1 - l_2}{l_1} = o(n^0)\,, \qquad \frac{k_1 - k_2}{k_1} = o(n^0)\,. \tag{E.62}$$

It is straightforward to show that a similar argument can be applied to a more general version of this deformation, where we couple $o(n)$ fundamental hypermultiplets at each of $O(n^0)$ nodes in the quiver, where the location of these nodes relative to the left endpoint of the quiver scales proportionally to the overall size of the quiver with n.

Another deformation of interest involves coupling an additional small quiver to the left endpoint of our initial quiver, i.e. the endpoint opposite that which is coupled directly to the 4D theory upon imposing our field theory boundary condition. Here, "small quiver" refers to a quiver described by an $O(1)$ number of parameters $(N_{D5}^{(A)}, N_{D3}^{A})$ and $(N_{NS5}^{(B)}, \hat{N}_{D3}^{B})$, all of which are dominated by our initial parameters $(N_{D5}, N_{NS5}, N_{D3}, \hat{N}_{D3})$. We can couple the large and small quivers together via bifundamental matter coupled to an extra $U(m)$ node, where m is also dominated by our initial parameters; the result will be a good quiver, provided that the small quiver is good. This procedure results in a boundary condition described by many distinct parameters, which we can denote by $(N_{D5}^{(A)}, N_{D3}^{A})_{A=1\ldots p}$ and $(N_{NS5}^{(B)}, \hat{N}_{D3}^{B})_{B=1\ldots q}$ with some abuse of notation (they are different from those describing the small quiver). Notably, $(N_{D5}^{(p)}, N_{NS5}^{(q)}, N_{D3}^{p}, \hat{N}_{D3}^{q})$ agree with the original parameters $(N_{D5}, N_{NS5}, N_{D3}, \hat{N}_{D3})$ at leading order. From

$$\begin{aligned} N_{D3}^{p} &= \sqrt{g} l_p + \frac{2}{\pi} \sum_B N_{NS5}^{(B)} \arctan\left(l_p / k_B\right) \\ \hat{N}_{D3}^{q} &= \frac{1}{\sqrt{g}} k_q + \frac{2}{\pi} \sum_A N_{D5}^{(A)} \arctan\left(k_q / l_A\right) \ , \end{aligned} \tag{E.63}$$

and the fact that $N_{D5}^{(A)}, N_{NS5}^{(B)} \ll N_{D5}^{(p)}, N_{NS5}^{(q)}$ for $A < p$ and $B < q$, we see that the leading behaviour of l_p, k_q will be the same as before the deformation. Moreover, the remaining equations for the linking numbers imply

$$l_A / k_q = O\left(L_A / N_{NS5}^{(q)}\right) \ , \qquad k_B / l_p = O\left(K_B / N_{D5}^{(p)}\right) \tag{E.64}$$

for $A < p$ and $B < q$. Consequently, the newly added parameters are suppressed compared to l, k, and contribute to Δ at subleading order; we therefore arrive again at a solution with a large $\mathrm{AdS}_5 \times S^5$ region.

E.6 Multi-wedge generalizations

Our goal in this section is to understand how to construct theories whose holographic description involves several wedges of $\mathrm{AdS}_5 \times S^5$ connected by

interface branes; this applies to the BCFT case as well as the case involving 3D SCFTs which descend from linear or circular quiver gauge theories. The intuition behind our construction is illustrated in Figure E.1.

Our construction in this section will begin with a list

$$(m_0, m_1, m_2, \ldots, m_{p-1}, m_p) \tag{E.65}$$

of non-negative integers, where we fix p for concreteness. In the linear quiver case, we will have $m_0 = m_p = 0$, in the circular quiver case, we will have $m_0 = m_0 = L \neq 0$, and in the BCFT case, we will have $m_0 = 0$ and $m_p = N$. We would then like to define the required field theory data

$$(N^1_{D3}, \ldots, N^p_{D3})\,,\ (\hat{N}^1_{D3}, \ldots, \hat{N}^p_{D3})\,,\ (N^{(1)}_{D5}, \ldots, N^{(p)}_{D5})\,,\ (N^{(1)}_{NS5}, \ldots, N^{(p)}_{NS5})\,, \tag{E.66}$$

where the linking numbers are listed in increasing order. We will define these via the brane configuration depicted in Figure E.1; we have "blocks" with large numbers of D5-branes and NS5-branes $N^{(A)}_{D5}, N^{(A)}_{NS5}$, each with large linking numbers $N^A_{D3}, \hat{N}^A_{D3}$ respectively, and the $(A-1)^{\text{th}}$ and A^{th} blocks are connected by m_A D3-branes. The quantities $(N^{(A)}_{D5}, N^{(A)}_{NS5}, N^A_{D3}, \hat{N}^A_{D3})$ which parametrize the A^{th} block may be constructed in a completely identical manner to the construction of the one-parameter families we considered in Section 6.4.3 and Appendix E.4, with the simple replacement $N \to (m_A - m_{A-1})$; in particular, the linking numbers $\bar{N}^A_{D3}, \hat{\bar{N}}^A_{D3}$ that we would obtain from that construction will be related to the correct linking numbers $N^A_{D3}, \hat{N}^A_{D3}$ in the full quiver of the present construction by

$$N^A_{D3} = \bar{N}^A_{D3} + \sum_{B=1}^{A-1} N^{(B)}_{NS5}\,, \qquad \hat{N}^A_{D3} = \hat{\bar{N}}^A_{D3} + \sum_{B=1}^{A-1} N^{(B)}_{D5}\,, \tag{E.67}$$

since we need to account for the fact that the linking numbers depend on the quantities of 5-branes present in previous blocks. Ultimately, we will take all of the m_A (and the number of blocks p) to be $O(1)$ in some large parameters which will determine the number of 5-branes and linking numbers in the A^{th} block.

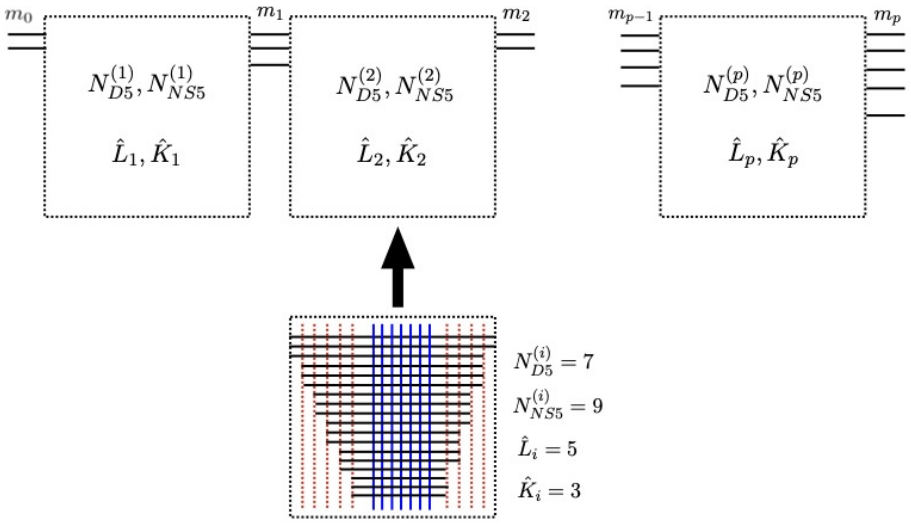

Figure E.1: D-brane construction giving rise to the class of boundary conditions considered in this appendix. We have "blocks" consisting of D3-branes stretched between $N_{D5}^{(i)}$ D5-branes and $N_{NS5}^{(i)}$ NS5-branes with fixed linking numbers L_i, K_i, where ultimately we will take $N_{D5}^{(i)}, N_{NS5}^{(i)}, L_i, K_i$ to scale with some large quantity. The $(i-1)^{\text{th}}$ and i^{th} blocks are connected by m_i D3-branes. We give an example of the brane configuration in one such block, with D3-branes shown in black, D5-branes in blue, and NS5-branes in red.

The above is the sense in which these boundary conditions correspond to "glued together" sub-quivers; the sub-quivers that are being coupled in this case are precisely those that arose in the discussion of Section 6.4.3, corresponding to boundary conditions described by single linking numbers $N_{D3}, \hat{N}_{D3}$, with the replacement $N \to (m_A - m_{A-1})$ in the present context.

We proceed to define $(\bar{N}_{D3}^A, \hat{\bar{N}}_{D3}^A, N_{D5}^{(A)}, N_{NS5}^{(A)})$, beginning in full generality with the case of arbitrary coupling g; in general, we construct these exactly as in Appendix E.4, taking

$$N_{D5}^{(A)} = b_n^{(A)} q_n^{(A)} f_n^{(A)} + \alpha_n^{(A)} , \qquad N_{NS5}^{(A)} = b_n^{(A)} p_n^{(A)} f_n^{(A)} + \beta_n^{(A)} \tag{E.68}$$

and

$$\bar{N}^A_{D3} = a_n^{(A)} p_n^{(A)} f_n^{(A)} + \gamma_n^{(A)} \,, \qquad \hat{\bar{N}}^A_{D3} = (b_n^{(A)} - a_n^{(A)}) q_n^{(A)} f_n^{(A)} + \delta_n^{(A)} \,, \tag{E.69}$$

where

$$\frac{a_n^{(A)}}{b_n^{(A)}} \to \frac{2}{\pi} \tan^{-1}(z_A/g) \,, \qquad \frac{p_n^{(A)}}{q_n^{(A)}} \to z_A \tag{E.70}$$

for some z_A, the quantities $\alpha_n^{(A)}, \beta_n^{(A)}, \gamma_n^{(A)}, \delta_n^{(A)}$ sastisfy

$$\alpha_n^{(A)} \gamma_n^{(A)} + \beta_n^{(A)} \delta_n^{(A)} - \alpha_n^{(A)} \beta_n^{(A)} = m_A - m_{A-1} \,, \tag{E.71}$$

and $f_n^{(A)}$ is quickly-scaling. Then, passing to the linking numbers by (E.67), we have that

$$\sum_{A=1}^{p} \left(N_{D5}^{(A)} N_{D3}^A + N_{NS5}^{(A)} \hat{N}_{D3}^A \right) = m_p - m_0 + N_{D5} N_{NS5} \tag{E.72}$$

and the linking numbers are increasing by construction, We will also require that $f_n^{(A)}$ scales sufficiently quickly relative to $f_n^{(A-1)}$ such that the parameters in block A scale at least as quickly as the parameters in block $A-1$. We can now consider how the SUGRA parameters behave for each case.

E.6.1 Multi-wedge dual of BCFT

Recalling that

$$\sum_{A=1}^{p} \left(\sqrt{g} N_{D5}^{(A)} l_A + \frac{1}{\sqrt{g}} N_{NS5}^{(A)} k_A \right) = N \,, \tag{E.73}$$

and all of the l_A, k_A are positive, we see that one must have

$$l_A < \frac{N}{N_{D5}^{(A)}} \,, \qquad k_A < \frac{N}{N_{NS5}^{(A)}} \,, \tag{E.74}$$

so that in particular

$$\lim_{n \to \infty} l_A, k_A = 0 \,. \tag{E.75}$$

We have from our definitions

$$\begin{aligned} N^A_{D3} &= a^{(A)}_n p^{(A)}_n f^{(A)}_n + \gamma^{(A)}_n + \sum_{B=1}^{A-1} \left(b^{(A)}_n p^{(A)}_n f^{(A)}_n + \beta^{(A)}_n \right) \\ \hat{N}^A_{D3} &= (b^{(A)}_n - a^{(A)}_n) q^{(A)}_n f^{(A)}_n + \delta^{(A)}_n + \sum_{B=1}^{A-1} \left(b^{(A)}_n q^{(A)}_n f^{(A)}_n + \alpha^{(A)}_n \right) , \end{aligned} \tag{E.76}$$

as well as the relations to SUGRA parameters

$$\begin{aligned} N^A_{D3} &= \sqrt{g} l_A + \frac{2}{\pi} \sum_{B=1}^{p} \left(b^{(A)}_n p^{(A)}_n f^{(A)}_n + \beta^{(A)}_n \right) \tan^{-1}\left(l_A / k_B \right) \\ \hat{N}^A_{D3} &= \frac{1}{\sqrt{g}} k_A + \frac{2}{\pi} \sum_{B=1}^{p} \left(b^{(A)}_n q^{(A)}_n f^{(A)}_n + \alpha^{(A)}_n \right) \tan^{-1}\left(k_A / l_B \right) . \end{aligned} \tag{E.77}$$

Comparing these expressions at leading order, we see that consistency is achieved by requiring

$$\lim_{n\to\infty} \frac{l_A}{k_A} = \frac{z_A}{g} \tag{E.78}$$

and

$$\lim_{n\to\infty} \frac{l_A}{l_B} = \lim_{n\to\infty} \frac{k_A}{k_B} = 0 , \qquad A < B . \tag{E.79}$$

Schematically, we can say that $g l_A \sim z_A k_A$ and

$$l_1 \ll l_2 \ll \ldots \ll l_p \ll 1 , \quad k_1 \ll k_2 \ll \ldots \ll k_p \ll 1 . \tag{E.80}$$

We therefore find

$$\lim_{n\to\infty} \Big| \sum_{A=1}^{p} \left(N^{(A)}_{D5} l_A - N^{(A)}_{NS5} k_A \right) \Big| = 0 , \tag{E.81}$$

as desired.

We have demonstrated that our construction thus far possesses a large $\mathrm{AdS}_5 \times S^5$ asymptotic region; to ensure that we recover a multi-wedge deep in the interior, we will actually consider a subset of the families defined so far for which the parameters $(N^{(A)}_{D5}, N^{(A)}_{NS5}, \bar{N}^A_{D3}, \hat{\bar{N}}^A_{D3})$ of block A are all taken

to scale with the same large parameter as the parameters of block $A-1$, as opposed to scaling strictly faster. Note that the "doubled" construction of Section 6.6.1 is an example of this choice. In this case, it suffices to note that for $l_A, k_A \ll r \ll l_{A+1}, k_{A+1}$, we find the leading behaviour of h_1, h_2 to be

$$\begin{aligned} h_1 &= \frac{\pi\ell_s^2}{2}\frac{r\cos\theta}{\sqrt{g}} + \frac{\ell_s^2}{4}\sum_A \frac{c_A}{\sqrt{g}}\ln\left(\frac{(r\cos\theta + l_A)^2 + r^2\sin^2\theta}{(r\cos\theta - l_A)^2 + r^2\sin^2\theta}\right) \\ &= \ell_s^2 \sum_{B\leq A} N_{D5}^{(B)}\left(\frac{l_B}{r}\cos\theta + O(l_B^3/r^3)\right) \\ &\quad + \ell_s^2 \sum_{B>A} N_{D5}^{(B)}\left(\frac{r}{l_B}\cos\theta + O(r^3/l_B^3)\right) \\ &\approx \ell_s^2\cos\theta\left(N_{D5}^{(A)}\frac{l_A}{r} + N_{D5}^{(A+1)}\frac{r}{l_{A+1}}\right) \end{aligned} \tag{E.82}$$

and

$$\begin{aligned} h_2 &= \frac{\pi\ell_s^2}{2}\sqrt{g}r\sin\theta + \frac{\ell_s^2}{4}\sum_A d_A\sqrt{g}\ln\left(\frac{r^2\cos^2\theta + (r\sin\theta + k_A)^2}{r^2\cos^2\theta + (r\sin\theta - k_A)^2}\right) \\ &= \ell_s^2 \sum_{B\leq A} N_{NS5}^{(B)}\left(\frac{k_B}{r}\sin\theta + O(k_B^3/r^3)\right) \\ &\quad + \ell_s^2 \sum_{B>A} N_{NS5}^{(B)}\left(\frac{r}{k_B}\cos\theta + O(r^3/k_B^3)\right) \\ &\approx \ell_s^2\sin\theta\left(N_{NS5}^{(A)}\frac{k_A}{r} + N_{NS5}^{(A+1)}\frac{r}{k_{A+1}}\right)\ . \end{aligned} \tag{E.83}$$

Since $z_B N_{D5}^{(B)} \sim N_{NS5}^{(B)}$ and $\sqrt{g}l_B \sim \frac{z_B}{\sqrt{g}}k_B$, the geometry in this region is approximately that of $\mathrm{AdS}_5 \times S^5$, where the value of r_0 is proportional to the geometric mean of l_A (or k_A) and l_{A+1} (or k_{A+1}), and the AdS radius in this wedge scales relative to the AdS radius in the asymptotic region as $L^4_{\text{wedge}}/L^4_{\text{AdS}} \sim \frac{N_{D5}^{(A)}N_{D5}^{(A+1)}}{N^2}\frac{l_A}{l_{A+1}}$.

E.6.2 Multi-wedge dual of SCFT: linear quiver

As at the end of last section, we will continue to restrict to the case where the linking numbers and charges for each block are all taken to scale with the same large parameter. The linking numbers $N^A_{D3}, \hat{N}^A_{D3}$ are related to parameters $N^{(A)}_3, \hat{N}^{(A)}_3$ by

$$N^{(A)}_3 = N_{NS5} - N^A_{D3}\,, \qquad \hat{N}^{(A)}_3 = \hat{N}^A_{D3}\,, \tag{E.84}$$

so we can write (6.74) as

$$\begin{aligned} N^A_{D3} &= \frac{2}{\pi}\sum_B \hat{N}^{(B)}_5 \tan^{-1}\left(e^{\hat{\delta}_B - \delta_A}\right) \\ \hat{N}^B_{D3} &= \frac{2}{\pi}\sum_A N^{(A)}_5 \tan^{-1}\left(e^{\delta_A - \hat{\delta}_B}\right)\,. \end{aligned} \tag{E.85}$$

It is immediate that we obtain the desired behaviour in this case, since this system of equations is identical to the system from the BCFT case up to subleading terms if we identify $l_A \leftrightarrow e^{-\delta_A}$ and $k_B \leftrightarrow e^{-\hat{\delta}_B}$, and the definitions of h_1, h_2 will have the same leading behaviour in the regions of interest.

E.6.3 Multi-wedge dual of SCFT: circular quiver

The solutions of type IIB supergravity describing the vacuum states of 3D SCFTs arising from circular quiver gauge theories have not yet been discussed in this note, but were first analyzed in [297]. These solutions are similar to those arising from linear quivers, with harmonic functions h_1, h_2 now given by

$$\begin{aligned} h_1 &= -\sum_{a=1}^{p}\gamma_a \ln\left(\prod_{n=-\infty}^{\infty}\tanh\left(\frac{\pi i}{4} - \frac{z-(\delta_a+2nt)}{2}\right)\right) + \text{c.c.}\,, \\ h_2 &= -\sum_{b=1}^{\hat{p}}\hat{\gamma}_b \ln\left(\prod_{n=-\infty}^{\infty}\tanh\left(\frac{\pi i}{4} - \frac{z-(\hat{\delta}_b+2nt)}{2}\right)\right) + \text{c.c.}\,, \end{aligned} \tag{E.86}$$

where t is a positive parameter satisfying $0 \leq \delta_a, \hat{\delta}_b \leq 2t$. These functions are periodic under $\mathrm{Re}(z) \to \mathrm{Re}(z)+2t$ by construction, and we can alternatively express them using Jacobi ϑ-functions as

$$\begin{aligned} h_1 &= -\sum_{a=1}^{p} \gamma_a \ln\left(\frac{\vartheta_1(\nu_a|\tau)}{\vartheta_2(\nu_a|\tau)}\right) + \text{c.c.}\,, \qquad i\nu_a = -\frac{z-\delta_a}{2\pi} + \frac{i}{4}\,, \\ h_2 &= -\sum_{b=1}^{\hat{p}} \hat{\gamma}_b \ln\left(\frac{\vartheta_1(\hat{\nu}_b|\tau)}{\vartheta_2(\hat{\nu}_b|\tau)}\right) + \text{c.c.}\,, \qquad i\hat{\nu}_b = \frac{z-\hat{\delta}_b}{2\pi} \end{aligned} \tag{E.87}$$

on a torus with modular parameter $\tau = it/\pi$.

The linking numbers and supergravity parameters are now related by

$$\begin{aligned} N^A_{D3} &= \frac{2}{\pi}\sum_B N^{(B)}_{NS5}\left(\sum_{n=0}^{\infty}\arctan\left(e^{-\hat{\delta}_B+\delta_A-2nt}\right)\right. \\ &\qquad \left. -\sum_{n=1}^{\infty}\arctan\left(e^{\hat{\delta}_B-\delta_A-2nt}\right)\right) \\ \hat{N}^A_{D3} &= \frac{2}{\pi}\sum_B N^{(B)}_{D5}\left(\sum_{n=0}^{\infty}\arctan\left(e^{\hat{\delta}_B-\delta_A-2nt}\right)\right. \\ &\qquad \left. -\sum_{n=1}^{\infty}\arctan\left(e^{-\hat{\delta}_B+\delta_A-2nt}\right)\right) \end{aligned} \tag{E.88}$$

and

$$\begin{aligned} N_{D3} &= \frac{2}{\pi}\sum_A\sum_B N^{(A)}_{D5}N^{(B)}_{NS5} \\ &\quad \times\sum_{s=1}^{\infty} s\left(\arctan(e^{\hat{\delta}_B-\delta_A-2st}) + \arctan(e^{\delta_A-\hat{\delta}_B-2st})\right)\,, \end{aligned} \tag{E.89}$$

where $N_{D3} = m_0 = m_p$.

The linking number conditions can again be satisfied by requiring

$$e^{-\delta_A}, e^{-\hat{\delta}_A} \ll e^{-\delta_{A+1}}, e^{-\hat{\delta}_{A+1}} \tag{E.90}$$

and

$$e^{\hat{\delta}_A - \delta_A} \sim \tan\left(\frac{\pi}{2}\frac{\bar{K}_A}{N_{D5}^{(A)}}\right) \sim \frac{g}{z_A}\,, \tag{E.91}$$

provided t is sufficiently large that

$$e^{-\hat{\delta}_B + \delta_A - 2t} \ll 1\,, \qquad e^{\hat{\delta}_B - \delta_A - 2t} \ll 1 \tag{E.92}$$

for all A, B. It is clear from the expression for N_{D3} that these conditions must be true, since $N_{D5}^{(A)}, N_{NS5}^{(B)} \gg N_{D3}$. Again, in the region $\delta_A \ll \mathrm{Re}(z) \ll \delta_{A+1}$, the harmonic functions h_1, h_2 agree with those from the linear quiver case at leading order, since the additional contributions coming from the $n \neq 0$ terms will be suppressed.